April 2006

UNIVERSITY OF CANTERBURY
Te Whare Wānanga o Waitaha
CHRISTCHURCH NEW ZEALAND

Late Pleistocene Glacial Geology of the Hope-Waiau Valley System in North Canterbury, New Zealand

A thesis submitted in partial fulfilment of the requirements
for the Degree of

Doctor of Philosophy
in Geology

in the University of Canterbury

by

Henrik Rother

The Hope – Boyle River confluence west of Hanmer Basin.

Table of Contents

List of figures..... 5

List of tables..... 10

Abstract..... 11

Chapter 1

Introduction

1.1. General Introduction..... 12
1.2. Objectives of this study..... 14
1.3. Thesis structure..... 15
1.4. Methodology / Field work..... 16

Chapter 2

Late Pleistocene glaciations in the Southern Alps: a review of the Canterbury valley systems

2.1. Geological, topographic and climatic setting..... 18
2.2. Historical Review..... 20
2.2.1. The beginnings: 1861 - 1910..... 20
2.2.2. The later pioneering phase: 1910 - 1958..... 22
2.2.3. Post - 1958…..... 23
2.3. Geochronological summary 32

Chapter 3

The Hope-Waiau Valley system

3.1. Physiography..... 38
3.2. Bedrock geology and tectonic setting..... 40
3.3. Previous glacial work..... 43

Chapter 4

Stratigraphy and tectonic implications of Late Pleistocene valley fill deposits in the lower Hope Valley

4.1. Introduction 50
4.2. Local setting: the lower Hope basin..... 51

4.3. Quaternary context....54
4.4. Methodology....56
4.4.1. Ground penetrating radar....57
4.4.2. Luminescence dating....58
4.5. Results....60
4.5.1. Glynn Wye outcrop....60
4.5.2. GPR results and interpretations....63
4.5.3. IRSL results....71
4.6. Discussion....73
4.7. Summary and conclusions....76

Chapter 5

Sedimentology of and depositional model for glacial sediments at Poplars Gully in the lower Hope Valley

5.1. Introduction....77
5.2. The Poplars Gully study site....77
5.3. Quaternary geological setting....79
5.4. Methods….....80
5.4.1. Sedimentary logging....80
5.4.2. IRSL methods....81
5.5. Results….....82
5.5.1. Lithofacies descriptions and interpretations....82
5.5.2. Luminescence results....93
5.6. Discussion....96
5.6.1. Site history and depositional....96
5.6.2. Regional glacial and tectonic implications....100
5.7. Summary and conclusions....103

Chapter 6

Chronology and sequence architecture of valley fill terraces between the middle Hope and lower Waiau Valleys

6.1. Introduction....105
6.2. Valley geomorphometry....107
6.3. Valley fill lithostratigraphy and geochronology....111
6.3.1.Methods....112
6.3.2. The terrace sequence....113
6.3.3. Valley fill stratigraphy and sedimentology….....115
6.3.3.1. Glynn Wye Stream....116
6.3.3.2. Carlyle Terrace....119
6.3.3.3. Middle Hope Valley....120
6.3.3.4. Horseshoe, Kakapo and Glynn Wye Terraces....123

6.4. IRSL results 125
6.5. Discussion and summary 128
6.5.1. Valley fill and sedimentary architecture 128
6.5.2. Geochronology 129

Chapter 7

Surface exposure dating of glacial moraines in the Hope-Waiau Valleys

7.1. Introduction 132
7.2. Cosmogenic dating: background 133
7.3. Methods 135
7.3.1. The sampling campaign 135
7.3.2. Chemical preparation and isotope measurement 137
7.3.3. Data correction 140
7.4. Results 142
7.5. Discussion and conclusion 143

Chapter 8

Glacial systems of the Southern Alps: Sensitivity to climate parameters and implications for the forcing of glaciations

8.1. Introduction 147
8.2. LGM and LGIT climates of New Zealand 149
8.3. Glaciological setting 151
8.4. Temperature effects on snow mass balances in the Southern Alps 154
8.5. Discussion 160

Chapter 9

Discussion and Conclusion

9.1. Geochronology 168
9.1.1. Valley fill sequence 170
9.1.2. Glacial advances 173
9.2. Sedimentary architecture of the Hope-Waiau valley fill 176
9.3. The New Zealand glacial system: Towards a model for glaciation in the Southern Alps 178

Acknowledgements 185

References 186

Appendices

Appendix 1A: Papers produced from this thesis to date:

1.1. Rother, H., Shulmeister, J. (in press). Synoptic climate change as a driver of late Quaternary glaciations in the mid-latitudes of the Southern Hemisphere, Climate of the Past..... 209

1.2. Rother, H., Jol, H.M., Shulmeister, J. (in press). Stratigraphy and tectonic implications of Late Pleistocene valley fill in the Hope Valley, Canterbury, South Island, New Zealand. In: Baker, G.S., Jol, H.M. (eds.). Progress in stratigraphic analyses using ground penetrating radar (GPR), Geological Society of America, Special Publication..... 228

1.3. Rother, H., Rieser, U., Shulmeister, J. (submitted). Stratigraphy and depositional model of a OIS 6 glacial sequence in the Hope Valley, Southern Alps, New Zealand. Quaternary Science Reviews..... 256

Appendix 1B: Co-authored papers

1.4. Nobes, D.C., Rother, H., Kruk, van der, J., Jol, H.M. (2006). Radar 'lensing' by a small river: Can a layer of surface water improve the signal?, Near Surface Geophysics, Special Issue on Ground Penetrating Radar 4: 69-74..... 292

Appendix 2: Sample details for age determinations

2.1. Luminescence dating..... 300
2.2. Cosmogenic surface exposure dating.....302
2.3. Radiocarbon dating..... 305

Appendix 3: Compilation of absolute age control for the eastern Southern Alps

3.1. Hope-Waiau Valleys..... 307
3.2. Waimakariri Valley.....311
3.3. Rakaia Valley.....313
3.4. Rangitata Valley.....316
3.5. Mackenzie Basin..... 317

Appendix 4: Data depository for glacial model of Chapter 8

4.1. Precipitation data: Rain/snow ratios and snowfall values.....319
4.2. Snow ablation and net accumulation data.....332

List of Figures

Chapter 2

Fig. 1. Overview summarizing locations and limits of Late Pleistocene glacial advances in the Waimakariri Valley.

Fig. 2. Overview summarizing locations and limits of Late Pleistocene glacial advances in the Rakaia Valley.

Fig. 3. Overview summarizing locations and limits of Late Pleistocene glacial advances in the Rangitata / Ashburton Valleys.

Fig. 4. Overview summarizing locations and limits of Late Pleistocene glacial advances in the Mackenzie Basin.

Fig. 5. Summary of the Late Pleistocene and Early Holocene absolute age control for the main Canterbury Valley systems.

Chapter 3

Fig. 6. General overview of locations, topography and tectonic setting of the study area in the central South Island of New Zealand.

Fig. 7. Downvalley accumulation of catchment area between Lewis Pass and Hanmer Basin.

Fig. 8. Fault trace of the Hope Fault on the Glynn Wye Terrace.

Fig. 9. The fault trace of the Kakapo Fault in the middle Kakapo Valley.

Fig. 10. Limits of Late Pleistocene glacial advances in the Hope-Waiau Valleys.

Fig. 11. Clayton's (1968) map of late Pleistocene glacial deposits in the lower Hope Valley.

Fig. 12. View of the Kakapo Hill surface.

Fig. 13. Erratic boulder on Kakapo Hill.

Fig. 14. Glacial erratic on the Horseshoe surface.

Fig. 15. Horseshoe aggradational gravels at Manuka Creek.

Fig. 16. Exposed Glynn Wye moraines in the lower Hope Valley.

Fig. 17. Glynn Wye moraine at Windy Point.

Chapter 4

Fig. 18. Location of the lower Hope Valley in the South Island, New Zealand.

Fig. 19. Overview of structural geology and fault controlled features in the Boyle-Hope-Waiau Valley system.

Fig. 20. View of Poplars Graben in the lower Hope Valley.

Fig. 21. Alexander McKay at the offset fence line near Glynn Wye Station following the 1888 North Canterbury earthquake.

Fig. 22. Position and elevation of bedrock gorges and strath terraces in the lower Hope Basin.

Fig. 23. Glynn Wye terrace with preserved channel pattern.

Fig. 24. Quaternary geology of the lower Hope Valley study area (modified from Clayton, 1968).

Fig. 25. Upriver view (west) into the lower Hope Valley.

Fig. 26. GPR field set and crew comprising computer, antennae and cable operators.

Fig. 27. Location, context and stratigraphy of aggradational deposits at Glynn Wye Station.

Fig. 28. The G2 fluvial sequence at Kakapo Delta.

Fig. 29. Location and orientation of GPR transects presented in Figs. 30, 31 and 33 and photos presented in Fig. 32.

Fig. 30. 50-MHz GPR profile A.

Fig. 31. 50-MHz GPR profile B.

Fig. 32. Deformed lacustrine muds exposed at river level in the lower Hope Valley.

Fig. 33. 25-MHz and 50 MHz GPR profiles.

Chapter 5

Fig. 34. Location of the Hope Valley and the Marlborough Fault Zone in the South Island, New Zealand.

Fig. 35. Oblique aerial view into the lower portion of Poplars Gully in September 1995.

Fig. 36. View down valley from the lower Hope Valley.

Fig. 37. Stratigraphic overview of deposits at Poplars Gully.

Fig. 38. Stratigraphy, depositional context and sedimentological summary log for deposits exposed at the base of Poplars Gully (Facies A, Facies B).

Fig. 39. Particle sizes of laminated to banded silts and fine sands of Facies A.

Fig. 40. Stratigraphy, depositional context and sedimentological summary log of Facies C and Facies D.

Fig. 41. Deformation in Facies D.

Fig. 42. Stratigraphy, depositional context and sedimentological summary log of deposits in the upper section of Poplars Gully including Facies E, F, G and H.

Fig. 43. Stratigraphic positions of luminescence samples from Poplars Gully.

Fig. 44. Depositional model for the Poplars Gully sequence.

Chapter 6

Fig. 45. Major glacial valley and lake systems in the South Island and approximate zoning of valley fill types in the central Southern Alps.

Fig. 46. Glacial valleys of the Hope-Waiau catchment.

Fig. 47. Oblique aerial photos showing glacial and aggradational features in the study area.

Fig. 48. Relief ratio of the trunk glacial channel in the Hope-Waiau Valley system.

Fig. 49. Aggradational and degradational terraces in the lower Hope-Waiau Valleys.

Fig. 50. Fluvial terraces and cross valley profiles in the Hope and Waiau Valleys.

Fig. 51. Stratigraphic details of terraces previously identified to represent aggradation associated with the late glacial Lewis advance.

Fig. 52. Overview of deposits and terrace stratigraphy at Glynn Wye Stream.

Fig. 53. Till overlying fluvial deposits at Glynn Wye Stream in the lower Hope Valley.

Fig. 54. Overview of sediments, depositional context and stratigraphy at the Carlyle terrace exposure in the lower Hope Valley.

Fig. 55. Overview of deposits and stratigraphy in the middle Hope Valley.

Fig. 56. Overview of sediments and stratigraphy of glacial outwash terraces in the Hope-Waiau Valleys.

Fig. 57. Sand and silt units sampled for IRSL dating.

Fig. 58. Postglacial paleo-lake remnants in the lower Lewis Valley, lower Hope Valley and lower Boyle Valley.

Chapter 7

Fig. 59. Moraine locations sampled for exposure dating.

Fig. 60. Trajectories of cosmic ray particles that approach Earth's magnetic dipole field.

Fig. 61. Boulders sampled for cosmogenic dating from (a) the Glynn Wye moraine, (b) Glenhope moraine, (c) Kakapo moraine, and (d) Kiwi Stream moraine.

Fig. 62. Cosmogenic sample preparation flow diagram.

Fig. 63. Scaling factors for production rates of *in-situ* produced cosmogenic nuclides.

Chapter 8

Fig. 64. Summary of the temporal variations of Milankovitch orbital parameters and their combined effect on solar insolation received at 65° N.

Fig. 65. Comparison of precipitation and ELA levels across the Southern Alps and European Alps.

Fig. 66. Comparison of the minimum cirque floor elevations in the western/central and eastern Southern Alps.

Fig. 67. Locations of study area, Hokitika climate station and Ivory Glacier in the Southern Alps and the physical relationship between mean monthly temperature and the snow-rain ratio.

Fig. 68. The three annual precipitation scenarios used for snow mass balance modelling.

Fig. 69. Annual snowfall under cooling as a result of changes to the snow-rain ratio and variations in total annual precipitation.

Fig. 70. Impact of cooling on snow ablation at present ELA as calculated by the degree day mass balance model.

Fig. 71. Projected annual net snow accumulation as a result of variations in annual precipitation, snow-rain proportions and ablation under -1 to -9ºC cooling.

Fig. 72. Total estimated ice cover in the South Island during the LGM.

Fig. 73. Observed annual precipitation distribution at Glacier in the central Southern Alps.

Fig. 74. DEM analysed hypsometry above 1400 m in the central Southern Alps showing the potential increase in low angle (less than 15°) surface areas above snowline from a 300 m ELA lowering (1700 m to 1400 m).

Chapter 9

Fig. 75. Map of the Waiho Loop moraine, Franz Josef and surrounding glaciers.

Fig. 76. Geochronological summary from valley fill deposits in the lower Hope Valley.

Fig. 77. Conceptual glacial model for the Southern Alps.

List of Tables

Chapter 2

Table 1. Correlations of glacial chronologies in Canterbury and Westland.

Chapter 4

Table 2. Sample and radioactivity data for luminescence samples from the Kakapo Delta exposure.

Table 3. Measured a-values and equivalent doses as well as calculated dose rates and resulting luminescence ages from the Kakapo Delta exposure.

Chapter 5

Table 4. Facies codes used for sedimentary logging at Poplars Gully.

Table 5. Sample and radioactivity data for luminescence samples from Poplars Gully.

Table 6. Measured a-values and equivalent doses as well as calculated dose rates and resulting luminescence ages from Poplars Gully.

Table 7. Relative proportions of logged deposits in the Poplars Gully glacial sequence. Note the dominance of aqueous deposition.

Chapter 6

Table 8. Sample and radioactivity data for luminescence dating in the Hope-Waiau Valleys.

Table 9. Measured a-value and equivalent dose and calculated dose rate and luminescence age.

Chapter 7

Table 10. Sample name, NZ grid location (1:50 000) and descriptions of reported moraine boulders. Sample GW-B comes from the same boulder as GW-I.

Table 11. ^{10}Be cosmogenic isotope exposure ages for moraine in the Hope-Waiau Valleys. All ages are reported with 1s errors.

ABSTRACT

This thesis presents stratigraphic, sedimentological and geochronological results from valley fill and glacial moraines of the Hope-Waiau Valleys in North Canterbury, New Zealand. The findings demonstrate that a substantial portion of the modern valley fill comprises *in-situ* sedimentary sequences that were deposited during the penultimate glaciation (OIS 6), the last interglacial (OIS 5) and during the mid-late last glacial cycle (OIS 3/2). The sediments survived at low elevations in the valley floor despite overriding by later glacial advances. Sedimentologically, the fill indicates deposition in an ice marginal zone and consists of paraglacial/distal-proglacial aggradation gravels and ice-proximal/marginal-subglacial sediments. Deposition during glacial advance phases was characterized by the sedimentation of outwash gravels and small push moraines while glacial retreat phases are dominated by glaciolacustrine deposits which are frequently interbedded with debris flow diamictons. The overall depositional arrangement indicates that glacial retreat from the lower valley portion occurred via large scale ice stagnation.

Results from infra-red stimulated luminescence (IRSL) dating gives evidence for five large aggradation and degradation phases in the Hope-Waiau Valleys over the last 200 ka. Combined with surface exposure dating (SED) of moraines the geochronological results indicate that glacial advances during OIS 6 were substantially larger in both ice extent and ice volume than during OIS 4-2. The last glacial maximum (LGM) ice advance occurred prior to 20.5 ka and glacial retreat from extended ice positions began by ~18 ka BP. A late glacial re-advance (Lewis Pass advance) occurred at ~13 ka BP and is probably associated with a regional cooling event correlated to the Antarctic Cold Reversal (ACR).

The findings from the Hope-Waiau Valleys were integrated into a model for glaciations in the Southern Alps which uses data from a snow mass balance model to analyse the sensitivity of glacial accumulation to temperature forcing. Model results indicate that in the central hyperhumid sector of the Southern Alps ice would expand rapidly with minor cooling (2-4°C) suggesting that full glaciation could be generated with little thermal forcing. Some Quaternary glacial advances in the Southern Alps may have been triggered by regional climate phenomena (e.g. changes in ENSO mode) rather than requiring a thermal trigger from the Northern Hemisphere.

CHAPTER 1

GENERAL INTRODUCTION

The New Zealand sub-continent constitutes a group of islands located in the humid-temperate South West Pacific region stretching between the latitudes 34˚S and 47˚S. The present glacial cover of New Zealand comprises a total of 3,155 glaciers and glacierettes (National Snow and Ice Data Center, 1999)[1] which are largely confined to the highest ranges of the Southern Alps (the total land area in New Zealand covered by glaciers is about 1150 km^2). At various times during the Quaternary, ice accumulation increased dramatically producing large scale glaciations during which alpine piedmont glaciers advanced beyond the limits of the Southern Alps reaching the Tasman Sea in the west and extending into the eastern alpine forelands of Canterbury and Otago. As a result glacial sediments and landforms cover extensive areas in New Zealand and provide an important record of past glacial processes and associated regional paleo-climates.

Glaciers and their environments undoubtedly represent one of the most dynamic and spectacular geological landsystems on Earth. Quaternary glaciations in New Zealand have had a profound effect on the evolution of the physical landscape and are associated with the production, transport and deposition of enormous volumes of sediment. In addition to the importance of these records for regional reconstructions, glacial records from the Southern Alps are also globally significant because New Zealand has become a key location for the debate on interhemispheric correlations of Late Quaternary glacial events (e.g. Denton and Hendy, 1994; Broecker, 1997; Ivy-Ochs et al., 1999; Vandergoes et al., 2005). Results from our region have proven to be critical for the reconstruction of the underlying mechanisms of global climate teleconnections (e.g. Denton et al., 1999; Lowell et al., 1995).

Since the recognition of formerly extensive glaciations in New Zealand in the second half of the 19th century numerous glacial studies have investigated glacial records from the Southern Alps. Following a relatively long pioneering phase, the modern

[1] Glaciers exceeding 0.01 km^2 in size.

glacial framework was only established during the period 1958 - 1980 (e.g. Gage, 1958; McKellar, 1960; Soons, 1963a; Speight, 1963; Suggate, 1965; Clayton, 1968; Nathan and Moar, 1973; Mabin, 1980). The main emphasis during this phase was on the systematic differentiation of glacial landform associations, primarily based on the mapping of moraine positions and the tracing and matching of aggradational and degradational terrace surfaces. This largely geomorphological approach, although modified for its application in New Zealand, followed the glacial model developed for the European Alps (Penck and Brueckner, 1909). The completion of this work for all major glacial valley systems in the Southern Alps led to the formulation of a first comprehensive geomorphological and chronological model for Quaternary glaciations in New Zealand (e.g. Suggate 1965, 1990).

During the past 20 years dramatic progress has been made in the field of glacial geology. Of particular importance is the development of systematic sedimentological approaches to the study of glacial sediments which have increased the precision with which glacio-depositional environments can be reconstructed. Also critical is the development of new numerical dating techniques for Quaternary glacial sequences (e.g. cosmogenic dating, luminescence dating, accelerator mass spectrometry ^{14}C dating) which permit the dating of previously undateable materials and time intervals. Few of these new tools and approaches, however, have yet been employed on glacial deposits in New Zealand. For example, little detailed sedimentological and stratigraphic work has been completed on glacial valley fills in the Southern Alps (e.g. Bull, 1987; Hart, 1996). Similarly, only a limited number of numerical geochronological investigations have been carried out (Williams, 1996; Shulmeister et al, 2005). At present, absolute age control for Quaternary glacial events in the Southern Alps is still relatively poor and the problems are accentuated for glacial events beyond 20 ka. This suggests there is a reservoir of yet unexplored geological information and a clear need to revisit our glacial valley sequences. This work will be critical for the development of conceptual, stratigraphic and geochronological frameworks for past glaciations in New Zealand.

1.2. Objectives of this study

The goal of this PhD project is to document the extent, timing and nature of Late Pleistocene glacial advances in the Hope-Waiau Valleys of the north-central Southern Alps. The project builds on the pioneering work of Clayton (1965) and Suggate (1965) who presented the first detailed investigations of the glacial geomorphology of the area. The specific aim of this thesis is to address the general absence of detailed stratigraphic data, the lack of absolute age control for moraine sequences and glacial deposits, and to study valley fills and river terraces for the reconstruction of glacially induced cycles of fluvial aggradation and degradation. To achieve these goals the thesis considers the Hope-Waiau valley system at a variety of scales and through a range of methods. The following eight main objectives are addressed:

1) Review, refine and revise the distribution of glacial deposits and moraines in the study area based on Clayton (1968).
2) Investigate the stratigraphy of the valley fill sequence and delineate its depositional architecture using outcrops and subsurface geophysical techniques.
3) Investigate the sedimentology of glacial sedimentary successions and develop case study based depositional models.
4) Obtain age control on the valley fill sequence through infrared stimulated luminescence dating of fine grained fluvial and lacustrine deposits.
5) Obtain age control for key glacial moraine sequences through cosmogenic dating using situ produced radionuclides (^{10}Be, ^{26}Al) in morainic boulders.
6) Develop an age model for glacial advances and cycles of large scale alluvial aggradation and degradation. Discuss implications for the global correlation of New Zealand glacial events.
7) Use stratigraphic and geochronological tools to update the local late Quaternary tectonic history and calculate a revised slip rate for the Hope Fault.
8) Develop a conceptual model for the glacial accumulation and glacial style of alpine glaciations in the Southern Alps.

1.3. Thesis structure

This thesis consists of a series of connected papers that investigate different aspects of the glacial geology of the Hope-Waiau Valley system. The chapters were written with the intention for publication and at this stage three of the chapters have been submitted to international journals (Rother et al., in press; Rother and Shulmeister, in press; Rother et al., submitted; Appendix 1). Several other chapters are being currently worked up for publication. Changes to the submitted manuscripts were made to meet the required thesis layout, but overall style and structure of all chapters reflect a research article format. Some minor adjustments to data and text were made *after* manuscript submission so this thesis contains the most recent analysis and interpretation. Each chapter is self-contained and begins with an introduction. The research methods are described in detail within each chapter.

The thesis is divided into nine chapters and an appendix:

Chapter One provides an introduction to the thesis project, identifies the thesis objectives and summarizes research methods as well as the thesis structure.

Chapter Two describes the overall geological and glacial setting of New Zealand and summarizes knowledge on Quaternary glaciations for the major valley systems of the eastern Southern Alps.

Chapter Three provides a detailed introduction into the physical setting of the Hope-Waiau Valleys, reviews previous work and outlines the overall methodology.

Chapter Four considers the valley fill stratigraphy of the southern portion of the lower Hope Valley by using sedimentary descriptions, geochronological data and near surface geophysical techniques.

Chapter Five presents an analyses of a large sequence of glacial deposits exposed on the northern side of the lower Hope Valley. The investigation uses

stratigraphic and sedimentary descriptions and presents a detailed depositional model.

Chapter Six presents a reconstruction of the history of glacial advances for the lower Hope, Boyle, and Lewis Valleys based on geomorphological mapping and cosmogenic dating of key moraine successions.

Chapter Seven analyses the overall valley fill sequence and presents stratigraphic and luminescence results from degradational and aggradational terraces.

Chapter Eight develops a snow mass balance model for the Southern Alps that is based on the relationships between climate parameters and topography. The chapter then discusses implications for the style of ice accumulation and considers potential drivers of Late Pleistocene glaciations in the Southern Alps.

Chapter Nine summarizes the geochronological data set and develops an age model for glacial events in the Hope-Waiau catchment. The chapter discusses the overall thesis results and makes suggestions regarding future work.

The *Appendix* includes additional documents such as luminescence and cosmogenic sample descriptions, data depositories for chapters 2 and 9, paper manuscripts and co-authored papers.

1.4. Methodology / Field work

Field work was undertaken between 2003 – 2005 and concentrated mainly on areas in the lower Hope, Boyle and Waiau Valleys. The larger Hope-Waiau catchment comprises several hundred kilometres of river valleys many of them inaccessible by road and logistical considerations for the planned field work had to be taken into account. Following a thorough reconnaissance phase during which most locations described by previous workers were visited at least once, a selection of key sites was

made on which detailed work began. Choices were based on the main project aims, first to establish absolute age control for the glacial sequence and second to resolve stratigraphy and sedimentology of valley fill successions. Chronological control was mainly obtained by cosmogenic and luminescence dating techniques and a key field work component was to locate suitable materials for dating that provided good stratigraphic control and allowed to test previously suggested correlations. Detailed descriptions of all methods are given with each Chapter.

Base maps used include the Department of Survey and Land Information map sheets M31, N31, L32, M32 and N32 (scale 1 : 50,000, 20 m contour lines). Although relatively little geomorphological mapping was conducted for this project aerial photographs that were especially useful include runs 1798, 1799, 2217 and 2219 (1950s series at 1 : 20,000 scale) and higher altitude air photographs at a scale of 1 : 50,000 (1998 series). Digital elevation models (DEM's) were created for the entire study area using the 1 : 50,000 base topographic information. Geographic positioning and absolute heights of terraces and longitudinal valley profiles were measured using two GPS systems, a handheld Garmin eTrex and a high accuracy differential Trimble ProXR comprising a base station and rover.

CHAPTER 2

LATE PLEISTOCENE GLACIATIONS IN THE SOUTHERN ALPS: A REVIEW OF THE CANTERBURY VALLEY SYSTEMS

2.1. Geological, topographic and climatic setting

New Zealand straddles the boundary between the Pacific and Indo-Australian plates in the South Pacific region. Convergent plate movement along the boundary zone is represented in a complex pattern of bi-directional plate subduction (e.g. Weissel et al., 1977; Norris et al., 1990) which has resulted in the development of mountain ranges since the early Pliocene (Suggate, 1978). Following the principle strike of the major tectonic contact zone, the Southern Alps (41º- 46º S) constitute an up to 3.7 km high mountain range. Principal rock formations in the alps originated as Upper Permian to Late Jurassic Gondwana shelf deposits (quartzofeldspathic greywackes) which were accreted as terranes during Mesozoic and Cenozoic collisions (Kamp, 2001; Pickard, et al. 2000). The Mesozoic (Rangitata) Orogeny caused the metamorphosis of extensive suites of South Island sedimentary rocks and the emplacement of granitoids and volcanic rocks (Suggate 1978). The inception of the present day oblique plate boundary (continental-continental transpressional collision) occurred during the mid-late Cenozoic (Kamp and Tippett, 1993). The event marks the onset of the Kaikoura Orogeny which causes ongoing uplift along the Alpine Fault (e.g. Carter and Norris, 1976; Kamp, 1986). While the height of the present Southern Alps is largely between 2 - 3 km, the total amount of uplift during the orogeny is estimated to be in the range of 15 - 20 km (Kamp et al., 1989). This implies extraordinarily large denudation rates across the Southern Alps which is confirmed by suspended sediment yields from New Zealand rivers which are amongst the highest in the world (Griffiths, 1981; Hicks, 1998).

Topographically, the Southern Alps constitute an ~800 km long but only 60 - 80 km wide axial mountain belt, ranging in elevation largely between 1800 - 2700 m while only few peaks reach above 3400 m (all heights in m a.s.l.). Due to the larger land extent east of the Southern Alps and the position of the topographic divide west of

the island's center line, valley systems of the eastern Southern Alps are substantially more extensive than those of the west. While short and steeply descending valleys are characteristic for the western areas, eastern valleys are longer and descend at a gentler gradient. The distribution of land implies that during glaciations only eastward flowing glaciers extended to their climatic termini (as controlled by mass balance) while, in contrast, many glaciers of the western Southern Alps reached the open Tasman Sea where they were terminated by non-climatic forces (i.e. wave action).

Climatically, New Zealand's narrow land mass is located in the temperate zone of the oceanic Southern Hemisphere. While the South Island is dominated by the circumpolar westerly vortex and the eastward passage of low pressure systems, the North Island protrudes into the subtropical high pressure cell. Mean annual temperatures at sea level range from 10˚C in the south of New Zealand to about 14˚C in the north. The regional climate of the South Island is profoundly affected by the NE-SW trending Southern Alps which constitute a large topographic obstruction in the pathway of the Southern Ocean westerlies. Through the interception and rapid orographic forcing of eastward flowing moist air masses, the central Southern Alps receive large amounts of precipitation which place these areas amongst the wettest regions on the planet. Annual precipitation near the alpine divide is commonly in excess of 9,000 mm with observed maximum values at around 16,000 mm (Griffiths and McSaveney, 1983; Henderson and Thompson, 1999). Precipitation maxima usually occur 5-10 km west of the Southern Alps divide but totals decrease exponentially with distance from the central alps and are usually below 1000 mm/a on the eastern edge of the Southern Alps (Sinclair et al., 1997; Chater, 1995). In Canterbury, areas within 25-35 km to the topographic divide receive most of their moisture through spill-over of westerly precipitation, while for areas in the eastern foothills southerly rainstorms are an additional significant moisture source. The marked cross-alpine precipitation contrast is critical for the glaciological setting as it defines a narrow hyperhumid sector which stretches along the full length of the Southern Alps. Virtually all of New Zealand's present glaciers are located in this sector.

2.2. Historical Review

Glacial geologists in New Zealand commonly refer to Suggate's (1965) seminal report on the "Late Pleistocene glacial geology of the northern part of the South Island" as the milestone that marks the end of a long pioneering phase and the establishment of the modern climate-stratigraphic framework for alpine glaciations in New Zealand (e.g. Gage, 1985). This division is justified insofar as that Suggate (1965) presents a first systematic polyglacial synthesis of the by then accumulated observations. Conceptually, his report was based on detailed field studies, many of them undertaken in Canterbury Valleys, that were published prior to 1965 (e.g. Gage and Suggate, 1958; Gage, 1958; Powers, 1962; Soons, 1963a; Speight, 1963). Of these, Gage's (1958) paper on the Waimakariri Valley can be regarded as the earliest comprehensive study on a glacial valley sequence in New Zealand that set the standard for all later investigations. This chapter will briefly summarize the major developments in the history of glacial geology in New Zealand. For this a threefold division into an early pioneering stage (1861 - 1909), a later pioneering phase (1909 – 1958) and a post-1958 period will be adopted. The review will lay emphasis on glacial records from the five largest valley systems in Canterbury, the Waimakariri, Rakaia, Rangitata/Ashburton Valleys as well as the valleys of the Mackenzie Basin. The glacial sequence of the Hope-Waiau Valleys will be reviewed in greater detail in Chapter 3.

2.2.1. The beginnings: 1861-1909

First accounts of formerly extended glaciers in the Southern Alps were published in the mid 19th century by Haast and Hochstetter from Lake Rotoiti (Haast, 1861) and the Mackenzie Basin (Hochstetter, 1863; Haast, 1864). During reconnaissance expeditions to South Canterbury they noted that the Lakes Ohau, Pukaki, and Tekapo are dammed behind large moraines and that lake formation was due to *"... the retreat of an enormous glacier*" (Haast, 1864; p. 96). "*No link is missing to show us that the formation of these magnificent alpine lakes is due to the former extension of the present glaciers …and we can follow the former lateral moraines to the altitude, where, in the glacial period, a uniform sheet of ice covered these mountain masses…"* (p. 92). This discovery of a 'New Zealand glacier period' came

remarkably early considering that it was contemporary with the wider recognition of the ice age theory in Europe and North America.

As elsewhere the early scientific debate on glaciations was dominated by the search for its causes. In the case of New Zealand, a major complication in explaining the growth of formerly vastly extended glaciers was the early discovery that, unlike in Europe and North America, New Zealand's late Pliocene and Quaternary biota gave little evidence that a "*...great reduction of temperature has occurred in these latitudes since those times ... sufficient to cause so great an extension of our glaciers as we know to have taken place*" (Hutton, 1872; p. 384). The problem is still central to glacial research in New Zealand and undoubtedly represents its most long standing issue. Early attempts to explain the apparent simultaneity of glaciation and near modern temperatures (Haast, 1864; Hector, 1865; Dobson, 1872; Hutton, 1872) often suggested that *"...the extension of the glaciers was owed to a greater elevation of the land*" (Hutton, 1872; p. 385). It was argued that during glacial times more land existed above snowline, which accounted for greater ice accumulation without requiring significant overall climate cooling. Accordingly, the end of glaciation was inferred to have been caused by a period of increased subsidence of the land: *"... we must either accept a change in climate of a very remarkable character, but of which we have no evidence whatever, or attribute the disappearance of such glaciers to a diminution of not less than 4000 to 5000 feet in the general height of the ranges in question…"* (Travers, 1873; p. 299). Although it was pointed out (e.g. Marshall, 1909) that the greater elevation of New Zealand during the post-Pliocene period would have connected some off-shore islands (e.g. Auckland Islands) to New Zealand, and that the existence of such land bridge would be in contradiction with the survival of the highly endemic biota on these islands, the overall model of an 'elevated glacial New Zealand' remained popular among glacial workers until the early 20th century (e.g. Hutton, 1900; Speight, 1907; Henderson, 1924; Morgan, 1927).

Further debate during the early pioneering phase in New Zealand centred on the question whether the past glaciation was of Pliocene or Pleistocene age and how the New Zealand event correlates to glaciation in North America and Europe (e.g. Hector, 1869; Hutton, 1872). Major discoveries during this period were the

recognition that the substantial gravel accumulations of the Canterbury Plains are *"... the product and record of a glacial period in the Southern Hemisphere*" (Hardcastle, 1890; p. 316) and that the widespread loess deposits are of aeolian origin and *"...belong to a glacial age"* (Hardcastle, 1889; p. 326). The general understanding of most geologists at the time was that the glaciation of New Zealand was a 'monoglacial' event while only a minority believed in more than one glaciation. In his review of the first century of glacial research Gage (1985) credited Alexander McKay (1893) to have been the first to suggest that the former glaciation of New Zealand comprised two glacial advances (Gage, 1985, p. 198). However, the extended literature search by this writer found a much earlier publication by Hutton and Ulrich (1875) to make the first clear duo-glaciation claim. They state *"...we have proofs not only of the great length of time that has elapsed since the greatest extension of the glaciers took place, but also ... of a second advance of the glaciers ...* [which] *... we may with much probability place between the Pareora and Wanganui formations and between the Wanganui and Pleistocene formations respectively, the earlier ... being the greater and the longer period."*[2] (p. 85).

2.2.2. The later pioneering phase: 1909 – 1958

Following the exploratory phase during which fundamental issues of glaciation in New Zealand were debated in a relatively broad sense, the period of the 1910s is marked by an increasing number of more detailed physiographic field studies which investigated geomorphic features of glaciated landscapes in the Southern Alps. First descriptions of glacial deposits and maps of moraine positions were published for parts of the Waimakariri Valley (Gudex, 1909; Speight, 1911), Waiau Valley (Park, 1910), Hurunui Valley (Speight, 1918), Rangitata Valley (Speight, 1923), Rakaia Valley (Cox, 1926; Speight, 1926) and Mackenzie Basin (Speight, 1921). The work by Cox (1926) and Speight (1926, 1933, 1938, 1942) provided for the first time relatively detailed sedimentological descriptions of glaciofluvial, glaciolacustrine and morainic deposits. Based on such observations Speight (1926) reconstructed a large glacial paleo-lake in the Rakaia Valley and presented a depositional model for its sedimentary fill that also incorporated more advanced concepts such as

[2] Hutton and Ulrich (1875) suggest a Pliocene and Pleistocene glaciation. The correlations of the Pareora formation has since changed and is now correlated to a Miocene stage.

glaciotectonic deformation. In his study of the Rakaia gorge district Cox (1926) presented detailed stratigraphic and sedimentological evidence for the existence of two glacial periods during Pleistocene. He states that there are *"...two independent glacial deposits ... which are separated by a considerable thickness of normal fluviatile or lacustrine sediments. It therefore follows that there must have been at least two periods in which ice extended as far down the Rakaia Valley as the present gorge. ...the thickness of intervening sediments ... shows that the duration of the interglacial phase was not short"* (p. 109). Other authorative New Zealand geologists, however, questioned evidence for repeated glaciation until the 1930's (e.g. Speight, 1933, 1938).

During the post-war period more stratigraphic evidence was found for older glaciations and intervening interglacials. Gage (1945) discovered the Late Pliocene 'Ross glaciation' in Westland (which remains the oldest recognized terrestrial glacial event in New Zealand) while Wellman (1951) found organic interglacial deposits at Bruce Bay (South Westland) leading to the formulation of a first three-glaciation alpine chronology (Fleming, 1956). A last major development in the 1950's was the establishment of a radiocarbon dating laboratory in New Zealand, the first such facility in the Southern Hemisphere.

2.2.2. Post-1958

Although a polyglacial model was widely accepted in New Zealand by the mid-1950's, field evidence for multiple glaciations in the Southern Alps was still very limited. In Canterbury two glacial advances had been described for the Rakaia and Waimakariri Valleys (Cox, 1926; Speight, 1933) but it was debated whether the advances represented ice front oscillations within one glaciation or indeed multiple glacial periods (e.g. Speight, 1938). A new approach followed the return of Maxwell Gage and arrival of Pat Suggate in the early 1950's from overseas (North America, Europe), where they had been exposed to classical glacial sequences as well as the field evidence for distinguishing and correlating valley glaciations after which Gage felt *"...that similar criteria should work in New Zealand"* (Gage, 1985; p. 203). Beginning with the Waimakariri Valley, Gage (1958) published a first systematic investigation of moraine-outwash systems in the eastern Southern Alps. The decade

following his seminal paper became the most productive period for glacial research in New Zealand during the 20 century. In a series of papers glacial maps and detailed glacio-geomorphological descriptions were published for nearly all major valley systems in Canterbury (e.g. Powers, 1962; Soons, 1963a; Carryer, 1965; Speight, 1963; Suggate, 1965; Rains, 1967; Gair, 1967; Clayton, 1968).

For the WAIMAKARIRI VALLEY, Gage (1958) suggested five Late Pleistocene glacial advances that occurred during two glacial cycles. The individual glacial sequences were separated based on differences in elevation, distribution, thickness, weathering characteristics and the degree of landscape dissection. Among these criteria, the elevations of moraine-outwash systems and the downvalley extent of glacial moraines were most important. The differentiation of successive glacial periods based on elevation generally assumes that older glaciations were more extensive than younger ones (Gage, 1958; Suggate, 1965) and that rapid tectonic uplift during the Quaternary has caused increasing vertical displacement of glacial landforms through time (Suggate, 1990). Based on this concept a relative elevation-age relationship was developed where outwash terraces and moraines at higher elevations are interpreted to be older than glacial features found at lower elevations. The early application of this model faced substantial difficulties mainly due to the limited availability of topographical maps with reliable contours.

The five glacial advances in the Waimakariri Valley were named (from oldest to youngest) Avoca, Woodstock, Otarama, Blackwater (two advances) and Poulter (Gage, 1958). Later field work extended this scheme by a Poulter-2 and Blackwater-3 advance (Gage, 1977; Bell, 1998). In addition a moraine sequence at Arthur's Pass that was previously considered to be of Holocene age (Burrows et al., 1976; Chinn, 1981b; Gellatly et al., 1988) has now been dated to the Latest Pleistocene (Ivy-Ochs et al., 1999). Further regrouping modified the original two-glaciation scheme (Gage, 1958) to three-glaciations (Gage, 1961) and more recently to a four-glaciation model (e.g. Suggate, 1990).[3] A summary of the moraine positions, localities and proposed correlations is shown in Fig. 1. A spectacular feature in the upper portion of the middle Waimakariri Valley are extensive beach ridges representing a ~20 km long

[3] This excludes the late Pliocene Ross and Porika glaciations of which no remnants have been found in the eastern Southern Alps (see Fitzsimons et al., 1996). All correlations are shown in Table 1 (p. 30).

glacial paleo-lake ('Lake Speight') that formed following ice retreat from the Poulter Moraines (Gage, 1958). In addition to the completeness of the Waimakariri glacial sequence its importance is also highlighted by last interglacial organic deposits from Joyce Stream in the lower Waimakariri catchment which represent the only such deposit known from the alpine portion of the eastern South Island (Moar and Gage, 1973).

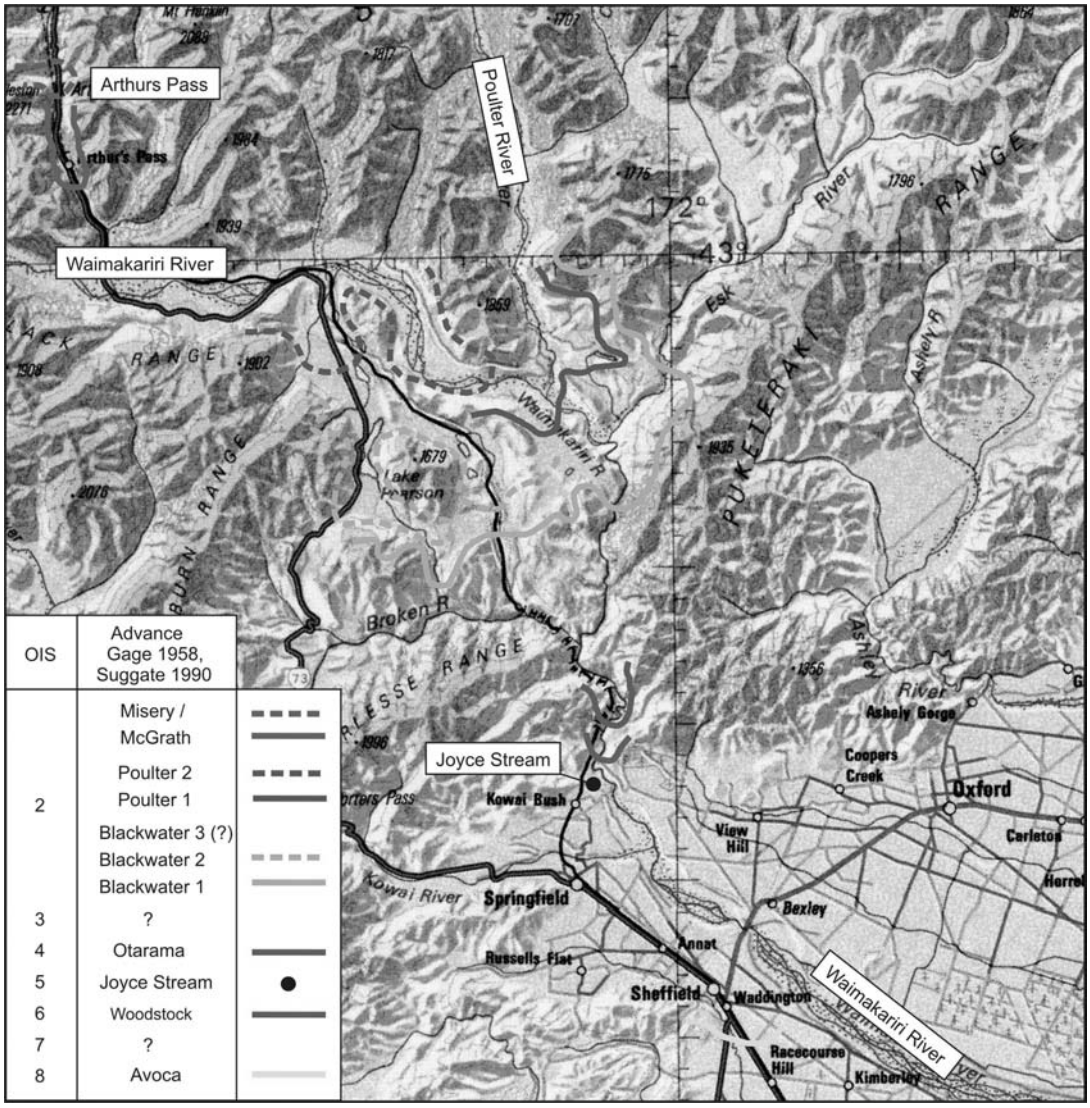

Fig. 1: Overview summarizing locations and limits of Late Pleistocene glacial advances in the Waimakariri Valley (based on Gage, 1958, 1977) and their correlations to Oxygen Isotope Stages (OIS).

Using a similar approach to Gage (1958), Soons (1963a) was the first to reconstruct the Late Pleistocene glacial geology of the RAKAIA VALLEY. Glacial advances in the valley were primarily fed through the coalescence of lobes from three large tributary valleys, the Rakaia, Mathias, and Wilberforce Valleys (Fig. 2). Based on

morainic deposits and associated outwash trains Soons (1963a) identified the limits of seven distinct ice advances named (oldest to youngest) Woodlands, Tui Creek, Bayfield (two advances), and Acheron (three advances). Correlations between the Rakaia and Waimakariri sequences was achieved by tracing glacial outwash surfaces from the two valleys to the Canterbury Plains where they merge (Suggate, 1965). Although the number of individual advances varied, the two records generally corresponded well. No morainic equivalent for the oldest Waimakariri glaciation (Avoca) was found in the Rakaia Valley, however, a correlated event is indicated by a high lying Rakaia outwash surface (Suggate, 1965). Later work on the Rakaia glacial sequence led to the subdivision of the Tui Creek advance into three separate ice re-advances (Soons and Gullentops, 1973) and the addition of a Bayfield-3 advance based on the re-examination of a moraine complex at the Lyndon-Acheron confluence (Soons and Burrows, 1978). During the two older advances (Woodlands, Tui Creek) ice extended beyond the Rakaia gorge onto the open Canterbury Plains,

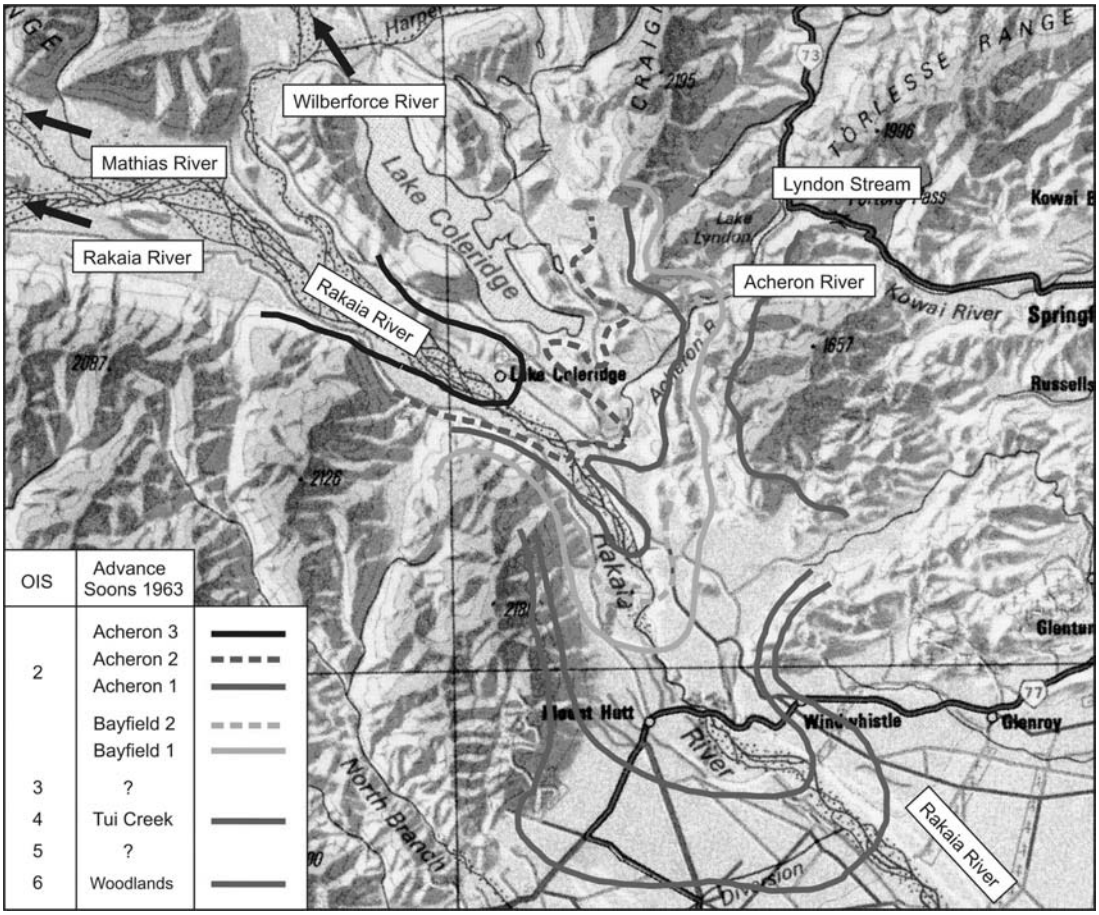

Fig. 2: Overview summarizing locations and limits of Late Pleistocene glacial advances in the Rakaia Valley (based on Soons, 1963a) and their correlations to Oxygen Isotope Stages (OIS).

whereas the terminal positions of all younger advances are located within 13 km upstream of the gorge. Soons (1963a) argued that the extensive glaciolacustrine deposits interpreted by Speight (1926) to represent a large glacial lake are more likely to have formed in a series of small ice marginal lakes. She noted that that the silts are found mainly in the lower valley fill stratigraphy which is overlain by thick aggradational gravels and moraines that relate to the surface morphology. Based on these stratigraphic relationships she suggested a pre-Bayfield age of the glaciolacustrine sequences (Soons, 1963a).[4] During later work Soons (1964) described a large drainage network of former ice marginal channels that is located on the extensive northeastern valley flank. She demonstrated that the drainage system was used during successive glacial advances and showed the effects of postglacial fluvial adjustments including drainage re-orientations and the re-use of former meltwater channels by the modern streams.

Of the major glacial systems in Canterbury the RANGITATA / ASHBURTON sequence was the last to be described in detail (Burrows, 1975; Burrows and Russel, 1975; Mabin, 1980, 1984). Although previous workers (e.g. Speight, 1941) had suggested that the former Rangitata glacier reached the open Canterbury plains, no attempt had been made to interpret the overall sequence in a polyglacial context. During glaciation a distributary lobe from the Rakaia Glacier extended into the Lake Heron Basin, while the Rangitata trunk glacier also split into two lobes, a southern lobe occupying the present Rangitata Valley and a northern lobe that extended into the Lake Clearwater Basin (Fig. 3). Mainly based on topography, weathering and landform preservation criteria, Mabin (1980) distinguished a total of five glacial advances. He found no evidence for a glacial event that correlates to the oldest Waimakariri glaciation (Avoca). During the three older glacial advances, named (from oldest to youngest) Pyramid, Dogs Hill, and Trinity, the Rakaia distributary lobe coalesced with the Cameron, Ashburton and northern Rangitata glaciers resulting in terminal positions near (Trinity advance) or downstream of the Ashburton and Rangitata gorges (Pyramid, Dogs Hill advances). Two later advances were less extensive and all lobes remained separate, with moraine positions named

[4] A pre-Bayfield age has recently been confirmed by luminescence dating (Shulmeister et al., subm.).

Hakatere and Spider Lake for the Rangitata Glacier and Emily and Lake Heron for the Rakaia lobe (Fig. 3).

Mabin (1980) interpreted the Rangitata / Ashburton sequence to comprise largely deglacial landforms that formed during the retreat of the Spider Lake and Lake Heron ice. This is indicated by the presence of extensive hummocky ground moraines (ablation moraines), dead-ice topography and ice disintegration moraines. Local differences in the morphology of these landforms suggests that their formation was heavily affected by differences in the distribution of supraglacial debris. Deglaciation was interpreted to have occurred via large scale stagnation and downwasting of passive ice with no evidence for re-advances during the ice decay

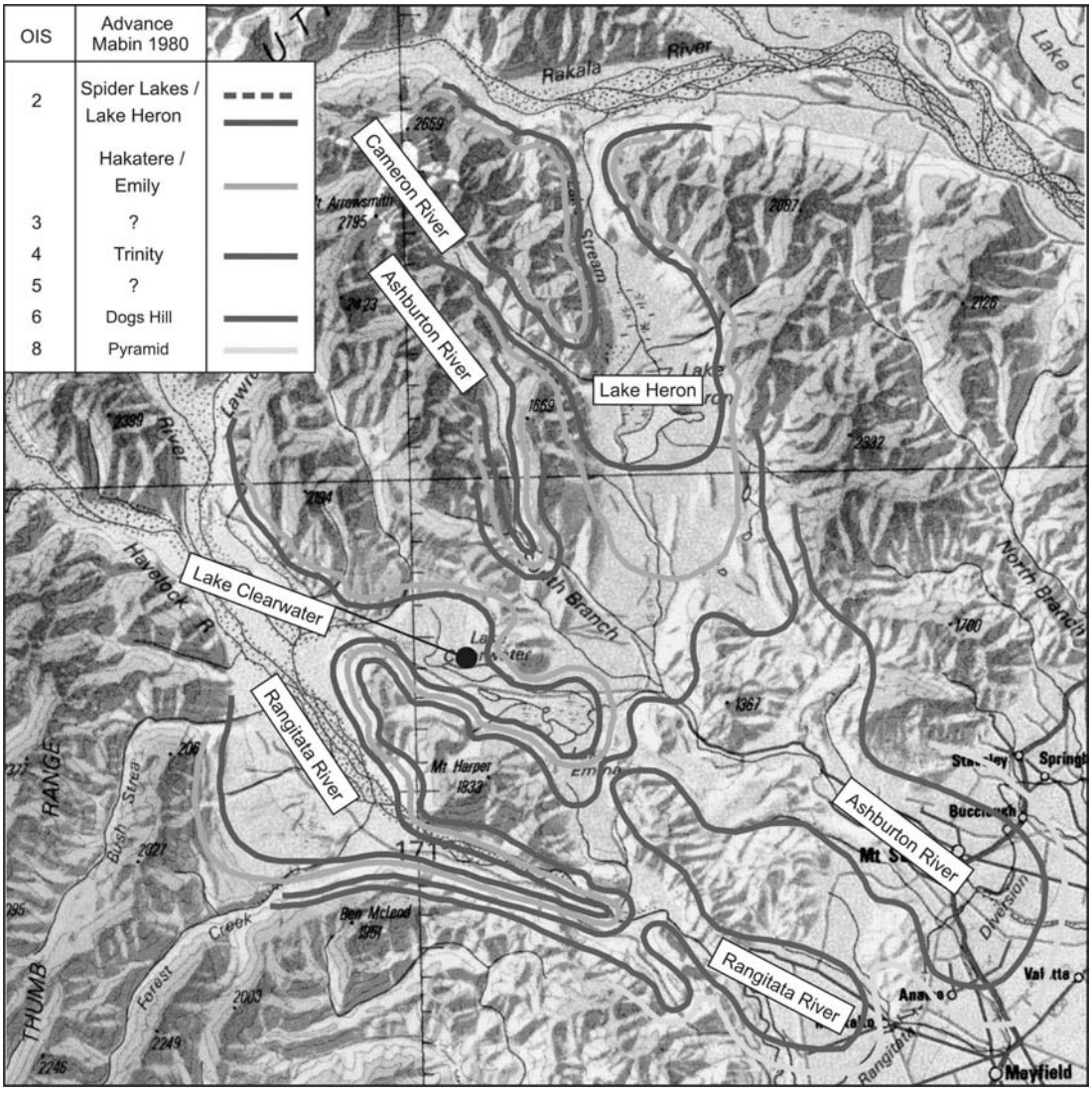

Fig. 3: Overview summarizing locations and limits of Late Pleistocene glacial advances in the Rangitata / Ashburton Valleys (based on Mabin, 1980) and their correlations to OISs.

phase (Mabin, 1980). Due to the separation into a system of distributary lobes, glacial advances in the Rangitata / Ashburton Valleys produced a complex glaciofluvial drainage pattern. During glacial maxima the Rangitata gorge was iceblocked (southern Rangitata lobe) and meltwaters from the Clearwater Basin drained via the Ashburton gorge. Multiple phases of glacial advance and retreat caused repeated switches between drainage outlets and adjustments of the drainage pattern.

As described earlier glacial landforms in the MACKENZIE BASIN were pivotal in the discovery of former glaciations in New Zealand. The basin formed as a tectonic depression during the Kaikoura Orogeny and holds a substantial thickness of alluvial and glacial debris (Read, 1976). Although various aspect of its glacial geology had been described in the first half of the 20th century (Park, 1910a; Kitson and Thiel, 1910; Speight, 1915, 1921, 1940a, 1942) a full treatment of the glacial sequence was not available before Speight's (1961, 1963) investigation of the Lake Pukaki area. Using Gage's (1958) methodology, Speight (1961, 1963)[5] refined this approach conceptually by grouping and describing glacial surface elements as 'glacial landform associations' which include landforms that show *"...an ordered arrangement, consistency of slopes, uniformity of erosional development, and degree of obliteration of detail as would indicate that they originated together as a land surface"* (Speight, 1963; p. 162). He assigned to each 'landform associations' a 'type area' and provided a description of the sedimentary facies. In the interpretation 'landform associations' then served as geomorphic units analogous to the concept of 'formation' in stratigraphy. The approach can be seen as a forerunner of the modern "landsystem" model which has gained increasing importance in recent years for glacial geomorphologists (e.g. Benn and Evans, 1998; Evans, 2003).

Speight (1963) distinguished five landform associations in the Lake Pukaki area. For reasons that are unclear his naming system for the advances was discontinued and replaced by a new terminology in the first edition of the New Zealand Geological Map (Mt Cook sheet; Gair, 1967) which identified the same number of glacial events (for a larger area). The new nomenclature which has commonly been used in the

[5] The author is J.G. Speight, not to be confused with his uncle R. Speight (1867-1949).

Chronology / Stratigraphy			Canterbury Sequences					Correlated Sequences		
Stratigraphic Nomenclature	Oxygen Isotope Stages (OIS)	ka BP Martinson 1987	**Waimakariri** Gage 1958, 1977 & Suggate 1965, 1990	**Rakaia** Soons 1963, Soons et al. 1973, 1978	**Waiau / Hope** Clayton 1965, 1968, Rother (this study)	**Rangitata / Ashburton** Mabin 1980	**Mackenzie Basin** Speight 1963, Gair 1967	**Westland** Suggate 1965, & 1990	**NW Canterbury Plains** Wilson 1989	**Christchurch** Brown et al. 1988
Otira (Glac)	2	24	Poulter 2, 1 Blackwater 3 (?) Blackwater 2 Blackwater 1	Acheron 3, 2, 1 Bayfield 3 Bayfield 2 Bayfield 1	Lewis Glynn Wye Glenhope	Spider Lake / Lake Heron Hakatere / Emily	Tekapo Mt John 2, 1	Kumara 3 Kumara 2/2	Burnham	Riccarton Gravel
	3	59	No deposits of this age identified							
	4	73	Otarama	Tui Creek 3, 2, 1	Leslie Hill	Trinity	Balmoral 2, 1	Kumara 2/1	Windwhistle	
Kaihinu (Int)	5	128	Joyce Stream	No deposits of this age identified				Sunday Creek	Bromley	Bromley
Waimea (Glac)	6	188	Woodstock	Woodlands	Horseshoe	Dogs Hill	Wolds	Kumara 1	Woodlands	Linwood Gravel
Karoro (Int)	7	241	No deposits of this age identified							Heathcote
Waimaunga (Glac)	8	291	Avoca	Hororata	Kakapo	Pyramid		Hohono	Hororata	Burwood Gravel
Nemona (Glac)	10	360	Hororata	Hororata	No deposits of this age identified			Cockeye	Hororata	Wainoni Gravel

Table 1: Correlations of glacial chronologies in Canterbury and Westland.

literature (Fig. 4) describes the following five major ice advances (from oldest to youngest) Wolds, Balmoral, Mt. John, Tekapo and Birch Hill.[6] The oldest advance (Wolds) has been correlated to either the early Otiran (Gair, 1967) or the penultimate glaciation (Speight, 1963; Suggate, 1990). There is general agreement on a last glacial age of the Balmoral (two advances), Mt. John (two advances) and Tekapo advances. The Birch Hill advance has been correlated to either the late Last-Glacial-Interglacial-Transition (LGIT), (Burrows, 1980; Gellatly et al., 1988) or Holocene (Gair, 1967). It is improbable that the recognized Late Pleistocene glacial advances in the Ohau, Pukaki, and Tekapo Valleys were large enough to produce a coalescing piedmont ice field in the Mackenzie Basin, although a small contact zone between the Ohau and Pukaki glaciers during Wolds time is likely (Mansergh, 1973). In each valley the maximum advance reached its terminal position approximately 8 km

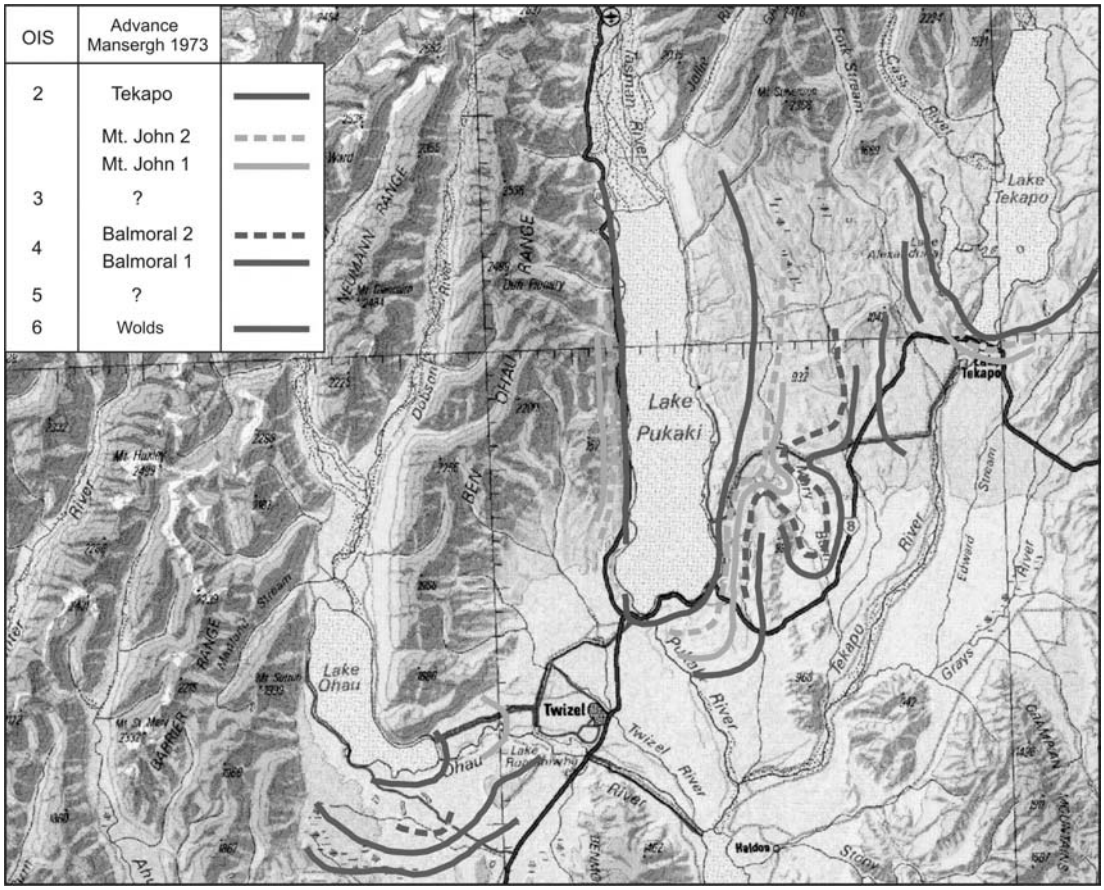

Fig. 4: Overview summarizing locations and limits of Late Pleistocene glacial advances in the Mackenzie Basin (based on Speight, 1963; Mansergh, 1973) and their correlations to Oxygen Isotope Stages.

[6] Speight's (1963) equivalent names for the landform associations were Stevenson, Irishman, Maryburn, Pukaki and Birch Hill.

(Ohau), 6 km (Pukaki) and 2 km (Tekapo) downstream of the respective lake outlets while all younger advance remained inside these ice limits. The original relative glacial chronology was confirmed by Maizels (1989) who compared landform associations around Lake Tekapo using terraces elevations and gradients as well as geomorphic indices to quantify the degree of channel network preservation, loess thicknesses, and the specific clast gravity of outwash deposits. She found significant differences in the ages between the Wolds and Balmoral sequences, and less pronounced but still consistent differences between the Balmoral, Mt John and Tekapo sequences.

Earlier workers had noted the presence of higher shorelines and beach deposits around Lake Pukaki (R. Speight, 1942; J.G. Speight 1961) which Read (1976) saw mainly as a result of the postglacial lowering of the Lake Pukaki level in response to downcutting of the Pukaki River. Wellman (1979), assuming constant uplift rates, demonstrated relative age differences using the differential tilting of shorelines and outwash terraces. Compared to the variety of geomorphological investigations, the sedimentology of glacial sequences has only rarely been investigated. Existing studies on extensive outcrops of glacial deposits in particularly around Lake Pukaki described the sediments as mainly stratified to massive silty fine to medium sands with gravels that often display intense contortions (Speight, 1942; Read, 1976). Although previous workers have described the deposits as till (Read, 1976; McGregor, 1981) more recent sedimentological investigation showed that the sequences comprise mainly glaciotectonically deformed glaciolacustrine and glaciofluvial diamictons (Hart, 1996).

2.3. Geochronological summary

As described above the post-1958 investigation of glacial sequences in the Southern Alps relied largely on relative morphological and stratigraphic criteria. None of the original glacial studies on the major Canternbury valleys had substantiative support from absolute dating which made definite correlations between valley systems and beyond the New Zealand region difficult. Over the past 50 years, however, a considerable number of numerical ages on the timings of glacial events has been obtained. Until very recently radiocarbon dating was the only method available,

which effectively limited age control to the younger part of the last glacial cycle and the Holocene neoglaciation. Despite this, beginning in the 1980's alpine sequences in New Zealand were linked to global Oxygen Isotope Stages (e.g. Nelson et al., 1985; Suggate, 1990) through which absolute ages dating back as far as ~360 ka (OIS 10) were assigned to Late Pleistocene glacial advances in the Southern Alps (Suggate, 1990; Tab. 1). This chapter aims to review the present Late Pleistocene absolute age control for the five largest valley systems in Canterbury.

The interpretation of the chronological data-set of numerical ages for glacial sequences in the Southern Alps has become a challenge for glacial workers in New Zealand. This is partially because no comprehensive compilation of relevant ages is available, and the accessibility of the numerous published and unpublished sources of these ages varies considerably. In addition, no standardized format has been followed in the reporting of absolute ages in the literature. For radiocarbon dating, difficulties in the assessment of a reported age often arise from the incompleteness of the published subsidiary set of information such as lab numbers, sample properties, precise location, stratigraphic context, method of calibration and which of the half-live was used for calculation. The review presented here is based on an up-to-date summary of all available Late Pleistocene geochronological data from Canterbury. A spreadsheet containing details on all available radiocarbon, luminescence and cosmogenic dates is included in the appendix (Appendix 3). The compilation adopts no upper age limit other than the technical limit provided by the dating method itself but excludes ages younger than 8,000 a BP. A Holocene lower age limit follows the recommendation of the New Zealand INTIMATE group to include the full OIS 2/1 transition when assessing Late Pleistocene glacial fluctuations (Alloway, 2004; Barrell et al., 2005). Results from relative dating techniques such as clast weathering rind dating or lichenometry have not been considered in the compilation.

A review of the general distribution, range and technical nature of the applied dating methods shows that to date, 104 Late Pleistocene and Early Holocene ages have accumulated for the considered valleys (Fig. 5). Based on a summary of research objectives and the selection of target materials in numerical dating studies, the available age control can be grouped into five categories which resolve timings of glacial advances (1), aggradation and degradation events (2), the formation and

cessation of paleo-lakes (3), the last glacial termination and valley deglaciation (4), and the accumulation of organic materials and vegetation developments. In the following a brief summary of the above categories will be provided for the Canterbury valleys in question.

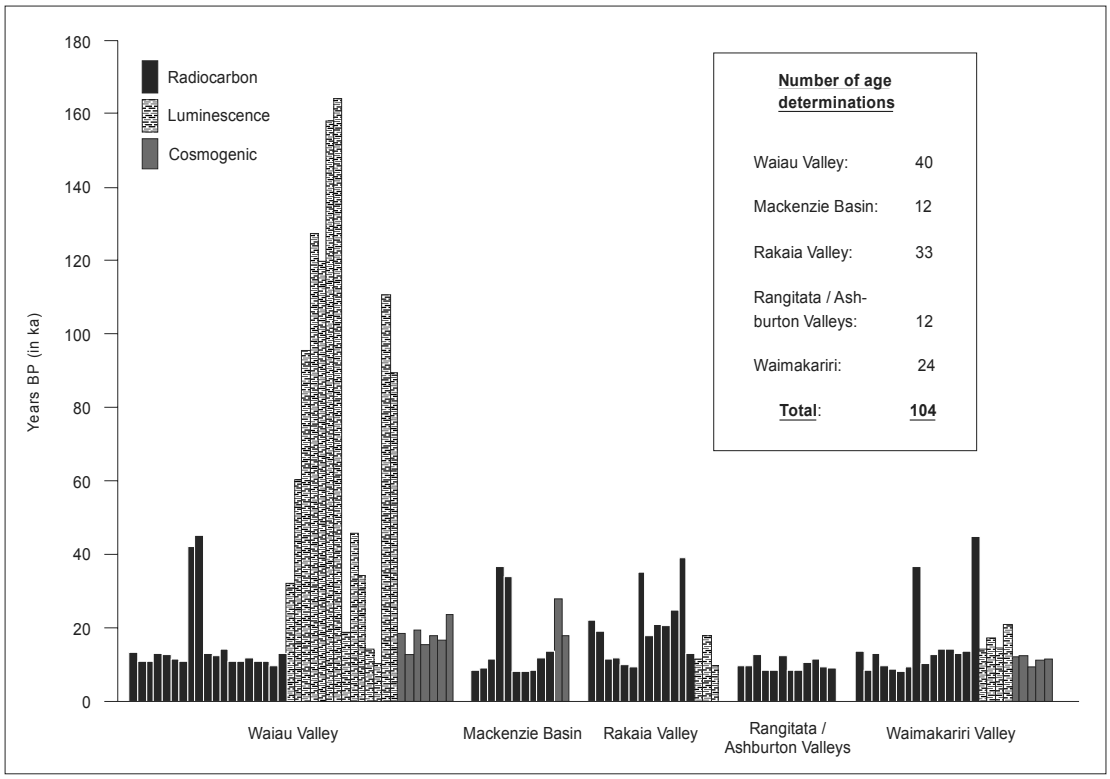

Fig. 5. Summary of the Late Pleistocene and Early Holocene absolute age control for the main Canterbury Valley systems. The compilation also includes 22 new age determinations on the Hope-Waiau-glacial sequence presented by this thesis and discussed in Chapters 4 – 8.

At higher resolution, the timings of Late Quaternary ice advances in the eastern Southern Alps are constrained by only a limited number of cosmogenic ages which were directly obtained from moraine boulders. This is complemented by a somewhat larger number of radiocarbon ages from organic deposits which are of varying association with the glacigenic sediments. Cosmogenic dating was used on a moraine complex at Arthur's Pass (Misery Moraines) yielding ages of 12,420 ± 1180; 12,050 ± 960; 11,410 ± 1030; 11,000 ± 1360 and 9,300 ± 990 a (Ivy-Ochs et al., 1999). Excluding the 9,300 ± 990 date as an outlier Ivy-Ochs et al. (1999) calculated a mean age of 11,720 ± 320 for the moraines and suggested that the advance occurred synchronous to the Younger Dryas chron. The ages show that the advance occured during a LGIT climate reversal thereby revising earlier suggestions that the moraines are of Mid or Early Holocene age (Burrows et al., 1976; Chinn, 1981b; Gellatly et al.,

1988). Schaefer et al. (2001) dated a sequence of LGM moraines at Lake Pukaki (using cosmogenic dating) to 27,800 ± 2500 (Mt. John advance) and 18,000 ± 2000 years ago (Tekapo advance).

In the Mackenzie Basin peat between tills of the Mt John advance and the early Otiran Balmoral advance of the Pukaki Glacier was dated to 36,400 ± 3150 a BP and 34,100 ± 2750 a BP, respectively (Mansergh, 1973; Porter 1975, Suggate, 1990). The ages support a pre-OIS 2 assignment of the Balmoral advances (Tab. 1). In the Rakaia Valley at High Peak Stream a radiocarbon date of >39,000 a BP (Grant-Taylor and Rafter, 1971) from sands deposited in front of the Tui Creek moraine supports Soon's (1963a) and Rains' (1967) suggestion that a distributary lobe from the Rakaia glacier pushed into the High Peak valley prior to the LGM. At Lyndon Stream, another tributary to the Rakaia Valley, lacustrine sediments deposited during a recessional phase, were dated to 22,200 ± 750 a BP and 19,200 ± 550 a BP (Soons and Burrows, 1978). The radiocarbon dates are now supported by a luminescence age of 18,100 ± 1,700 a BP from the top of the same lacustrine unit (Rieser, 2001). In the Waimakariri Valley a minimum age of >45,000 ^{14}C a BP from peat found at Joyce Stream (Moar and Gage, 1973) was interpreted to indicate organic deposition during the last interglacial (OIS 5). The unit is overlain by thick gravels (~60 m) which are associated with aggradation during the last glacial cycle.

In addition to the direct dating of moraines, age control for glacial periods in New Zealand has often been obtained by dating periods of large scale paraglacial aggradation and loess accumulation which are interpreted to be directly associated with glacial advances. In Canterbury, phases of loess deposition have been luminescence dated to 73 ka, 41 ka, and 27 ka (Berger et al., 2001), while deposition at 23 ka and during OIS 5d / OIS 6 (90 – 130 ka) has been confirmed from Banks Peninsula (Shulmeister et al., 1999). Several South Island loess records contain Kawakawa tephra indicating dust accumulation during the ~22.6 ka BP eruption (Eden and Frogatt, 1988). Loess deposits in the Waimakariri have luminescence ages of 17,000 ± 900 a; 14,300 ± 900 a, and 14,000 ± 600 a (Rieser, 2001). Problems in the inference of glacial conditions from South Island loess records arise from the fact that loess is also deposited under modern conditions. The onset of large scale fluvial aggradation in eastern New Zealand is constrained by radiocarbon dates of 35,170 ±

580 a BP from Bayfield outwash below the Rakaia gorge (Bal and Browne, 1997) and a 37,000 ± 200 a BP age from Blackwater outwash in the Waimakariri Valley (Burrows and Moar, 1996). The ages indicate that the onset of last glacial aggradation in Canterbury pre-dates the LGM and falls into OIS 3. A minimum age for the cessation of large scale valley aggradation and the begin of postglacial fluvial downcutting is indicated by a radiocarbon date of 14,100 ± 220 a BP from organic silts that overlie LGM aggradational gravels in the Waiau Valley suggesting the abandonment of this floodplain level (Suggate 1965). An age of 15,250 ± 250 a BP dates the end of alluvial aggradation at Greta Valley of the Hurunui catchment (Moar 1980).

Final last glacial ice retreat from valleys in the eastern Southern Alps is constrained by a number of minimum ages which mainly date the onset of limnic-telmatic deposition and soil development in freshly deglaciated valley portions. Radiocarbon ages from the Waimakariri Valley demonstrate that ice had retreated from the Poulter moraines by 13,750 ± 200 a BP at the very latest as indicated by near basal organic sediments in Kettlehole Bog (Burrows, 1983). In the Hope-Waiau Valleys retreat from LGM positions commenced prior to 13,309 ± 203 a BP (Clayton, 1968) and 13,050 ± 200 a BP (Burrows, 1988) as suggested by radiocarbon dates on lacustrine deposits near the Doubtful River confluence. In the Mackenzie Basin (Tasman Valley) ice had retreated to about the modern upper valley margin of Lake Pukaki by 13,500 ± 250 a BP as shown by a radiocarbon dated peat from a kame depression (Moar, 1980). Dates of 12,624 ± 75 a BP and 12,552 ± 133 a BP from Sandys Basin in the upper Rangitata Valley (Forsyth et al., 2003) indicate that by this time the trunk Rangitata glacier had retreated more than 38 km upvalley from the LGM position. Similarly, organic deposits at Quagmire Tarn in the upper Rakaia Valley provide evidence that by 11,900 ± 200 a BP (Burrows and Russel, 1975) the distributary Lake Heron lobe had disintegrated and the trunk Rakaia glacier was at least within 20 km of the headwaters. It is worthwhile noting that although the general deglaciation of most lower and middle valley reaches in Southern Alps can be confidently dated to about 14,500 -13,500 ^{14}C a BP, age control for the deglaciation of the alpine headwaters and the abandonment of cirques is almost entirely lacking.

All of the reviewed Canterbury valleys show evidence that following ice retreat from the extended LGM terminal positions large lakes formed in the abandoned glacial troughs. Many of these lakes survived to the present day (e.g. Lakes Ohau, Pukaki, Tekapo, Heron, Coleridge, Sumner) while evidence for paleo-lakes of similar or smaller dimensions have been found in nearly all other valley systems including the Rakaia Valley (Speight, 1926; Soons, 1963a), Waimakariri Valley (Gage, 1958), Hope-Waiau Valleys (Clayton, 1968) and the Rangitata Valley (Mabin, 1987). Ages on these lake have been reported from the Hope-Waiau Valleys (13,309 ± 203 a BP - 10,660 ± 60 a BP; Clayton, 1968, Burrows, 1988, Turney et al., 2003), the Rakaia Valley (11,650 ± 200 a BP; Soons and Gullentops, 1973), the Rangitata Valley (9780 ± 140 a BP; Mabin, 1987), Tekapo Valley (11,650 ± 200 yr BP; Burrows 1976), but the most spectacular paleo-lake, 'Glacial Lake Speight' (Gage, 1958), remains undated.

In summary, despite the accumulation of more than 104 Late Pleistocene and Early Holocene numerical ages, absolute chronological control for Quaternary glacial events in the Southern Alps is still relatively poor. Few directly dated glacial advances during the LGM and older periods are available and these difficulties have led to the use of glacio-fluvial outwash terraces as the means for the relative discrimination between glacial events. Age control is better for the post-14 ka period providing some insight into the timing of valley deglaciation and Early Holocene glacial re-advances. Although glacial sequences in Canterbury valleys commonly include landforms and deposits inferred to represent older glaciations during OIS 4, OIS 6, OIS 8 and OIS 10 (e.g. Suggate 1990) direct age control for such sequences is entirely missing and the correlations are tentative at best. However, the increasing application of newly advanced dating techniques (i.e. cosmogenic dating, luminescence dating), has the potential to substantially improve the age control for Quaternary glacial advances.

CHAPTER 3

THE HOPE-WAIAU VALLEY SYSTEM

3.1. Physiography

The upper portion of the Hope-Waiau catchment in the central South Island comprises an alpine and subalpine area of about 2000 km^2 located roughly between Mt. Una in the north, Kiwi Saddle in the south and Hanmer Basin in the east (Fig. 6). The highest point in the catchment is Mt. Una (2300 m) in the Spenser Range but throughout most of the area the average peak height lies between 1600 – 1800 m. While the ranges in the headwaters are characterized by a steep and rugged topography most peaks have a rounded and gentle morphology. The largest tributary valleys are the Waiau Valley which extends far north into the Spenser Range and the Hope Valley which drains the southwestern portion of the catchment. Secondary tributaries are formed by the Doubtful, Boyle, Nina, Kakapo and Lewis Rivers (Fig. 7). The only significant level plains in the area are Hanmer Basin (10 x 20 km) and a number of smaller intermontane depression. Dominant trends in the orientation of most valleys are SW – NE (e.g. lower Hope Valley) following a course parallel to the strike of the major transcurrent faults in the area and a secondary, roughly perpendicular to the first, N – S orientation (e.g. upper Waiau Valley). The middle and lower valley portions are often deeply incised with spectacular flights of terraces, while the upper valley reaches are characterized by a fresh U-shaped morphology where terraces are usually missing. In particular the upper portions of the Waiau and Hope Valleys preserve extensive unincised fluvial and alluvial fill sequences. Knickpoints between the incised and unincised valley reaches are common. Near Lewis Pass, the Maruia River has beheaded the upper trunk valley which now drains into the Tasman Sea (Fig. 6).

Annual precipitation yields in the catchment vary dramatically and range from 5000 mm near the alpine divide to about 1200 mm in areas between Glynn Wye and Hanmer Springs (Bowden, 1974). The high yields in the headwaters are associated

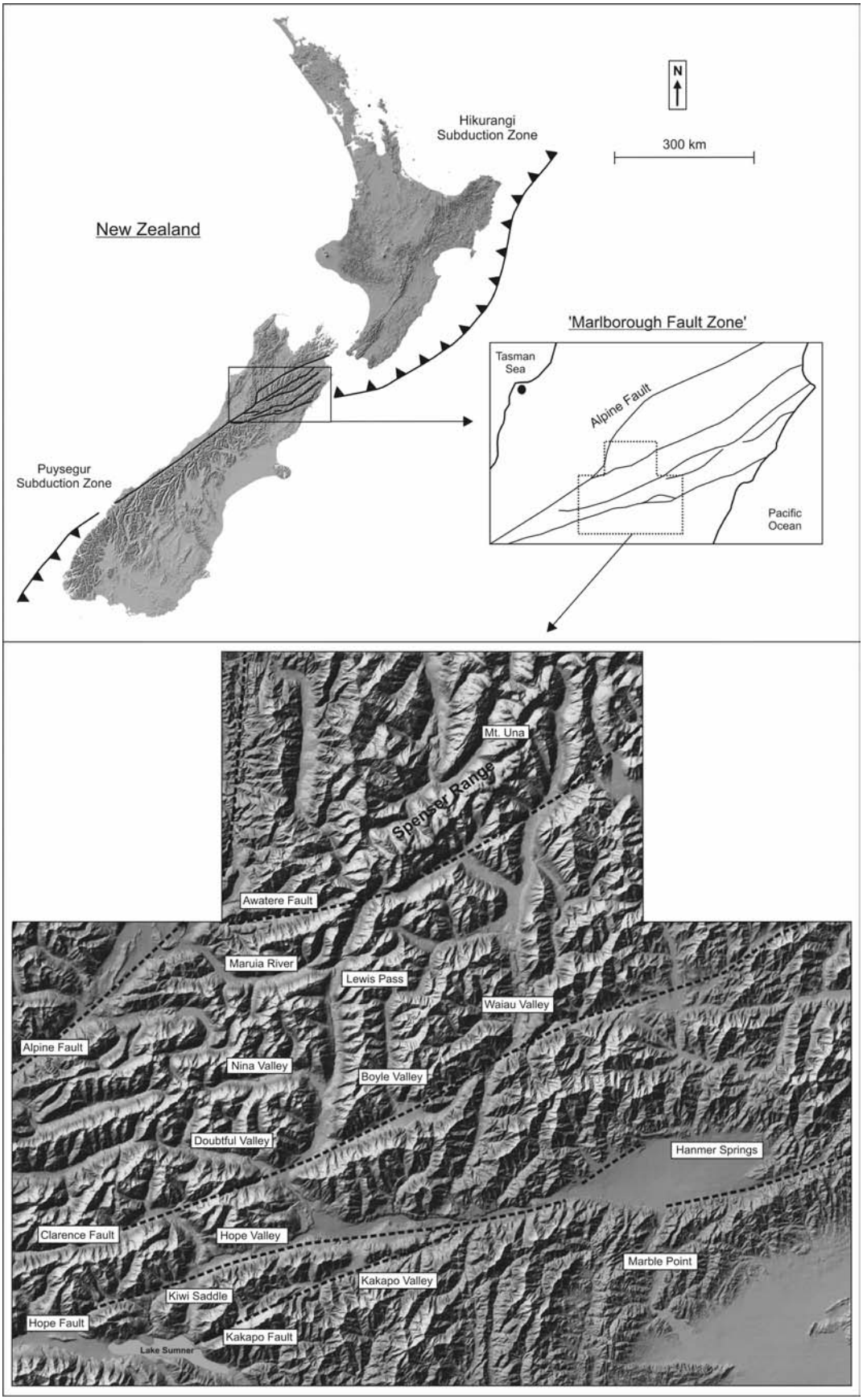

Fig. 6: General overview of locations, topography and tectonic setting of the study area in the central South Island of New Zealand.

with strong north-westerly airflow while precipitation totals in the eastern catchment also reflect the influence of moist southerly and easterly airflows. About 90 % of the total drainage of the Waiau River at its mouth is generated in the upper catchment (above Marble Point) with the Hope River contributing about 40 % to the overall drainage. Mean flow at Marble Point is 101 m^3/s (1975 - 2002) with a recorded maximum of 1,650 m^3/s (Mosley, 2004). Snowlines in the area range between 1950 - 2050 m a.s.l. (Lamont et al., 1999) and only the highest peaks in the Spenser Range are permanently above snowline. The New Zealand Glacier Inventory lists 18 glacierettes for the Waiau catchment, however, updated glacier data have not been published in recent years and it is not known if all of the glaciers still exist.

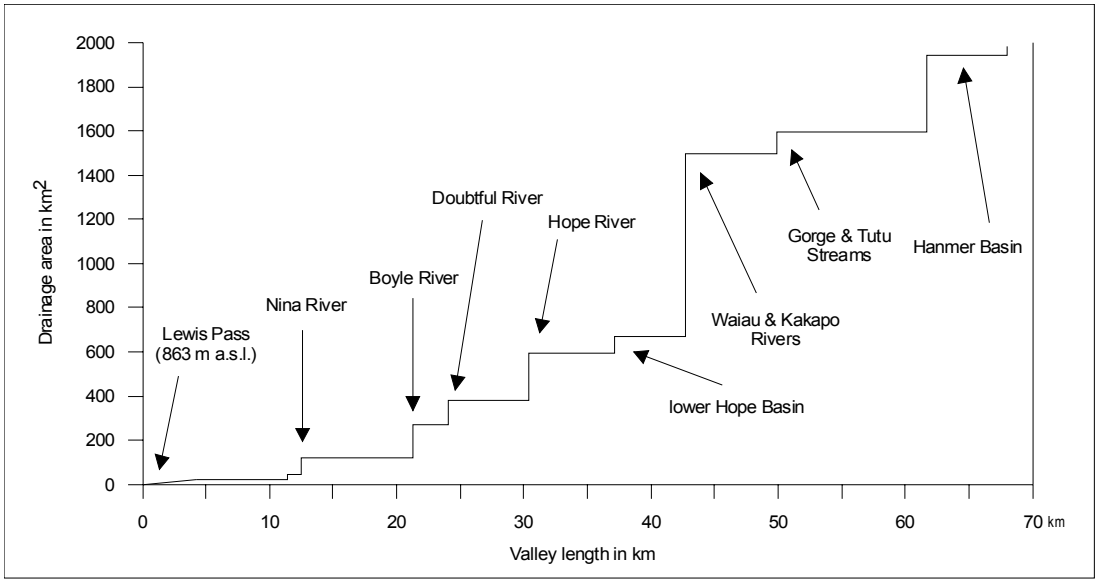

Fig. 7: Downvalley accumulation of catchment area between Lewis Pass and Hanmer Basin.

3.2. Bedrock geology and tectonic setting

The regional basement is dominated by suites of strongly indurated and folded Triassic greywackes and argillites of the Torlesse Supergroup. Secondary rock types comprise basic volcanics, minor beds of conglomerates and Tertiary limestone (Gregg, 1964). Tectonically, the study area is part of the 80-km-wide Marlborough Transform Fault Zone, which accommodates relative plate motion between the Pacific and Indo-Australian plates via a system of transpressional and transtensional faults (Walcott, 1984; Wood et al., 1994; Eusden et al., 2001). Beginning in the middle Pleistocene the fault system has slowly propagated southward as suggested

by the deceleration of offset in faults in the north (e.g. Clarence Fault; Pettinga, 2002) and the inception of new faults in the south (e.g. Kakapo Fault; Yang, 1991). The effects of intense strike–slip faulting in the study area are highlighted by the marked dextral offset of major valleys along the Clarence Fault (Waiau Valley, lower Boyle Valley, Fig. 6) and fault escarpments in the lower Hope and Kakapo Valleys (Fig. 7 and 8). Including the Porter's Pass fault, the Marlborough Transform Zone accommodates ~38 mm/a or ~81% of the total relative plate motion (Yang, 1991). The most active of the Marlborough Faults is the Hope Fault which ruptured

Fig. 8: The fault trace of the Hope Fault displacing Late Pleistocene aggradational deposits in the lower Hope Valley at Glynn Wye.

Fig. 9: The fault trace of the Kakapo Fault in the middle Kakapo Valley.

last in 1888 during an estimated 7.0-7.3 magnitude earthquake (McKay, 1890; Cowan, 1991). Cowan and McGlone (1991) calculated an average re-ocurrence interval of seismic events along this fault segment of 81-200 years. Using offset basement rocks, Freund (1971) estimated the total Pliocene and Pleistocene displacement along the fault to be about 19 km. The overall regional uplift rate is not well constrained but is estimated to be about 2 mm/yr (Wellman, 1979).

The largest morphological feature to form as a result of motion along the Hope Fault is Hanmer Basin (10 x 20 km) which was first described as a tectonic depression by Cotton (1947). Although the basin has frequently been cited as a classic example of a pull-apart basin (e.g. Mann et al., 1983; Sylvester, 1988) a more recent seismic investigation by Wood et al. (1994) suggested a more complex basin evolution in the step-over region between two Hope fault segments. They argued that the basin represents a combination of a fault-wedge and pull-apart basin. The results also showed that the depression contains between 500 - 1000 m of Pleistocene soft-sediments (Wood et al., 1994). The basin shallows towards the east and older basin fill, age constrained by a beyond-range radiocarbon date of > 45,000 a BP, is uplifted and recycled through transpressional tectonics (Wood et al., 1994).

Between the Southern Alps Divide and the coast the Hope Fault comprises four segments, the Hurunui, Hope, Conway and Seaward fault sections which appear to be seismically independent of each other (Wood et al., 1994). The intensity of late Quaternary tectonism in the immediate study area is highlighted by a spectacular fault trace in the lower Hope Valley along which last glacial terrace and moraine landforms have been dextrally offset (Fig. 8). The partially displaced Glynn Wye Moraine with a presumed age of 17 – 20,000 a (Suggate, 1965) has been the key feature used to determine a 10-14 mm/a Late Quaternary fault slip rate of this fault segment of the Hope Fault (Cowan, 1990; Cowan and McGlone, 1991). Slip rates of the other fault sections are estimated to be 18-23 mm/a for the Conway segment (Van Dissen, 1989; Pope, 1994) with a re-occurrence interval of seismic events between 180-310 years (Bull, 2003; Langridge et al., 2003) and 8-13 mm/a at the Hurunui segment with a re-occurrence interval of 310-490 years (Langridge and Berryman, 2005).

3.3. Previous glacial work

The first reference to glaciation in the wider study area was made by Haast (1879) who suggested that during the Pleistocene the Hurunui glacier extended onto the Culverden Plains and Hutton (1900) who noted that "*...large glaciers went down the Clarence and Waiau Valleys, the latter being no less than fourteen miles in length*." (p. 173). Park (1910b) mapped what he presumed to be roches moutounées and moraines east of Hanmer Springs and concluded that the former Waiau glacier extended to the sea. Speight (1918) rejected such great ice extension and noted that for the Hurunui Valley unambiguous evidence for glaciation is only found in the valley reaches above the junction between the northern and southern Hurunui branches. Speight (1918) also recognized that ice from the trunk Hurunui glacier fed into neighbouring valleys, however it appears that he did not recognize the ice overflow into the Hope Valley via Kiwi Saddle (see map in Speight, 1939). Pleistocene ice limits for north-west and central New Zealand were also presented in a map by Henderson (1931) suggesting that the glaciers of the Hope, Doubtful, Boyle and Waiau Valleys remained separate during their maximum extension.

Glacial deposits of the Hope-Waiau Valleys were first mapped during early 1960's for the 1 : 250,000 Geological Map of New Zealand (Gregg, 1964). This information also formed the basis for Suggate's (1965) Geological Survey Bulletin on the "Late Pleistocene geology of the northern part of the South Island" which included a description and glacial map of the Hope-Waiau Valleys. Substantially greater detail was added by Clayton (1965) who mapped glacial deposits in the Hope Valley, Edwards Valley and Culverden Plains. His conclusions form the basic framework for the presently accepted interpretation of the Waiau glacial sequence (Fig. 10 and 11; Clayton 1968, Suggate 1973, 1990). More recent investigations with relevance to the glacial geomorphology and chronology include a number of neotectonic studies (e.g. Cowan, 1989, 1990, 1991; Cowan and McGlone, 1991; Yang 1991; Wood et al., 1994; Langridge and Berryman, 2005) and two paleo-ecological investigations of late glacial lacustrine deposits in the lower Boyle and Doubtful Valleys (Burrows, 1988; Turney et al., 2003).

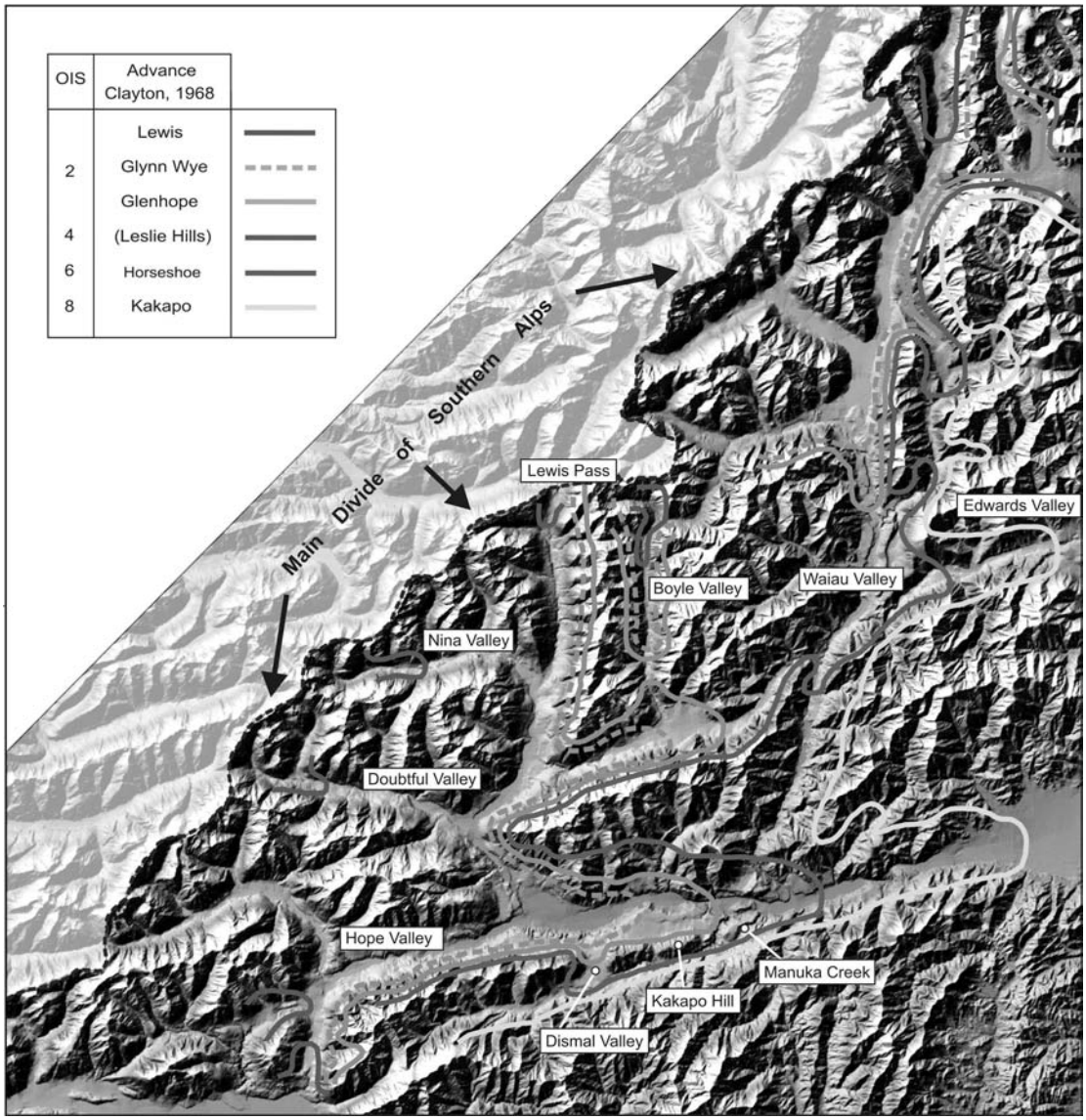

Fig. 10: Overview of the wider study area summarizing locations mentioned in the text and the limits of Late Pleistocene glacial advances in the Hope-Waiau Valleys (based on Clayton, 1965; 1968) and their correlations to Oxygen Isotope Stages (OIS).

Based on differences in elevation, down valley position of moraines and weathering characteristics, Clayton (1968) distinguished six late Pleistocene glacial advances in the Hope-Waiau Valleys (Fig. 10). The oldest advance ('Kakapo advance') was reconstructed based on several high lying surfaces that include the ice scoured flat mountaintop of Kakapo Hill (Fig. 12 and 13; 850 m a.s.l.), a high lying outwash terrace in a tributary valley of Culverden Basin (Lottery-Mason Valley), and a subdued terminal moraine in the Edwards Valley. Since remains associated with the Kakapo advance are extremely scarce the reconstruction of the Kakapo glaciation ice limits shown in Fig. 10 is largely hypothetical. Clayton (1965) correlated the Kakapo advance to the Avoca glaciation of the Waimakariri Valley (Gage, 1958) which today

Fig. 11: Reproduced A3 map of Clayton (1968); see full page in hard copy

implies an absolute age of about 290 – 240 ka (OIS 8). If this assumed age is correct several kilometres of horizontal displacement on the Hope and Clarence faults and about 0.5 km of vertical uplift have since occurred rendering an accurate reconstruction of the Kakapo glaciation highly problematic. All proposed correlations between the Hope-Waiau Valleys and other glacial systems are summarized in Table 1 (p. 30).

Fig. 12: Ice scoured surface of Kakapo Hill located 430 m above the present river (~850 m a.s.l.). The surface is bedrock-cored and covered by a veneer of till, gravel and loess of less then 3 m thickness. Several large erratics and streamlined bedrock features indicate that the Kakapo surface was ice overrun.

Fig. 13: Erratic boulder on Kakapo Hill during sampling for cosmogenic dating.

The next younger glaciation, the penultimate Horseshoe glaciation, was named after Horseshoe Lake near the Kakapo Brook - Hope River junction. Horseshoe surfaces are located 680 – 700 m a.s.l., roughly ~300 m above present river level but ~150

below the Kakapo surface (Fig. 14 and 15). The distinction of the Horseshoe sequence was based on its lower elevation and a lesser degree of weathering and landform dissection compared to the Kakapo sequence. Horseshoe aggradation terraces, alluvial fans, glacial erratics and moraines were mainly found in the lower Hope and Kakapo Valleys. Although these landforms are better preserved than the Kakapo landforms they are morphologically more subdued than those of the last glacial Glynn Wye and Glenhope sequences (see below). Clayton (1968) found that Horseshoe terraces adjacent to hill sides have usually smooth contact zones suggesting relatively widespread alluvial debris blankets which were derived over time from the adjacent

Fig. 14: Glacial erratic on Horseshoe surface (~700 m a.s.l.) in the lower Hope Valley.

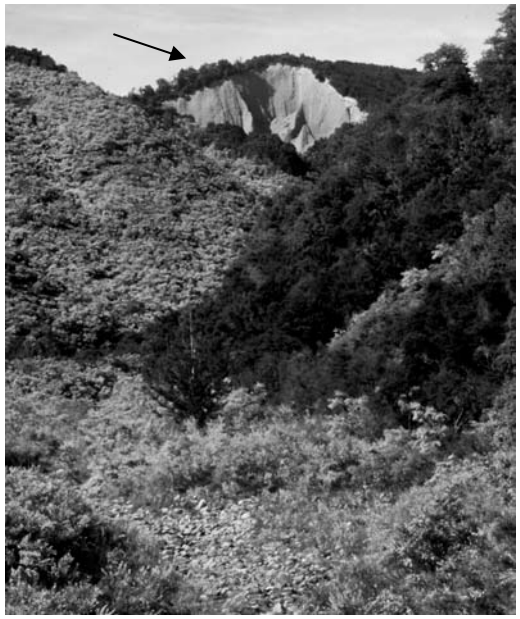

Fig. 15: Horseshoe aggradational gravels exposed ~280 m above river level.

slopes. Exposures of Horseshoe gravels are characterized by a yellowish oxidised colour (Munsell 10 YR 7/4), a greater degree of compaction and little remaining open pore spaces between clasts. Several high lying terraces in the Waiau Valley (120 – 170 m above river, between Jones Stream and Lake Guyon) and a small number of surfaces in the north-eastern Culverden Plains are correlative to the Horseshoe glaciation Clayton (1968). Similar to the Kakapo sequence, glacial deposits and landforms of the Horseshoe advance are relatively scarce and the ice limits shown in Fig. 10 are only a rough estimate. Prior to this study no direct age control was available for either the Kakapo and Horseshoe glaciations.

The subsequent Otira glaciation (OIS 4 – 2) was divided into four stadials based on moraine positions and terrace elevations (Clayton, 1968). The earliest reconstructed advance, named Leslie Hills advances, is poorly constrained and no deposits or landforms have been identified in the area depicted in Fig. 10 and 11. The advance is based on only few scattered aggradational terrace remnants in Culverden Basin, some 45 km downstream of Kakapo Hill. No attempt was made to reconstruct the ice limits during the advance (Clayton, 1968). The Glenhope advance during the early last glacial maximum is represented by moraines east of Kakapo Hill, in Dismal Valley and in the upper Waiau Valley. The advance is associated with outwash terraces located about 150 m above river level but about 100 m below the surfaces of the preceding Horseshoe glaciation. This advance is followed by the Glynn Wye advance which is associated with extensive outwash terraces in the Hope Valley and a series of moraines in the Hope and Waiau Valleys. Clayton (1968) suggested that during the advance glacial tongues of the Hope, Doubtful, Nina and Lewis Valleys coalesced whereas glaciers of the upper Boyle and Waiau Valleys remained separate. The Glenhope and Glynn Wye advances are correlated to the Blackwater and Bayfields sequences of the Waimakariri and Rakaia Valleys. None of the Otiran advances in the Hope-Waiau Valleys has numerical age control and all correlations are based on relative criteria only.

Ice retreat and onset of postglacial fluvial incision in the Hope-Waiau Valleys is constrained by a radiocarbon date from organic silts deposited between Glynn Wye aggradation gravels and fan debris yielding an age of 14,100 ± 220 a BP (Suggate, 1965). Pollen from this deposit indicate a dominantly grass and herb vegetation. A

second minimum age on the retreat from extended LGM ice positions is provided by a date of 13,309 ± 203 a BP (Clayton, 1968) from lacustrine muds in the lower Boyle River deposited in a glacial lake which formed following ice evacuation from this valley reach. The general retreat phase was interrupted by a late glacial re-advance (Lewis advance) which is represented by moraines in the headwaters of nearly all valleys but most prominently at Lewis Pass. The advance was comparatively small and did not produce a coalescing network of valley glaciers which characterized the earlier glacial advances. A recent radiocarbon from McMillan Stream 8 km up valley from the Lewis moraine at the Hope-Kiwi lodge yielded and age of 12,897 ± 65 a BP (Langridge and Berryman, 2005) suggesting that the Lewis advance occurred prior to this date.

Fig. 16: Exposed Glynn Wye moraines in the lower Hope Valley

Fig. 17: Glynn Wye moraine at Windy Point with glacial erratic sampled for cosmogenic dating.

CHAPTER 4

STRATIGRAPHY AND TECTONIC IMPLICATIONS OF LATE PLEISTOCENE VALLEY FILL DEPOSITS IN THE LOWER HOPE VALLEY

4.1. Introduction

This chapter aims to describe and interpret a spectacular sedimentological outcrop exposed by river erosion on the southern bank of the Hope River ('Glynn Wye outcrop' at New Zealand grid ref. M32 E 24629 / N 58445). The exposed sequence comprises a sedimentary succession of roughly 120 m thickness representing a nearly complete cross-section of the valley fill sequence in this valley portion. A distinctive feature of glacio-depositional sequences in valleys of the Southern Alps is the extraordinarily large scale of alluvial aggradation fans which often exceed 100 m in thickness. These fill successions represent the dominant 'glacial' deposit in the Southern Alps and as a consequence, the traditional focus of glacial geologists in New Zealand has been on the correlation of outwash terraces for the discrimination of glacial events (e.g. Gage, 1958; Suggate, 1965; Nathan and Moar, 1973; Mabin, 1983; Suggate, 1985; Maizels, 1989). However, despite the importance of glacial valley fills there have been only few detailed investigations aimed at deciphering the sedimentology, stratigraphy and numerical chronology of such sequences. In the lower Hope Valley spectacular outwash terraces give evidence for the large scale of valley aggradation that occurred during the last glacial cycle and the intensity of subsequent periods of postglacial fluvial downcutting. This chapter investigates aggradational deposits in the lower Hope Valley where excellent outcrop allowed detailed sedimentary logging and sampling for luminescence dating. The sedimentological investigation of outcrops at river level was complemented by geophysical information from the adjacent floodplain using ground penetrating radar (GPR) to analyse depositional structures of the subsurface. GPR data collection was supported by Dr. Harry Jol (Department of Geography and Anthropology, University of Wisconsin-Eau Claire, USA) who visited the Department of Geological Sciences (UoC) in 2003.

4.2. Local setting: the lower Hope Basin

The Hope River (mean flow 45.9 m^3/s) originates SE of Mt. Ajax (Lat/Long: S 42˚35'35"/ E172˚03'97") and drains an area of ~700 km^2 of alpine terrain east of the topographic divide. The studied valley reach, the lower Hope Valley, constitutes a 9 km long and 4 km wide valley segment located between the Windy Point and Glynn Wye gorges near the confluence of the Hope and Boyle Rivers (Fig. 18). The area is tectonically highly active and several NE trending dextral strike-slip faults traverse the catchment. Of these, the Hope Fault follows roughly the course of the Hope and lower Waiau Rivers. Cowan (1991) suggested that the broad lower Hope Valley represents a tectonic depression that formed along a releasing bend of the fault. Other features including the repeated succession of narrow bedrock gorges and intermediate wider valley segments are also interpreted to be fault controlled (Fig. 19). Faulting

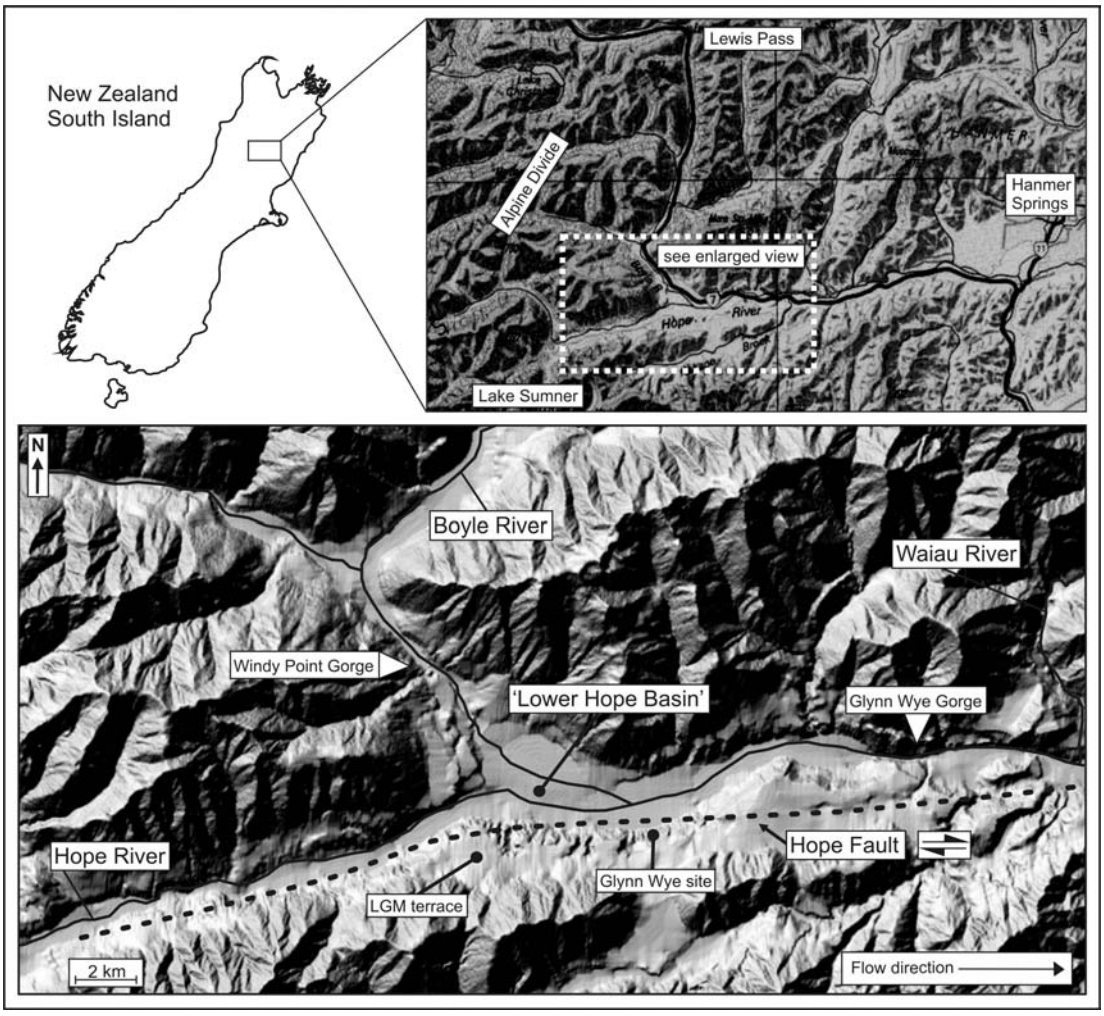

Fig. 18: Location of the lower Hope Valley in the South Island, New Zealand. The shaded relief map shows the course of the Hope Fault and the location of the studied outcrop (Glynn Wye site).

along the investigated segment of the Hope Valley offset a glacial moraine complex at Glynn Wye station which is inferred to be 17 – 20 ka BP old (Knuepfer, 1988; Cowan, 1990). The lateral displacement of the moraine was surveyed by several workers but because of differences in the geomorphological interpretation the suggested offset varied from 348 ± 7 m (Knuepfer, 1984), and 286 ± 6 m (Cowan, 1989) to 230 ± 20 m (Cowan, 1990). Accordingly, estimates of the slip rate of the Hope Valley segment of the Hope Fault range between 21-14 mm/a. Extensional faulting was also responsible for the formation of Poplars Graben near Glynn Wye Station along a small releasing bend of the fault. Surveys of the graben (Freund,

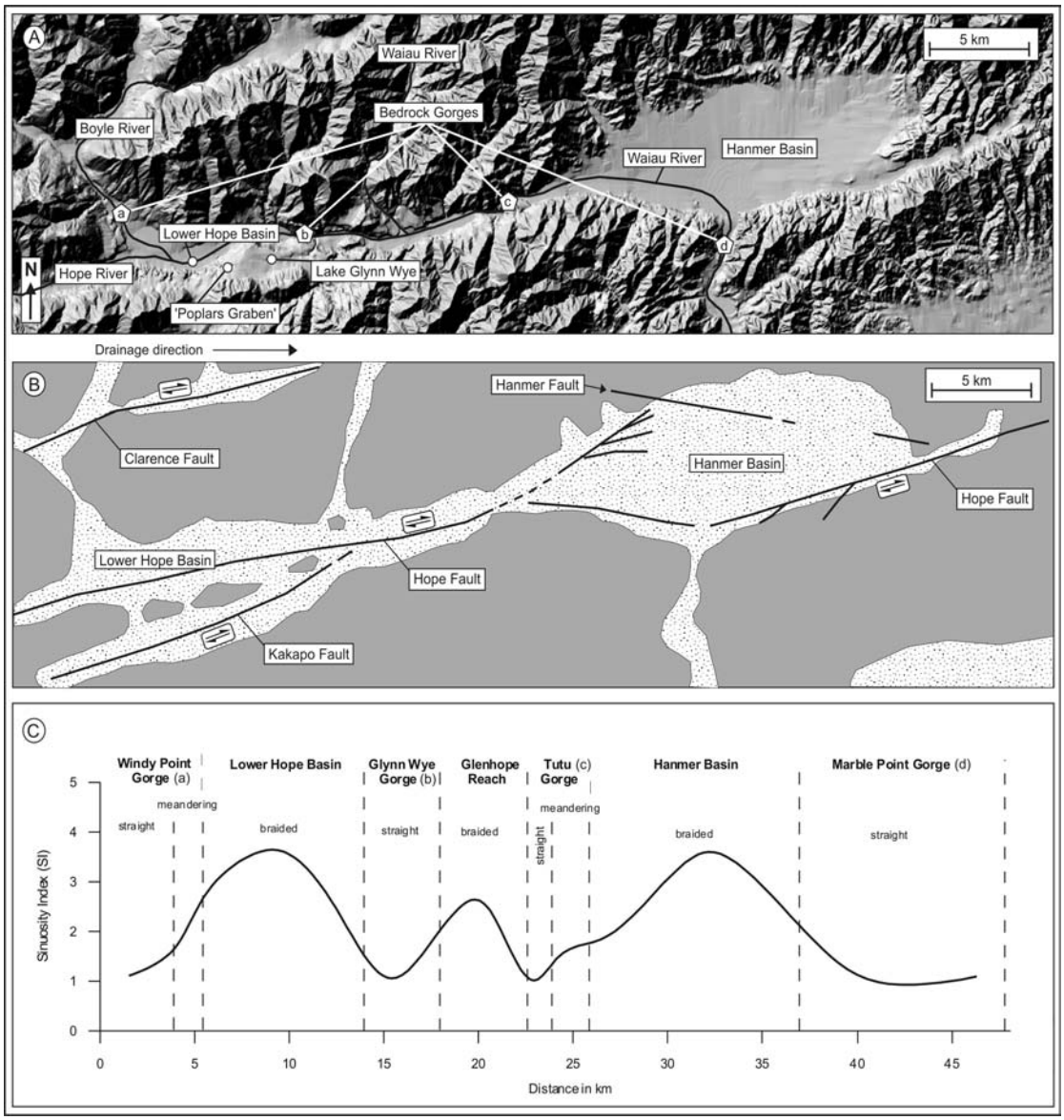

Fig. 19. Overview of structural geology and fault controlled features of the Boyle-Hope-Waiau Valley system (A & B). Note the succession of gorges and wider valley segments which are associated with rapid changes from braided to single thread channel geometries as indicated by the Sinuosity Index (SI) in C. SI is the ratio between totals channel length and thalweg length.

1971; Cowan, 1989) found the central part of the structure to be downthrown by roughly 40 m. The graben formed in last glaciation aggradational deposits also estimated to be 17-20 ka BP old (Fig. 20, Clayton, 1965; Hardy and Wellman, 1984). The lower Hope Basin is the inferred initiation point of the large 1888 North Canterbury earthquake (Cowan, 1991) which caused widespread ground shaking throughout the region and damaged the Christchurch cathedral 110 km to the south.

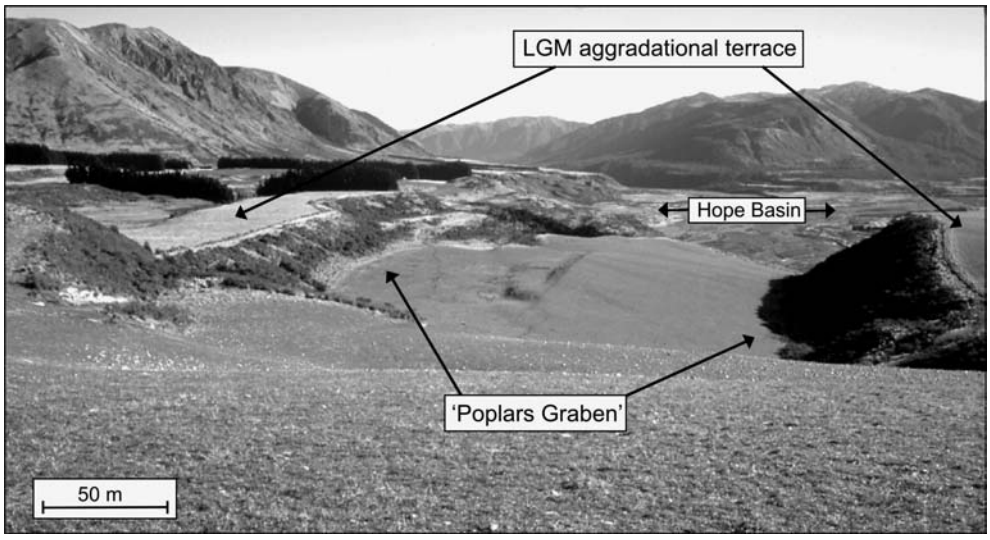

Fig. 20. Poplars Graben is located on the main aggradational terrace within the Hope Basin. The photo shows a view through the graben towards W. The graben is displacing last glacial aggradational deposits and represents a secondary tectonic structure within the larger Hope Basin.

Fig. 21. Alexander McKay at the fence line near Glynn Wye Station which was off-set by the 1888 magnitude ~7 earthquake in the Hope Valley.

During the event the ~30 km Hope Valley fault segment (between the lower Hope Valley and Hanmer Plains) ruptured and produced dextral offsets of 1.5 – 2.6 m which were observed on displaced fence-lines. The effects were documented in detail by McKay (1890) whose report is recognized to be the first published record of pure strike-slip motion during an earthquake (Fig. 21; Freund, 1971; Sylvester, 1988). Apart from Cowan's (1990, 1991) references to the lower Hope Basin, little is known about the geomorphological and sedimentological effects of local basin formation and the total basin depth is as yet unknown. The configuration of the basin is best expressed by highlighting the distribution of bedrock and strath terraces along the lower Hope Valley reach. Although deeply incised bedrock gorges are found on the immediate upstream and downstream ends of the reach, no bedrock is found at surface level within the lower Hope Valley itself (Fig. 22). Postglacial strath terraces at Windy Point Gorge (upstream) and Glynn Wye Gorge (downstream) range in elevation from 490 – 536 m a.s.l., yet in the depression (~450 m a.s.l.) no basement rock is exposed. The absence of knickpoints in the longitudinal valley profile is related to the sedimentary infilling of the Hope Basin.

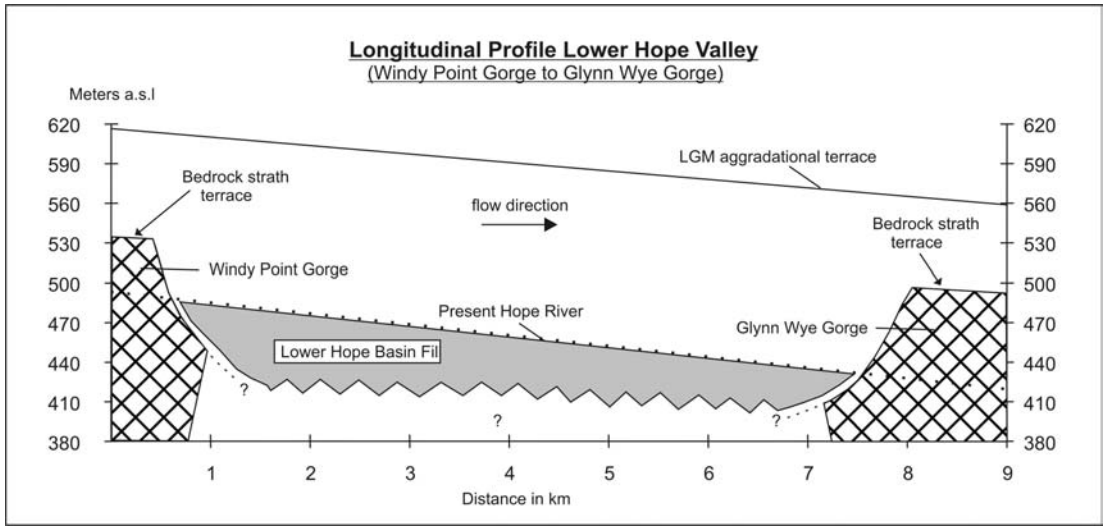

Fig. 22. Position and elevation of bedrock gorges and strath terraces in the lower Hope Basin.

4.3. Quaternary context

Several times during the Late Pleistocene valley glaciers extended 30-40 km from the central Southern Alps causing the former Hope, Boyle and Doubtful glaciers to coalesce in the lower Hope Basin. Clayton (1968) recognized six glacial advances in

the overall catchment, four of which have their 'type location' in the lower Hope Valley. Glacial surfaces are found over a wide range of elevations above the present river. The inferred LGM glacial moraines and correlated outwash are situated 160 m above the present river (Fig. 23), while the highest (and presumably oldest) glacial surface is located on Kakapo Hill 430 m above the Hope River (Kakapo advance). Between these two advances an intermediate level of outwash surfaces is preserved at about 300 m above river level (Horseshoe advance). Although Clayton (1965, 1968) and Suggate (1965) recognized greater weathering and a more subdued topography associated with the Kakapo and Horseshoe surfaces, which they interpreted to indicate formation during more distant Pleistocene glaciations, numerical age control of the higher (and older?) surfaces was absent and no quantified weathering parameters have been presented. The lack of good sedimentological exposure adds to the difficulty in using relative criteria to 'date' these surfaces. Therefore, although the premise of the general 'elevation-age-model' (e.g. Gage, 1958; Suggate, 1965) is reasonable, it should be noted that the model is valid only if it can be demonstrated beyond doubt that younger ice advances never reached the elevation level(s) of previous glacial advance(s) and overrode the older surfaces. A summary of the Late Pleistocene geology in the lower Hope Valley area is given in Fig. 24.

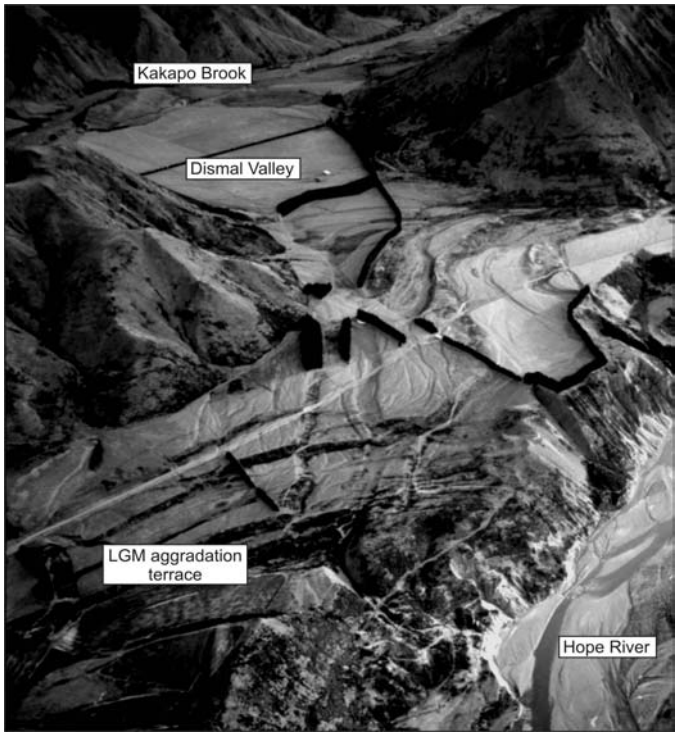

Fig. 23: Glynn Wye terrace with preserved channel pattern ~160 m above present Hope River (photo courtesy J. Pettinga).

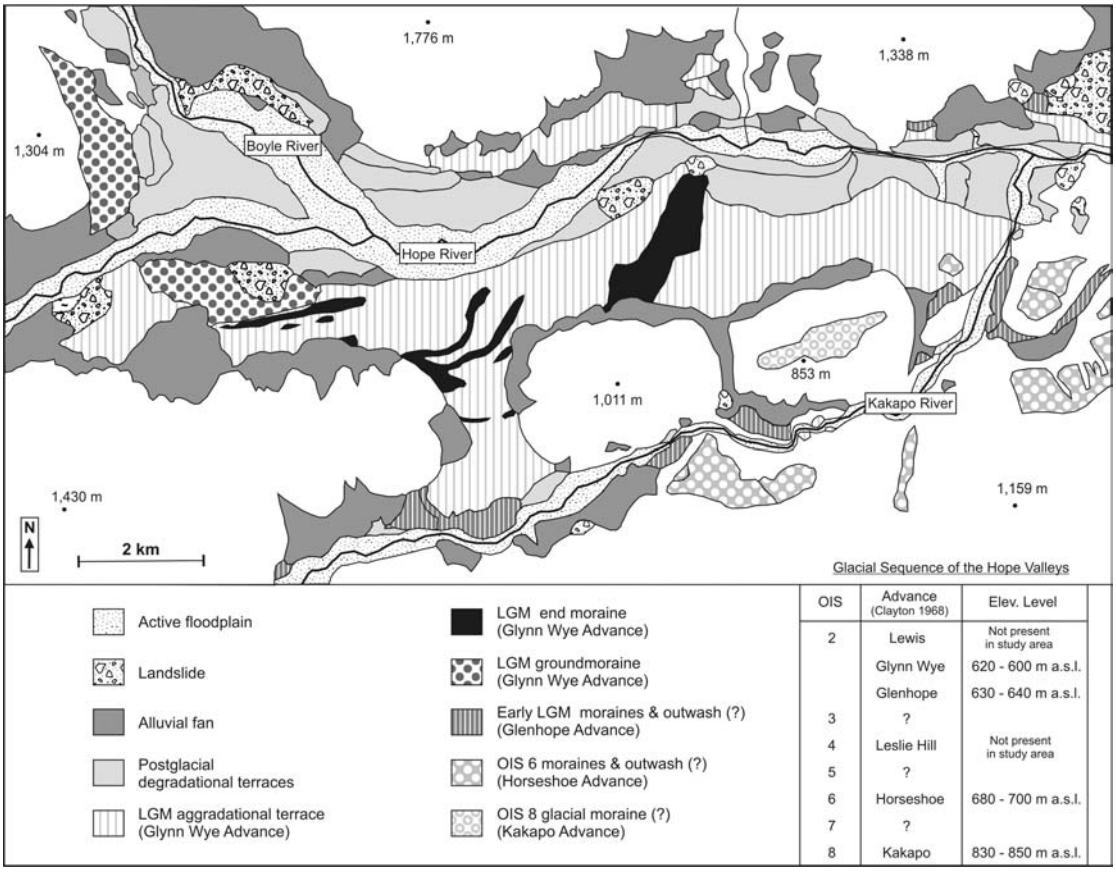

Fig. 24. Quaternary geology of the lower Hope Valley study area (modified from Clayton 1968). Note the distinct elevation levels of landforms associated with advances during OIS 8, 6, and 2 (see table).

4.4. Methodology

The described outcrop is a prominent feature in the lower Hope Valley and can be easily spotted from SH 7 on route to Lewis Pass. Apart from a brief description in Cowan (1989) the stratigraphy and sedimentology of the exposure has never been investigated. Clayton (1965, 1968) made no mention of the sequence probably because, as contemporary aerial photos show, during the 1960's the Hope River flowed in the central part of the floodplain and large scree slopes covered most of the Glynn Wye exposure. Field work started with reconnaissance mapping in the Kakapo and Hope Valleys which was supported by airphoto interpretation to provide the necessary context for the Quaternary geology of the study area (Fig. 25). For sedimentological descriptions standard logging techniques were employed. Units were distinguished based on bedding angles, sediment composition, texture, grain size, and sorting. Only the lower portion of the outcrop was directly accessible as the

middle and upper section form a ~75 m high vertical cliff. The sediments exposed in this section were logged from several vantage points. Data on clast imbrication and clast angularity were collected from all accessible units for at least 30 clasts at each site.

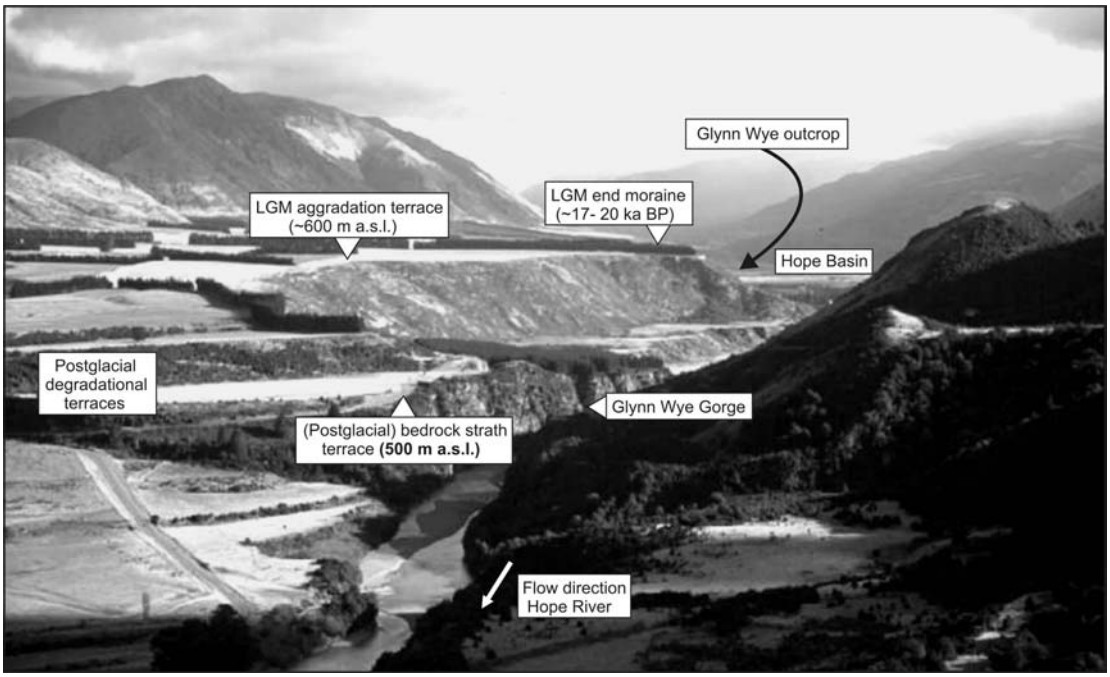

Fig. 25: Upriver view (west) into the lower Hope Valley showing the context of landforms and deposits discussed in the text. The investigated Glynn Wye outcrop is located in the Hope Basin (black arrow). Following postglacial fluvial incision through the LGM aggradational terrace, the Hope River formed a bedrock strath terrace at Glynn Wye Gorge (500 m a.s.l).

4.4.1. Ground penetrating radar

A portable digital pulseEKKOTM IV radar system was used to collect GPR reflection profiles to investigate the relationship between exposed sediments and the sub-floodplain sedimentary fill. Near surface geophysical tools such as GPR use high-frequency electromagnetic pulses which are transferred into the ground via a transmitter antenna (Fig. 26). The radiated energy waves are reflected back to the surface from interfaces of sediments with different dielectric properties due to variations in water content, grain size, porosity and compaction (Jol and Bristow, 2003; Nobes, 2000). The returning radar echoes are recorded by a receiver antenna. Signal penetration and signal resolution depend on a variety of factors that include most importantly the energy frequency chosen (commonly between 400-25 MHz) and the properties of the investigated sediments with grain size and water content

being the most influential. Penetration depths can vary between few meters in saturated fines to about 20 m in saturated gravel to hundreds of meters in hard rock and ice. After tests with various antennae a 50 MHz antenna was selected for the survey in the lower Hope Valley and a low frequency 25 MHz antenna for the survey at Glynn Wye gorge which provided the best signal penetration and profile resolution. The GPR system was operated in 'step-wise reflection mode' where a reading is taken at a fixed position every 0.50 m (for 50 Mhz) and 1.0 m (25 MHz) respectively. Each digital trace was vertically stacked 32 times at a sampling time interval of 800 picoseconds. Profiles were processed and plotted using pulseEKKO™ software. Several common mid-point (CMP) surveys were performed to determine the near-surface signal velocity in the investigated sediments. From the results an average velocity of the radar waves of 0.11 m/ns was calculated.

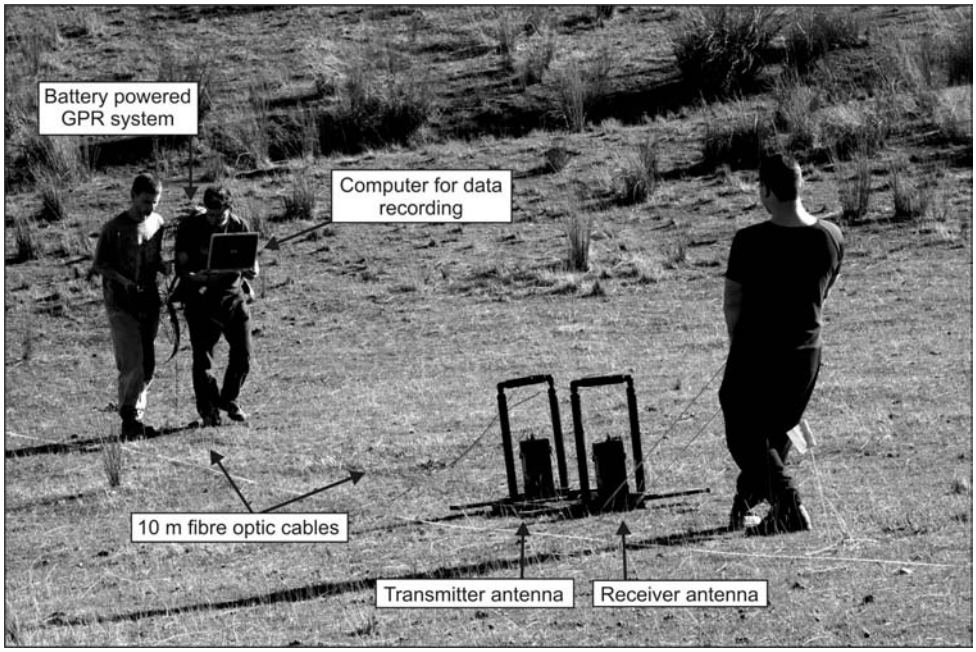

Fig. 26. GPR field set and crew comprising computer, antennae and cable operators. GPR has become a powerful tool for sedimentological studies because the system is comparably mobile and provides real-time recorded depictions of subsurface structures (bedding angles, sediment deformation etc.).

4.4.2. Luminescence dating

Samples for Infrared Stimulated Luminescence (IRSL) dating were obtained by forcing a 220 mm long steel tube (75 mm diameter) into fine sediments or by excavating a coherent sediment block (15 x 15 cm) from the outcrop. Samples were

tightly wrapped to prevent light exposure and to contain its moisture content. All samples were submitted to Victoria University Dating Laboratory (Wellington, New Zealand) where they were analyzed using the silt fraction following the procedure of Rieser (2004). Sample preparation was conducted under subdued orange light and included the removal of carbonates (10%-HCL), organic matter (10%-H_2O_2) and iron oxide coatings (Na-citrate, Na-bicarbonate, Na-dithionate). Between each step the samples were carefully rinsed with distilled water. After extracting the 4-11 μm grain size the samples was brought into suspension in pure acetone and deposited evenly in a thin layer on small aluminium discs (10 mm diameter).

Luminescence measurements were performed using a RISO TL-DA15 system, equipped with Kopp 5-58 and Schott BG39 optical filters to select the luminescence blue band. Optical stimulation was carried out at ~30mW/cm^2 using infrared diodes. For beta irradiations a Daybreak 801E ^{90}Sr, ^{90}Y irradiator was used that was calibrated to ~3% accuracy against a standard at the SFU luminescence facility, Vancouver, Canada. Alpha irradiations were completed on a ^{241}Am irradiator supplied and calibrated by ELSEC, Littlemore, UK. The paleodose, (i.e. the radiation dose accumulated in the sample after the last light exposure) was determined by measuring the blue light output during infrared optical stimulation of feldspar minerals using a multiple aliquot additive-dose method. Following measurements the disks were stored in the dark for four weeks to relax the crystal lattice after irradiation. After storage the discs were heated (220˚C) to remove unstable signal components and then measured for 100sec each to obtain the shinedown curves. The dry homogenised samples were counted using a high resolution gamma spectrometer with a broad energy GE detector for a minimum time of 24h. The spectra were analysed using GENIE2000 software. The doserate calculation is based on the activity concentration of the nuclides ^{40}K, ^{208}Tl, ^{212}Pb, ^{228}Ac, ^{214}Bi, ^{214}Pb, ^{226}Ra.

4.5. Results

The following results consist of sedimentary log data (Glynn Wye outcrop) and a GPR survey comprising three 65 m, 100 m, and 115 m long profiles from the southern and central parts of the Hope Basin. These complimentary data sets allow for the reconstruction of depositional processes in the Hope Basin.

4.5.1. Glynn Wye outcrop

The local valley fill stratigraphy was studied using an exposure at Glynn Wye Station which comprises 120 m of deposits that constitute the main aggradational terrace in this valley reach (Fig. 27). Variation in dominant clast lithology, colour and bedding orientation separates two well defined gravel units which are visually distinct (Fig. 27C). The ~55 m thick basal unit (G1 gravels) comprises ~45 m of steeply dipping beds (~33º, unit 1) which are overlain by a ~10 m thick unit of nearly horizontal beds (unit 2, Fig. 27D). The orientation of the dipping beds ranges between 330 - 030˚. The gravels are dark grey in colour (Munsell colour: N 3/0). Both units are clast supported and are lithologically very similar. They are dominated by large pebble and cobble clasts ranging in size between 40-120 mm. Most clasts are subangular in shape. The units contain a high proportion of argillite lithologies.

Interpretation: Unit 1 is interpreted as a delta foreset deposit and the overlying unit 2 is interpreted as delta topset beds (Fig. 27D). The internal structure of the overall deposit resembles a Gilbert-type delta where fluvial gravels avalanched into a lake at the subaqueous angle of repose which was then followed by the progradation of a subaerial fluvial system that deposited the flat lying topset beds (Gilbert, 1890). Gilbert style deltas can be used to limit the former lake depth because the contact between foreset and topset units represents the migrating delta lip which closely approximates the former lake level. Based on this datum and because the basal contact of the foreset unit is not exposed the reconstructed former Hope paleo-lake had a minimum water depth of ~45 m.

A compositionally different gravel package (G2 gravels) comprising ~65 m of coarse clast supported gravels overlies the delta deposit. The maximum clast size is about

400 mm but most clasts are between 150-250 mm in diameter. The lighter sediment colour of these gravels (Munsell Colour: N 6/0) is due to a higher proportion of greywacke lithologies which provides a contrast to the underlying units which are dominated by darker coloured argillite. Most clasts of the G 2 gravels are well rounded. Several subunits of upwards coarsening gravels and rare beds of sand and silt can be distinguished. In some places the individual gravel units have sharp erosional basal contacts (Fig. 28) but no erosional scour was found at the contact between the delta gravels and the G 2 gravels.

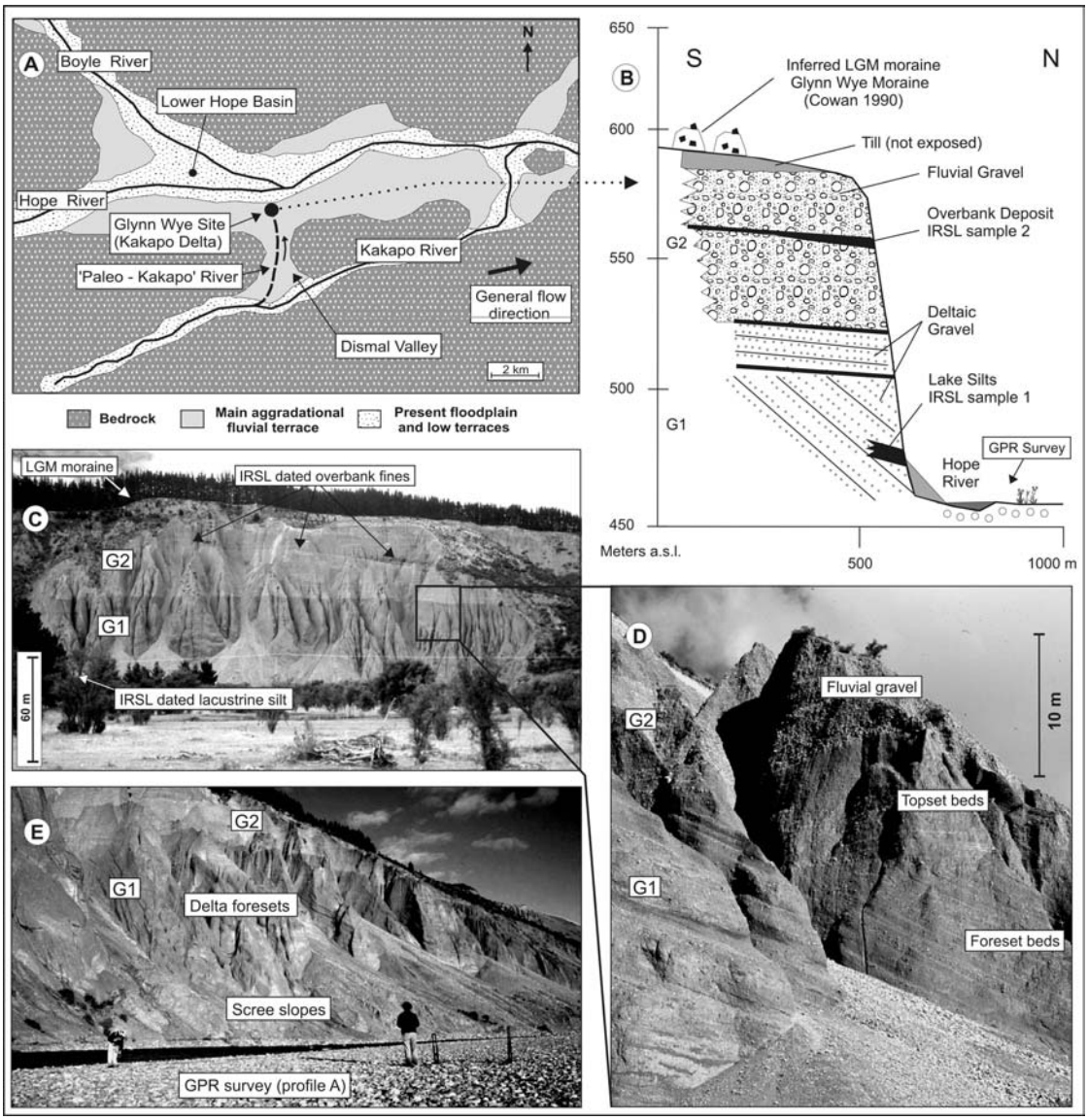

Fig. 27. Location, context and stratigraphy of aggradational deposits at Glynn Wye Station. Figure 27C shows the studied outcrop a seen from SH 7 near Hope River bridge. The positions of the two major gravel units (G1 & G2) are marked for better orientation. Note that Fig. 27B and Fig. 27E show the location of the transect for the GPR profile presented in Fig. 30.

Interpretation: This unit resembles in composition and clast shape sediments of the present floodplain and is interpreted as a fluvial deposit. Several channel fills can be distinguished within the G2 unit comprising erosionally bound packages of gravels which are interbedded with finer sediments interpreted to represent flood overbank deposits. The sequence was deposited on an aggrading braid plain characterized by frequent channel evulsions. No evidence for significant scouring at the contact between the lacustrine (G1) and fluvial (G2) units was found, indicating that none or only very minor erosion occurred between the deposition of the two sequences. The overall contact is therefore interpreted to be depositional in nature, which is supported by the completeness of the underlying delta sequence which includes fully preserved topset beds.

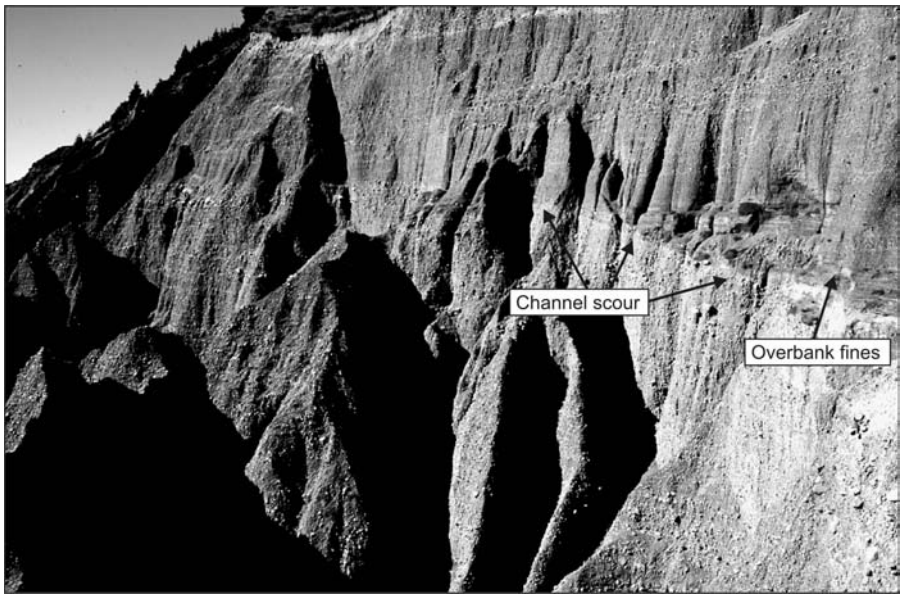

Fig. 28: The G2 fluvial sequence. Note the upwards coarsening gravel unit on the right.

The aforementioned lithological difference between the G1 and G2 gravel units has relevance for the reconstruction of the source areas for both gravel sequences. The argillite clasts of the delta deposit are dominantly of subangular shapes indicating a relatively short distance of fluvial transport whereas the overlying coarse fluvial gravels are mainly rounded suggesting longer distance fluvial transport. The depositional orientation of the foreset beds (330 - 030˚) indicates that the delta was deposited into the Hope paleolake from the south which is inconsistent with the W-E drainage orientation of the lower Hope River. The only potential stream outlet from this direction is through Dismal Valley, which at present, does not carry any drainage

into the Hope Basin. Therefore, the data suggest that during delta deposition the Kakapo River, which presently flows further to the south, drained across Dismal Valley directly into the Hope paleolake ('Kakapo Delta') (Fig. 27A). This reconstruction is consistent with the measured orientation of the foreset beds and also accounts for the subangularity of the clasts in the delta beds because the fluvial transport distance out of the Kakapo catchment into the lower Hope Basin would not have exceeded ~10 km. A subsequent change in the depositional direction is recorded by the overlying fluvial unit (G2) which was deposited from west to east by the Hope River. Stratigraphic control is provided by a glacial moraine system deposited on top of the Glynn Wye sequence (Fig. 27C). By correlation to other New Zealand glacial systems the moraines are regarded as the terminal position of a LGM ice advance (Clayton, 1968). Knuepfer (1988) reported a dubious 'composite' clast weathering rind age from the moraine of 18.7 ± 3.8 ka BP which is consistent with an LGM interpretation but no direct ages are available.

4.5.2. GPR results and interpretation

GPR was used at several locations in the lower Hope Valley to determine the depth to bedrock and to investigate sedimentary structures of the basin fill (Fig. 29). In this chapter three of the profiles are presented in detail. The first survey (profile A, Fig. 30) was collected on the south side of the Hope River floodplain along a transect line located ~15 m away from the described Glynn Wye outcrop. The recorded reflections delineate three radar facies (lower, middle, upper) with a total signal penetration depth of ~12 m. The lower radar facies displays continuous to semi-continuous, horizontal to sub-horizontal reflection patterns. The 11-m thick middle facies is dominated by continuous to semi-continuous reflections with a dip angle ranging from 31º to 38º. Between positions 0 – 20 m (horizontal distance) reflections are sub-horizontal, and are onlapping the steeply inclined unit in the center of the profile. At the eastern end of the profile (position 45 - 55 m) reflections become less continuous with the inclination of the bedding reduced to ~ 21º. The middle radar facies is separated from the nearly horizontal upper facies by a truncation and the contact is interpreted as an erosional unconformity. The upper facies is ~1.50 m thick and consists of sub-horizontal to horizontal continuous to semi-continous reflection patterns.

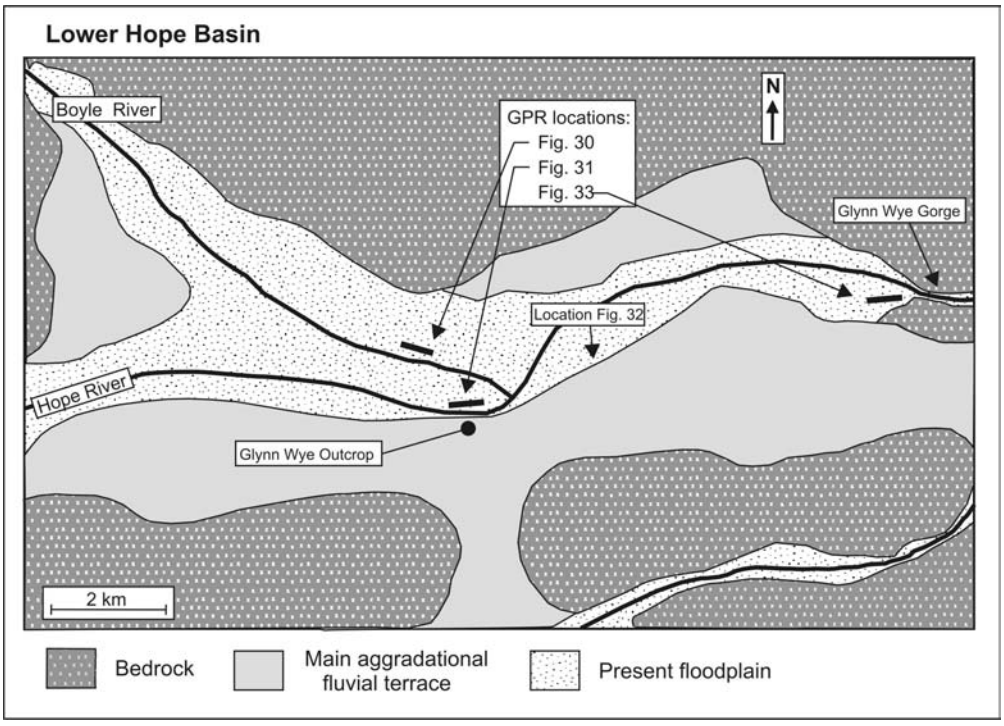

Fig. 29: Location and orientation of GPR transects presented in Figs. 30, 31 and 33 and photos presented in Fig. 32.

In the context of the inclined bedding of the middle radar facies the nearly horizontal reflections of the lower radar facies are interpreted to represent delta bottomset beds. Rapid signal attenuation within the facies is probably due to the fine-grained nature of the sediment, such as is observed in exposed lacustrine beds at the base of the adjacent Glynn Wye outcrop. The overlying radar facies (middle) comprises steeply dipping beds, interpreted as delta foresets. The deltaic sediments indicated by the lower and middle radar facies give evidence for an older lake phase in the Hope Basin. GPR profile A shows no bedrock contact to a depth of 12 m below the Hope River floodplain. Separated by an erosional unconformity, the thin uppermost facies (~1.50 m) represents a veneer of gravels which are part of the active channel facies of the Hope River. The deposit comprises mainly of boulders representing the coarse bed load component which is not moved under standard flow conditions. However, the moderate thickness of the channel facies and the sharp erosional nature of the basal contact suggests that during frequent flooding, the present river is capable of moving its bedload and of incising into the underlying lacustrine facies.

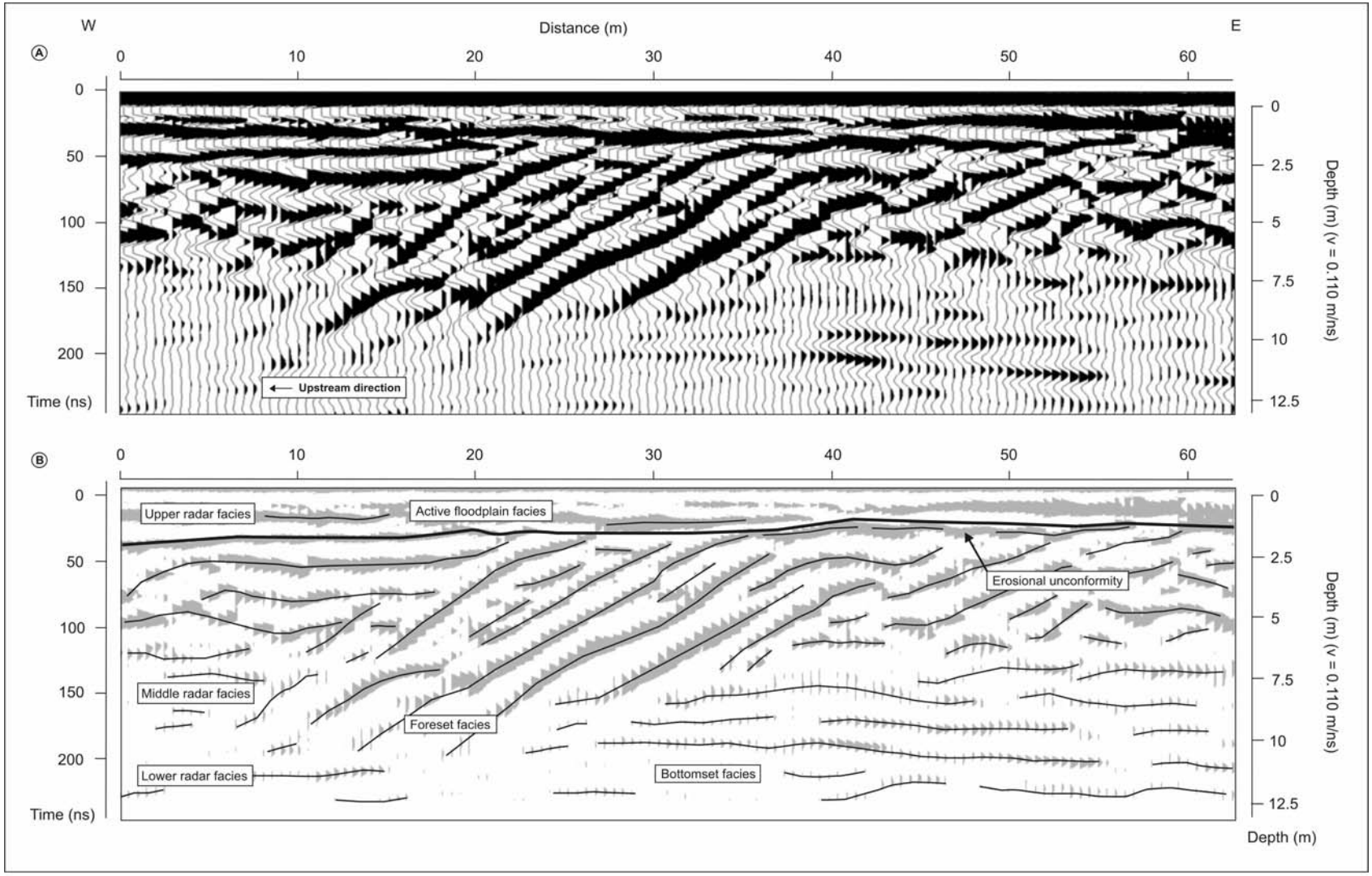

Fig. 30. 50-MHz GPR profile A showing radar reflections and interpretation of sedimentary structures below the Hope River floodplain.

The second GPR survey line (profile B, Fig. 31) was located near the center of the Hope Basin about 1.4 km northwest of the Glynn Wye outcrop (see Fig. 29). The 115 m long survey line was oriented parallel to the river (WNW-ESE). Radar reflections were recorded to a depth of 16-17 m. The profile is summarized into three radar facies (lower, middle, upper). The lower facies is poorly constrained with only three slightly dipping (2º downstream), continuous to semi-continuous reflections between 10-70 m (horizontal distance). The middle facies is ~12 m thick and displays continuous to semi-continuous reflections with varying dip angles and dip directions. A prominent 30 m long, 5 m high anticlinal reflection pattern is centered at 28 m (Fig. 31). In the central section of the profile (position 64-71 m) reflections indicate the presence of a steeply dipping unit (42º) with a depth ranging from 2.5 to 9 m. Between 70-110 m (horizontal distance) dipping reflections indicate a bedding inclination of ~18º. Reflections at both positions dip in an upstream direction. The middle radar facies is separated from the nearly horizontal upper facies by a truncation which is interpreted as an erosional unconformity. The upper facies is ~1.50 m thick and consists of sub-horizontal to horizontal continuous to semi-continous reflection patterns.

Profile B extends to a depth of 17 m below the floodplain, and fails to intercept bedrock which is consistent with results from profile A. The weak reflection pattern of the lowest radar facies is interpreted as an undeformed, nearly parallel bedded and slightly downstream dipping sedimentary unit. The overlying middle radar facies, in contrast, displays substantial sediment deformation. Structures include a slightly asymmetrical anticlinal fold (centered at 28 m horizontal distance) which appears in three dimensions to be mound shaped. The steeply dipping reflections (between 64-71 m) are interpreted to be oversteepened gravel beds (>40º dip) since they exceed the natural angle of repose for loose sediment. The profile segment between 70-110 m dips at ~18º in a WNW direction. Because of the dip angle and dip direction (upstream) it is improbable that the deposit is of primary fluvial origin. An interpretation as delta foresets is also unlikely because the direction of dip points upstream and neither of the larger streams in the Hope Basin (Hope and Boyle Rivers) can be the depositing agent. Other tributary streams that drain into the Hope Basin are also unlikely candidates for potential delta deposition because the structure is located in the central part of the Hope Basin (~1.5 km from either valley side) and none of the

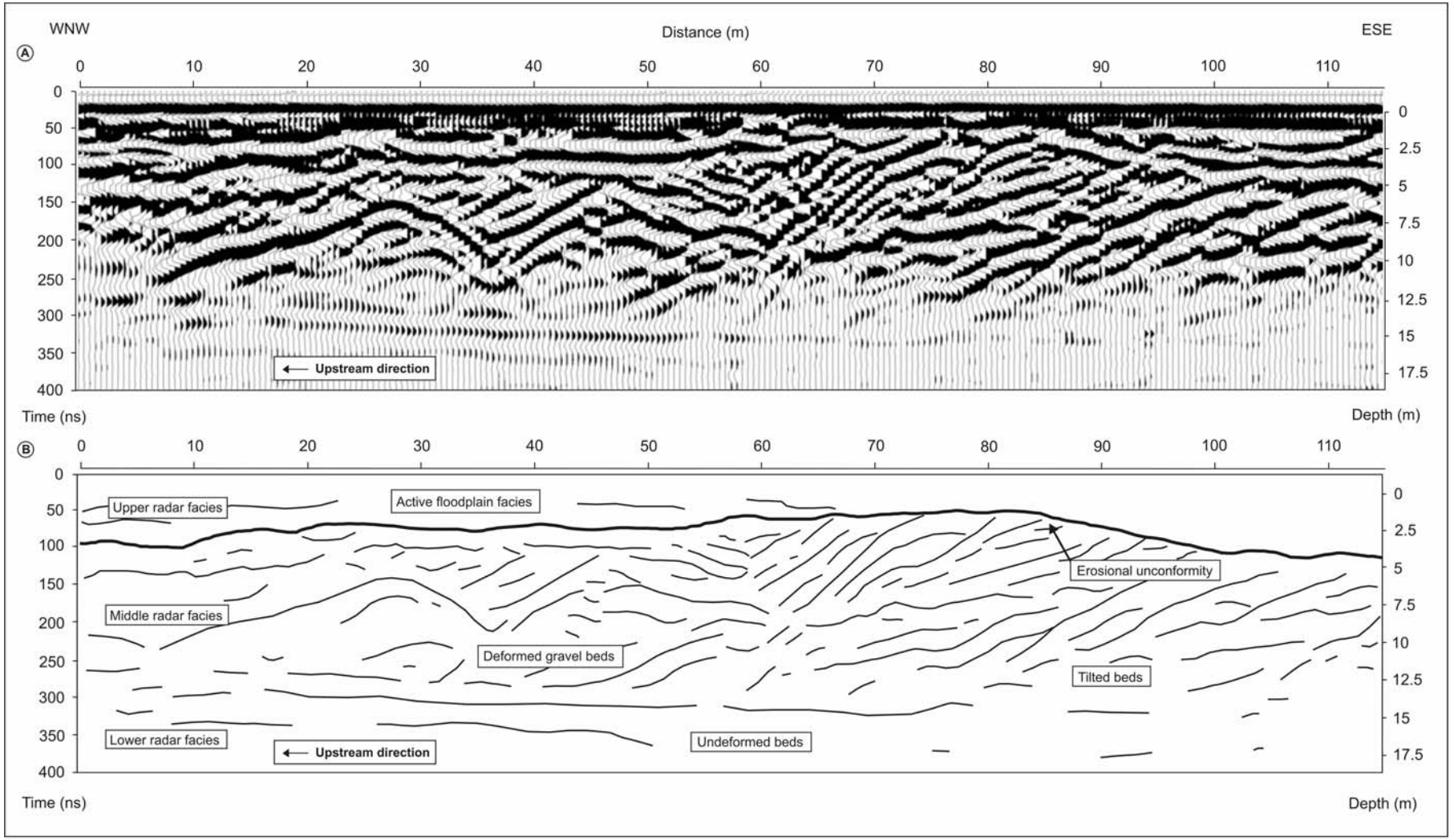

Fig. 31. 50-MHz GPR profile B from the central part of the Hope Basin showing radar reflections interpreted to represent deformational structures. Note that deformation occurs only in the middle facies while the bottom facies is undeformed.

tributaries are considered large enough to build a delta that extends over such distance from the valley side into the central basin. A more likely explanation for the reflection pattern is sediment deformation caused by tilting and folding.

The upper radar facies consists of nearly horizontal reflections and is interpreted as the channel deposit of the active river which truncates underlying deposits (i.e. middle radar facies). The presence of an erosional unconformity below the channel deposit in profile B is consistent with results from profile A and supports the view that the lower Hope River is presently incising into older valley fill. Despite some uncertainty about the mechanism that produced the sediment deformation observed in profile B, it is important to note that the lower facies (> 14.0 m depth) appears to be undeformed. Since the deformational structures are clearly restricted to near surface sediments it is improbable that the deformation is tectonic as this would also have disturbed the underlying beds. A more probable explanation for the structures is deformation caused by slumping and similar sediment deformation in lacustrine muds is exposed in a nearby outcrop at river level (Fig. 32).

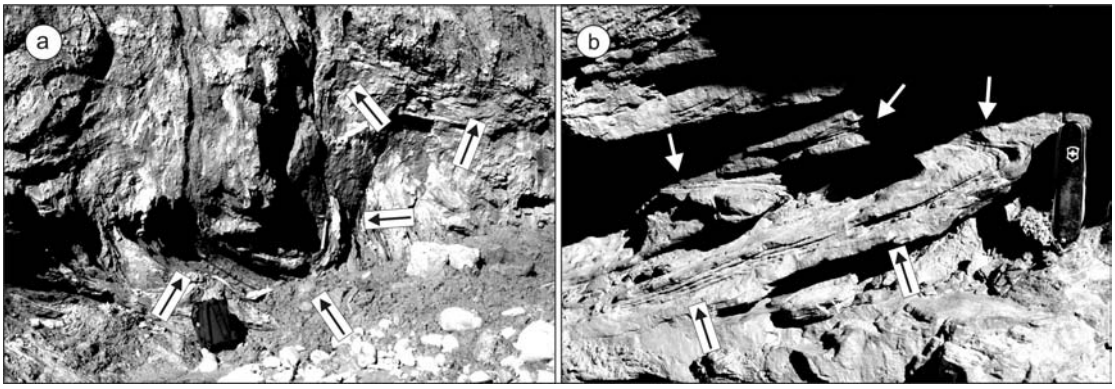

Fig. 32: Deformed lacustrine muds exposed at river level in the lower Hope Valley (for location see Fig. 29). Deformation (see arrows) was caused by subaqueous slumping and a similar process is inferred to explain deformation of the middle radar facies in profile B. Backpack in (a) and knife in (b) for scale.

The third radar transect (profile C, Fig. 33) was collected at Glynn Wye gorge on the southern side of the floodplain roughly 6 km downstream of Profile B. The 100 m long survey line was oriented parallel to the river and data collection started about 20 m upstream of the outcropping bedrock face of the gorge. To combine good signal resolution and maximum signal penetration the survey was repeated twice along the same line, first using a 50 MHz antenna and then a low frequency 25 MHz antenna.

Fig. 33 (A) presents results from the 25 MHz survey which yielded a ~35 % greater signal penetration than the 50 MHz survey. The recorded reflections delineate three radar facies (lower, middle, upper). The lower radar facies displays continuous sub-parallel and sub-horizontal to horizontal reflections mainly occurring between positions 45-100 m (horizontal distance). They are interpreted as offline reflections from a nearby ~2 m high terrace edge which runs roughly parallel to the survey line. The reflections were recorded at t = 300-350ns which is consistent with a surface distance to the terrace edge of ~45 m (air travel wave velocity: 0.3 m/ns). Similarly, the package of dipping and parallel reflectors at the eastern end of the profile (10-45 m) is interpreted to represent offline signal contamination caused by reflections from the nearby exposed bedrock face. The reflections appear to gain depth because the air wave travel time increases as the recording device moves away from the face. The lower radar facies is overlain by the 9-m thick middle radar facies which displays continuous to semi-continuous reflections that dip in a downstream direction between positions 42-65 m. Further to the west (65-100 m) the reflections are undulating and comprise m-scale anticlines. The middle radar facies is truncated by the ~4 m thick upper radar facies which consists of sub-horizontal to horizontal reflections.

To test if the anticlinal reflection pattern of the middle radar facies represents true bedding features or alternatively diffractions as caused by scattering objects in the subsurface (e.g. large boulders) the data were migrated using fk-migration pulse EKKO-42 software. Migration collapses diffraction tails while flatlying surfaces and reflections of truly dipping contacts or layers do not migrate. Results (Fig. 33C) show that some of the anticlinal reflections collapse, indicating that they were caused by diffractions while other reflectors remain which are then interpreted to represent true subsurface bedding or contact features. Plotting the 50 MHz data at a 0.1 m/ns wave velocity (Fig, 33D) causes overcorrection of the diffraction pattern (‘smiles’) suggesting that the correct wave velocity is slower in the western portion of the profile (~0.06 m/ns) than in the east where no such overcorrections occur. Similarly, the velocity decreases vertically in the west as seen at position ~80m (Fig. 33D) where the upper radar facies remains flatlying, while the middle radar facies is overcorrected at 0.1 m/ns. The vertical and horizontal variations in wave velocity are

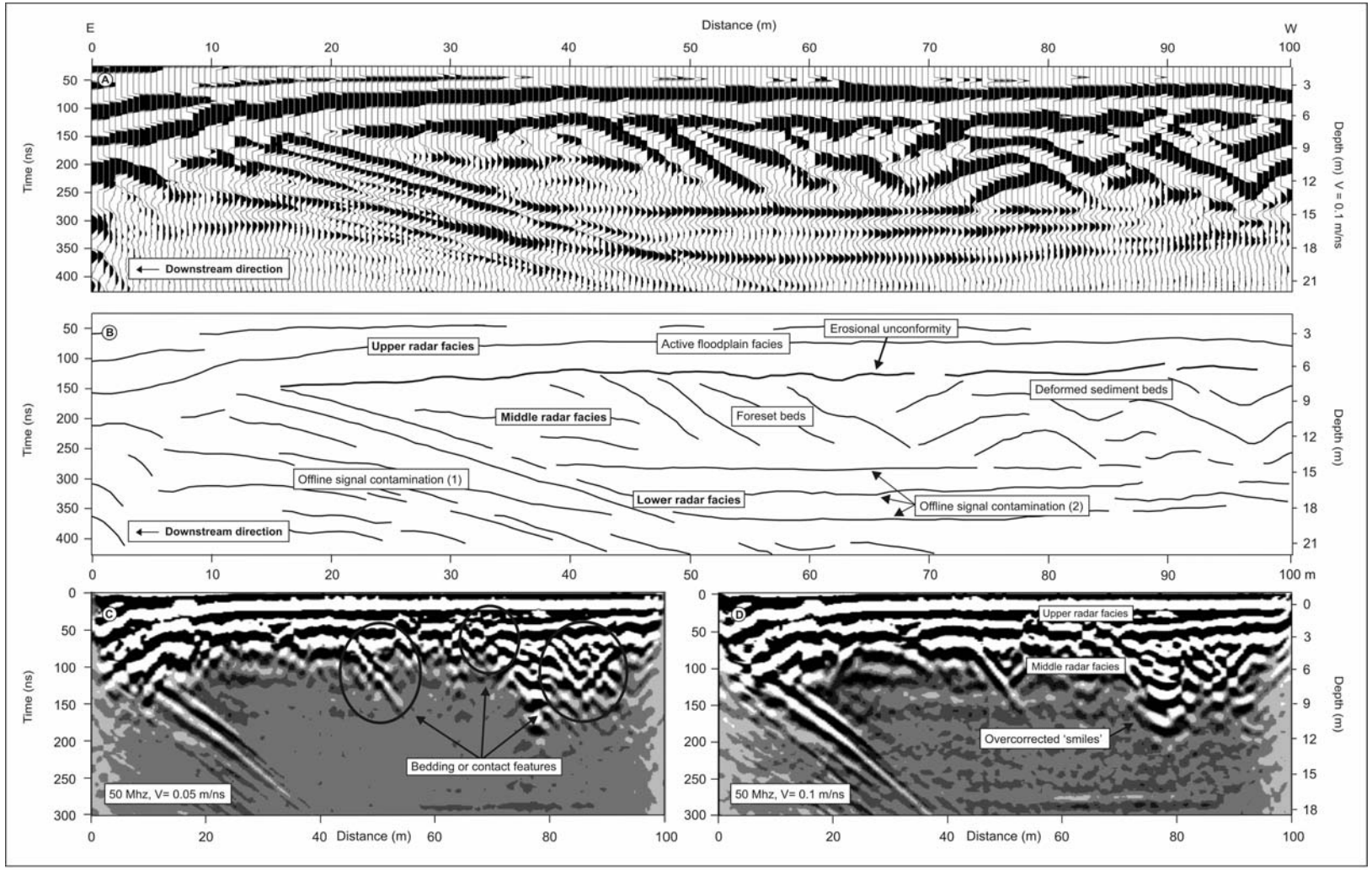

Fig. 33: 25-MHz (A) and 50 MHz (C,D) GPR profile from the valley reach upstream of Glynn Wye gorge showing raw radar data (A), interpretations (B) and migrated data (C, D). The profile shows offline signal contamination from a nearby bedrock outcrop and a terrace edge which runs parallel to the survey line (offline contaminations 1 & 2).

interpreted as indicating differences in the sedimentary properties. All of the depicted radar facies represent water saturated deposits situated below the local water table. The most probable explanation for the velocity variations are differences in the water or matrix content of the sediments. Velocity differences as seen in profile C would be expected if the faster velocity represents coarse to medium gravels and the slower velocity matrix rich gravels or silts. A similar material difference is indicated between the upper and middle radar facies in the western end of the profile where the velocity decreases near the contact between the two facies. This interpretation is consistent with the truncation of the middle radar facies by the upper radar facies which is interpreted as an erosional unconformity. Based on this the upper radar facies represents the active channel facies which eroded into rheologically different sediments of the middle radar facies.

In summary, profile C confirms results from profile A and B which indicate that bedrock is at least 15-17 m below the floodplain. GPR profiles A and B display sedimentary structures (delta foreset in profile A; deformational pattern in profile B), which suggest that the sub-valley fill is not associated with recent fluvial activity of the present Hope River. This is consistent with profile C where sediments at greater depth have different dielectric properties indicating the presence of lithologically different sediments at greater depths, possibly lacustrine silts. Erosional unconformities were found in all radar transects between the active channel deposit and underlying sediments suggesting that the present Hope River is incising into sedimentary basin fill. The buried delta foreset and bottomset found in GPR profile A adjacent to the Glynn Wye outcrop are interpreted to represent the sub-floodplain continuation of the exposed foreset units. Both the exposed and buried sediment facies provide therefore evidence for a large paleolake that existed in the Hope Basin. The GPR results from the lower Hope Valley show that in none of the profiles bedrock contact was found and that the sedimentary fill of the Hope Basin extends to at least 17 m below the present floodplain.

4.5.3. IRSL results

Two infrared stimulated luminescence ages (IRSL) were obtained from the Glynn Wye sequence. Sediment samples were taken from a ~3 m thick unit of laminated

lacustrine silts (Sample 1) and from well sorted ~0.60 m thick fluvial overbank deposits (Sample 2). The stratigraphically lower sample comes from a bed of lacustrine mud exposed within the deltaic gravels (G1) while the second sample was retrieved from fines found within the overlying fluvial gravels (G2). The dated overbank silt layer was traced across the outcrop and sampled in an accessible gully 150 m east of the main exposure. Both units are interpreted to have had a good probability of signal zeroing before deposition. Locations, stratigraphic positions and lithology of the sampled units are shown in Fig. 27. The sediment recovered from the sample steel tube (~1 kg) was used to measure the luminescence signal as well as the amount of dose rate relevant elements (K, Th, U). All dosimetric data are summarized in Table 2. For luminescence dating a multiple-aliquot additive-dose method was used to determine the equivalent dose rates (D_e), from which the paleodose was calculated. The D_e values and resulting luminescence ages are shown in Table 3.

Table 2: Sample and radioactivity data for luminescence samples from the Kakapo Delta exposure.

Sample[a]	Grain size (µm)	Water content (δ)[b]	U (µg/g) from ^{234}Th	U (µg/g)[c] ^{226}Ra, ^{214}Pb, ^{214}Bi	U (µg/g) from ^{210}Pb	Th (µg/g)[c] from ^{208}Tl, ^{212}Pb, ^{228}Ac	K (%)	dD_e/dt (Gy/ka)[d]
1	4-11µm	1.280	4.09 ± 0.51	3.42 ± 0.06	3.70 ± 0.50	17.02 ± 0.14	2.78 ± 0.06	0.0018 ± 0.0001
2	4-11µm	1.229	2.93 ± 0.40	2.75 ± 0.04	2.66 ± 0.40	10.22 ± 0.16	1.90 ± 0.04	0.0226 ± 0.0011

[a] Lab codes: 1) WLL-356; 2) WLL-351
[b] Ratio wet to dry sample weight. Errors assumed 50% of (δ-1).
[c] U and Th contents are calculated from the error weighted mean of the isotope equivalent contends.
[d] Contribution of cosmic radiation to the total doserate, calculated following Prescott & Hutton (1995).

Table 3: Measured a-values and equivalent doses as well as calculated dose rates and resulting luminescence ages from the Kakapo Delta exposure.

Sample	a-value	D_e(GY)	dD/dt (Gy/ka)	**IRSL age (ka)**
1	0.036 ± 0.007	265.4 ± 8.6	4.40 ± 0.39	**60.3 ± 5.6**
2	0.049 ± 0.004	105.8 ± 4.1	3.29 ± 0.24	**32.1 ± 2.6**

The lacustrine muds from the delta sequence yielded an age of 60.3 ± 5.6 ka suggesting a late OIS 4 age for the Hope paleolake. Since this IRSL sample was obtained from above the basal contact of the lacustrine unit (not exposed) the lake initiation must necessarily pre-date the IRSL age. The second sample from silts within the G2 gravels and 80 m above sample 1 gave an age of 32.1 ± 2.6 ka.

Because the date comes from the approximate middle of the 60 m thick gravel unit, it is suggested that major fluvial aggradation in the lower Hope Valley began during mid/late-OIS 3. Both IRSL ages are stratigraphically consistent and are corroborated by the inferred LGM age of the Glynn Wye moraine on top of the sequence (Clayton, 1968). In summary, the results show that deposition at Glynn Wye began probably during late OIS 4 with the formation of a paleolake. Following the termination of the lake during mid/late-OIS 3 and the onset of large scale fluvial aggradation, valley infilling continued until the LGM ice advances.

4.6. Discussion

Transtensional motion along the Hope Valley segment of the Hope Fault produced various structural depressions of different dimensions (Hanmer Basin, Lake Glynn Wye, Poplars Graben, Hope Basin; for locations see Fig. 19. This chapter has described the stratigraphy of one such depression, the Hope Basin, where relative subsidence trapped a thick aggradational sequence of Late Pleistocene deposits. Postglacial degradation by the Hope River resulted in 160 m of fluvial incision which partially exposed fill deposits preserved in the Hope Basin. Mapping of bedrock levels upstream and downstream of the lower Hope Valley indicate that ~70 m of the total amount of incision occurred into the basin fill which is exposed in the lower section of the Glynn Wye outcrop. Although the total basin depth is not yet known, the GPR data indicate that at least 17 m of additional fill is preserved below the Hope River floodplain, suggesting a minimum total basin depth of ~87 m.

An estimate of the Late Quaternary subsidence rate for the Hope Basin can be obtained from Poplars Graben. The graben, which has a maximum downthrow of ~40 m (Cowan 1990), is located on the southern side of the Hope Basin and has disrupted parts of the main aggradational terrace. Cosmogenic dating (see results Chapter 7) of the Glynn Wye moraine, which overlies the terrace, indicates a mean age of 18.5 ± 1.9 ka for the moraine, and it is reasonable to assume a similar age for the top of the terrace. Based on this terrace age a Late Quaternary graben subsidence rate of 2.1 ± 0.3 mm/a is calculated. An extrapolation of this subsidence rate from Poplars Graben to the entire Hope Basin must take into account that the graben represents a smaller secondary structure within the Hope Basin, but the 2.1 mm/a rate

is probably a reasonable minimum estimate for the Late Pleistocene subsidence of the Hope Basin.

In the context of the continuing regional uplift the formation of the Hope Basin must be regarded as a result of relative rather than absolute subsidence. The rise of the adjacent hill ranges occurs at approximately 2 mm/a (Wellman 1979), while basin downfaulting follows at a similar rate (~2.1 mm/a). With both the average basin subsidence and the regional uplift rate around ~2 mm/a the absolute basin floor elevation in the lower Hope Valley has remained roughly static during the latest Pleistocene. Under these tectonic conditions, the sedimentary history of the basin was largely dominated by superimposed effects of climatically induced periods of aggradation and degradation.

The basal contact of the delta deposit at Glynn Wye outcrop is not exposed at river level indicating a possible continuation of the foreset beds into the subsurface. This was investigated using GPR. Profile A (Fig. 30), which was recorded only ~15 m away from the outcrop, confirms the presence of foreset beds below the Hope River floodplain. Dip angle and orientation of the foresets as indicated by GPR are consistent with the exposed foresets and it is suggested that both the buried and the exposed foreset facies belong to the same delta deposit. The total thickness of exposed (45 m) and buried (11 m) foreset beds amounts to 56 m, indicating the combined minimum depth of the Hope paleolake during delta deposition. The lake terminated sometime during OIS 3 and its delta was subsequently buried under 65 m of glaciofluvial outwash gravels. A later glacial advance during the LGM overran the valley fill and deposited terminal moraines over the top of the sequence.

Luminescence dating on lacustrine silts exposed at Glynn Wye station show that a large paleolake occupied the lower Hope Valley at the end of OIS 4 (60.3 ± 5.6 ka BP). With the GPR data indicating the continuation of exposed delta foresets into the subsurface, it is implied that at the time of lake formation the local valley floor was below its present level. The low elevation of the valley floor at the end of OIS 4 (~180 m below the level of the LGM aggradational terrace) may reflect glacial overdeepening at the confluence of the Hope and Boyle glaciers. Under this model

the Hope paleo-lake formed in the overdeepened valley trough following glacial retreat at the termination of OIS 4.

Although the residence time for the lake is not known, a luminescence age from the overlying fluvial deposit shows that the lake disappeared prior to 32.1 ± 2.6 ka BP. The absence of erosional scouring and the preservation of the delta topset beds indicate that no or only minor erosion occurred between the termination of the lake and the deposition of the overlying fluvial gravels. It is therefore probable that the lake infilled. Rivers in the catchment originate in tectonically very active mountain environments with high erosion rates. Present suspended sediment yields from New Zealand rivers are known to rank among the highest in the world (Griffiths 1981, Hicks 1998). It has been shown that sediment supply in New Zealand during OIS 4 and OIS 3 was larger than at present (Brown et al., 1988; Suggate, 1990; Browne and Naish, 2003) and infilling of the Hope paleolake may have occurred over a relatively short period of time (~1–10 ka). Intense OIS 4 to OIS 2 aggradation not only entirely filled the Hope Basin (to a level of ~ 520 m a.s.l.), but exceeded this level by ~90 m, with the LGM aggradational terrace located at ~ 610 m a.s.l.. The aggradation and associated build up of sediment in the lower Hope Valley caused the deflection of the paleo-Kakapo River from Dismal Valley into its present course as its original drainage outlet into the Hope Basin became blocked by the Hope River aggradation fan. Overall results from luminescence dating show that the most recent phase of large scale valley aggradation in the Hope Valley began during mid/late-OIS 3.

Following LGM ice retreat and the establishment of interglacial conditions which resulted in decreased sediment supply and increased flow values, the Hope River began its recent history of postglacial fluvial degradation. Incision rates quickly outpaced rates of basin subsidence leading to rapid downcutting into the basin. Erosional unconformities between thin active channel deposits and underlying basin fill (GPR results) and the presence of low degradational terraces (5-10 meters above river level) indicate that the present Hope River continues to incise in the lower Hope Valley. The modern incision rate is controlled by bedrock gorges upstream and downstream of the Hope Basin (Windy Point Gorge and Glynn Wye Gorge).

An interesting aspect of the stratigraphic sequence at Glynn Wye station is its survival in a central Hope Valley position despite overriding by late last glacial ice advances, which deposited moraines over the top of the sequence. The luminescence results suggests a substantial pre-LGM age for the sedimentary succession below the moraines, implying that the LGM glacial advance overrode the site but was comparably ineffective in eroding underlying soft sediments. Whether this represents a local anomaly or constitutes a general feature of the LGM advance that reached the lower Hope Valley is the subject of further investigation in chapters 5 and 7.

4.7. Summary and conclusions

A thick sequence (~177 m) of aggradational deposits was studied in the lower Hope Valley. Valley fill is preserved in a tectonic depression, the Hope Basin, which is associated with a releasing bend on the active strike slip Hope Fault. Local basin subsidence since the last glacial maximum (LGM) is estimated to have occurred at a rate of 2.1 ± 0.3 mm/a, which matches the known regional tectonic uplift rate. The approximate balance between uplift and basin subsidence has resulted in climate driven sedimentation patterns which dominated during the Late Pleistocene. The deposition of the sediments described here started near the termination of OIS 4 and continued throughout the following interstadial and stadial (OIS 3 and OIS 2). Aggradation began with the infilling of a large paleolake that occupied the Hope Basin. Luminescence dating (IRSL) on lake beds indicates an OIS 4 age for the formation of this lake. The lake terminated during OIS 3 as a result of complete infilling. The subsequent phase of fluvial aggradation buried paleolake deposits under 65 m of glaciofluvial outwash before the progression of a late OIS 3 or early OIS 2 advance over the valley fill. A luminescence age (IRSL) of 32.1 ± 2.6 ka BP from outwash deposits below the LGM terminal moraine indicates that the aggradation phase leading to the LGM advance began during late OIS 3. Postglacial fluvial degradation caused 160 m of incision into the lower Hope Valley thereby partially excavating the pre-LGM basin fill.

CHAPTER 5

SEDIMENTOLOGY OF AND DEPOSITIONAL MODEL FOR GLACIAL SEDIMENTS AT POPLARS GULLY IN THE LOWER HOPE VALLEY

5.1. Introduction

This chapter investigates valley fill deposits on the northern side of the lower Hope Valley at Poplars Gully (M32 E 24630 / N 58461) located directly opposite of the Glynn Wye exposure that was described in the previous chapter. Both outcrops expose sediments of the same paired aggradational terrace ('Glynn Wye terrace') which has been inferred to represent the maximum level of valley aggradation during the LGM (Clayton, 1968; Knuepfer, 1988; Cowan, 1990). Because of this, the stratigraphy and sedimentology of the Poplars Gully sequence was expected to resemble deposits exposed on the southern valley side. However, major differences were found and this chapter describes the lithostratigraphy of the 110 m thick Poplars Gully sequence. The study identifies depositional processes and characterizes the associated glacio-depositional environments. Stratigraphic data and limiting age control from luminescence dating of fine grained glacio-fluvial and glacio-lacustrine deposits are used to reconstruct the glacial site history. The outcrop has been exposed by a recent landslide (10.1994) and is described for the first time in this chapter. The overall findings have implications for both the regional glacial and tectonic history.

5.2. The Poplars Gully study site

The studied outcrop is located at Poplars Station and exposes a section of the main valley fill terrace on the northern side of the Hope Basin. Following the initial landslide a series of smaller slips due to heavy rainfall and structural instabilities further enlarged the original escarpment during the subsequent months. The resulting gully complex is approximately 130 m wide, 120 m deep and about 200 m long (Fig. 34B). The landslide generated a ~500 m wide and several meter high debris flow fan which flowed across SH 7 and blocked the road. To mitigate these effects two earthen ramps with an intermediate bridge segment were constructed but because of continuing slumping and slurrying of material out of the gully, the structure was

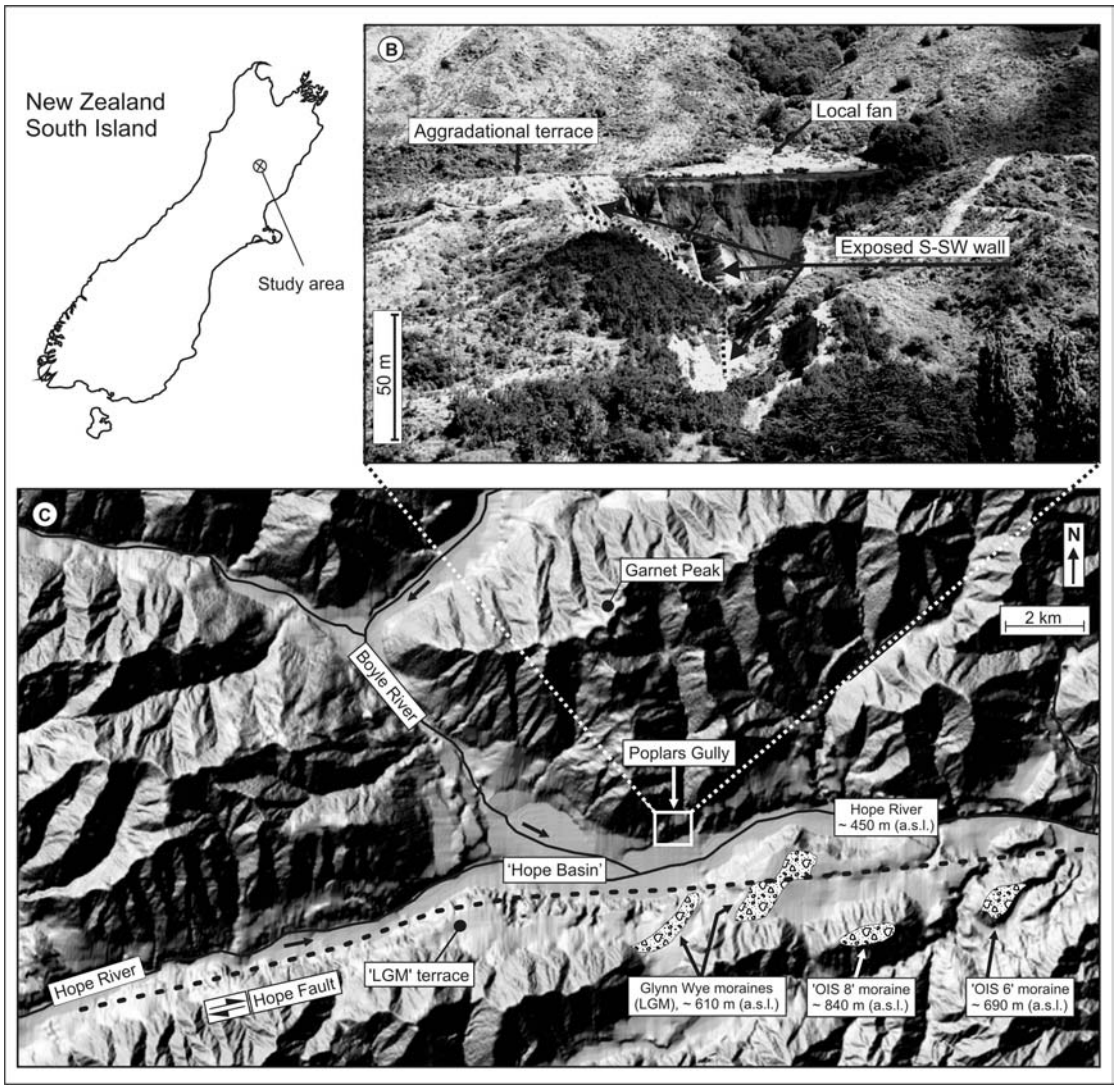

Fig. 34. Location of the Hope Valley and the Marlborough Fault Zone in the South Island, New Zealand. The photo in Figure 34B shows a view from the south into Poplars Gully in 2005. The shaded DEM in Figure 1C shows the Hope Basin, the course of the Hope Fault and the general location of the studied outcrop ('Poplars Gully' site). Note the positions and elevations of the principal glacial moraines in Fig. 34C (modified from Clayton, 1968).

eventually abandoned and SH 7 relocated by about 400 m to the south (Fig. 35). Although no formal investigation into the cause of the landslide was undertaken it is likely that the event was indirectly triggered by the Arthur's Pass earthquake of 18.06.1994 (pers. com. T. Davies). Following the earthquake a marked drop in the volume of groundwater flow, which previously seeped through the terrace and re-surfaced at its toe, was observed by local residents. As none of the other streams increased in drainage volume it is likely that this water was retained within the terrace itself, which in combination with the large proportion of fine grained terrace sediments is the probable cause for the landslide. A similar landslide scarp, generated by an earlier event, is preserved to the west of Poplars Gully.

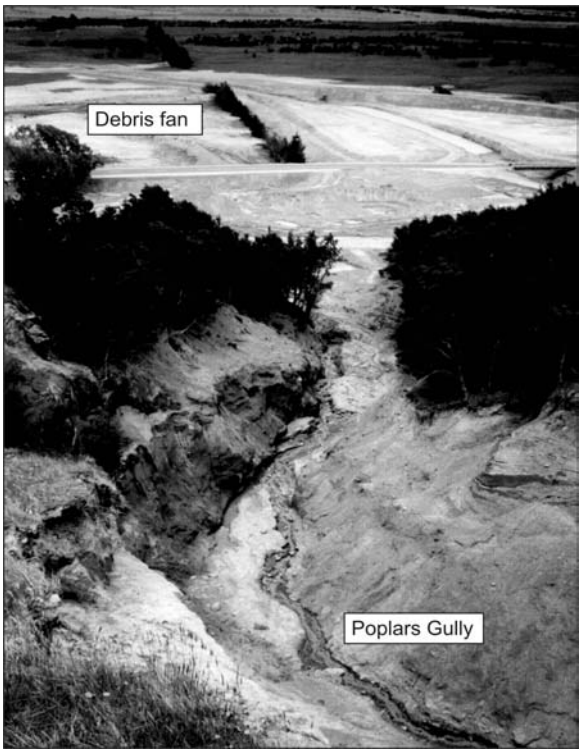

Fig. 35: Oblique aerial view into the lower portion of Poplars Gully in September 1995. At this stage the gully was still structurally unstable and widening. Note reconstructed SH 7 and improvised bridge with debris channel in upper right prior to the eventual highway relocation (photo: T. Davies).

5.3. Quaternary geological setting

The general tectonic and glacial geology of the lower Hope Valley was introduced in Chapter 4 (sections 4.2 and 4.3) and also forms the background for this investigation. The main glacial and tectonic features are summarized in Figs. 34C and 36. Deposits at Poplars Gully comprise mainly of glacial sediments which dominate the fill sequence in this part of the valley. Favourable conditions for local sediment preservation at Poplars Gully were provided by a bedrock spur that extends from Garnet Peak and shielded local deposits from erosion (Fig. 34).

Generally rapid tectonic uplift in New Zealand has provided an effective mechanism by which older glacial sequences were raised above the central valley train thereby reducing the possibility for erosion by later glacial or fluvial processes. Consequently, in many valleys of the Southern Alps remnants of glacial surfaces at higher elevations are interpreted to predate the last glacial cycle (Suggate, 1965, 1990). At the same time, although little published, it is widely considered improbable that older glacial sequences (pre-last glacial cycle) can have survived in the central valley trough

without removal by later glaciations or interglacial fluvial incision. Therefore, the volumetrically dominant portion of remaining valley fills in glacial valleys of the Southern Alps has been inferred to represent sedimentary products of the last glacial cycle. Results of Chapter 4, however, suggest that the majority of the terrace stratigraphy at Glynn Wye Station substantially predates OIS 2 and survived ice overrun during the LGM. Based on this, glacial aggradation in the Hope Valley commenced at least ~60 ka ago and continued throughout OIS 3 until the LGM glacial advances. This chapter addresses these questions through an investigation of the valley fill sequence in the northern Hope Valley.

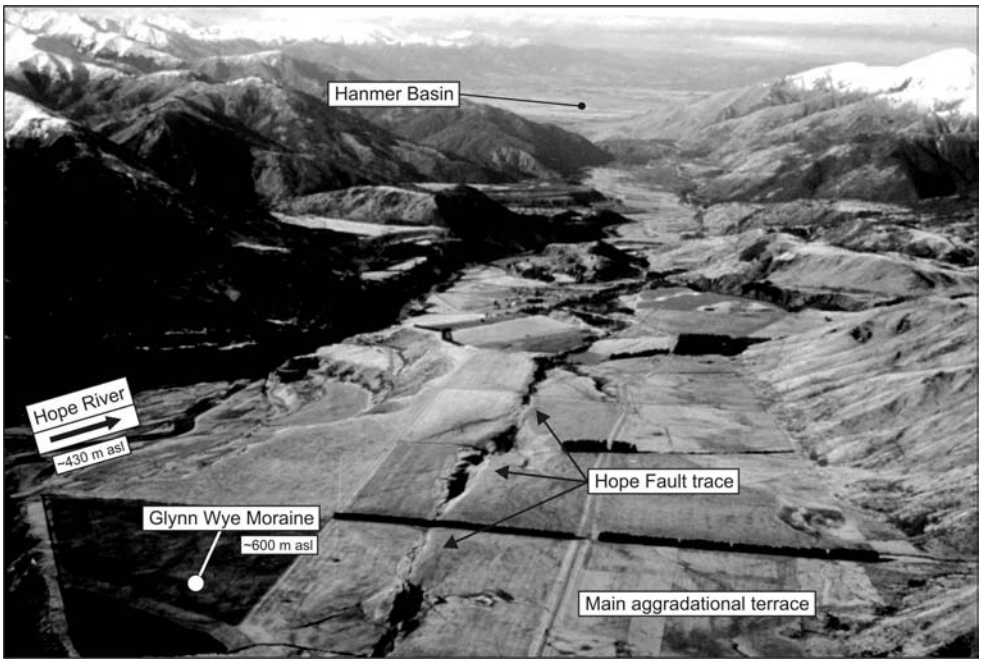

Fig. 36: View down valley from the lower Hope Valley showing locations and landforms mentioned in the text (photo: J. Pettinga).

5.4. Methods

5.4.1. Sedimentary logging

This study used standard sedimentary logging techniques and applied a modified facies code from Eyles et al. (1983). The individual sediments were grouped in lithofacies assemblages on the basis of sediment composition, texture, grain size, sorting, and structures (Table 4). Representative clast orientation data were collected from all units defined as diamictons. The a-axis orientation and the dip were measured

together with the clast roundness for elongate and prolate stones with long axes between 20 – 250 mm (Evans and Benn, 2004). The data were recorded for at least 30 clasts at each site, and normally collected over an area of less than 1 square meter. Paleo-flow directions from aqueous units were obtained from small-scale ripple cross laminations and clast imbrication. Grain sizes from selected fine grained deposits were determined using a laser particle analyzer (Saturn DigiSizer 5200). Sedimentological data are presented for four stratigraphic columns which are shown in Figure 37.

Table 4: Facies codes used for sedimentary logging at Poplars Gully (modified from Eyles et al., 1983).

Facies codes:

Fines (<0.063mm)
- Fl - Laminated mud, silt and fine sand
- Fe - Laminated silts and clays with dropstones
- Fd - Deformed laminated silt
- Fm - Massive silt and clay

Sands (0.063 – 2mm)
- Sh - Plane bedded medium sand
- Sm - Massive sand
- Sd - Deformed sand
- Sx - Cross-laminated sand
- Sr - Ripple cross-laminated sand

Diamictons
- Dmm - Matrix supported, masive
- Dms - Matrix supported, stratified

Granules (2-8mm)
- GRo - Openwork granules
- GRmc - Massive granules, with isolated clasts
- Grch - Channelled massive granules
- GRmp - Massive with pebble stringers

Gravels (8-256mm)
- Gms - Muddy matrix supported gravel, subrounded to subangular, poor sorting and crude bedding
- Gm - Massive clast supported, crudely bedded gravel, poor to moderate sorting
- Gni - Normal-inversely graded gravels
- Gh - Horizontally bedded gravel
- Gs - Matrix supported gravel
- GRh - Stratified granules

5.4.2. IRSL methods

Four luminescence samples were obtained by forcing a 220 mm long steel tube (75 mm diameter) into sediments ranging in grain size from silt to medium sand. The cylinder was then sealed and carefully excavated to prevent light exposure and sediment mixing. All samples were submitted to Victoria University Dating Laboratory (Wellington, New Zealand) where they were analyzed using the 4-11 μm grain size fraction. Sample preparation and measurement followed the procedure by Rieser (2004) which was described in detail in Chapter 4 (section 4.4). Each sample was measured for 100sec each to obtain the shinedown curves. Counting was done using a high resolution gamma spectrometer with a broad energy GE detector for a minimum time of 24h. The doserate calculation is based on the activity concentration of the nuclides ^{40}K, ^{208}Tl, ^{212}Pb, ^{228}Ac, ^{214}Bi, ^{214}Pb, ^{226}Ra.

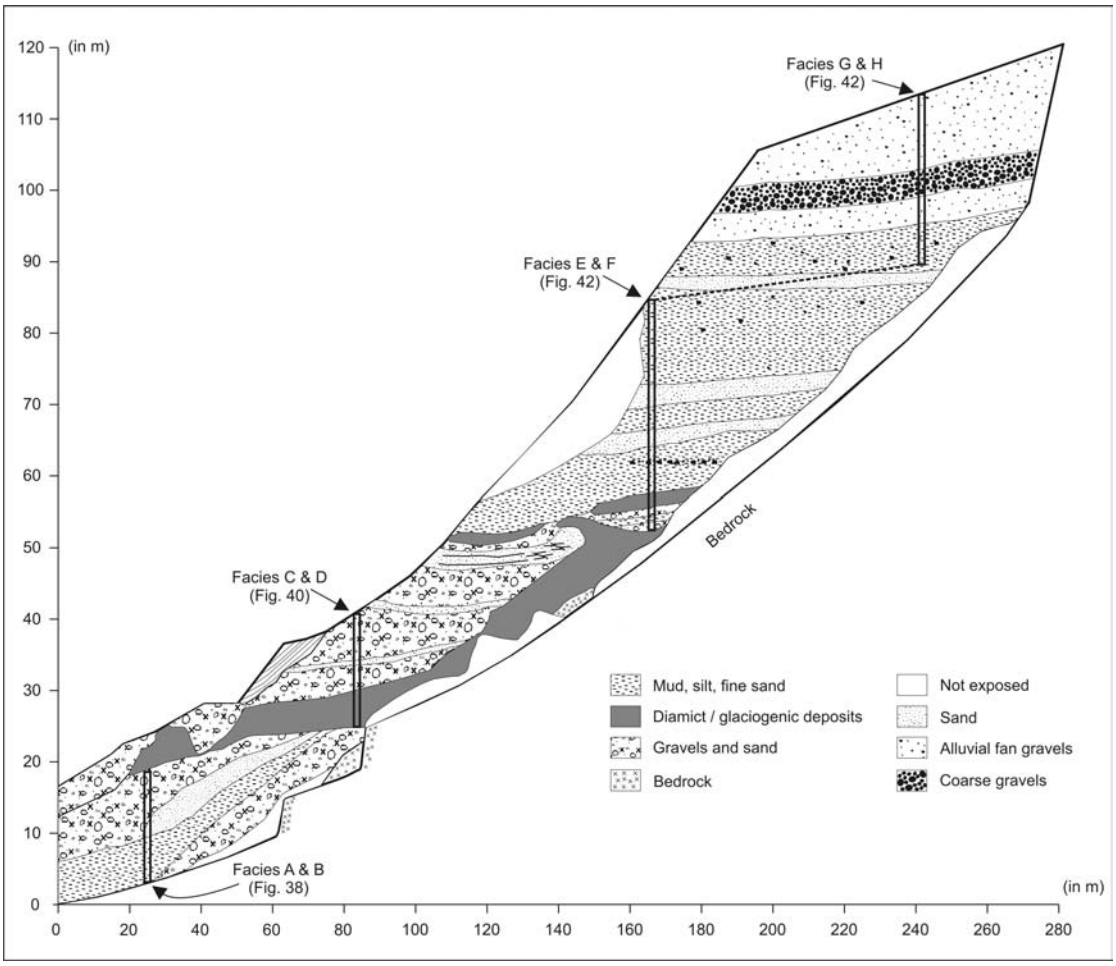

Fig. 37: Stratigraphic overview of deposits at Poplars Gully.

5.5. Results

5.5.1. Lithofacies descriptions and interpretations

The outcrop at Poplars Gully exposes a 110 m thick depositional sequence. Eight lithofacies assemblages were identified on the basis of sediment properties, structures and stratigraphic context. The following section presents sedimentological descriptions and interpretations:

Facies A: stratified & massive sand, stratified gravel, rhythmically laminated clay, silt and fine sand: Sh, Sm, Gh, Fl, Fd, Fe

Facies A comprises just under 6 m of laminated to banded silts and sands (Fig. 38). The whole unit dips ~18º (SSW) towards the centre of the Hope Valley. The lowest

beds are planar bedded medium sands to granules with interbedded laminated silts overlain by 0.4 m of stratified gravel. The main body of the unit overlies this. It is composed of a 2.1 m thick deposit of mm-scale laminae alternating between fine and coarse silt (Fig. 38b and 39a). There is a thin (0.15 m) cobbly diamicton above this (Fig. 38c) followed by 2.2 m of normally graded, 10-30 mm thick banded sands to silts which cap the unit. Convolute bedding (Fig. 38a) and small scale normal faulting (Fig. 38b) are widespread throughout, especially in the finer beds. Larger m-scale normal faults are also present, all of which are confined within the unit. Structures associated with contorted beds range from cm-scale flame structures at silt-sand contacts to 300 mm thick bands where originally planar laminations are intensely folded. Small compressional folds occur within fines at the base of the thin diamicton in the central part of the unit (Fig. 38c). The bedding of the lower sand units is contorted with local mobilization of silt which was injected into higher units (Fig. 38d).

Interpretation: The laminated fines of Facies A are a slack water deposit reflecting rapid sedimentation into a small lake. The high sediment flux is indicated by the incomplete dewatering of the beds which produced hydroplastic deformations and small scale flame structures (e.g. Fig. 38a). Such deformations are common in glaciolacustrine deposits where materials of varying densities accumulate rapidly (e.g. Shaw, 1975; Donelly and Harris, 1989; Teller, 2003). Several dropstones and a thin diamicton with associated impact folding in the underlying fines (Fig. 38c) represent dump structures of ice rafted debris (e.g. Thomas and Connell, 1985). Metre scale normal faults show an incremental decrease of displacement in the direction of sediment younging and represent syndepositional deformation related to melting of underlying dead ice during deposition. The overall ~18º dip (SSW) of the sediment package affects all units of facies A and is interpreted as postdepositional deformation caused by the removal of large scale structural support, probably due to the collapse of dead ice in the trunk glacial valley. The overall facies was deposited subaqueously in an ice marginal valley edge position and is interpreted as a kame deposit. Earlier ice overriding of the site is indicated by loading of deposits at the base of Facies A which caused the injection of silts into overlying sands.

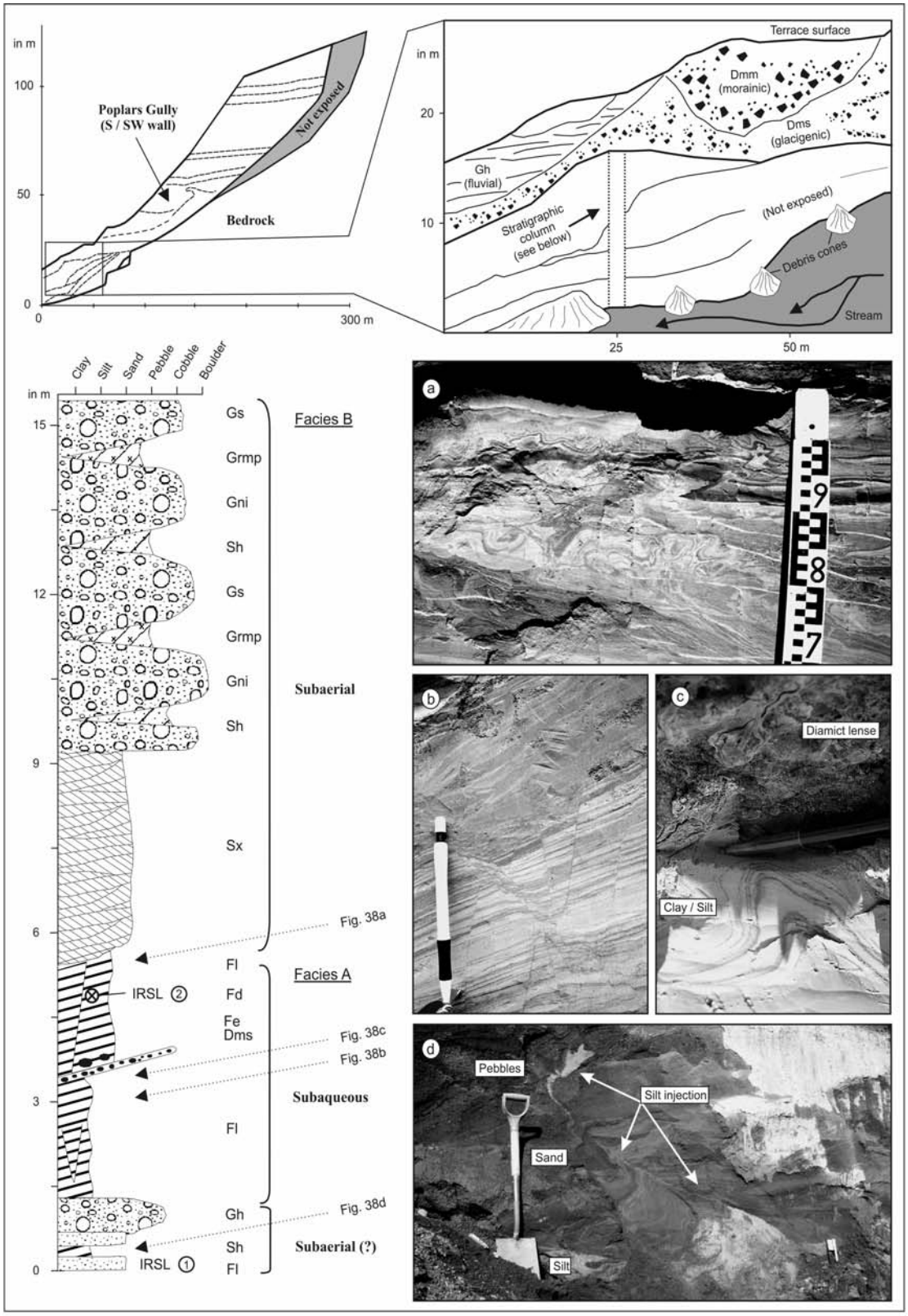

Fig. 38: Stratigraphy, depositional context and sedimentological summary log for deposits exposed at the base of Poplars Gully (Facies A, Facies B). Facies A comprises dominantly of laminated silts and sands with normal faulting that is interpreted as meltout deformation while underlying sand units show deformation through ice loading. Facies B consists of sand and gravel representing ice proximal glaciofluvial outwash. Note that Facies A & B dip as a block by 18 degrees towards the central valley (SSW).

Facies B: stratified sand, normally & inversely graded gravel, massive gravels: Sx, Gm, Gms, Gni

Facies B is a ~10 m thick sand and gravel unit that dips concordantly with facies A (18º / SSW). The deposits were not fully accessible for logging at the face. The basal 3.7 m comprise trough cross-bedded medium sands which truncate underlying deposits of Facies A (Fig. 38). This in turn is truncated by matrix supported stratified to variably graded cobble sized gravels which contain sandy interbeds and patches of openwork gravels.

Interpretation: Gravels and sands of Facies B occupy a ~15 m wide channel and represent a fluvial input. Although the gravels were not directly accessible for imbrication measurements, the overall orientation of the exposed channel cross-section indicates that flow was generally eastward (down the modern valley). The mainly matrix supported gravels are gravel sheets which were deposited during flood events. The succession from sand to gravel indicates that deposition followed the infilling of the prior kettlehole pond (Facies A) and suggests that Facies B was deposited subaerially. There is probably very little age difference between these deposits and the underlying Facies A. After deposition and consolidation of both facies they were tilted as a block towards the main valley floor (SSW direction). This is interpreted to have been caused by the removal of support following the general collapse of the trunk valley glacier.

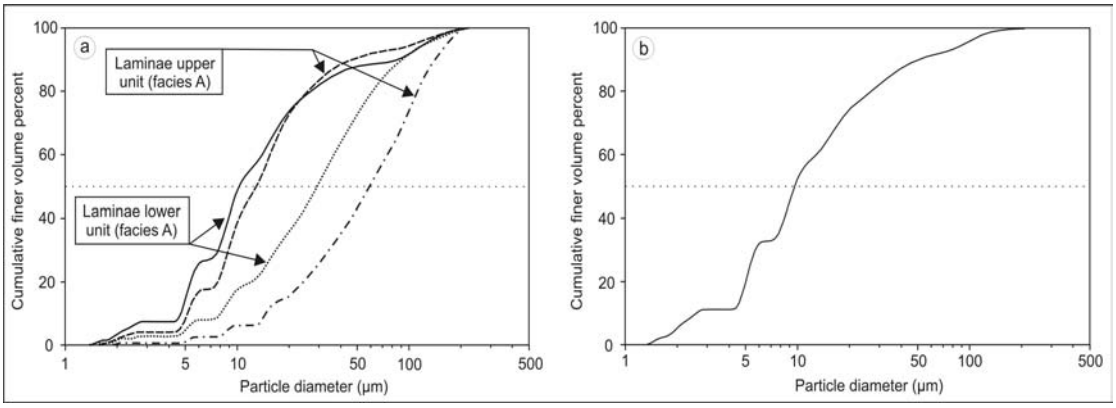

Fig. 39: Particle sizes of laminated to banded silts and fine sands of Facies A (38a). Figure 39b shows the grain size distribution of a 20 mm thick band that drapes clasts a diamicton of Facies C (shown in Figure 40a).

Facies C: stratified and massive diamictons: Dms, Dm

Facies C comprises a 6.5 m thick package of diamictons (Fig. 40). The unit dips at low angles (1-5º dip) and truncates underlying beds of Facies A & B. Towards the valley edge Facies C is deposited directly onto a bedrock bench. The facies is sub-divided into 6 units of stratified and moderately compacted diamictons with variable lateral extent. Most clasts are subrounded to rounded. Fabric data from representative diamicton units show a dominant SW-NE long axis orientation. Based on differences in the composition and stratification five diamict types have been distinguished (I, II, III, IV, V). Type I diamictons consist of clast to matrix supported crudely stratified gravels that overly an erosional unconformity. The deposit is associated with local loading and drag structures in the underlying sediments. The type II diamicton is a single matrix dominated unit that is ~300 mm thick and has limited lateral extension. This unit is massive and includes small cobbles with a strong NE clast fabric orientation. The diamicton overlies a deformed sand and mud unit with shear planes (Fig. 40c). Type III diamictons show generally coarse stratification but include lenses of well sorted sand and granules. The 200-300 mm thick sorted sediment packages are characterized by small scale extensional faulting (Fig. 40d). Type IV diamicts are generally well stratified and consist of 10-30 mm thick bands that range in grain size from mud to granules. Pebble and cobble clasts in these diamictons are draped by bands of silt and sand (Fig. 40a, 39b). Type V diamicts are also stratified and comprise mainly of steeply dipping beds and include deformed lenses, of medium to coarse sand. Characteristic features are pervasive ductile deformation and flow structures (Fig. 40b). Where the beds dip less steeply the original stratification of alternating 2-5 cm thick bands of diamict and coarse sorted sand is preserved (Fig. 40e).

Interpretation: This facies assemblage comprises a series of ice proximal mass flow diamictons and subglacial till which were deposited following a re-advance of the main valley glacier into the lower Hope Valley. Type I and V diamictons are interpreted as mass flow deposits based on their crude stratification and the ductile deformation of incorporated sediment lenses (e.g. Fig. 40b). These diamictons also have a greater variability in their macro-fabrics. Diamicton types III and IV are interpreted as basal melt-out tills as indicated by their stratification, the draping of

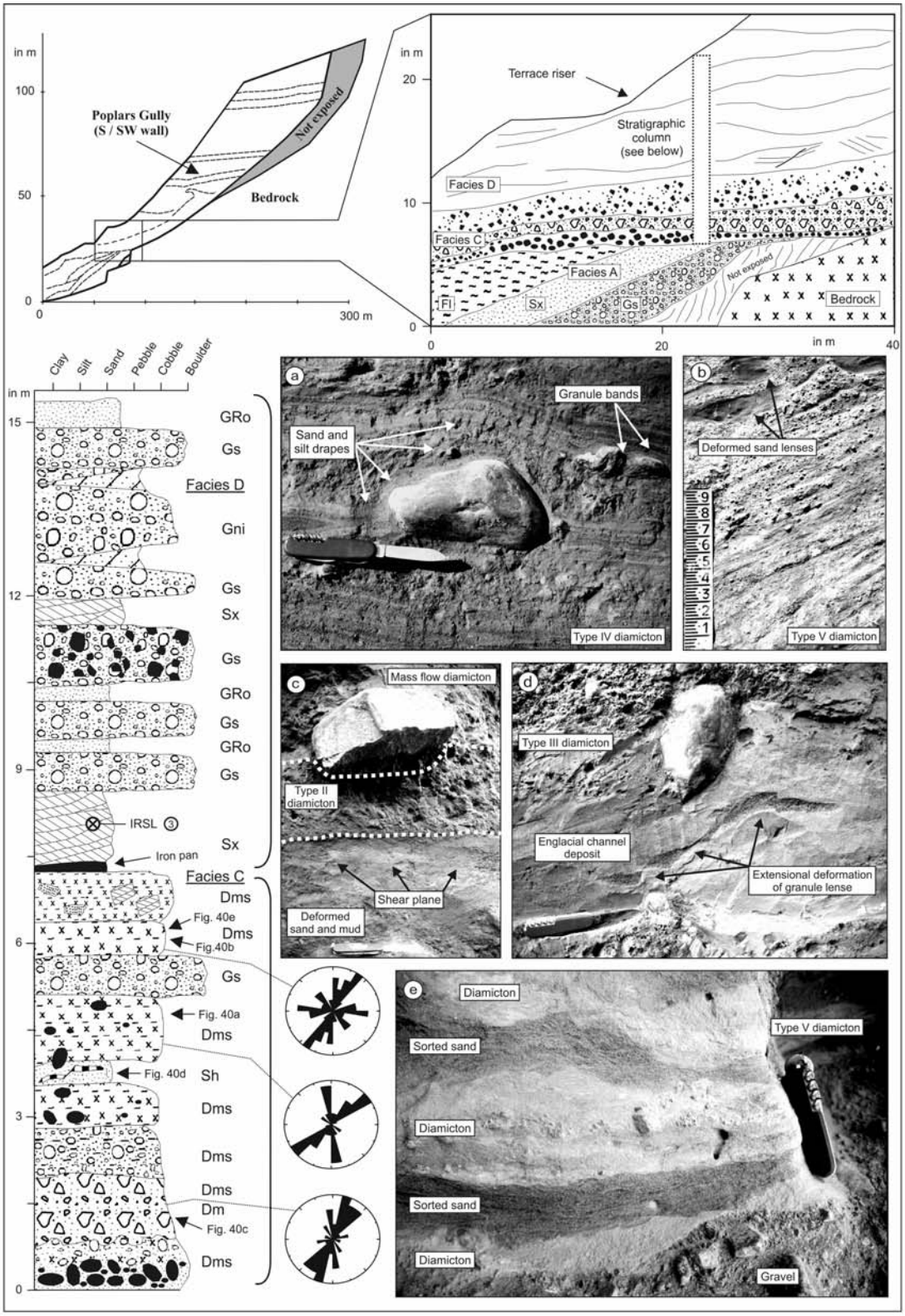

Fig. 40: Stratigraphy, depositional context and sedimentological summary log of Facies C and Facies D. Facies C truncates underlying facies and comprises a series of stratified and massive diamictons interpreted as ice proximal mass flows and till. Facies D consists of clast and matrix supported gravels and cross stratified sands representing glaciofluvial outwash.

sorted sediment bands over lodged clasts (Haldorsen and Shaw, 1982; Dreimanis, 1988) and the presence of interbedded englacial channel fills which were extensionally deformed during basal meltout (Fig. 40d). Little modification of the primary meltout features indicates that deposition occurred by mainly passive meltout from stagnant ice. Only one of the diamictons (type II) is interpreted to represent subglacial deposition from actively moving ice. This ~300 mm thick massive diamicton is found near the base of the facies C and is associated with shear planes in the underlying sediment (Fig. 40c). The diamicton shows a strong fabric signal suggesting ice flow from SW.

In summary, the diamict facies C represents a series of ice proximal mass flow deposits, stratified melt-out tills and massive subglacial till indicating an ice re-advance into the lower Hope Valley. The glacial diamictons cross-cut Facies A & B and show a much lower dip than these underlying deposits suggesting that Facies C was deposited after Facies A & B were block tilted during the preceding ice collapse phase.

Facies D: normally & inversely graded gravel, stratified and deformed sand: Sx, Sh, Sd, Gs, Gms

This is a ~23 m thick assemblage of clast and matrix supported gravels and cross stratified sands with an average thickness of individual beds of less than 0.6 m. The facies is not fully accessible and only the basal 8 m were logged in detail (Fig. 40). Individual units comprise moderately sorted and conformably bedded gravel and sand sheets that are laterally continuous. Facies D overlies the glacial diamictons of Facies C. Intense extensional deformation that resulted in the disruption and block rotation of several units is noted in the basal part of Facies D. Bedding planes of the middle and upper Facies D are less deformed, displaying only a downward bend with a deflection estimated to be less than 1.5 m. A spectacular deformational feature in Facies D is a ~4 m high asymmetrical fold shown in Fig. 41. The deformation incorporated diamictons from Facies C into strata of Facies D. Measurements on the excavated fold limb and on several thrust planes show a W to WSW orientation, respectively (Fig. 41).

Interpretation: Sediments of Facies D are interpreted as outwash representing the stratigraphic transition from tills and mass flows (facies C) to collapsed ice proximal glaciofluvial gravels (basal facies D) to less deformed sand and gravel beds of the middle and upper Facies D. Paleo-current directions from ripple cross-stratified sands indicate a dominant flow direction towards ENE. The limited thickness of individual units (<0.6 m) and the considerable range in grain size suggests frequently fluctuating flow conditions. Deformation of Facies D includes the gentle downwarping of the originally plane bedding, which was presumably caused by buried ice meltout and consequent loss of volume in lower beds. The overall interpretation of Facies D as a glaciofluvial assemblage relies partially on the depositional context provided by the underlying melt dominated (upper) Facies C and lower Facies D. Following this logic Facies D was deposited subaerially in a proglacial / ice lateral position after ice retreat from the Poplars Gully site. The large deformational structure shown in Fig. 41 is a postdepositional feature that involved later compressional folding and thrust faulting of Facies C & D deposits (see interpretation of Facies E).

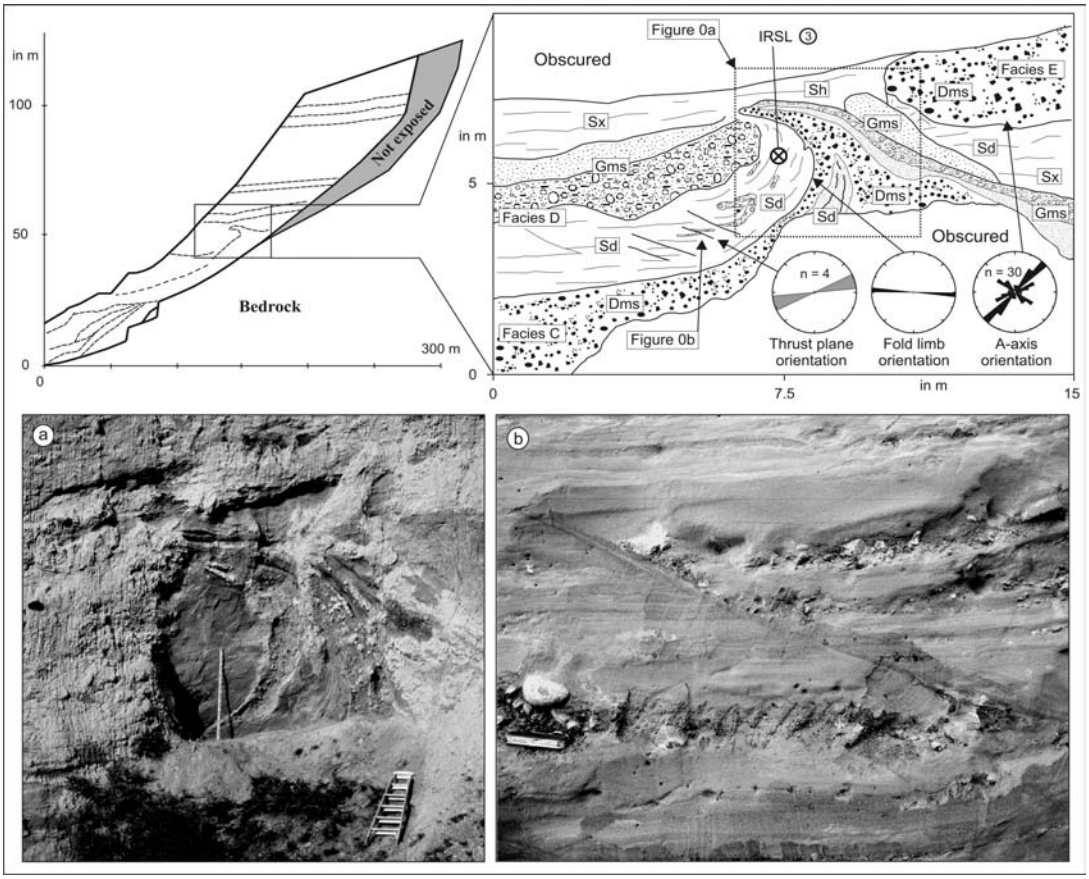

Fig. 41: Deformation in Facies D (Fig. 41a). This asymmetrical fold has deformed sand and gravel of Facies D as well as diamictons of the underlying Facies C. It is interpreted as a glaciotectonic structure associated with a later glacial re-advance (see facies E, Fig. 42).

Facies E: stratified diamictons, clast supported gravel, laminated fines: Dms, Gm, Fl

Facies E is a 6.5 m thick sediment assemblage comprising two 1.5 m thick units of stratified and sandy interbedded diamictons, an intermediary 1.5 m thick unit of laminated silt and fine sand as well as 2.0 m of clast supported gravel (Fig. 42, 42a). The sorted intra-diamict layers are usually 2-5 cm thick bands of undeformed and conformably bedded sand. The diamicton closely resembles diamict type V in Facies C (Fig. 40e). Clasts in the diamictons comprise well rounded to subrounded cobbles showing a dominant NE long axis orientation with a SW dip. The diamicton at the base of Facies E is overlain by a 1.5 m thick unit of silt and fine sand consisting of 2-5 mm thick laminae. Locally, the laminations are intensely deformed through micro-scale faulting and ductile distortions of beds (Fig. 42c). The unit is overlain by a 2.0 m thick deposit of laterally confined cobbly gravels that shows crude bedding and a NE clast (a-axis) imbrication (Fig. 42a).

Interpretation: Stratified diamictons of Facies E are interpreted as ice proximal mass flows that were deposited following a glacial re-advance. Ice overrun or proximity of active ice is also indicated by intense compressional deformation in underlying sediments of Facies D. Towards the valley edge where Facies D pinches out, deformation also extends into Facies C. The advance produced the previously described asymmetrical fold shown in Fig. 41 which is interpreted to have resulted from compressional proglacial glaciotectonics. The fold structure combines dominant ductile folding of matrix supported diamictons and brittle thrust faulting in adjacent sands and gravels (Fig. 41b). Orientational data obtained from the excavated fold limb as well as from thrust planes suggests compression from W and WSW, respectively. This is broadly consistent with the reconstructed SW fabric in the diamictons of Facies E (Fig. 42). Sediments between the two till units comprise deformed units of laminated mud and fine sand as well as glaciofluvial gravels. The micro-scale deformation on laminae of the fine grained unit is interpreted as a postdepositional feature presumably caused by ice overran or during freeze-on and subglacial transport of a pre-existing block of lacustrine muds.

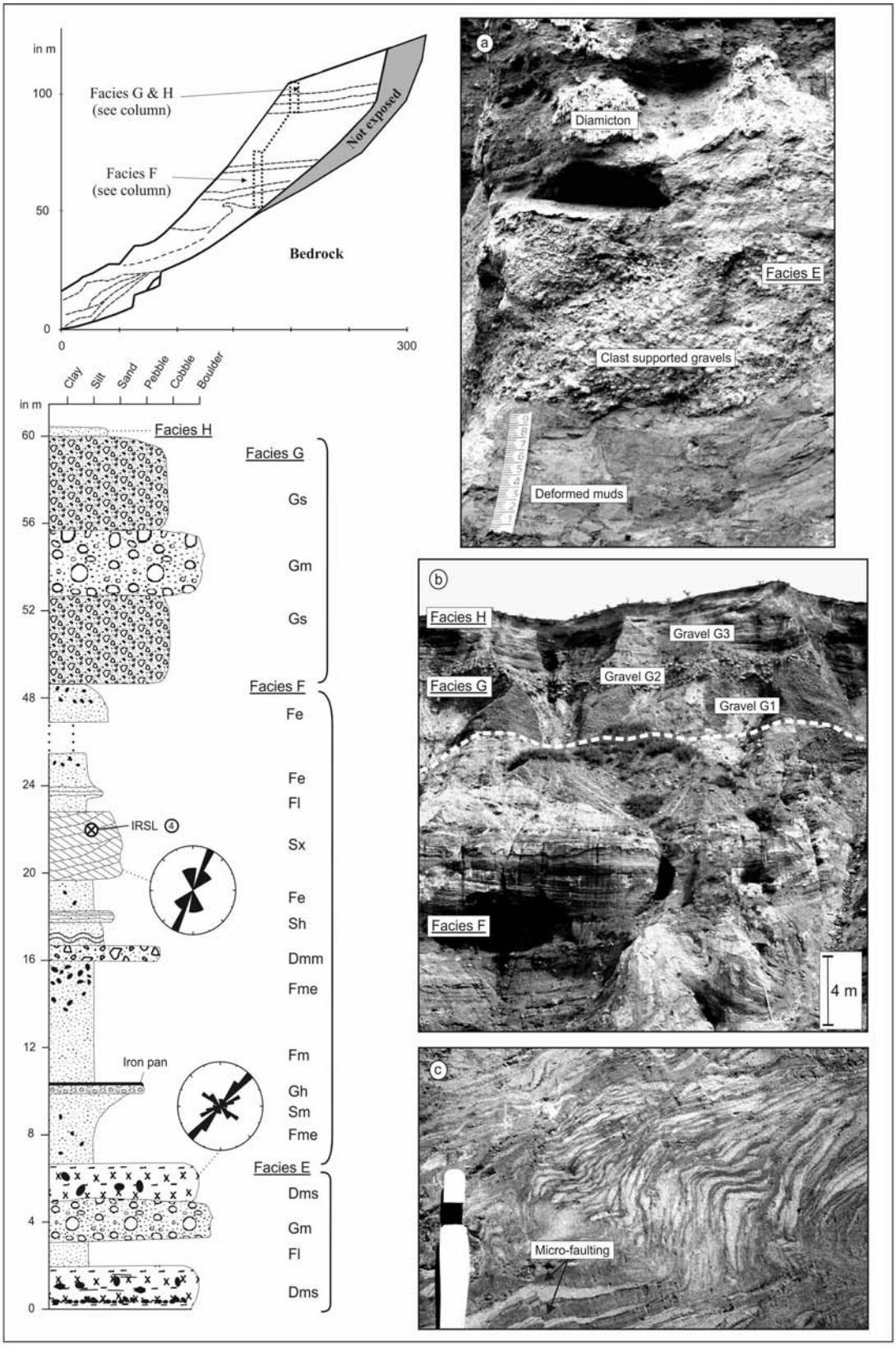

Fig. 42: Stratigraphy, depositional context and sedimentological summary log of deposits in the upper section of Poplars Gully including Facies E, F, G and H. Facies E consists of glacial diamictons interpreted as ice proximal mass flows and indicating a glacial re-advance. Muds and sands of the overlying Facies F represent glaciolacustrine deposition associated with a proglacial lake that formed following glacial retreat. Facies G comprises alluvial and fluvial gravel which are overlain by loess of Facies H.

Facies F: massive & laminated mud, cross-stratified sand, diamicton: Fm, Fl, Fe, Sm, Sx, Dmm

This ~44 m thick fine grained facies consists of alternating units of laminated to massive muds and sands, interbedded with ripple cross-stratified fine to medium sands (Fig. 42). Dispersed stones with impact structures in underlying beds are present throughout the mud units but increase in frequency below a thin diamicton found ~9 m above the base of the facies. The 0.35 m thick matrix supported diamicton is characterized by a high proportion of angular cobble clasts. The mud sequence is capped by a 3 m thick cross-laminated medium sand with sinuous-crested subcritically climbing ripples. Orientational measurements on ripple crests indicate a mean NNE paleo-flow direction. Above this there are 26 m of massive to stratified muds and sandy muds. Dispersed stones with deformed underlying bedding are frequent and about 15% of the clasts are angular in shape.

Interpretation: Sediments of Facies F were laid down in a proglacial lake that formed in the lower Hope Valley following renewed glacial retreat. In the context of the glacial re-advance (Facies E) it is probable that the lake was moraine dammed. Granulometric changes within the facies suggest varying lake levels where units of ripple cross-stratified fluvial sands represent either extreme lake low stands or higher energy environments when the glacier re-advanced towards the site. The dropstones suggest that the lake was in proglacial position and received debris loaded icebergs through glacier calving. The 0.35 m thick diamicton found within the muds is laterally continuous (~8 m) and was probably laid down as a subaqueous gravity flow deposit. The modern margin of the Tasman Glacier (Southern Alps) where calving into a recently formed proglacial lake has become the dominant form of ice loss (Purdie and Fitzharris, 1999) may provide a good analogue for the depositional environment of Facies F.

Facies G: clast & matrix supported gravels: Gs, Gh, Gm

Facies G comprises three gravel beds with a total thickness ~13.5 m. The upper and lower beds (G1 & G3 in Fig. 42b) comprise clast to matrix supported subangular to subrounded cobbly gravels. The matrix consists of silty sand and granules. The

intermediary bed (G 2) consists of 3 m of well rounded clast supported bouldery gravel.

Interpretation: The lower and upper gravel beds of Facies G (G1 & G3) are alluvial sediments which are interbedded with coarse fluvial gravels (G2). Deposition started when a talus fan built out from the adjoining hill onto the northern part of Hope River floodplain (G1). As the fan accumulated, channel evulsion of the Hope River caused relocation of a braid channel to this section of the floodplain where it eroded part of the fan and deposited a veneer of coarse fluvial gravel (G2). As the channel avulsed away fan building recommenced burying the fluvial deposit (G3). The mature sorting and roundness of boulders in the fluvial gravel (G2) suggests medium to long distance transport. This represents a depositional environment markedly different from the previously described glacial sequence. Therefore a substantial time break between the deposition of all underlying facies and Facies G is inferred. The fan and fluvial gravel assemblage of Facies G can be visually correlated to fan/fluvial gravels at similar elevation and identical stratigraphic position on the southern side of the valley. A luminescence age of 32.1 ± 2.6 ka BP (IRSL sample: WLL 351) was obtained from a silt inter-bed in those gravels (section 4.5.3.) and a similar age is inferred for gravels of Facies G.

Facies H: massive silt and fine sand: Fm

This is a massive sandy silt unit of ~0.5 m thickness overlying alluvial fan deposits associated with Facies G. Numerous large angular boulders are scattered on its gently climbing surface.

Interpretation: The deposit is a loess which covers the underlying alluvial fan. The boulders are rockfall debris derived from the adjoining hill side.

5.5.2. Luminescence results

The sediments of the Poplars Gully section are derived from glacigenic deposits and are potentially problematic as a target for luminescence dating. Difficulties are usually

related to insufficient signal zeroing prior to deposition due to high suspended sediment loads in glaciofluvial streams and due to generally short proglacial transport distances (e.g. Mejdahl and Funder, 1994; Duller et al., 1995). In more recent years, refined IRSL and OSL techniques have considerably reduced required exposure times for signal zeroing and Gemmell (1999) showed that (for IRSL dating) sediments in glaciofluvial streams can be effectively bleached by only short exposure to strong sunlight even in streams with suspended sediment yields of >150 mg l^{-1}.

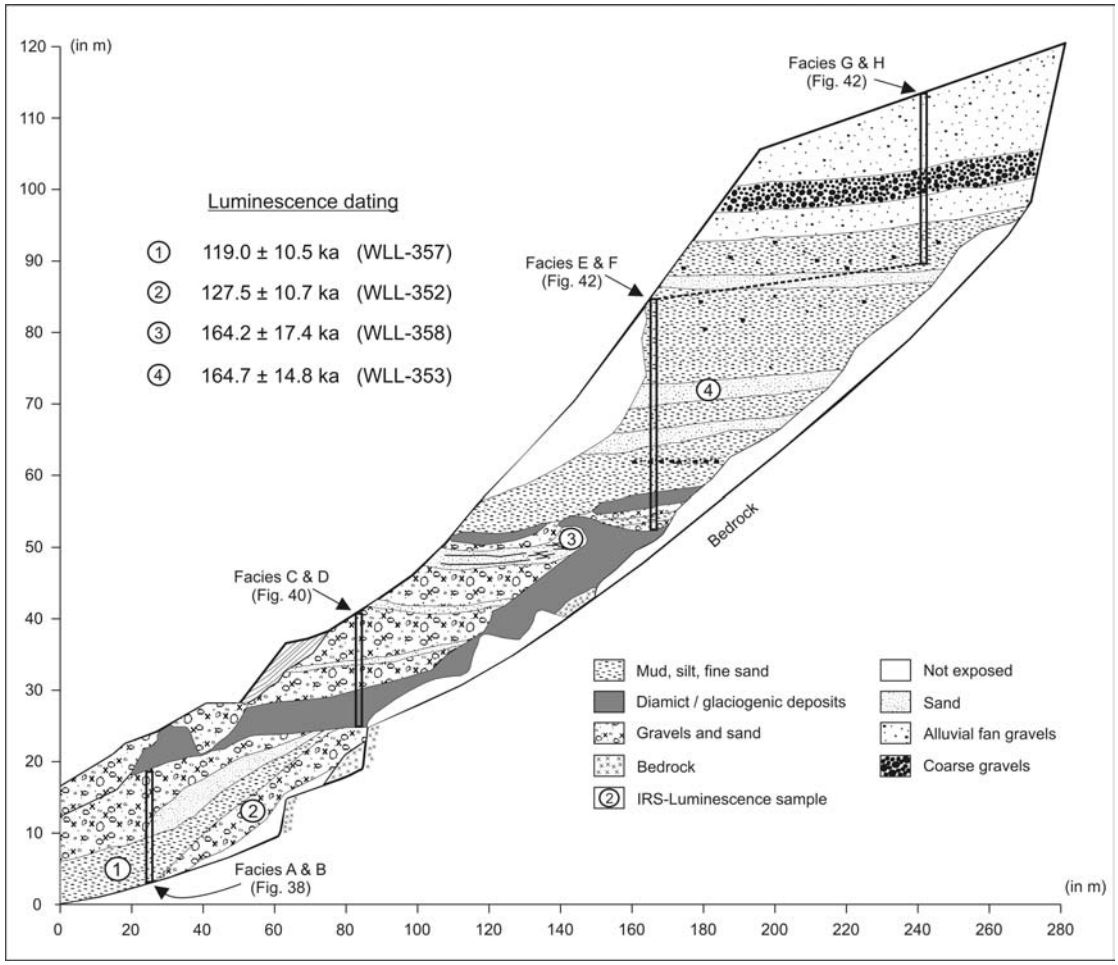

Fig. 43: Stratigraphic positions of luminescence samples from Poplars Gully.

Four samples for IRSL dating were obtained from fine to medium sand beds. The sampled units are at least 1.5 m thick and consist of either well sorted laminated lacustrine sand (No. 1) or homogeneous ripple cross-stratified fluvial sand (No. 2,3,4). Stratigraphic positions and lithology of the sampled units are shown in Fig. 43. The units were selected because all of them are interpreted to have been deposited pro- or paraglacially with a good possibility of zeroing before deposition. The samples were

obtained from different facies assemblages (A, D, and F) and cover a considerable portion of the Poplars Gully stratigraphy (65 m vertical distance between samples 1 and 4).

The sediment recovered from the sample steel tube (~1 kg) was used to measure the luminescence signal and the amount of dose rate relevant elements (K, Th, U). Radioactive disequilibria within the ^{238}U chain pose potential problems for some water-laid deposits (Krbetschek et al., 1994). One of the samples (No. 4) displayed a minor radioactive disequilibrium (significant at 2σ-level) between ^{226}Ra and ^{210}Pb. The effect was probably caused by the influx of Radon which is sometimes absorbed from the atmosphere (e.g. Murray and Aitken, 1982). Two samples (No. 1, 3) were near saturation and a second dating method, the Single Aliquot Regenerative (SAR) technique, was applied to check the reliability of the results (Murray and Wintle, 2000). SAR dates a sub-sample of quartz and therefore represents an independent test for the multiple aliquot additive-dose method which dates feldspar minerals and was used for all other samples. The SAR ages agree within error, which gives more confidence than a near saturation IRSL age alone. All dosimetric data are summarized in Table 5. Extrapolation from the shine down curve to the dose-axis gave the equivalent dose (D_e) which was used to estimate the paleodose. The D_e values and resulting luminescence ages are shown in Table 6.

Table 5: Sample and radioactivity data for luminescence samples from Poplars Gully.

Sample[a]	Grain size (µm)	Water content (δ)[b]	U (µg/g) from ^{234}Th	U (µg/g)[c] ^{226}Ra, ^{214}Pb, ^{214}Bi	U (µg/g) from ^{210}Pb	Th (µg/g)[c] from ^{208}Tl, ^{212}Pb, ^{228}Ac	K (%)	dD_c/dt (Gy/ka)[d]
1	4-11µm	1.203	2.15 ± 0.37	2.40 ± 0.04	2.20 ± 0.37	10.18 ± 0.15	2.14 ± 0.05	0.0018 ± 0.0001
2	4-11µm	1.156	2.81 ± 0.36	2.09 ± 0.04	2.65 ± 0.36	9.74 ± 0.14	2.39 ± 0.05	0.0226 ± 0.0011
3	4-11µm	1.182	2.10 ± 0.33	1.62 ± 0.03	2.10 ± 0.34	7.58 ± 0.13	1.83 ± 0.04	0.0071 ± 0.0004
4	4-11µm	1.199	2.12 ± 0.26	1.81 ± 0.03	2.42 ± 0.26	7.92 ± 0.11	1.63 ± 0.03	0.0852 ± 0.0043

[a] Lab codes: 1) WLL-357; 2) WLL-352; 3) WLL-358; 4) WLL-353
[b] Ratio wet to dry sample weight. Errors assumed 50% of (δ-1).
[c] U and Th contents are calculated from the error weighted mean of the isotope equivalent contends.
[d] Contribution of cosmic radiation to the total doserate, calculated following Prescott & Hutton (1995).

The four IRSL ages from Poplars Gully range from 164.7 ± 14.8 ka to 119.8 ± 10.5 ka. Two samples (1, 3) were near or at saturation indicating that the result may be an underestimate. It is noted that the ages are stratigraphically reversed with the two

younger dates at the bottom and the two older ages at the top. A distinct possibility is that the stratigraphically younger material was not fully zeroed prior to deposition. On environmental grounds this interpretation is unlikely because Facies F is very clearly a proglacial unit and a good chance of zeroing is expected. In addition, ages 3 and 4 coincide, which is unlikely if inherited signals are involved, unless all the material was recycled from the same local source. It is more likely that the reversal is related to

Table 6: Measured a-values and equivalent doses as well as calculated dose rates and resulting luminescence ages from Poplars Gully.

Sample[a]	a-value	D_e(GY)	dD/dt (Gy/ka)	**IRSL age (ka)**
1[b]	0.048 ± 0.010	397.0 ± 19.2 (413.4 ± 21.2)	3.45 ± 0.25	**115.0 ± 9.9** **(119.8 ± 10.5)**
2	0.040 ± 0.006	467.0 ± 28.8	3.66 ± 0.21	**127.5 ±10.7**
3[b]	0.055 ± 0.014	514.1 ± 30.0 (465.6 ± 37.4)	2.84 ± 0.20	**181.3 ± 16.4** **(164.2 ± 17.4)**
4[c]	0.040 ± 0.020	441.0 ± 15.4	2.79 ± 0.22 (2.68 ± 0.22)	**157.8 ± 14.8** **(164.7 ± 14.8)**

[a] Lab codes: 1) WLL-357; 2) WLL-352; 3) WLL-358; 4) WLL-353
[b] Samples 1 and 3 were near saturation. The bracketed values were calculated using a Single Aliquot Regenerative Method.
[c] This sample showed a minor radioactive disequilibrium (bracketed values) and the given age has been corrected.

the relatively great age of the samples which approach the upper limit of IRSL dating in this environment. This reduces the stratigraphic and chronological resolution of the results. However, all four samples, which were obtained from widely spaced units, returned ages of ≥120 ka and it is highly probable that this rules out deposition during the last glacial cycle. Samples 2 and 4 are unsaturated and provide upper limit ages. In summary, the IRSL results are interpreted to indicate that deposition of the Poplars Gully sequence occurred during OIS 6.

5.6. Discussion

5.6.1. Site history and depositional model

Prior to this study, deposits at Poplars Gully had no direct age control, but the valley fill terrace in which the sediments were found has generally been inferred to represent LGM aggradation (Suggate, 1965; Clayton, 1968; Knuepfer, 1984, 1988; Cowan,

1990). The four IRSL samples presented in this study consistently show a ≥120 ka age suggesting that deposition at Poplars Gully occurred during the OIS 6 glacial. On stratigraphic and sedimentological grounds it is argued that only the uppermost gravel facies (facies G) is likely to represent deposition during the LGM. Glaciofluvial gravels of this facies form the terrace surface that can be correlated by height across the valley. All underlying sediments, however, predate the LGM on both valley sides.

Poplars Gully sediments were laid down in a dominantly ice-marginal and pro-glacial position and most of the sequence is interpreted to have formed as a kame terrace during multiple phases of ice incursion, stagnation and withdrawal from the lower Hope Valley. The general depositional setting at Poplars Gully is a lower valley reach which was repeatedly transgressed by a valley glacier and where sedimentation was mainly associated with stagnating ice during phases of glacial retreat. The sequence exposes the lateral transition from glacial deposition onto bedrock at the valley side to deposition over pre-deposited soft sediments in the middle of the valley. The basal bedrock contact of the sequence dips steeply from the valley side and disappears below the present Hope River floodplain. The remaining depth of fill below valley floor is unknown. However, a ground penetrating radar survey on the floodplain (section 4.5.1.) showed that unconsolidated sediments extend to at least 20 m below the present floodplain surface. Sedimentary facies at Poplars Gully preserve an intact stratigraphy allowing the reconstruction of the site history for this portion of the lower Hope Valley. Nine phases are identified, depicted in Fig. 44a –i, which place deposition in the context of an oscillating ice lobe followed by final ice evacuation and fluvial/alluvial infilling.

Prior to the onset of sedimentation a significant erosional phase in the valley is deduced from the presence of bedrock strath terraces which are buried by Poplars Gully deposits. This period of incision, probably similar to the last post-glacial (Holocene) fluvial degradation, excavated and largely removed any pre-existing (> OIS 6) valley fill (Fig. 44a), though older deposits may still be preserved under the valley floor. Following an initial ice advance (Fig. 44b), basal units at Poplars Gully record sedimentation associated with the retreat phase of that advance. This is represented through extensive dead ice meltout and collapse features (Facies A) as well as ice-marginal glacio-fluvial deposits (Facies B) (Fig. 44c). It is probable that

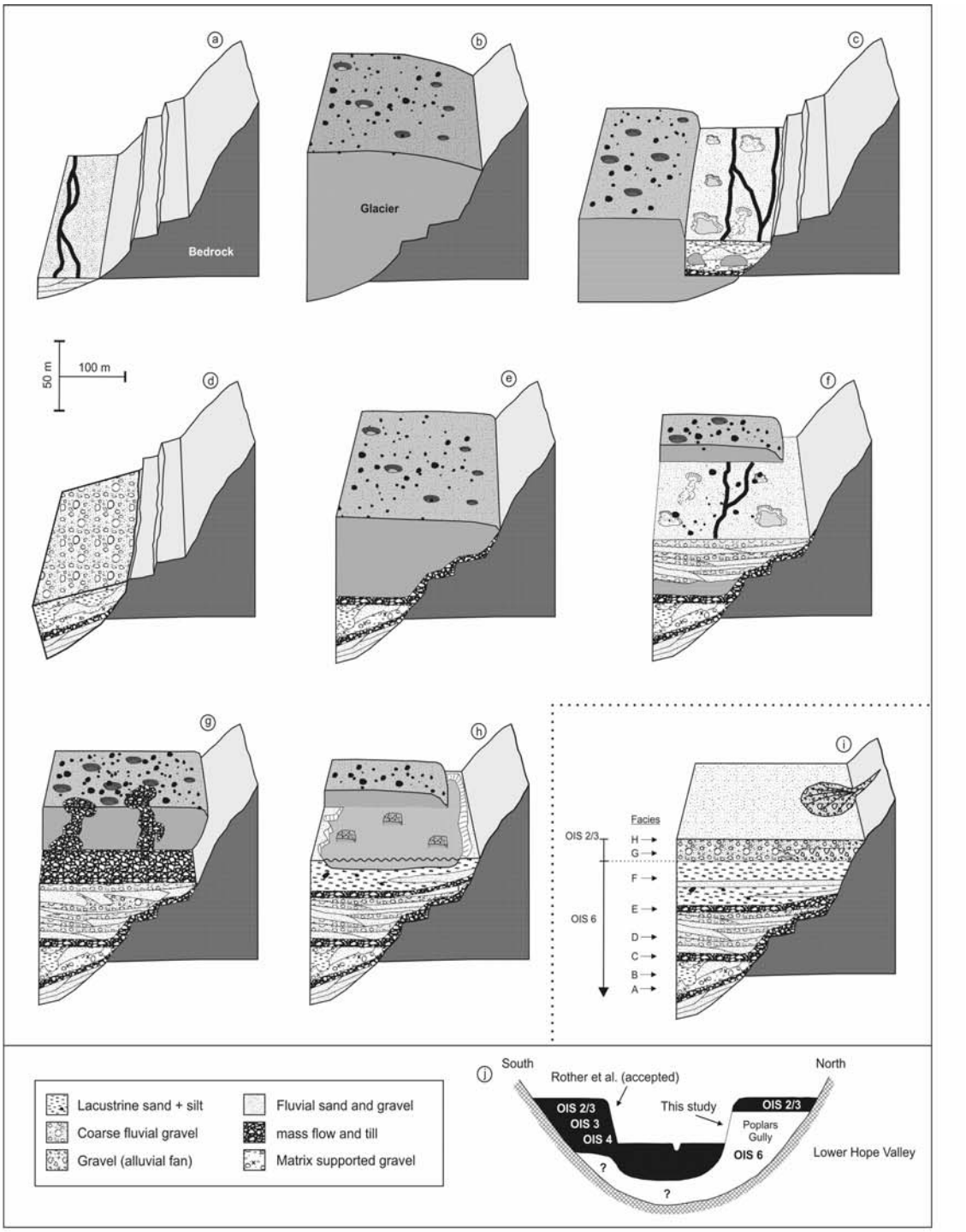

Fig. 44: Depositional model for the Poplars Gully sequence based on sediment properties and depositional context. Nine phases are identified (44a-i) beginning with an (interglacial?) erosional phase (a) that was followed by a substantial glacial advance (b). Basal deposits at Poplars Gully are interpreted as ice marginal ice contact deposits (c) which show post-depositional deformation including block tilting and collapse features (d). This is followed by a glacial re-advance (e) which truncated deposits laid down during the previous retreat. Overlying glaciofluvial deposits indicated a period of retreat (f) before a glacial re-advance deposited diamictons and glaciotectonized the proglacial sequence (g). Renewed glacial retreat resulted in the formation of a proglacial lake (h). Figure (h) summarizes the stratigraphic composition and geochronological model for Poplars Gully. Figure (i) shows the context and depositional architecture of valley fill deposits in the Hope Valley.

the retreat eventually resulted in complete ice evacuation from this part of the Hope Valley as indicated by widespread and relatively large scale collapse deformation. The removal of structural ice support is inferred to have caused the topple failure and forward collapse of a kame terrace block that resulted in the observed concordant tilting of heterogeneous lacustrine and fluvial deposits of Facies A & B (Fig. 44d).

Ice retreat and block failure was followed by a substantial glacial re-advance into the lower Hope Valley (Fig. 44e). Mass flows and tills from the advance (Facies C) unconformably truncate underlying sediments. Fabric characteristics and the general absence of active ice deformation indicate that deposition occurred mainly during passive melt-out from a stagnant body of ice. Sedimentation associated with progressive ice downwasting is consistent with the observed succession from basal meltout tills to mass flows (Facies C) through to dominantly glacio-fluvial sediments (Facies D). During the deposition of Facies D the site may either have been proglacial or again formed part of a kame terrace system as depicted in Fig. 44f.

A re-advance then occurred as suggested by the glacial diamictons of Facies E and the presence of glaciotectonic deformation structures in Facies D and the top of Facies C (Fig. 41, 44g). Following a renewed phase of glacial retreat a proglacial lake formed in the lower Hope Valley (Fig. 44h). Glacio-lacustrine deposits (Facies F) are ~40 m thick and include ice rafted debris. Although it is difficult to estimate the size of the lake, the considerable thickness of Facies F suggests that the lake was extensive. Fluvial beds in the lacustrine sediments suggest either repeated lake low stands when fluvial sands were deposited or changes in the glacier front up valley with sand beds deposited during ice incursions.

As previously indicated a major hiatus is inferred between the deposition of glacio-lacustrine sediments of Facies F and the overlying gravel units of Facies G (OIS 2/3?). How much material of the original OIS 6 sequence was eroded prior to sedimentation of Facies G is not known. The elevation of the fluvial-alluvial gravels (c. 610 m asl) matches the terrace level of the main (last glacial) aggradation surface at the opposite valley side. It is suggested that deposits of Facies G correlate to aggradation during the last glacial cycle that overtopped and buried the penultimate valley fill remnant at Poplars Gully. Following this interpretation, Facies G represents an ‘overlapping’

secondary valley fill as shown in Fig. 44j. Rapid incision following the last deglaciation changed base levels, stopped fan building on the high surface and eventually triggered the landslide which exposed the Poplars Gully sequence.

5.6.2. Regional glacial and tectonic implications

Past glacial research in New Zealand has mainly focussed on establishing the ice limits of former glacial advances and their relative chronology, while by comparison, relatively little attention has gone to the sedimentology of NZ's glacial sequences. The study of sedimentary and structural parameters, however, can substantially improve our understanding of the glaciological conditions of formerly extended valley glaciers (e.g. Shaw, 1987; Benn, 1995; Boulton et al., 2001; Benn et al., 2003; Evans and Hiemstra, 2005). Such reconstructions are particularly important for New Zealand where Quaternary glaciations occurred under perhumid conditions with ice accumulation and ice turn-over rates that ranked among the highest on Earth. The consequent glacial style is therefore likely to differ from the more continental glaciations of North America and Europe. This notion is supported by observations from the Southern Alps where glacial workers have long been aware of some distinct features of glacial valley sequences. Of these, the very large scale of glacio-fluvial aggradation fans, the generally small size of terminal moraines, and the widespread occurrence of atypical stratified and only weakly compacted 'tills' have been described (e.g. Speight, 1940b, 1942; Gage, 1965, 1985; Suggate, 1990) but detailed studies on these phenomena are very rare (e.g. Hart, 1996).

Four IRSL ages from Poplars Gully obtained from different facies assemblages and covering a considerable portion of the exposed stratigraphy suggest that deposition at Poplars Gully occurred during OIS 6 / early OIS 5. The overall sequence is interpreted as a remnant of the penultimate glacial valley fill which was protected from last interglacial erosion in a sheltered position behind a bedrock spur and then incorporated into the aggradational fan of the last glacial cycle. The *in situ* OIS 6 sedimentary sequence survived later ice overriding in the central lower Hope Valley without modification. The findings support earlier results of Chapter 4 and challenge the notion that glacial advances during the LGM were sufficiently erosive to effectively remove all pre-existing valley fill deposits in the Hope Valley. Sediments

at Poplars Gully preserve an excellent record of glacial deposition during OIS 6. The interpretation lays emphasis on the reconstruction of the local glacial history and the sedimentological style of pre-LGM glacial deposition. Stratigraphic data from Poplars Gully provide evidence for a total of three glacial advances which are separated by one major and one minor ice retreat phase. The more substantial retreat occurred between the two older advances and resulted in complete ice evacuation from the lower Hope Valley. This was followed by a later glacial re-advance which truncated the underlying successions. The re-advance is subdivided into two phases separated by a minor ice terminal oscillation. These data are significant because Poplars Gully is located 30 – 40 km down valley from the glacial accumulation areas and only substantial ice advances reach the lower Hope Valley. Based on the stratigraphic data it is suggested that the previously undivided OIS 6 in the Southern Alps of New Zealand (e.g. Suggate, 1990) comprises at least two large scale glacial advance phases

Facies type	Facies description	Facies code	% total
Mud	Laminated silt and mud	Fl	6.0
	Laminated silt and mud with dropstones	Fe	19.7
	Massive silt and mud	Fm	3.8
	Massive silt and mud with dropstones	Fme	14.8
		Total mud	**44.3**
Sand	Massive sand, moderately to well sorted	Sm	2.2
	Horizontally laminated sand, moderately to well sorted	Sh	3.4
	Cross-stratified sand	Sx	9.6
		Total sand	**15.2**
Gravel	Massive, clast supported gravels	Gm	5.3
	Stratified & normally and inversely graded gravels	Gh & Gni	6.6
	Matrix supported gravels	Gs	14.4
	Granules (openwork)	Gro	2.2
		Total gravel	**28.5**
Diamict	Massive diamict, boulder to silt size	Dmm	2.2
	Stratified diamict, boulder to silt size	Dms	9.8
		Total diamict	**12.0**

Table 7: Relative proportions of logged deposits in the Poplars Gully glacial sequence. Note the dominance of aqueous deposition.

A summary of the relative abundance of logged deposits (Table 7) highlights the dominance of water driven or water influenced sedimentation at Poplars Gully. This can partially be explained by the deglacial context of the overall sedimentary succession in which meltwater dominated deposition and extensive fluvial reworking is to be expected. However, the characteristically large volumes of such sequences in glacial valleys of the Southern Alps implies extraordinary large sediment supply,

while the dominant fluvial-lacustrine appearance of the majority of these sequences clearly requires the abundant availability of free water.

The survival of thick OIS 6 deposits in the Hope Valley despite ice occupation during the LGM poses intriguing questions regarding the mechanism of preservation. For an explanation the local tectonic setting must be considered first. As introduced earlier the area is part of the Marlborough Fault Zone and the active strike-slip Hope Fault follows the course of the middle and lower part of the valley. Chapter 4 showed that the lower Hope Valley constitutes a structural depression that formed at a releasing fault bend and that Late Quaternary basin subsidence occurred at a rate that approximately matches the overall regional uplift rate of ~2 mm/a^{-1} (Wellman, 1979). Dating of fluvial and lacustrine valley fill deposits at Glynn Wye Station (Chapter 4) showed a long term aggradation trend in the lower Hope Valley at least over the last ~60 ka. These results suggest that relative basin subsidence was undoubtedly significant in the preservation of penultimate glacial deposits at Poplars Gully. Conditions changed only during the postglacial period when downcutting by the Hope River outpaced basin subsidence leading to partial excavation of the basin fill.

Despite the importance of local tectonic influences, however, it is noted that this does not account for the marked difference in the volume of glacial deposits generated during OIS 6 and the LGM. There is clear evidence that glaciers reached the lower Hope Valley during both periods (Clayton, 1968; Suggate, 1990; this study), however, it appears that sedimentary sequences deposited during OIS 6 (i.e. Poplars Gully) are substantially thicker than the locally widespread but relatively thin LGM deposits. Similar results were obtained from Glynn Wye Station where most of the sequence was OIS 4 / 3 in age with LGM deposits forming a thin cap. The terminal position of the LGM advance is preserved through a moraine complex at Glynn Wye Station while the glacial downvalley extent during OIS 6 is not known. No glacial deposits associated with OIS 4 have so far been found in the lower Hope Valley (Suggate, 1965; Clayton, 1968; Cowan, 1989). The variation in depositional volume is unlikely to be related to regional tectonics as faulting and associated subsidence along the Hope Valley segment has been continuous from the mid-Pleistocene (Wood et al., 1994) to the last major seismic event in 1888 (McKay, 1890).

Since local tectonism does not explain the significant difference in thickness between penultimate and last glacial deposits it is considered it to be a genuine glacial feature. It seems that OIS 6 or earlier advances carved a deep glacial through in the lower Hope Valley which was subsequently sediment filled during ice stagnation and deglaciation (e.g. Poplars Gully), while no such glacial valley erosion occurred in the lower Hope Valley during the LGM. Generally, deep glacial troughs are common in high-turnover glacio-alpine environments (e.g. Hooke and Pohjola, 1994; Spedding and Evans, 2002; Baker et al., 2003) and is a feature of the present day Tasman Glacier in New Zealand which occupies a 120 m deep ice–marginal trough behind its outwash barrier (Nobes and Owens, 1995).

The data suggest that ice advances during OIS 2 (or late 3) produced much thinner glacial sequences in the lower Hope Valley and caused significantly less erosion of pre-existing sedimentary sequences than the OIS 6 advances. This may be explained by the substantially greater downvalley ice extent during OIS 6, and hence may reflect variations in total ice volume or alternatively, may be related to a shorter duration of ice occupation during the LGM. Both options would indicate that the OIS 6 glaciation was larger than glaciation during the LGM. Larger glaciation during OIS 6 (compared to LGM) has also been recognized in Tasmania where OIS 6 ice limits are far more extensive than during OIS 2 and 4 (Colhoun, 1985; Augustinus 1999; Colhoun 2004). The results from the Hope Valley are likely to represent a similar signal in New Zealand (see general discussion, Chapter 9).

5.7. Summary and conclusions

A 110 m thick succession of glacial and proglacial deposits is described from Poplars Gully, Hope Valley, South Island, New Zealand. The section consists of eight principle lithofacies assemblages that represent different stages of ice occupation in the valley. After an initial ice advance basal sediments record an ice retreat phase which is indicated by laminated kettlehole deposits with meltout deformation and large scale ice collapse structures. This was followed by a substantial glacial re-advance which truncated the underlying facies and deposited mass flow diamictons and till. The subsequent glacial retreat is evidenced by the stratigraphic transition to ice proximal glaciofluvial gravels. A last, probably short lived ice advance, caused

folding and thrusting of the proglacial fan sequence and deposited mass flows. Final ice retreat from the lower Hope Valley was followed by the formation of a large proglacial lake. Most sediments at Poplars Gully are associated with glacial retreat while ice advances are represented by thin sequences of mass flow diamictons and minor till deposits. The general dominance of aqueous deposition in the ice proximal environment which implies that climatic conditions during deposition were mild enough to provide nearly year-round availability of large volumes of melt-water.

Poplars Gully provides evidence for three glacial oscillations which are separated by one major and one minor ice retreat phase. The more substantial retreat occurred between the two older advances and probably resulted in complete ice evacuation from the lower Hope Valley. Infrared stimulated luminescence (IRSL) dating on fine grained glacio-fluvial and glacio-lacustrine deposits place deposition of the Poplars Gully sequence into Oxygen Isotope Stage 6 (OIS). Based on the stratigraphic data it is suggested that the previously undivided OIS 6 in the Southern Alps comprises at least two substantial glacial advances.

CHAPTER 6

CHRONOLOGY AND SEQUENCE ARCHITECTURE OF VALLEY FILL TERRACES BETWEEN THE MIDDLE HOPE AND LOWER WAIAU VALLEYS

6.1. Introduction

This chapter presents sedimentological and geochronological results from terrace deposits exposed in the valley reach from the middle Hope Valley to the confluence with the Waiau River. This will extend results of Chapters 4 and 5 which showed that fill deposits of the lower Hope Valley are sedimentologically diverse and comprise complex lacustrine, fluvial and glacial sequences, while results from luminescence dating demonstrated that the majority of the stratigraphy predates OIS 2. The sedimentological and structural fill properties reflect the unique regional tectonic and climatic setting that is characterized by exceptionally high erosion rates and the consequent production of very large volumes of clastic sediment (Hovius et al., 1997). As stated before under equilibrium conditions sediments are transported by powerful rivers that are primarily fed by the high rainfall zone of the central Alps causing sediment yields of New Zealand rivers to rank among the highest in the world

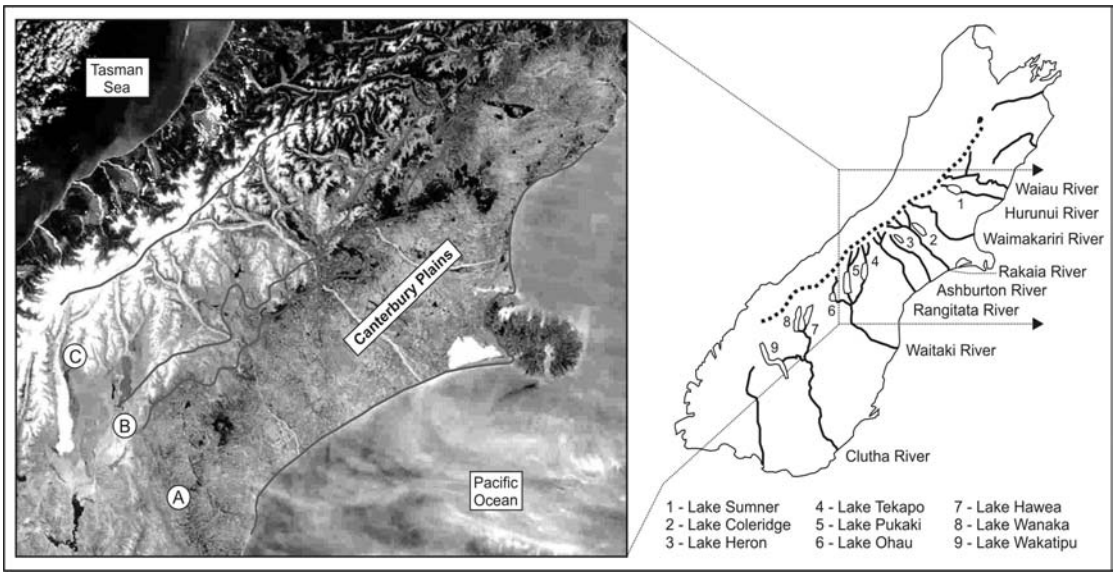

Fig. 45: Major glacial valley and lake systems in the South Island (right) and approximate zoning of valley fill types in the central Southern Alps (left). The fills can be differentiated into paraglacial foreland sequences (A), paraglacial alpine valley sequences (B), and proglacial ice-proximal alpine sequences (C).

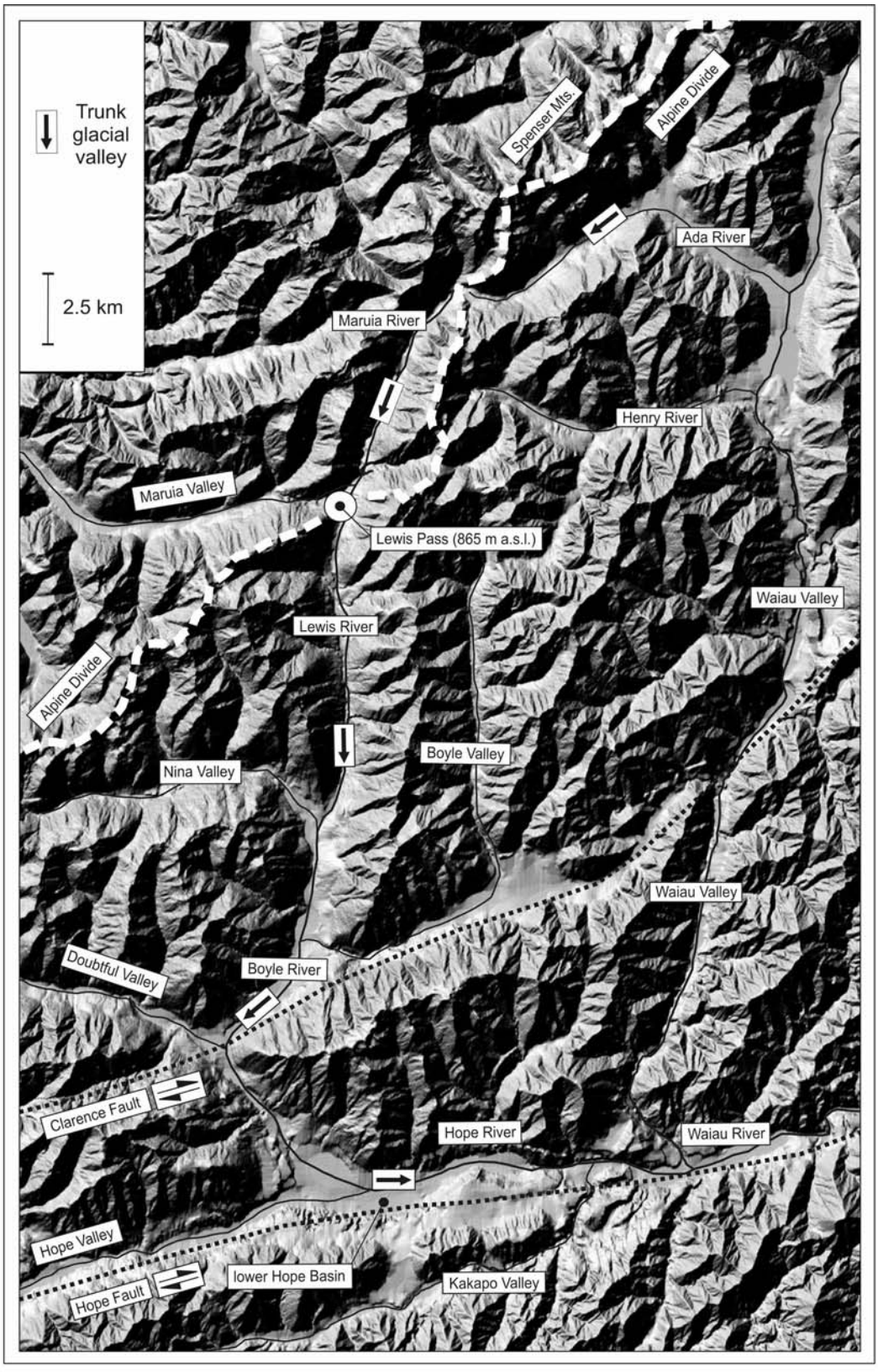

Figure 46: Glacial valleys of the Hope-Waiau catchment. The main Pleistocene trunk glacier extended from the Spenser Range in the north down the Ada-Maruia-Lewis-Boyle-Hope Valley channels while a less extensive lobe occupied the upper Waiau Valley. Note the transition of the U-shaped upper to the dominantly V-shaped lower Waiau Valley. Tributary ice lobes from the Nina, Doubtful and upper Hope Valleys joined the main trunk glacier which reached the lower Hope Basin during the LGM and earlier glaciations. Note the fluvial beheading of the upper trunk valley through the west flowing Maruia River. Marked dextral channel deflections of the Waiau and lower Boyle Valleys are associated with transcurrent motion along the Clarence Fault.

(Griffiths, 1981; Hicks, 1998). Major perturbations of this system occurred during the Pleistocene when under glacial conditions debris production was probably further increased while the fluvial transport capacity was reduced, which rapidly overwhelmed fluvial systems and resulted in the deposition of large glacio-aggradational valley fans. In New Zealand, alluvial valley fill successions can be differentiated into paraglacial sequences deposited on extensive alpine foreland plains (A), paraglacial valley fills deposited in the non-glaciated lower alpine valley reaches (B) and proglacial valley fills of the glaciated middle and upper valleys (C) (Fig.45). The deposits described in this chapter belong to the type B and C valley fills.

6.2. Valley geomorphometry

The glacial trunk valley comprises portions of six channels belonging to the Ada, Maruia, Lewis, Boyle, Hope, and Waiau Rivers (Fig. 46). Low and smooth mountain passes in most headwater regions (e.g. Lewis Pass, Amuri Pass, Hope Pass, Harper Pass) suggest that under full glacial conditions at least some ice flowed from west to east across the topographical divide, thereby reflecting the greater ice accumulation on the windward western side of the Southern Alps (Gage, 1965). Further differences between the former glacial ice flow pattern and the present day fluvial pattern are highlighted by the drainage capture of the upper trunk valley by the west flowing Maruia River (Fig. 46).

The upper catchment is characterized by broad U-shaped valleys that generally preserve a fresh glacial morphology, which has been little modified by fluvial incision (Fig. 47a). This is contrasted by most middle valley reaches which are incised and characterized by often spectacular flights of fluvial terraces. The morphological difference between the upper and middle reaches is reflected in the relief ratio (S) which is a measure for the overall catchment ruggedness. The relief ratio (S) is defined as $\Delta H/L$, where ΔH is the difference between the highest and lowest point of each valley reach and L is the length of the reach (Schumm, 1954). Results in Fig. 48A show, as expected, that the uppermost valley portion in the Spenser Range is the most rugged. The relief ratio then drops markedly in the downvalley direction, before climbing again and reaching a second maximum in the middle Hope Valley

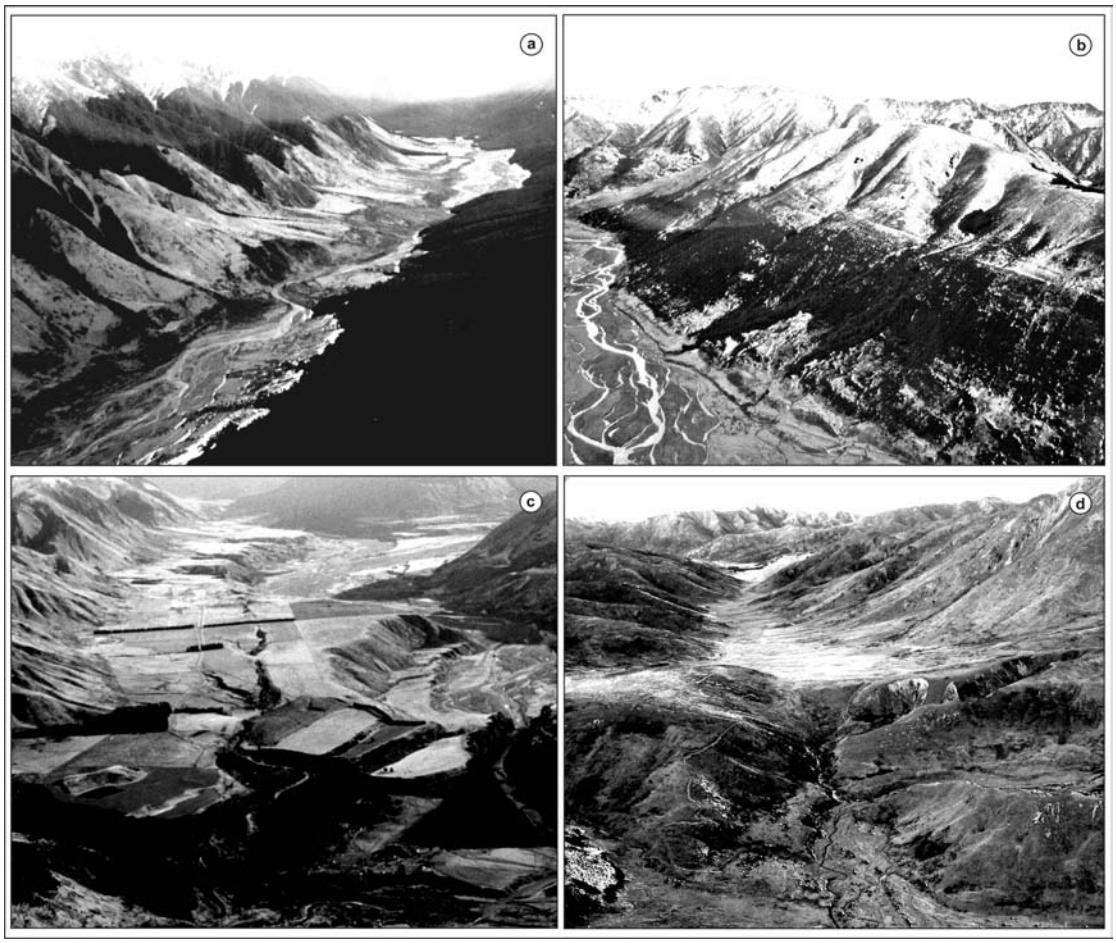

Fig. 47: Oblique aerial photos showing glacial and aggradational features in the study area. The broad U-shaped middle Hope Valley with truncated spurs and postglacial debris fans (a), glacial trimlines and rounded mountain tops in the upper Waiau Valley (b), extensive aggradational terraces in the lower Hope Valley (c), and undissected valley fill of the upper Edwards Valley (d) (photo 47c: J. Pettinga).

(Hope Basin reach). The effect is explained by changes in ΔH, as maximum heights (max. H) along the middle valley reaches are relatively constant (1750 – 1850 m) while, at the same time, fluvial valley incision increases in the downstream direction which accounts for markedly lower valley floor positions (min H) resulting in higher relative relief ratios. In the middle Hope Valley, the reach with the second highest relief ratio, postglacial fluvial downcutting has exceeded 160 m (Fig. 47c).

For the trunk valley a morphological transition is observed near the Boyle River junction from the bedrock dominated upper valley to the fill and terrace dominated middle trunk valley. In the middle reach the valley constitutes a succession of broad valley segments with braid plains, which are separated by several narrow gorges. Bedrock in the gorges consists of highly fractured greywacke of low competency which was found at one location (Tutu Gorge) to be interbedded with fault gouge.

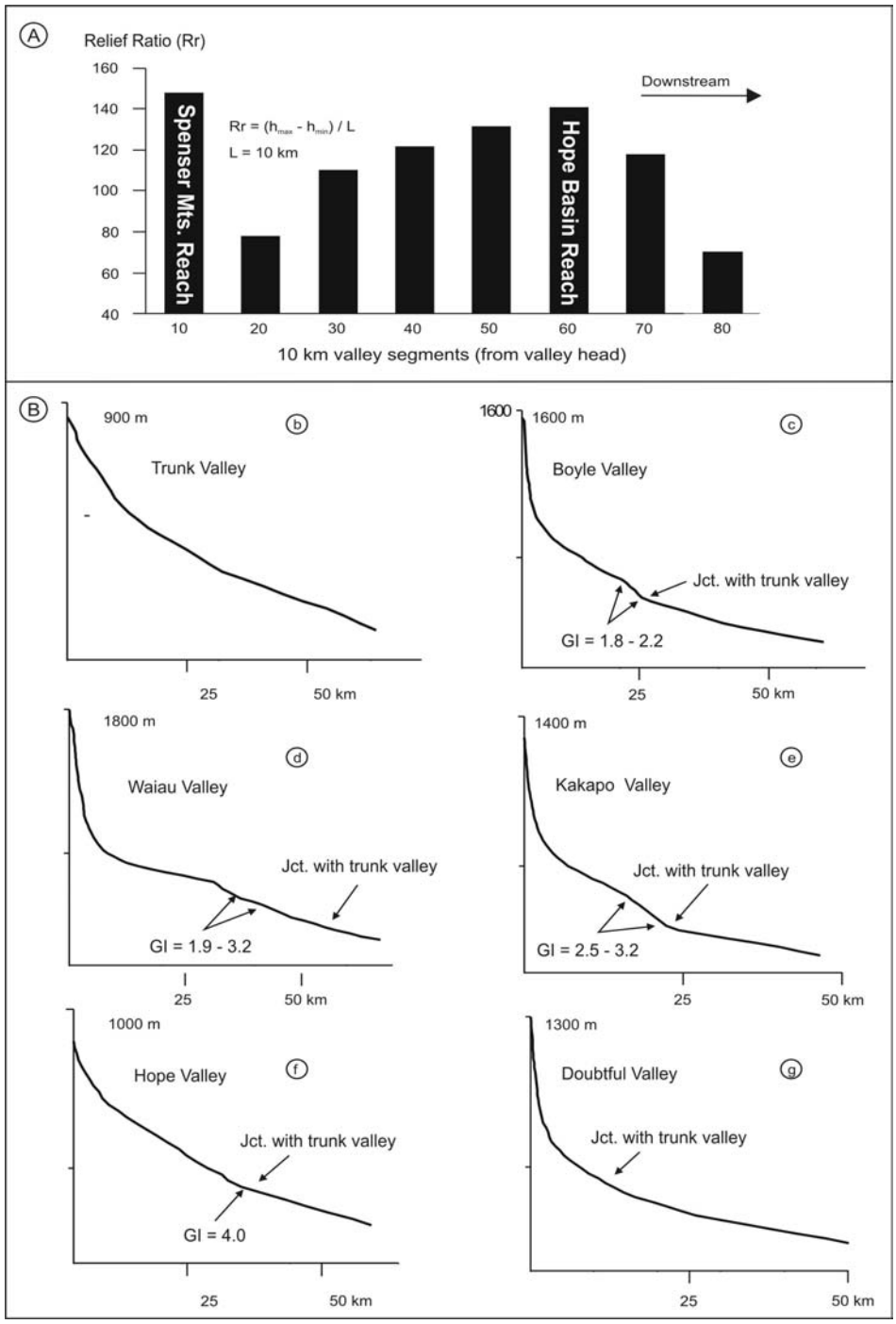

Fig. 48: Relief ratio of the trunk glacial channel as shown in Fig. 46 (A). Figure (B) shows longitudinal valley profiles for the trunk and tributary valleys. Note the low elevation (b) of the new trunk valley head (865 m a.s.l.) following fluvial beheading of the upper valley portion by the Maruia River.

Figure 48 (B) analyses the longitudinal channel profiles of the largest valleys in the catchment using a stream gradient index (GI) (Hack, 1973). GI is defined as the product of the channel slope of a reach and the length of the channel measured from the headwaters of the valley (Hack, 1973) and is calculated as:

$$GI = \Delta H / \Delta L \times L$$

where ΔH is the vertical difference between the upper and lower end of the reach, ΔL is the length of the reach and L is the overall stream length. The GI of each reach was then compared to the gradient index of the entire profile (SL) defined by:

$$SL = \frac{H_1 - H_2}{\log_e L_2 - \log_e L_1}$$

where $H_1 - H_2$ is the vertical difference between the highest and lowest map contour line crossed by the stream, L_2 is the valley distance from the source to its downstream limit, and L_1 is the highest map contour line crossed by the river. GI / SL ratios near 1 are typical for ideally shaped and mature valley profiles which resemble exponential curves, while values differing significantly from 1 indicate valley profile perturbations where channel gradients differ from those expected for an ideal profile.

The longitudinal valley profiles shown in Fig. 48b-g indicate that channel perturbations (knickpoints) occur in most tributary valleys whereas the trunk valley (Fig. 48b) is characterized by a comparatively smooth profile despite the presence of four bedrock gorges (Fig. 19A, pg. 52). A likely explanation for the absence of knickpoints in the trunk valley is a combination between the low competency of the highly fractured greywacke basement along the Hope Fault and the presence of intermediate wider valley segments which represent sediment filled structural depressions that smooth potential channel perturbations (see GPR results Chapter 4). In nearly all cases where knickpoints are present they occur at or near the junction between tributary valleys and the trunk valley (e.g. Fig. 48c,e,f). Although this pattern could be attributed to differential strength of tributary and trunk glacier erosion, the survival of the knickpoints at the junctions more probably reflects differences in the postglacial fluvial incision of the main and tributary rivers. This interpretation is supported by the profile of the Kakapo Valley which was not glaciated yet a knickpoint occurs at the junction with the trunk valley. Present day incision in the main valley is indicated by low degradational terraces 5-10 m above river level and erosional unconformities between channel deposits and the underlying fill sequence as indicated by ground penetrating radar (Chapter 4).

A variation from the general profile pattern is noted for the Waiau Valley (Fig. 48d), where a marked knickpoint is located near the Henry River mouth roughly 20 km upstream of the junction with the trunk valley (M31 720770), which itself is not associated with a channel perturbation. Although moraines in the upper Waiau Valley demonstrate the extension of former glaciers, the reconstructed ice limits suggest that neither during the last glacial cycle nor OIS 6 did ice reach the lower valley portion or the junction with the trunk valley (Clayton, 1968; see map of Fig. 10, pg. 44). The knickpoint near the Henry River mouth marks the morphological transition from the V-shaped lower valley to the previously glaciated, broad and fill dominated upper valley (Fig. 46). It is therefore likely that the knickpoint is of older Pleistocene age which accounts for the greater distance of upvalley knickpoint migration (from the trunk valley junction), than is observed for knickpoints in all other tributary valleys. This was possible because the bedrock profile of the middle and lower Waiau reaches received little glacial modification during the last glacial cycles thereby preserving the knickpoint, possibly buried under sedimentary fill. This interpretation implies that the knickpoint has been re-activated during several interglacials once the sedimentary fill sequence was removed.

6.3. Valley fill lithostratigraphy and geochronology

The morphology of the Hope and Waiau reaches of the trunk valley has a ‘trench-like’ appearance and is characterized by paired and unpaired alluvial terraces which extend to more than 450 m above river level. Thick alluvial sequences at distinct elevation levels represent periods of large scale valley aggradation that reflect dramatic changes in the balance between debris supply and fluvial transport capacity which are commonly associated with periods of major glacial expansion. Subsequent interglacial periods cause a reversal of the imbalance and lead to re-excavation of the valleys thereby producing flights of degradational terraces. The recognition of aggradational and degradational terrace landforms is therefore of stratigraphic and paleo-climatic significance.

6.3.1. Methods

Study sites were selected based on accessibility and the desire to log the vertical span of the fill stratigraphy at several locations in the valley. Because several of the valley fill units can be traced laterally for considerable distances, the presented analysis is thought to be representative for the fill stratigraphy in the Hope-Waiau Valleys. Terraces elevations were measured using a handheld global positioning system (GPS) with an average vertical uncertainty of ± 6 m. Exposures were measured, photographed and logged using techniques described in the method sections of Chapters 5 (section 5.4.1.). Numerical age control on sediments was obtained by IRSL dating of fine grained deposits. Sediment sampling and laboratory preparation followed the procedure described in Chapter 4 (section 4.4.2.).

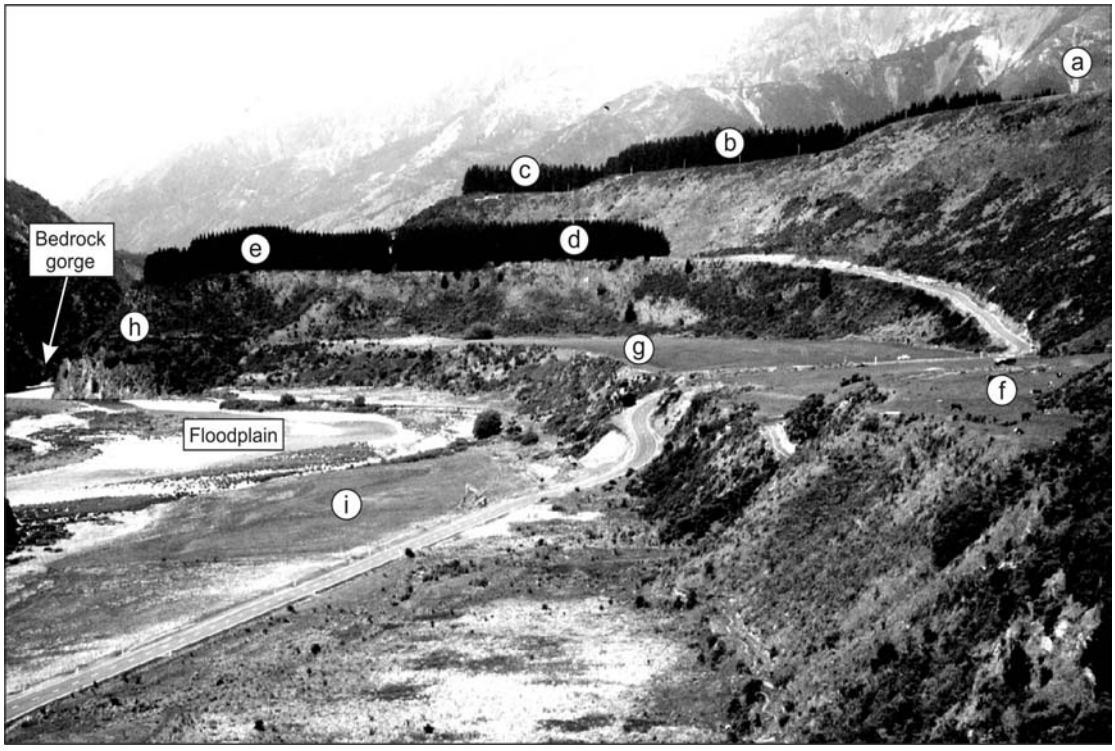

Fig. 49: Aggradational and degradational terraces in the lower Hope-Waiau Valleys. The high terrace (a) is the LGM aggradational terrace. Terraces (b), (c), (d), and (e) are postglacial degradational terraces, of which (d) and (e) are bedrock strath terraces. Clayton (1968) interpreted terraces (f), (g), and (h) as aggradational terraces associated with the Lateglacial Lewis advance, however, (h) is a bedrock strath terrace and (f) and (g) are incised into older lacustrine deposits (see text and Fig. 51). Note digger near road on terrace (i) for scale.

6.3.2. The terrace sequence

In the study area sets of mainly discontinuous terraces were grouped based on stratigraphy and height above river level. Aggradational terraces form the uppermost members of each terrace tread. The geographic distribution of the terraces is shown in Fig. 50. Degradational terraces were grouped into three treads, consisting mainly of unpaired surfaces distributed over ~110 vertical meters. The mapping of degradational terraces was based on criteria used by Wilson (1989) where such surfaces were identified by thin veneers of degradational gravels, which overlie and are recognizably different from deeper gravels. In a number of cases the distinction between gravel units proved difficult due to a lack of exposure and the general similarity of the gravel packages. However, an unambiguous identification of degradational terraces was usually possible because most of these terrace, despite being cut into soft sedimentary fill, could also be matched with bedrock strath terraces at the gorges. The largest number of degradational terraces is preserved in the reaches downstream of Carlyle Gorge whereas the number decreases up valley (Fig. 50).

As introduced in previous chapters (sections 3.4. and 4.3), Clayton (1968) found evidence for five advances in the lower Hope and Waiau Valley reaches. The most continuous outwash surface stretches for ~13 km on the south side of the lower Hope Valley and is associated with several well preserved LGM moraine ridges. Most of the assemblage is associated with a surface 130-160 m above river level, but one of the moraine ridges is connected to a surface level 20-30 m higher and Clayton (1968) interpreted the sequence to represent two glacial advances (Glynn Wye and Glenhope advances).

Late glacial moraines (Lewis advance) are preserved at Lewis Pass approximately 30 km upstream from the lower Hope Basin. Clayton (1968) suggested that the advance caused aggradation in the lower valley as represented by several terraces situated roughly 30 m above the present floodplain. However, exposures in the two most extensive remnants of these terraces (Carlyle terrace, Poplars terrace, Fig. 51) show that their stratigraphy comprises thin veneers (<2 m) of coarse gravel which overlie 10-15 m of laminated lacustrine sand/silt (Fig. 51b-e). The terrace level can also be matched with bedrock strath terraces at the Glynn Wye gorge, the Waiau

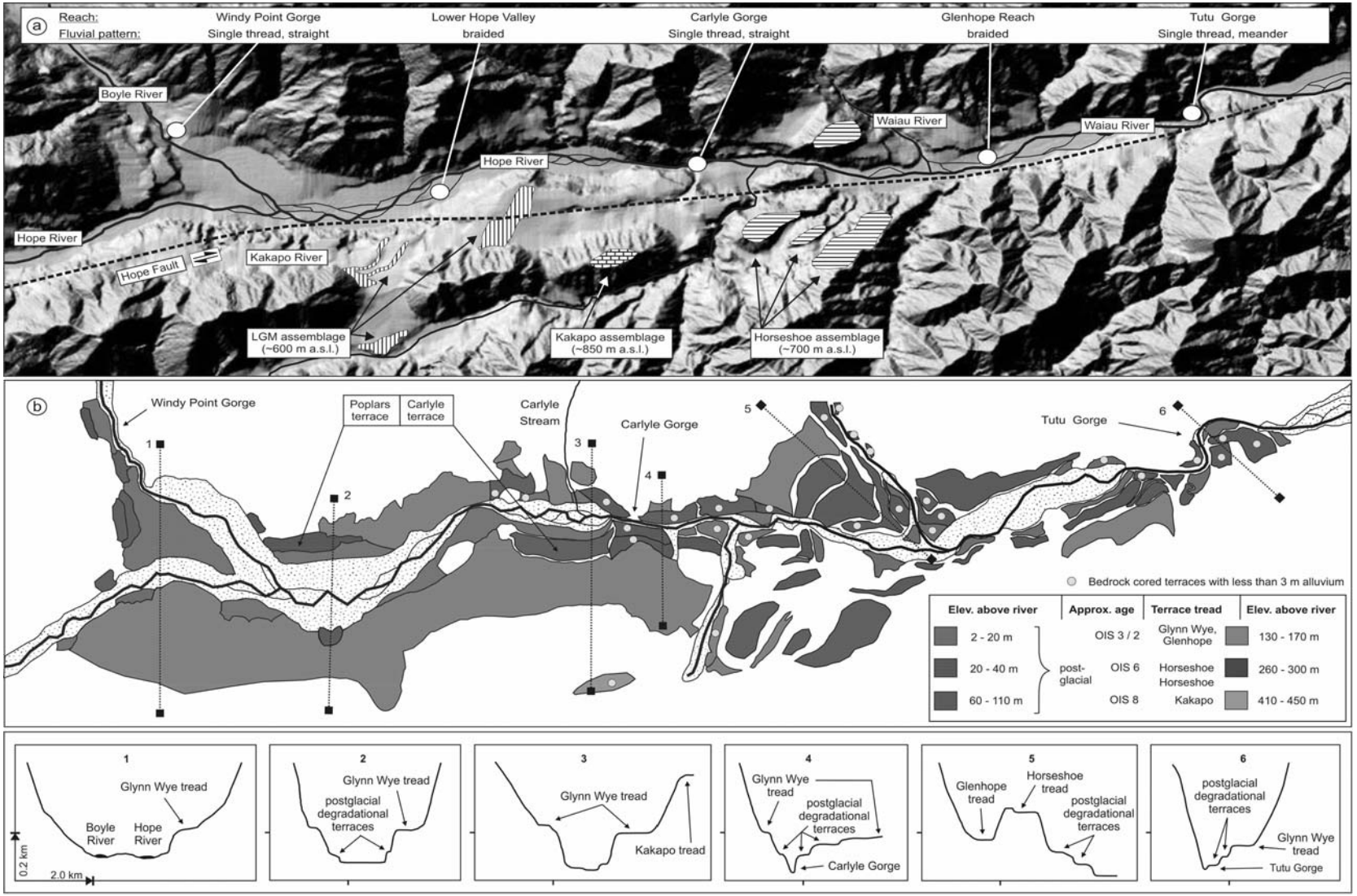

Fig. 50: Fluvial terraces and cross valley profiles in the Hope and Waiau Valleys

Mouth, and Tutu Gorge. Therefore these terraces are unlikely to represent aggradation during the Lewis advance but instead postglacial degradation by the Hope and Boyle Rivers. Additional evidence to support this interpretation comes from luminescence dating and is presented in section 6.4.

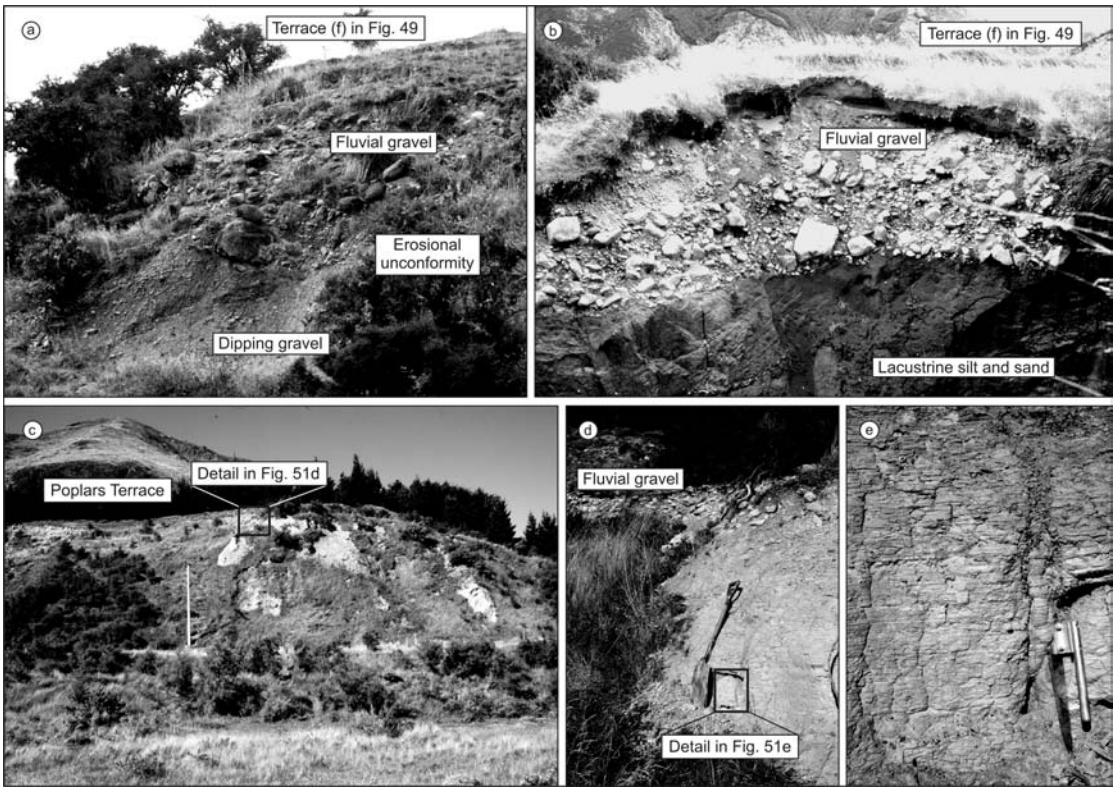

Fig. 51: Stratigraphic details of terraces previously identified to represent aggradation associated with the late glacial Lewis advance (Clayton, 1968). But exposures in terraces near the Carlyle Stream mouth (a and b) and at Poplars Station (c-e) show that the terrace stratigraphy comprises thin veneers of fluvial gravel at the top which unconformably overlie deeper deposits (for locations see Fig. 50). This indicates that the terrace is not aggradational but instead was formed by postglacial degradation.

6.3.3. Valley fill stratigraphy and sedimentology

The Quaternary fill sequence described here is exposed over a down valley distance of ~30 km in the Hope-Waiau trunk valley. In the upper and middle part of this reach glacial deposits are widespread and include sets of LGM terminal moraines as well as older moraines at higher elevations. In contrast, no glacigenic deposits or landforms are present in the lower portion of the valley segment. This suggests that the valley reaches examined cover the sedimentary transition from glacial to proglacial to paraglacial deposition. Such composite valley fill sequences are expected to be

sedimentologically and structurally complex as they are associated with an oscillatory glacier system. This usually produces a variable mixture of glacigenic, glaciofluvial and glaciolacustrine sediments which in turn are often interbedded with paraglacial floodplain and alluvial fan deposits (e.g. Ballentyne, 2002). The section below presents section descriptions and interpretations. Results from luminescence dating are shown in the accompanying figures and are discussed in detail in section 6.4.

6.3.3.1. Glynn Wye Stream

Glynn Wye Stream (GWS; NZ grid M32 E 24691 / N 58457), a small tributary to the Hope River, flows across the LGM aggradational terrace before cutting a steep gully through a terrace sequence of alluvial fill (Fig. 52). At its base, the fill sequence rests on bedrock which is exposed in stream banks near the junction between GWS and the Hope River. Sediments overlying bedrock comprise several m-scale units of well to crudely stratified gravels interbedded with units of coarse sand and granules. Above this there is a ~15 m thick unit of mainly planar bedded fine sand and silt with few beds of medium to coarse sand. Both the bedrock contact as well as the overlying sediments dip 2-8˚ in a southward direction, which is inconsistent with the present drainage orientations of GWS (N to S) and the Hope River (W to E). The basal sequence is truncated by 1.5 m of coarse gravel overlain by a 0.5 m of fine sand which form the surface of the T 5 terrace (Fig. 52b, c). The sand-silt unit below the T 5 terrace surface is laterally extensive and can be traced below the adjacent T 4 terrace.

The stratigraphically higher terrace sequence (T 1-3) comprises relatively uniform units of stratified and poorly sorted gravels with clasts up to 0.5 m but mainly below 0.3 m in diameter. All gravel units are clast supported and are loosely packed with a matrix of sand and granules. A marked feature within the gravels is the occurrence of an at least 6 m thick unit of fines in the lower portion of the upper terrace sequence (Fig. 52d) The basal contact is not exposed but the unit is laterally extensive and can be traced over ~250 m. The fines are coarsening from laminated silt at the bottom to cross-stratified medium and coarse sand above. At several positions sand beds dip at ~30˚. Normal faulting is pervasive in the fines, yet despite the apparent continuation of several of the faults into the overlying gravels their traces disappear quickly. The

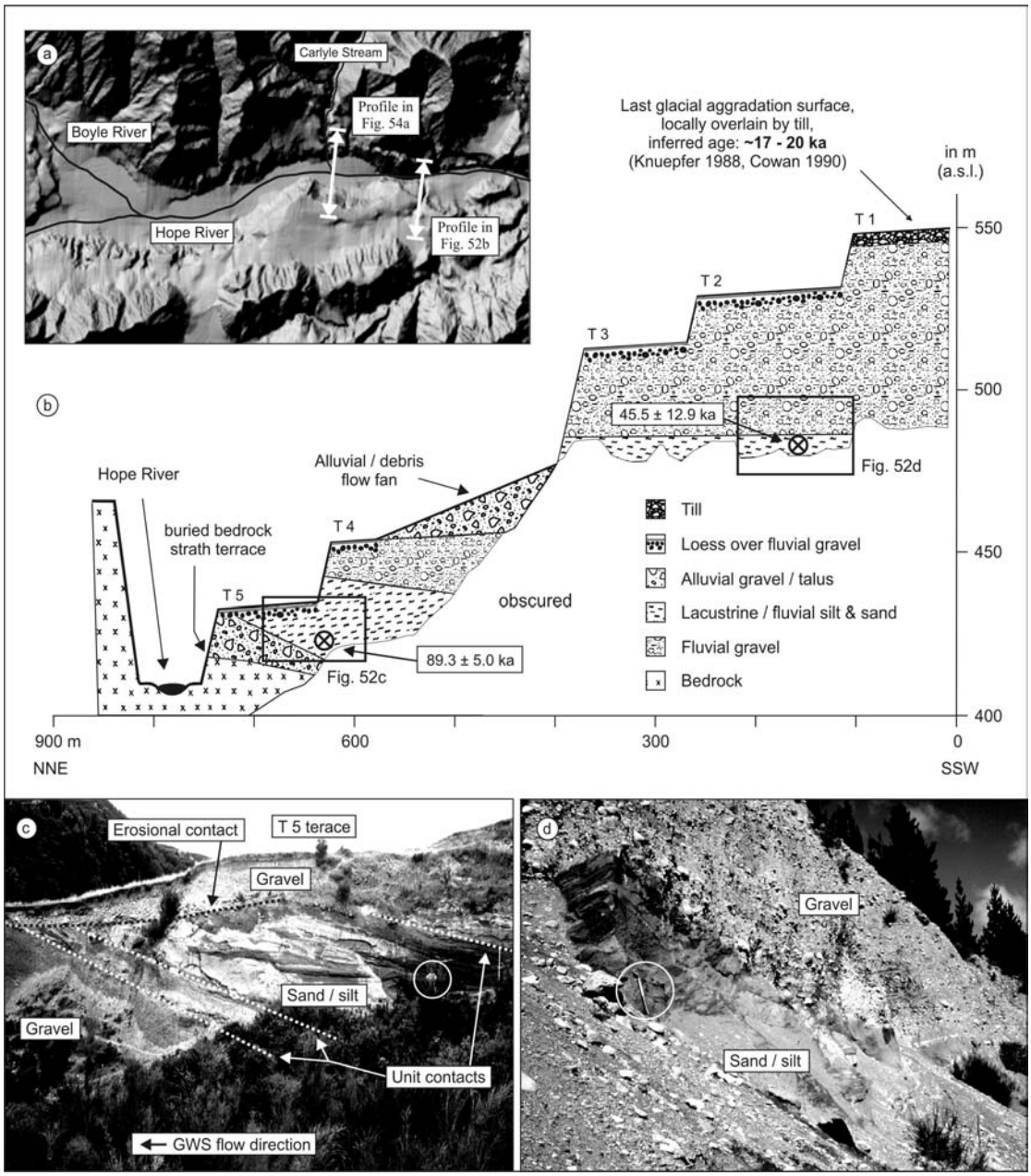

Fig. 52: Overview of deposits and terrace stratigraphy at Glynn Wye Stream (GWS). Note the dip of sedimentary units in (c). Luminescence samples were retrieved from the sand and silt units shown in (c) and (d). Note that the sand / silt unit below T 5 laterally extends and is part of the T 4 terrace fill also. Circled person (c) and spade (d) for scale.

interbeds are overlain by ~55 m of coarse fluvial gravel which in turn is capped by a well indurated diamicton containing angular and rounded boulders of up to 0.7 m in diameter (Fig. 53).

Interpretation: Coarse sediments at the base of GWS are interpreted as alluvial gravels overlain by lacustrine silt and sand. The units rest on a flat bedrock surface which represents a bedrock strath terrace. The terrace and the directly overlying sedimentary

units dip southward (Fig. 52c) which is interpreted to have resulted from post-formation tilting. This is supported by small scale faulting in the fine grained units above the strath terrace and by the proximity of the site to the Hope Fault. The basal sequence near the junction of GWS with the Hope River is truncated by coarse fluvial gravel overlain by loess which form the surfaces of the T 5 and T 4 terraces. The lateral continuation of T 5 terrace fill units under the T 4 terrace (Fig. 52b) and the presence of veneers of truncating fluvial gravels at the terrace surfaces suggest that both terraces are degradational and were cut by the Hope River.

The transition from the lower (T 4-5) to the upper terrace sequence (T 1-3) is accompanied by a marked narrowing and deepening of the gully. Exiting the narrower upper gully GWS deposited an alluvial fan onto the former T 4 floodplain (Fig. 52b). The fan was subsequently entrenched as GWS incised in response to downcutting by the Hope River. The upper gravel sequence comprises mainly fluvial deposits. Variability of clast sizes and sorting suggests deposition on a braid plain and the sedimentary pattern resembles floodplain deposits of the present Hope River. The gravels are interbedded with 6 m of laterally continuous and upwards coarsening silt and sand. The overall deposit is interpreted as a slack water facies which grades upwards into low flow regime fluvial sands. The limited thickness of the fines indicate deposition of these units as flood overbank or shallow lacustrine sediments. Fine grained deposits near the base of GWS were sampled for IRSL dating and yielded an age of 89.3 ± 5.0 ka indicating deposition during OIS 5. A second age was

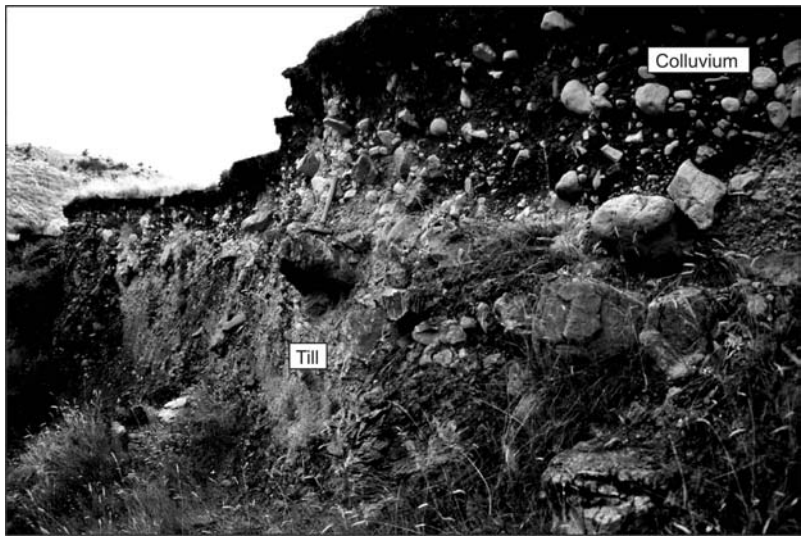

Fig. 53: Till overlying fluvial deposits (not shown in photo) at GWS.

obtained from sands interbedded with the stratigraphically higher gravels (Fig. 52d) and gave an age of 45.4 ± 12.9 ka. The top of the sequence is overlain by till deposited by the inferred LGM ice advance (Fig. 53).

6.3.3.2. Carlyle Terrace

The Carlyle terrace surface is situated in the lower Hope Valley ~150 m below the last glacial aggradational terrace and ~30 m above present river level (Fig. 54). Clayton (1968) suggested that the terrace formed during aggradation associated with a Late glacial ice advance (Lewis Advance), that deposited terminal moraines ~30 km up valley (at Lewis Pass). However, as shown earlier (Fig. 51), the stratigraphic and sedimentological context suggests that the terraces formed by postglacial downcutting of the Hope and Boyle Rivers. Sediments of the Carlyle terrace were logged in detail on the south side of the Hope Valley opposite the Carlyle Stream mouth (Fig. 54; NZ grid M 32 E 24670 / N 58459). The local sequence comprises mainly of alternating thin layers of fine sand and silt with interbeds of medium sand and rare beds of coarse sand, granules and pebbles. Contacts between laminae often undulate and form gradationally bound sets of small scale climbing ripples. Bedding contortions are common at silts-sand contacts where originally planar laminae are disrupted by cm-scale flame structures. The gravels and the overlying 0.4 m of fine sand form the T 4 terrace surface.

Interpretation: Fine grained sediments of the Carlyle terrace sequence are interpreted as lacustrine deposits. Grain size distributions indicate deposition in slack water with the cross laminated sand interbeds suggesting a lower flow regime fluvial input. At the top of the section a 1.9 m thick veneer of sand beds may reflect deposition during lake low stands. The lacustrine sequence is truncated by a 1.8 m thick unit of coarse fluvial degradational gravels overlain by loess. IRSL ages from the basal lacustrine units indicate deposition at 95.7 ± 6.8 ka (WLL-355) while the loess overlying the degradational gravels yielded an age of 18.2 ± 1.6 ka (WLL-359).

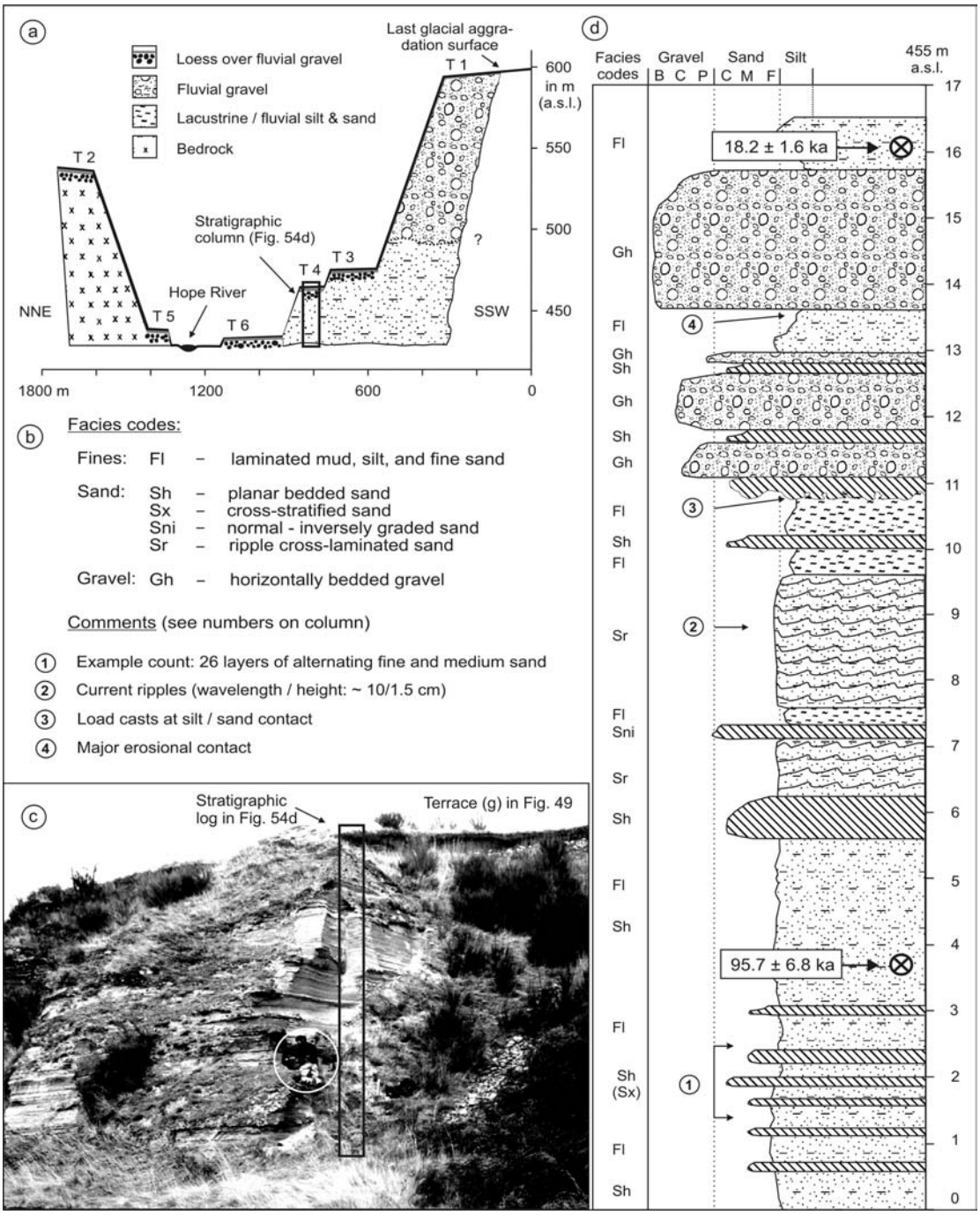

Fig. 54: Overview of sediments, depositional context and stratigraphy at the Carlyle terrace exposure. The logged section is shown in the photo (c). Note person for scale.

6.3.3.3. Middle Hope Valley

The logged outcrop is located in the middle Hope Valley approximately 5 km upstream of the confluence between the Hope and Boyle Rivers (Fig. 55; NZ grid M32 E 24563 / N 58441). Erosion at the north bank exposed a roughly 40 m thick sequence of sediments above the modern river. Basal deposits comprise a 20 m thick

unit of slightly downstream dipping laminated muds with a dominant grain size in clay. The basal contact of the muds is not exposed and probably lies below the modern floodplain. Individual laminae range in thickness between 5-15 mm and are highly cohesive. Small scale normal faulting with offsets between 20-50 mm is common. A block of sediment from this deposit was sampled for luminescence dating. At the top the muds grade into 1.5 m of planar bedded sand which is not accessible at the face. Above this there are 15 m of gravels which dip distinctly at ~32˚ in a downstream direction. The unit consists of 200-400 mm thick beds of clast supported pebbles and small cobbles. Interbeds of openwork gravel and sand occur. These gravel beds are truncated and are overlain by a at least 30 m of near horizontally bedded cobbly gravels which are exposed over a lateral distance of 200 m.

Interpretation: Laminated muds exposed at river level are of lacustrine origin and probably continue below river level indicating that the lake in which they were deposited extended below the present floodplain. The deposit yielded an IRSL age of 34.4 ± 2.5 ka (WLL-411) suggesting deposition during OIS 3. Coarsening upwards into lacustrine sand both basal units are interpreted as delta bottomset deposits which are overlain by dipping gravel beds that represent a prograding delta foreset sequence. The planar bedded gravel package is coarser (cobbles) than the underlying foreset unit (pebbles). The upper unit is interpreted as a delta topset deposit which grades upwards into fluvio-aggradational gravels. Clasts in the aggradational gravel package (mainly cobbles) are smaller in size than the boulder dominated fluvial deposit of the present floodplain. Lacustrine deposition at ~34 ka in the middle Hope Valley indicates that the valley portion was still ice free, although glaciers may have occupied the valley at some distance upstream. The cause for local lake formation during OIS 3 is not known but a possible explanation is damming by a rapidly accumulating aggradation fan in the trunk valley which outpaced aggradation in the middle Hope Valley and blocked this valley segment. A similar event probably caused the deflection of the Kakapo River from Dismal Valley to its present course further to the south (see Chapter 4). A large aggradation fan in the trunk valley would have reduced valley gradient and stream power in the middle Hope Valley which would explain the relatively smaller clast sizes of the glacio-aggradational gravels, compared to the present floodplain deposit.

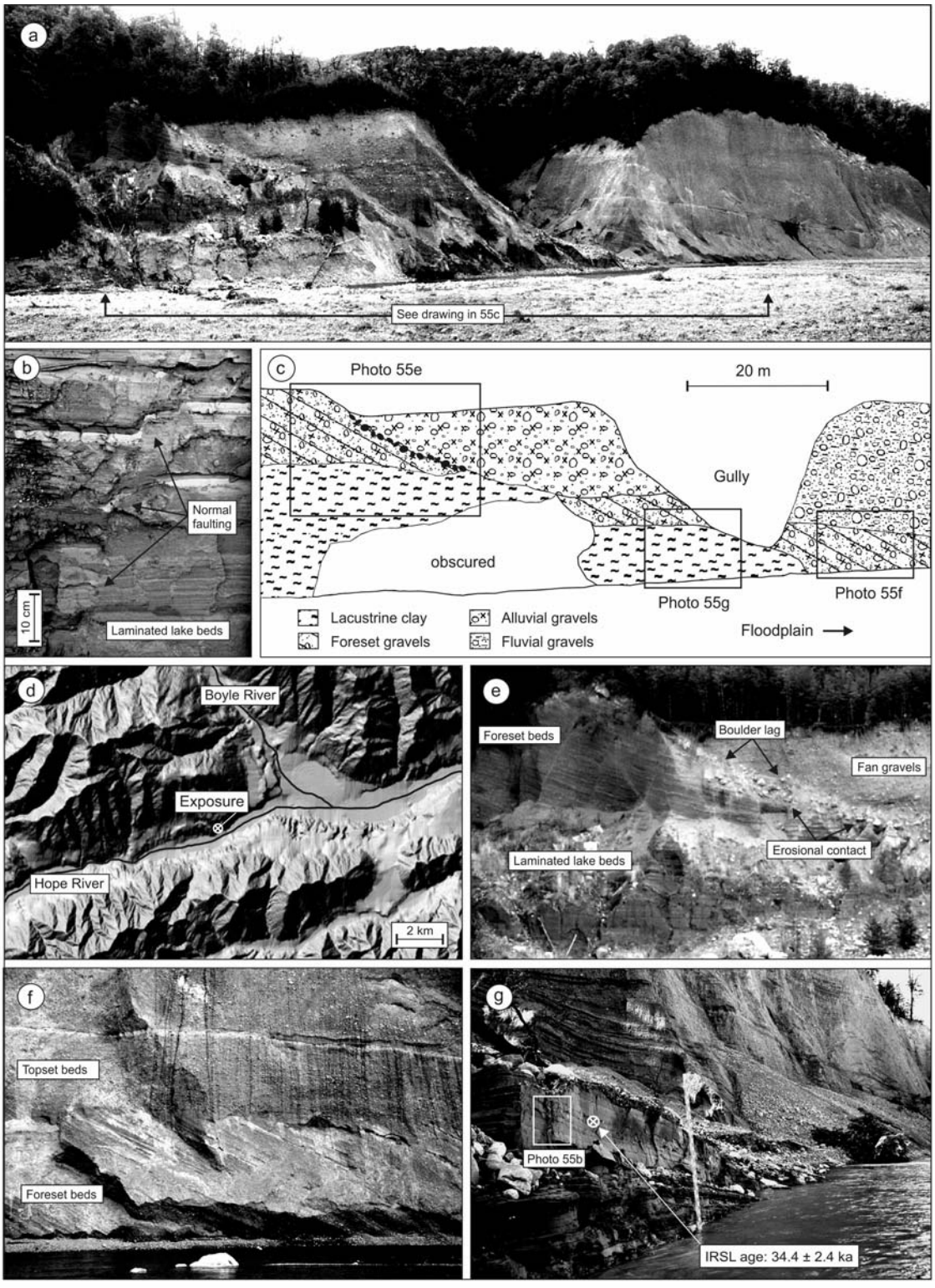

Figure 55: Overview of deposits and stratigraphy in the middle Hope Valley. The location of the logged exposure relative to the confluence of the Hope and Boyle Rivers is shown in (d). Laminated and faulted lacustrine muds are exposed at river level (b, g) and were sampled for IRSL dating. The muds are overlain by a delta sequence which is capped by glacio-fluvial gravels (e,f).

6.3.3.4. Horseshoe, Kakapo and Glynn Wye Terraces

Terrace landforms in the lower Hope Valley occur up to 450 m above river level. The highest surface remnants are preserved at 850 m a.s.l. and 700 m a.s.l. and have been associated with aggradation during OIS 6 and OIS 8 (Clayton, 1968). Exposures of deposits that form these surfaces are rare and sedimentary logging was limited to

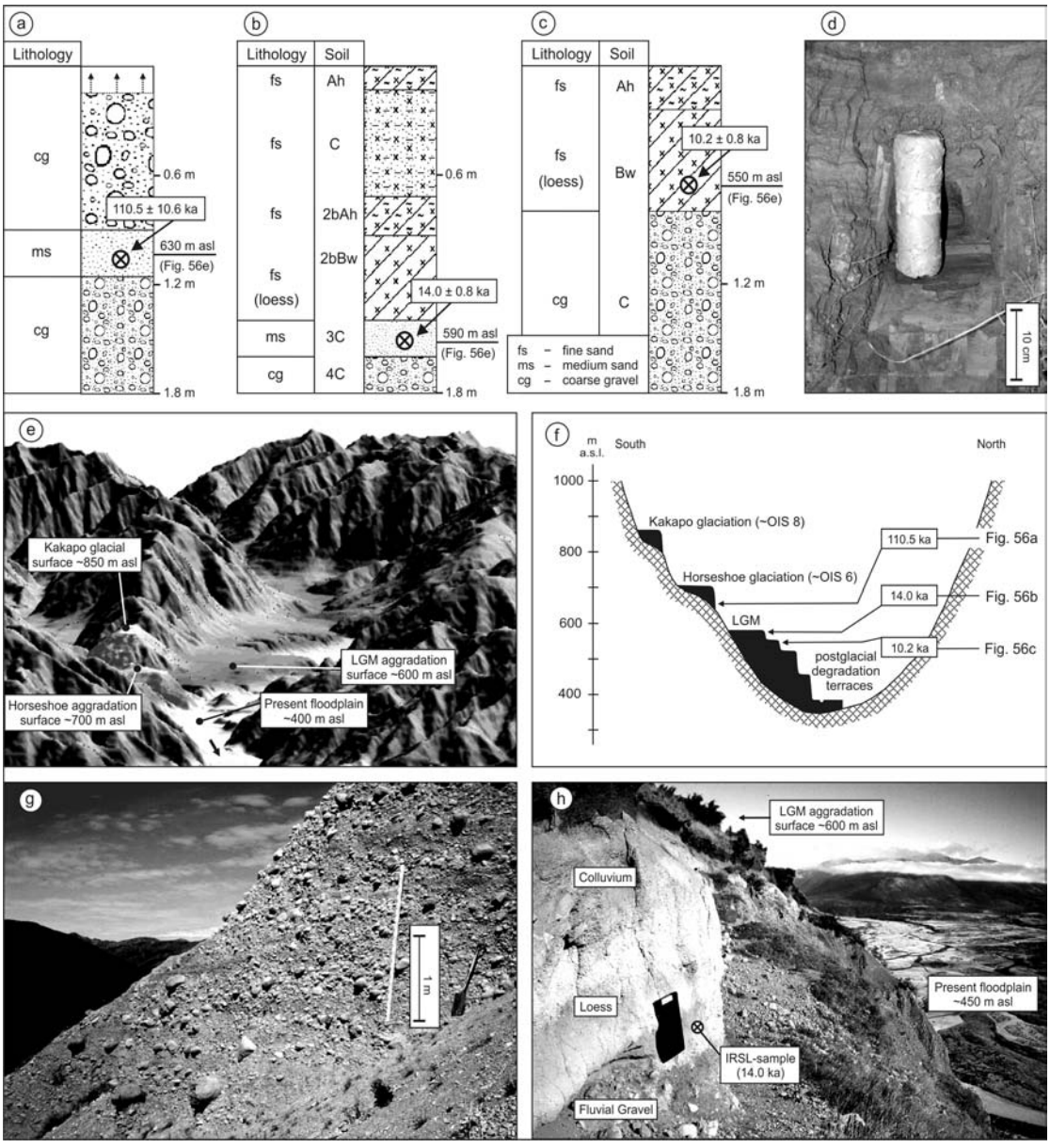

Fig. 56: Overview of sediments and stratigraphy of glacial outwash terraces in the Hope-Waiau Valleys. Figures 56e and 56f show location and context of sediments and IRSL samples from profiles shown in (a-c). The view into the Waiau and lower Hope Valley presented in (d) is DEM generated. Photo (f) shows Horseshoe aggradation gravels situated ~250 above modern river level, and (d) shows LGM gravels near the terrace surface ~150 above floodplain level.

outcrops caused by two larger slips and along farm tracks. Horseshoe surface exposures (Fig. 57a) display largely uniform packages of stratified and well rounded gravels which resemble in sorting and grain size the floodplain deposits of the present Hope River. Marked differences, however, are noted with regard to sediment colour, matrix abundance and overall sediment compaction. While gravels of the present floodplain and the last glacial aggradation surfaces are mainly grey coloured (Munsell codes 10YR 5/1 and 6/1), gravels associated with higher surfaces often display light orange colours (Munsell codes 10YR 6/6 to 7/6, Fig. 57). Fresh surfaces on split clasts indicate that the colour tone is associated with mm-thick coatings on weathering rinds of the clasts. Spaces and pores between grains are almost completely filled with

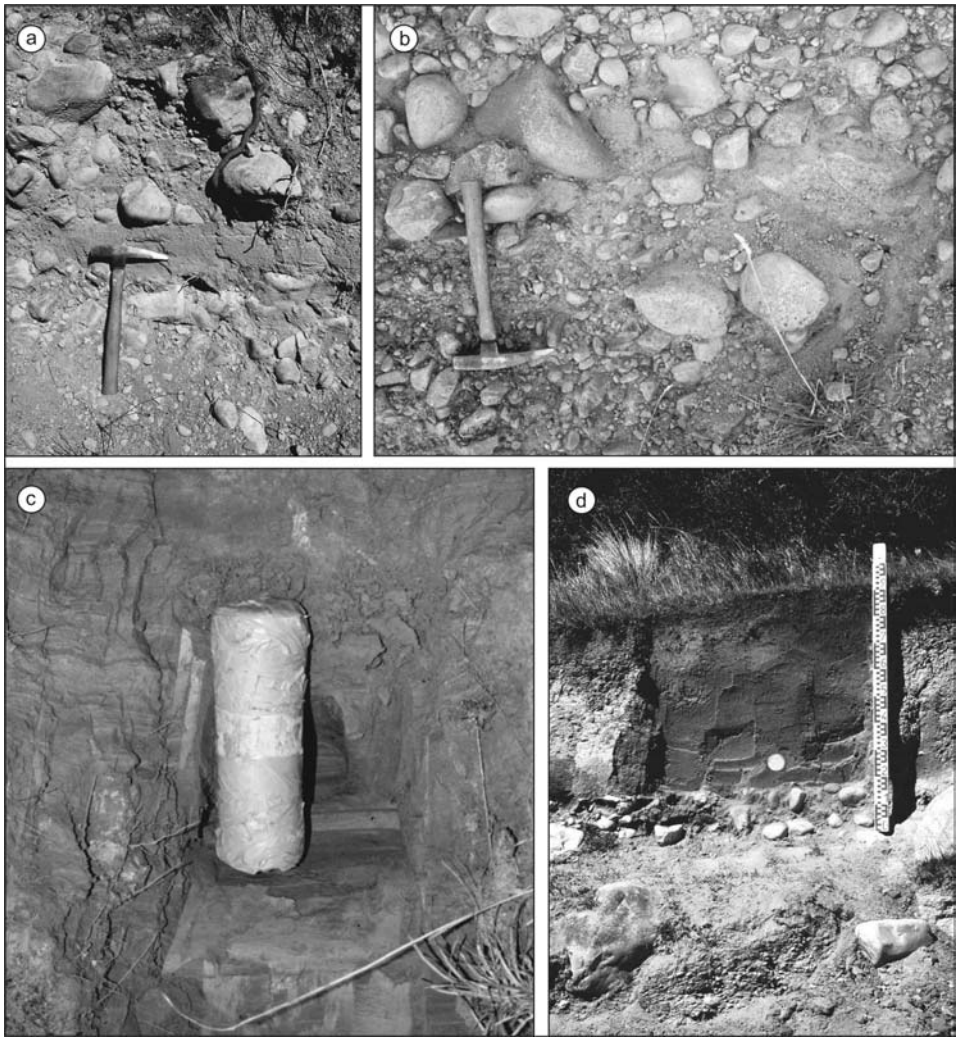

Fig. 57: Sand and silt units sampled for IRSL dating. The thin sand bed within Horseshoe gravels at the hammer head in (a) yielded an age of ~110.5 ± 10.6 ka, the loess sheet overlying degradational gravels in (d) gave an age of 14.0 ± 0.8 ka. Photo (c) shows the 22 cm long and 7 cm wide metal cylinder after recovery from the sediment. Photo (d) shows the IRSL sample cylinder after it was hammered into the face. Note the oxidized colours of Horseshoe gravels shown in (a-b).

fines which contributes to the greater induration of these gravels. The features are interpreted to have resulted from weathering over extended periods of time, which has formed the basis for suggesting that these higher gravel packages are of greater relative age than those at lower elevations (Clayton, 1968). Terrace surfaces in the lower Hope Valley are overlain by loess that varies in thickness between 0.3 – 1.5 m and comprises up to two identifiable sheets. Luminescence samples were recovered from sands within Horseshoe aggradation gravels (NZ grid M32 E 24722 / N 58440; Fig. 56a and 57a), as well as from the basal portions of loess cover beds on the LGM aggradation surface (NZ grid M32 E 24683 / N 58458; Fig. 56c, g) and degradational terraces (NZ grid M 32 E 24670 / N 58459; Fig. 57d; M32).

6.4. IRSL results

Eight IRSL samples were retrieved from fine sediments interpreted as lake beds, overbank deposits, sand interbeds in coarse gravels and loessial cover beds. All measurements were conducted at the Victoria University Dating Laboratory in Wellington, New Zealand. The sampled lacustrine, fluvial and aolian sediments were all subaerially deposited and are interpreted to have had a good chance of signal zeroing prior to sedimentation. Seven of the IRSL ages were determined using a multiple-aliquot additive-dose method on silt sized grains of feldspars. One of the samples (WLL-354) did not contain enough silt material and a Single Aliquot Regenerative (SAR) method was used using sand sized grains of quartz. Both techniques were summarized in chapters 4 and 5 (sections 4.4.2. and 5.4.2.). Two samples (WLL-359, WLL-422) displayed a minor radioactive disequilibrium (significant on 2σ-level) between ^{234}Th and ^{226}Ra probably due to Radium migration associated with water flow. One sample (WLL-412) showed a small radioactive disequilibrium between ^{226}Ra and ^{210}Pb probable due to influx of Radium. Since the level of disequilibrium over time is unknown, the result is provided as an estimate of the true age only. A summary of the dosimetric data is provided in Table 8 and all equivalent doses (D_e) and resulting luminescence ages in Table 9.

The oldest IRSL age was obtained from a medium sand lens (shown in Fig. 57a) interbedded with coarse gravels situated ~ 250 m above the modern river level. The gravels are located at an elevation ~50 m above the LGM sequences and Clayton

(1968) associated the deposits with aggradation during the penultimate Horseshoe glaciation. The sample gave an age of 110.5 ± 10.6 ka (WLL-422) suggesting deposition during early OIS 5 or late OIS 6 which broadly confirms the correlation of Clayton (1968).

Tab. 8: Sample and radioactivity data for luminescence dating.

Sample	Grain size (µm)	Water content (δ)[a]	U (µg/g) from ^{234}Th	U (µg/g)[b] ^{226}Ra, ^{214}Pb, ^{214}Bi	U (µg/g) from ^{210}Pb	Th (µg/g)[b] from ^{208}Tl, ^{212}Pb, ^{228}Ac	K (%)	dD_e/dt (Gy/ka)
WLL-354	90-200 µm	1.101	2.15±0.34	1.98±0.04	2.07±0.34	8.97±0.13	2.14±0.05	0.0309±0.0015
WLL-355	4-11µm	1.194	2.50±0.37	2.08±0.04	1.95±0.36	9.37±0.14	2.13±0.05	0.0852±0.0043
WLL-359	4-11µm	1.241	3.11±0.32	2.16±0.04	2.26±0.30	10.69±0.14	2.16±0.04	0.2052±0.0103
WLL-411	4-11µm	1.211	3.22±0.21	3.11±0.04	3.45±0.20	12.46±0.13	2.30±0.05	0.0195±0.0010
WLL-412	4-11µm	1.130	2.10±0.25	1.94±0.04	2.71±0.24	8.61±0.12	1.88±0.04	0.1853±0.0093
WLL-413	4-11µm	1.210	2.92±0.29	2.44±0.04	2.11±0.24	11.30±0.15	1.81±0.04	0.1853±0.0093
WLL-422	4-11µm	1.266	2.67±0.19	1.96±0.03	2.01±0.16	10.66±0.11	2.13±0.04	0.1185±0.0059
WLL-423	4-11µm	1.130	2.17±0.22	2.20±0.03	2.34±0.20	9.65±0.12	2.21±0.05	0.0943±0.0047

[a] Ratio wet sample to dry sample weight.
[b] U and Th-content is calculated from the error weighted mean of the isotope equivalent contents.

Table 9: Measured a-value and equivalent dose and calculated dose rate and luminescence age.

Sample	a-value	D_e (GY)	dD/dt (Gy/ka)	**IRSL age (ka)**
WLL-354	N/A	139.9 ± 39.1	3.07 ± 0.13	**45.5 ± 12.9**
WLL-355	0.041 ± 0.009	319.0 ± 6.4	3.33 ± 0.23	**95.7 ± 6.8**
WLL-359	0.052 ± 0.004	66.8 ± 3.3	3.67 ± 0.25 (3.56 ± 0.25)	**18.2 ± 1.6** (18.8 ± 1.6)
WLL-411	0.093 ± 0.006	154.1 ± 5.1	4.48 ± 0.29	**34.4 ± 2.5**
WLL-412	0.057 ± 0.003	50.3 ± 1.6	3.59 ± 0.15 (3.44 ± 0.15)	**14.0 ± 0.8** (14.6 ± 0.8)
WLL-413	0.066 ± 0.006	36.8 ± 1.7	3.61 ± 0.23	**10.2 ± 0.8**
WLL-422	0.053 ± 0.018	375.5 ± 10.7	3.40 ± 0.30 (3.32 ± 0.30)	**110.5 ± 10.6** (113.2 ± 10.6)
WLL-423	0.058 ± 0.004	344.6 ± 1067	3.86 ± 0.18	**89.3 ± 5.0**

IRSL results from Glynn Wye Stream (Fig. 52) yielded ages of 89.3 ± 5.0 ka (WLL-423) for lake beds near the base of the sequence and 45.5 ± 12.9 ka (WLL-354) for overbank fines in the stratigraphically higher gravels. The latter age was obtained

from ~65 m below the Glynn Wye terrace surface, which is traditionally considered to represent the LGM aggradation terrace (Knuepfer, 1988; Cowan, 1990). The ages are stratigraphically consistent and suggest that deposition of the Glynn Wye sequence commenced during late OIS 5. The basal OIS 5 deposits overlie a tilted bedrock strath terrace which indicates a period of fluvial incision that preceded the onset of substantial valley sedimentation in the lower Hope Valley. The strath terrace suggests that pre-OIS 5 fluvial incision reached a valley floor level similar to or below that of the present day.

The OIS 5 units are overlain by a thick sequence of gravels. An IRSL sample from gravels stratigraphically ~80 m above the basal sample indicates aggradation of these units during early-mid OIS 3 (<45 ka, WLL-354). No major erosional breaks are apparent in the GWS sequence that would suggest glacial erosion during OIS 4. Similarly, the exposed sequence shows no evidence to infer glacial deposition, ice proximity or potential glacial overriding during OIS 4. A substantial portion of the stratigraphy has no numerical age control (i.e. between 420 – 490 m a.s.l., Fig. 52). Therefore, although sediments at GWS cover the time span from OIS 5 to OIS 3/2, the sequence provides little information about the depositional (or erosional) processes during OIS 4 (73 – 59 ka).

At Carlyle terrace (Fig. 54), 2 km upstream from the GWS site, basal lacustrine deposits were dated to 95.7 ± 5.0 ka (WLL-355). The result supports the dating of stratigraphically correlated lacustrine sediments at the base of GWS (i.e. ~20 m above modern river level) and suggest the presence of a large paleo-lake during OIS 5. The loessial cover beds that overlie degradational fluvial gravels at Carlyle terrace (~450. m a.s.l.) gave an age of 18.2 ± 1.6 ka (WLL-359). Two further samples from loess overlying the LGM aggradational terrace (~590 m a.s.l.) and an intermediate degradational terrace (~550 m a.s.l.) returned ages of 14.0 ± 0.8 ka (WLL-412) and 10.2 ± 0.8 ka (WLL-413), respectively. Because the 18.2 ka age comes from the lowest of the three dated terraces, it conflicts with the stratigraphically consistent 14.0 ka and 10.2 ka ages from the higher terraces. The 18.2 ka age also conflicts with results from cosmogenic dating (presented in Chapter 7) and is therefore considered an outlier.

6.5. Discussion and summary

6.5.1. Valley fill and sedimentary architecture

Volumetrically, the majority of the fill sequence in the Hope-Waiau Valleys consists of coarse and poorly sorted fluvial gravels which were laid down by mainly paraglacial braided river systems. The well rounded clasts of these deposits are predominantly of cobble to boulder size and consist almost entirely of local sandstones (greywacke) with only minor contributions from conglomerate and argillite lithologies. In addition to fluvial gravels a substantial portion of the valley fill stratigraphy comprises of fine grained lacustrine sediments that were found at GWS, Carlyle Terrace, the middle Hope Valley, as well as at the previously described Glynn Wye and Poplars Gully sites (Chapters 4 and 5). Based on stratigraphic context and luminescence data all of the lacustrine sequences predate the LGM and represent previously unrecognized early lake phases in the Hope-Waiau Valleys. Younger (i.e. postglacial) paleo-lakes have been confirmed from the lower Boyle (Clayton, 1965; 1968) and Lewis Valleys (Fig. 58). In the lower Doubtful Valley wood from laminated delta bottomsets was dated to 12,450 ± 200 a BP (Chinn, 1981a). The overall lake sizes varied from relatively small (GWS) to substantial (Kakapo Delta, Carlyle Terrace, Poplars Gully). Sedimentological, structural and geochronological properties of the lake sequences indicate a range of lacustrine environments varying from ice proximal (Poplars Gully), through ice distal (Kakapo Delta; lower Boyle Delta; Clayton, 1968) to ice free and interglacial conditions (GWS).

Volumetrically small components of the overall fill succession are contributed by alluvial fan sediments and even less by glacigenic deposits. Based on the relative sedimentary proportions it becomes apparent that fluvio-lacustrine deposits form the principal component of the local glacio-aggradational fill sequence. The dominant ‘aqueous’ sedimentary style, which characterizes even clearly ice proximal and subglacial sedimentary successions (e.g. Poplars Gully, Chapter 5), suggests that glacigenic sedimentation of valley glaciers in this part of the Southern Alps is insignificant, or, alternatively and more likely, that fluvial reworking appears to be

highly effective in re-depositing nearly all glacigenic sediments and consequently the glacigenic character of the original sediments is lost.

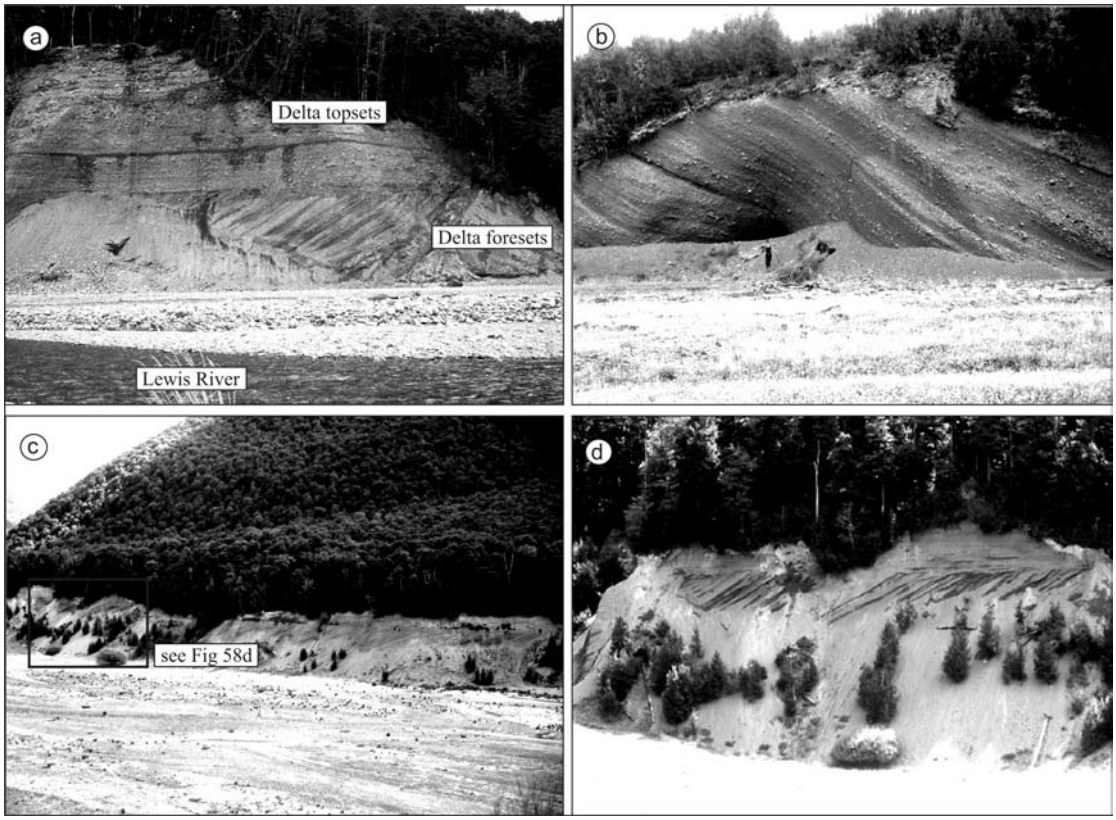

Fig. 58: Postglacial paleo-lake remnants in the lower Lewis Valley (a), lower Hope Valley (b) and lower Boyle Valley (c,d). The paleo-lake in the lower Boyle Valley has age control from ten radiocarbon dates giving ages between 13,3 - 10,7 ka BP (^{14}C ages in Clayton, 1968; Chinn, 1981a; Burrows, 1988, 1997; Turney et al., 2003).

6.5.2. Geochronology

The numerical dating of fill deposits between the middle Hope and Waiau Valleys show that sediments which have traditionally been considered to represent aggradation during the LGM, are in fact substantially older and instead were aggraded during OIS 5 and OIS 3. The IRSL dates confirm earlier results from previous chapters which also found that the valley fill sequence comprises mainly of sediments deposited during OIS 4/3 (Kakapo Delta) and OIS 6 (Poplars Gully). Because all luminescence ages were obtained from a 30 km long valley reach the results provide a relatively detailed record of the local Late Pleistocene valley sedimentation and exhumation during which sedimentary infilling and subsequent fluvial downcutting exceeded a vertical distance of at least 250 m.

The oldest date was obtained from gravels of the Horseshoe high surface (110 ± 10.6 ka) and falls into OIS 5 or possibly late OIS 6. Although age control of this surface is limited to this one age the result confirms Clayton's (1968) correlation of the Horseshoe glaciation with OIS 6. Following the OIS 6 glacial termination a period of postglacial fluvial downcutting is inferred to have exhumed the valley segment during OIS 5. This is indicated by fine grained lake sediments deposited at low elevation in the newly excavated valley trough (~300 m below Horseshoe surface). The sediments were dated at Glynn Wye Stream and Carlyle Terrace to 95.7 ± 6.8 ka and 89.3 ± 5.0 ka, respectively. At Glynn Wye Stream, these deposits overlie a bedrock strath terrace that is situated roughly 10 m above modern river level suggesting that the incised OIS 5 valley floor was at or below the present valley floor level (~405 m a.s.l.). Because the GWS site is located downstream and outside of the lower Hope Basin, it is improbable that the result reflects local basin subsidence. The survival of OIS 5 deposits at GWS and Carlyle terrace implies that possible erosion by an inferred but unconstrained OIS 4 glacial advance into the lower Hope and Waiau Valleys cannot have reached bedrock. This also suggests that the volume and ice extent during OIS 4 was smaller than that associated with the OIS 6 glaciation. Because OIS 5 deposits overly bedrock it is inferred that glaciation during OIS 6 eroded to bedrock and removed all earlier fills.

At both sites the basal sediments are overlain by gravel dominated aggradational sequences of more than 150 m thickness. A pre-LGM lake deposit dated to 34.4 ± 2.5 ka from the middle Hope Valley, which survived later ice overriding by the main LGM advances, indicates ice free conditions in the middle and lower valley at this time. The preservation of these deposits roughly 16 km upstream of the main LGM ice terminus (Glenhope advance) suggests that the LGM advance did not erode to bedrock in this part of the valley. Suggate (1973, p. 103) reported a 41,200 ± 2400 a BP radiocarbon age from a carbonaceous band found between two fans and below terrace gravels at Goings Creek 3 km south of Lewis Pass[1]. The age was considered dubious because Suggate (1973) expected pre-LGM deposits to have no chance of surviving the extensive LGM ice advances. However, results presented in this and earlier chapters have demonstrated that older deposits have survived ice overrun at

[1] Pollen from this deposit comprised grass, herb and podocarp Phyllocladus vegetation and is probably indicative of a cool climate.

many sites in the Hope-Waiau Valleys, and it is likely that the age from Goings Creek is correct also, with the proviso that 41.2 ka is a minimum age only.

The end of valley aggradation and onset of postglacial fluvial downcutting into the local sedimentary fill is constrained by a radiocarbon date of 14.1 ± 0.2 ka BP (17.5 ± 0.3 cal. ka BP) from organic silts in the Waiau Valley (Suggate, 1965) and an IRSL age of 14.0 ± 0.8 ka (WLL-412) from loessial cover beds overlying the main aggradational terrace in the lower Hope Valley. Both ages were derived from deposits indicating cessation of fluvial aggradation and abandonment of the last glacial aggradational floodplain level.

In summary, stratigraphic and geochronological results presented in this chapter suggest that extensive deposits dating to the penultimate and early last glacial cycles are preserved in the lower fill stratigraphy of the Hope Valley. Sedimentologically, the majority of the fill sequence is composed of (glacio-) fluvial and (glacio) lacustrine deposits while alluvial and glacial deposits are volumetrically less important. Paleo-lakes of various dimensions occupied the Hope Valley around ~90 ka, ~35 ka and 13 – 11 ka BP.

CHAPTER 7

SURFACE EXPOSURE DATING OF GLACIAL MORAINES IN THE HOPE-WAIAU VALLEYS

7.1. Introduction

The review of the available geochronological data on Late Pleistocene glaciations in New Zealand (section 2.3) has shown that few direct ages constrain the timings of former glacial advances in the eastern Southern Alps. The temporal response of Southern Hemisphere glaciers to Quaternary climate signals, however, has become a prime research focus in the global climate dynamics debate (e.g. Ivy-Ochs et al., 1999; Kaplan et al., 2004; Shulmeister et al., 2005). The lack of high resolution absolute dating limits the usefulness of New Zealand data in this debate despite the fact that the Southern Alps provide one of the key glacial records from the mid-latitude Southern Hemisphere. It is also a major obstacle for resolving the controversy on the paleo-climatological interpretation of New Zealand glacial data (e.g. Ivy-Ochs et al., 1999; Easterbrook, 2004; Shulmeister et al., 2005; Anderson and Mackintosh, 2006a; see also Chapter 8). To address this, this chapter presents results from Surface Exposure Dating (SED) of glacial moraines in the Hope-Waiau Valleys which uses an *in-situ* produced cosmogenic radionuclide (^{10}Be) from moraine boulders. SED measures the length of time that a freshly eroded boulder (or bedrock) surface has been exposed to cosmic rays. For the technique to work there must be at least 1 – 3 m of rock eroded from any pre-exposed surface. Because glacial plucking and abrasion are highly effective in eroding rocks, SED has shown to be reliable for dating glacial events. Critical advantages over other dating techniques are that ^{10}Be SED can directly date moraines as it uses quartz minerals from common lithologies in moraines and ice carved bedrock (e.g. sandstones, granites) and that ^{10}Be has a half live of 1.5 Ma which theoretically allows age determinations far beyond the range of luminescence and radiocarbon dating. A brief summary of the SED technique and descriptions of the sampling procedure, chemical sample preparation, and the isotopic measurement process are given in sections 7.2 and 7.3.

As part of the effort to obtain age control on the overall glacial sequence in the Hope-Waiau Valleys all key moraines of the trunk glacial valley were sampled. This chapter presents ^{10}Be results from three moraine systems (1,5,7 in Fig. 59). However, because of substantial delays in the chemical rock preparation none of the ^{10}Be results from the other moraines and no ^{26}Al age determinations are available at the completion of this thesis despite all samples having been submitted for laboratory processing in early 2004. Final age determinations are expected within the next six months and the complete cosmogenic geochronology is intended for publication once all ages are available.

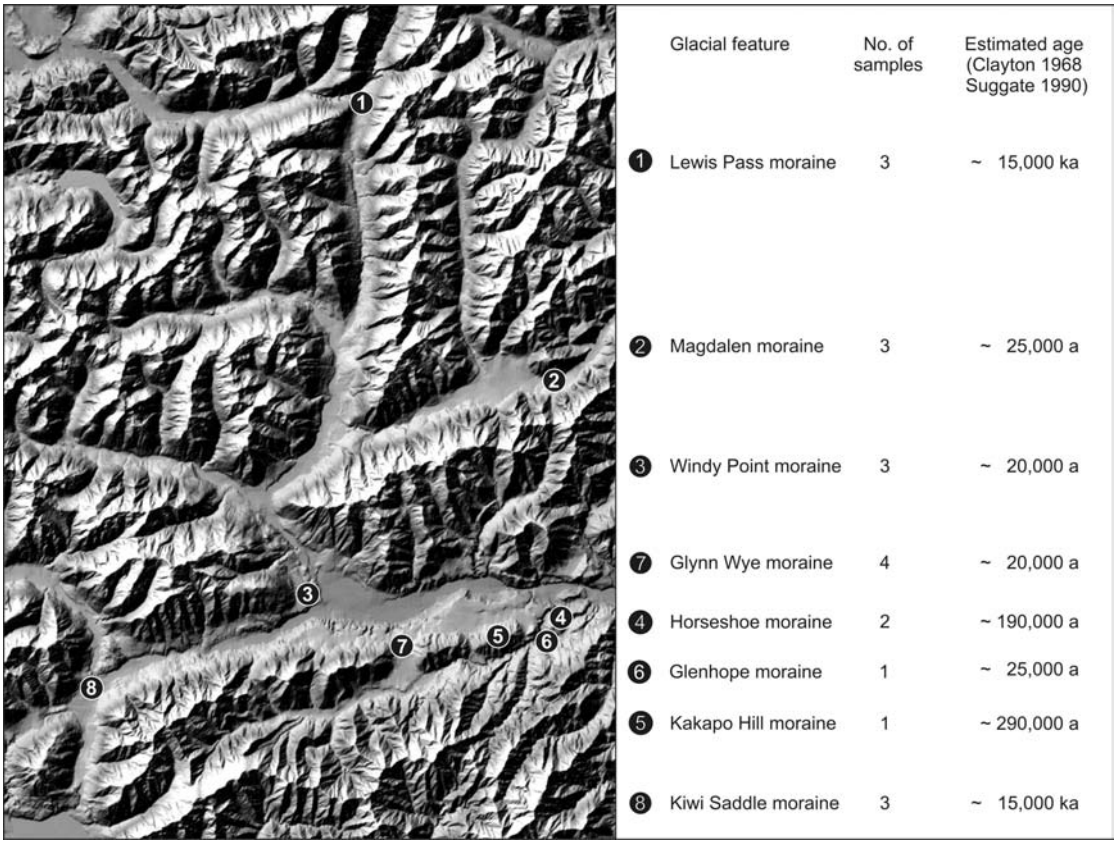

Fig. 59: Moraine locations sampled for exposure dating. ^{10}Be results for moraine sequences 1, 5, and 7 are reported in this chapter. All sample grid locations are given in Appendix 2.2.

7.2. Cosmogenic dating: background

The time dependent production of measurable amounts of cosmogenic nuclides in terrestrial rock surfaces allows the use of cosmogenic isotopes as geochronometers. *In situ* produced terrestrial cosmogenic nuclides (TCNs) are defined as sub-atomic elements which are produced through the bombardment of rock by cosmic rays

(Gosse and Phillips, 2001). Cosmic radiation received on Earth is primarily composed of high energy nucleons, which originate from the sun and deep space. Upon contact with Earth's upper atmosphere the particles cause nuclear disintegrations and create a wide array of secondary particles (e.g. protons, neutrons, mesons, muons) which in turn cause further nuclear interactions resulting in a complex cascading particle shower (Fig. 60). The trajectory and momentum of the incoming particles are heavily influenced by Earth's magnetic field and past variations in the dipole field strength must be accounted for to correctly calculate the terrestrial nuclide production rates through time.

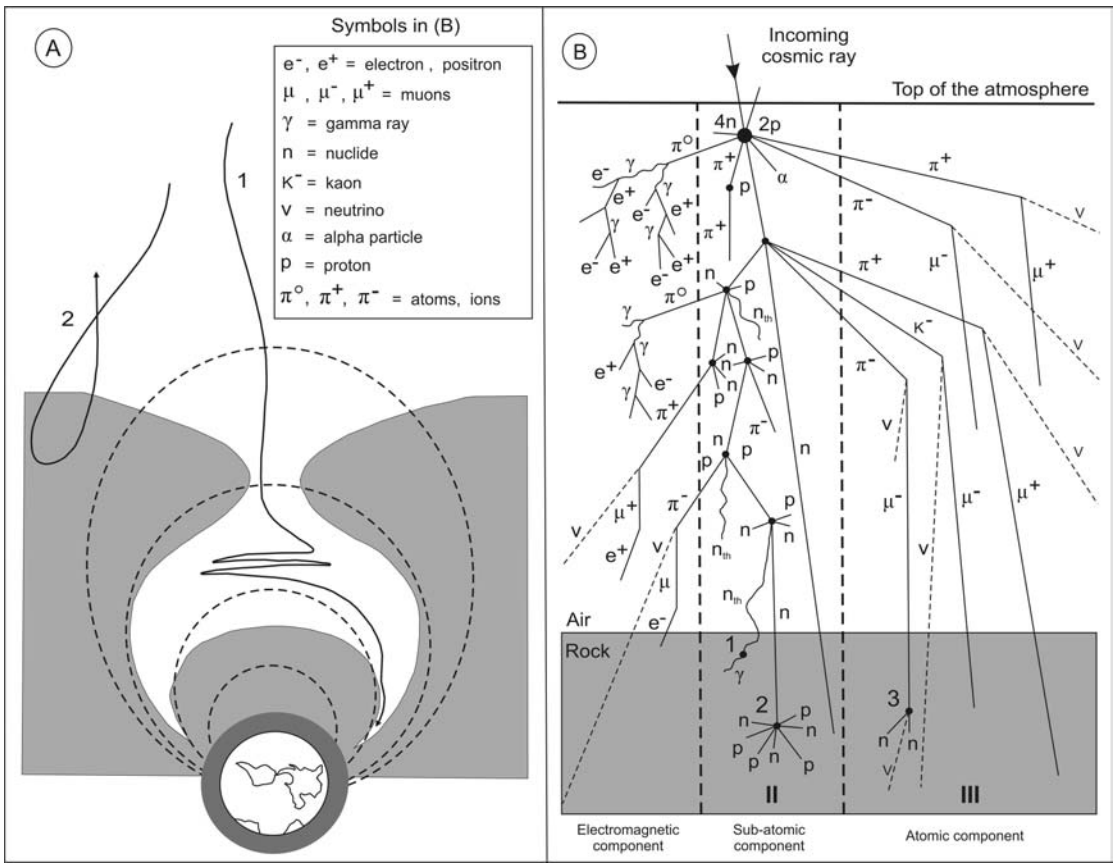

Fig. 60: Trajectories of cosmic ray particles that approach Earth's western magnetic dipole field (A). Low energy particles are mostly deflected away from Earth while higher energy flux may penetrate the magnetic field. Non-elastic interaction with atmospheric particles (B) initiates extensive nuclear disintegrations resulting in a cascading shower of descending secondary particles. Most of the charged particles are slowed down due to loss of ionization energy but uncharged secondary neutrons remain highly energetic and can cause nuclear disintegrations in the shallow lithosphere. It is this sub-atomic component that produces ^{10}Be from ^{16}O and ^{28}Si in SiO_2 minerals (modified from Gosse and Phillips, 2001; Zondervan, 2004)

Secondary particles produced in the upper atmosphere hit terrestrial surfaces and can penetrate the upper few meters of the lithosphere. ^{10}Be isotopes are produced *in situ*

largely from spallation of ^{16}O and ^{28}Si in Quartz. During the process a high energy neutron collides with the^{16}O and ^{28}Si targets and breaks off several lighter nuclei including ^{10}Be. Empirical ^{10}Be production rates in rock (at sea level and >60° latitude) range from 4.74 atoms g^{-1} yr^{-1} (Clark et al., 1995) to 6.4 atoms g^{-1} yr^{-1} (Brown et al., 1991). The ^{10}Be ages presented in this chapter are based on the more recently measured and now widely accepted production rate of 5.1 ± 0.3 atoms g^{-1} yr^{-1} of Stone (2000). ^{10}Be atoms accumulate in quartz minerals at the rock surface and samples can be analysed for miniscule amounts of ^{10}Be using ultrasensitive accelerator mass spectrometry (AMS). The measurable $^{10}Be/^{9}Be$ ratios spans 4 orders of magnitude, from 10^{-10} to 10^{-14}, with a detection limit of 3.0×10^{-14} atoms per gram. Because the production rate and half life of ^{10}Be are known the measured concentration can be used to calculate the amount of time that has elapsed since ^{10}Be production began (i.e. exposure). In order to calculate correct exposure ages, the 'raw' age determinations must be corrected for a variety of factors such as geomagnetic field variations and potential loss of surface material through mm-scale erosion (see section 7.3.3.).

7.3. Methods

7.3.1. The sampling campaign

The Quaternary geology and moraine positions of the Hope-Waiau Valleys were reviewed in detail in earlier chapters (sections 3.3., 4.3., 5.3.) and a map with all ice limits is shown on p. 44. Sampling for exposure dating concentrated on erratics associated with the key moraines in the trunk valley. Boulders were selected based on size and geomorphic setting while sampling usually targeted the largest available block (Fig. 61). In seismically active regions like the Hope-Waiau Valleys ground shaking associated with earthquakes is a potential problem for SED as this may cause boulders to move after primary deposition which would change the orientation of the exposed boulder surface in relation to the incoming cosmic rays. Because the geometric parameters, which in part determine the local ^{10}Be production rate, are assumed to have remained constant throughout the exposure time, post-depositional boulder movement would result in an incorrect (young) age. To avoid this problem only large boulders (minimum diameter: ~1.5 m) were sampled, while boulders in

Fig. 61: Boulders sampled for cosmogenic dating from the Glynn Wye moraine (a), Glenhope moraine (b), Kakapo moraine (c) and Kiwi Stream moraine (d). Photos (e) and (f) show quartz veins of erratics from the Windy Point and Lewis Pass moraines. Generally, 1-2 kg of rock was chiseled from the top 1-4 cm of each boulder (g, h). The sample from Kakapo Hill (c) comes from the only large boulder suitable for cosmogenic dating. The sample was obtained from the steep (~40°) eastern side of the boulder (indicated by the person on boulder in photo c).

potentially unstable positions were avoided (e.g. on steep slopes). All samples come from boulder surfaces which were at least 0.6 m above the surrounding ground to reduce the possibility of sampling a formerly buried boulder. Boulders near erosional features (e.g. channels, gullies) were avoided, as were blocks that showed signs of splitting and spallation. Rock samples were obtained by chiselling off an up to 4 cm thick piece of rock preferable from the centre of flat boulder surfaces. Most samples are whole-rock greywackes (quartz-arenites and feldsarenites) while in a small number of cases protruding secondary quartz veins were sampled (Fig. 61e-f). In total 22 samples of 1.5 - 4 kg weight were collected. Data recorded at each boulder include the grid position, altitude, sample thickness, angle of sampled surface and horizon shielding. The principle sample details are given in Table 10 and Appendix 2.2.

Table 10: Sample name, NZ grid location (1:50,000) and description of reported moraine boulders. Sample GW-B comes from the same boulder as GW-I.

Sample	Moraine site	Grid reference	Altitude	Size (L x W x H)	Sample material
GW-I	7	M32 6254/4339	640 m	560 x 340 x 220	Sandstone
GW-II	7	M32 6254/4339	645 m	270 x 330 x 160	Sandstone
GW-III	7	M32 6257/4341	647 m	270 x 85 x 75	Sandstone
GW-B	7	M32 6254/4339	640 m	560 x 340 x 220	Sandstone
LP-I	1	M31 6066/6975	870 m	170 x 120 x 60	Sandstone
LP-II	1	M31 6062/6980	880 m	200 x 110 x 75	Quartz vein
KH-I	5	M32 6745/4362	830 m	250 x 150 x 170	Sandstone / quartz vein

7.3.2. Chemical preparation and isotope measurement

The chemical extraction of ^{10}Be isotopes from quartz of the sampled rock was undertaken at the newly established cosmogenic preparation laboratory of the Department of Geological Sciences (UoC.) and was supervised by lab manager Rob Spiers. The Hope-Waiau rocks were part of the first batch of samples processed in the lab and extensive equipment and procedure calibration was necessary before the extraction process could be started. Although cosmogenic dating was used previously in New Zealand (e.g. Ivy-Ochs et al., 1999; Shulmeister et al., 2005) chemical sample preparation for these studies was completed overseas while the results presented in this chapter are based on isotope extractions performed in New Zealand. The

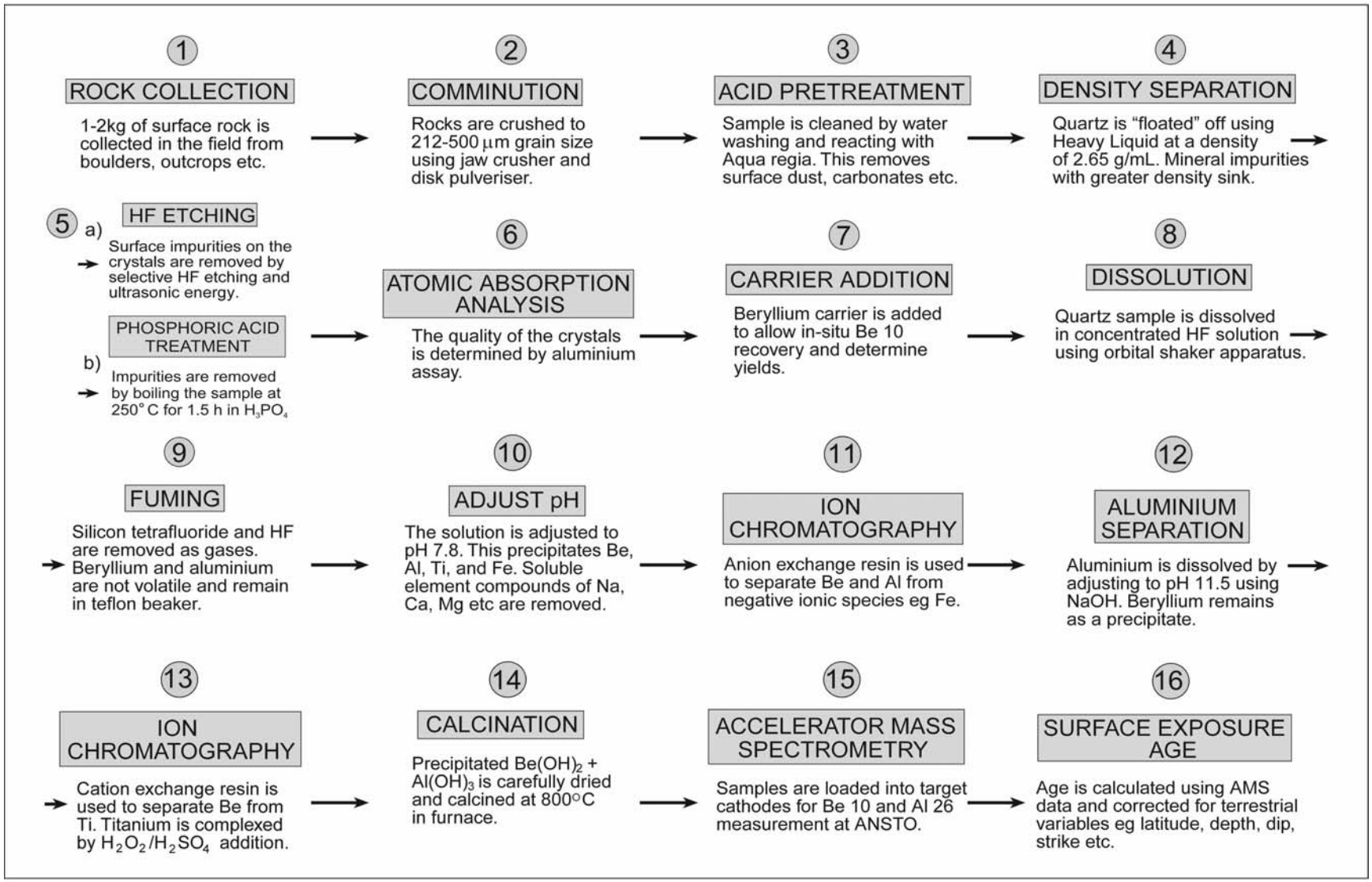

Fig. 62: Cosmogenic sample preparation flow diagram (modified procedure from ANSTO).

preparation process is time and labour intensive and Fig. 62 provides a summary of all necessary steps before final ^{10}Be concentrations could be measured using AMS.

During the first stages of laboratory preparation the rock is crushed and sieved to obtain grain sizes of 212-500 µm (step 2 in Fig. 62). About 300 g of the rock flour was used for further processing which ensured that a minimum of 30-50 g of pure quartz was available at the end of the cleaning process. Because ^{10}Be is also produced in the atmosphere (at a rate roughly 1000 times greater than within the rock) the sample was carefully cleaned (step 3) to ensure that the extracted ^{10}Be from the rock is not contaminated with atmospherically produced ^{10}Be. A substantial problem in the purification process was posed by the impurity of the quartz in nearly all greywacke samples. Repeated HF etching proved to be insufficient to clean the samples and an alternative phosphoric acid treatment was eventually used which yielded better results and was more time efficient (step 5). After each sample was checked for impurities using Atomic Absorption Analysis (step 6) the chemically identical but stable ^{9}Be isotope is added as a chemical carrier. This is necessary because ^{10}Be concentrations are usually too low to allow chemical extraction (step 7). Since the amount of added carrier is precisely known, only the ratio between ^{9}Be and ^{10}Be need to be measured by final AMS analysis. The isotope dilution method can be compared to the addition of exotic pollen to pollen sub-samples in order to control relative abundances (Gosse and Phillips, 2001). After several intermediary steps to dissolve, concentrate and pH-adjust the sample (steps 8 – 10), ion chromatography (steps 11 and 13) was performed to separate Be from anions and cations (e.g. Ti, Fe). Aluminium was precipitated by adjusting the ph-value to 11.5. The remaining Beryllium hydroxide was then oxidized in a furnace at 800˚C to produce the final pellet target that was measured using AMS.

The TCN concentration of the sample was analysed by counting individual ^{10}Be atoms using the ANTARES accelerator at ANSTO in Sydney. Measurement began by focussing a Cs^{+} beam at the sample producing ions from the ^{10}Be source which were then magnetically deflected into the eight million volt (MV) accelerator where the ions are accelerated to about 10% the speed of light. Based on the known atomic mass of Be radioisotopes magnetic deflection was used to filter all atoms that do not have the correct mass or energy level while bending the target isotope trajectory into an ion

detector where individual atoms were counted by means of measuring the released ionization energy.

7.3.3. Data correction

From the seven samples of the Hope-Waiau Valleys four come from the inferred main LGM moraine complex at Glynn Wye Station, two from the late glacial Lewis Pass moraine, and one sample from the high surface of Kakapo Hill which is thought to represent glaciation during OIS 8 (correlations from Clayton, 1968; Suggate, 1990). Exposure ages were calculated based on the local ^{10}Be production rates which were adjusted to geographic latitude and sample altitude. For the central South Island (41°-47°) production rates roughly double from sea level to 1000 m a.s.l. (Fig. 63). Based on these adjustments a 'raw' exposure age was reported by the AMS laboratory which is shown in table 11. The final ages, which include corrections for geomagnetic variations, horizon/slope shielding, and sample thickness have not yet been provided by the laboratory. Because the corrections usually move final ages in both directions

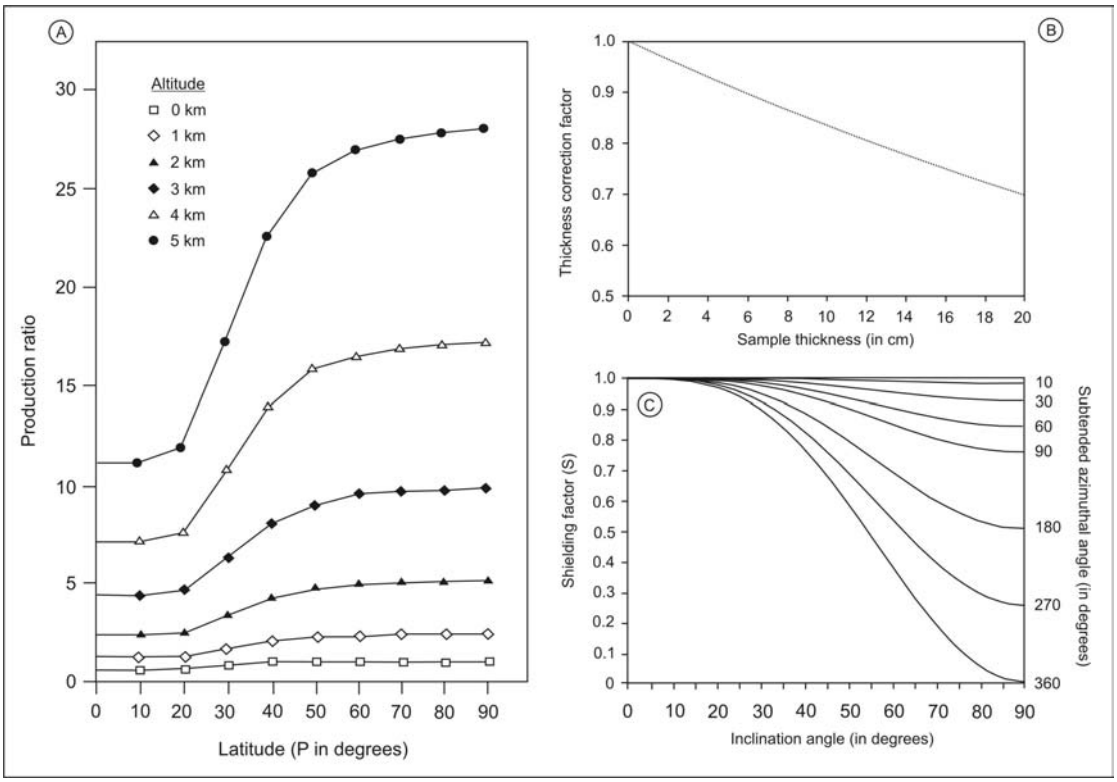

Fig. 63: Scaling factors for production rates of *in-situ* produced cosmogenic nuclides. Graph (A) shows the altitudinal increase, (B) the exponential decrease with sample thickness, and (C) the impact of horizon and slope shielding on nuclide production (Fink, 2003).

(e.g. sample thickness increases the age while geomagnetic corrections reduces it) fully corrected ages usually agree within 10% with the uncorrected age. Preliminary age corrections based on average values were performed by the writer and are explained in the following section.

Changes in the paleo-intensity of Earth's magnetic field, as indicated by marine sediment cores (Guyodo and Valet, 1999), are associated with slight temporal variations in the flux of cosmic rays that reach terrestrial surfaces. This can result in variations in the TCN production rate throughout the time of exposure. To account for the effect an average late Pleistocene geomagnetic correction factor of 1.05 was applied (Duna, 2000). Horizon shielding either from the slope of the sampled rock surface (internal shielding) or horizon blockage from surrounding mountain ranges (external shielding) reduces the amount of incoming cosmic rays and decreases the local TCN production rate. In the case of the reported boulders slope/horizon shielding was for most samples below 15˚ and thus necessary corrections for shielding were small (factors 0.85-0.95) and needed only to be applied to three samples (KH-1, LP-I. LP-II). As the capacity of cosmic rays to penetrate rock attenuates exponentially with depth, the production rate at the surface of a 10 cm thick sample is roughly 20 % higher than at the bottom (Fink, 2003). To minimize the error related to this effect rock sampling in the field targeted only the top 4 cm of the boulder. Variations in TCN production over this thickness were corrected by applying a depth integrated correction factor of 0.96 (Shulmeister et al., 2005). A further source of error for SED is potential erosion of the boulder surface which would cause loss of material and in an apparent age decrease. For the sampled boulders some surface erosion was indicated by protruding quartz veins (Fig. 61e-f) but the precise erosion rate is unknown. As erosion is likely to have affected the boulder surface an average erosion rate of 2 mm/ka was assumed and included in the age correction which increased the final exposure ages by ~4%. No variations in the solar particle flux and TCN loss due to radioactive decay were considered as they have negligible effects for samples younger than ~100 ka.

7.4 Results

Exposure ages from the Glynn Wye moraine range between 12.5 – 18.8 ka (Table 11). Two of the dates are statistically identical (GW-I, GW-II), one sample is younger (GW-III), and GW-B substantially younger. The age of GW-B (12.5 ± 2.8 ka) conflicts with results for GW-I (18.2 ± 1.7 ka) which was obtained as a b-sample from the same boulder and is supported by the 18.8 ± 2.0 ka of sample GW-II. A potential 12.5 ka age for the moraine is inconsistent with radiocarbon dates for a postglacial paleo-lake at the Boyle-Doubtful River junction (~10 km upstream from the Glynn Wye moraine) which suggest that deglaciation of the lower Hope and Boyle Valleys was complete by 15.0 - 14.5 cal. ^{14}C ka BP (Clayton, 1968; Chinn, 1981; Burrows, 1988).[1] The GW-B exposure age must therefore be erroneous and is considered an outlier. The boulder from Kakapo Hill (KH-I) yielded a date of 20.5 ± 1.7 ka. KH-I was the only sample where the corrected age deviates by more than 10% from the raw age. The effect is due to the higher than average internal shielding correction (factor 0.85) because the sample was taken from the steep eastern face of the boulder (Fig. 61c). Results for moraines at Lewis Pass, which are located roughly 30 km upvalley

Fig. 11: ^{10}Be cosmogenic isotope exposure ages for moraine in the Hope-Waiau Valleys. All ages are reported with 1σ errors.

Sample	Moraine (no. in Fig.0)	^{10}Be / ^{9}Be ratio (x 10^{-16})[a]	^{10}Be (x 10^{4} atoms / g)[b]	'Raw' minimum exposure age (ka)[c]	Corrected exposure age[d]
GW-I	Glynn Wye (7)	320	15.6 ± 1.0	18.6 ± 1.7	18.2 ± 1.7
GW-II	Glynn Wye (7)	167	16.1 ± 1.3	19.2 ± 2.0	18.8 ± 2.0
GW-III	Glynn Wye (7)	338	13.0 ± 0.6	15.5 ± 1.2	15.2 ± 1.2
GW-B	Glynn Wye (7)	253	10.8 ± 2.2	12.8 ± 2.8	12.5 ± 2.8
LP-I	Lewis Pass (1)	321	14.8 ± 0.6	14.6 ± 1.3	13.5 ± 1.3
LP-III	Lewis Pass (1)	421	13.9 ± 1.0	13.7 ± 1.6	12.7 ± 1.6
KH-I	Kakapo Hill (5)	259	23.0 ± 0.8	23.4 ± 1.7	20.5 ± 1.7

[a] The measured ratio were corrected by full chemistry procedural blanks (max. 3% with 1% correction).
[b] Concentration at site location based on accepted AMS standards (Fink et al., 2000). The uncertainty represents quadrature addition of 1σ errors in final AMS isotope ratio, masses and a 2% systematic variability.
[c] The raw ages includes basic production rate adjustments for geographic latitude and altitude derived from Duna (2000).
[d] Corrections include adjustments for shielding, geomagnetic variations, sample thickness and surface erosion (see text).

[1] Cosmogenic exposure ages closely correspond to calendar years and are therefore compared to calibrated radiocarbon years. The ^{14}C dates were calibrated using OxCal software version 3.5.

from the Glynn Wye moraine, indicate ages for the moraine of 13.5 ± 1.3 ka and 12.7 ± 1.6 ka. Both samples agree within error. In summary all the dated boulders yielded ages <21 ka. In addition to being largely internally consistent the persistent young ages suggest that lack of erosive zeroing was not an issue in the valley. This matches observations by Ivy-Ochs et al. (1999) and Shulmeister et al. (2005) for other New Zealand glacial valleys.

7.5. Discussion and conclusion

The Waiau-Hope Valleys preserve an excellent glacial moraine record but because of the general lack of organic deposits associated with glacial moraines in the eastern Southern Alps, numerical age control has so far been very limited. However, due to the ubiquity of quartzofeldspathic sandstones in most eastern valleys cosmogenic exposure dating is ideally suited to provide direct age control for glacial events. Based on the statistical spread of the exposure ages the results identify three discernable periods during which the dated moraines were deposited. The sample from Kakapo Hill, the highest glacial surface in the Hope-Waiau Valleys, yielded an age of 20.5 ± 1.7 ka, which is substantially younger than the previously suggested OIS 8 age (~290 - 240 ka) for this surface (see correlations in Clayton, 1968; Suggate, 1990). The boulder (photo 61c) is clearly a glacial erratic as it is located on a gently undulating moraine surface. No higher ground exists from where this boulder could have been derived. Because the exposure date is based on one sample only caution is necessary when considering the age. However, even including the error, the age still deviates by at least 200 ka from the suggested OIS 8 age for the Kakapo surface and the result is therefore significant. Based on the 20.5 ± 1.7 ka age it is suggested that the surface was ice overrun during the LGM. This does not exclude the possibility that the Kakapo surface itself was formed during an earlier glaciation.

The dated boulder on Kakapo Hill is located on a moraine surface which does not represent a terminal ice position. The boulder exposure age suggests that Kakapo Hill was ice overrun during the largest of the LGM advances. This cannot be the Glynn Wye advance as this advances formed a terminal moraine 200 m below Kakapo Hill. A more likely candidate is the inferred early LGM Glenhope advance (Clayton, 1968). Although remnants of this advance, in particular glacial erratics are extensive,

no moraine terminus was preserved and the precise down-valley ice extent of the Glenhope advance remains unclear. Since the dated boulder is located on a undulating ground moraine it is likely that the boulder was deposited during the deglaciation of the Kakapo surface which is consistent with the exposure age of the boulder.

Of the three ages considered for the Glynn Wye moraine two indicate an age between 18.8 – 18.2 ka (GW-I, GW-II) while one sample yielded an age of 15.2 ± 1.2 ka (GW-III). When including all errors GW-III does not overlap with the two older ages. A possible explanation for the younger GW-III boulder is that the block rolled during the stabilization phase of the Glynn Wye moraine or during an earthquake which exposed a fresh rock surface some time after the original moraine deposition. Because the two older ages are statistically identical we consider them as more reliable. Nevertheless, all three ages are younger than would be expected if the Glynn Wye moraine were to represent the main LGM terminal position in the lower Hope Valley. In New Zealand, the largest OIS 2 ice advance occurred prior to ~23.0 cal. ^{14}C ka as indicated by records from the western and eastern Southern Alps (e.g. Suggate, 1965; Suggate and Moar, 1970; Moar, 1980; Soons and Burrows, 1978; Almond et al., 2001; Suggate and Almond, 2005; Alloway, et al., subm.). The probable 19 – 18 ka age of the Glynn Wye moraine suggests that the moraine is more likely to be associated with either a true LGM ice re-advance or alternatively a recessional halt during the initial glacial retreat. Either interpretation is consistent with recent surface exposure dating of moraines in the Cobb Valley of North-West Nelson (Shulmeister et al., 2005). There, results indicate that major ice retreat from the LGM ice position (21 km distance to headwaters) began by 18.3 ± 1.3 ka producing a series of younger recessional moraines (Shulmeister et al., 2005). Because of the resemblance in age and down-valley position, the Glynn Wye moraine is interpreted to represent a similar ice advance which was at least 10 km short of the full LGM ice extent. This interpretation implies that Clayton's (1968) Glenhope advance represents a larger OIS 2 / late OIS 3 while the smaller Glynn Wye advance, dates to a later LGM retreat phase and is probably correlated to the Bayfield-3 or alternatively the Poulter-1/Acheron-1 advances of the Waimakariri and Rakaia Valleys, respectively. Until direct age control for these advances improves these correlations will remain tentative.

In addition to the reconstruction of the glacial history of the Hope-Waiau Valleys, absolute dating of the Glynn Wye moraine has important implications for the regional tectonic geology. As has been described earlier (section 3.2.) the moraine has been dextrally offset by transcurrent motion along the Hope Fault and the moraine has been the principle geomorphic feature from which the late Quaternary strike-slip rate of the Hope Valley segment of the Hope Fault was determined (Knuepfer, 1984, 1988; Cowan, 1989, 1990). The fault is the most active of the Marlborough fault system and is the second fastest moving fault in New Zealand. Cowan (1990) surveyed the moraine in detail and measured the offset to be 230 ± 20 m. Given the lack of absolute dating Cowan (1990) used an assumed moraine age of 17.0 ± 2.0 ka and calculated an average late Quaternary strike-slip rate of 14 ± 3 mm/a. The new surface exposure ages suggest that the Glynn Wye moraine has a mean age of 18.5 ± 1.9 ka, thereby roughly confirming Cowan's (1990) assumed age. Based on the 18.5 ± 1.9 ka moraine age a refined strike slip rate of 12 ± 2 mm/a was calculated which is about 2 mm/a lower than the previous estimate.

Moraines at Lewis Pass yielded exposure ages of 13.5 ± 1.3 ka and 12.7 ± 1.6 ka resulting in a combined age of 13.1 ± 1.5 ka. This suggests the advance is younger than would be expected if Clayton's (1968) correlation of the Lewis advance to the Poulter/Acheron advances in the Waimakariri and Rakaia Valleys (Gage, 1958; Soons 1963a) were correct. The late glacial Poulter/Acheron complex of the eastern South Island is constrained by radiocarbon dates from locations at Kettlehole bog and Cass River, which are inside the Poulter moraine loop, and indicate that the advance terminated prior to 16. 4 ± 0.4 cal. ^{14}C ka BP and 15.9 ± 450 cal. ^{14}C ka BP, respectively (Burrows, 1983). A younger-than Poulter/Acheron age for the Lewis advance is suggested by the valley positions of the respective moraines. While the Poulter and Acheron moraines are about ~50 km distant from the headwaters, the Lewis Pass moraines are within 15 km of the ~2,200 m high Spenser Range.

A combined exposure age of 13.1 ± 1.5 ka for the Lewis Pass moraine puts this advance into the last glacial – interglacial transition (LGIT). In New Zealand there has been intense debate about whether a LGIT glacial advance represents a New Zealand climate signal or the Northern Hemisphere Younger Dryas event (12.7 – 11.5 cal. ka BP; Denton and Hendy, 1994; Mabin, 1996, Singer et al., 1998; Ivy-Ochs et al., 1999;

Shulmeister et al., 2005). The Lewis Pass moraine ages confirm a LGIT re-advance for the Southern Alps but suggest that the advance pre-dates the onset of the Younger Dryas chron and a causal correlation is therefore improbable. Based on the exposure ages it is more likely that the Lewis Pass advance is associated with a Southern Hemisphere cooling event known as the Antarctic Cold Reversal (ACR; 14.0 - 12.5 cal. ka BP; Jouzel et al., 2001) which interrupted Antarctic warming during the deglaciation before the Northern Hemisphere Younger Dryas. An ACR signal has been found in New Zealand pollen and maar lake records (McGlone; 1995, McGlone et al., 2004; Pepper et al., 2004). The debate is complicated by the fact that the YD and ACR overlap between 13.0 – 12.5 ka BP and more and tighter absolute dating is required to confirm the ACR correlation of the Lewis Pass moraine.

In summary, cosmogenic exposure dating in the Waiau-Hope Valleys yielded three key observations. Firstly, that the high surface of Kakapo Hill, may represent an older glaciation as it was originally mapped, but the surface was ice overrun during the LGM. This is a problem for the simple uplift and preservation model (e.g. Gage, 1958) of older glacial remnants in the Southern Alps (see discussion Chapter 9). Secondly, that the Glynn Wye moraine represents a late glacial re-advance which is correlated to the late Bayfield or early Poulter/Acheron complex, and thirdly that the headwater moraines at Lewis Pass represent an LGIT glacial re-advance such as the Misery/McGrath moraines (Arthur's Pass) and that they are *not* correlated to the more extensive Poulter or Acheron advances of the Waimakariri and Rakaia Valleys.

CHAPTER 8

GLACIAL SYSTEMS OF THE SOUTHERN ALPS: SENSITIVITY TO CLIMATE PARAMETERS AND IMPLICATIONS FOR THE FORCING OF GLACIATIONS

8.1. Introduction

Chapters 4-7 presented sedimentological and geochronological investigations from the Hope-Waiau Valleys which highlighted new information on the timing and nature of the local glaciation. This chapter considers the larger scale perspective of glaciations in the Southern Alps by using a snow mass balance model to analyse the style of glaciation. On the largest scale, glacial theory states that variations in the receipt of solar energy as caused by regular changes in Earth's orbital parameters are responsible for the cyclic pattern of Quaternary glaciations (Hays et al., 1976). Large scale global glaciations are forced by summer insolation in the Northern Hemisphere mid-high latitudes (Fig. 64; e.g. Broecker, 1968; Ruddiman, 2003). Because it has been demonstrated that the timing of glaciations in the Southern Hemisphere (SH) roughly coincides with those of the Northern Hemisphere (NH) (e.g. Suggate, 1990; Ehlers and Gibbard, 2004), it has been suggested that the interhemispheric transfer of NH climate signals is the principal driver of large glaciations in the SH (e.g. Denton et al., 1999; Clapperton, 2000).

Recent research on the absolute timings of mid-latitude SH glacial signals, in particular in New Zealand and southern South America, has focussed on the level of correspondence between the hemispheric glacial signals, and resulted in hypotheses on the mechanisms of interhemispheric climate teleconnections (Ivy-Ochs et al., 1999; Kaplan et al., 2004). Two sets of ideas have emerged and it has been argued that glacial synchrony is indicative of direct NH forcing of SH glaciation via the atmosphere (e.g. Kaplan et al., 2004) whereas asynchrony is seen to support an oceanic NH to SH link through the thermohaline conveyor (e.g. Lowell et al., 1995). Results from New Zealand were initially interpreted as demonstrating interhemispheric synchrony of LGIT[2] glacial advances (e.g. Denton and Hendy, 1994)

[2] Late-Glacial-Interglacial-Transition

and it has been suggested that a specific LGIT climate event from the North Atlantic region (the Younger Dryas) can be directly correlated to mountain glacier advances in New Zealand (Ivy-Ochs et al., 1999). More recent work has highlighted asynchronous changes suggesting a link through the thermohaline circulation (e.g. Turney et al., 2003).

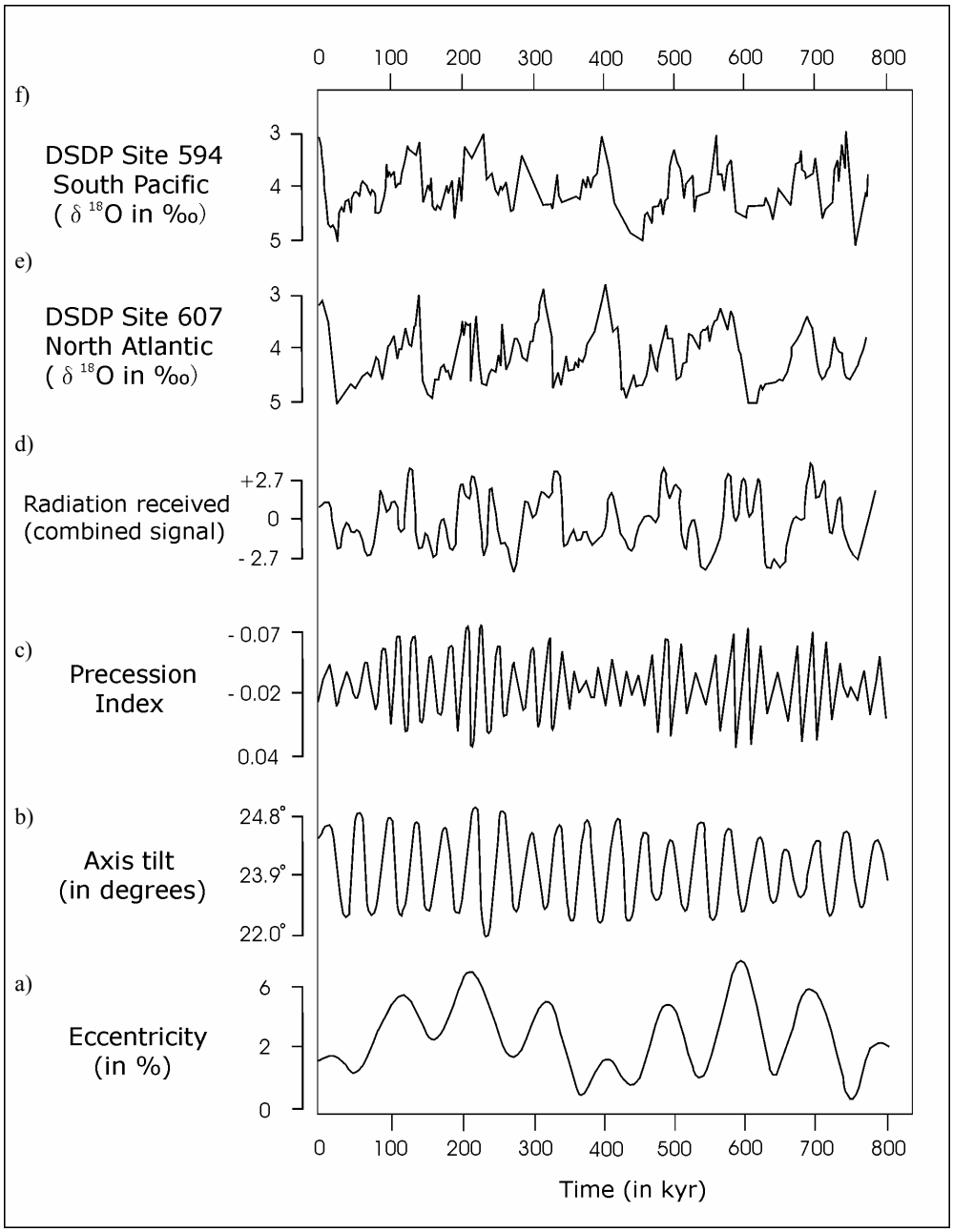

Fig. 64: Summary of the temporal variations of Milankovitch orbital parameters (a, b, c) and their combined effect on solar insolation received at 65˚ N (d) (Muller and MacDonald, 2000). Oxygen isotope records from Deep Sea Drilling Project sites 607 (North Atlantic, Ruddiman, et al., 1987) and 594 (east of New Zealand, Nelson et al., 1985; Heusser and van de Geer, 1994) demonstrate the general global correspondence of ocean climate signals during the Quaternary as derived from benthic (site 594) and planktonic (site 607) foraminifera.

A critical component of the synchrony hypothesis is that the SH mid-latitudes respond directly to the NH cooling. Work in this thesis has highlighted that glacial deposits suggest a comparatively mild cooling during glaciations and the whole issue of thermal forcing of New Zealand glaciations needs examination. In this chapter the sensitivity of glacial systems in the Southern Alps to thermal forcing will be analysed using a snow mass-balance model that highlights the specific pattern of glacial accumulation under the conditions of the perhumid and temperate Southern Alps. The model calculates snow accumulation for various cooling scenarios to simulated potential temperature decline. The results are used to argue that NH climate forcing may not have been the exclusive driver of Quaternary glaciations in New Zealand and to suggest an alternative forcing mechanism.

8.2. LGM and LGIT climates of New Zealand

Glacial advances in New Zealand during the late last glacial cycle appear to have occurred broadly synchronous to those of the Northern Hemisphere (e.g. Suggate, 1990), however, despite this, the paleo-climatological interpretation of the proposed correlations is not straightforward. It has long been known that no severe cooling occurred in New Zealand during the Pliocene and Pleistocene periods as indicated by the continuous presence of a temperate marine fauna and a flora which *"...has a semitropical aspect, inconsistent with the probability of its co-existence with severe glacial conditions, many of the most hardy plants being unable to withstand the rigour even of an English winter."* (Travers, 1874; p. 419). Early quantified estimates of the mean temperature decline during glaciation in New Zealand varied between 3˚C (Haast, 1879), 5˚C (Park, 1909) and 4-6˚C (Morgan, 1927). Willett (1950) used elevations of cirque floor basins to approximate an average LGM regional snowline depression of ~1000 m which he estimated to be equivalent to a 6˚C cooling in mean temperature. A similar estimate for the LGM was derived from an early isotopic study on speleothems (Hendy and Wilson, 1968). Relatively mild glacial conditions are also suggested by geomorphic and sedimentological proxies. Soons (1963b) found that evidence for former periglacial processes in the South Island is limited to relatively high altitudes while these features disappear entirely towards the West Coast. Gage (1965) noted that glacial deposits in New Zealand suggest the plentiful availability of flowing water during glaciation thereby indicating above freezing temperatures for

most months of the year. Based on these results Soons (1979) pointed out that focussing on temperature depression alone for explaining former glaciation may be misleading as *"glaciation in New Zealand may … be as much a response to increased precipitation as to depressed temperatures…"* (p. 20).

More recent numerical paleo-environmental reconstructions of last glacial climate conditions have generally confirmed the earlier estimates. Studies using speleothems and fossil beetle assemblages show that LGM cooling was very moderate (Hellstrom et al., 1998) and possibly as little as 1 - 4°C (Marra et al., 2004; in press). These results are supported by General Circulation Model (GCM) calculations that predict 2 to 3°C lower sea-surface temperature (SST) in the Tasman Sea during the LGM (Hewitt and Mitchell, 1997) while sea-surface temperature reconstructions from forams suggest slightly stronger cooling at c. 4°C (Barrows and Juggins, 2005). For the LGIT, at least one glacial re-advance has been demonstrated for the Southern Alps (Denton and Hendy, 1994; Mabin, 1996; Ivy-Ochs et al., 1999). However, this re-advance, which was originally correlated to the Younger Dryas Chronozone (Denton and Hendy, 1994), is neither universally detected in NZ's glacial records (e.g. Shulmeister et al., 2005) nor, critically, is a significant simultaneous cooling apparent from pollen or other paleoecological records (e.g. Singer et al., 1998; Turney et al., 2003). The New Zealand pollen records suggest a pause or minor reversal in the post-glacial warming only between 14.6 – 13.6 cal.^{14}C years (McGlone, 1995; McGlone et al., 2004) which pre-dates the above advance and instead correlates better to the Antarctic Cold Reversal (ACR). Results from surface exposure dating of moraines at Lewis Pass in the Hope-Waiau Valleys suggest that the New Zealand LGIT glacial re-advance occurred during the ACR rather than the Younger Dryas (Chapter 7).

In summary, none of the reconstructions suggest a cooling of more than 5-7˚C during the LGM while the lower end of the reconstructions suggest cooling similar to the modern interannual temperature variability associated with ENSO and other oscillatory systems. Despite the debate about the precise timing and correlation of LGM and LGIT glacial advances in New Zealand, the broader glacio-chronological and paleoecological data appear robust, and it has been difficult to resolve the occurrence of significant glacial expansions contemporaneous with only moderate cooling. The problem has wider implications because similar confusion has

characterized the LGIT debate in southern South America with various authors proposing cooling or an absence thereof during the LGIT (e.g. Moreno et al., 2001; Bennett et al., 2000).

The snow mass balance model presented in this chapter tests the sensitivity of glacial accumulation in the Southern Alps to thermal changes. By doing so it analyses whether the emerging glacio-chronological and paleoecological records from New Zealand are in fact compatible and if minor thermal forcing is sufficient to cause full-scale glacial expansion in the Southern Alps. The question has wider relevance because under such a scenario we must consider the possibility that some Quaternary glacial advances in NZ, and by implication in parts of South America, were generated by synoptic climate variations alone, requiring little (during the LGM) or no (during the LGIT) climate forcing from the NH.

8.3. Glaciological setting

New Zealand's glaciological setting is profoundly affected by the interception and rapid orographic forcing of west flowing moist air masses by the NE-SW trending Southern Alps. Annual precipitation in the central Alps is commonly in excess of 9,000 mm with observed maximum values at around 16,000 mm (Griffiths and McSaveney, 1983; Henderson and Thompson, 1999). Critical for the glaciological setting is the marked cross-alpine precipitation distribution and the presence of a narrow hyperhumid sector which stretches along the full length of the Southern Alps. Virtually all of New Zealand's c. 3,100 present glaciers are located in this sector (National Snow and Ice Data Center, 1999). Glaciers of these perhumid environments are characterized as high turn-over systems with large positive and negative mass balances, high glacial flow velocities and relatively short climatic reaction times (Woo and Fitzharris, 1992; Benn and Evans, 1998).

Glacial Equilibrium Line Altitudes (ELAs) separate glacial accumulation from ablation areas and represent the altitude at which the glacial mass balance is zero. Key factors influencing the position of the ELA are long term mean temperatures and total precipitation. In the Southern Alps the ELA closely reflects the steep windward-leeward precipitation contrast, which causes ELA gradients in New Zealand to be up

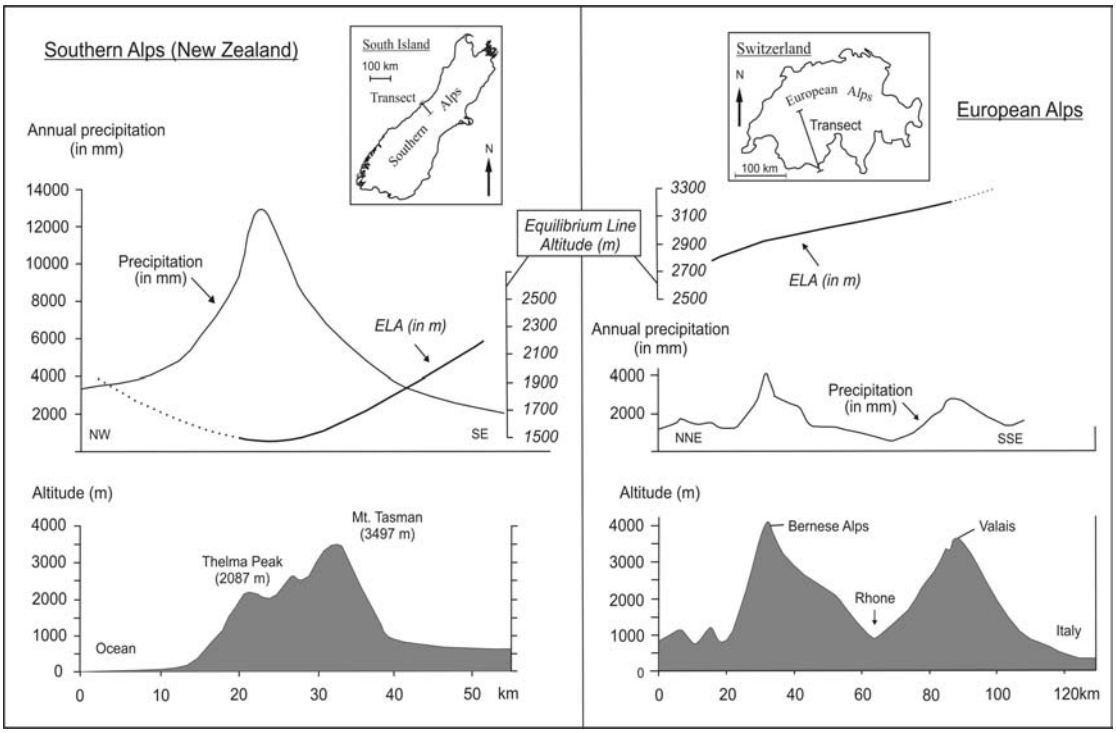

Fig. 65: Comparison of precipitation and ELA levels across the Southern Alps (Griffiths and McSaveney, 1983; Chinn and Whitehouse, 1980) and European Alps (Sturman and Wanner, 2001, Mueller et al., 1976) plotted at equal scales (except horizontal distances). In New Zealand heavy orographic precipitation is concentrated in a 15 – 20 km wide sector along the alpine divide with annual totals 3 - 4 times greater than in the European Alps. The marked distribution of precipitation causes a strong ELA depression and very steep ELA gradients. In the European Alps, the NNW-SSE rise in ELA is mainly due to the meridional temperature increase.

to 20 times steeper than those reported for arctic and subarctic regions (Chinn and Whitehouse, 1980; Andrews and Miller, 1972). Despite this distinct glaciological setting, Quaternary glacial records from the Southern Alps are often directly correlated to records from other mid-latitude mountain belts, in particular to those from the European Alps (e.g. Ivy-Ochs et al., 1999). A comparison of key glacial parameters of the two ranges (Fig. 65) shows that despite substantially greater mean elevations, the European Alps receive only a quarter to a third of the NZ precipitation values while its distribution is far more even. A direct consequence of the hyper-humidity in the Southern Alps is a strong depression of ELAs (Chinn and Whitehouse, 1980), which are generally about 1000 m lower than those in the European Alps (Mueller et al., 1976). The differences have important implications for mechanisms of glacial accumulation and the resulting glacial styles in the two mountain belts. Because New Zealand's glaciological configuration is fundamentally related to the interaction between the Southern Alps and the Westerly wind belt, studies of regional paleo-circulation patterns are critical to the reconstruction of

former glacial base conditions. Evidence for enhanced ocean upwelling east of New Zealand (Fenner et al., 1992; Weaver et al., 1998) and maxima in dust flux (Thiede, 1979; Stewart and Neall, 1984; Carter et al., 1995) have generally been attributed to persistent and strong westerly flow during the LGM (e.g. Markgraf et al., 1992; Shulmeister et al., 2004). In addition, glacio-eustatic sea level lowering, increased the relative height of the Southern Alps which in turn intensified the orographic forcing of moist westerly air masses. It is therefore reasonable to assume that the pattern of a strong windward-leeward gradient of precipitation across the Southern Alps remained intact during Quaternary glacial periods. Such a scenario is supported by reconstructed paleo-ELAs from cirque floor elevations comparing the western/central alps to those of the eastern alps (Fig. 66). Results show that despite an estimated ~800 m ELA lowering (Porter, 1975), steep paleo-ELA gradients persisted during past glaciations.

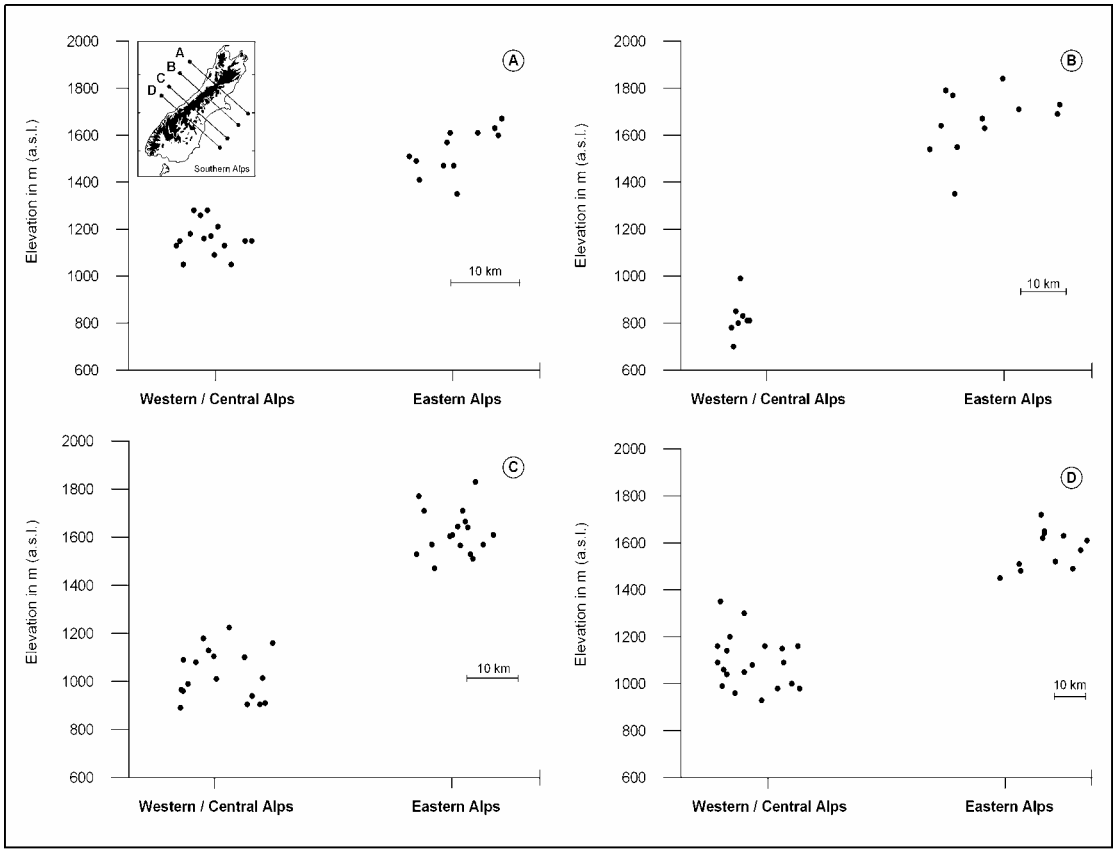

Figure 66: Minimum cirque floor elevations of the western/central and eastern Southern Alps. Clearly defined cirque basins were mapped along four 30 km wide transects as shown in A. The data indicate that steep West – East precipitation and snowline gradients persisted during Quaternary glaciations.

To summarise, the combination of hyper-humidity and a steep paleo-ELA gradient during Late Quaternary glaciations in the Southern Alps is responsible for a specific nature of glaciation in New Zealand. Firstly, very high levels of snowfall occurred in a 15 - 30 km wide sector near the alpine divide which corresponded with the area of minimum ELA. Secondly, due to rainshadow effects and because the ELA rises sharply east of the divide, alpine areas only a short distance from the divide received significantly less snowfall and only the highest peaks penetrated the annual snowline. This resulted in a glacial pattern where large scale ice accumulation was concentrated in the narrow perhumid sector, while the contribution of all other areas to overall glacial accumulation in the Southern Alps was orders of magnitude smaller.

8.4. Temperature effects on snow mass balances in the Southern Alps

In the central Southern Alps present ELAs range between 1500 m – 2100 m (Lamont et al., 1999). Critically, at these ELAs atmospheric temperatures remain above freezing for considerable periods of the year. This means that a significant portion of the large annual precipitation at and around ELA level falls as rain. This constitutes a substantial snow resource if climate cooling occurs as additional snow is generated without any synoptic changes. By comparison, in the European Alps present ELAs are on average 1000 m higher (2500 m – 3500 m) and corresponding atmospheric temperatures remain too cold for rain to form a significant portion in the annual precipitation at ELA (Fig. 65b).

To investigate temperature effects on glacial accumulation in the perhumid Southern Alps a snow mass balance model is used. The full details of the model are provided in the appendix (appendix 4). The model calculates annual net snow accumulation for various cooling scenarios (-1 to -9°C in mean T) by analysing temperature related changes to the snow-rain-ratio, total annual precipitation and snow ablation rates. Data are calculated for the central perhumid alpine sector (Fig. 67a) with an ELA of 1600 m (Chinn and Whitehouse, 1980; Clare et al., 2002) and a total annual precipitation of 9000 mm (Griffiths and McSaveney, 1983; Henderson and Thompson, 1999). The overall topography, ELA position and the amount of annual precipitation in this area represent average condition for substantial portions in the

central alps. Temperature data used in the model are from the nearest climate station (Hokitika, Fig. 67a) and were converted to the ELA altitude by using a standard environmental lapse rate of 6°C/km. Cooling related changes to net snow accumulation were calculated for the ELA (1600 m) where the current snow mass balance is zero. Mean temperatures were then incrementally lowered to simulate potential atmospheric cooling.

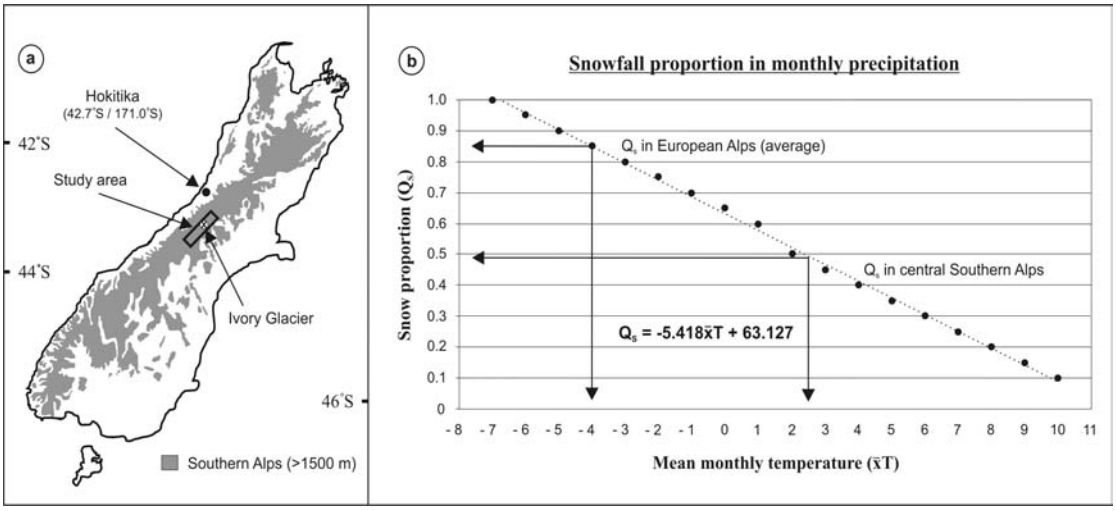

Figure 67: Locations of study area, Hokitika climate station and Ivory Glacier in the Southern Alps (a). Figure b shows the physical relationship between mean monthly temperature and the snow-rain ratio as derived from the Swiss Alps (Sevruk, 1992). The presented data apply to altitudes 1400 – 1600 m. Average rain-snow ratios at ELA in the European Alps and Southern Alps are marked (b).

Observations on snow proportions (Q_S) in total precipitation (P_{total}) are not available for the Southern Alps but it has been shown that snow proportions correlate well to mean monthly temperatures (Lauscher, 1954; Cehak-Trock, 1958). Q_S in P_{total} was calculated using a regression function derived empirically from 32 stations in the Swiss Alps (Sevruk, 1992) (Fig. 67b). Q_S results for the Southern Alps were then adjusted for the seasonal variation in precipitation by applying weighted averages from the observed monthly precipitation at the nearby Ivory Glacier (Anderton and Chinn, 1978; Fig. 67a). At ELA (1600 m) mean annual temperature is 2.3°C with a monthly range from -2.1°C (July) to 6.4°C (February). Results show that at this elevation 49.2 % (mm water equivalent) of the annual total of 9000 mm fall currently as snow while the remaining 50.8 % (4570 mm) fall as rain. This provides an enormous potential additional snow source. For every 1°C of cooling in mean

monthly temperature the percentage of snow as a proportion of precipitation grows by 5.5% (Fig. 67b).

Atmospheric cooling is likely to affect the amount of total annual precipitation received by the Southern Alps. Recent studies have suggested relatively wet conditions in New Zealand associated with enhanced Westerlies during the LGM (e.g. Eden and Hammond, 2003; Shulmeister et al., 2004) and LGIT (e.g. Pepper et al., 2004), while others argue that humidity was somewhat reduced during glacial periods (e.g. Hope et al., 2004). At present no quantified paleo-data on the response of precipitation in the New Zealand region to LGM and LGIT cooling exist. In general precipitation will respond to cooling by adjusting to changes in air mass saturation vapour pressure, evaporation and to variations in the route and velocity of atmospheric transport. In order to demonstrate the general relationships between precipitation, temperature, snow-rain ratios and snow accumulation in the New Zealand setting, three simple precipitation scenarios are used to account for a range of possible precipitation values (Fig. 68). Scenario 1 assumes a cooling related decrease in annual precipitation and approximates the non-linear reduction through the temperature related variation in air mass saturation vapour pressure (SVP). In this

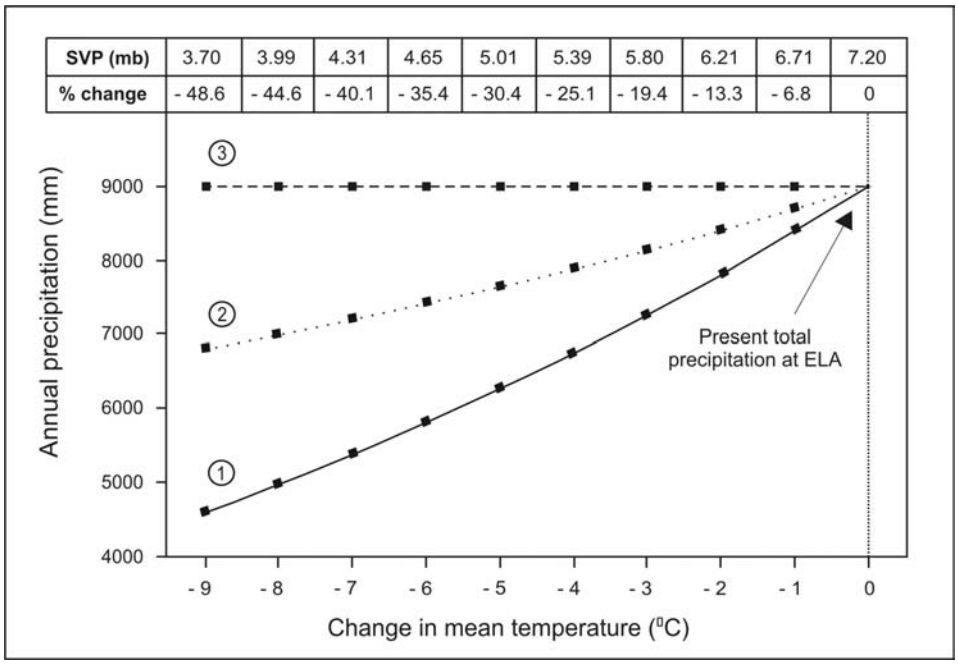

Figure 68: The three annual precipitation scenarios (a). Scenario 1 approximates cooling related changes through variations in air saturation vapour pressure (SVP) (see table). Scenario 2 assumes half the change of scenario 1, and scenario 3 assumes no change in precipitation.

scenario, variations in overall precipitation are calculated from SVP changes which are used as a proxy for the moisture capacity of the air and where a cooling of -5˚C would reduce overall humidity by ~30%. In scenario 2, the reduction in annual precipitation is assumed to be half of that of scenario 1 and scenario 3 assumes wet conditions where precipitation totals remain at the present levels even under increasingly colder conditions. It should be noted that the above scenarios were designed for the purpose of this model study with no claim to accurately describing the complex response of precipitation to past cooling in New Zealand.

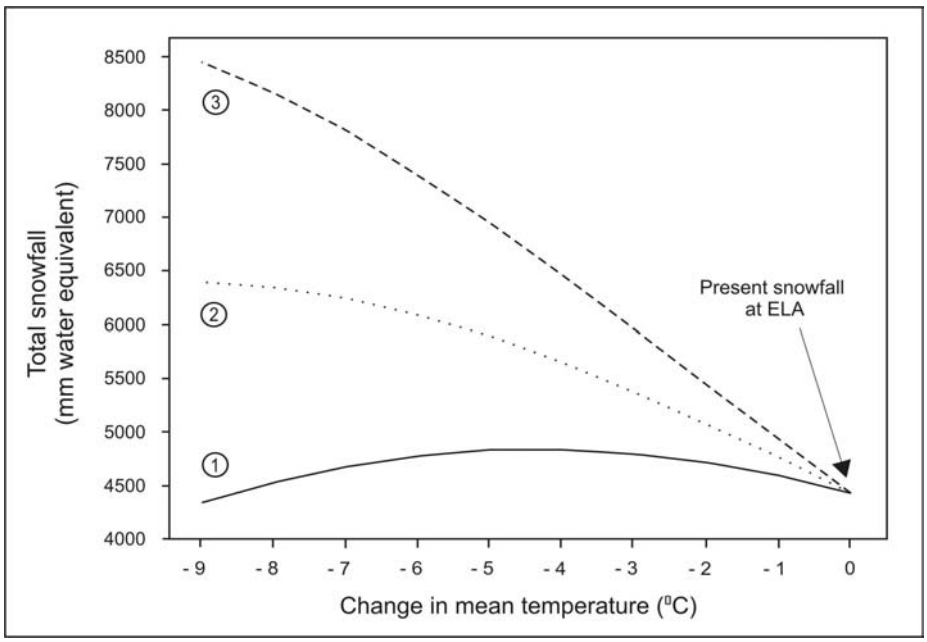

Figure 69: shows annual snowfall under cooling as a result of changes to the snow-rain ratio and variations in total annual precipitation. Snowfall is adjusted to the seasonal variation in precipitation.

Results in figure 69 show total annual snowfall for increasingly colder conditions as calculated when the precipitation scenarios are combined with the dynamic snow-rain ratio. As expected snowfall totals vary greatly depending on the assumed annual precipitation. The data generally reflect two compensating trends during cooling, firstly the continuing increase of Q_S in P_{total}, and secondly a cooling related decline in P_{total} (scenarios 1 and 2). Results indicate that the addition of large amounts of extra snow from the rain-snow conversion causes a dramatic effect on snow mass balances in perhumid environments. Snowfall increases (scen. 2) or remains high (scen. 1) even if annual precipitation declines substantially. If conditions are wetter (scen. 3) snowfall will expand vastly as large amounts of snow are added.

The projected annual snowfall total was then related to ablation for assessing net snow accumulation (Fig. 70). Snow ablation was calculated by using a degree day mass balance (DDMB) model in which mean daily temperatures are taken as an integrated index of the heat budget and where ablation is assumed to occur proportionally to the mean air temperature (e.g. Linsley et al., 1947). DDMB models have been widely tested under field conditions where they have shown to predict ablation reliably (e.g. Komarov et al., 1969; Braithwaite and Olesen, 1989; Johannesson et al., 1995; Braithwaite and Zhang, 2000). The calculation uses the formula:

$$a(z) = kT_{sum}(z) + H_S \quad T > 0C°$$

where ablation (a) is computed for elevation (z), using the sum of positive mean daily temperatures (T_{sum}) at z. The positive degree days are multiplied with k representing an empirically derived degree day factor. The calculation uses a degree day factor of 4.5 mm day-1 deg-1 as was derived for Franz Josef Glacier in the central Southern Alps (Anderson, 2003). HS is ablation from latent heat (rain on snow) which contributes ~2% to annual ablation in the Southern Alps (Hay and Fitzharris, 1988). The model was tested by predicting ablation at the present ELA where annual

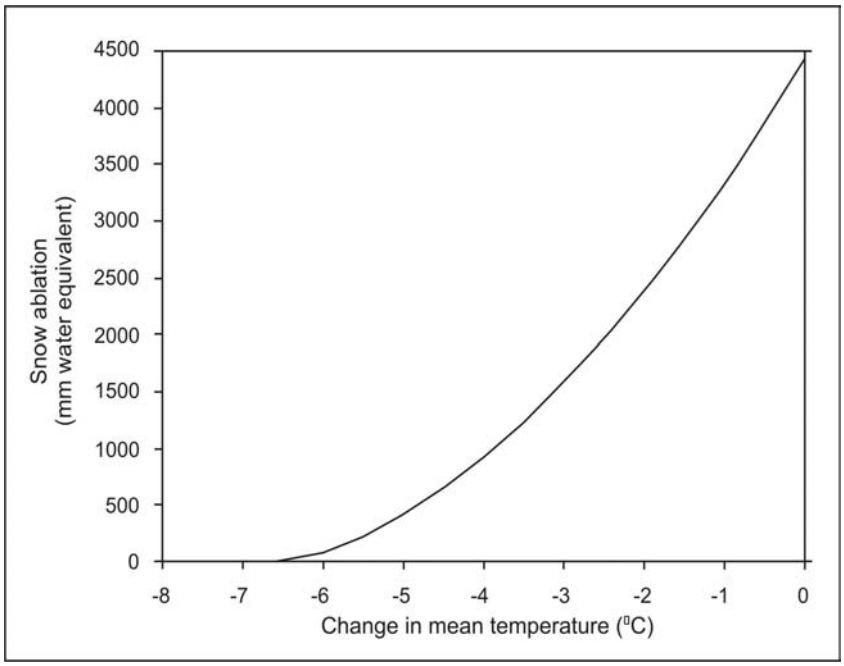

Figure 70: Impact of cooling on snow ablation at present ELA as calculated by a degree day mass balance model.

snowfall is 4432 mm and no net accumulation occurs (mass balance 0). The model indicates 4359 mm of ablation, underestimating actual ablation by only 1.7 %. Overall results in figure 70 show how snow ablation decreases at ELA under intensifying cooling from 4432 mm/a (present temperature conditions) until it virtually stops at 6.5˚C cooling.

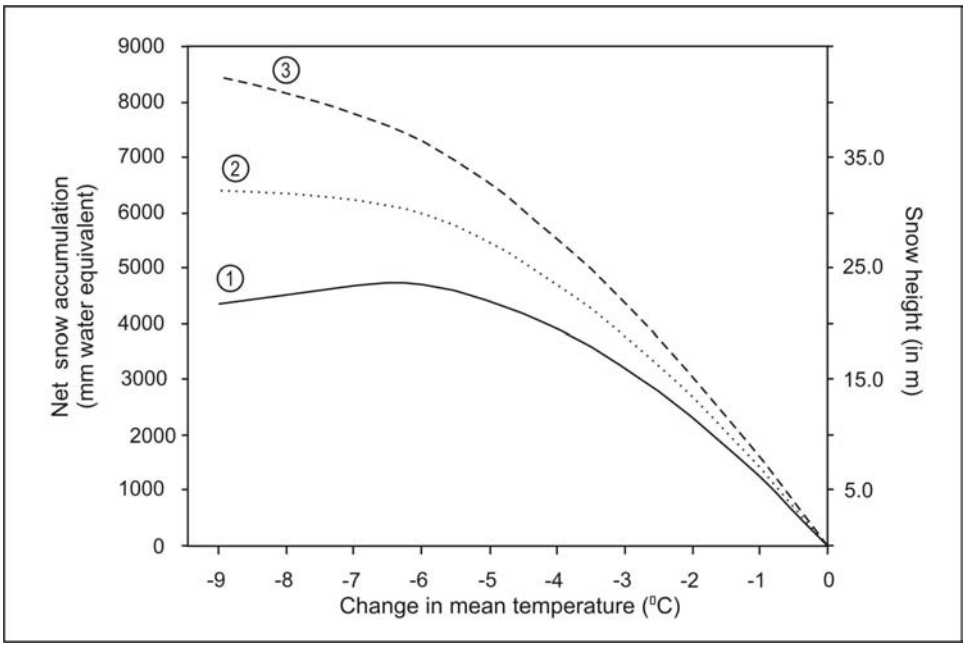

Figure 71: Projected annual net snow accumulation as a result of variations in annual precipitation, snow-rain proportions and ablation under -1 to -9ºC cooling. Note the steep increase in snow accumulation at moderate cooling.

All analyzed parameters (snow-rain proportions, total precipitation, snow ablation) were then integrated to predict net snow accumulation in the central alps under increasingly cooler conditions. Results are shown in Fig. 71 where 0°C change (x-axis) represents the current temperature conditions at the ELA with no net accumulation. The outcome indicates that net snow accumulation in the hyperhumid Southern Alps responds strongly positively to moderate cooling. Snow accumulation grows dramatically under all precipitation scenarios even when overall humidity declines substantially. A striking feature is the steep increase recorded for the early part of the cooling (1 - 4˚C), where snow accumulation grows markedly mainly due to the rapid conversion from rain to snow. A cooling of only 2 - 3˚C at present ELA would result in the net annual addition of ~15 vertical meters of snow (Fig. 71). Interestingly, the gain generally slows with more severe cooling. For precipitation scenario 1 (driven by SVP changes) the snow accumulation trend will even reverse at

around -6°C cooling with net annual accumulation starting to decline. The effect is caused by high snow proportions at this cooling and the effective halt of ablation after which the continuing decrease of total annual precipitation drives net accumulation down.

8.5. Discussion

Heavy orographic precipitation in the central parts of the long (~800 km) but narrow (~80 km) Southern Alps results in some of the steepest recorded glacial ELA gradients on Earth. During Quaternary glaciations and associated low sea level stands, the relative height of the Southern Alps as a barrier for moist westerly air masses was further enhanced and ELA gradients were maintained or even steepened.

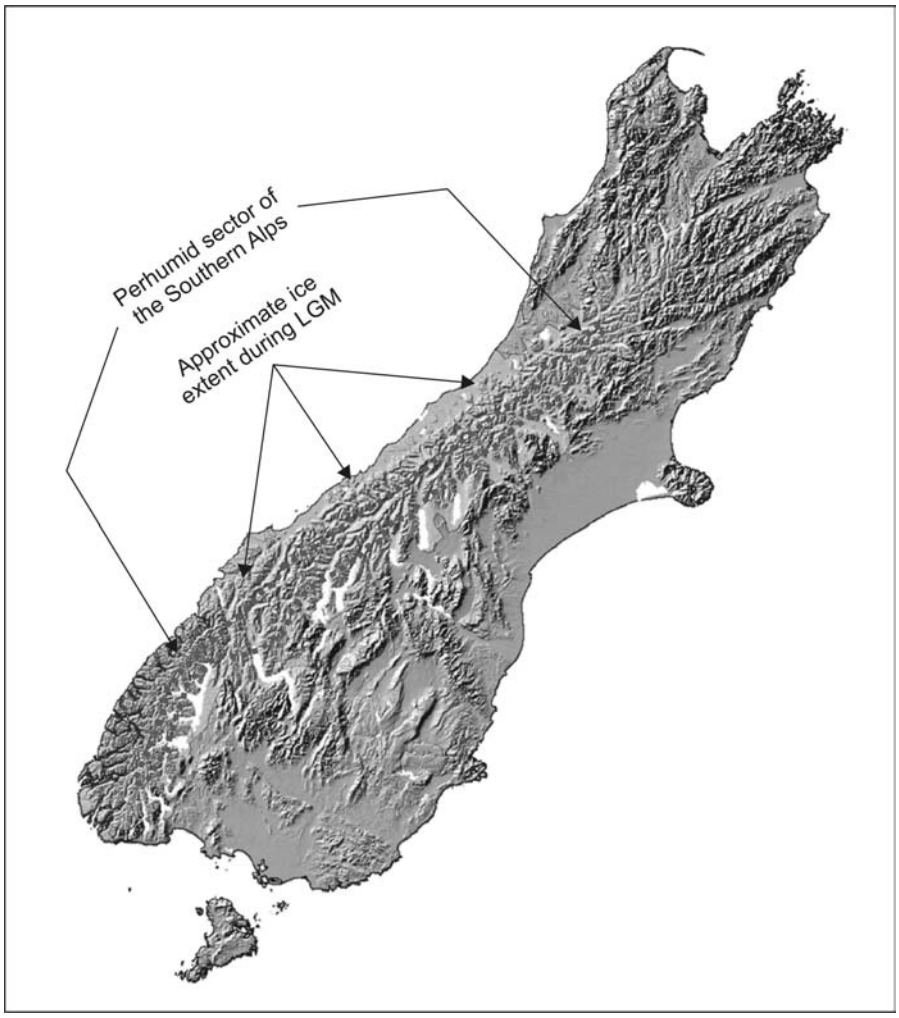

Figure 72: Total estimated ice cover in the South Island during the LGM. The red dashed line shows the perhumid alpine sector with >8,000 mm/a which generally dominates glacial accumulation in New Zealand (base map courtesy M. McGlone).

Reconstructed paleo-ELAs (Porter 1975; Chinn and Whitehouse, 1980) imply that ice accumulation during the LGM was concentrated in the perhumid central alps. These conditions produced a narrow ice cap, which covered a ~30 km wide sector near the alpine divide. From this high turn-over ice cap valley glaciers extended 50 - 70 km to their LGM terminal positions (Fig. 72). The snow mass balance model indicates that glacial accumulation in the Southern Alps is sensitive to small thermal changes. Moderate cooling (3 - 5˚C) is sufficient to increase snowfall dramatically and trigger large positive excursions in glacial mass balances. If this cooling is sustained under a 5000 - 8000 mm precipitation regime it would generate glacial advances of the scale recorded for the LGM. The sensitivity of glacial systems in New Zealand to moderate cooling is mainly due to extreme perhumidity and associated low ELA levels which cause present glacial accumulation areas in the Southern Alps to receive substantial amounts of rain. It is suggested that the rain-snow conversion would impact rapidly as present precipitation maxima occur during the cooler Autumn and Spring seasons thereby requiring only moderate further cooling to initiate full rain-snow conversion (Fig. 73).

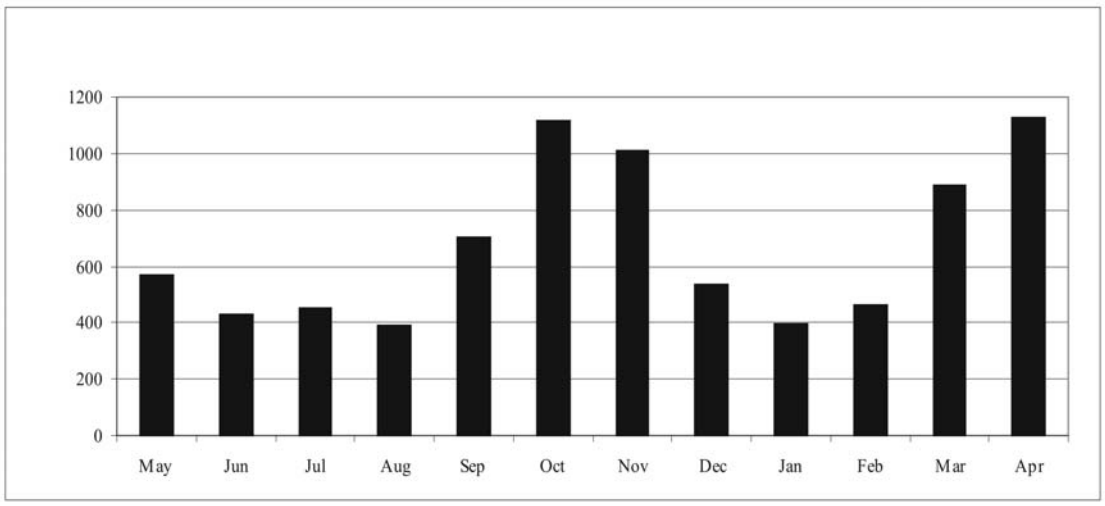

Fig. 73: Observed annual precipitation distribution at Glacier in the central Southern Alps (Anderton and Chinn, 1978). The total annual precipitation is 8,247 mm.

The model assumptions account for a cooling related decrease in total annual precipitation, which is consistent with LGM humidity estimates suggested from New Zealand pollen (McGlone, 1995). Likewise, regional paleo-temperature reconstructions using speleothems and fossil beetle assemblages indicate that cooling during LGM and LGIT glacial advances was possibly as little as -2°C (e.g. Hellstrom

et al., 1998; Marra et al., in press). The benefit of the presented mass balance model is that it provides a mechanism that resolves the occurrence of substantial glacial advances in New Zealand contemporaneous with reconstructed drier conditions and under only moderate atmospheric cooling. It should be noted that under a scenario where total precipitation in glacial New Zealand would noticeable increase (for example due to higher wind speeds or altered atmospheric transport pathways) glaciation in the Southern Alps could be generated with even less cooling then suggested by the present study.

In New Zealand, hypsometric characteristics of areas immediately below snowline (~1400 -1700) in the perhumid zone, suggest that a moderate drop in ELA levels would bring extensive low angle surface areas above snowline. This factor is important because new permanent snow accumulations can only occur if slope angles are suitable. The effect is demonstrated for the study area where hypsometric integrals were calculated for a 10 km wide and 60 km long sector (S 43°17′1" / E 170°53′4" to S 42°50′1" / E 171°29′0") (Fig. 74). Results indicate that an ELA lowering of only

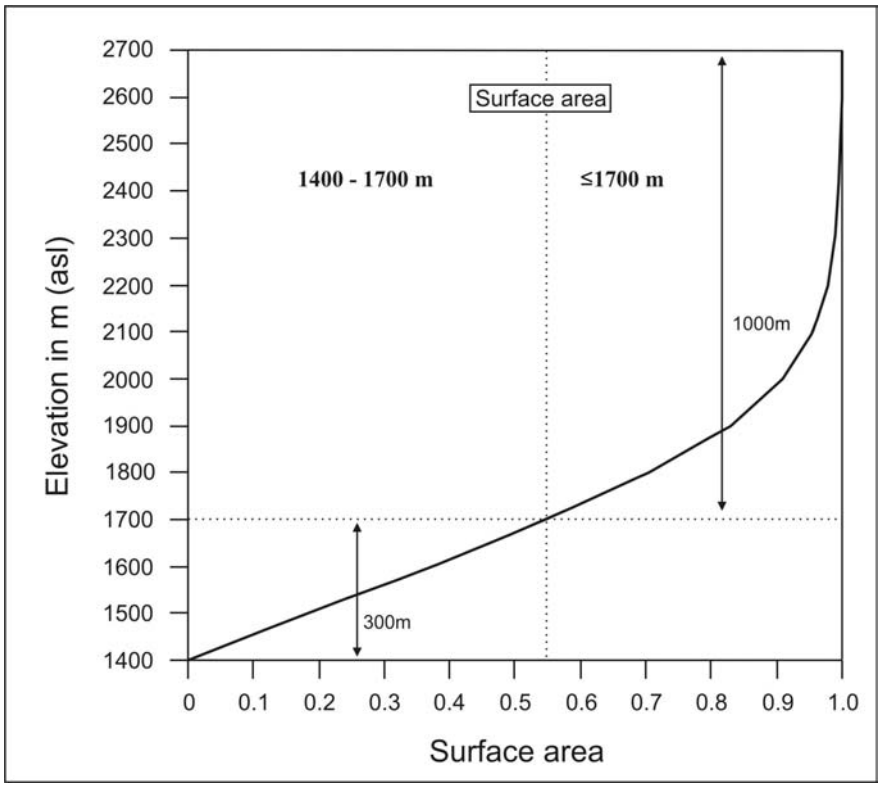

Figure 74: DEM analysed hypsometry above 1400 m in the central Southern Alps showing the potential increase in low angle (less than 15°) surface areas above snowline from a 300 m ELA lowering (1700 m to 1400 m) The analysed alpine area is the study area as shown in Fig. 67a. The lowering would increase low angle surface area by 121.5 %.

300 m would more than double the low angle surface area above snowline. In reality, the increase in suitable snow accumulation surfaces would be further enhanced by the extension of glacial tongues into the upper valleys where they raise the effective elevation of the valley floor.

Moderate cooling as a driver of Quaternary glacial advances in New Zealand has several important implications. Firstly, it accounts for sedimentological peculiarities associated with glacial sequences in the Southern Alps. Commonly noted features are the enormous scale of glacio-fluvial aggradation fans, the large proportions of water lain deposits in ice-proximal sequences and the widespread occurrence of stratified and only weakly compacted tills (e.g. Speight, 1942; Gage, 1965, 1985; Hart, 1996; see also chapter 5). The overall climatic implication is that conditions during deposition were clearly mild enough to provide nearly year-round availability of large volumes of melt-water.

Secondly, the low thermal forcing mechanism for glaciation in New Zealand implies that large glacial advances can be generated rapidly, and conversely, shut down rapidly since glacial conditions are sensitive to small thermal changes. This 'flickering switch' feature of Quaternary glacial advance in the Southern Alps is likely to have resulted in a larger number of individual glacial oscillation than for example is observed in the more continental European Alps. This pattern may complicate attempts to directly correlate glacial signals from the NH to New Zealand.

Thirdly, moderate cooling as a glacial driver in New Zealand highlights the distinct possibility that regional (synoptic) climate phenomena were the principle cause for some Late Quaternary glacial events. It has been shown that modern glaciers in western New Zealand respond to synoptic circulation changes, where enhanced zonal flow (westerly/south-westerly) is associated with glacial advances and stronger meridional flow is associated with retreats (Lamont et al., 1999; Hooker and Fitzharris, 1999). The reason is that strengthened westerly flow increases orographic precipitation over the mountains and reduces ablation through enhanced cloud cover, while conversely, more persistent meridional circulation is associated with reduced precipitation and clear skies that cause increased ablation. Strong westerly flow, associated with glacial advances, mirrors the impact of El Niño on New Zealand.

Recent spectral analyses on varved lake sediments have highlighted the possibility of a periodically enhanced inter-annual El Niño Southern Oscillation (ENSO) signal during the LGIT over New Zealand (Pepper et al., 2004). Speleothem data from the South Island (Hellstrom et al., 1998) now supported by uranium isotope data (Robinson et al., 2004) also indicate a period of enhanced precipitation over New Zealand at around 13 ka which may be linked to a late glacial Southern Hemisphere climate event known as the Antarctic Cold Reversal (ACR) (Jouzel et al., 2001) that has recently been recognized in New Zealand pollen (McGlone et al., 2004) and maar lake records (Pepper et al., 2004). Alternatively, a ~13 ka New Zealand climate event may represent a directly transmitted NH Younger Dryas signal (e.g. Morigi et al., 2003). Enhanced precipitation, in association with very minor cooling, would trigger glacial re-advances in the central parts of the Southern Alps such as at Franz-Josef Glacier (Denton and Hendy, 1994). These changes, however, would not impact on already deglaciated mountain systems such as the Tasman Mountains in NW Nelson (Shulmeister et al., 2005), nor on the pollen record (McGlone, 1995; Singer et al., 1998; Turney et al., 2003). A synoptic 'wet' event as a driver of the LGIT re-advance in New Zealand is therefore consistent with the available glacial record.

Recently, Anderson and Mackintosh (2006a) presented results of a numerical ice flow model for Franz Josef Glacier (FJG). In this paper they argue for the predominance of temperature change in driving LGIT glacial advances in New Zealand and downgrade precipitation effects to a minor factor. They suggest that a cooling of ~4.0˚C in mean annual temperature is required for FJG to advance to its late glacial Waiho Loop moraine, which represents an ice limit far less extensive than that of the LGM. Based on their modelling, Anderson and Mackintosh (2006a) conclude that minor cooling would be insufficient to expand FJG and by implication all New Zealand glaciers to their LGM and late glacial ice positions, respectively. They therefore argue that *"... the late glacial climate of New Zealand was significantly colder than previously estimated"* (p. 122). Because these conclusions conflict with the views presented in this thesis, the following section discusses their study.

Anderson and Mackintosh's (2006a) numerical calculations are based on a coupled mass balance and ice flow model for Franz Josef Glacier. Model parameters were based on field measured mass balance and glacier flow data (Anderson, 2003) and the

glacier dynamics were simulated using a flow line model (Oerlemans, 1986). Climate data were derived from Hokitika some 100 km to the north, the same station used for the snow mass balance calculation in this chapter. Anderson and Mackintosh (2006a) simulated the Little Ice Age advance, one advance to Canavans Knob, and the LGIT advance to the Waiho Loop moraine (Fig. 75). They found that without a change in precipitation a mean annual cooling of ~1˚C would expand the glacier to its Little Ice Age limit, ~3˚C to Canavans Knob, while a more substantial cooling of ~4.5˚C is required to drive the glacier to the Waiho Loop moraine. Alternatively, if

Fig. 75: Topographic map view of the Waiho Loop moraine with Franz Josef and surrounding glaciers (transparent white areas represent the glacial extent as derived from the NZ 1 : 50,000 topographic map). The LGIT age of the Waiho Loop moraine (Denton and Hendy, 1994) was derived from dated wood found between tills at Canavans Knob. Anderson and Mackintosh (2006a) modelled the advance under the assumption that ice was derived entirely from Franz Josef Glacier.

temperature were to have remained stable, they state that precipitation is required to increase by roughly ~400% or to several times the present world precipitation maximum, to simulate the Waiho Loop advance. Anderson and Mackintosh (2006a) consider a combination of cooling and a slight increase in precipitation as the most realistic scenario, but they conclude that a cooling of at least 3-4˚C is necessary to account for the Waiho Loop advance. Although the authors do not use their model to analyse the amount of cooling required to drive the glacier to the LGM ice limit (terminal position is offshore) their results imply that this cooling would be required to significantly exceed ~5˚C.

In their model Anderson and Mackintosh (2006a) assume that the Waiho Loop advance represents exclusively an expansion of Franz Josef Glacier. They state that *"…there was no ice-cap in the central Southern Alps. All of the ridges in this area are extremely steep and pointy, not round and smooth as would be expected if they had been over-ridden by ice"* (Anderson and Mackintosh, 2006b; p. 164). The modelling therefore accounts only for a scenario where no ice was added into FJG via ice overspill or glacier confluence with the Callery or Tatere Glaciers (Fig. 75). As all of FJG's potential glacial catchment is already glaciated and no input of additional ice from neighbouring catchments was considered, the modelled Waiho Loop advance was driven exclusively by the thickening of the existing névé while an expansion of the accumulation area was not considered.

These parameters in Anderson and Mackintosh's (2006a) numerical model, however, are unlikely to represent a realistic reconstruction of FJG during the Waiho Loop advance. Firstly, several presently smaller glaciers in the Fritz Range (Fig. 75) as well as a number of unglaciated cirques which lie outside the modelled accumulation area would expand and feed ice into FJG if ELAs are moderately lowered. In addition, some ice from the upper Fox Glacier would almost certainly spill into FJG. Secondly, and more important, ELA lowering would significantly expand glaciers in the upper Callery Valley (Spencer Gl., Johannes Gl., Burton Gl.) and it is likely that the combined Callery glacier would have extended to the foreland where its tongue would have coalesced with FJG. Therefore, it is speculative to assume that the Waiho Loop advance can be accurately modelled by considering FJG ice production alone. If, however, the interpretation proposed here is correct, and substantial ice from

neighbouring catchments coalesced with FJG, the required cooling to produce the Waiho Loop advance would be significantly less then is suggested by Anderson and Mackintosh (2006a).

If Anderson and Mackintosh's (2006a) model results and parameterization of the FJG Waiho Loop advance were correct, their conclusions would still be problematic, because FJG is not a good choice from which to infer general mechanisms of last glacial ice accumulation in the wider Southern Alps. Following Anderson and Mackintosh's (2006a) model parameterization the topographical constraints of FJG's névé make it virtually impossible to add new ice accumulation areas with moderate cooling. These conditions, however, are not representative for most parts of the Southern Alps where existing or potential glacial accumulation areas are topographically far less confined. The DEM based hypsometrical calculation for a 60 km long sector in the central Alps (Fig. 74) shows that a 300 m ELA drop would more than double the surface area of low angle slopes which is expected to caused considerable increase of potential ice accumulation areas. High-mass-balance (HMB) feedbacks, in particular in the less steeply descending eastern valleys would further increase the extent of new ice accumulation areas. None of this applies to FJG where the possibility of adding new ice accumulation areas is extremely limited.

In summary, it is unlikely that Anderson and Mackintosh's (2006a) are correct in assuming that the Waiho Loop advance was exclusively driven through the thickening of the FJG, while in addition, glacial catchments in most other parts of the Southern Alps will expand much faster with moderate cooling than is the case at FJG. This suggests that (a) climatic conditions during the Waiho Loop advance were probably milder than is suggested by Anderson and Mackintosh (2006a) and (b) that glacial accumulation areas (and therefore glaciers) would expand more rapidly with moderate cooling in most parts of the Southern Alps than is the case at FJG.

CHAPTER 9

DISCUSSION AND CONCLUSION

This thesis has considered the Quaternary geomorphology, sedimentology and geochronology of the Hope-Waiau valley system at a variety of scales. Key aims were (1) to obtain age control for glacial moraines and valley fill deposits in order to reconstruct the timings of past glacial fluctuations and large valley aggradation and degradation; (2) to study the stratigraphy and sedimentology of the valley fill sequence and (3) to analyse the key elements that controlled former glacial accumulation in the Southern Alps and to develop a conceptual model for Quaternary glaciations in the Southern Alps. In the following sections the individual chapter results will be brought together and the main thesis outcomes will be discussed.

9.1. Geochronology

A total of 23 new numerical ages were presented, divided into 14 infrared stimulated luminescence (IRSL) ages, 7 cosmogenic exposure ages and 2 radiocarbon ages (see sample summary in appendix 2). Considered together the dating provides age control for the period 165 ka – 10 ka BP. Almost all age determinations are internally and stratigraphically plausible and only three ages are likely to be outliers. A fundamental result of the dating campaign is the recognition that a volumetrically significant portion of the sedimentary fill in the Hope-Waiau Valleys pre-dates the LGM (OIS 2 / late OIS 3) and instead represents deposition during OIS 5 and OIS 3. Additionally, a thick sequence of OIS 6 glacial deposits was documented at Poplars Gully. In summary, pre-LGM fluvial, lacustrine and glacial deposits were found and dated at five different sites located on both sides of the valley and the geochronological results, which are discussed in the following section, are considered robust.

The survival of penultimate and early last glacial deposits in the central valley through despite overriding by later ice advances poses intriguing questions regarding the mechanism of preservation. Because pre-LGM sediments are preserved also in the middle Hope Valley, 16 km upvalley of the LGM terminus, the phenomenon does not

represent the relatively common process where a thin glacial tongue pushes over ice marginal proglacial deposits without removing them (e.g. Speight, 1942). Instead in the case of the Hope Valley a valley glacier, likely to have been several hundred meters thick, overrode pre-existing sedimentary successions without destroying them. Although it has long been known that buried and successively older outwash sequences are preserved in actively subsiding foreland basins such as the Canterbury Plains, for the glaciated portions of the Southern Alps pre-last-glaciation deposits have so far only been associated with uplifted glacial terraces and surfaces. Accordingly, tectonic uplift has been considered to be the principal factor permitting the preservation of older deposits, while the possibility that such sequences could survive in the valley floor was either not considered or regarded as extremely improbable. Suggate (1985) states that the *"... preservation of glacial deposits ... is critically dependent on rate and timing of uplift ..."* (cited in Suggate 1990, pg. 182) and that the *"...general change from aggradation to erosion, accompanied by uplift, has led to the preservation of successively younger formations at successively lower heights in the each catchment"* (Suggate 1965, p. 8). He further noted that *"owing to subsequent re-advances of the ice, deposits formed during the retreat are rarely preserved"* and that such sequences are *"... brought into prominence only with respect to the retreat from the last major maximum..."* (p. 9). Results of this thesis, however, demonstrate that the modern Hope-Waiau Valley fill consists predominantly of sediments older than the last major maximum and that ages are substantially greater at successively *lower* elevations in the valley.

A contrary view to the mainstream position outlined above was provided by Soons (1963a) who described the sedimentological divisions between the lower and upper fill stratigraphy in the Rakaia Valley. She noted that the widespread contorted lacustrine sediments of the lower fill stratigraphy were probably *"...laid down in a number of ice-marginal lakes related to different advances and in particular to retreat stages of these advances..."* (p. 755) and concluded that on stratigraphic grounds a *"... pre-Bayfield* [pre-OIS 2] *age for these deposits is therefore certain"*(p. 755). Soons' (1963a) stratigraphic interpretation that pre-LGM deposits are preserved at low elevation in the Rakaia Valley was recently confirmed by luminescence dating which demonstrated that practically the entire lower valley fill stratigraphy consists of sediments which were deposited during OIS 6 - OIS 4 (Shulmeister et al., submitted).

Soons' (1963a) showed that in some cases the presence of older deposits may be deduced from stratigraphic relationships, but because of the depositional complexity of fill sequences in question, the interpretation without numerical age control is limited. Because the geochronological findings of this thesis are supported by results from the Rakaia Valley it is unlikely that the Hope-Waiau findings are due to a local, potentially tectonic, anomaly. Instead it is more probable that the phenomenon represents a wider trend and that similar results will be obtained from other glacial valleys in the Southern Alps. The results from the Hope-Waiau Valleys indicate that New Zealand alpine valley fills present an important, yet largely unexploited, terrestrial glacial record.

9.1.1. Valley fill sequence

Sedimentological and geochronological results from the Hope-Waiau Valleys are used to reconstruct several late Pleistocene phases of valley infilling and re-excavation. The majority of the absolute ages were recovered from the lower Hope Valley and a summary of these data is shown in Fig. 76. The record starts with an undated period of significant valley erosion, inferred to be OIS 7, during which the valley was incised and all potentially older valley fills removed. This is indicated by several bedrock strath terraces which are buried below OIS 6 deposits at Poplars Gully. The relatively low height of the strath terraces suggests that the OIS 7 valley floor was at a similar elevation than that of the modern valley. Erosion was followed by infilling associated with glacial advances during OIS 6 as represented by ice proximal sediments from Poplars Gully (ages A–D in Fig. 76) and proglacial fluvial sediments further downvalley (E). In total the OIS 6 / early OIS 5 aggradational sequence in the lower Hope Valley comprises a vertical thickness of more than 250 m.

The Poplars Gully sequence contains 110 m of dominantly ice proximal sediments which are exposed as part of the main aggradational terrace. Terrace remnants on both sides of the lower Hope Valley correspond in elevation and were therefore interpreted as representing the main LGM aggradational terrace (Clayton, 1965; Suggate, 1965; Knuepfer, 1984, 1988; Cowan, 1990). However, despite their position in the same aggradational terrace, ice-proximal deposits at Poplars Gully are sedimentologically

inconsistent with ice distal lacustrine and glacio-fluvial deposits exposed at the same elevations at Glynn Wye Station. The problem was resolved by IRSL dating which showed that both sequences are unrelated as deposits at Poplars Gully are roughly 100 ka older than sediments at Glynn Wye Station.

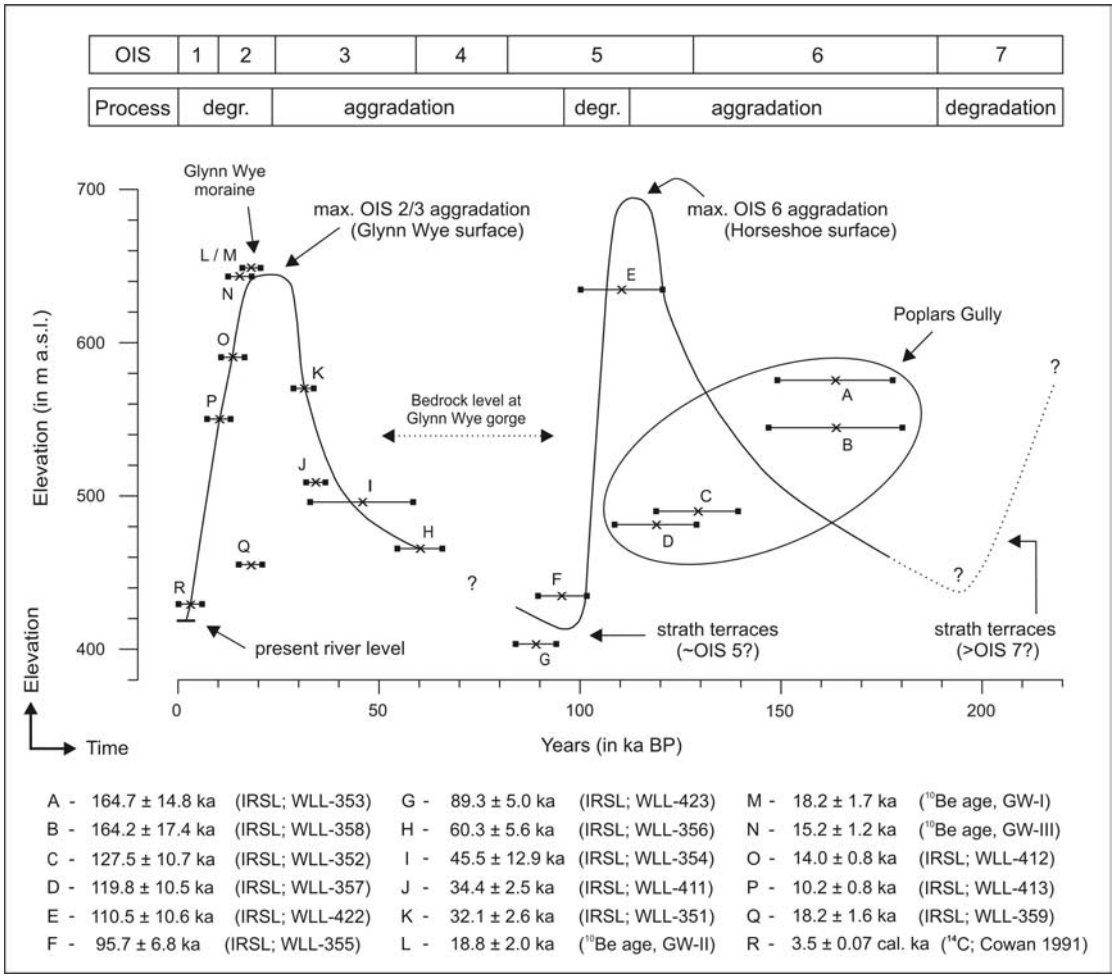

Fig. 76. Geochronological summary from valley fill deposits in the lower Hope Valley. Numerical ages are plotted against elevation and provide a detailed record of multiple phases of valley filling and exhumation over the past ~200 ka. The results show that the modern valley fill represents a composite of at least two generations of deposits from OIS 6 and OIS 4-2, respectively. Based on numerical ages and stratigraphic context five Late Pleistocene phases of large scale aggradation and degradation were identified with a vertical spread of 220 m. Because the minimum valley floor elevation during each of the exhumed stages was below the level of the Glynn Wye gorge it is probable that the gorge was re-used and repeatedly buried and re-excavated, or alternatively, that other gorges existed which are still buried under the remaining fill sequence.

Postglacial downcutting that followed OIS 6 glaciation rapidly exhumed the valley until mid-OIS 5. A new phase of valley aggradation began at around ~90 ka, as indicated by fine grained sediments deposited at low elevation in the newly excavated valley at 95.7 ± 6.8 ka and 89.3 ± 5.0 ka (F, G, Glynn Wye Stream site, Carlyle

Terrace site). At Glynn Wye Stream, OIS 5 deposits overlie a bedrock strath terrace located 10 m above modern river level (~415 m) and indicating that the incised OIS 5 valley floor was at or below present valley floor (~405 m). At both sites the dated sediments are overlain by gravel dominated aggradational sequences of more than 150 m thickness. IRSL dates from fine grained interbeds within these gravels and cosmogenic ages from the overlying moraine provide a series of stratigraphically consistent ages (ages H, I, J, K, L, M, N in Fig. 76). The ages trace the progressive infilling of the lower Hope Valley during late OIS 4 and throughout OIS 3. Between ~60 ka and ~30 ka aggradation raised the lower Hope Valley floor by at least 110 m suggesting that the majority of last glacial aggradation occurred significantly before the LGM (late OIS 3 / 2). An IRSL age of 34.4 ka (J) obtained from lacustrine deposits in the middle Hope Valley indicates that by this time the middle and lower valley were still ice free. The lake in this tributary valley was probably dammed by the rapidly accumulating aggradation fan in the trunk valley suggesting that the onset of large scale last glacial valley aggradation occurred prior to ~34 ka. This interpretation is consistent with an IRSL age of 32.1 (K) from the aggradation gravels in the trunk valley itself.

With respect to the timing of the last glacial maximum, the Hope-Waiau results show that aggradation was well advanced by ~34 ka thereby supporting the recent notion that the New Zealand LGM signal has a much earlier onset than 23 ka which is traditionally considered the begin of the 'global' LGM of (e.g. Mix et al., 2001). In New Zealand the LGM onset is now seen to significantly predate the OIS 2 boundary (~24 ka, Martinson et al., 1987), and is more accurately placed at around 28.5 – 30.5 ka as based on pollen (Vandergoes et al., 2005), at around 27.0 ka as shown by speleothem records (Hellstrom et al., 1998), at ~30.0 ka as seen in DSDP 594 (Heusser and van de Geer, 1994), and at around 28–32 ka from geomorphic and glacial records of the western South Island (Suggate and Almond, 2005).

The end of valley aggradation and onset of postglacial fluvial downcutting into the local sedimentary fill is constrained by a minimum radiocarbon age of 17.5 ± 0.3 cal. ka BP from organic silts near the top of the main aggradational terrace in the Waiau Valley (Suggate, 1965). If the age is considered close to the onset of degradation it suggests that fluvial downcutting started with some delay following glacial retreat.

This would be expected since many of the unglaciated tributary valleys (e.g. Kakapo Valley) were filled with thick sedimentary sequences as removal via the main valley was blocked by the trunk glacier. These and other depositoral systems were responsible for the high sediment supply immediately following glacial retreat, thereby preventing an immediate post-deglaciation begin of fluvial downcutting. An IRSL age from loessial cover beds on lower degradational terraces (10.2 ka) and an earlier radiocarbon age from organic silts of an abandoned low terrace (3.5 ± 0.07 cal. ka BP, Cowan 1991) permit the construction of a rough late OIS 2 and Holocene fluvial downcutting curve (Fig. 76). Results indicate a relatively linear downcutting profile with incision rates of 10.0 – 12.8 mm/a during late OIS 2 and 4.9 mm/a during the late Holocene.

9.1.2. Glacial advances

Although results from cosmogenic dating are available only for a third of the sampled moraines in the Hope-Waiau Valleys, the ages on hand constrain the timings of several key moraines and by combining cosmogenic and luminescence dating a number of new insights were found. The oldest glacial deposits in the valley were dated to OIS 6 and based on the stratigraphic context and sedimentological properties (Poplars Gully) three glacial advances were recognized and a subdivision of OIS 6 into two glacial phases proposed. OIS 6 deposits in the lower Hope Valley overlie bedrock and are volumetrically substantially thicker than the OIS 4 and OIS 2/3 sequences. A possible explanation for the relatively minor depositional volume associated with OIS 4/2 could be that these glacial advances were mainly erosive in this part of the valley but such scenario is inconsistent with the extensive survival of older deposits. The results are interpreted to indicate that OIS 6 glacial advances were considerably larger than those of the last glacial cycle. This suggestion is mainly based on the larger size of the OIS 6 glacial trough in the lower Hope Valley which extended at least 150 m below the inferred LGM base level in the same valley segment. A similar observation has been made for the Rakaia Valley where OIS 6 deposits occupy a much greater trough than those of the LGM (Shulmeister, et al., submitted). Although it has been pointed out that the ice extents of Late Pleistocene glacial advances are roughly comparable (Suggate, 1990), the Hope-Waiau data

indicate that the respective ice volumes in OIS 6 and OIS 4-2 differed substantially. These results are not consistent with Suggate's (1990) model were the *"...generally similar extents of glaciers ... during the last 0.35 Ma"* (p. 182) would indicate that *"... conditions during all of these were similar to those inferred for the Otira glaciations"* (p. 182). Instead the findings of this thesis are similar to results from Tasmania were a substantially larger OIS 6 and even larger mid-Quaternary glaciations (compared to OIS 2/3 and OIS 4) have been recognized (Colhoun, 1985; Augustinus, 1999; Colhoun, 2004).

No OIS 4 glacial deposit was found and all of the dated aggradational deposits either pre- or postdate OIS 4. Similarly, none of the glacial landforms returned an OIS 4 age and it is therefore difficult to assess whether OIS 4 glacial advances were predominantly erosional or depositional in character, although it may be said that potential OIS 4 advances must have been smaller than those of OIS 6. The results mirror earlier uncertainties by Clayton (1968) who could not find evidence for an early Otiran (OIS 4) glaciation in the middle and upper Hope-Waiau Valleys. OIS 4 advances, however, have been recognized (Soons, 1963a) and numerically dated in the Rakaia Valley (Shulmeister et al., submitted).

Cosmogenic dating of three moraines and glacial surfaces yielded ages between 20.5 ka and 13.5 ka suggesting that all of them are associated with glacial advances during OIS 2. This was particularly unexpected for the Kakapo Hill surface which was previously inferred to represent glaciation during OIS 8 (Clayton, 1968). The data suggest that, although the Kakapo deposits may have formed during an earlier glaciation, the surface was overrun by a glacial advance during the LGM. Although age control for the LGM ice overrun is limited, the result must be taken seriously, because overriding of higher (and assumingly older) glacial surfaces by younger ice advances poses a potential problem for one of the more fundamental assumptions in the glacial model of the Southern Alps. Namely that the vertical arrangement of glacial surfaces is a representation of vertically stacked and successively older glacial surfaces which were uplifted through time. Instead the result from Kakapo Hill indicates that this surface was overrun by younger ice. Higher surfaces may therefore have a more complex history than previously recognized. More and tighter numerical

age control from higher elevation glacial surfaces in the Southern Alps is essential to resolve this question.

Late LGM and LGIT ages from the Glynn Wye (~18.5 ka) and Lewis Pass (12.7 -13.5 ka) moraines indicate that they are associated with last glacial recessional still-stands or, and more probable, with brief glacial re-advances following the onset of general glacial retreat. In the case of the Glynn Wye moraine the results suggest a correlation to the later Blackwater/Bayfield or alternatively early Poulter/Acheron advances of the Waimakariri and Rakaia Valleys. Based on this interpretation the earlier, but as yet undated Glenhope advance of the Hope-Waiau Valleys (Clayton, 1968) is likely to be the main Blackwater/Bayfield correlative and not an early Otiran advance as suggested by Cowan (1989). A revised correlation is also suggested for the Lewis Pass moraine which was associated by Clayton (1968) to the late glacial Poulter/Acheron complex. The Lewis advance was a much smaller ice fluctuation near the headwaters of this system and thus represents a late stage re-advance.

In summary, the Glynn Wye dates indicate that recession from the LGM in New Zealand commenced close to 20-19 ka which is generally consistent with data from the Cobb Valley in the northern South Island (Shulmeister et al., 2005) and other locations in the Southern Hemisphere such as the Chilean Lake District and the Argentinean Lago Buenos Aires (Denton et al., 1999; Kaplan et al., 2004). The recession was interrupted by short lived ice re-advances at ~18 ka and during the LGIT at ~13 ka. Other LGIT advances in New Zealand have been reported from Arthur's Pass and Franz Josef Glacier but the dating of the advances has been controversial (Ivy-Ochs et al., 1999; Denton and Hendy, 1994; Mabin, 1996). In the case of the Waiho Loop a Younger Dryas interpretation was based on a mean age of 13.1 ± 0.08 cal. ka BP (Denton and Hendy, 1994) obtained from wood at Canavans Knob which is in fact 2 km upvalley from the Waiho Loop terminus (Anderson and Mackintosh, 2005). Similarly, the Misery moraines at Arthur's Pass were interpreted to represent a Younger Dryas advance based on a mean cosmogenic age of 11.7 ± 0.3 ka (Ivy-Ochs et al., 1999). The dating provides a minimum age only, because, firstly the Misery moraines are about 2 km upvalley of the maximum re-advance limit (McGrath moraines) secondly, because the shielding factor of 0.99 - 0.98 used by Ivy-Ochs et al. (1999) to calculate the ages significantly overestimates the local TCN

production rate (pers. com. D. Fink) which makes the age appear younger. Thirdly, Ivy-Ochs et al. (1999) used a ^{10}Be production rate that is ~18 % higher (6.0 atoms g^{-1} yr^{-1}) than the more widely accepted Stone (2000) values (5.1 atoms g^{-1} yr^{-1}). This makes the Misery moraine ages reported by Ivy-Ochs et al. (1999) younger than would be reported by other cosmogenic groups. It is therefore likely that the true ages of both advances are between 0.5 – 2 ka older. This would put both advances close to the dates for the Lewis Pass re-advance of the Hope-Waiau Valleys which predates the Northern Hemisphere Younger Dryas cooling and is therefore more likely to represent a New Zealand climate signal associated with the Antarctic Cold Reversal (ACR). This is consistent with recent pollen studies from New Zealand who suggest a minor climate reversal during the postglacial warming between 14.6 – 13.6 cal.^{14}C years (McGlone, 1995; McGlone et al., 2004) and recent results from surface water uranium ratios (^{234}U/^{238}U) which indicate minor cooling and increased precipitation over New Zealand during the same period (Robinson et al, 2004).

9.2. Sedimentary architecture of the Hope-Waiau valley fill

The deposition of glacial valley fills is controlled by a great variety of geological processes and valley fills of the Southern Alps permit to reconstruct past combinations of glaciological, geomorphological and tectonic parameters. Deposition occurred in a setting that was characterized by very high erosion rates and sediment fluxes as well as high-throughput / high-capacity glacial and fluvial systems (e.g. Kirkbride and Spedding, 1996; Benn et al., 2003). Glacial valley landsystems of New Zealand represent exceptionally well connected glacial and fluvial transport systems in which proglacial fluvial reworking is dominant while very little material is incorporated into terminal moraines. This predominance of fluvial deposits is typical of ice advances phases in this type of glacier system. Deposition during retreat phases differs and is dominated by glaciolacustrine sediments and gravity driven ice collapse processes. The associated deposits are surprisingly well preserved in the Hope-Waiau Valleys.

Fill deposits in the Hope-Waiau Valleys comprise deformed and undeformed morainic, (glacio-) fluvial, (glacio-) lacustrine, till, debris flow, fan and aeolian

sediments. The overall sedimentological arrangement indicates a range from glacial to proglacial to paraglacial deposition with a sedimentary inventory that is typical for ice marginal zones. The Hope-Waiau valley fill can be classified as a polygenetic-composite fill sequence (Ballantyne, 2002; Owen, 1989). The fill consists of a paraglacial/distal-proglacial portion, which is dominated by a braided river facies consisting of gravels and overbank sediments, and an ice-proximal/marginal-subglacial portion, which comprises glacio-lacustrine silts and sands, poorly sorted glaciofluvial gravels, subaqueous mass flows and stratified glacial diamictons.

Glacial sediments at Poplars Gully (ice-proximal/marginal-subglacial fill portion) contain a high proportion of waterlain sediments and sub-aqueous mass flows. Widespread evidence for extensional deformation is interpreted to indicate removal of ice-support shortly after deposition. The overall stratigraphic architecture is chaotic and it was problematic to differentiate between subglacial and ice proximal proglacial deposits. The sedimentary style indicates rapid deposition often in conjunction with probably short lived proglacial lakes. The overall sequence is interpreted to represent sedimentation during the retreat of the Hope-Waiau glacier. Glaciolacustrine deposits are typical of recessional valley fills since proglacial lakes often form behind terminal moraines and outwash heads following ice thinning and glacial retreat (e.g. Evans, 2003). The lakes act as sediment traps for ice contact deposits. Sedimentation along the retreating ice margin was mainly via subaqueous and subaerial ice contact fans, deposited by conduits, as well as ice marginal and supraglacial streams. These sequences are often interbedded with mass flows that derived from the nearby active and stagnant ice or alternatively from collapsing kame or glaciofluvial terraces. Because of the inherent instability of these environments the individual fans are usually small and the lateral extent of most units limited. Ice proximity is indicated by glaciotectonic deformation, which in most cases represents only minor re-advances. Deformation of the proglacial sediment barrier can range from small scale open folding to m-scale shearing of units. Brief re-advances into proglacial lake fills are a likely explanation for push moraines which have been described as anomalous from other New Zealand valleys (e.g. Speight, 1942) because they appeared to *"...show a marked departure from the ordinary structure of moraines"* as they consist of *"...rounded stones in a finer matrix, and with no sign of included morainic material"* (p. 151).

Regarding the initial question concerning the mechanism for the preservation of ice overrun older soft sediments in the Hope-Waiau Valleys, it may be pointed out that the ice advanced largely over its own coarse outwash gravels which in turn were aggraded over older depositional sequences. The gravels probably constituted a well drained glacier bed which largely prevented formation of subglacial glaciofluvial channels and associated erosion by pressurized subglacial meltwaters. Dry glacier beds would have reduced glacial sliding suggesting that ice flow in the lower portions of extended valley glaciers in the Southern Alps occurred mainly via internal ice deformation. Additionally, conditions at the glacier bed were probably above pressure melting point for most parts of the year which limited the possibility of subglacial freeze on and removal of material. Exceptionally well drained glacier beds, as provided by ice overrunning coarse gravel sequences, may be the explanation for the observed low erosional capacity associated with the *lower* portions of large valley glaciers in the Southern Alps. This may suggest that although New Zealand's temperate glaciers are associated with exceptionally high erosion rates over bedrock (e.g. Hallet et al., 1996), their erosive capacity over well drained soft sediments is small. Because the preservation of ice overrun older deposits appears to be a more common phenomenon in New Zealand (e.g. Rakaia Valley, Shulmeister et al., submitted) a general distinction between a highly erosive upper, bedrock dominated, and a low-erosive lower, sediment dominated, glacial zone is suggested.

9.3. The New Zealand glacial system: Towards a model for glaciation in the Southern Alps

As was highlighted in Chapter 8, former glacier systems of the Southern Alps operated under hyperhumid conditions with large annual mass balances and some of the highest glacial ice turn-over rates on Earth. As a result glacio-depositional sequences in New Zealand differ in both morphology and sedimentology from the drier, higher-latitude / higher-elevation systems that have traditionally formed the basis for glacier-climate models in paleo-glaciology (e.g. Sugden and John, 1976; Benn and Evans, 1998). At the same time modern mid-latitude perhumid glacial systems (e.g. Southern Chile, Pacific NW) are substantially smaller in scale and it is dubious whether glacial models derived from higher latitude temperate glaciers (e.g.

Iceland, Alaska, Norway) can fully apply to the lower mid-latitude setting of New Zealand.

Ice accumulation during Quaternary glaciations was concentrated in a narrow sector of the central Southern Alps from which fast flowing valley glaciers extended to the alpine forelands and to low elevations above sea level. Steeply rising ELAs meant that glacial tongues often extended far below the regional ELA where, even during glacials, relatively mild maritime conditions caused high levels of ice ablation (Takeuchi et al., 1999). This resulted in an almost year-round availability of large volumes of free melt-water in glacial and paraglacial environments (Gage, 1965; Soons, 1979). As a direct consequence ice proximal depositional sequences in most glacial valleys of the Southern Alps contain an unusually large portion of water lain or water derived sediments.

Chapter 8 suggested that (a) large scale glaciations in the Southern Alps can be generated with very moderate cooling (2-4˚C), that (b) synoptic climate phenomena in the New Zealand region are capable to generate a cooling of this scale and that (c) such synoptic event was the likely cause for the much debated LGIT re-advance in New Zealand and not Northern Hemisphere climate forcing as suggested by Denton and Hendy (1994) and Ivy-Ochs et al. (1999). The modelled response of snow mass balances to moderate cooling indicates that glacial systems of the Southern Alps are highly temperature sensitive, however, the results also show that this thermal sensitivity fundamentally depends on the availability of very large annual precipitation totals.

The results of this thesis have yielded some new insights into the nature, extent and timing of former glaciations in the Hope-Waiau Valleys of North Canterbury. Though the main focus of the study was to understand the local glacial pattern, the findings have implications for the larger scale interpretation of Quaternary glaciations in New Zealand. The following section will discuss the larger perspective and summarize a conceptual model for the growth and decay of glaciations in the Southern Alps which uses both existing and new ideas. An outline of the model is shown in Fig. 77.

I have argued that glacial accumulation in the Southern Alps can expand dramatically in response to minor climatic perturbations. While this can be seen as a general feature of glaciers in perhumid and maritime settings (Benn and Evans, 1998), the style of glacial accumulation in New Zealand has some distinct characteristics. Under present conditions (A in Fig. 77) comparatively small mountain glaciers remain on both sides of the topographic divide with the majority of glacial accumulation occurring in ice fields above 1800 m (Clare et al., 2002). Positive and negative mass balances are greatest on the western side of the divide where precipitation is largest and glaciers descend to near sea level.

Following cooling at the begin of glaciation (B in Fig. 77) mountain glaciers expanded to valley glaciers and large ice fields formed in the central Alps from which outlet glaciers descended downvalley. Maximum last glacial cooling in New Zealand is estimated to be 4-5˚C (Porter, 1975; Soons, 1979). The early phases of glaciation are unlikely to record maximum cooling and a forcing of 2-3˚C during the initial glacial phases is probable, which is consistent with regional sea surface temperature estimates (e.g. Barrows and Juggins, 2005). Based on an average environmental lapse rate of 0.6˚C/100m this cooling drops ELAs in the Southern Alps by about ~400 m (Fig. 77). As a result, the available glacial accumulation area, in particular in the central Alps where interglacial ELAs were already at comparatively low elevations, rapidly increased in size. The expanding ice volumes causes separate glacier fields to merge and form large ice fields with the highest peaks standing proud as nunataks. Even at this stage a separation between the topographic and glacial divides developed with the centre of ice accumulation shifting westward to the area of maximum precipitation. This initiates ice overflow from areas west of the topographic divide into eastern catchments and most of the lower passes at the divide, as at Lewis Pass in the Hope Waiau Valleys, probably become operative at this time. Substantial ice overspill is indicated by rounded mountaintops, smooth ice confluence saddles and low mountain passes in the headwater regions of most glacial valleys. Due to steeper valley gradients, glaciers in the west descended to lower elevations than in the east and experienced greater ablation losses which is likely to have caused higher ice flow velocities in the west than in the east. As shown in Fig. 77 glacial maxima in New Zealand are probably associated with enhanced westerly wind flow in response to globally increased pole-equator pressure differences (Shulmeister et al., 2004) and

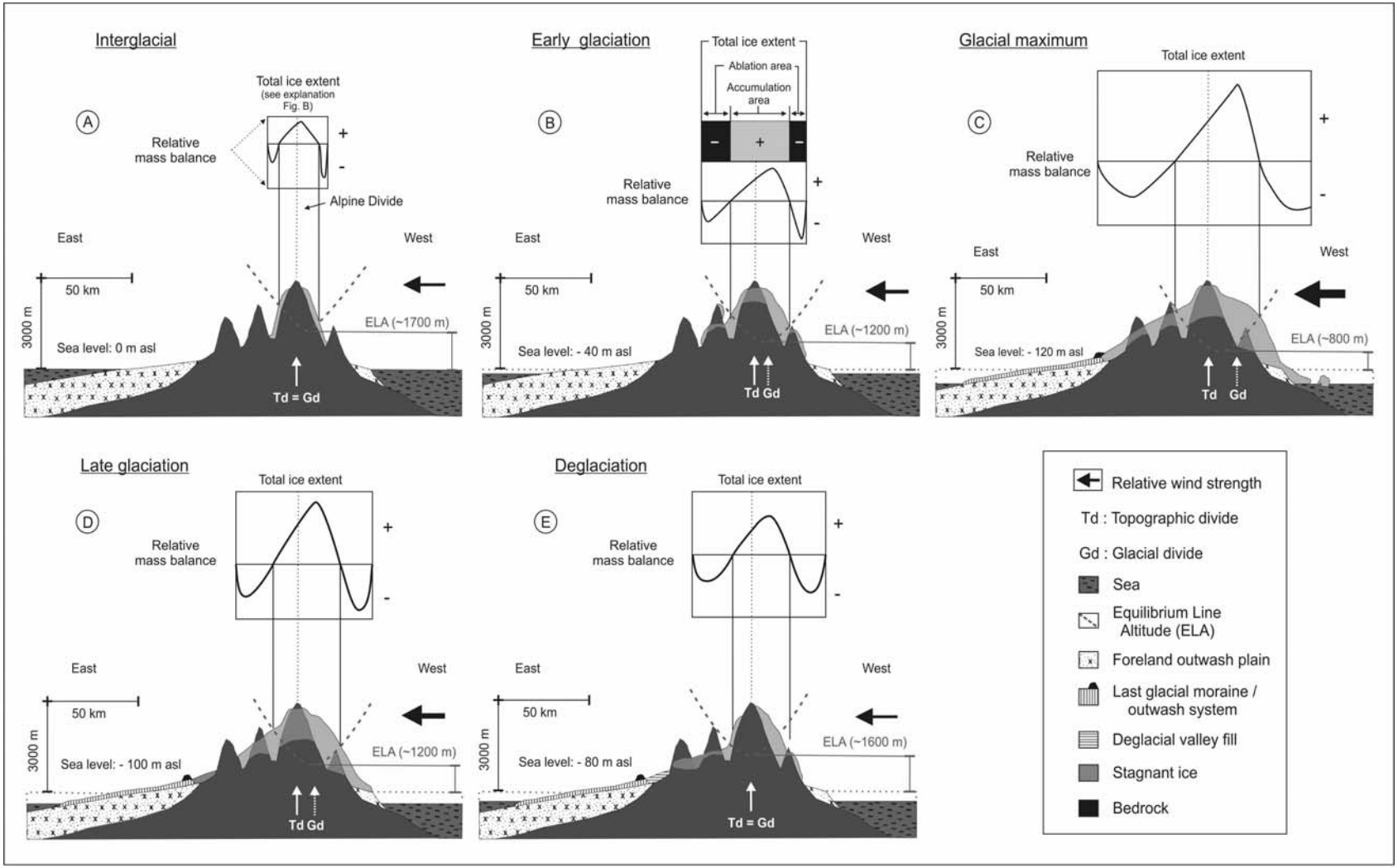

Fig. 77: Conceptual glacial model for the Southern Alps reconstructing changes in ELA, relative mass balance, ice extent, topographic and glacial divides, sea level and westerly strength throughout the growth and decay of a glaciation in New Zealand. The depicted ELA levels are averages.

positive ENSO modes (Pepper et al., 2004). In addition, lower sea levels pronounced the relative height of the Southern Alps which in turn intensified orographic forcing of moist westerly air masses causing persistent or possibly increased precipitation over the western Alps.

During each of the late Pleistocene glacial maxima (C in Fig. 77) ice drained from the central Alps via the existing valley network and glaciers reached the alpine forelands in the east and calved into the Tasman Sea in the west. Central ELAs were depressed by 800 – 1000 m (Willet, 1950; Suggate, 1990) which transformed most of the central Alps into a highly productive glacial accumulation zone. The continuing growth of connected ice fields increased the separation distance between topographic and glacial divides and enlarged the ice volume that flowed from west to east. The location of the maximum ice thickness is likely to have migrated westwards thereby reflecting the asymmetric growth of ice fields in the Southern Alps and the successively further westward interception of moist westerly air masses. This effect probably enhanced the east-west precipitation contrast. Geomorphologically this phase is associated with substantial gravel accumulations on the foreland plains.

Glacial ELAs in New Zealand rose steeply so areas east of the central Alps could not have contributed substantial amounts of ice. This is indicated by the high elevation, small size and general low number of cirques in ranges east of the central Alps. It implies a glacial pattern where ice occupied the headwaters and extended through large trunk glaciers far downvalley, blocking most of the ice free or only partically glaciated tributaries valleys. Blocking by the trunk glaciers resulted in extensive sediment storage and lake damming in the tributary valleys.

The deglaciation sequence (D and E in Fig. 77) starts with climatic amelioration which raised the regional ELAs. The response to the initial warming signal was not immediate because the ice fields in the central Alps had raised the active terrestrial surface by hundreds of meters, thereby maintaining large areas above ELA. This partially isolated the accumulation zone from raising ELAs during the begin of the late glacial stage. The situation is shown in Fig. 77D where the ELA is at ~1200 m, the same level as during the early part of the glaciation (B), yet a substantially larger ice volume can be maintained. As long as thick ice fields remain, ice produced west of

the topographic dived will flow east. The warming nevertheless increased ice ablation at the glacier termini and this phase is associated with gradual glacial retreat from the maximum moraine positions.

Deglaciation markedly intensified when the thinning of the central alpine ice fields reached a point where ice overspill from western to eastern catchments ceased. This cut off a significant ice source for the now overextended glaciers in the eastern valleys which can no longer support the extended ice positions. Fig. 77E depicts this situation which is likely to have rapidly reduced ice gradients and consequently led to the stagnation of large portions of the lower valley glaciers. Conditions similar to these are likely to have occurred during the deposition of the deglacial Hope-Waiau Valley fill which is associated with formation of large proglacial lakes. Following the recession from the extended late glacial ice positions in the Southern Alps (Poulter/Acheron/Kumara-3 complex) no major glacial re-advances is recognized while smaller scale ice terminal oscillations reflect only minor (seasonal?) variations.

The pattern of inception and growth of large glaciations in the Southern Alps is controlled by the rapid expansion of ice accumulation in the hyperhumid central sector of the Alps. Steeply rising ELA levels imply that ice accumulation in nearly all other mountainous areas was small by comparison and in consequence did not have significant influence on the dynamics of glacial fluctuations in New Zealand. Glacial termini in the eastern Southern Alps were climatically overextended and could only be maintained so long ice from western New Zealand was fed into the eastern valley systems. The pattern of glacial decay was characterized by the initial survival of large ice fields in the central Alps due to the elevated ice surfaces, followed by an accelerated deglaciation via large scale ice stagnation.

In summary, this thesis has produced a variety of new information on the Hope-Waiau glacial system. The recognition and documentation of extensive older fill sequences is a key finding and preliminary work from other New Zealand valleys (e.g. Rakaia Valley) indicates that the studied system is not unique. Further work on this issue is needed and should target other major valley systems such as the Waimakariri, Rangitata and Clutha Valleys as well as the Mackenzie Basin. The sedimentology and stratigraphy of valley fill sequences provides detailed insights into the glaciological

modes and depositional environments associated with former New Zealand glacier systems. Although this thesis was primarily concerned with glacial valleys of the eastern Southern Alps, similar work is needed for western New Zealand to highlight glaciological and sedimentological similarities and differences between eastern and western systems.

The combined application of IRSL and cosmogenic dating has provided detailed information on the geomorphological evolution of the Hope-Waiau Valley system over the last two glacial cycles. Similar dating campaigns are needed for more major valleys to improve absolute age control for glaciations in New Zealand and substantiate the presented timings of glacial oscillations and aggradation-degradation cycles from the Hope-Waiau Valleys. Better absolute age control on glacial signals in New Zealand will unlock the full potential of this record for the debate on interhemispheric glacial correlations and global climate research. Finally, the model approach used by this thesis to analyse the sensitivity of glacial accumulation in the Southern Alps has demonstrated that large glaciation in New Zealand can be triggered by only moderate cooling. An expansion of the model work for the whole of the Southern Alps is needed and should integrate mass balance and ice flow characteristics with a digital elevation model. However, none of above approaches will provide a final solution when applied separately, the combination of *all* of them is essential for the formulation of a comprehensive glacial model for the Southern Alps.

Acknowledgements

During this thesis project I have had the privilege to work with several outstanding people who have contributed greatly to this study and provided me with invaluable personal and scientific guidance. Of those, my academic supervisor Dr. Jamie Shulmeister, has been an inspiration from the first to the last day and I would like to thank him for his unfailing support, his excellent advise and for putting me on the scientific path. I am also grateful to him and his wife Val for being great friends and fantastic hosts. Dr. Phil Tonkin has shared his encyclopaedic knowledge on New Zealand geomorphology with me and has stimulated my thinking during many discussions. Thanks to Dr. David Nobes who helped me collecting and interpreting ground penetrating radar profiles and Dr. David Fink for the AMS measurements of cosmogenic ^{10}Be. The Department of Geological Sciences has been a wonderful place to be and I am grateful to all of the teaching staff for their support but in particular to Mr. Dave Bell and Dr. Tim Davies. I would like to thank all the technical staff, especially Rob Spiers and Sacha Baldwin-Cunningham for their excellent job in the cosmogenic sample preparation, Pat Roberts, our secretary, for solving every problem she was presented with, and Cathy Higgins and John Southward for their help throughout this thesis project. I have discussed many of the field problems with several overseas visitors to the department and would like to thank Dr. Harry Jol, Dr. Chris Smart and Dr. Dave Evans for their contributions. I was assisted in the field by Craig Woodward, Flo Buech and Guyon Smith. The work on this thesis and the last 3½ years of my life in New Zealand, however, were made unforgettably special by my partner Marie-Elaine who I thank for her unshakable support and love. I am so much looking forward to a future with you.

References

Alloway, B.V., 2004. NZ-INTIMATE meeting, GNS Rafter Laboratory, Wellington, August 2004. Institute of Geological and Nuclear Sciences, Report 2004/22, 43p.

Alloway, B.V., Almond, P.C., Augustinus, P.C., Barrell, D.J.A., Bertler, N.A.N., Carter, L., Litchfield, N.J., Lowe, D.J., McGlone, M. S., Newnham, R.M., Shulmeister, J., Vandergoes, M.J., Williams, P.W., and NZ-INTIMATE Members (submitted). Towards a climate event stratigraphy for New Zealand over the past 30,000 years. Journal of Quaternary Science.

Almond, P., Moar, N.T., Lian, O.B., 2001. Reinterpretation of the glacial chronology of South Westland. New Zealand Journal of Geology and Geophysics 44: 1-15.

Anderson, B., 2003. The response of 'Ka Roimata o Hine Hukatere' Franz Josef Glacier to climate change. Unpublished Ph.D. thesis, University of Canterbury, Christchurch, 114p.

Anderson, B., Mackintosh., A., 2006a. Temperature change is the major driver of late-glacial and Holocene glacier fluctuations in New Zealand. Geology 34(2): 121-124.

Anderson, B., Mackintosh., 2006b. Interactive comment on: Synoptic climate change as a driver of late Quaternary glaciations in the mid-latitudes of the Southern Hemisphere, H. Rother and J. Shulmeister. Climate of the Past Discussions 1: 161-167. 1814-9359/cpd/2005-1-1.

Anderton, P.W., Chinn, T.J., 1978. Ivory Glacier, New Zealand, an I.H.D. representative basin study. Journal of Glaciology 20: 67-84.

Andrews, J.T., Miller, G.H., 1972. Quaternary history of the northern Cumberland Peninsula, Baffin Island, N.W.T. Canada. Arctic and Alpine Research 4: 45-59.

Augustinus, P.C., 1999. Reconstruction of the Bulgobac glacial system, Pieman River Basin, western Tasmania. Australian Geographical Studies 37(1): 24-36.

Baker, G. S., Strasser, J.C., Evenson, E.B., Lawson, D.E., Pyke, K., Bigl, R.A., 2003. Near-surface seismic reflection profiling of the Matanuska Glacier, Alaska Geophysics 68(1): 147-156.

Bal, A.A., Browne, G.H., 1997. Geological Society of New Zealand, Fossil Record Form (unpublished record), University of Canterbury, File K35-f61.

Ballantyne, C.K., 2002. Paraglacial geomorphology. Quaternary Science Reviews 21: 935-2017.

Barrell, D.J.A., Alloway, B.V., Shulmeister, J., Newnham, R.M. (eds.), 2005. Towards a climate event stratigraphy for New Zealand over the past 30,000 years. Science Report 2005/07. Wellington, Institute of Geological & Nuclear Sciences: 12p and poster.

Barrows, T.T., Juggins, S., 2005. Sea-surface temperatures around the Australasian margin and Indian Ocean during the Last Glacial Maximum. Quaternary Science Reviews 24: 1017-1047.

Bell, D.H., 1998. Glacial History of Cass. Geological Society of New Zealand, Miscellaneous Publication Field Trip 4, 101B: 12p.

Benn, D.I., 1995. Fabric signature of subglacial till deformation, Breidamerkurjoekull, Iceland. Sedimentology 42: 735-747.

Benn, D.I., Evans, D.J.A., 1998. Glaciers and Glaciation. Arnold, London, 734p.

Benn, D.I., Kirkbride, M.P., Owen, L.A., Brazier, V., 2003. Glaciated valley landsystems. Evans, D.J.A. (ed.), 2003. Glacial landsystems: 373-406.

Bennett, K.D., Haberle, S.G., Lumley, S.H., 2000. The last glacial-Holocene transition in southern Chile. Science 290: 325-328.

Berger, G.W., Tonkin, P.J., Pillans, B.J., 1996. Thermoluminescence ages of post-glacial loess, Rakaia River, South Island, New Zealand. Quaternary International 34-36: 177-181.

Berger, G.W., Almond, P.C., Pillans, B.J., 2001. Luminescence dating on glacial stratigraphy in Westland, New Zealand. New Zealand Journal of Geology and Geophysics 44: 25-35.

Boulton, G.S., Dobbie, K.E., Zatsepin, S., 2001. Sediment deformation beneath glaciers and its coupling to the subglacial hydraulic system. Quaternary International 86: 3-28.

Bowden, M.J., 1974. The water resources of the Waiau catchment, North Canterbury Catchment Board.

Braithwaite, R.J., Olesen, O.B., 1989. Calculation of glacier ablation from air temperature, West Greenland. Oerlemans, J. (ed.). Glacier fluctuations and climatic change. Amsterdam, Kluwer Academic Publishers: 219-233.

Braithwaite, R.J., Zhang, Y., 2000. Sensitivity of mass balances of five Swiss glaciers to temperature changes assessed by tuning a degree-day model. Journal of Glaciology 46: 7-14.

Broecker, W.S., 1997. Future directions of paleoclimate research. Quaternary Science Reviews 16: 821-825.

Broecker, W.S., Thurber, D.L., Goddard, J., Ku, T., Matthews, R.K., Mesolella, K.J., 1968. Milankovitch hypothesis supported by precise dating of coral reefs and deep-sea sediments. Science 159: 297-300.

Brown, L.J., Wilson, D.D., Moar, N.T., and Mildenhall, D.C., 1988. Stratigraphy of the late Quaternary deposits of the northern Canterbury Plains, New Zealand. New Zealand Journal of Geology and Geophysics 31: 305-335.

Brown, E.T., Edmond, J.M., Raisbeck, G.M., Yiou, F., Kurz., M.D., Brook, E.J., 1991. Examination of surface exposure ages of Antarctic moraines using *in situ* produced 10Be and 26Al. Geochimica et Cosmochimica Acta 55: 2269-2283.

Browne, G.H., Naish, T.R., 2003. Facies development and sequence architecture of a late Quaternary fluvial-marine transition, Canterbury Plains and shelf, New Zealand: implications for forced regressive deposits. Sedimentary Geology 158: 57-86.

Bull, W.B., 1987. Adjustments by the Charwell River, New Zealand, to uplift and climatic changes. Geomorphology 1: 15-32.

Bull, W.B., 2003. Lichenometry dating of coseismic changes to a New Zealand landslide complex. Annals of Geophysics 46: 1155-1168.

Burrows, C.J., 1975. Late Pleistocene and Holocene moraines of the Cameron Valley, Arrowsmith Range, Canterbury, New Zealand. Arctic and Alpine Research 7(2): 125-140.

Burrows, C.J., 1979. A chronology for cool-climate episodes in the Southern Hemisphere 12 000 - 1000 yr. B.P. Paleogeography, Paleoclimatology, Paleoecology 27: 287-347.

Burrows, C.J., 1980. Radiocarbon dates for post-Otiran glacial activity in the Mt. Cook region, New Zealand. New Zealand Journal of Geology and Geophysics 23: 239-248.

Burrows, C.J., 1983. Radiocarbon dates from late Quaternary deposits in the Cass District, Canterbury, New Zealand. New Zealand Journal of Botany 21: 443-454.

Burrows, C.J., 1988. Late Otiran and early Aranuian radiocarbon dates from South Island localities. New Zealand Journal of Science 15: 25-36.

Burrows, C.J., 1997. A macrofossil flora from early Aranuian lake bed deposits, Doubtful River, Waiau-uhu catchment, North Canterbury, New Zealand. New Zealand Journal of Botany 35: 545-553.

Burrows, C.J., Russel, J.B., 1975. Moraines of the upper Rakaia Valley. Journal of the Royal Society of New Zealand 5(4): 463-477.

Burrows, C.J., Chinn, T., Kelly, M., 1976. Glacial activity in New Zealand near the Pleistocene-Holocene boundary in the light of new radiocarbon dates. Boreas 5(2): 57-60.

Burrows, C.J., Gellatly, A.F., 1982. Holocene glacier activity in New Zealand. Striae 18: 41-47.

Burrows, C.J., Russel, J.B., 1990. Aranuian vegetation history of the Arrowsmith Range, Canterbury I. Pollen diagrams, plant macrofossils, and buried soil from Prospect Hill. New Zealand Journal of Botany 28: 323-345.

Burrows, C.J., Duncan, K.W., Spence, J.R., 1990. Aranuian vegetation history of the Arrowsmith Range, Canterbury II. Revised chronology for moraines of the Cameron Glacier. New Zealand Journal of Botany 28: 455-466.

Burrows, C.J., Moar, N.T., 1996. A mid Otira glaciation palaeosol and flora from the Castle Hill Basin, Canterbury, New Zealand. New Zealand Journal of Botany 34: 539-545.

Carryer, S.J., 1965. The glacial deposits along the northern flank of the Mount Hutt Range. New Zealand Journal of Geology and Geophysics 10: 1136-1144.

Carter, R.M., Norris, R.J., 1976. Cainozoic history of southern New Zealand; an accord between geological observations and plate tectonic predictions. Earth and Planetary Science Letters 31: 85-94.

Carter, L., Nelson, C.S., Neil, H.L., Froggatt, P.C., 1995. Correlation , dispersal, and preservation of the Kawakawa tephra and other late Quaternary tephra layers in the southwest Pacific Ocean. New Zealand Journal of Geology and Geophysics 38: 29-46.

Cehak-Trock, H., 1958. Der feste Niederschlag im atlantischen Klimagebiet., Arch. Meteorologie, Geophysik, Bioklimatologie. Serie B, 8 (3/4): 352-368.

Chater, A.M., 1995. A study on the spillover of westerly rainfall into the upper Waimakariri catchment. M.Sc. thesis, Department of Geography, University of Canterbury, 189p.

Chinn, T.J., 1981a. Geological Society of New Zealand, Fossil Record Form (unpublished record), University of Canterbury, File M32-f4.

Chinn, T.J., 1981b. Use of rock weathering rind thickness for Holocene absolute age-dating in New Zealand. Arctic and Alpine Research 13(1): 33-45.

Chinn, T.J., Whitehouse, I.E., 1980. Glacier snow line variations in the Southern Alps, New Zealand. IAHS-AISH Publ. 126: 219-228.

Clapperton, C.M., 2000. Interhemispheric synchroneity of Marine Oxygen Isotope Stage 2 glacier fluctuations along the American Cordilleras transect. Journal of Quaternary Science 15(4): 435-468.

Clare, G.R., Fitzharris, B.B., Chinn, T.J.H., Salinger, M.J., 2002. Interannual variation in end-of-summer snowlines of the Southern Alps of New Zealand, and relationships with Southern Hemisphere atmospheric circulation and sea surface temperature patterns. International Journal of Climatology 22: 107-120.

Clark, D.H., Bierman, P.R., Larsen, P., 1995. Improving *in situ* cosmogenic chronometers. Quaternary Research 44(3): 366-376.

Clayton, L.S., 1965. Late Pleistocene geology of the Waiau Valleys, North Canterbury, New Zealand. Unpublished Ph.D. thesis, University of Illinois, 93p.

Clayton, L.S., 1968. Late Pleistocene glaciations of the Waiau Valleys, North Canterbury. New Zealand Journal of Geology and Geophysics 11: 753-767.

Colhoun, E.A., 1985. The glaciations of the West Coast range, Tasmania. Quaternary Research 24: 39-59.

Colhoun, E.A., 2004. Quaternary glaciations of Tasmania and their ages. Quaternary glaciations extent and chronology. Ehlers, J., Gibbard, P.L. (eds.). Elsevier, Amsterdam, III: 353-360.

Cotton, C.A., 1947. The Hanmer Plain and the Hope Fault. The New Zealand Journal of Science and Technology 29: 10-17.

Cowan, H.A., 1989. An evaluation of the late Quaternary displacements and seismic hazards associated with the Hope and Kakapo Faults, Amuri District, North Canterbury. Unpublished M.Sc. thesis, Department of Geological Sciences University of Canterbury, 239p.

Cowan, H.A., 1990. Late Quaternary displacements on the Hope Fault at Glynn Wye, North Canterbury. New Zealand Journal of Geology and Geophysics 33: 285-293.

Cowan, H.A., 1991. The north Canterbury earthquake of September 1, 1888. Journal of the Royal Society of New Zealand 21(1): 1-12.

Cowan, H.A., McGlone, M.S., 1991. Late Holocene displacements and characteristic earthquakes on the Hope River segment on the Hope Fault, New Zealand. Journal of the Royal Society of New Zealand 21(4): 373-384.

Cox, P.T., 1926. Geology of the Rakaia gorge district. Transactions and Proceedings of the New Zealand Institute 56: 91-111.

Davies, T.R.H., Smart, C.C, Turnbull, J.M., 2003. Water and sediment outbursts from advanced Franz Josef Glacier, New Zealand. Earth Surface Processes and Landforms 28: 1081-1096.

Denton, G.H., Hendy, C.H., 1994. Younger Dryas age advance of Franz-Josef Glacier in the Southern Alps of New Zealand. Science 264: 1434-1437.

Denton, G.H., Heusser, C.J., Lowell, T.V., Moreno, P.I., Andersen, B.G., Heusser, L.E., Schluechter, C., Marchant, D.R., 1999. Interhemispheric linkage of paleoclimate during the last deglaciation. Geografiska Annaler (A) 81(2): 107-153.

Dobson, A.D., 1872. On the traces of ancient glaciers in Nelson Province. Transactions and Proceedings of the New Zealand Institute 4: 336-341.

Donelly, R., Harris, C., 1989. Sedimentology and origin of deposits from a small ice dammed lake, Leirbreen, Norway. Sedimentology 36: 581-600.

Dreimanis, A., 1988. Tills: their genetic terminology and classification. Genetic classification of glacigenic deposits. Goldthwait, R.P., Matsch, C.L. Rotterdam: 17-83.

Duller, G.A.T., Wintle, A.G., Hall, A.M., 1995. Luminescence dating and its application to key pre-Late Devensian sites in Scotland. Quaternary Science Reviews 14: 495-519.

Duna, T.J., 2000. Scaling factors for production rates of *in situ* produced cosmogenic nuclides: a critical reevaluation. Earth and Planetary Science Letters 176: 157-169.

Easterbrook, D.J., 2004. Synchronous, global, late Pleistocene ice sheet and alpine glacial fluctuations. Geological Society of America, 2004 annual meeting, Denver, CO, U.S.A. Abstracts with Programs, vol. 36, no. 5, 344p.

Eden, D.E., Frogatt, P.C., 1988. Identification and stratigraphic significance of distal Aokautere Ash in three loess cores from eastern South Island, New Zealand. Loess - its distribution, geology and soils. Eden, D.E., Furkert, R.J. Rotterdam, Balkema: 47-58.

Eden, D.E., Hammond, A.P., 2003. Dust accumulation in the New Zealand region since the last glacial maximum. Quaternary Science Reviews 22: 2037-2052.

Ehlers, J., Gibbard, P.L., 2004. Quaternary glaciations extent and chronology, Part 2: South America, Asia, Africa, Australasia, Antarctica. Elsevier, Amsterdam, 380p.

Eusden, J.D., Pettinga, J.R., Campbell, J.K., 2000. Structural evolution and landscape development of a collapsed transpressive duplex on the Hope Fault, North Canterbury, New Zealand. New Zealand Journal of Geology and Geophysics 43: 391-404.

Evans, D.J.A. (ed.), 2003. Glacial Landsystems. London, 532p.

Evans, D.J.A., Hiemstra, J.F., 2005. Till deposition by glacier submarginal, incremental thickening. Earth Surface Processes and Landforms 30: 1633-1662.

Evans, D.J.A., Benn., D.I., 2004. A practical guide to the study of glacial sediments, Arnold.

Eyles, N., Eyles, C., Miall, A.D., 1983. Lithofacies types and vertical profile methods; an alternative approach to the description and environmental interpretation of glacial diamict and diamictite sequences. Sedimentology 30: 393-410.

Fenner, J., Carter, L., Stewart, R., 1992. Late Quaternary paleoclimatic and paleo-oceanographic change over northern Chatham Rise, New Zealand. Marine Geology 108: 383-404.

Fink, D., 2003. *In situ* cosmogenic radionuclides for dates and rates. Biennial Conference of the Australasian Quaternary Association, Westport, New Zealand. Programme and Abstracts, 16p.

Fink, D., McKelvey, B., Hannan, D., Newsome, D., 2000. Cold rocks, hot sands - *in situ* cosmogenic applications in Australia at ANTARES. Nucl. Instrum. Methods B 17: 838-846.

Fitzsimons, S.J., Pollington, M., Colhoun, E.A., 1996. Palaeomagnetic constraints on the ages of glacial deposits in North-West South Island, New Zealand. Zeitschrift fuer Geomorphologie 105: 7-20.

Fleming, C.A., 1956. Quaternary geochronology in New Zealand. Actes du IV Congress International du Quaternaire 1953: 925-930.

Freund, R., 1971. The Hope Fault, New Zealand Geological Survey Bulletin. Wellington, 47p.

Forsyth, P.J., Barrell, D.J.A., Basher, L.R., Berryman, K.R., 2003. Holocene landscape evolution of the Havelock and upper Rangitata Valleys, South Canterbury, New Zealand. Wellington, Institute of Geological & Nuclear Sciences,.Science Report no. 2003/22: 45.

Gage, M., 1945. The Tertiary and Quaternary geology of Ross, Westland. Transactions of the Royal Society of New Zealand 75(2): 138-159.

Gage, M., 1958. Late Pleistocene glaciations of the Waimakariri Valley, Canterbury, New Zealand. New Zealand Journal of Geology and Geophysics 1: 123-155.

Gage, M., 1961. New Zealand Glaciations and the duration of the Pleistocene. Journal of Glaciology 3: 940-943.

Gage, M., 1965. Some characteristics of Pleistocene cold climates in New Zealand. Transactions of the Royal Society of New Zealand 3: 11-21.

Gage, M., 1977. Glacial Geology. Cass - History and Science in the Cass District, Canterbury. C. J. Burrows. Christchurch, University of Canterbury: 67-77.

Gage, M., 1985. Glaciations in New Zealand - the first century of research. Quaternary Science Reviews 4: 189-214.

Gage, M., Suggate, R.P., 1958. Glacial Chronology of the New Zealand. Pleistocene Bulletin of the Geological Society of America 69: 589-598.

Gair, H.S., 1967. Geological Map of New Zealand, 1 : 250 000, Sheet 20, Mt. Cook, Department of Scientific and Industrial Research, Wellington.

Gellatly, A.F., Chinn, T.J.H., Roethlisberger, F., 1988. Holocene glacier variations in New Zealand. Quaternary Science Reviews 7: 227-242.

Gemmell, A.M.D., 1999. IRSL from fine-grained glacifluvial sediment. Quaternary Geochronology 18: 207-215.

Gilbert, G.K., 1890. Lake Bonneville. Monograph - U. S. Geological Survey, Report: M 0001, 438p.

Gosse, J.C., Philips, F.M., 2001. Terrestrial in situ cosmogenic nuclides: theory and application. Quaternary Science Reviews 20: 1475-1560.

Grant-Taylor, T.L., Rafter, T.A., 1971. New Zealand Radiocarbon Measurements - 6. New Zealand Journal of Geology and Geophysics 14(2): 364-402.

Gregg, D.R., 1964. Geological Map of New Zealand, 1: 250 000, Sheet 18 – Hurunui, Department of Industrial and Scientific Research, Wellington.

Griffiths, G.A., 1981. Some suspended sediment yields from South Island catchments, New Zealand. Water Resource Bulletin, American Water Resources Association 27(4): 662-671.

Griffiths, G.A., McSaveney, M.J., 1983. Distribution of mean annual precipitation across some steepland regions of New Zealand. New Zealand Journal of Science 26: 197-209.

Gudex, M.C., 1909. Some striated stones from the St. Bernard Saddle, upper Waimakariri Valley. Transactions and Proceedings of the New Zealand Institute 41: 33.

Guyodo, Y., Valey, J.P., 1999. Global changes in intensity of the Earth's magnetic field during the past 800 kyr. Nature 399: 249-252.

Haast, von, J., 1861. Report of the topographical and geological exploration of the western districts of the Nelson Province, New Zealand.

Haast, von, J., 1864. Notes on the mountains and glaciers of the Canterbury Province, New Zealand. Journal of the Royal Geographical Society of London 34: 87-96.

Haast, von, J., 1879. The geology of the provinces Canterbury and Westland.

Hack, J.T., 1973. Stream profile analysis and stream gradient index. Journal of Research, U.S. Geol. Survey 1(4): 421-429.

Haldorsen, S., Shaw, J., 1982. The problem of recognizing melt-out till. Boreas 11: 261-277.

Hallet, B., Hunter, L., Bogen, J., 1996. Rates of erosion and sediment evacuation by glaciers: A review of field data and their implications. Global and Planetary Change 12: 213-235.

Hardcastle, J., 1889. On the Timaru loess as a climate register. Transactions and Proceedings of the New Zealand Institute 23: 324-332.

Hardcastle, J., 1890. On the drift in South Canterbury. Transactions and Proceedings of the New Zealand Institute 23: 311-324.

Hardy, E.F., Wellman, H.W., 1984. The Alpine, Wairau, and Hope Faults. Victoria University of Wellington Geology Department publication, v. 27, 15p.

Hart, J.K., 1996. Proglacial glaciotectonic deformation associated with glaciolacustrine sedimentation, Lake Pukaki, New Zealand. Journal of Quaternary Science, 11(2): 149-160.

Hay, J.E., Fitzharris, B.B., 1988. The synoptic climatology of ablation on a New Zealand Glacier. Journal of Climatology 8: 201-215.

Hays, J.D., Imbrie, J., Shackleton, N.J., 1976. Variations in the Earth's orbit; pacemaker of the ice ages. Science 194: 1121-1132.

Hector, J., 1865. On the geology of Otago, New Zealand. Quarterly Journal of the Geological Society of London 21: 124-128.

Hector, J., 1869. On mining in New Zealand. Transactions and Proceedings of the New Zealand Institute 2: 361-384.

Hellstrom, J., McCulloch, M., Stone, J., 1998. A detailed 31,000-year record of climate and vegetation change, from the isotope geochemistry of two New Zealand speleothems. Quaternary Research 50: 167-178.

Henderson, J., 1924. The post-Tertiary history of New Zealand. Transactions and Proceedings of the New Zealand Institute 55: 580-600.

Henderson, J., 1931. The ancient glaciers of Nelson. New Zealand Journal for Science and Technology 13: 154-160.

Henderson, R.D., Thompson, S.M., 1999. Extreme rainfalls in the Southern Alps of New Zealand. Journal of Hydrology (N.Z.) 38(2): 309-330.

Hendy, C.H., Wilson, A.T., 1968. Paleoclimate data from speleothems. Nature 219: 48-51.

Heusser, L.E., Geer, van de, G., 1994. Direct correlation of terrestrial and marine paleoclimatic records from four glacial-interglacial cycles - DSDP Site 594 Southwest Pacific. Quaternary Science Reviews 13: 273-282.

Hewitt, C.D., Mitchell, J.F.B., 1997. Radiative forcing and response of a GCM to ice age boundary conditions: cloud feedback and climate sensitivity. Climate Dynamics 13: 821-834.

Hicks, M.D., 1998. Suspended sediment in New Zealand rivers; indications from 40 years of data, National Institute of Water and Atmospheric Research (NIWA), Dunedin, 46p.

Hochstetter, von, F., 1863. Neuseeland. Stuttgart, Germany, 555p.

Hooke, R.L., Pohjola, V.A., 1994. Hydrology of a segment of a glacier situated in an overdeepening, Storglaciären, Sweden. Journal of Glaciology 40(134): 140-148.

Hooker, B.L., Fitzharris, B.B., 1999. The correlation between climatic parameters and the retreat and advance of Franz Josef Glacier, New Zealand. Global and Planetary Change 22: 39-48.

Hope, G., Kershaw, A.P., Kaars, van de, S., Xiangjun, S., Liew, P-M., Heusser, L.E., Takahara, H., McGlone, M., Miyoshi, N., Moss, P.T., 2004. History of vegetation and habitat change in the Austral-Asian region. Quaternary International 118-119: 103-126.

Hovius, N.S., Colin, P., Allen, P.A., 1997. Sediment flux from a mountain belt derived by landslide mapping. Geology 25(3): 231-234.

Hutton, F.G.S., 1872. On the date of the last great glacier period in New Zealand. Transactions and Proceedings of the New Zealand Institute 5: 384-393.

Hutton, F.G.S., 1900. The geological history of New Zealand. Transactions and Proceedings of the New Zealand Institute 32: 159-183.

Hutton, F.W., Ulrich, G.H.F., 1875. Report on the geology and gold fields of Otago. Dunedin, 244p.

Ivy-Ochs, S., Schluechter, C., Kubik, P.W., Denton, G.H., 1999. Moraine exposure dates imply synchronous Younger Dryas glacier advances in the European Alps and in the Southern Alps of New Zealand. Geografiska Annaler 81A: 313-323.

Johannesson, T., Sigurdsson, O., Laumann, T., Kennett, M., 1995. Degree-day glacier mass-balance modelling with applications to glaciers in Iceland, Norway and Greenland. Journal of Glaciology 41(138): 345-358.

Jol, H.M., Bristow, C.S., 2003. GPR in sediments: advice on data collection, basic processing and interpretation, a good practice guide. In: Bristow, C.S. and Jol, H.M. (eds.). GPR in Sediments. Geological Society of London, Special Publication 211: 9-27.

Jouzel, J., Masson, V., Cattani, O., Falourd, S., Stievenard, M., Stenni, B., Longinelli, A., Johnsen, S.J., Steffenssen, J.P., Petit, J.R., Schwander, J., Souchez, R., Barkov, N.I., 2001. A new 27 ky high resolution East Antarctic climate record. Geophysical Research Letters 28: 3199-3202.

Kamp, P.J.J., 1986. The mid-Cenozoic Challenger Rift System of western New Zealand and its implications for the age of the Alpine Fault inception. Bulletin of the Geological Society of America 97: 255-281.

Kamp, P.J.J., 2001. Possible Jurassic age for part of the Rakaia Terrane: implications for tectonic development of the Torlesse accretionary prism. New Zealand Journal of Geology and Geophysics 44: 185-203.

Kamp, P.J.J., Green, P.J., White, S.H., 1989. Fission track analysis reveals the character of collisional tectonics in New Zealand. Tectonics 8: 169-195.

Kamp, P.J.J., Tippett, J.M., 1993. Dynamics of the Pacific plate crust in the South Island (New Zealand) zone of oblique continent-continent convergence. Journal of Geophysical Research 98: 16105-16118.

Kaplan, M.R., Ackert, Jr., R.P., Singer, B.S., Douglass, D.C., Kurz, M.D., 2004. Cosmogenic nuclide chronology of millennial-scale glacial advances during O-isotope stage 2 in Patagonia. Geological Society of America Bulletin 116: 308-321.

Kirkbride, M.P., 1989. The influence of sediment budget on geomorphic activity of the Tasman Glacier, Mount Cook National Park, New Zealand. Unpublished Ph.D. thesis, University of Canterbury, 395p.

Kirkbride, M.P., Spedding, N., 1996. The influence of englacial drainage on sediment-transport pathways and till texture of temperate valley glaciers. Annals of Glaciology 22: 60-166.

Kitson, A. E., Thiel, E.O., 1910. The geography of the upper Waitaki basin. New Zealand Geographic Journal 36(537-554).

Komarov, V.P., Makarova, T.T., Sinegub, E.S., 1969. The estimation of snowmelt runoff hydrograph of small plain rivers using snowmelt data. Transactions of the Hydro-meteorological Centre of the USSR N37: 3-36.

Knuepfer, P.L.K., 1984. Tectonic geomorphology and present day tectonics of the alpine shear system, South Island, New Zealand, Unpublished Ph.D. thesis, University of Arizona, 480p.

Knuepfer, P.L.K., 1988. Estimating ages of late Quaternary stream terraces from analysis of weathering rinds and soils: Geological Society of America Bulletin 100: 1224-1236.

Krbetschek, M.R., Rieser, U., Zoeller, L., Heinicke, J., 1994. Radioactive disequilibria in palaeodosimetric dating of sediments. Radiation Measurements 24: 485-489.

Lamont, G.N., Chinn, T.J., Fitzharris, B.B., 1999. Slopes of glacier ELAs in the Southern Alps of New Zealand in relation to atmospheric circulation patterns. Global and Planetary Change 22: 209-219.

Langridge, R.M., Campbell, J., Hill, N., Pere, V., Pettinga, J., Estrada, B., Berryman, K., 2003. Paleoseismicity and slip rate of the Conway segment of the Hope fault at Greenburn Stream, South Island, New Zealand. Annals of Geophysics 46: 1119-1139.

Langridge, R.M., Berryman, K.R., 2005. Morphology and slip rate of the Hurunui section of the Hope Fault, South Island, New Zealand. New Zealand Journal of Geology and Geophysics 48: 43-57.

Lauscher, F., 1954. Klimatologische Probleme des festen Niederschlages. Arch. Meteorologie, Geophysik, Bioklimatologie, Serie B, 6 (1/2): 60-65.

Lawson, D.E., Strasser, J.C., Evenson, E.B., Alley, R.B., Larson, G.J., Arcone, S.A., 1998. Glaciohydraulic supercooling: a freeze-on mechanism to create stratified, debris-rich basal ice: I. Field evidence. Journal of Glaciology, 44(148): 547-569.

Linsley, R.K., Kohler, M.A., Paulhus, I.L., 1947. Applied Hydrology. New York, McGraw Hill, 432p.

Lowell, T.V., Heusser, C.J., Andersen, B.G., Moreno, P.I., Hauser, A., Heusser, L.E., Schluechter, C., Marchant, D.R., Denton, G.H., 1995. Interhemispheric correlation of Late Pleistocene glacial events. Science 269: 1541-1549.

Mabin, M.C.G., 1980. The glacial sequences in the Rangitata and Ashburton Valleys, South Island, New Zealand. Ph.D. thesis, University of Canterbury, 238p.

Mabin, M.C.G., 1984. Late Pleistocene glacial sequence in the Lake Heron basin, mid Canterbury. New Zealand Journal of Geology and Geophysics 27: 191-202.

Mabin, M.C.G., 1987. Early Aranuian sedimentation in the Rangitata Valley, mid Canterbury. New Zealand Journal of Geology and Geophysics 30: 87-90.

Mabin, M.C.G., 1996. The age of the Waiho Loop glacial event. Science 271: 668.

Maizels, J.K., 1989. Differentiation of late Pleistocene terrace outwash deposits using geomorphic criteria: Tekapo Valley, South Island, New Zealand. New Zealand Journal of Geology and Geophysics 32: 225-241.

Mann, P., Hempton, M.R., Bradley, D.C., Burke, K., 1983. Development of pull-apart basins. Journal of Geology 91: 529-554.

Mansergh, G.D., 1973. Quaternary Geology of the Mackenzie Basin. Guidebook for Excursion 7, XI. INQUA Congress in Christchurch, New Zealand: 102-112.

Markgraf, V., Dodson, J.R., Kershaw, A.P., McGlone, M.S., Nicholls, N., 1992. Evolution of late Pleistocene and Holocene climates in the circum-South Pacific land areas. Climate Dynamics 6: 193-211.

Marra, M.J., Shulmeister, J., Smith, E., (in press). Reconstructing temperature during the Last Glacial Maximum from Lyndon Stream, South Island, New Zealand using beetle fossils and maximum likelihood envelopes. Quaternary Science Reviews.

Marshall, P., 1909. The glaciation of New Zealand. Transactions and Proceedings of the New Zealand Institute 42: 334-348.

Martinson, D.G., Pisias, N.G., Hays, J.D., Imbrie, J., Moore, T.C., Shackleton, N.J., 1987. Age dating and the orbital theory of the Ice Ages: development of a high resolution 0 to 300,000-year chronostratigraphy. Quaternary Research 27: 1-29.

McGlone, M.S., 1995. Late-glacial landscape and vegetation change and the Younger Dryas climatic oscillation in New Zealand. Quaternary Science Reviews 14: 867-881.

McGlone, M.S., Turney, C.S.M., Wilmshurst, J.M., 2004. Late-glacial and Holocene vegetation and climatic history of the Cass Basin, central South Island, New Zealand. Quaternary Research 62(3): 267-279.

McGregor, G.R., 1981. Weathering characteristics of Late Pleistocene tills. New Zealand Journal of Geology and Geophysics 24: 107-113.

McKay, A., 1890. On the earthquakes of September, 1888, in the Amuri and Marlborough Districts of the South Island. New Zealand Geological Survey, Report of Geological Exploration 2: 11-16.

McKay, A., 1893. Geological explorations of the northern part of Westland. Parliamentary Papers, C (Mines Rep.): 132-186.

McKellar, I.C., 1960. Pleistocene deposits of the upper Clutha Valley, Otago, New Zealand. New Zealand Journal of Geology and Geophysics 3: 432-460.

Mejdahl, V., Funder, S., 1994. Luminescence dating of Late Quaternary sediments from East Greenland. Boreas 23: 525-535.

Mix, A.C., Bard, E., Schneider, R., 2001. Environmental processes of the ice age: land oceans, glaciers (EPILOG). Quaternary Science Reviews 20: 627-657.

Moar, N.T., 1980. Late Otiran and early Aranuian grassland in central South Island. New Zealand Journal of Ecology 3: 4-12.

Moar, N.T., Gage, M., 1973. Interglacial deposits in Joyce Stream (S74), Waimakariri Valley, Canterbury. New Zealand Journal of Geology and Geophysics 16: 321-331.

Moar, N.T., Lintott, W.H., 1977. Post-glacial history of vegetation at Cass. Cass - History and Science in the Cass District, Canterbury, New Zealand. Burrows, C.J. Christchurch, University of Canterbury: 147-157.

Moreno, P.I., Jacobson, G.L., Lowell, T.V., Denton, G.H., 2001. Interhemispheric climate links revealed by a late-glacial cooling episode in southern Chile. Nature 409: 804-808.

Morgan, P.G., 1927. The definition, classification and nomenclature of the Quaternary periods. New Zealand Journal for Science and Technology 8: 273-282.

Morigi, C., Capotondi, L., Giglio, F., Langone, L., Brilli, M., Turi, B., Ravaioli, M., 2003. A possible record of the Younger Dryas event in deep-sea sediments of the Southern Ocean (Pacific sector). Paleogeography, Paleoclimatology, Paleoecology 198(1-2): 265-278.

Mosley, M.P., 2004. Waiau River - instream values and flow regime. Christchurch, Environment Canterbury, Report R04/02: 218.

Mueller, F., Caflisch, T., Mueller, G., 1976. Firn und Eis der Schweizer Alpen. Geographisches Institut, ETH Zuerich, Publ. No. 57: 293p.

Muller, R.A., MacDonald, G.J., 2000. Ice ages and astronomical causes. London, New York, 318p.

Murray, A.S., Aitken, M.J., 1982. The measurement and importance of radioactive disequilibria in TL samples. Journal of the Council of Europe PACT 6: 155-169.

Murray, A.S., Wintle, A.G., 2000. Luminescence dating of quartz using an improved single-aliquot regenerative-dose protocol. Radiation Measurements 32: 57-73.

Nathan, S., Moar, N.T., 1973. Age and correlation of late Quaternary terraces in the lower Inangahua Valley, West Coast, South Island, New Zealand. Journal of the Royal Society of New Zealand 3(3): 409-414.

National Snow and Ice Data Center, 1999 (updated 2003). World Glacier Inventory. World Glacier Monitoring Service and National Snow and Ice Data Center / World Data Center for Glaciology. Boulder, CO.

Nelson, C.S., Hendy, C.H., Jarrett, G.R., and Cuthbertson, A.M., 1985. Near-synchroneity of New Zealand alpine glaciations and Northern Hemisphere continental glaciations during the past 750 kyr: Nature 318: 361-363.

Nobes, D.C., 2000. Geophysics in industry - ground penetrating radar. New Zealand Geophysical Society Newsletter 57: 34-39.

Nobes, D., Owens, I.F., 1995. Preliminary results of the 1995 programme of radar profiling of the Tasman Glacier and the nevé of the Franz Josef Glacier. Annual Conference of the Geological Society of New Zealand, Geological Society of New Zealand Annual Conference Programme and Abstracts, p. 158, Auckland, New Zealand.

Nobes, D.C., Rother, H., Kruk, van der, J., Jol, H.M., 2006. Radar 'lensing' by a small river: Can a layer of surface water improve the signal? Near Surface Geophysics Special Issue on Ground Penetrating Radar(4): 69-74.

Norris, R.J., Koons, P.O., Cooper, A.F., 1990. The obliquely-convergent plate boundary in the South Island of New Zealand: implications for ancient collision zones: Journal of Structural Geology 12(5-6): 715-725.

Oerlemans, J., 1986. An attempt to simulate historic front variations of Nigardsbreen, Norway. Theoretical and Applied Climatology 37: 126-135.

Oerlemans, J., 1997. Climate sensitivity of Franz Josef Glacier New Zealand, as revealed by numerical modelling. Arctic and Alpine Research 29: 233-239.

Owen, L.A., 1989. Terraces, uplift and climate in the Karakoram Mountains, Northern Pakistan: Karakoram intermontane basin evolution. Zeitschrift fuer Geomorphologie, N.F., suppl.-bd. 76: 117-146.

Park, J., 1909. The great ice age of New Zealand. Transactions and Proceedings of the New Zealand Institute 42: 589-612.

Park, J., 1910a. Geology of New Zealand. Whitcombe & Tombs, Dunedin, 488p.

Park, J., 1910b. Some notes on the Marlborough coastal moraines and Waiau glacial valley. Transactions of the Royal Society of New Zealand 43: 520-524.

Penck, A., Brueckner, E., 1909. Die Alpen im Eiszeitalter. Leipzig, 3 volumes.

Pepper, A.C., Shulmeister, J., Nobes, D.C., Augustinus, P.A., 2004. Possible ENSO signals prior to the Last Glacial Maximum, during the last deglaciation and the early Holocene, from New Zealand. Geophysical Research Letters 31: L15206.

Pettinga, J., 2002. Active tectonics and landscape evolution in the Australia-Pacific plate boundary zone, northern South Island, New Zealand. Gondwana 11 Correlations and Connections, Field trip guide, Christchurch.

Pickard, A.L., Adams, C.J., Barley, M.E., 2000. Australian provenance of Upper Permian to Cretaceous rocks forming accretionary complexes on the New Zealand sector of the Gondwanaland margin. Australian Journal of Earth Sciences 47: 987-1007.

Pope, J.G., 1994. Secondary structures, Holocene displacements and paleoseismicity of the Conway segment of the Hope fault, Greenburn Stream to Sawyers Creek. Honours thesis, Department of Geology. University of Canterbury, Christchurch.

Porter, S.C., 1975. Equilibrium-line altitudes of late Quaternary glaciers in the Southern Alps, New Zealand. Quaternary Research 5: 27-47.

Powers, W.E., 1962. Terraces of the Hurunui River, New Zealand. New Zealand Journal of Geology and Geophysics 5: 114-129.

Purdie, J., Fitzharris, B., 1999. Processes and rates of ice loss at the terminus of Tasman Glacier, New Zealand. Global and Planetary Change 22: 79-91.

Rains, R.B., 1967. The late Pleistocene glacial sequence of the High Peak Valley, Canterbury. New Zealand Journal of Geology and Geophysics 10: 1145-1158.

Read, S.A.L., 1976. Upper Waitaki power development scheme, Pukaki control engineering geological completion report. Engineering Geology Report, EG 268, Department of Scientific and Industrial Research, Wellington, 43p.

Rieser, U., 2001. Determination of sediment deposition ages by luminescence dating. Technical Report, Luminescence Dating Laboratory, Victoria University, Wellington, 4p.

Rieser, U., 2004. Determination of sediment deposition ages by luminescence dating. Technical Report, Luminescence Dating Laboratory, Victoria University, Wellington, 4p.

Robinson, L.F., Henderson, G.M., Hall, L., Matthew, I., 2004. Climate control of riverine and seawater uranium-isotope ratios. Science 305: 851-854.

Roethlisberger, F., 1987. 10000 Jahre Gletschergeschichte der Erde. Aarau, Verlag Sauerlaender.

Rother, H ., Jol, H.M., Shulmeister, J., in press. Stratigraphy and tectonic implications of Late Pleistocene valley fill in the Hope Valley , Canterbury , South Island , New Zealand. Baker, G.S., Jol, H.M. (eds.). Progress in stratigraphic analyses using ground penetrating radar (GPR), Geological Society of America (GSA), Special Publication.

Rother, H., Shulmeister, J., in press. Synoptic climate change as a driver of Late Quaternary glaciations in the mid-latitudes of the Southern Hemisphere. Climates of the Past.

Rother, H., Rieser, U., Shulmeister, J., submitted. Stratigraphy and depositional model of a OIS 6 glacial sequence in the Hope Valley, Southern Alps, New Zealand. Quaternary Science Reviews.

Ruddiman, W.F.K., 2003. Orbital insolation, ice volume, and greenhouse gases. Quaternary Science Reviews 22: 1597-1629.

Ruddiman, W.F.K., Robert B; Baldauf, J.G., Clement, B.M., Dolan, J.F., Eggers, M.R., Hill, P.R., Keigwin, L.D., Jr, Mitchell, M., Philipps, I., Robinson, F., Salehipour, S.A.. Takayama, T., Thomas, E., Unsold, G., Weaver, P.E., 1987. Site 607. Initial Reports of the Deep Sea Drilling Project 94(1-2): 75-147.

Sevruk, B. (ed.), 1992. Snow cover measurements and aerial assessment of precipitation and soil moisture. World Meteorological Organization, Geneva, Operational Hydrological Report No. 35, WMO-No. 749: 129.

Schaefer, J.M., Ninnemann, U., Denton, G.H., Schluechter, C., Ivy-Ochs, S., Wieler, R., Kubik, P.W., Anderson, B.G., Schlosser, P., 2001. Structure of the Last Glacial Maximum in New Zealand - terrestrial and marine evidence from southern mid-

latitudes. American Geophysical Union, Fall Meeting 2001, abstract PP42B-0499, AGU.

Schumm, S.A., 1954. The relation of drainage basin relief to sediment loss. International Association of Hydrology, IUGG, General Assembly 10th, Rome, Proceedings 1: 216-219.

Shaw, J., 1975. Sedimentary successions in Pleistocene ice-marginal lakes. Glaciofluvial and glaciolacustrine sedimentation. In: Jopling, A.V., McDonald, B.C. (eds.). Glaciofluvial and glaciolacustrine sedimentation, Special Publication - Society of Economic Paleontologists and Mineralogists, Tulsa, Oklahoma, U.S.A.: 281-303.

Shaw, J., 1987. Glacial sedimentary processes and environmental reconstruction based on lithofacies. Sedimentology 34: 103-116.

Shulmeister, J., Soons, J.M., Berger, G.W., Harper, M., Holt, S., Moar, N., Carter, J.A., 1999. Environmental and sea-level changes on Banks Peninsula (Canterbury, New Zealand) through three glaciation-interglaciation cycles. Palaeogeography Palaeoclimatology, Palaeoecology 152: 101-127.

Shulmeister, J., Goodwin, I., Renwick, J., Harle, K., Armand, L., McGlone, M.S., Cook, E., Dodson, J., Hesse, P.P., Mayewski, P., Curran, M., 2004. The southern hemisphere westerlies in the Australasian sector over the last glacial cycle: a synthesis. Quaternary International 118-119: 23-53.

Shulmeister, J., Fink, D., Augustinus, P., 2005. A cosmogenic nuclide chronology of the last glacial transition in North-West Nelson, New Zealand - new insights in Southern Hemisphere climate forcing during the last deglaciation. Earth and Planetary Science Letter 233: 455-466.

Shulmeister, J., Thackray, G.D, Rieser, U., Rother, H., Smart, C.C., Evans, D.J.A., Hyatt, O. (submitted). The stratigraphy and timing of glaciation in the middle Rakaia Valley, South Island, New Zealand with some implications for understanding past glaciations in New Zealand. Quaternary Science Reviews.

Sinclair, M.R., Wratt, D.S., Henderson, R.D., Gray, W.R., 1997. Factors affecting the distribution and spillover of precipitation in the Southern Alps of New Zealand - a case study. Journal of Applied Meteorology 36: 428-442.

Singer, C., Shulmeister, J., McLea, B., 1998. Evidence against a significant Younger Dryas cooling event in New Zealand. Science 281: 812-814.

Soons, J.M., 1963a. The glacial sequence in part of the Rakaia Valley, Canterbury, New Zealand. New Zealand Journal of Geology and Geophysics 6: 735-756.

Soons, J.M., 1963b. A survey of periglacial features in New Zealand. Land and Livelihood, Geographical essays in honour of George Jobberns. M. McCaskill. Christchurch, New Zealand Geographical Society Special Publication: 74-87.

Soons, J.M., 1964. Ice-marginal drainage channels in the Rakaia Valley. New Zealand Geographer 19: 153-164.

Soons, J.M., 1979. Late Quaternary environments in the central South Island of New Zealand. New Zealand Geographer 35(1): 16-23.

Soons, J.M., Gullentops, F.W., 1973. Glacial advances in the Rakaia Valley, New Zealand. New Zealand Journal of Geology and Geophysics 16(3): 425-438.

Soons, J.M., Burrows, C.J., 1978. Dates for Otiran deposits, including plant microfossils and macrofossils, from Rakaia Valley. New Zealand Journal of Geology and Geophysics 21: 607-615.

Spedding, N., Evans, D.J.A., 2002. Sediments and landforms at Kvíárjökull, southeast Iceland: a reappraisal of the glaciated valley landsystem. Sedimentary Geology 149: 21-42.

Speight, R., 1907. Some aspects of the terrace development in the Valleys of the Canterbury Rivers. Transactions and Proceedings of the New Zealand Institute 40: 16-43.

Speight, R., 1911. Glaciated surfaces and boulder clay near Bealey. Transactions and Proceedings of the New Zealand Institute 44: 98.

Speight, R., 1915. The intermontane basins of Canterbury. Transactions and Proceedings of the New Zealand Institute 47: 336-353.

Speight, R., 1918. Structural and glacial features of the Hurunui Valley. Transactions of the New Zealand Institute 50: 93-105.

Speight, R., 1921. Geological Excursion to Lake Tekapo. Transactions and Proceedings of the New Zealand Institute 51: 269-281.

Speight, R., 1923. Note on the hanging valleys of the upper Rangitata Valley. Transactions of the Royal Society of New Zealand 54: 90-98.

Speight, R., 1926. Varved glacial silts from the Rakaia Valley. Records of the Canterbury Museum 3(1): 55-82.

Speight, R., 1933. The Rakaia Valley. Transactions and Proceedings of the New Zealand Institute 63(4): 457-496.

Speight, R., 1938. Morainic deposits of the Waimakariri. Transactions and Proceedings of the New Zealand Institute 68: 143-160.

Speight, R., 1939. Some aspects of glaciation in New Zealand. Australian and New Zealand Association of the Advancement of Science, Report, 24th Meeting in Canberra Australia, 1939: 49-71.

Speight, R., 1940a. The gravels of the Mackenzie Intermont. Transactions and Proceedings of the New Zealand Institute 70: 175-187.

Speight, R., 1940b. Ice wasting and glacier retreat in New Zealand. Journal of Geomorphology 3: 131-143.

Speight, R., 1941. The Rangitata Glacier - The question of its maximum extension. Transactions and Proceedings of the New Zealand Institute 71: 169-180.

Speight, R., 1942. A detail of the Pukaki moraine. Transactions and Proceedings of the Royal Society of New Zealand, 72(2): 148 - 157.

Speight, J.G., 1961. Pleistocene historical geomorphology of the area about Lake Pukaki, New Zealand. unpublished M.Sc. thesis, University of Canterbury: 129p.

Speight, J.G., 1963. Late Pleistocene historical geomorphology of the Lake Pukaki area, New Zealand. New Zealand Journal of Geology and Geophysics 6: 160-188.

Stewart, R.B., Neall, V.E., 1984. Chronology of palaeoclimatic change at the end of the last glaciation. Nature 311: 47-48.

Stone, J.O., 2000. Air pressure and cosmogenic isotope production. Journal of Geophysical Research 105: 23753-23759.

Sturman, A., Wanner, H., 2001. A comparative review of the weather and climate of the Southern Alps of New Zealand and the European Alps. Mountain Research and Development 21: 359-369.

Sugden, D.E., John, B.S., 1976. Glaciers and landscape. London, Arnold, 376p.

Suggate, R.P., 1965. Late Pleistocene geology of the northern part of the South Island, New Zealand. New Zealand Geological Survey Bulletin 77, 90p.

Suggate, R.P., 1973. The glacial sequence in the Hope and tributary valleys. Guidebook for Excursion 5, Northern South Island, XI. INQUA Congress in Christchurch, New Zealand: 101-108.

Suggate, R.P. (ed.), 1978. The Geology of New Zealand, New Zealand Geological Survey, Wellington, 2 volumes, 820p.

Suggate, R.P., 1985. The glacial/interglacial sequence of North Westland, New Zealand. New Zealand Geological Survey, Record 7.

Suggate, R.P., 1990. Late Pleistocene and Quaternary glaciations of New Zealand. Quaternary Science Reviews 9: 175-197.

Suggate, R.P., Moar, N.T., 1970. Revision of the Chronology of the Late Otira Glacial. New Zealand Journal of Geology and Geophysics 13: 742-746.

Suggate, R.P., Almond, P.C., 2005. The Last Glacial Maximum (LGM) in western South Island, New Zealand: implications for the global LGM and MIS 2. Quaternary Science Reviews 24: 1923-1940.

Sylvester, A.G., 1988. Strike-slip faults. Geological Society of America Bulletin 100: 1666-1703.

Takeuchi, Y., Naruse, R., Satow, K., Ishikawa, N., 1999. Comparison of heat balance characteristics from five glaciers in the Southern Hemisphere. Global and Planetary Change 22: 201-208.

Teller, J.T., 2003. Subaquatic landsystems: large proglacial lakes. Glacial landsystems, Evans, D.J.A. (ed.). London, 532p.

Thiede, J., 1979. Wind regimes over the late Quaternary southwest Pacific Ocean. Geology 7: 259-262.

Thomas, G.S.P., Connell, R.J., 1985. Iceberg drop, dump, and grounding structures from Pleistocene glacio-lacustrine sediments, Scotland. Journal of Sedimentary Petrology 55(2): 243-249.

Travers, W.T.L., 1873. On the extinct glaciers of the middle Island of New Zealand. Transactions and Proceedings of the New Zealand Institute 6: 297-309.

Travers, W.T.L., 1874. Notes on Dr. Haast's supposed Pleistocene glaciation of New Zealand. Transactions and Proceedings of the New Zealand Institute 7: 409-440.

Turney, C.S.M., McGlone, M.S., Wilmhurst, J.M., 2003. Asynchronous climate change between New Zealand and the North Atlantic during the last deglaciation. Geology 31(3): 223-226.

Van Dissen, R., 1989. Late Quaternary faulting in the Kaikoura region, southeastern Marlborough, New Zealand. Oregon State University. Corvallis: 68.

Vandergoes, M.J., Newnham, R.M., Preusser, F., Hendy, C.H., Lowell, T.V., Fitzsimmons, S.J., Hogg, A.G., Kasper, H.U., Schluechter, C., 2005. Regional insolation forcing of late Quaternary climate change in the Southern Hemisphere. Nature 436: 242-245.

Walcott, R.I., 1984. The kinematics of the plate boundary zone through New Zealand; a comparison of short- and long-term deformations. Geophysical Journal of the Royal Astronomical Society 79(2): 613-633.

Weaver, P.P.E., Carter, L., Neil, H.L., 1998. Response of surface water masses and circulation to late Quaternary climate change, east of New Zealand. Paleo-oceanography, 13: 70-83.

Weissel, J.K., Hayes, D.E., Herron, E.M., 1977. Plate tectonics synthesis; the displacements between Australia, New Zealand, and Antarctica since the late Cretaceous. Marine Geology 25(1-3): 231-277.

Wellman, H.W., 1951. The geology of Bruce Bay - Haast River, South Westland. New Zealand Geological Survey Bulletin, 48.

Wellman, H.W., 1979. An uplift map for the South Island of New Zealand, and a model for uplift of the Southern Alps. In: Walcott, R.I., Cresswell, M.M. (eds.). The origin of the Southern Alps. The Royal Society of New Zealand Bulletin: 13-20.

Willett, R.W., 1950. The New Zealand Pleistocene snowline, climatic conditions, and suggested biological effects. New Zealand Journal of Science and Technology B32(1): 18-48.

Williams, P.W., 1996. A 230 ka record of glacial and interglacial events from Aurora Cave, Fiordland, New Zealand. New Zealand Journal of Geology and Geophysics 39: 225-241.

Williams, P.W., King, D.N.T., Zhao, J.-X., Collerson, K.D., 2005. Late Pleistocene to Holocene composite speleothem 18O and 13C chronologies from the South Island, New Zealand - did a global Younger Dryas really exist?, Earth and Planetary Science Letters 230: 301-317.

Wilson, D.D., 1989. Geology of northwestern Canterbury Plains, New Zealand Geological Survey, Misc. Series Map 14, 35p.

Woo, M., Fitzharris, B.B., 1992. Reconstruction of mass balance variations for Franz Josef Glacier, New Zealand, 1913-1989. Arctic and Alpine Research 24: 281-290.

Wood, R.A., Pettinga, J.R., Bannister, S., Lamarche, G., McMorran, T.J., 1994. Structure of the Hanmer strike-slip basin, Hope Fault, New Zealand. Geological Society of America Bulletin 106: 1459-1473.

Yang, J.S., 1991. The Kakapo Fault: a major active dextral fault in the central north Canterbury - Buller region of New Zealand. New Zealand Journal of Geology and Geophysics 34: 137-143.

Zondervan, A., 2004. Introductory notes on the use and application of the cosmogenic nuclides 10Be, 7Be, 14C, and 26Al. In: Prior, C., Faure, K. (eds.). First Quaternary

technique workshop, Institute of Geological and Nuclear Sciences, Information Series, 63: 105-110.

Clim. Past, 2, 1–9, 2006
www.clim-past.net/2/1/2006/

Climate of the Past

Synoptic climate change as a driver of late Quaternary glaciations in the mid-latitudes of the Southern Hemisphere

H. Rother and J. Shulmeister

Department of Geological Sciences, University of Canterbury, Private Bag 4800, Christchurch, New Zealand

Received: 23 September 2005 – Published in Clim. Past Discuss.: 1 December 2005
Revised: 8 March 2006 – Accepted: 28 March 2006 – Published:

Abstract. The relative timing of late Quaternary glacial advances in mid-latitude (40–55° S) mountain belts of the Southern Hemisphere (SH) has become a critical focus in the debate on global climate teleconnections. On the basis of glacial data from New Zealand (NZ) and southern South America it has been argued that interhemispheric synchrony or asynchrony of Quaternary glacial events is due to Northern Hemisphere (NH) forcing of SH climate through either the ocean or atmosphere systems. Here we present a glacial snow-mass balance model that demonstrates that large scale glaciation in the temperate and hyperhumid Southern Alps of New Zealand can be generated with moderate cooling. This is because the rapid conversion of precipitation from rainfall to snowfall drives massive ice accumulation at small thermal changes (1–4°C). Our model is consistent with recent paleo-environmental reconstructions showing that glacial advances in New Zealand during the Last Glacial Maximum (LGM) and the Last Glacial Interglacial Transition (LGIT) occurred under very moderate cooling. We suggest that such moderate cooling could be generated by changes in synoptic climatology, specifically through enhanced regional flow of moist westerly air masses. Our results imply that NH climate forcing may not have been the exclusive driver of Quaternary glaciations in New Zealand and that synoptic style climate variations are a better explanation for at least some Late Quaternary glacial events, in particular during the LGIT (e.g. Younger Dryas and/or Antarctic Cold Reversal).

Correspondence to: H. Rother
(h.rother@geol.canterbury.ac.nz)

1 Introduction

Quaternary glacial signals from mountain belts in the mid-latitude Southern Hemisphere (mlSH), in particular from locations in New Zealand and southern South America, have become important for testing models of past and present interhemispheric climate teleconnections (e.g. Broecker, 1997; Moreno, 2001). It has been argued that synchrony of past glacial advances would be indicative of direct interhemispheric climate forcing via the atmosphere (e.g. Kaplan et al., 2004; Denton et al., 1999) whereas, asynchrony has been interpreted as a climate link through the thermohaline conveyor (e.g. Lowell et al., 1995). The focus in this debate has been on the absolute dating of Quaternary mlSH glacial advances, which are used as proxies to identify the level of global correspondence between distinct Northern Hemisphere (NH) and Southern Hemisphere (SH) climate signals.

In recent years, progress in cosmogenic and luminescence dating techniques has permitted the direct dating of glacial landforms and deposits in mlSH mountain belts. Initial results from the Southern Alps of New Zealand and the southern Andes have been interpreted as demonstrating interhemispheric synchrony of LGM glacial advances and it has also been suggested that specific LGIT climate events known from the North Atlantic region (e.g. the Younger Dryas) can be directly correlated to mountain glacier advances in the mlSH (Denton and Hendy, 1994; Ivy-Ochs et al., 1999). It has further been argued that such level of correspondence is compelling for a model of direct NH atmospheric forcing of glaciations in the SH (Kaplan et al., 2004; Denton et al., 1999).

Despite some indications for interhemispheric synchrony of a limited number of LGM and LGIT glacial advances, the paleo-climatological interpretation of the data is not straightforward. In the case of New Zealand, numerical paleo-environmental reconstructions using speleothems and

Published by Copernicus GmbH on behalf of the European Geosciences Union.

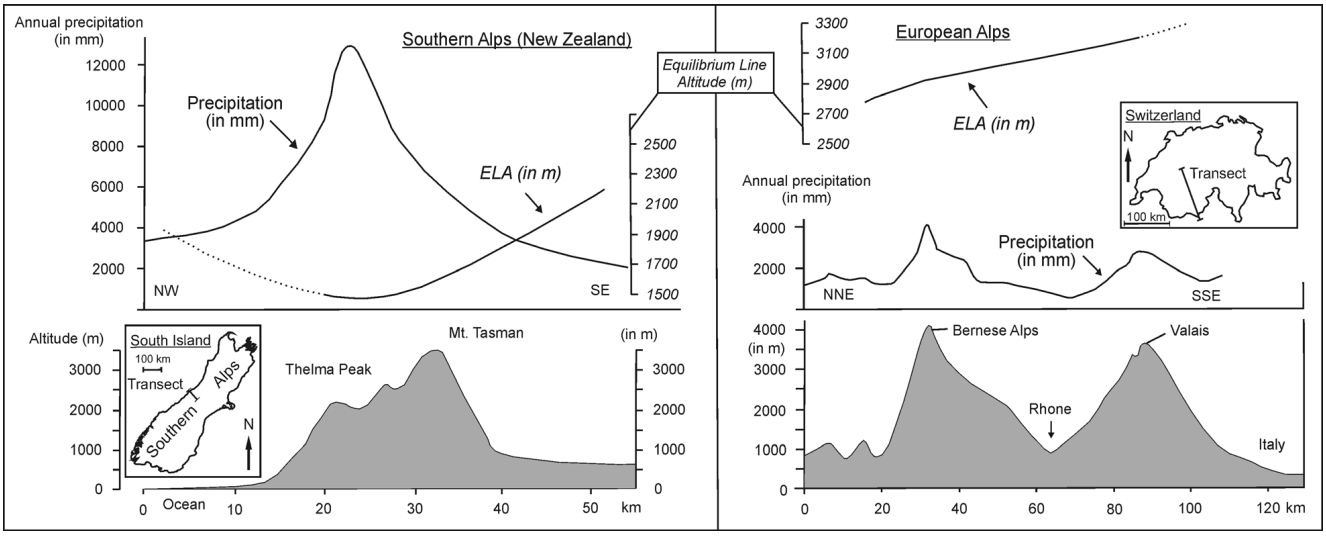

Fig. 1. Comparison of precipitation and ELA levels across the Southern Alps and European Alps (data from Mueller, 1976; Chinn and Whitehouse, 1980; Griffiths and McSaveney, 1983) plotted at equal scales (except horizontal distances) (modified from Sturman and Wanner, 2001). In New Zealand heavy orographic precipitation is concentrated in a 15–20 km wide sector along the alpine divide with annual totals 3–4 times greater than in the European Alps. The marked distribution of precipitation causes a strong ELA depression and very steep ELA gradients. In the European Alps, the NNW-SSE rise in ELA is mainly due to the meridional temperature increase.

fossil beetle assemblages show that LGM cooling was very moderate (Hellstrom et al., 1998) and possibly as little as 2 to 3°C (Marra et al., 2006). The paleo-ELA[1] depression suggests a cooling in the vicinity of 4–5°C (Porter, 1975; Soons, 1979). These results are supported by General Circulation Model (GCM) calculations that predict a 2 to 3°C lower sea-surface temperature (SST) in the Tasman Sea during the LGM (Hewitt and Mitchell, 1997) while SST reconstructions from forams suggest slightly stronger cooling at c. 4°C (Barrows and Juggins, 2005). In short, none of the reconstructions suggest a cooling of more than 5–7°C in NZ during the LGM while the lower end of the reconstructions suggest cooling similar to the modern interannual variability associated with ENSO and other oscillatory systems.

For the LGIT, at least one glacial re-advance has been demonstrated for the Southern Alps (Denton and Hendy, 1994; Ivy-Ochs et al., 1999), however, this re-advance, which was originally correlated to the Younger Dryas (YD) (Denton and Hendy, 1994), is neither universally detected in NZ's glacial records (e.g. Shulmeister et al., 2005) nor, critically, is a significant simultaneous cooling apparent from pollen or other paleoecological records (e.g. Singer et al., 1998; Turney et al., 2003). The New Zealand pollen records suggest a pause or minor reversal in the post-glacial warming only between 14.6–13.6 cal.^{14}C ka (McGlone, 1995, 2004) while warming resumed during the following YD chronozone (12.7–11.5 ka). Despite ongoing debate about the precise timing and correlation of LGM and LGIT glacial advances in New Zealand, the broader paleoecological data appear robust, and it has been difficult to resolve the occurrence of significant glacial expansions contemporaneous with only moderate cooling. The problem has wider implications because similar confusion has characterized the LGIT debate in southern South America with various authors proposing cooling or an absence thereof during the LGIT (e.g. Moreno et al., 2001; Bennett et al., 2000).

In this paper we present a snow mass balance model from the Southern Alps of New Zealand to test the sensitivity of glacial accumulation to thermal changes. By doing so we analyse whether the emerging glacio-chronological and paleoecological records from New Zealand are in fact compatible and if minor thermal forcing is sufficient to cause full-scale glacial expansion in the Southern Alps. The question has wider relevance because under such a scenario we must consider the possibility that some Quaternary glacial advances in NZ, and by implication in parts of South America, were generated by synoptic climate variations alone, requiring little (during the LGM) or no (during the LGIT) climate forcing from the NH.

2 Glaciological setting: New Zealand

New Zealand is located in the Southern Hemisphere westerly wind belt and is characterized by an oceanic climate. The

[1]The ELA separates glacial accumulation from ablation areas and represents the altitude at which the glacial mass balance is zero. Key factors influencing the position of the ELA are long term mean temperatures and precipitation.

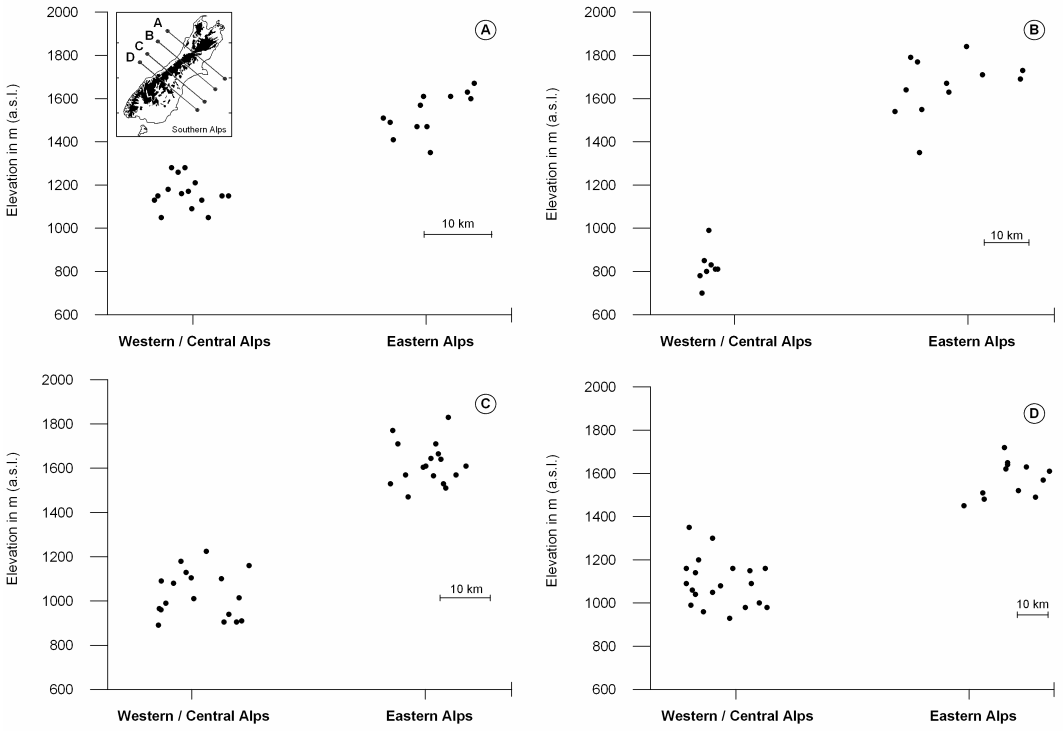

Fig. 2. Minimum cirque floor elevations of the western/central and eastern Southern Alps. Clearly defined cirque basins were mapped along four 30 km wide transects as shown in the inset of 2A. The data indicate that steep west-east precipitation and snowline gradients persisted throughout the late Quaternary.

regional climate is profoundly affected by the NE-SW trending Southern Alps (41°–46° S) which constitute a ∼3 km high topographic barrier in the pathway of the Southern Ocean Westerlies. Due to the interception and rapid orographic forcing of west flowing moist air masses, the central Southern Alps are amongst the wettest places on the planet. Annual precipitation near the alpine divide is commonly in excess of 9000 mm with observed maximum values at around 16 000 mm (Griffiths and McSaveney, 1983; Henderson and Thompson, 1999; Fig. 1). Critical for the glaciological setting is the marked cross-alpine precipitation distribution and the presence of a narrow hyperhumid sector which stretches along the full length of the Southern Alps. Virtually all of New Zealand's c. 3100 present glaciers are located in this sector (National Snow and Ice Data Center, 1999). Glaciers of perhumid environments are generally characterized as high ice turn-over systems with large positive and negative mass balances, high glacial flow velocities and relatively short climatic reaction times (Woo and Fitzharris, 1992; Benn and Evans, 1998).

Glacial Equilibrium Line Altitudes (ELAs) in the Southern Alps closely reflect the steep windward-leeward precipitation contrast which causes ELA gradients in New Zealand to be up to 20 times steeper than those reported for arctic and subarctic regions (Chinn and Whitehouse, 1980; Andrews and Miller, 1972). Despite this distinct glaciological setting, Quaternary glacial records from the Southern Alps are often directly correlated to records from other mid-latitude mountain belts, in particular to those from the European Alps (e.g. Ivy-Ochs et al., 1999). A comparison of key glacial parameters of the two ranges (Fig. 1) shows that despite substantially greater mean elevations, the European Alps receive only a quarter to a third of the NZ precipitation values while its distribution is far more even. A direct consequence of the hyperhumidity in the central Southern Alps is a strong depression of the ELA (Chinn and Whitehouse, 1980), which is generally about 1000 m lower than in the European Alps (Mueller, 1976). The differences in the physical setting have important implications for mechanisms of glacial accumulation and the resulting styles of glaciations in the two mountain belts.

Because New Zealand's glaciological configuration is fundamentally related to the interaction between the Southern Alps and the Westerly wind belt, studies of regional paleocirculation patterns are critical to the reconstruction of former glacial base conditions. Evidence for enhanced ocean upwelling east of New Zealand (Fenner et al., 1992; Weaver et al., 1998) and maxima in dust flux (Thiede, 1979; Stewart and Neall, 1984; Carter et al., 1995) have generally been attributed to persistent and strong westerly flow during the LGM (e.g. Markgraf et al., 1992; Shulmeister et al., 2004). Glacio-eustatic sea level lowering increased the relative height of the Southern Alps which in turn intensified

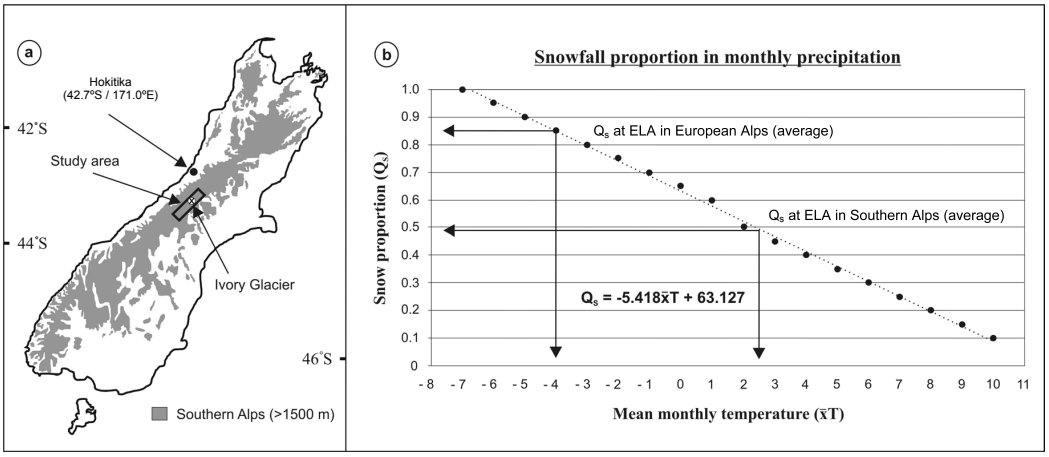

Fig. 3. Locations of study area, Hokitika climate station and Ivory Glacier in the Southern Alps **(a)**. **(b)** shows the physical relationship between mean monthly temperature and the snow-rain ratio (Q_S) as derived empirically from the Swiss Alps (Sevruk, 1992).

orographic forcing of moist westerly air masses. It is therefore probable that strong windward-leeward gradients in precipitation and ELA across the Southern Alps remained intact during Quaternary glacial periods. This is supported by reconstructed paleo-ELAs from cirque floor elevations comparing the western/central to the eastern alps (Fig. 2). Results show that despite an estimated ∼800 m ELA lowering (Porter, 1975), steep paleo-ELA gradients persisted during past glaciations.

To summarise, the combination of hyperhumidity and steep paleo-ELA gradients during Late Quaternary glaciations is responsible for a specific style of glacial accumulation in New Zealand. Firstly, very high levels of snowfall occurred in a 15–30 km wide sector near the alpine divide which corresponded with the area of minimum ELA. Secondly, due to rainshadow effects and because the ELA rose sharply east of the divide, alpine areas only a short distance from the divide received significantly less snowfall and only the highest peaks penetrated the annual snowline. This resulted in a glacial pattern where large scale ice accumulation was concentrated in the narrow perhumid sector of the central alps, while the contribution of all other areas to overall glacial accumulation in the Southern Alps was orders of magnitude smaller.

3 Temperature effects on snow mass balances in the Southern Alps

In the central Southern Alps present ELAs range between 1500 m–2100 m (Lamont et al., 1999). Critically, at these ELAs atmospheric temperatures remain above freezing for considerable periods of the year. This means that a significant portion of the large annual precipitation at and around ELA level falls as rain. This constitutes a substantial snow resource if climate cooling occurs as additional snow is generated without any synoptic changes. By comparison, in the European Alps present ELAs are on average 1000 m higher (2500 m–3500 m) and corresponding atmospheric temperatures remain too cold for rain to form a significant portion in the annual precipitation at ELA (Fig. 3b).

To investigate temperature effects on glacial accumulation in the perhumid Southern Alps we use a snow mass balance model[2]. The model calculates annual net snow accumulation for various cooling scenarios (−1 to −9°C in mean T) by analysing temperature related changes to the snow-rain-ratio, total annual precipitation and snow ablation rates. Data are calculated for the central perhumid alpine sector (Fig. 3a) with an ELA of 1600 m (Chinn and Whitehouse, 1980; Clare et al., 2002) and a total annual precipitation of 9000 mm (Griffiths and McSaveney, 1983; Henderson and Thompson, 1999). The overall topography, ELA position and the amount of annual precipitation in this area represent average condition for substantial portions in the central alps. Temperature data used in the model are derived from the nearest climate station (Hokitika, Fig. 3a) and were converted to the ELA altitude by using a standard environmental lapse rate of 6°C/km. We calculated cooling related changes to net snow accumulation at ELA (1600 m) where the current snow mass balance is zero. Mean temperatures were then incrementally lowered to simulate potential atmospheric cooling.

Observations on snow proportions (Q_S) in total precipitation (P_{total}) are not available for the Southern Alps but it has been shown that snow proportions correlate well to mean monthly temperatures (Lauscher, 1954; Cehak-Trock, 1958). We calculated Q_S in P_{total} using a regression function derived empirically from 32 stations in the Swiss Alps (Sevruk, 1992) (Fig. 3b). Q_S results for the Southern Alps were then

[2]Full details on the model are provided in the attached data depository available under: http://www.clim-past.net/2/1/2006/cp-2-1-2006-supplement.zip

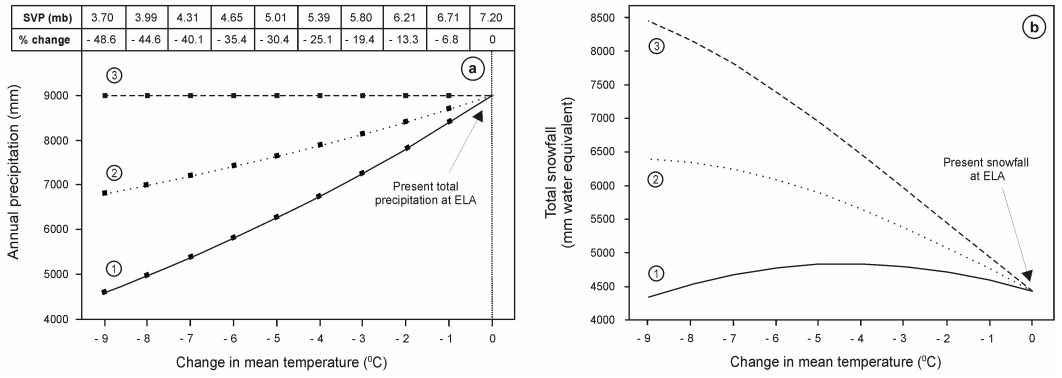

Fig. 4. The three annual precipitation scenarios **(a)**. Scenario 1 approximates cooling related changes through variations in air saturation vapour pressure (SVP) (see table in 4a). Scenario 2 assumes half the change of scenario 1, and scenario 3 assumes no change in precipitation with cooling. Figure 4b shows annual snowfall under cooling as a result of changes to the snow-rain ratio and variations in total annual precipitation. Snowfall is adjusted to the seasonal variation in precipitation.

adjusted for the seasonal variation in precipitation by applying weighted averages from the observed monthly precipitation at the nearby Ivory Glacier (Anderton and Chinn, 1978; Fig. 3a). At ELA (1600 m) mean annual temperature is 2.3°C with a monthly range from −2.1°C (July) to 6.4°C (February). Results show that at this elevation 49.2% (4430 mm water equivalent) of the annual total of 9000 mm fall as snow while the remaining 50.8% (4570 mm) fall as rain. This provides an enormous potential additional snow source. For every 1°C of cooling in mean monthly temperature the percentage of snow as a proportion of precipitation grows by 5.5% (Fig. 3b).

Atmospheric cooling is likely to affect the amount of total annual precipitation received by the Southern Alps. Recent studies have suggested relatively wet conditions in New Zealand associated with enhanced Westerlies during the LGM (e.g. Eden and Hammond, 2003; Shulmeister et al., 2004) and LGIT (e.g. Pepper et al., 2004), while others argue that humidity was somewhat reduced during glacial periods (e.g. Hope et al., 2004). At present no quantified paleo-data on the response of precipitation in the New Zealand region to LGM and LGIT cooling exist. In general, precipitation will respond to cooling by adjusting to changes in air mass saturation vapour pressure, evaporation and to variations in the route and velocity of atmospheric transport. In order to demonstrate the general relationships between precipitation, temperature, snow-rain ratios and snow accumulation in the New Zealand setting we use three simple precipitation scenarios to account for a range of possible precipitation values (Fig. 4a). Scenario 1 assumes a cooling related decrease in annual precipitation and approximates the non-linear reduction through temperature related variations in air mass saturation vapour pressure (SVP). In this scenario, the precipitation decrease is calculated from SVP changes which are used to approximate the moisture capacity of the air where a cooling of −5°C would reduce overall humidity by ∼30%. In scenario 2, the reduction in annual precipitation is assumed to be half of that of scenario 1 and scenario 3 assumes wet conditions where precipitation totals remain at the present levels even under increasingly colder conditions. The scenarios are designed for the purpose of this model study only and do not accurately describe the actual response of precipitation to past glacial cooling in New Zealand, however the scenarios cover the generally suggested last glacial precipitation estimates.

Results in Fig. 4b show total annual snowfall for increasingly colder conditions as calculated when the precipitation scenarios are combined with the dynamic snow-rain ratio. As expected snowfall totals vary greatly depending on the modelled annual precipitation. The data generally reflect two compensating trends during cooling, firstly the continuing increase of Q_S in P_{total}, and secondly a cooling related decline in P_{total} (scenarios 1 and 2). Results indicate that the addition of large amounts of extra snow from the rain-snow conversion would have dramatic effects on snow mass balances in perhumid environments. Snowfall increases (scen. 2) or remains high (scen. 1) even if annual precipitation declines substantially. If conditions are wetter (scen. 3) snowfall will expand vastly as P_{total} remains very high.

The projected annual snowfall total must be related to ablation for assessing net annual snow accumulation. We calculated snow ablation by using a degree day mass balance (DDMB) model in which mean daily temperatures are taken as an integrated index of the heat budget and where ablation is assumed to occur proportionally to the mean air temperature (e.g. Linsley, 1947). DDMB models have been widely tested under field conditions where they have shown to predict ablation reliably (e.g. Komarov et al., 1969; Braithwaite and Olesen, 1989; Jóhannesson et al., 1995; Braithwaite and Zhang, 2000). Calculation use the formula:

$$a(z) = kT_{\text{sum}}(z) + H_S/, T > 0\text{C}^\circ \quad (1)$$

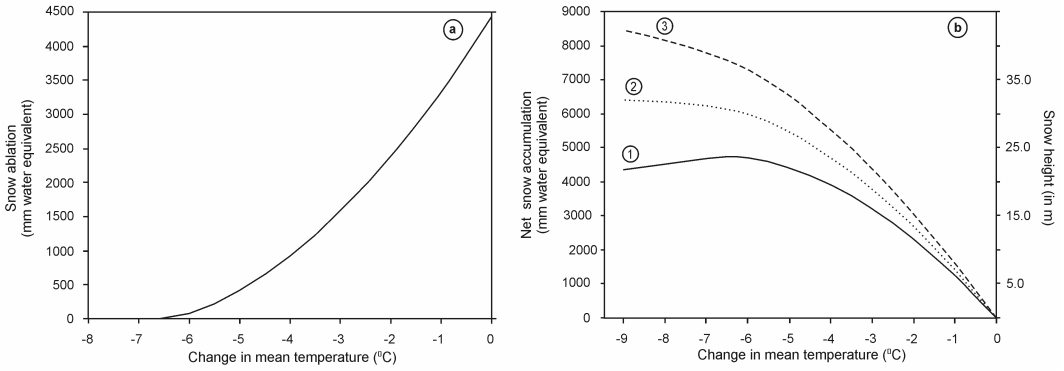

Fig. 5. Impact of cooling on snow ablation at present ELA as calculated by a degree day mass balance model **(a)**. **(b)** shows projected annual net snow accumulation as a result of variations in annual precipitation, snow-rain proportions and ablation under −1 to −9°C cooling. Note the steep increase in snow accumulation at moderate cooling.

where ablation (a) is computed for elevation (z), using the sum of positive mean daily temperatures (T_{sum}) at z. The positive degree days are multiplied with k representing an empirically derived degree day factor. We use a degree day factor of 4.5 mm day-1 deg-1 as was derived for Franz Josef Glacier in the central Southern Alps (Anderson, 2003). H_S is ablation from latent heat (rain on snow) which contributes ∼2% to annual ablation in the Southern Alps (Hay and Fitzharris, 1988). We tested the model by predicting ablation at the present ELA where annual snowfall is 4432 mm and no net accumulation occurs (mass balance 0). The model indicates 4359 mm of ablation, underestimating actual ablation by only 1.7%. Overall results in Fig. 5a show how snow ablation decreases at ELA under intensifying cooling from 4432 mm/a (at present temperature conditions) until it virtually stops at −6.5°C cooling.

We then integrated all previously analyzed parameters (snow-rain proportions, total precipitation, snow ablation) to predict net snow accumulation in the central alps under increasingly cooler conditions. Results are shown in Fig. 5b where 0°C represents current climate conditions at the ELA with no net accumulation. The outcome indicates that net snow accumulation in the Southern Alps responds strongly positive to moderate cooling. Snow accumulation grows dramatically under all precipitation scenarios even when overall humidity declines substantially. A striking feature is the steep increase recorded for the early part of the cooling (1–4°C), where snow accumulation grows markedly mainly due to the rapid conversion from rain to snow. A cooling of only 2–3°C at present ELA would result in the net annual addition of ∼15 vertical meters of snow (Fig. 5b). Interestingly, the gain generally slows with more severe cooling. For precipitation scenario 1 (driven by SVP changes) the snow accumulation trend will even reverse at around −6°C cooling when net annual accumulation starts to decline. The effect is caused by high snow proportions at this cooling and the effective halt of ablation after which the continuing decrease of total annual precipitation drives net accumulation down.

4 Discussion and conclusion

Heavy orographic precipitation in the central parts of the long (∼800 km) but narrow (∼80 km) Southern Alps results in some of the steepest recorded glacial ELA gradients on Earth. During Quaternary glaciations and associated low sea level stands, the relative height of the Southern Alps as a barrier for moist westerly air masses was further enhanced and ELA gradients were maintained or even steepened. Reconstructed paleo-ELAs (Porter, 1975; Chinn and Whitehouse, 1980) imply that ice accumulation during the LGM was concentrated in the perhumid central alps. These conditions produced extensive ice fields or possibly a narrow ice cap, which covered the ∼30 km wide hyperhumid sector near the alpine divide. From the central alpine accumulation zone valley glaciers extended on average 50–70 km to their LGM terminal positions.

Our snow mass balance data indicate that glacial accumulation in the Southern Alps is sensitive to small thermal changes. Moderate cooling (2–4°C) is sufficient to increase snowfall dramatically and trigger large positive excursions in glacial mass balances. If this cooling is sustained under a 5000–8000 mm precipitation regime it is possible to generate glacial advances of the scale recorded for the LGM. The high temperature sensitivity of glacial systems in New Zealand is mainly due to extreme perhumidity and associated low ELA levels which cause present glacial accumulation areas in the Southern Alps to receive substantial amounts of rain. The rain-snow conversion would impact rapidly as present precipitation maxima occur during the cooler Autumn and Spring seasons thereby requiring only moderate further cooling to initiate full rain-snow conversion.

The model assumptions account for a cooling related decrease in total annual precipitation, which is consistent with LGM humidity estimates suggested from New Zealand pollen (McGlone, 1995). Likewise, regional paleotemperature reconstructions using speleothems and fossil beetle assemblages indicate that cooling during the LGM

and LGIT glacial advances was only moderate (Hellstrom et al., 1998) and possibly as little as −2 to −3°C (Marra et al., 2006). The benefit of our mass balance model is that it provides a mechanism that resolves the occurrence of substantial glacial advances in New Zealand contemporaneous with reconstructed drier conditions and with only moderate atmospheric cooling. We note that under a scenario where total precipitation in glacial New Zealand would noticeable increase (for example due to higher wind speeds or altered atmospheric transport pathways) glaciation in the Southern Alps could be generated with even less cooling then suggested by the present study.

For the central Southern Alps, hypsometric characteristics of areas immediately below snowline (∼1400–1700) suggest that a moderate drop in ELA would bring extensive low angle surface areas above snowline. This factor is important because new permanent snow accumulations can only occur if slope angles are suitable. The effect is demonstrated for our study area where we calculated hypsometric integrals for a 10 km wide and 60 km long sector (S 43°17′1″/E 170°53′4″ to S 42°50′1″/E 171°29′0″) (Fig. 6). Results indicate that an ELA lowering of only 300 m would more than double the low angle surface area above snowline. In reality, the increase in suitable snow accumulation surfaces would be further enhanced by the extension of glacial tongues into the upper valleys where they raise the effective elevation of the valley floor (high-mass-balance feedback).

Moderate cooling as a driver of Quaternary glacial advances in New Zealand has several important implications. Firstly, it accounts for sedimentological peculiarities associated with glacial sequences in the Southern Alps. Commonly noted features are the enormous scale of glacio-fluvial aggradation fans, the large proportion of glacio-lacustrine deposits in ice-proximal sequences and the widespread occurrence of stratified and only weakly compacted glacial diamictons (e.g. Speight, 1942; Gage, 1965, 1985; Hart, 1996). The overall climatic implication is that conditions during deposition were clearly mild enough to provide nearly year-round availability of large volumes of melt-water.

Secondly, the low thermal forcing mechanism for glaciation in New Zealand implies that large glacial advances can be generated rapidly, and conversely, shut down rapidly since glacial conditions are sensitive to small thermal changes. This "flickering switch" feature of Quaternary glacial advances in the Southern Alps is likely to have produced a larger number of individual glacial oscillation than for example is observed in the more continental European Alps. This pattern may complicate attempts to directly correlate glacial signals from the NH to New Zealand.

Thirdly, moderate cooling as a glacial driver in New Zealand highlights the distinct possibility that regional (synoptic) climate phenomena were the principle cause for some Late Quaternary glacial events. It has been shown that modern glaciers in western New Zealand respond to synoptic circulation changes, where enhanced zonal flow

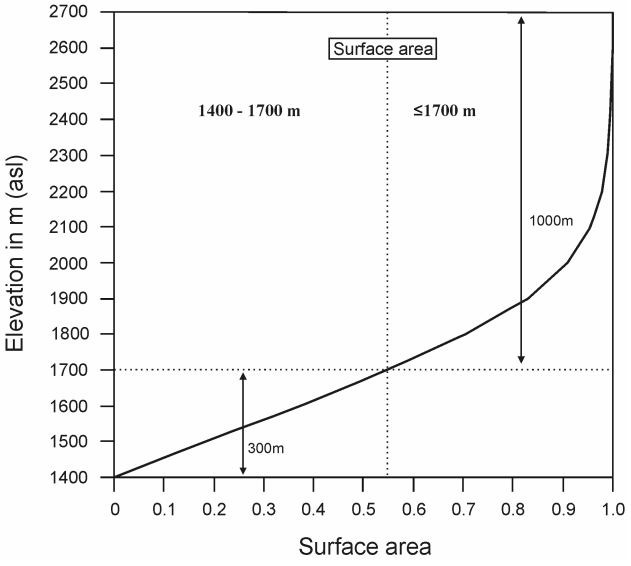

Fig. 6. DEM analysed hypsometry above 1400 m in the central Southern Alps showing the potential increase in low angle (less than 15°) surface areas above snowline from a 300 m ELA lowering (1700 m to 1400 m) The analysed alpine zone is the study area as shown in Fig. 3a. ELA lowering would increase the aerial extent of low angle surfaces by 121.5%.

(westerly/south-westerly) is associated with glacial advances and stronger meridional flow is associated with retreats (Lamont et al., 1999; Hooker and Fitzharris, 1999). The reason is that strengthened westerly flow increases orographic precipitation over the mountains and reduces ablation through enhanced cloud cover, while conversely, more persistent meridional circulation is associated with reduced precipitation and clear skies that cause increased ablation. Strong westerly flow, associated with glacial advances, mirrors the impact of El Niño on New Zealand. Recent spectral analyses on varved lake sediments have highlighted the possibility of a periodically enhanced inter-annual El Niño Southern Oscillation (ENSO) signal during the LGIT over New Zealand (Pepper et al., 2004). Speleothem data from the South Island (Hellstrom et al., 1998) now supported by uranium isotope data (Robinson et al., 2004) also indicate a period of enhanced precipitation over New Zealand at around 13 ka which may be linked to a late glacial Southern Hemisphere climate event known as the Antarctic Cold Reversal (ACR) (Jouzel et al., 2001). An ACR signal has recently been recognized in New Zealand pollen (McGlone et al., 2004) and maar lake records (Pepper et al., 2004). Alternatively, it has been suggested that a ∼13 ka New Zealand climate event could represent a directly transmitted NH Younger Dryas signal (e.g. Morigi et al., 2003). Regardless of its correlation neither period is associated with marked larger scale cooling in New Zealand. Enhanced precipitation, in association with very minor cooling, would have been capable of triggering glacial re-advances in the central parts of the Southern Alps such as at Franz-Josef Glacier (Ivy-Ochs et

al., 1999). These changes, however, would not have impacted on already deglaciated mountain systems such as the Tasman Mountains in NW Nelson (Shulmeister et al., 2005), nor on the pollen record (McGlone, 1995; Singer et al., 1998; Turney et al., 2003). A synoptic 'wet' event as the driver of the LGIT (ACR or YD) re-advance in New Zealand is therefore consistent with the available glacial record.

Synoptic climatology as the cause for late Quaternary glacial advances in hyperhumid mountain environments of the Southern Alps may provide an explanation for inconsistencies in glacial records of the SHml (Southern Alps, southern Andes), where climate signals and glacial advances have been recorded as both synchronous and asynchronous to Northern Hemisphere cooling events. The situation in South America is somewhat different in that part of the discrepancy is created by the larger geographical area covered, but at least some of the records may be reconcilable using our model. However, even if our model does not apply in all cases, the likelihood that major advances in the SHml can be explained without invoking inter-hemispheric forcing, or indeed major thermal changes, challenges current understanding of global climate linkages.

Acknowledgement. We thank C. Smart, I. Owens and P. Tonkin for comments on the manuscript and D. Richter for assistance with the hypsometric calculations. The comments by an anonymous referee helped to improve this paper. We would like to acknowledge the critical comments by B. Anderson and A. Mackintosh during the CPD online discussion. This work was supported by the University of Canterbury Research Grant No. U 6508 and through the Marsden Grant contract UoC 301 (NZ).

Edited by: A. Paul

References

Anderson, B.: The response of 'Ka Roimata o Hine Hukatere' Franz Josef Glacier to climate change, Unpublished Ph.D. thesis, University of Canterbury, Christchurch, 114pp., 2003.

Anderson, B. and Mackintosh., A.: Temperature change is the major driver of late-glacial and Holocene glacier fluctuations in New Zealand, Geology, 34(2), 121–124, 2006.

Anderton, P. W. and Chinn, T. J.: Ivory Glacier, New Zealand, an I.H.D. representative basin study, J. Glaciol., 20, 67–84, 1978.

Andrews, J. T. and Miller, G. H.: Quaternary history of the northern Cumberland Peninsula, Baffin Island, N.W.T., Canada, Arctic and Alpine Res., 4, 45–59, 1972.

Barrows, T. T. and Juggins, S.: Sea-surface temperatures around the Australasian margin and Indian Ocean during the Last Glacial Maximum, Quaternary Sci. Rev., 24, 1017–1047, 2005.

Benn, D. I. and Evans, D. J. A.: Glacier and Glaciation, London, 734p., 1998.

Bennett, K. D., Haberle, S. G., and Lumley, S. H.: The last glacial-Holocene transition in southern Chile, Science, 290, 325–328, 2000.

Braithwaite, R. J. and Olesen, O. B.: Calculation of glacier ablation from air temperature, West Greenland, Glacier fluctuations and climatic change, J. Oerlemans. Amsterdam, Kluwer Academic Publishers, 219–233, 1989.

Braithwaite, R. J. and Zhang, Y.: Sensitivity of mass balances of five Swiss glaciers to temperature changes assessed by tuning a degree-day model, J. Glaciol., 46, 7–14, 2000.

Broecker, W. S.: Future directions of paleoclimate research, Quaternary Sci. Rev., 16, 821–825, 1997.

Carter, L., Nelson, C. S., Neil, H .L., and Froggatt, P. C.: Correlation, dispersal, and preservation of the Kawakawa tephra and other late Quaternary tephra layers in the southwest Pacific Ocean, New Zealand J. Geol. Geophys., 38, 29–46, 1995.

Cehak-Trock, H.: Der feste Niederschlag im atlantischen Klimagebiet, Arch. Meteorologie, Geophysik, Bioklimatologie, Serie B, 8(3/4), 352–368, 1958.

Chinn, T. J. and Whitehouse, I. E.: Glacier snow line variations in the Southern Alps, New Zealand, IAHS-AISH Publ., 126, 219–228, 1980.

Clare, G. R., Fitzharris, B. B., Chinn, T. J. H., and Salinger, M. J.: Interannual variation in end-of-summer snowlines of the Southern Alps of New Zealand, and relationships with Southern Hemisphere atmospheric circulation and sea surface temperature patterns, Int. J. Climatol., 22, 107–120, 2002.

Denton, G. H. and Hendy, C. H.: Younger Dryas age advance of Franz-Josef Glacier in the Southern Alps of New Zealand, Science, 264, 1434–1437, 1994.

Denton, G. H., Heusser, C. J., Lowell, T. V., Moreno, P. I., Andersen, B. G., Heusser, L. E., Schluechter, C., and Marchant, D. R.: Interhemispheric linkage of paleoclimate during the last deglaciation, Geografiska Annaler (A), 81(2), 107–153, 1999.

Eden, D. E. and Hammond, A. P.: Dust accumulation in the New Zealand region since the last glacial maximum, Quaternary Sci. Rev., 22, 2037–2052, 2003.

Fenner, J., Carter, L., and Stewart, R.: Late Quaternary paleoclimatic and paleoceanographic change over northern Chatham Rise, New Zealand, Mar. Geol., 108, 383–404, 1992.

Gage, M.: Some characteristics of Pleistocene cold climates in New Zealand, Transact. Roy. Soc. New Zealand, 3, 11–21, 1965.

Griffiths, G. A. and McSaveney, M. J.: Distribution of mean annual precipitation across some steepland regions of New Zealand, New Zealand J. Sci., 26, 197–209, 1983.

Hart, J. K.: Proglacial glaciotectonic deformation associated with glaciolacustrine sedimentation, Lake Pukaki, New Zealand, J. Quaternary Sci., 11(2), 149–160, 1996.

Hay, J. E. and Fitzharris, B. B.: The synoptic climatology of ablation on a New Zealand Glacier, J. Climatol., 8, 201–215, 1988.

Hellstrom, J., McCulloch, M., and Stone, J.: A detailed 31 000-year record of climate and vegetation change, from the isotope geochemistry of two New Zealand speleothems, Quaternary Res., 50, 167–178, 1998.

Henderson, R. D. and Thompson, S. M.: Extreme rainfalls in the Southern Alps of New Zealand, J. Hydrol. (N.Z.), 38(2), 309–330, 1999.

Hewitt, C. D. and Mitchell, J. F. B.: Radiative forcing and response of a GCM to ice age boundary conditions: cloud feedback and climate sensitivity, Climate Dyn., 13, 821–834, 1997.

Hooker, B. L. and Fitzharris, B. B.: The correlation between climatic parameters and the retreat and advance of Franz Josef Glacier, New Zealand, Global Planet. Change, 22, 39–48, 1999.

Hope, G., Kershaw, A. P., Kaars, S. v. d., Xiangjun, S., Liew, P.-

M., Heusser, L. E., Takahara, H., McGlone, M., Miyoshi, N., and Moss, P. T.: History of vegetation and habitat change in the Austral-Asian region, Quaternary Int., 118–119, 103–126, 2004.

Ivy-Ochs, S., Schluechter, C., Kubik, P. W., and Denton, G. H.: Moraine exposure dates imply synchronous Younger Dryas glacier advances in the European Alps and in the Southern Alps of New Zealand, Geografiska Annaler, 81A, 313–323, 1999.

Johannesson, T., Sigurdsson, O., Laumann, T., and Kennett, M.: Degree-day glacier mass-balance modelling with applications to glaciers in Iceland, Norway and Greenland, J. Glaciol., 41(138), 345–358, 1995.

Jouzel, J., Masson, V., Cattani, O., Falourd, S., Stievenard, M., Stenni, B., Longinelli, A., Johnsen, S. J., Steffenssen, J. P., Petit, J. R., Schwander, J., Souchez, R., Barkov, N. I.: A new 27 ky high resolution East Antarctic climate record, Geophys. Res. Lett., 28, 3199–3202, 2001.

Kaplan, M. R., Ackert Jr., R. P., Singer, B. S., Douglass, D. C., Kurz, M. D.: Cosmogenic nuclide chronology of millennial-scale glacial advances during O-isotope stage 2 in Patagonia, Geol. Soc. Amer. Bull., 116, 308–321, 2004.

Komarov, V. P., Makarova, T. T., and Sinegub, E. S.: The estimation of snowmelt runoff hydrograph of small plain rivers using snowmelt data, Transactions of the Hydro-meteorological Centre of the USSR, N37, 3–36, 1969.

Lamont, G. N., Chinn, T. J., and Fitzharris, B. B.: Slopes of glacier ELAs in the Southern Alps of New Zealand in relation to atmospheric circulation patterns, Global Planet. Change, 22, 209–219, 1999.

Lauscher, F.: Klimatologische Probleme des festen Niederschlages, Arch. Meteorologie, Geophysik, Bioklimatologie, Serie B, 6(1/2), 60–65, 1954.

Linsley, R. K., Kohler, M. A., and Paulhus, I. L.: Applied Hydrology, New York, McGraw Hill, 432p., 1947.

Lowell, T. V., Heusser, C. J., Andersen, B. G., Moreno, P. I., Hauser, A., Heusser, L. E., Schluechter, C., Marchant, D. R., and Denton, G. H.: Interhemispheric correlation of Late Pleistocene glacial events, Science, 269, 1541–1549, 1995.

Markgraf, V., Dodson, J. R., Kershaw, A. P., McGlone, M. S., and Nicholls, N.: Evolution of late Pleistocene and Holocene climates in the circum-South Pacific land areas, Climate Dyn., 6, 193–211, 1992.

Marra, M. J., Shulmeister, J., and Smith, E.: Reconstructing temperature during the Last Glacial Maximum from Lyndon Stream, South Island, New Zealand using beetle fossils and maximum likelihood envelopes, Quaternary Sci. Rev., accepted, 2006.

McGlone, M. S.: Late-glacial landscape and vegetation change and the Younger Dryas climatic oscillation in New Zealand, Quaternary Sci. Rev., 14, 867–881, 1995.

McGlone, M. S., Turney, C. S. M., Wilmshurst, J. M.: Late-glacial and Holocene vegetation and climatic history of the Cass Basin, central South Island, New Zealand, Quaternary Res., 62(3), 267–279, 2004.

Moreno, P. I., Jacobson, G. L., Lowell, T. V., and Denton, G. H.: Interhemispheric climate links revealed by a late-glacial cooling episode in southern Chile, Nature, 409, 804–808, 2001.

Morigi, C., Capotondi, L., Giglio, F., Langone, L., Brilli, M., Turi, B., and Ravaioli, M.: A possible record of the Younger Dryas event in deep-sea sediments of the Southern Ocean (Pacific sector), Paleogeography, Paleoclimatology, Paleoecology, 198(1–2), 265–278, 2003.

Mueller, F., Caflisch, T., and Mueller, G.: Firn und Eis der Schweizer Alpen, Geographisches Institut, ETH Zuerich, Publ. No. 57, 293p., 1976.

National Snow and Ice Data Center: World Glacier Inventory, World Glacier Monitoring Service and National Snow and Ice Data Center/World Data Center for Glaciology. Boulder, CO, 1999, updated 2003.

Pepper, A. C., Shulmeister, J., Nobes, D. C., and Augustinus, P. A.: Possible ENSO signals prior to the Last Glacial Maximum, during the last deglaciation and the early Holocene, from New Zealand, Geophys. Res. Lett., 31, L15206, doi: 10.1029/2004GL020236, 2004.

Porter, S. C.: Equilibrium-line altitudes of late Quaternary glaciers in the Southern Alps, New Zealand, Quaternary Res., 5, 27–47, 1975.

Robinson, L. F., Henderson, G. M., Hall, L., and Matthew, I.: Climate control of riverine and seawater uranium-isotope ratios, Science, 305, 851–854, 2004.

Sevruk, B. (Ed.): Snow cover measurements and aerial assessment of precipitation and soil moisture, World Meteorological Organization, Geneva, Operational Hydrological Report No. 35, WMO-No. 749, 283p., pg. 129, 1992.

Shulmeister, J., Goodwin, I., Renwick, J., Harle, K., Armand, L., McGlone, M. S., Cook, E., Dodson, J., Hesse, P. P., Mayewski, P., and Curran, M.: The southern hemisphere westerlies in the Australasian sector over the last glacial cycle: a synthesis, Quaternary Int., 118–119, 23–53, 2004.

Shulmeister, J., Fink, D., and Augustinus, P.: A cosmogenic nuclide chronology of the last glacial transition in North-West Nelson, New Zealand – new insights in Southern Hemisphere climate forcing during the last deglaciation, Earth Planet. Sci. Lett., 233, 455–466, 2005.

Singer, C., Shulmeister, J., and McLea, B.: Evidence against a significant Younger Dryas cooling event in New Zealand, Science, 281, 812–814, 1998.

Speight, R.: A detail of the Pukaki moraine, Transactions and Proceedings of the Royal Society of New Zealand, 72(2), 148–157, 1942.

Stewart, R. B. and Neall, V. E.: Chronology of palaeoclimatic change at the end of the last glaciation, Nature, 311, 47–48, 1984.

Sturman, A. and Wanner, H. A comparative review of the weather and climate of the Southern Alps of New Zealand and the European Alps, Mountain Res. Dev., 21, 359–369, 2001.

Suggate, R. P.: Late Pleistocene and Quaternary glaciations of New Zealand, Quaternary Sci. Rev., 9, 175–197, 1990.

Thiede, J.: Wind regimes over the late Quaternary southwest Pacific Ocean, Geology, 7, 259–262, 1979.

Turney, C. S. M., McGlone, M. S., and Wilmhurst, J. M.: Asynchronous climate change between New Zealand and the North Atlantic during the last deglaciation, Geology, 31(3), 223–226, 2003.

Weaver, P. P. E., Carter, L., and Neil, H. L.: Response of surface water masses and circulation to late Quaternary climate change, east of New Zealand, Paleoceanography, 13, 70–83, 1998.

Woo, M. and Fitzharris, B. B.: Reconstruction of mass balance variations for Franz Josef Glacier, New Zealand, 1913–1989, Arctic Alpine Res., 24(4), 281–290, 1992.

Stratigraphy and tectonic implications of Late Pleistocene valley fill in the Hope Valley, Canterbury, South Island, New Zealand

Henrik Rother*, Harry M. Jol**, James Shulmeister *

* Department of Geological Sciences, University of Canterbury, Private Bag 4800, Christchurch, New Zealand

** Department of Geography and Anthropology, University of Wisconsin-Eau Claire, Eau Claire, WI, 54702, USA

Abstract

A thick sequence (~177 m) of aggradational deposits was studied in the lower Hope Valley. Valley fill is preserved in a tectonic depression, the Hope Basin, which is associated with a releasing bend on the active strike slip Hope Fault. Local basin subsidence since the last glacial maximum (LGM) is estimated to have occurred at a rate of 1.4 – 2.5 mm/yr, which matches the known regional tectonic uplift rate. The approximate balance between uplift and basin subsidence has resulted in climate driven sedimentation patterns which dominated during the Late Pleistocene.

The deposition of the sediments described here started near the termination of OIS 4 (Oxygen Isotope Stage) and continued throughout the following interstadial and stadial (OIS 3 and OIS 2). Aggradation began with the infilling of a large paleolake that occupied the Hope Basin. Luminescence dating (IRSL) on lake beds indicates an OIS 4 age for the formation of this lake. The lake terminated during OIS 3 as a result of complete infilling. The subsequent phase of fluvial aggradation buried paleolake deposits under 65 m of glaciofluvial outwash before the progression of a late OIS 3 or early OIS 2 advance over the valley fill. A luminescence age (IRSL) of 32.1 ± 2.6 ka BP from outwash deposits below the LGM terminal moraine indicates that the aggradation phase leading to the LGM advance

began during late OIS 3. Postglacial fluvial degradation caused 160 m of incision into the lower Hope Valley thereby partially excavating the pre-LGM basin fill.

Keywords: New Zealand, glaciation, aggradation, degradation, ground penetrating radar (GPR), Late Quaternary, infrared stimulated luminescence (IRSL), Hope Valley, Southern Alps

Introduction

The Southern Alps of New Zealand experienced numerous glaciations within the Late Pleistocene during which large valley glaciers advanced beyond the limits of the Southern Alps reaching the Tasman Sea in the west and extending into the eastern alpine forelands (Suggate 1990). Marine and terrestrial records show that New Zealand's Pleistocene glaciations were broadly synchronous with glacial climate fluctuations in the Northern Hemisphere (Nelson et al. 1985, Suggate 1990). However, accurate correlations are limited by inadequate age control for New Zealand's glacial sequences and problems are accentuated for events prior to the Last Glacial Maximum (LGM). Recently, renewed interest in improving the resolution of New Zealand's glacial chronology follows the recognition that New Zealand data are of key importance for the high precision correlation of paleo-climatic events between the Northern and Southern Hemispheres (e.g. Broecker 1997, Singer et al.1998, Ivy-Ochs et al. 1999).

A distinctive feature of glacial sequences in the Southern Alps is their strong association with waterlain sediments. Thick fluvial aggradation fans, often exceeding 100 m in thickness, represent the dominant deposit in the major glacial valleys east of the alpine divide. Consequently, the traditional focus of glacial geologists in New Zealand has been on

the correlation of outwash terraces for the discrimination of glacial events (e.g. Gage 1958, Suggate 1965, Nathan & Moar 1973, Mabin 1983, Suggate 1985, Maizels 1989). Despite the importance of glacio-aggradational deposits in the Southern Alps there are few investigations aimed at deciphering the sedimentary pattern and numerical chronology of the glacial aggradation sequence. In this paper we present a case study on aggradational deposits from the Hope Valley in North Canterbury, New Zealand. The valley was chosen because it displays a typical glacial sequence and contains excellent outcrops that allow detailed sedimentary logging and sampling for luminescence dating

Remnants of uplifted aggradational terraces in many New Zealand valleys provide evidence of older valley fills. However interglacial valley re-excavation, enhanced by rapid tectonic uplift, has often led to the complete removal of previous valley fill sequences. Only in rare cases are older aggradational deposits preserved. We highlight such a sedimentary sequence from the lower Hope Valley. Subsurface information on sedimentary structures of the basin fill was provided by ground penetrating radar (GPR).

Regional setting: the Hope Valley

The Hope River (mean flow 45.9 m^3/s) in North Canterbury is part of the Waiau catchment which drains ~1980 km^2 situated on the eastern side of the Southern Alps (Fig. 1). Bedrock in the area is dominated by highly folded and faulted Triassic greywacke with rare beds of conglomerate, limestone and volcanics (Torlesse Group) (Gregg 1964). The highest peaks in the catchment are approximately 2300 m (a.s.l.) but present glaciation is limited to a small number of cirque glaciers in the headwater ranges of the Waiau Valley. However, the presence of U-shaped valleys, till plains, terminal moraines, and frequent erratics provide evidence for extensive past glaciations.

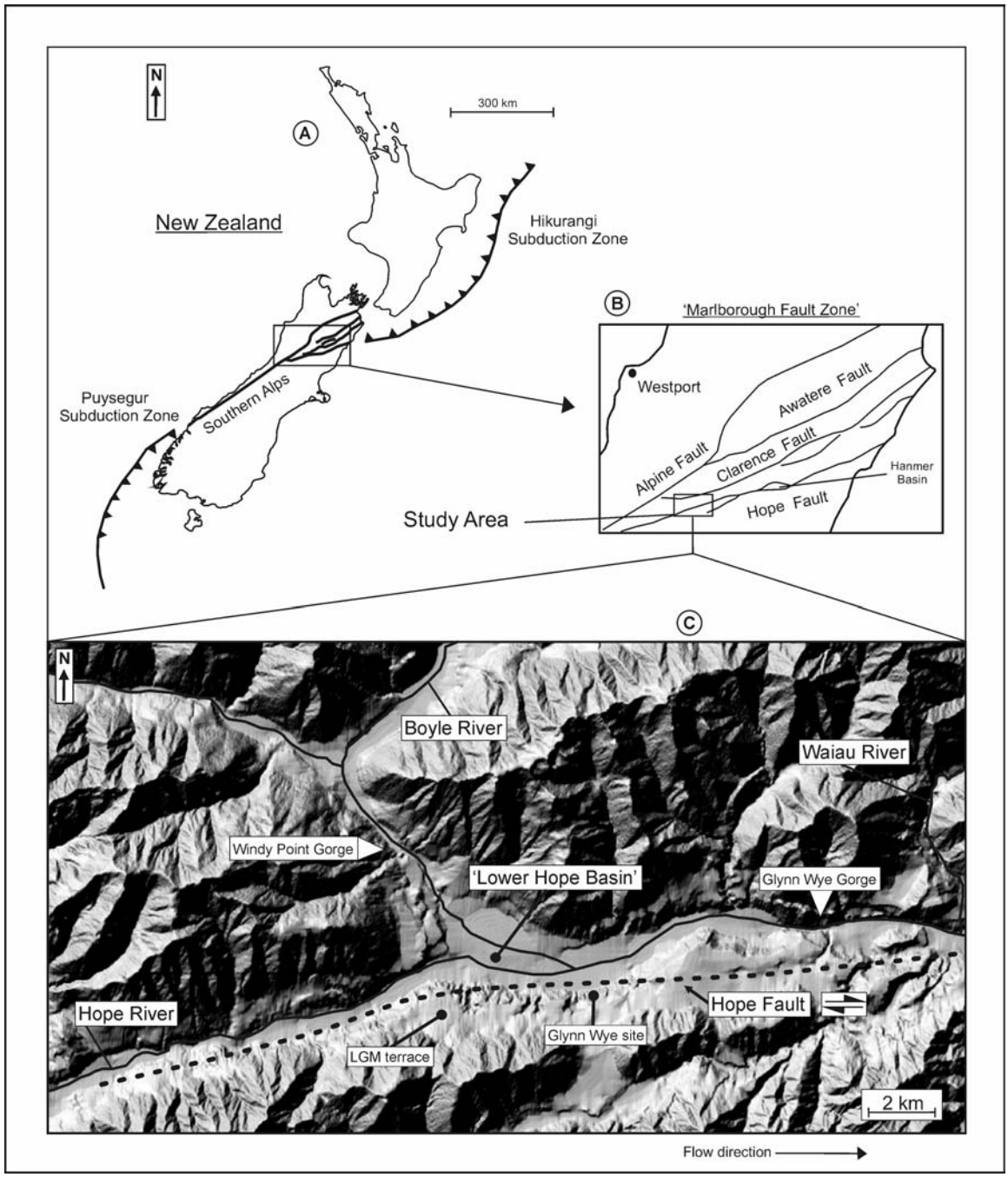

Fig. 1. Location of the Hope Valley and the 'Marlborough Fault Zone' in the South Island, New Zealand (A, B). The shaded relief map (from a DEM) in Figure 1C shows the Hope Basin, the course of the Hope Fault and the location of the studied outcrop (Glynn Wye site).

The study area is part of the highly active tectonic Marlborough Fault Zone, where ongoing deformation is related to the oblique collision of the Australian and Pacific plates (Norris et al. 1990). Several NE trending dextral strike-slip faults traverse the area and control overall valley and drainage orientation. The most active fault is the Hope Fault with

an estimated Late Pleistocene-Holocene strike-slip rate of 10-14 mm/yr (Cowan 1990, Cowan & McGlone 1991). Recent rupture events along the Hope Fault include a magnitude 7.0-7.3 earthquake in 1888 (McKay 1890). The average recurrence interval of major seismic events along the Hope Valley segment of the Hope Fault ranges between 80-200 years (Cowan 1991).

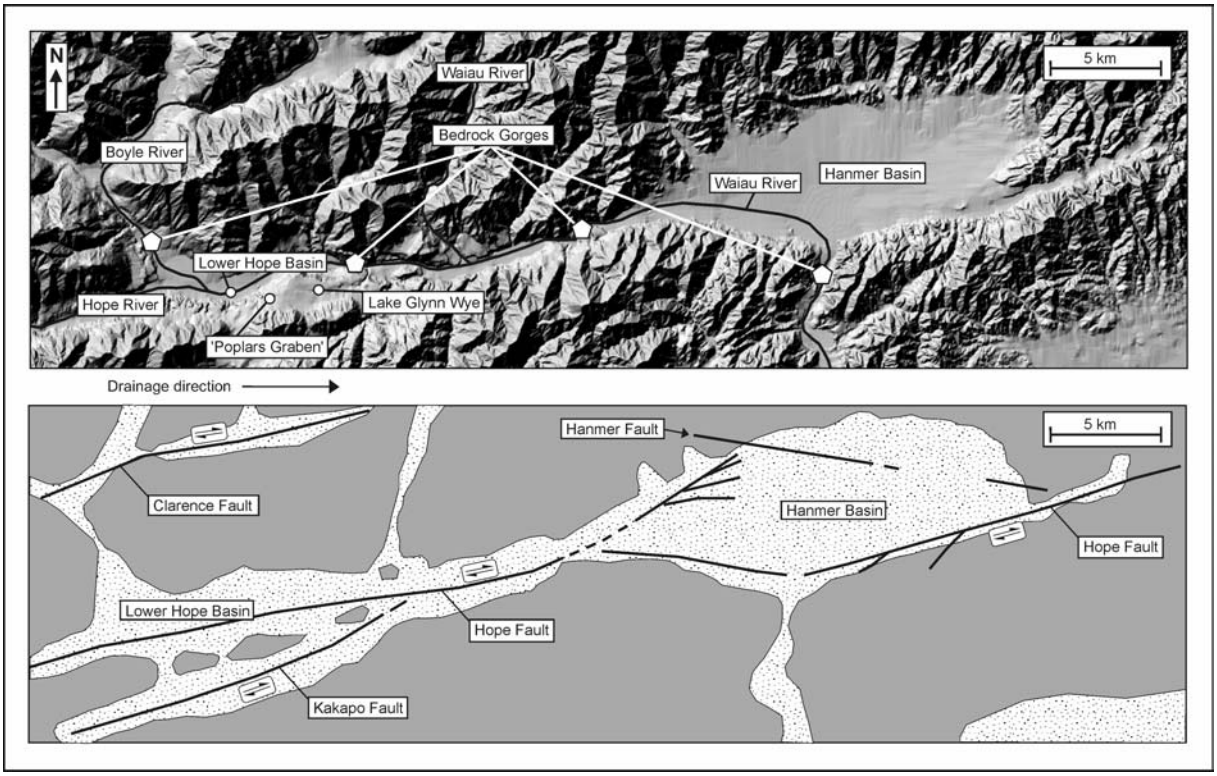

Fig. 2. Overview of structural geology and fault controlled features of the Boyle-Hope-Waiau Valley system. Note the succession of gorges and wider valley segments, all of which are associated with rapid changes from braided to single thread channel geometry.

The largest morphological feature to form as a result of transcurrent motion on the Hope Fault is the Hanmer Basin (10 x 20 km) in the middle Waiau Valley (see Fig. 2, Cotton 1947, Clayton 1965, Freund 1971). A seismic survey by Wood et al. (1994) found the basin depocenter to contain ~1000 m of sediments. They interpreted the basin origin to be related to a pull-apart motion in a step over region on the Hope Fault. The fault line follows the course of the Hope Valley and various other morphological features, in particular the

repeated succession of narrow bedrock gorges and intermediate wider valley segments appear to be fault controlled.

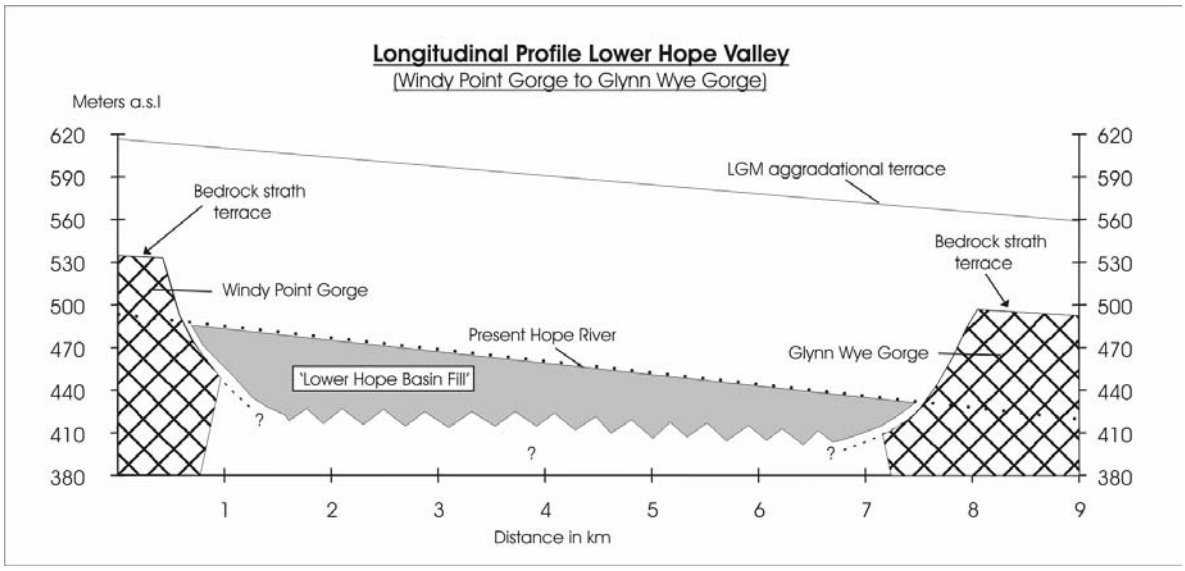

Fig. 3. Position and elevation of bedrock gorges and strath terraces in the lower Hope Valley. Although bedrock is exposed at gorges upstream and downstream of the lower Hope Valley (= Hope Basin), no bedrock is found at surface level within the lower Hope Valley itself. Postglacial strath terraces at Windy Point Gorge (upstream) and Glynn Wye Gorge (downstream) range in elevation from 490 – 536 m a.s.l., yet in the lower Hope Valley bedrock is not exposed at river level (~450 m a.s.l. in central basin). The absence of knickpoints in the longitudinal valley profile is caused by the sedimentary infilling of the Hope Basin.

The Hope Basin

The Hope Basin is located in the lower Hope Valley constituting a 9.0 km long and 4 km wide valley segment at the confluence of the Hope and Boyle Rivers. Cowan (1991) suggested that the structure represents a tectonic depression (7 x 3 km) that formed at a releasing bend of the Hope Fault. Apart from Cowans' (1990, 1991) references to the Hope Basin, little is known about geomorphic and sedimentary effects of local basin formation and total basin depth is unknown. The configuration of the basin is best expressed by highlighting the distribution of bedrock and strath terraces along the lower Hope Valley. Although deeply incised bedrock gorges are found on the immediate upstream and

downstream ends of the lower Hope Valley (Windy Point Gorge and Glynn Wye Gorge), no bedrock is exposed for several kilometers at river level within this valley reach (Fig. 3).

Late Quaternary tectonic activity in the Hope Valley is demonstrated by a marked fault trace along which late glacial landforms have been dextrally offset. The key feature frequently used to determine the fault slip rate, is the presumed LGM moraine ridge at Glynn Wye Station (Glynn Wye moraine). The lateral offset of the moraine has been measured by several studies (Knuepfer 1984, 1988, Cowan 1989, 1990), but due to different geomorphic interpretations results varied between 230 ± 20 m and 348 ± 7 m. Other effects of Late Quaternary extensional faulting in the lower Hope Valley are expressed at the surface through the Poplars Graben (Freund 1971), which formed along a small scale releasing bend of the Hope Fault. The graben is located within the Hope Basin and formed in late last glaciation aggradational deposits. Freund (1971) and Cowan (1989) surveyed the graben and found the central part of the structure to be downthrown by 38 m and 40 m, respectively (Fig. 4).

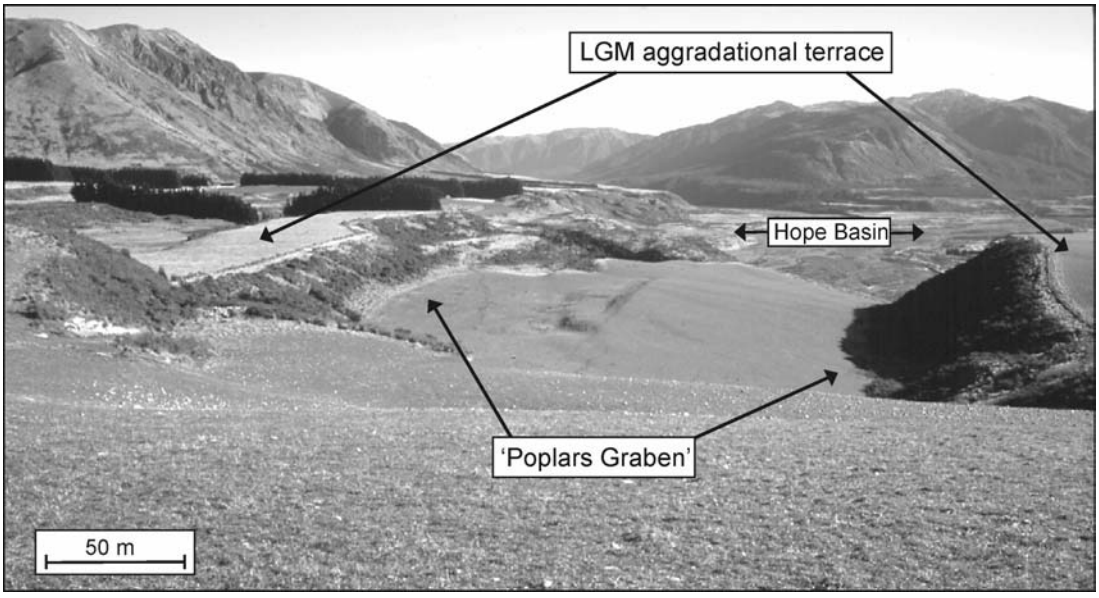

Fig. 4. Poplars Graben is located on the main aggradational terrace within the Hope Basin (see Fig. 2). The photo shows a view through the graben towards W. The graben is displacing LGM aggradational deposits and represents a secondary tectonic structure within the larger Hope Basin. Maximum downthrow of the graben is 40 m (Cowan 1990).

Quaternary context

The current chronology of Late Pleistocene glacial fluctuations in the Hope and Waiau Valleys was established by Clayton (1968) who mapped distinct levels of moraines and associated outwash surfaces upon which he identified six glacial advances. Remnants of four of these advances are found in the lower Hope Valley (Fig. 5). During glacial periods valley glaciers extended 30-40 km from a long but narrow ice cap which formed over the central perhumid sector of the Southern Alps. Several times during the Late Pleistocene glacial advances were extensive enough to reach the Hope Basin where the Hope and Boyle glaciers coalesced to form a single glacier tongue.

The general model developed to establish the present chronology for New Zealand's glacial periods relies on the assumption that rapid tectonic uplift has caused increasing vertical displacement of glacial landforms through time. The concept uses a relative elevation-age relationship where outwash terraces and moraines at higher elevations are interpreted to be older than glacial features found at lower elevations (Gage 1958, Suggate 1965). Although the premise of the model is reasonable, independent numerical age control of higher (and older?) glacial deposits is usually absent. Also the model is valid only if younger glacial advances did not reach the elevation level(s) of the previous glacial advance(s).

Glacial surfaces in the Hope Valley are found over a wide range of elevations above the present river. The inferred LGM glacial moraines and correlated outwash (inferred age) are situated 160 m above the present river, while the highest (and presumably oldest) glacial surface is located on Kakapo Hill 430 m above the Hope River (Kakapo Advance). Between these two advances an intermediate level of outwash surfaces is found at about 300 m above river level (Horseshoe Advance). The table in Fig. 5 summarizes Clayton's (1968) relative

chronology and provides an updated correlation to marine Oxygen Isotope Stages (OIS). None of the geomorphic features or deposits associated with Late Pleistocene glacial advances in the Hope-Waiau catchment have direct age control and correlations remain tentative.

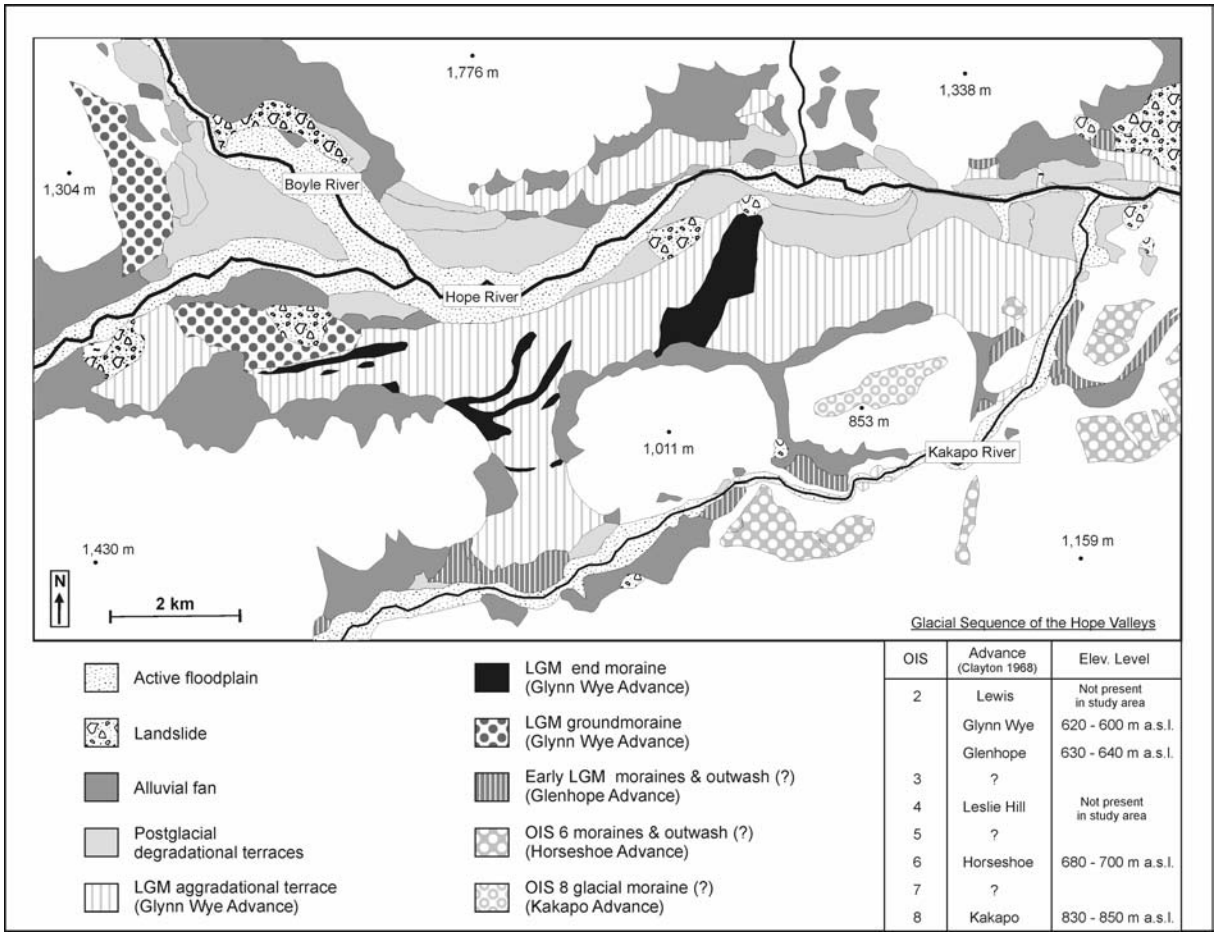

Fig. 5. Quaternary geology of the lower Hope Valley study area (modified from Clayton 1968). Note that landforms and deposits from glacial advances during OIS 8, 6, and 2 (all ages inferred) are associated with distinct elevation levels.

Methodology

A detailed investigation of the Hope Basin was undertaken as part of a larger project aimed at remapping and dating glacial deposits in the Hope & Waiau Valleys. Field work started with a reconnaissance mapping campaign of the entire glacial sequence in the Hope

Valley during which most of the glacial sites described in Clayton's (1965) original study were revisited. This was combined with airphoto interpretation, to provide the necessary context for the Quaternary geology of the study area (Fig. 6).

A portable digital pulseEKKO™ IV radar system was used to collect GPR reflection profiles. After tests with various antennas, a low frequency 50 MHz antenna was selected for the survey (Jol and Bristow, 2003). The system was operated in 'step-wise reflection mode' with a step size of 0.50 m. Each digital trace was vertically stacked 32 times at a sampling time interval of 800 picoseconds. Profiles were processed and plotted using pulseEKKO ™ software. From several common mid-point surveys an average near-surface velocity of 0.11 m/ns was calculated for the sediment.

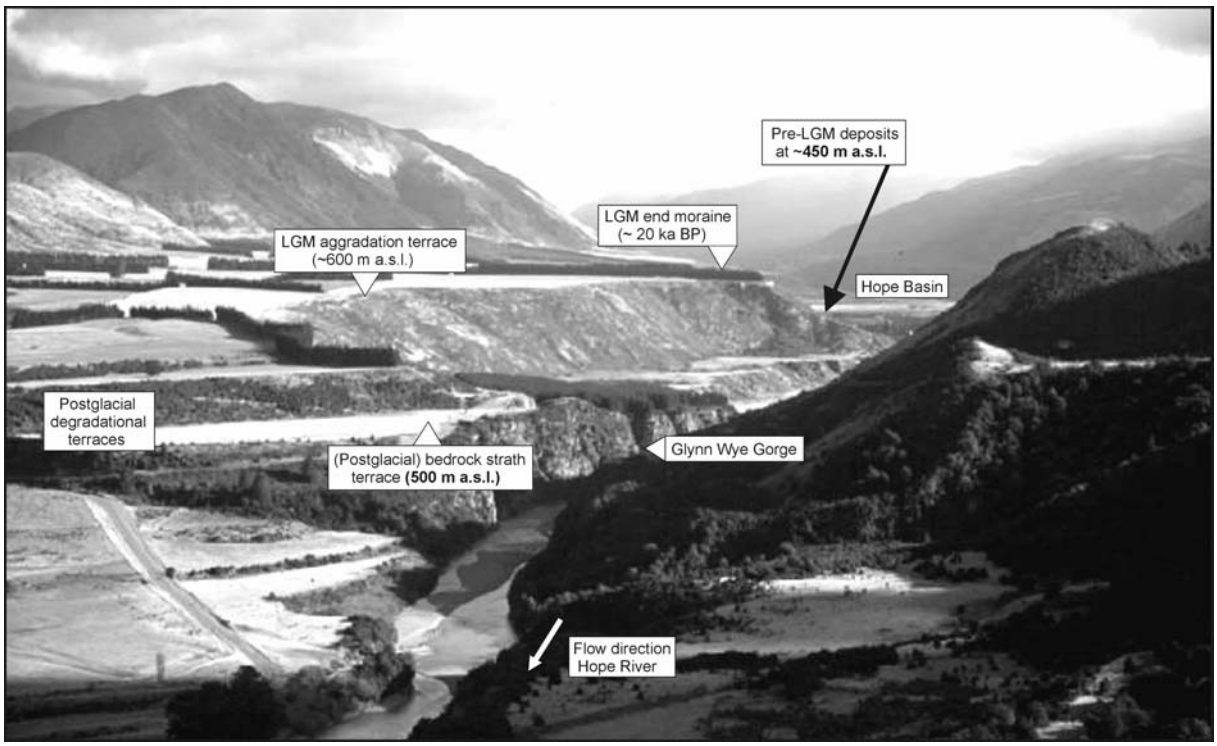

Fig. 6. Upriver view (west) into the lower Hope Valley showing the context of landforms and deposits discussed in the text. The basin configuration of the lower Hope Valley is demonstrated by the elevations of some key features. Following postglacial fluvial incision through the LGM aggradational terrace, the Hope River formed a bedrock strath terrace at Glynn Wye Gorge (500 m a.s.l). However, older pre-LGM fill deposits are exposed upriver at an elevation of only 450 m a.s.l. (black arrow). Note that LGM ages for local end moraines and aggradational terraces are inferred and rely on correlations to other valley systems in the Southern Alps (Clayton 1968, Knuepfer 1984, Cowan 1990).

Results

The following results consist of a GPR survey of sub-floodplain deposits and log data from an adjacent sedimentary exposure (Glynn Wye outcrop). These complimentary data sets allow for the reconstruction of depositional processes in the Hope Basin.

GPR results and interpretation

In the Hope Basin, GPR was used at two locations to determine the depth to bedrock and to investigate sedimentary structures of the basin fill (Fig. 7). The first survey (profile A, Fig. 8) was collected on the south side of the Hope River floodplain along a survey line located ~15 m away from the Glynn Wye outcrop (see outcrop description next section). Reflections delineate three radar facies (lower, middle, upper) with a total signal penetration depth of ~12 m. The lower radar facies displays continuous to semi-continuous, horizontal to

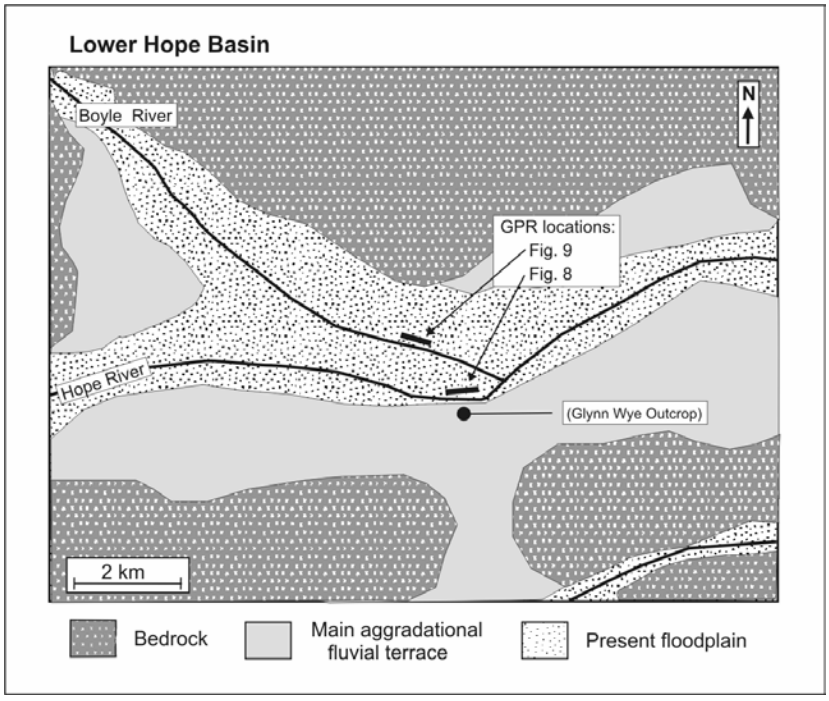

Fig. 7. Location and orientation of transects for GPR profiles presented in Figs. 8 and 9.

sub-horizontal reflection patterns. The 11-m thick middle facies is dominated by continuous to semi-continuous reflections with a dip angle ranging from 31º to 38º. Between positions 0 – 20 m (horizontal distance) reflections are sub-horizontal, and are onlapping the steeply inclined unit in the center of the profile. At the eastern end of the profile (horizontal position 45 - 55 m) reflections become less continuous with the inclination of the bedding reduced to ~ 21º. The middle radar facies is separated from the nearly horizontal upper facies by a truncation and we interpret the contact as an erosional unconformity. The upper facies is ~1.50 m thick and consists of sub-horizontal to horizontal continuous to semi-continous reflection patterns.

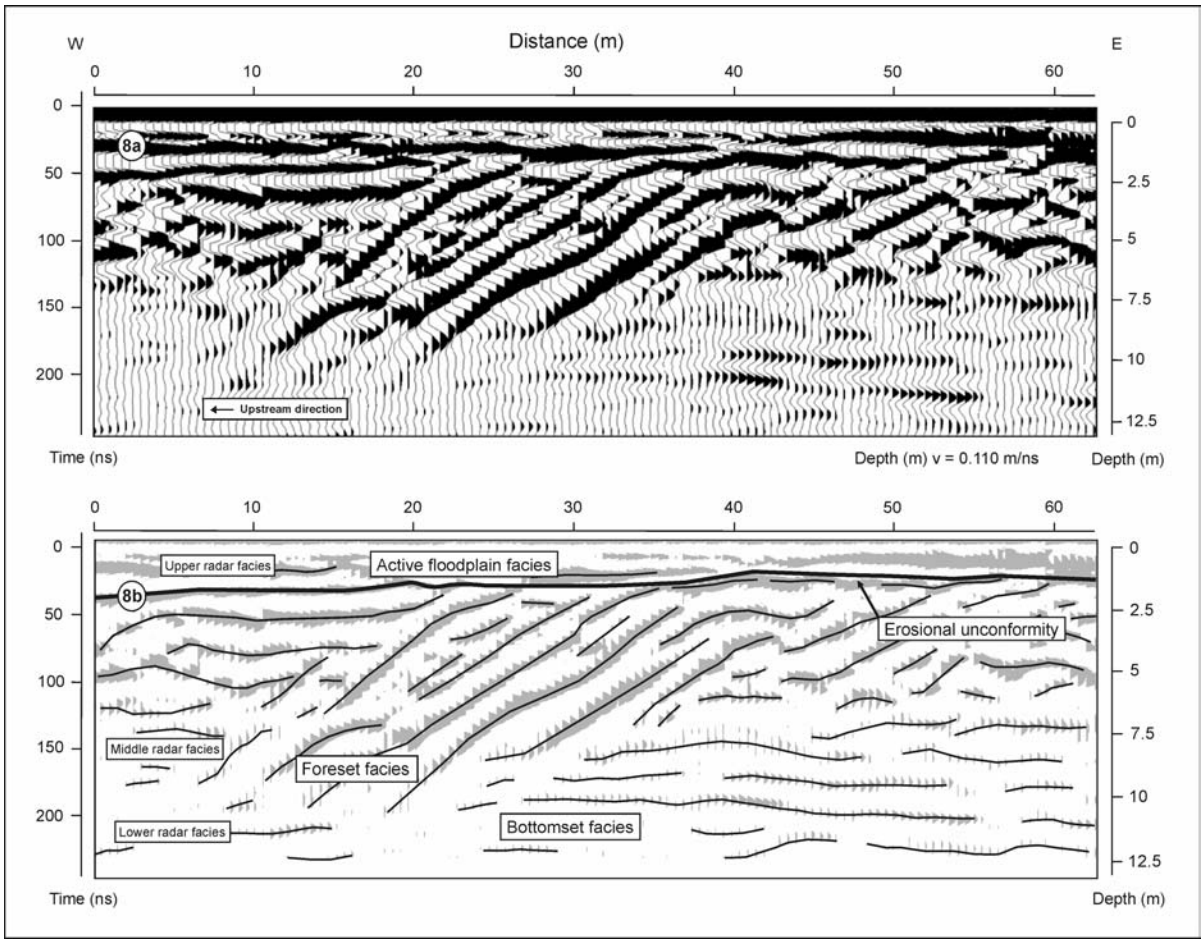

Fig. 8. 50-MHz GPR profile A showing radar reflections (a) and interpretation of sedimentary structures (b) below the Hope River floodplain.

In the context of the inclined bedding of the middle radar facies we interpret the nearly horizontal reflections of the lower radar facies to represent a delta bottomset deposit. Rapid signal attenuation within the facies might be explained by the fine-grained nature of the sediment, such as is observed in exposed beds at the base of the adjacent Glynn Wye outcrop. The overlying radar facies (11 m) comprises of steeply dipping beds, which are interpreted as delta foresets. The deltaic sediments indicated by the lower and middle radar facies represent an older lake phase in the Hope Basin. GPR profile A shows no bedrock contact to a depth of 12 m below the Hope River floodplain.

Separated by an erosional unconformity, the thin uppermost facies (~1.50 m) represents a veneer of coarse gravels which form the active channel deposit of the Hope River. The deposit comprises of mainly boulders representing the coarse bed load component which is not moved under standard flow conditions. However, the moderate thickness of the channel facies and the erosional nature of the basal contact suggests that during frequent flooding, the present Hope River is capable of moving its bedload and of incising into the underlying lacustrine facies.

The second GPR survey line (profile B, Fig. 9) was located near the center of the Hope Basin about 1.4 km northwest of the Glynn Wye outcrop (see Fig. 7). The 115 m long survey line was oriented parallel to the lower Boyle River (WNW-ESE). Radar reflections were recorded to a depth of 16-17 m.

The profile is summarized into three radar facies (lower, middle, upper). The lower facies is poorly constrained with only three slightly dipping (2º downstream), continuous to semi-continuous reflections between 10-70 m (horizontal distance). The middle facies is ~12 m thick and displays continuous to semi-continuous reflections with varying dip angles and dip directions. A prominent 30 m long, 5 m high anticlinal reflection pattern is centered at 28 m (horizontal distance). In the central section of the profile (64-71 m horizontal position)

reflections indicate the presence of a steeply dipping unit (42º) with a depth ranging from 2.5 to 9 m. Between 70-110 m (horizontal distance) dipping reflections indicate a bedding inclination of ~18º. It is important to note that the reflections at both positions dip in an upstream direction. The middle radar facies is separated from the nearly horizontal upper facies by a truncation which is interpreted as an erosional unconformity. The upper facies is ~1.50 m thick and consists of sub-horizontal to horizontal continuous to semi-continous reflection patterns.

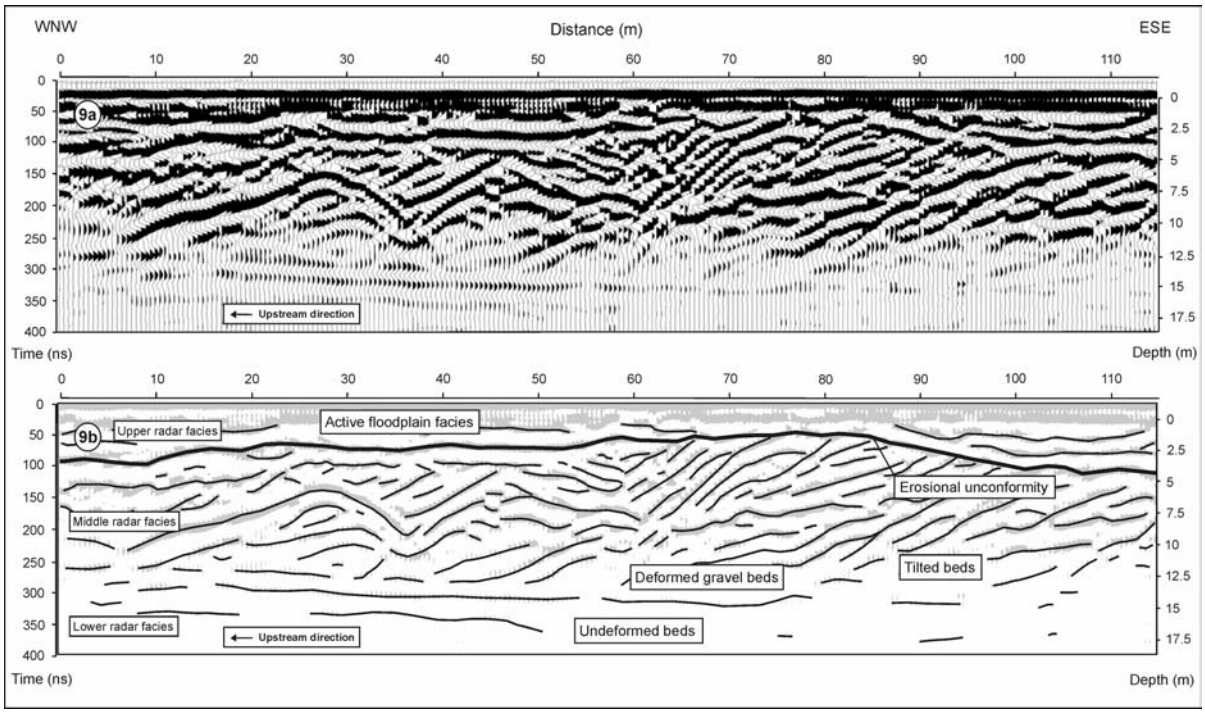

Fig. 9. 50-MHz GPR profile B from the central part of the Hope Basin showing radar reflections (a) interpreted to represent deformational structures (b). Note that deformation occurs only in the middle facies while the bottom facies is undeformed.

Profile B shows no indication of bedrock to a depth of 17 m below the floodplain, which is consistent with results from profile A. The weak reflection pattern of the lowest radar facies is interpreted as an undeformed, nearly parallel bedded and slightly downstream dipping sedimentary unit. The overlying middle radar facies, in contrast, displays a remarkable degree of sediment deformation. Structures include a slightly asymmetrical

anticlinal fold (centered at 28 m horizontal distance) which appears in three dimensions to be mound shaped based on perpendicular GPR survey lines. The steeply dipping reflections (see position 64-71 m in Fig. 9) are interpreted to be oversteepened gravel beds (~42º dip) which exceed the natural angle of repose for loose sediment.

The profile segment between 70-110 m dips at ~18º in a WNW direction. With respect to dip angle and dip direction (upstream) the deposits cannot be of primary fluvial origin and an interpretation as delta foresets is unlikely because the structure is located in the central part of the Hope Basin (~1.5 km distance to either valley side). With the direction of dip pointing upstream neither the Hope River nor the Boyle River are candidates for potential delta foreset deposition at the site while all other streams draining into the basin are too small to produce a delta that would be required to extend 1.5 km from the valley side into the central basin. A more likely explanation for the reflection pattern is sediment deformation caused by tilting and folding.

The upper radar facies consists of nearly horizontal reflections and is interpreted as the active channel deposit which truncates underlying deposits (i.e. middle radar facies). The presence of an erosional unconformity below the channel deposit in profile B is consistent with results from profile A and supports the view that the lower Hope River is presently incising into the older valley fill.

Despite some uncertainty about the mechanism that produced the sediment deformation observed in profile B, it is important to note that the lower facies (> 14.0 m depth) appears to be undeformed. Since the deformational structures are clearly restricted to near surface sediments we consider it improbable that they are associated with a seismic event on the Hope Fault as this would likely also have disturbed underlying beds (i.e. lower radar facies). A more likely explanation for the structures is deformation caused by slumping or glaciotectonic processes, however, alternative processes cannot be ruled out at this stage.

In summary, the GPR results show that the sedimentary fill of the Hope Basin extends to at least 17 m below the present floodplain. Both GPR profiles display sedimentary structures (delta foreset in Fig. 8a; deformational pattern in Fig. 9a), which imply that the sub-valley fill is not associated with fluvial aggradation of the present Hope River. This view is also supported by erosional unconformities found below the active channel deposit in both profiles. The delta foreset and bottomset seen in Fig. 8a provide evidence for a paleolake that existed in the Hope Basin.

Glynn Wye outcrop

Large outwash terraces in the Hope Valley are evidence for the massive extent of valley aggradation during glacial periods and the intensity of postglacial fluvial downcutting. The local stratigraphy of valley fill deposits is exposed in a spectacular outcrop on the south side of the Hope Basin at Glynn Wye Station (Lat/Long: S 42º36'16"/E 172º25'42"; NZ grid ref. M32 448631). The outcrop comprises 120 m of deposits which form the main aggradational terrace in the lower Hope Valley (Fig. 10).

Variation in dominant clast lithology, color and bedding orientation separates two well defined gravel units that are visually distinct from the distance (Fig. 10C). The ~55 m thick basal unit (G1) comprises ~45 m of steeply dipping foreset beds (33º), which are overlain by ~10 m of nearly horizontal topset beds (Fig. 10D). A compositionally different unit (G2) comprising 65 m of coarse fluvial gravel (max. clast Ø ~0.4 m) overlies the delta deposit. The lighter sediment color of the G2 gravels (Munsell Colour: N 6/0) is explained by a high proportion of greywacke lithologies while underlying deltaic gravels (G1) contain a higher proportion of darker colored argillite (Munsell colour: N 3/0). The fluvial unit consists mainly of well rounded boulders and resembles in composition and clast shape to

the present floodplain deposit. The absence of erosional scouring at the contact between lacustrine and fluvial gravels indicates that none or only minor erosion occurred between the deposition of the two units and that the contact is depositional in nature. This view is supported by the fact that the delta sequence is complete including the fully preserved topset beds.

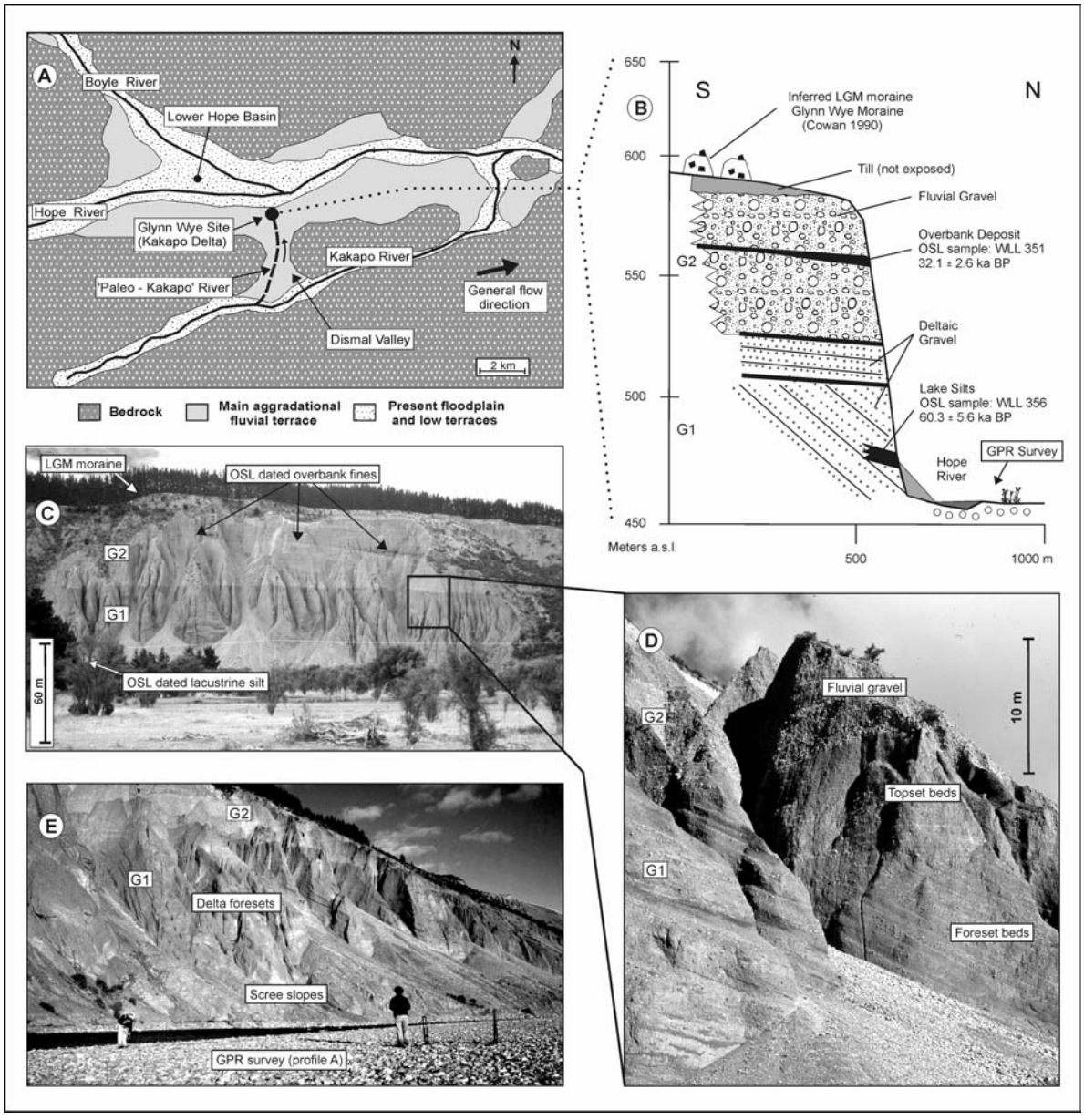

Fig. 10. Location and stratigraphy of aggradational deposits exposed at Glynn Wye Station on the south side of the Hope Basin. The positions of the two major gravel units (G1 & G2) are marked for better orientation. Note that Fig. 10B and Fig. 10E show the location of the transect for the GPR profile presented in Fig. 8.

The aforementioned lithological difference between the two major gravel units G1 and G2 is relevant when considering the source areas for both gravel packages. Argillite clasts of the delta deposit (G1) are mainly 4-12 cm in size (a-axis) and are dominated by subangular shapes indicating a short distance of fluvial transport while the overlying fluvial gravel (G2) contains mainly well rounded boulders suggesting longer distance transport. Measurement of the depositional orientation of the foreset beds indicate that the delta was deposited into the Hope paleolake from the south. The only potential stream outlet from this direction is Dismal Valley which is presently dry. However, our data indicate that at the time of delta deposition the present Kakapo River drained across Dismal Valley directly into the Hope paleolake (the Kakapo Delta) (Fig. 10A). In addition to being consistent with the observed foreset orientations, this reconstruction also accounts for the high proportion of subangular argillite clasts as fluvial transport distances out of the Kakapo catchment cannot have exceeded 15 km. In contrast to the deltaic gravels, the overlying fluvial unit (G2) was deposited by the main Hope River flowing from west to east.

Stratigraphic control on the deposition of the aforementioned units is provided by a glacial moraine system deposited on top of the Glynn Wye sequence (see photo in Fig. 10C). The moraines overlie glaciofluvial outwash of the main aggradational terrace in the Hope Valley. By correlation to other New Zealand glacial systems, Suggate (1965), Clayton (1968) and Cowan (1990) suggested that the moraines represent the terminal position of the main LGM advance. Knuepfer (1988) reported a dubious clast weathering rind age of 18.7±3.8 ka BP for the moraine.

We obtained two infrared stimulated luminescence ages (IRSL) from the Glynn Wye sequence. The stratigraphically lower sample was taken from a block of lacustrine silt exposed within deltaic gravels (G1) in the lower part of the sequence (Figs. 10B, 10C). The silt deposit has an age of 60.3 ± 5.6 ka BP (OSL sample: WLL 356) suggesting that the

Hope paleolake occupied the valley during late OIS 4. Since our IRSL sample was obtained from above the basal contact of the lacustrine unit (base is not exposed) the lake formation must pre-date our IRSL ages. A second sample for IRSL dating was retrieved from a 0.6 m thick silty overbank deposit, which was found within fluvial gravels (G2) in the upper part of the outcrop (Figs. 10B, 10C). The dated silt layer was traced across the sequence and sampled in an accessible gully 150 m east of the main outcrop. The sample yielded an age of 32.1 ± 2.6 ka BP (OSL sample: WLL 351) indicating that major aggradation in the lower Hope Valley occurred during OIS 3. This suggests that the Glenn Wye moraine may precede the global LGM by up to 10 ka as the accumulation of gravels during a glacial advance would have been fairly rapid above this bed.

The basal contact of the delta foresets at the Glynn Wye Station outcrop is not exposed at river level indicating a possible continuation of the foreset beds into the subsurface. This was investigated using GPR. Profile A (Fig. 8), which was recorded only ~15 m away from the outcrop, confirms the presence of foreset beds below the Hope River floodplain (see photo in Fig. 10E). Dip angle and orientation of the foresets as indicated in the GPR profiles are consistent with the exposed foresets and it is suggested that both the buried and the exposed foreset facies belong to the same delta deposit. The total thickness of exposed (45 m) and buried (11 m) foreset beds amounts to 56 m, indicating the minimum depth of the Hope paleolake during delta deposition. The lake terminated sometime during OIS 3 and was subsequently buried under 65 m of glaciofluvial outwash. The subsequent glacial advance overran the valley fill and deposited terminal moraines over the top of the sequence.

Discussion and summary

Transtensional motion along the Hope Valley segment of the Hope Fault produced various structural depressions of different dimensions (Hanmer Basin, Lake Glynn Wye, Poplars Graben, Hope Basin; for location see Fig. 2). We describe the stratigraphy of one such depression, the Hope Basin, where relative subsidence trapped a thick aggradational sequence of Late Pleistocene deposits. Postglacial degradation by the Hope River resulted in 160 m of fluvial incision which partially exposed fill deposits preserved in the Hope Basin. Mapping of bedrock levels upstream and downstream of the lower Hope Valley indicate that ~70 m of the total amount of incision occurred into the basin fill which is exposed in the lower part of the Glynn Wye station outcrop. Although the total basin depth is not yet known, our GPR data indicate that at least 17 m of additional fill is preserved below the Hope River floodplain, suggesting a minimum total basin depth of ~87 m.

An estimate of the Late Quaternary subsidence rate for the Hope Basin can be obtained from Poplars Graben (Fig.4). The graben, which has a maximum downthrow of ~40 m (Cowan 1990), is located on the southern side of the Hope Basin and has disrupted parts of the main aggradational terrace. Although no reliable dates have been established for the terrace deposits, Knuepfer (1988) and Cowan (1990) have suggested ages between 18.7 ± 3.8 ka BP and 17.0 ± 2.0 ka BP, while others have assumed a generalized LGM age of 20 ka BP for the terrace (Clayton 1968, Freund 1971, Hardy & Wellman 1984). There is a distinct possibility that this moraine complex is actually late OIS 3, rather than LGM in age. If we apply a conservative age range of 15-30 ka BP, which covers both the LGM and late OIS 3 options we get an average Late Quaternary graben subsidence rate of ~1.35 -2.5 mm/yr. An extrapolation of the Poplars Graben subsidence rate to the entire Hope Basin must take into account that the graben represents a smaller secondary structure within the Hope Basin, but

we suggest that 1.35 -2.5 mm/yr represents a reasonable minimum estimate for Late Pleistocene subsidence of the Hope Basin.

In the context of the continuing regional uplift of the overall catchment area the formation of Hope Basin is a result of relative rather than absolute subsidence. The rise of adjacent hill ranges is estimated to occur at approximately 2mm/yr (Wellman 1979), while basin downfaulting follows at a similar rate (~1.35-2.5 mm/yr). With both the average basin subsidence and the regional uplift rate to be around 2 mm/yr the absolute basin floor elevation in the lower Hope Valley has remained roughly static. Under these conditions superimposed effects of climatically induced periods of aggradation and degradation dominated the sedimentary history of the basin.

Luminescence dating on lacustrine silts exposed at Glynn Wye station show that a large paleolake occupied the lower Hope Valley at the end of OIS 4 (60.3 ± 5.6 ka BP). GPR data indicate the continuation of exposed delta foresets into the subsurface of the lower Hope Valley, implying that at the time of lake formation the local valley floor was below its present level. The low position of the valley floor at the end of the glacial OIS 4 (~180 m below the level of the LGM aggradational terrace) may be explained as a result of glacial overdeepening at the confluence of the Hope and Boyle glaciers. The subsequent lake is likely to have formed in the overdeepened valley trough following glacial retreat at the termination of OIS 4.

Although the residence time for the lake is not known, a luminescence age from the overlying fluvial deposit shows that the lake disappeared prior to 32.1 ± 2.6 ka BP. The absence of erosional scouring and the preservation of the delta topset beds indicate that none or only minor erosion occurred between the termination of the lake and the deposition of the overlying fluvial gravels. It is therefore probable that the lake vanished due to infilling rather than through rapid drawdown as caused by a catastrophic drainage event. Rivers in the

catchment originate in tectonically very active mountain environments with high erosion rates. Present suspended sediment yields from New Zealand rivers are known to rank among the highest in the world (Griffiths 1981, Hicks 1998). It has been shown that sediment supply in New Zealand during OIS 4 and OIS 3 was larger than at present (Brown et al. 1988, Suggate 1990, Browne & Naish 2003) and infilling of the Hope paleolake may have occurred in a period of only a few thousand years. Intense OIS 4 to OIS 2 aggradation not only entirely filled the Hope Basin (to a level of ~ 520 m a.s.l.), but exceeded this level by ~90 m, with the LGM aggradational terrace located at ~ 610 m a.s.l.. The aggradation and associated build up of sediment in the lower Hope Valley caused the deflection of the paleo-Kakapo River from Dismal Valley into its present course as its original drainage became increasingly constricted. Overall results from luminescence dating indicates that the most recent phase of large scale valley aggradation in the Hope Valley, which led to the late OIS 3/ LGM glacial advances, began during OIS 3.

Following LGM ice retreat and the establishment of interglacial conditions which resulted in decreased sediment supply and increased flow values, the Hope River began its recent history of postglacial fluvial degradation. Incision rates quickly outpaced rates of basin subsidence leading to rapid downcutting into the basin. Erosional unconformities between thin active channel deposits and underlying basin fill (GPR results) and the presence of low degradational terraces (5-10 meters above river level) indicate that the present Hope River continues to incise in the lower Hope Valley. The modern incision rate is controlled by bedrock gorges upstream and downstream of the Hope Basin (Windy Point Gorge and Glynn Wye Gorge).

An interesting aspect of the stratigraphic sequence at Glynn Wye station is its survival in a central Hope Valley position despite overriding by a late OIS 3/LGM glacial advance, which deposited moraines over the top of the sequence. Our luminescence results

suggests a substantial pre-LGM age for the sedimentary succession below the moraines, implying that the LGM glacial advance overrode the site but was comparably ineffective in eroding underlying soft sediments. Whether this represents a local anomaly or constitutes a general feature of the LGM advance that reached the lower Hope Valley demands further study.

Acknowledgments

This study was financially supported by University of Canterbury internal grant U6508 to JS, a D.W. Lewis Grant to HR, an University of Canterbury Visiting Erskine Fellowship as well as a University of Wisconsin-Eau Claire Sabbatical leave to HJ. The paper benefited from discussions with Phil Tonkin and Jarg Pettinga and the review comments by John Degenhardt. We would like to thank Uwe Rieser (Victoria University of Wellington) for processing the luminescence samples. Marie Elaine van Egmond, Guyon Smith, and Craig Woodward provided tenacious assistance in the field. Sincere thanks go to Kevin and Jules Henderson of Poplars Station for their hospitality and a bumpy ride across the floodplain.

References

Broecker, W., 1997, Future directions of paleoclimate research: Quaternary Science Reviews, v. 19, p. 821-825.

Browne, G. H., and Naish, T.R., 2003, Facies development and sequence architecture of a late Quaternary fluvial-marine transition, Canterbury Plains and shelf, New Zealand: implications for forced regressive deposits: Sedimentary Geology, 158: 57-86.

Brown, L. J., Wilson, D.D., Moar, N.T., and Mildenhall, D.C., 1988, Stratigraphy of the late Quaternary deposits of the northern Canterbury Plains, New Zealand: New Zealand Journal of Geology and Geophysics 31: 305-335.

Clayton, L. S., 1965, Late Pleistocene geology of the Waiau Valleys, North Canterbury, New Zealand [Ph.D. thesis]: University of Illinois, 93 p.

Clayton, L. S., 1968, Late Pleistocene glaciations of the Waiau Valleys, North Canterbury: New Zealand Journal of Geology and Geophysics, v. 11, p. 753-767.

Cotton, C. A., 1947, The Hanmer Plain and the Hope Fault: The New Zealand Journal of Science and Technology, v. 29, p. 10-17.

Cowan, H. A., 1989, An evaluation of the late Quaternary displacements and seismic hazards associated with the Hope and Kakapo Faults, Amuri District, North Canterbury [M.Sc. thesis]: University of Canterbury, 239 p.

Cowan, H. A., 1990, Late Quaternary displacements on the Hope Fault at Glynn Wye, North Canterbury: New Zealand Journal of Geology and Geophysics, v. 33, p. 285-293.

Cowan, H. A., 1991, The north Canterbury earthquake of September 1, 1888: Journal of the Royal Society of New Zealand, v. 21, no. 1, p. 1-12.

Cowan, H. A., and McGlone, M.S., 1991, Late Holocene displacements and characteristic earthquakes on the Hope River segment on the Hope Fault, New Zealand: Journal of the Royal Society of New Zealand, v. 21, no. 4, p. 373-384.

Freund, R., 1971, The Hope Fault, New Zealand Geological Survey Bulletin: Wellington, 49p.

Gage, M., 1958, Late Pleistocene glaciations of the Waimakariri Valley, Canterbury, New Zealand: New Zealand Journal of Geology and Geophysics, v. 1, p. 123-155.

Gregg, D. R., 1964, Geological Map of New Zealand, 1: 250 000, Sheet 18 – Hurunui, Department of Industrial and Scientific Research, Wellington.

Griffiths, G. A., 1981, Some suspended sediment yields from South Island catchments, New Zealand: Water Resource Bulletin, American Water Resources Association, v. 27, no. 4, p. 662-671.

Hardy, E. F., and Wellman, H. W., 1984, The Alpine, Wairau, and Hope Faults, Victoria University of Wellington Geology Department publication, v. 27, 15 p.

Hicks, M.D., 1998, Suspended sediment in New Zealand rivers; indications from 40 years of data, National Institute of Water and Atmospheric Research (NIWA), Dunedin, 46p.

Ivy-Ochs, S., Schluechter, C., Kubik, P.W., and Denton, G.H., 1999, Moraine exposure dates imply synchronous Younger Dryas glacier advances in the European Alps and in the Southern Alps of New Zealand: Geografiska Annaler, v. 81A, no. 2, p. 313-323.

Jol, H. M., and Bristow, C. S., 2003. GPR in sediments: advice on data collection, basic processing and interpretation, a good practice guide. In: Bristow, C.S. and Jol, H.M. (eds.), GPR in Sediments, Geological Society of London, Special Publication 211, 9-27.

Knuepfer, P. L. K., 1984, Tectonic geomorphology and present day tectonics of the alpine shear system, South Island, New Zealand [Ph.D. thesis]: University of Arizona, 480 p.

Knuepfer, P. L. K., 1988, Estimating ages of late Quaternary stream terraces from analysis of weathering rinds and soils: Geological Society of America Bulletin, v. 100, p. 1224-1236.

Mabin, M. C. G., 1983, Late Otiran sedimentation and glacial chronology in the Warwick Valley, southeast Nelson: New Zealand Journal of Geology and Geophysics, v. 26, p. 189-195.

Maizels, J. K., 1989, Differentiation of late Pleistocene terrace outwash deposits using geomorphic criteria: Tekapo Valley, South Island, New Zealand: New Zealand Journal of Geology and Geophysics, v. 32, p. 225-241.

McKay, A., 1890, On the earthquakes of September, 1888, in the Amuri and Marlborough Districts of the South Island: New Zealand Geological Survey, Report of Geological Exploration, no. 2, pp. 11-16.

Nathan, S., and Moar, N.T., 1973, Age and correlation of late Quaternary terraces in the lower Inangahua Valley, West Coast, South Island, New Zealand: Journal of the Royal Society of New Zealand, v. 3, no. 3, p. 409-414.

Nelson, C. S., Hendy, C.H., Jarrett, G.R., and Cuthbertson, A.M., 1985, Near-synchroneity of New Zealand alpine glaciations and Northern Hemisphere continental glaciations during the past 750 kyr: Nature, v. 318, p. 361-363.

Norris, R. J., Koons, P.O., and Cooper, A.F., 1990, The obliquely-convergent plate boundary in the South Island of New Zealand: implications for ancient collision zones: Journal of Structural Geology, v. 12, no. 5/6, p. 715-725.

Singer, C., Shulmeister, J., and McLea, B., 1998, Evidence against a significant Younger Dryas cooling event in New Zealand: Science, v. 281, p. 812-814.

Suggate, R. P., 1965, Late Pleistocene geology of the northern part of the South Island, New Zealand, New Zealand Geological Survey Bulletin 77.

Suggate, R. P., 1985, The glacial/interglacial sequence of North Westland, New Zealand: New Zealand Geological Survey, Record 7.

Suggate, R. P., 1990, Late Pleistocene and Quaternary glaciations of New Zealand: Quaternary Science Reviews, v. 9, p. 175-197.

Wellman, H. W., 1979, An uplift map for the South Island of New Zealand, and a model for uplift of the Southern Alps, *in* Walcott, R. I., and Cresswell, M.M., ed., The origin of the Southern Alps: The Royal Society of New Zealand Bulletin, p. 13-20.

Wood, R. A., Pettinga, J.R., Bannister, S., Lamarche, G., and McMorran, T.J., 1994, Structure of the Hanmer strike-slip basin, Hope Fault, New Zealand: Geological Society of America Bulletin, v. 106, p. 1459-1473.

Stratigraphy and depositional model of a OIS 6 glacial sequence in the Hope Valley, Southern Alps, New Zealand

Henrik Rother[a1], Uwe Rieser[b] James Shulmeister[a]

a Department of Geological Sciences, University of Canterbury, Private Bag 4800, Christchurch, New Zealand (hro13@student.canterbury.ac.nz) and (James.Shulmeister@canterbury.ac.nz)
1 from May 1st 2006 at Institute for Environmental Research, ANSTO, PMB1, Menai, 2234 , Australia
b Luminescence Dating Laboratory, School of Earth Sciences, Victoria University of Wellington, P.O. Box 600, Wellington, New Zealand (Uwe.Rieser@vuw.ac.nz)

Abstract

A 110 m thick succession of glacial and proglacial deposits is described from Poplars Gully in the Hope Valley, South Island, New Zealand. The section consists of eight lithofacies assemblages that represent different stages of ice occupation in the valley. Basal sediments record an ice retreat phase as indicated by laminated kettlehole deposits with meltout deformation and large scale ice collapse structures. This was followed by a glacial re-advance which truncated the underlying facies and deposited mass flow diamictons and till. The subsequent glacial retreat is evidenced by the stratigraphic transition to ice proximal glaciofluvial gravels. A last, probably short lived advance, caused folding and thrusting of the proglacial fan sequence and deposited mass flows. Final ice retreat from the lower Hope Valley was followed by the formation of a large proglacial lake. Most sediments at Poplars Gully are associated with glacial retreat. Ice advances are represented by thin sequences of mass flow diamictons and minor till deposits.

Poplars Gully provides evidence for three glacial oscillations. A significant retreat occurred between the two older advances and probably resulted in complete ice evacuation from the lower Hope Valley. Infrared stimulated luminescence (IRSL) ages place deposition

of the Poplars Gully sequence into Oxygen Isotope Stage 6 (OIS). Based on our stratigraphic data we suggest that the previously undivided OIS 6 in the Southern Alps contains at least two substantial glacial advances.

Keywords: New Zealand, glaciation, glacilacustrine, OIS 6, sedimentology, kame terrace

1.1. Introduction

During the Pleistocene mountain glaciers of the South Island, New Zealand repeatedly advanced beyond the limits of the Southern Alps reaching the Tasman Sea in the west and extending into the eastern alpine forelands of Canterbury and Otago (e.g. Suggate 1990). Glacial sediments and landforms cover extensive areas in New Zealand and provide an important record of past glacial signals in the mid-latitude Southern Hemisphere (e.g. Denton and Hendy 1994, Ivy-Ochs et al. 1999, Shulmeister et al. 2005a). Until recently, the chronology of Quaternary glacial events in the Southern Alps was largely based on a relative uplift-model where the elevation of glacial surfaces and terraces combined with weathering characteristics were used to infer relative ages of glacial sequences (e.g. Gage 1958, Suggate 1965). From this, it has generally been argued that Quaternary glacial advances in New Zealand are broadly correlated to glaciations in the Northern Hemisphere (e.g. Suggate 1990), however, major uncertainties remain regarding the absolute and higher resolution timings of glacial events (e.g. Denton & Hendy 1994, Mabin 1996, Ivy-Ochs et al. 1999,). These difficulties are greatly accentuated for glacial advances older than Oxygen Isotope Stage 2.

With so much of the attention on glacio-chronological and stratigraphic problems, there has been little work undertaken on the sedimentology of NZ's glacial deposits. This is despite the progress made elsewhere in reconstructing former glacial conditions from sedimentary and structural parameters (e.g. Shaw 1987, Benn et al. 2003). New Zealand

provides a case where glaciations occurred under perhumid conditions with high ice accumulation and turn-over rates. There is a need for this research as modern perhumid glacial systems (e.g. Southern Chile, Pacific NW and New Zealand) are substantially smaller in scale and it is dubious whether glacial models derived from higher latitude glaciers (e.g. Iceland, Alaska, Norway) can fully apply to the lower mid-latitude setting of New Zealand.

Glacial workers have long been aware of some unusual features in the glacial sequences of the Southern Alps. Of these the enormous scale of glacio-fluvial aggradation fans, the often small size of terminal moraines, and the widespread occurrence of stratified and only weakly compacted 'drift deposits' have previously been described (e.g. Speight 1940, 1942; Gage 1965). Speight (1942, p. 151) noted that the sedimentology of terminal moraines near Lake Pukaki (Mackenzie Basin) showed "*...marked departures from the ordinary structure of moraines*". The moraines consisted of highly distorted and stratified fines, which included some angular gravel but "*…no signs of morainic material*" (Speight 1942, p. 152). Hart (1996) who revisited the Lake Pukaki moraines interpreted the deposits as ice-proximal subaqueous sediments which were subsequently deformed by proglacial glacio-tectonics. Similar sediments have been described from the Clutha (McKellar 1960) and Rakaia (Shulmeister et al. 2005b) valleys.

In the Hope Valley of North Canterbury previous glacial investigations have concentrated on geomorphological mapping (Clayton 1968, Cowan 1989) and the radiocarbon dating of a prominent postglacial lake remnant in the lower Boyle Valley (Clayton 1968, Burrows 1988, 1997, Turney et al. 2003). In this paper we describe a 110 m thick sequence of glacial deposits found at Poplars Gully on the northern side of the lower Hope Valley (Fig. 1). Our investigation represents the first detailed sedimentological description of glacial and proglacial deposits in the Hope Valley. The findings have implications for both ice dynamics and the regional tectonic history.

Fig.1: Location of the Hope Valley and the Marlborough Fault Zone in the South Island, New Zealand (A). The photo in Figure 1B shows a view from the south into Poplars Gully after the 1994 landslide. The shaded DEM in Figure 1C shows the Hope Basin, the course of the Hope Fault and the general location of the studied outcrop ('Poplars Gully' site). Favourable conditions for sediment preservation at Poplars Gully were provided by a bedrock spur that extends from Garnet Peak and has shielded deposits from erosion. Note the positions and elevations of the principal glacial moraines in Fig. 1C (modified from Clayton, 1968).

1.2 Geological setting

New Zealand is located along the convergent plate boundary between the Australian and Pacific plates and is associated with a complex pattern of plate subduction and transcurrent movement (e.g.Norris et al. 1990). Principal rock formations in the Southern Alps originated as Upper Permian to Late Jurassic Gondwana shelf deposits (quartzofeldspathic greywackes)

which were accreted as terranes during Mesozoic and Cenozoic collisions (Kamp 2001). The inception of the present day oblique plate collision occurred during the mid-late Cenozoic. It marks the onset of the Kaikoura Orogeny associated with ongoing uplift of the Southern Alps along the Alpine Fault (e.g. Kamp 1986).

Tectonically, the study area is part of the highly active Marlborough Fault Zone which comprises a system of dominantly NE trending dextral strike-slip faults (Fig. 1A). The most active of the faults, the Hope Fault, follows the course of the Hope Valley and has an estimated Late Pleistocene-Holocene strike-slip rate of 10-14 mm/yr (Cowan 1990, Cowan & McGlone 1991). The last major rupture event along the Hope Fault was the North Canterbury earthquake of 1888 (McKay 1890) with an estimated 7.0-7.3 magnitude (Cowan 1991). The largest morphological feature to form as a result of transcurrent motion on the Hope Fault is the Hanmer Basin (10 x 20 km) in the middle Waiau Valley, which has a sedimentary fill c. 1 km deep. (Wood et al. ,1994, Cotton 1947).

The study area is located ~30 km upstream of Hanmer Basin in a smaller tectonic depression here referred to as the 'Hope Basin' (Fig. 1C). The basin forms a 9.0 km long and 4 km wide valley segment (lower Hope Valley) at the confluence of the Hope and Boyle Rivers. The basin formed at a releasing bend of the Hope Fault. Although geomorphic and sedimentary effects of the local basin formation have been investigated by Rother et al. (accepted), the total depth of sediment in the Hope Basin is as yet unknown.

1.3 Quaternary geology and study site

The Hope River is a tributary to the Waiau River which drains 1980 km^2 of the northeastern Southern Alps into the Pacific Ocean. Present glaciation in the catchment is limited to a small number of cirque glacierettes in the Spenser Range of the Waiau headwaters (max. peak elevation ~2300 m a.s.l.). During the Pleistocene large valley glaciers

extended 30 - 40 km from the central alps. Low and smooth mountain passes in most headwater regions (e.g. Lewis Pass, Amuri Pass, Hope Pass, Harper Pass) suggest that under full glacial conditions at least some ice flowed from west to east across the topographical divide, thereby reflecting greater ice accumulation on the windward western side of the Southern Alps. Several times during the Late Pleistocene glacial advances were extensive enough to reach the Hope Basin where the Hope and Boyle glaciers coalesced to form a single glacier tongue.

Glacial landforms in the Waiau Valleys were first systematically investigated by Clayton (1968) who mapped different elevation levels of moraines and associated outwash surfaces to provide evidence for six separate Late Pleistocene glacial advances. The general glacial model for the Southern Alps relies on the assumption that tectonic uplift has caused increasing vertical displacement of glacial landforms through time. Although the premise of the model is reasonable, independent numerical age control of higher (and older?) glacial deposits has not been generally available. In addition, the model is only valid if younger glacial advances were not large enough to overtop and modify landforms associated with previous glacial advances. In lower Hope Valley Clayton (1968) recognized sets of glacial moraines and outwash surfaces which are correlated but not dated to advances during OIS 8, OIS 6 and OIS 2 (Clayton 1968, Suggate 1990). LGM moraines and outwash are situated ~160 m above the present river, while the highest (and presumably oldest?) glacial surface is located on Kakapo Hill ~430 m above the Hope River (Kakapo Advance) (Clayton 1968). Between these two an intermediate level of outwash surfaces is found at about ~300 m above river level (Horseshoe Advance) (Clayton 1968).

It is generally considered improbable that older valley fills can survive re-newed valley glaciation in the central valley trough and hence, most workers assume that the present day sedimentary fills in glacial valleys of the Southern Alps are dominated by products of the last glacial cycle (e.g. Gage 1958, Soons, 1963, Suggate 1965, Clayton 1968, Maizels 1989).

The most extensive valley fill remnant in the Hope Valley is the formerly inferred LGM aggradational terrace (Fig. 1C, Fig. 2) (e.g. Clayton 1968, Cowan 1990). Recent work by Rother et al. (accepted) shows that while the terrace surface is likely to have been active during the LGM, valley aggradation in the Hope Valley commenced at least ~60 ka ago and continued throughout OIS 3 until the fill sequence was overrun by the LGM glacial advances.

In this paper we present a sedimentological investigation of valley fill deposits located within the main aggradational terrace on the northern side of the valley. The exposure described here was caused by a landslide in 1994 which exposed a spectacular 110 m thick sequence of valley fill deposits.

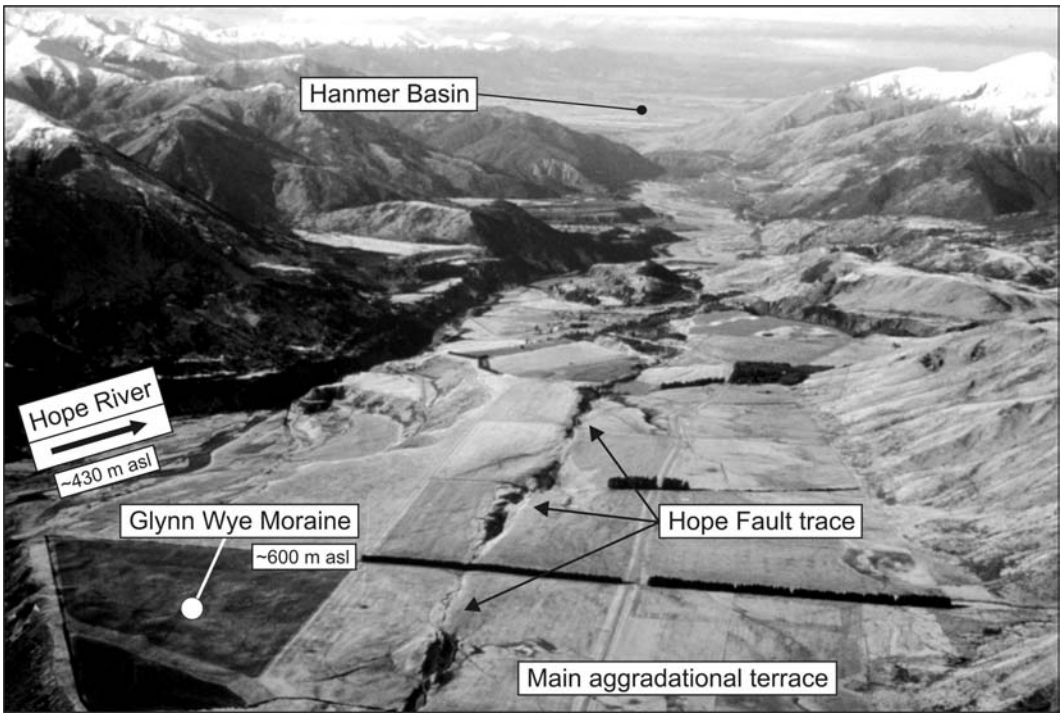

Fig. 2: View down valley from the lower Hope Valley showing locations and landforms mentioned in the text.

2.1 Methods

This study used standard sedimentary logging techniques and applied a modified facies code from Eyles et al. (1983). The individual sediments were grouped in lithofacies assemblages

on the basis of sediment composition, texture, grain size, sorting, and structures (Table 1). Representative clast orientation data were collected from all units defined as diamictons. The a-axis orientation and the dip were measured together with the clast roundness for elongate and prolate stones with long axes between 20 – 250 mm. The data were recorded for at least 30 clasts at each site, and collected over an area of less than 1 square meter. Paleo-flow directions from aqueous units were obtained from ripple cross laminations and clast imbrication. Grain sizes from selected fine grained deposits were determined using a laser particle analyzer (Saturn DigiSizer 5200). Age control was provided by Infrared Stimulated Luminescence (IRSL) dating of fine grained aqueous deposits.

Facies codes:

Fines (<0.063mm)
Fl - Laminated mud, silt and fine sand
Fe - Laminated silts and clays with dropstones
Fd - Deformed laminated silt
Fm - Massive silt and clay

Sands (0.063 – 2mm)
Sh - Plane bedded medium sand
Sm - Massive sand
Sd - Deformed sand
Sx - Cross-laminated sand
Sr - Ripple cross-laminated sand

Diamictons
Dmm - Matrix supported, massive
Dms - Matrix supported, stratified

Granules (2-8mm)
GRo - Openwork granules
GRmc - Massive granules, with isolated clasts
Grch - Channelled massive granules
GRmp - Massive with pebble stringers

Gravels (8-256mm)
Gms - Muddy matrix supported gravel, subrounded to subangular, poor sorting and crude bedding
Gm - Massive clast supported, crudely bedded gravel, poor to moderate sorting
Gni - Normal-inversely graded gravels
Gh - Horizontally bedded gravel
Gs - Matrix supported gravel
GRh - Stratified granules

Table 1: Facies codes used for sedimentary logging at Poplars Gully (modified from Eyles et al. 1983).

2.2. IRSL dating methods

Four luminescence samples were recovered. The sampled units are at least 1.5 m thick and consist of either well sorted laminated lacustrine sand (sample 1) or homogeneous ripple cross-stratified fluvial sand (samples 2,3 and 4). Luminescence samples were obtained by forcing a 220 mm long steel tube (75 mm diameter) into fines (silt to medium sands). The cylinder was then sealed and carefully excavated to prevent light exposure and sediment

mixing. All samples were submitted to Victoria University Dating Laboratory (Wellington, New Zealand) where they were analyzed using the silt fraction. Sample preparation was conducted under subdued orange light and included the removal of carbonates (10%-HCL), organic matter (10%-H_2O_2) and iron oxide coatings (Na-citrate, Na-bicarbonate, Na-dithionate). After extracting the 4-11 μm grain size the samples were deposited evenly in a thin layer on small aluminium discs (10 mm diameter).

Luminescence measurements were carried out using a RISO TL-DA15 measurement system, equipped with Kopp 5-58 and Schott BG39 optical filters to select the luminescence blue band. Optical stimulation was carried out at ~30mW/cm^2 using infrared diodes. For beta irradiations a Daybreak 801E ^{90}Sr, ^{90}Y irradiator was used that was calibrated to ~3% accuracy against a standard at the SFU luminescence facility, Vancouver, Canada. Alpha irradiations were completed on a ^{241}Am irradiator supplied and calibrated by ELSEC, Littlemore, UK. The paleodose was determined by measuring the blue light output during infrared optical stimulation of feldspar minerals using a multiple aliquot additive-dose method. Following measurements the disks were stored in the dark for four weeks to relax the crystal lattice after irradiation. After storage the discs were heated (220˚C) to remove unstable signal components and then measured for 100sec each to obtain the shine down curves. The dry homogenised samples were counted using a high resolution gamma spectrometer with a broad energy GE detector for a minimum time of 24h. The spectra were analysed using GENIE2000 software.

The doserate calculation is based on the activity concentration of the nuclides ^{40}K, ^{208}Tl, ^{212}Pb, ^{228}Ac, ^{214}Bi, ^{214}Pb, ^{226}Ra.

3.1 Lithofacies descriptions and interpretations

Sedimentological data are presented for four stratigraphic columns summarized in Figure 3. Eight lithofacies assemblages were identified on the basis of sediment properties, structures and stratigraphic context.

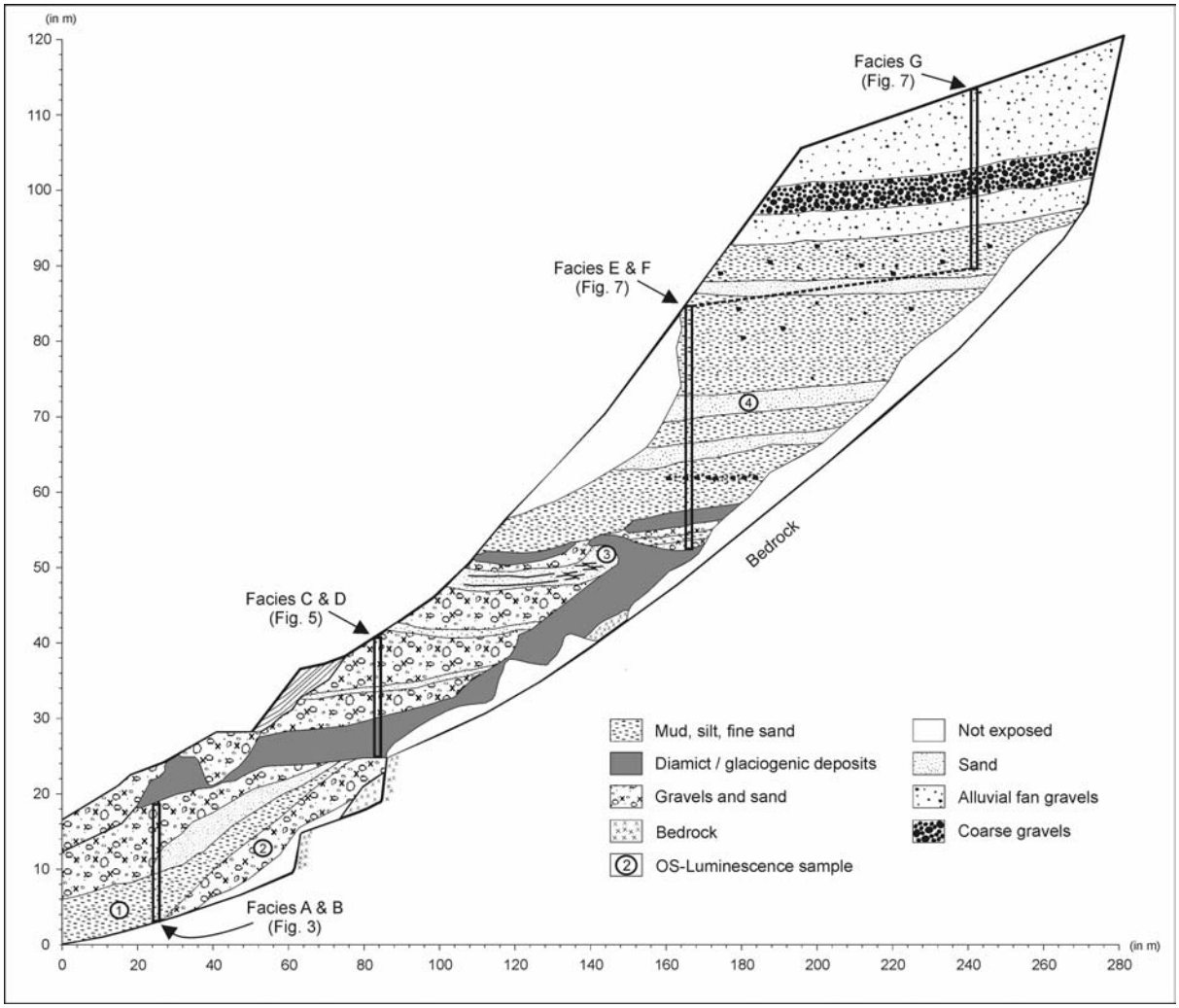

Fig. 3: Stratigraphic overview and locations of the luminescence samples from Poplars Gully.

3.1.1 Facies A: stratified & massive sand, stratified gravel, rhythmically laminated clay, silt and fine sand: Sh, Sm, Gh, Fl, Fd, Fe

Facies A comprises just under 6 m of laminated to banded silts and sands (Fig. 4). The whole unit dips ~18º (SSW) towards the centre of the Hope Valley. The lowest beds are plane bedded medium sands to granules with interbedded laminated silts overlain by 0.4 m of stratified gravel. The main body of the unit overlies this. It is composed of a 2.1 m thick deposit of mm-scale laminae alternating between fine and coarse silt (Fig. 4b, 5a). There is a thin (0.15 m) cobbly diamicton above this (Fig. 4c) followed by 2.2 m of normally graded, 10-30 mm thick banded sands to silts which cap the unit. Convolute bedding (Fig. 4a) and small scale normal faulting (Fig 4b) are widespread throughout, especially in the finer beds. Larger m-scale normal faults are also present, all of which are confined within the unit. Structures associated with contorted beds range from cm-scale flame structures at silt-sand contacts to 300 mm thick bands where originally planar laminations are intensely folded. Small compressional folds occur within fines at the base of the thin diamicton in the central part of the unit (Fig. 4c). The bedding of the lower sand units is contorted with local mobilization of silt which was injected into higher units (Fig 4d).

Interpretation: The laminated fines of Facies A are a slack water deposit reflecting rapid sedimentation into a small lake. The high sediment flux is indicated by the incomplete dewatering of the beds which produced hydroplastic deformations and small scale flame structures (e.g. Fig. 4a). Such deformations are common in glaciolacustrine deposits where materials of varying densities accumulate rapidly (e.g. Shaw 1975, Donelly & Harris 1989, Teller 2003). Several dropstones and a thin diamicton with associated impact folding in the underlying fines (Fig. 3c) represent dump structures of ice rafted debris (e.g. Thomas & Connell 1985).

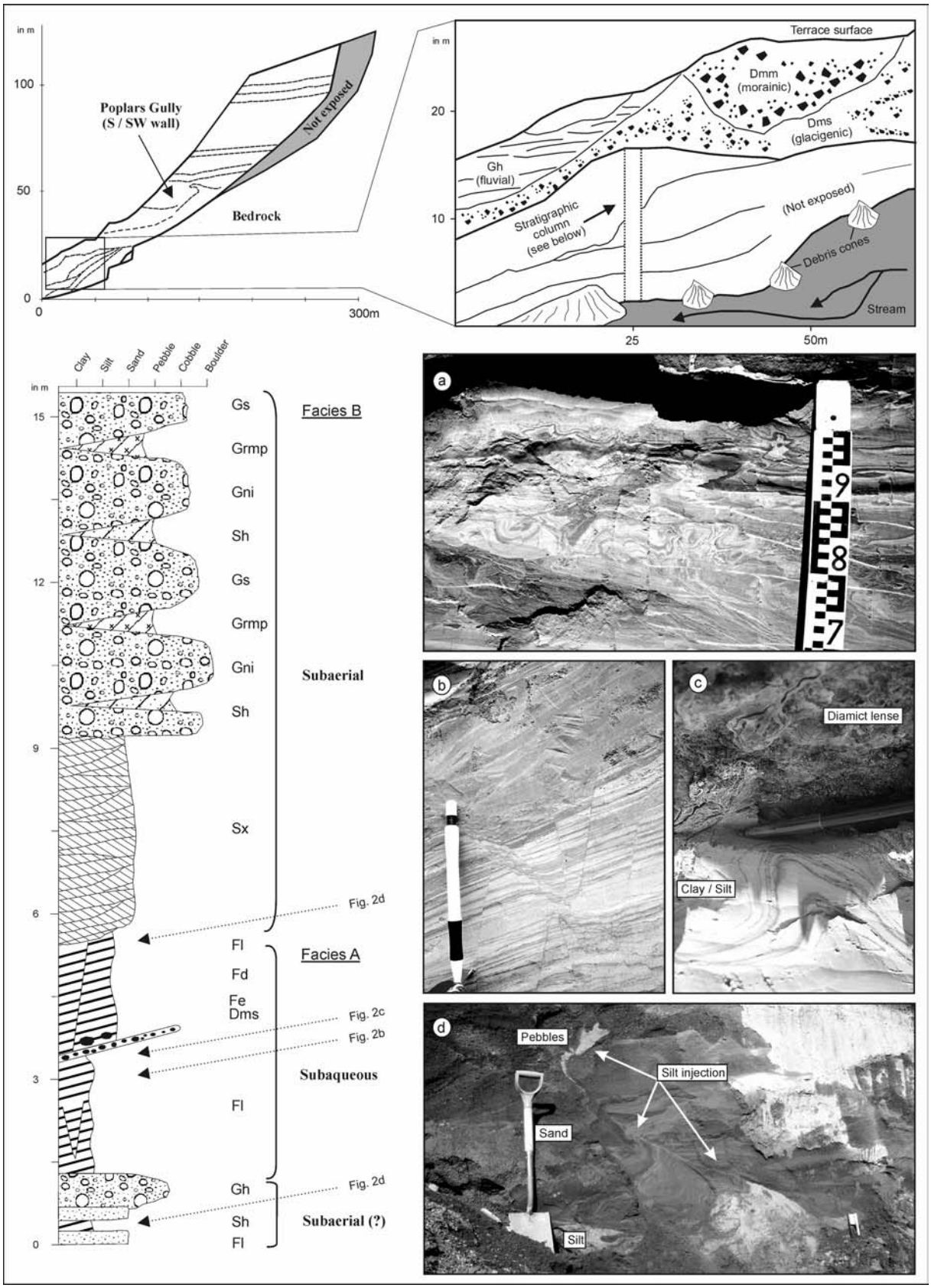

Fig. 4: Stratigraphy, depositional context and sedimentological summary log for deposits exposed at the base of Poplars Gully (Facies A, Facies B). Facies A comprises dominantly of laminated silts and sands with normal faulting that is interpreted as meltout deformation while underlying sand units show deformation through ice loading. Facies B consists of sand and gravel representing ice proximal glaciofluvial outwash. Note that Facies A & B dip as a block by 18 degrees towards the central valley (SSW).

Metre scale normal faults show an incremental decrease of displacement in the direction of sediment younging and represent syndepositional deformation related to melting of underlying dead ice during deposition. The overall ~18º dip (SSW) of the sediment package affects all units of facies A and is interpreted as postdepositional deformation caused by the removal of large scale structural support probably due to the collapse of dead ice in the trunk glacial valley. The overall facies was deposited subaqueously in an ice marginal valley edge position and is interpreted as a kame deposit. Earlier ice overriding of the site is indicated by loading of deposits at the base of Facies A which caused the injection of silts into overlying sands.

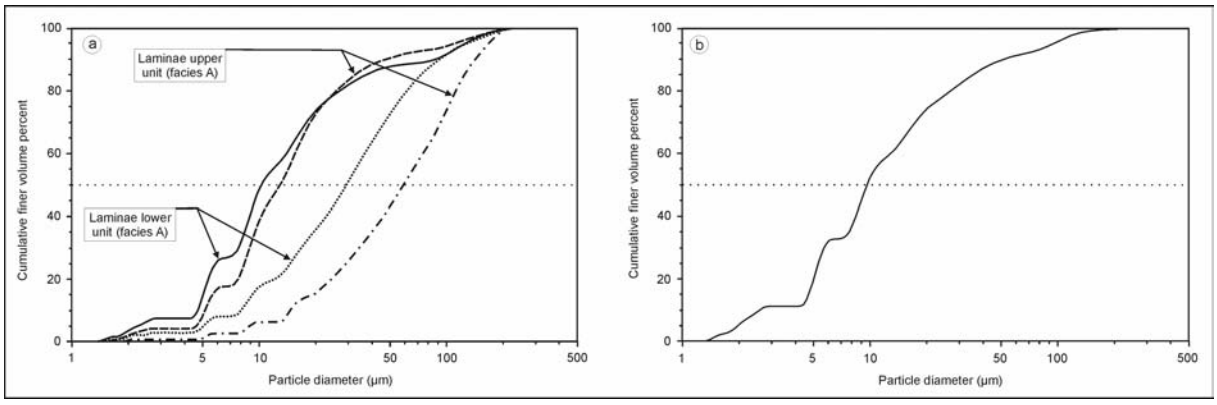

Fig. 5: Particle sizes of laminated to banded silts and fine sands of Facies A (5a). Figure 5b shows the grain size distribution of a 20 mm thick band that drapes clasts a diamicton of Facies C (shown in Figure 6a).

3.1.2. Facies B: stratified sand, normally & inversely graded gravel, massive gravels: Sx, Gm, Gms, Gni

Facies B is a ~10 m thick sand and gravel unit that dips concordantly with facies A (18º / SSW). The deposits were not fully accessible for logging at the face. The basal 3.7 m comprise of trough cross-bedded medium sands which truncate underlying deposits of Facies A (Fig 4). This in turn is truncated by matrix supported stratified to variably graded cobble sized gravels which contain sandy interbeds and patches of openwork gravels.

Interpretation: Gravels and sands of Facies B occupy a ~15 m wide channel and represent a fluvial input. Although the gravels were not directly accessible for imbrication measurements, the overall orientation of the exposed channel cross-section indicates that flow was generally eastward (down the modern valley). The mainly matrix supported gravel deposit are gravel sheets which were deposited during flood events. The succession from sand to gravel indicates that deposition followed the infilling of the prior kettlehole pond (Facies A) and suggests that Facies B was deposited subaerially. There is probably very little age difference between these deposits and the underlying Facies A. After deposition and consolidation of both facies they were tilted as a block towards the main valley floor (SSW direction). We interpret this to have been caused by the removal of support following the general collapse of the trunk valley glacier.

3.1.3. Facies C: stratified and massive diamictons: Dms, Dm

Facies C comprises a 6.5 m thick package of diamictons (Fig. 6). The unit dips at low angles (0-5º dip) and truncates underlying beds of Facies A & B. Towards the valley edge Facies C is deposited directly onto a bedrock bench. Sedimentologically the facies is sub-divided into 6 units of stratified and moderately compacted diamictons with variable lateral extent. Most clasts are subrounded to rounded. Orientational data measured on representative diamicton units show a dominant SW-NE long axis orientation. Based on differences in the composition and stratification five diamict types have been distinguished (I, II, III, IV, V).

Type I diamictons consist of clast to matrix supported crudely stratified gravels that overly an erosional unconformity. The deposit is associated with local loading and drag structures in the underlying sediments. The type II diamicton is a single matrix dominated unit of ~300 mm thickness and limited lateral extension. This unit is massive and includes small cobbles with a strong NE clast fabric orientation. The diamicton overlies a deformed

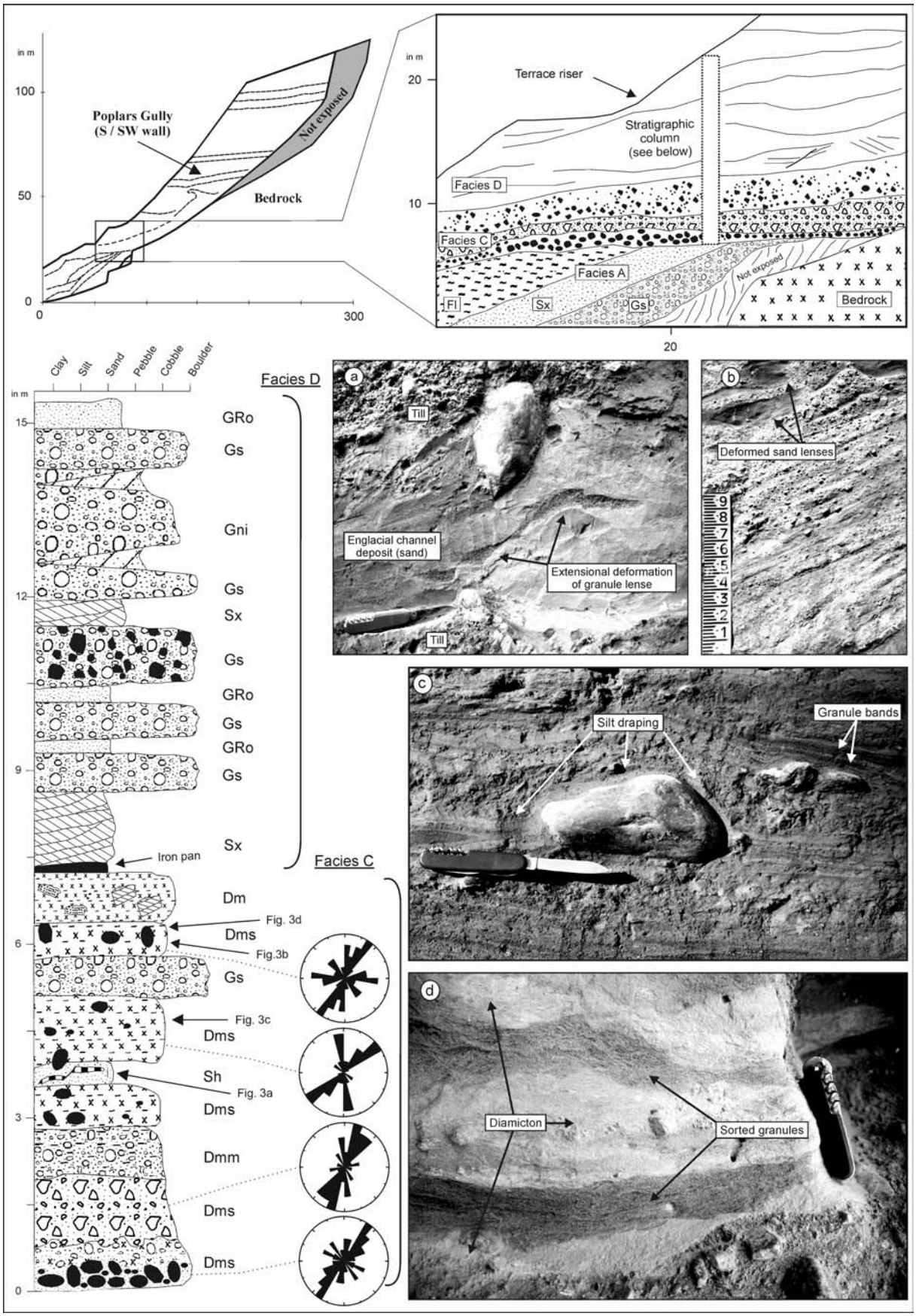

Fig. 6: Stratigraphy, depositional context and sedimentological summary log of Facies C and Facies D. Facies C truncates underlying facies and comprises a series of stratified and massive diamictons interpreted as ice proximal mass flows and till. Facies D consists of clast and matrix supported gravels and cross stratified sands representing glaciofluvial outwash.

sand and mud unit with shear planes (Fig. 6c). Type III diamictons show generally coarse stratification but include lenses of well sorted sand and granules. The 200-300 mm thick sorted sediment packages are characterized by small scale extensional faulting (Fig. 6d). Type IV diamicts are generally well stratified and consist of 10-30 mm thick bands that range in grain size from mud to granules. Pebble and cobble clasts in these diamictons are draped by bands of silt and sand (Fig. 6a, 5b). Type V diamicts are also stratified and comprise mainly of steeply dipping beds and include deformed lenses of medium to coarse sand. Characteristic features are pervasive ductile deformation and flow structures (Fig. 6b). Where the beds dip less steeply the original stratification of alternating 2-5 cm thick bands of diamict and sorted coarse sand is preserved (Fig. 6e).

Interpretation: This facies assemblage comprises a series of ice proximal mass flow diamictons and subglacial till which were deposited following a re-advance of the main valley glacier into the lower Hope Valley. Type I and V diamictons are interpreted as mass flow deposits based on their crude stratification and the ductile deformation of incorporated sediment lenses (e.g. Fig. 6b). These diamictons also display a greater orientational variability in their macro-fabrics. Diamicton types III and IV are interpreted as basal melt-out tills as is indicated by their stratification, the draping of sorted sediment bands over lodged clasts (Haldorsen & Shaw 1982, Dreimanis 1988, Fig. 6d) and the presence of interbedded englacial channel fills which were extensionally deformed during basal meltout (Fig. 6d). Little modification of the primary meltout features indicates that deposition occurred by mainly passive meltout from stagnant ice. Only one of the diamictons (type II) is interpreted to represent subglacial deposition from the actively moving ice. This ~300 mm thick massive diamict is found near the base of the facies C and is associated with shear planes in the underlying sediment (Fig. 6c). The diamicton shows a strong fabric signal suggesting ice flow from SW.

In summary, the diamict facies C represents a series of ice proximal mass flow deposits, stratified melt-out tills and massive subglacial till indicating an ice re-advance into the lower Hope Valley. The glacial diamictons cross-cut Facies A & B and show a much lower dip than these underlying deposits suggesting that Facies C was deposited after Facies A & B were block tilted during the preceding ice collapse phase.

3.1.4. Facies D: normally & inversely graded gravel, stratified and deformed sand, : Sx, Sh, Sd, Gs, Gms

This is a ~23 m thick assemblage of clast and matrix supported gravels and cross stratified sands with an average thickness of individual beds of less than 0.6 m. The facies is not fully accessible and only the basal 8 m were logged in detail (Fig. 6). Individual units comprise moderately sorted and conformably bedded gravel and sand sheets that are laterally continuous. Facies D overlies the glacial diamictons of Facies C. Intense extensional deformation that resulted in the disruption and block rotation of several units is noted in the basal part of Facies D. Bedding planes of the middle and upper Facies D are less deformed displaying only a downward bending with the deflection estimated to be less than 1.5 m. A spectacular deformational feature in Facies D is a ~4 m high asymmetrical fold shown in Fig. 7. The deformation incorporated diamictons from Facies C into strata of Facies D. Measurements on the excavated fold limb and on several thrust planes show a W to WSW orientation, respectively (Fig. 7).

Interpretation: Sediments of Facies D are interpreted as outwash representing the stratigraphic transition from tills and mass flows (facies C) to collapsed ice proximal glaciofluvial gravels (basal facies D) to less deformed sand and gravel beds of the middle and upper Facies D. Paleo-current directions from ripple cross-stratified sands indicate a dominant flow direction towards ENE. The limited thickness of individual units (<0.6 m) and the

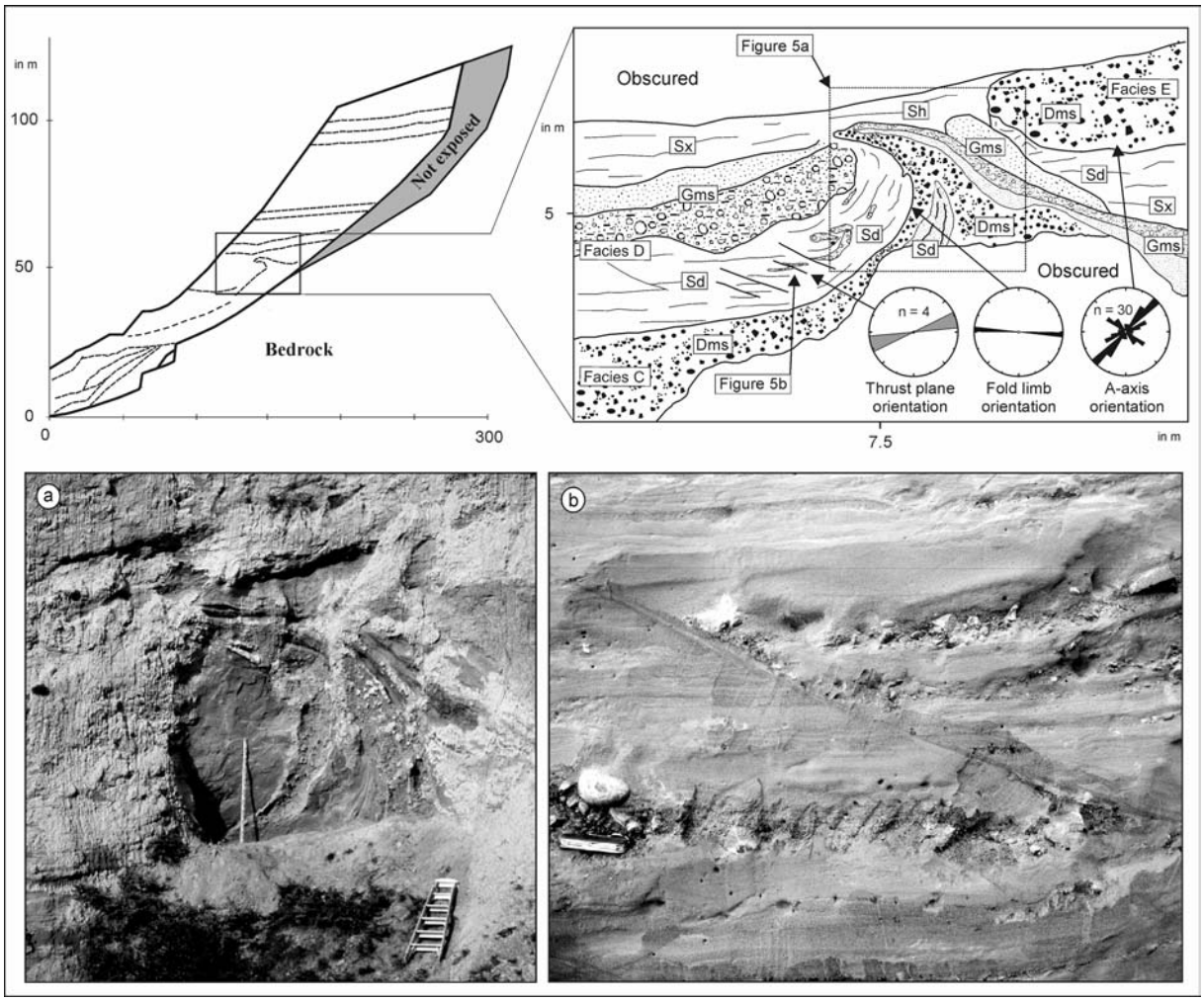

Fig. 7: Deformation in Facies D. This asymmetrical fold has deformed sand and gravel of Facies D as well as diamictons of the underlying Facies C. It is interpreted as a glaciotectonic structure associated with a later glacial re-advance (see facies E).

considerable range in grain size suggests frequently fluctuating flow conditions. Deformation of Facies D includes the gentle downwarping of the originally plane bedding, which was presumably caused by buried ice meltout and consequent loss of volume in lower beds. Our overall interpretation of Facies D as a glaciofluvial assemblage relies partially on the depositional context provided by the underlying melt dominated (upper) Facies C and lower Facies D. Following this logic Facies D was deposited subaerially in a proglacial / ice lateral position after ice retreat from the Poplars Gully site. The large deformational structure shown in Fig. 7 is a postdepositional feature that involved later compressional folding and thrust faulting of Facies C & D deposits (see interpretation of Facies E).

3.1.5 Facies E: diamictons, clast supported gravel, laminated fines: Dms, Gm, Fl

Facies E is a 6.5 m thick sediment assemblage comprising two 1.5 m thick units of stratified and sandy interbedded diamictons, an intermediary 1.5 m thick unit of laminated silt and fine sand as well as 2.0 m of clast supported gravel (Fig. 8, 8a). The sorted intra-diamict layers are usually 2-5 cm thick bands of undeformed and conformably bedded sand. The diamicton closely resembles diamict type V in Facies C (Fig. 6e). Clasts in the diamictons comprise well rounded to subrounded cobbles showing a dominant NE long axis orientation with a SW dip. The diamicton at the base of Facies E is overlain by a 1.5 m thick unit of silt and fine sand consisting of 2-5 mm thick laminae. Locally, the laminations are intensely deformed through micro-scale faulting and ductile distortions of beds (Fig. 8c). The unit is overlain by a 2.0 m thick deposit of laterally confined cobbly gravels that shows crude bedding and a NE clast (a-axis) imbrication (Fig. 8a).

Interpretation: Stratified diamictons of Facies E are interpreted as ice proximal mass flows that were deposited following a glacial re-advance. Ice overrun or proximity of active ice is also indicated by intense compressional deformation in underlying sediments of Facies D. Towards the valley edge where Facies D pinches out, deformation also extends into Facies C. The advance produced the previously described asymmetrical fold shown in Fig. 7 which we interpret as a result of compressional proglacial glaciotectonics. The fold structure combines dominant ductile folding of matrix supported diamictons and brittle thrust faulting in adjacent sands and gravels (Fig. 7b). Orientational data obtained from the excavated fold limb as well as from thrust planes suggests compression from W and WSW, respectively. This is broadly consistent with the reconstructed SW fabric in the diamicton of Facies E (Fig. 7). Sediments between the two till units comprise deformed units of laminated mud and fine sand as well as

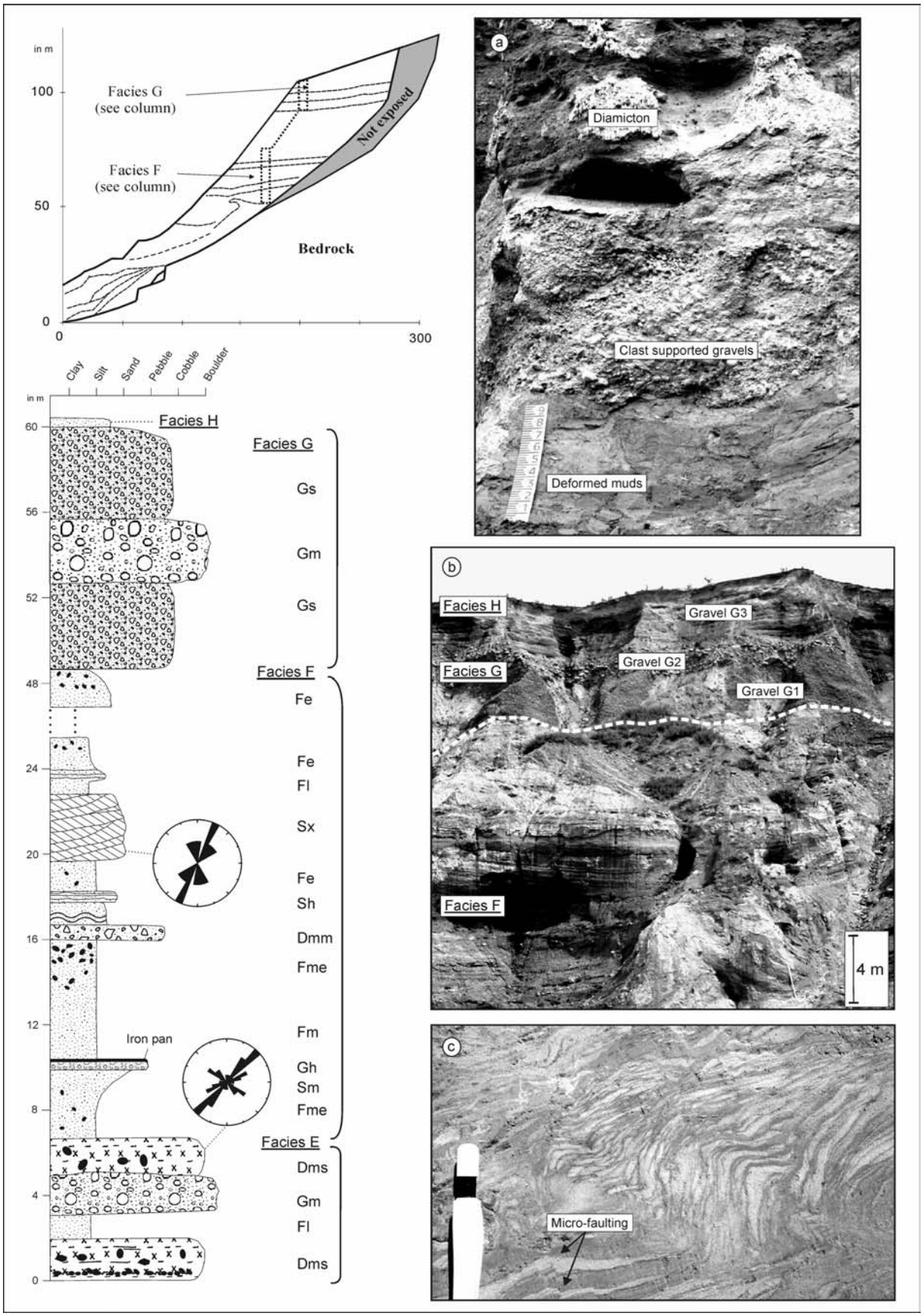

Fig. 8: Stratigraphy, depositional context and sedimentological summary log of deposits in the upper section of Poplars Gully including Facies E, F, G and H. Facies E consists of glacial diamictons interpreted as ice proximal mass flows and indicating a glacial re-advance. Muds and sands of the overlying Facies F represent glaciolacustrine deposition associated with a proglacial lake that formed following glacial retreat. Facies G comprises alluvial and fluvial gravel which are overlain by loess of Facies H.

glaciofluvial gravels. We interpret the micro-scale deformation on laminae of the fine grained unit as a postdepositional feature presumably caused by ice overran or during freeze-on and subglacial transport of a pre-existing block of lacustrine muds.

3.1.6. Facies F: massive & laminated mud, cross-stratified sand, diamicton: Fm, Fl, Fe, Sm, Sx, Dmm

This ~44 m thick fine grained facies consists of alternating units of laminated to massive muds and sands, interbedded with ripple cross-stratified fine to medium sands (Fig. 8, 8a). Dispersed stones with impact structures in underlying beds are present throughout the mud units but increase in frequency below a thin diamicton found ~9 m above the base of the facies. The 0.35 m thick matrix supported diamicton is characterized by a high proportion of angular cobble clasts. The mud sequence is capped by a 3 m thick cross-laminated medium sand with sinuous-crested subcritically climbing ripples. Orientational measurements on ripple crests indicate a mean NNE paleo-flow direction. Above this there are 26 m of massive to stratified muds and sandy muds. Dispersed stones with deformed underlying bedding are frequent and about 15% of the clasts are angular in shape.

Interpretation: Sediments of Facies F were laid down in a proglacial lake that formed in the lower Hope Valley following renewed glacial retreat. In the context of the aforementioned glacial re-advance (Facies E) it is probable that the lake was moraine dammed. Granulometric changes within the facies suggest varying lake levels where units of ripple cross-stratified fluvial sands represent either extreme lake low stands or higher energy environments when the glacier re-advanced towards the site. The dropstones suggest that the lake was in proglacial position and received debris loaded icebergs through glacier calving. The 0.35 m thick diamicton found within the muds is laterally continuous (~8 m) and was probably laid down as a subaqueous gravity flow deposit. The modern margin of the Tasman Glacier

(Southern Alps) where calving into a recently formed proglacial lake has become the dominant form of ice loss (Purdie & Fitzharris 1999) may provide a good analogue for the depositional environment of Facies F.

3.1.7. Facies G: clast & matrix supported gravels: Gs, Gh, Gm

Facies G comprises three gravel beds with a total thickness ~13.5 m. The upper and lower beds (G1 & G3 in Fig. 8a) comprise clast to matrix supported subangular to subrounded cobbly gravels. The matrix consists of silty sand and granules. The intermediary bed (G 2) consists of 3 m of well rounded clast supported bouldery gravel.

Interpretation: The lower and upper gravel beds of Facies G (G1 & G3) are alluvial sediments which are interbedded with coarse fluvial gravels (G2). Deposition started when a talus fan built out from the adjoining hill onto the northern part of Hope River floodplain (G1). As the fan accumulated, channel evulsion of the Hope River caused relocation of a braid channel to this section of the floodplain where it eroded part of the fan and deposited a veneer of coarse fluvial gravel (G2). As the channel avulsed away fan building recommenced burying the fluvial deposit (G3).

The mature sorting and roundness of boulders in the fluvial gravel (G2) suggests medium to long distance transport. This represents a depositional environment markedly different from the previously described glacial sequence. We therefore infer a substantial time break between the deposition of all underlying facies and Facies G. The fan and fluvial gravel assemblage of Facies G can be visually correlated to fan/fluvial gravels at similar elevation and identical stratigraphic position on the southern side of the valley. A luminescence date of 32.1 ± 2.6 ka BP (WLL 351) was obtained by Rother et al. (accepted) from a silt inter-bed in those gravels and we infer a similar age for gravels of Facies G.

3.1.8. Facies H: massive silt and fine sand: Fm

This is a massive sandy silt unit of ~0.5 m thickness overlying alluvial fan deposits associated with Facies G. Numerous large angular boulders are scattered on its gently climbing surface.

Interpretation: The deposit is a loess which covers the underlying alluvial fan. The boulders are rockfall debris derived from the adjoining hill side.

Table 2: Sample and radioactivity data for luminescence samples from Poplars Gully.

Sample[a]	Grain size (μm)	Water content (δ)[b]	U (μg/g) from ^{234}Th	U (μg/g)[c] ^{226}Ra, ^{214}Pb, ^{214}Bi	U (μg/g) from ^{210}Pb	Th (μg/g)[c] from ^{208}Tl, ^{212}Pb, ^{228}Ac	K (%)	dD_e/dt (Gy/ka)[d]
1	4-11μm	1.203	2.15 ± 0.37	2.40 ± 0.04	2.20 ± 0.37	10.18 ± 0.15	2.14 ± 0.05	0.0018 ± 0.0001
2	4-11μm	1.156	2.81 ± 0.36	2.09 ± 0.04	2.65 ± 0.36	9.74 ± 0.14	2.39 ± 0.05	0.0226 ± 0.0011
3	4-11μm	1.182	2.10 ± 0.33	1.62 ± 0.03	2.10 ± 0.34	7.58 ± 0.13	1.83 ± 0.04	0.0071 ± 0.0004
4	4-11μm	1.199	2.12 ± 0.26	1.81 ± 0.03	2.42 ± 0.26	7.92 ± 0.11	1.63 ± 0.03	0.0852 ± 0.0043

[a] Lab codes: 1) WLL-357; 2) WLL-352; 3) WLL-358; 4) WLL-353
[b] Ratio wet to dry sample weight. Errors assumed 50% of (δ-1).
[c] U and Th contents are calculated from the error weighted mean of the isotope equivalent contends.
[d] Contribution of cosmic radiation to the total doserate, calculated following Prescott & Hutton (1995).

3.2 Luminescence dating results

The stratigraphic positions and lithology of the sampled units are shown in Fig. 3. The samples were obtained from different facies assemblages (A, D, and F) and cover a considerable portion of the Poplars Gully stratigraphy (65 m vertical distance between samples 1 and 4). All dosimetric data are summarized in Table 2. One of our samples (No. 4) displayed a minor radioactive disequilibrium (significant at 2σ-level) between ^{226}Ra and ^{210}Pb. The D_e values and resulting luminescence ages are shown in Table 3. Two samples (No. 1, 3) were near saturation and a second dating method, Single Aliquot Regenerative (SAR), was applied to the quartz fraction to test the reliability of the results. The SAR ages

agree within error, which gives more confidence than a near saturation age alone. The four IRSL ages from Poplars Gully range from 164.7 ± 14.8 ka to 119.8 ± 10.5 ka.

Table 3: Measured a-values and equivalent doses as well as calculated dose rates and resulting luminescence ages from Poplars Gully.

Sample[a]	a-value	D_e (GY)	dD/dt (Gy/ka)	**IRSL age (ka)**
1[b]	0.048 ± 0.010	397.0 ± 19.2 (413.4 ± 21.2)	3.45 ± 0.25	**115.0 ± 9.9** **(119.8 ± 10.5)**
2	0.040 ± 0.006	467.0 ± 28.8	3.66 ± 0.21	**127.5 ±10.7**
3[b]	0.055 ± 0.014	514.1 ± 30.0 (465.6 ± 37.4)	2.84 ± 0.20	**181.3 ± 16.4** **(164.2 ± 17.4)**
4[c]	0.040 ± 0.020	441.0 ± 15.4	2.79 ± 0.22 (2.68 ± 0.22)	**157.8 ± 14.8** **(164.7 ± 14.8)**

[a] Lab codes: 1) WLL-357; 2) WLL-352; 3) WLL-358; 4) WLL-353
[b] Samples 1 and 3 were near saturation. The bracketed values were calculated using a Single Aliquot Regenerative Method.
[c] This sample showed a minor radioactive disequilibrium (bracketed values) and the given age has been corrected.

4.1 Discussion

4.1.1. Age results

Luminescence ages from glacigenic deposits are potentially problematic due to issues of insufficient signal zeroing prior to deposition and short (if any) proglacial transport paths (e.g. Mejdahl & Funder 1994, Duller et al. 1995). IRSL and OSL techniques have considerably reduced the exposure times needed for signal zeroing and Gemmell (1999) showed that (for IRSL dating) sediments in glaciofluvial streams can be effectively bleached by only short exposure to strong sunlight even in streams with suspended sediment yields of >150 mg l^{-1}. Both zeroing and the considerable age of the sediments are a concern in this study.

We note that the ages are stratigraphically reversed with the two younger dates at the bottom and the two older ages at the top. A possibility is that the stratigraphically younger material was not fully zeroed prior to deposition. On paleo-environmental grounds we are uncomfortable with this interpretation because Facies F is very clearly a proglacial unit and

we would expect a good chance of zeroing. In addition, ages 3 and 4 coincide, which is unlikely if inherited signals are involved, unless all the material was recycled from the same local source. It is more likely that the reversal is related to the relatively great age of the samples which may approach the upper limit of IRSL dating in this environment. This reduces the stratigraphic and chronological resolution of the results. However, all four samples returned ages of ≥120 ka and we are confident that this rules out deposition during the last glacial cycle. Similarly, samples 2 and 4 are unsaturated and provide upper limit ages within OIS 6. In summary, we limit our interpretation of the IRSL results to the observation that deposition of the Poplars Gully sequence occurred during OIS 6.

4.2 Site history and depositional model

Poplars Gully sediments were laid down in a dominantly ice-marginal and pro-glacial position and we interpret most of the sequence to have formed as a kame terrace during multiple phases of ice incursion, stagnation and withdrawal from the lower Hope Valley. The general depositional setting at Poplars Gully is a lower valley reach which was repeatedly transgressed by a valley glacier and where sedimentation was mainly associated with stagnating ice during phases of glacial retreat. The sequence exposes the lateral transition from glacial deposition onto bedrock at the valley side to deposition over pre-deposited soft sediments in the middle of the valley. The basal bedrock contact of the sequence dips steeply from the valley side and disappears below the present Hope River floodplain. The remaining depth of fill below valley floor is unknown but unconsolidated sediments extend to at least 20 m below the present floodplain surface (Rother et al., accepted).

Sedimentary facies at Poplars Gully preserve an intact stratigraphy and we can reconstruct the site history for this portion of the lower Hope Valley. We identify nine phases,

depicted in Fig. 9a –9i, which place deposition in the context of an oscillating ice lobe followed by final ice evacuation and fluvial/alluvial infilling.

Prior to the onset of sedimentation a significant erosional phase in the valley is deduced from the presence of two bedrock strath terraces which are buried by Poplars Gully deposits. This period of incision, probably similar to the last post-glacial (Holocene) fluvial degradation, excavated and largely removed any pre-existing (> OIS 6) valley fill (Fig. 9a), though older deposits may still be preserved under the valley floor. Following an initial ice advance (Fig. 9b), basal units at Poplars Gully record sedimentation associated with the retreat phase of that advance. This is represented through extensive dead ice meltout and collapse features (Facies A) as well as ice-marginal glacio-fluvial deposits (Facies B) (Fig. 9c). It is probable that the retreat eventually resulted in complete ice evacuation from this part of the Hope Valley as indicated by widespread and relatively large scale collapse deformation. We infer the removal of structural ice support to have caused the topple failure and forward collapse of a kame terrace block that resulted in the observed concordant tilting of heterogeneous lacustrine and fluvial deposits of Facies A & B (Fig. 9d).

Ice retreat and block failure was followed by a substantial glacial re-advance into the lower Hope Valley (Fig. 9e). Mass flows and tills from the advance (Facies C) unconformably truncate underlying sediments. Fabric characteristics and the general absence of active ice deformation indicate that deposition occurred mainly during passive melt-out from a stagnant body of ice. Sedimentation associated with progressive ice downwasting is consistent with the observed succession from basal meltout tills to mass flows (Facies C) through to dominantly glacio-fluvial sediments (Facies D). During the deposition of Facies D the site may either have been proglacial or again formed part of a kame terrace system as depicted in Fig. 9f.

A re-advance then occurred as suggested by the glacial diamictons of Facies E and the presence of glaciotectonic deformation structures in Facies D and the top of Facies C (Fig. 7, Fig. 9g). Following a renewed phase of glacial retreat a proglacial lake formed in the lower

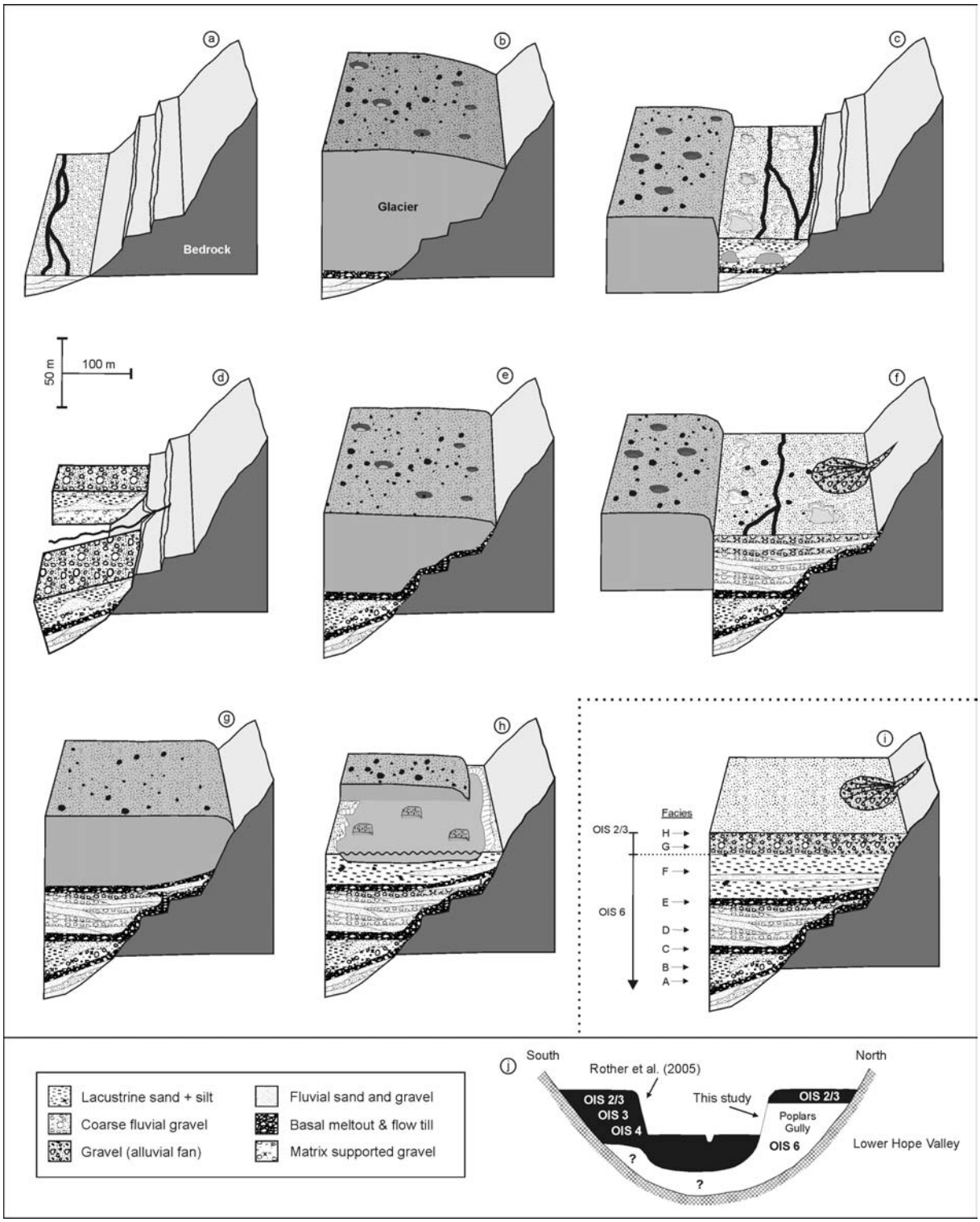

Fig. 9: Depositional model for the Poplars Gully sequence based on sediment properties and depositional context. We identify nine phases (9a-i) beginning with an (interglacial?) erosional phase (9a) that was followed by a substantial glacial advance (9b). Basal deposits at Poplars Gully are interpreted as ice marginal ice contact deposits (9c) which show post-depositional deformation including block tilting and collapse features (9d). This is followed by a glacial re-advance (9e) which truncated deposits laid down during the previous retreat. Overlying glaciofluvial deposits indicated a period of retreat (9f) before a glacial re-advance deposited diamictons and glaciotectonized the proglacial sequence (9g). Renewed glacial retreat resulted in the formation of a proglacial lake (9h). Figure 9h summarizes the stratigraphic composition and geochronological model for Poplars Gully. Figure 9i shows the context and depositional architecture of valley fill deposits in the Hope Valley.

Hope Valley (Fig. 9h). Glacio-lacustrine deposits (Facies F) are ~40 m thick and include ice rafted debris. Although it is difficult to estimate the original size of the lake, the considerable thickness of Facies F suggests that the lake was extensive. Fluvial beds in the lacustrine sediments suggest either repeated lake low stands when fluvial sands were deposited or changes in the glacier front up valley with sand beds deposited during ice incursions.

As previously indicated we infer a major hiatus between deposition of glacio-lacustrine sediments of Facies F and the overlying gravel units of Facies G (OIS 2/3?). How much material of the original OIS 6 sequence was eroded prior to sedimentation of Facies G is not known. The elevation of the fluvial-alluvial gravels (c. 610 m asl) matches the terrace level of the main (last glacial) aggradation surface at the opposite valley side. We suggest that deposits of Facies G correlate to aggradation during the last glacial cycle that overtopped and buried the penultimate valley fill remnant at Poplars Gully. According to this, Facies G represents an 'overlapping' secondary valley fill as shown in Fig. 9j. Rapid incision following the last deglaciation changed base levels, stopped fan building on the high surface and eventually triggered the landslide which exposed the Poplars Gully sequence.

4.3 Regional glacial and tectonic implications

Generally rapid tectonic uplift in New Zealand can provide an effective mechanism by which older glacial sequences were raised above the central valley train which reduced the possibility for erosion by later glacial or fluvial processes. Because of the inferred uplift, it is generally considered improbable that older glacial sequences (pre-last glacial cycle) can have survived in the central valley trough without removal by valley incision. In this investigation, however, we highlight an example of a thick *in situ* OIS 6 sedimentary sequence which survived river down cutting and ice overriding without modification in the central lower Hope

Valley. The results challenge the notion that glacial advances during the LGM were sufficiently erosive to effectively remove pre-existing valley fill deposits.

Stratigraphic data from Poplars Gully provide evidence for a total of three glacial advances which are separated by one major and one minor ice retreat phase. The more substantial retreat occurred between the two older advances and resulted in complete ice evacuation from the lower Hope Valley. This was followed by a later glacial re-advance which truncated the underlying successions. The re-advance is subdivided into two phases separated by a minor ice terminal oscillation. These data are significant because Poplars Gully is located 30 – 40 km down valley from the glacial accumulation areas and only substantial ice advances reach the lower Hope Valley. Based on our stratigraphic data we suggest that the previously undivided OIS 6 in the Southern Alps of New Zealand (e.g. Suggate 1990) comprises at least two larger scale glacial advance phases.

A summary of the relative abundance of logged deposits (Table 4) highlights the dominance of water driven or water influenced sedimentation at Poplars Gully. This can partially be explained by the deglacial context of the overall sedimentary succession in which we expect meltwater deposition and extensive fluvial reworking to be common. However, the characteristically large volumes of such sequences in glacial valleys of the Southern Alps implies extraordinary large sediment supply, while the dominant fluvial-lacustrine appearance of the majority of these sequences clearly requires the abundant availability of free water. This is unsurprising in a setting where glacial tongues extended tens of kilometres into the ablation zone. They generate facies and land systems which are distinctive to these environments.

Facies type	Facies description	Facies code	% total
Mud	Laminated silt and mud	Fl	6.0
	Laminated silt and mud with dropstones	Fe	19.7
	Massive silt and mud	Fm	3.8
	Massive silt and mud with dropstones	Fme	14.8
		Total mud	**44.3**
Sand	Massive sand, moderately to well sorted	Sm	2.2
	Horizontally laminated sand, moderately to well sorted	Sh	3.4
	Cross-stratified sand	Sx	9.6
		Total sand	**15.2**
Gravel	Massive, clast supported gravels	Gm	5.3
	Stratified & normally and inversely graded gravels	Gh & Gni	6.6
	Matrix supported gravels	Gs	14.4
	Granules (openwork)	Gro	2.2
		Total gravel	**28.5**
Diamict	Massive diamict, boulder to silt size	Dmm	2.2
	Stratified diamict, boulder to silt size	Dms	9.8
		Total diamict	**12.0**

Table 4: Relative proportions of logged deposits in the Poplars Gully glacial sequence. Note the dominance of aqueous deposition.

The survival of thick OIS 6 deposits in the Hope Valley despite ice occupation during the LGM is unexpected. For an explanation we must first consider the local tectonic setting. The area is part of the Marlborough Fault Zone (Norris et al. 1990) and an active strike-slip fault, the Hope Fault, follows the course of the middle and lower part of the valley. A more recent stratigraphic investigation by Rother et al. (accepted) suggests that the lower Hope Valley constitutes a structural depression that formed at a releasing fault bend. They estimated that late Quaternary basin subsidence has occurred at a rate that approximately matches the estimated regional uplift rate of ca. 2-3 mm/a^{-1} (Wellman 1979). Dating of fluvial and lacustrine valley fill deposits showed a long term aggradation trend in the lower Hope Valley at least over the last ~60 ka (Rother et al. accepted). The results show that relative basin subsidence was undoubtedly significant in the preservation of penultimate glacial deposits at Poplars Gully. Conditions changed only during the postglacial period when downcutting by the Hope River outpaced subsidence leading to partial excavation of the basin fill.

Despite the importance of local tectonic influences, however, we note that this does not account for the marked difference in the volume of glacial deposits generated during OIS

6 and the LGM. There is clear evidence that glaciers reached the lower Hope Valley during both periods (Clayton 1968, Suggate 1990, this study), however glacially sourced sediments during OIS 6 (i.e. Poplars Gully) are many tens of metres thick whereas LGM glacial sediments (as opposed to outwash) is only a few metres thick at most (Rother et al. accepted). The terminal position of the LGM advance is preserved in a moraine complex at Glynn Wye Station (Fig. 1) while the glacial extent during OIS 6 is not known. No glacial deposits associated with OIS 4 have so far been found in the lower Hope Valley (Suggate 1965, Clayton 1968, Cowan 1989). The variation in depositional volume is unlikely to be related to regional tectonics as faulting and associated subsidence along the Hope Valley segment has been continuous from the mid-Pleistocene (Wood et al. 1994) to the present.

It appears that OIS 6 or earlier advances carved a deep glacial through in the lower Hope Valley which was subsequently infilled during ice stagnation and deglaciation (e.g. Poplars Gully), whereas negligible glacial valley erosion occurred in the lower Hope Valley during the LGM. Generally, deep glacial troughs are common in high-turnover glacio-alpine environments (e.g. Hooke & Pohjola 1994, Spedding & Evans 2002, Baker et al. 2003) and is a feature of the present day Tasman Glacier in New Zealand which occupies a 120 m deep ice–marginal trough behind its outwash barrier (Nobes & Owens 1995).

Our data suggest that ice advances during OIS 2 (or late 3) produced much thinner glacial sequences in the lower Hope Valley and caused significantly less erosion of pre-existing sedimentary sequences than the OIS 6 advances. This may be explained by the substantially greater down valley ice extent during OIS 6, and hence may reflect variations in total ice volume or alternatively, may be related to a shorter duration of ice occupation during the LGM. Both options would indicate that the OIS 6 glaciation was more significant than glaciation during the LGM. However, this remains speculative until more detailed stratigraphic information and improved age control on glacial deposits from other New

Zealand valleys are available to test whether our results are due to local anomalies or if they indeed represent a diminishing trend in the size of glaciation from OIS 6 to the LGM.

Acknowledgements

We would like to thank Chris Smart, Phil Tonkin and Dave Evans for their comments in the field and during the manuscript production. H.R. would like to acknowledge the great hospitality of the Henderson family of Poplars Station who provided shelter and access to 'Henry's Hole'. Marie-Elaine van Egmond, Florian Bűch, and Craig Woodward provided assistance in the field. This study was financially supported by a Royal Society of New Zealand Marsden Grant (contract UoC 301) and a Mason Trust Award through the Department of Geological Sciences / University of Canterbury (New Zealand).

References

Baker, G. S., Strasser, J.C., Evenson, E.B., Lawson, D.E., Pyke, K., Bigl, R.A., 2003. Near-surface seismic reflection profiling of the Matanuska Glacier, Alaska. Geophysics 68(1): 147-156.

Benn, D. I., Kirkbride, M.P., Owen, L.A., Brazier, V., 2003. Glaciated valley landsystems. Glacial landsystems. D. J. A. Evans. London, 532 p.

Burrows, C. J., 1988. Late Otiran and early Aranuian radiocarbon dates from South Island localities. New Zealand Journal of Science 15: 25-36.

Burrows, C. J., 1997. A macrofossil flora early Aranuian lake bed deposits, Doubtful River, Waiau-uhu catchment, North Canterbury, New Zealand. New Zealand Journal of Botany 35: 545-553.

Clayton, L. S., 1968. Late Pleistocene glaciations of the Waiau Valleys, North Canterbury. New Zealand Journal of Geology and Geophysics 11: 753-767.

Cotton, C. A., 1947. The Hanmer Plain and the Hope Fault. The New Zealand Journal of Science and Technology 29: 10-17.

Cowan, H. A., 1989. An evaluation of the late Quaternary displacements and seismic hazards associated with the Hope and Kakapo Faults, Amuri District, North Canterbury. MSc thesis, Department of Geological Sciences, University of Canterbury: 239.

Cowan, H. A., 1990. Late Quaternary displacements on the Hope Fault at Glynn Wye, North Canterbury. New Zealand Journal of Geology and Geophysics 33: 285-293.

Cowan, H. A., 1991. The north Canterbury earthquake of September 1, 1888. Journal of the Royal Society of New Zealand 21(1): 1-12.

Cowan, H. A., McGlone, M.S., 1991. Late Holocene displacements and characteristic earthquakes on the Hope River segment on the Hope Fault, New Zealand. Journal of the Royal Society of New Zealand 21(4): 373-384.

Denton, G. H., Hendy, C.H., 1994. Younger Dryas age advance of Franz-Josef Glacier in the Southern Alps of New Zealand. Science 264: 1434-1437.

Donelly, R., Harris, C., 1989. Sedimentology and origin of deposits from a small ice dammed lake, Leirbreen, Norway. Sedimentology 36: 581-600.

Dreimanis, A., 1988. Tills: their genetic terminology and classification. Genetic classification of glacigenic deposits. R. P. Goldthwait, Matsch, C.L. Rotterdam: 17-83.

Duller, G. A. T., Wintle, A.G., Hall, A.M., 1995. Luminescence dating and its application to key pre-Late Devensian sites in Scottland. Quaternary Science Reviews 14: 495-519.

Eyles, N., Eyles, C., Miall, A.D., 1983. Lithofacies types and vertical profile methods; an

alternative approach to the description and environmental interpretation of glacial diamict and diamictite sequences. Sedimentology 30: 393-410.

Gage, M., 1958. Late Pleistocene glaciations of the Waimakariri Valley, Canterbury, New Zealand. New Zealand Journal of Geology and Geophysics 1: 123-155.

Gage, M., 1965. Some characteristics of Pleistocene cold climates in New Zealand. Transactions of the Royal Society of New Zealand 3: 11-21.

Gemmell, A. M. D. 1999. IRSL from fine-grained glacifluvial sediment. Quaternary Geochronology 18: 207-215.

Haldorsen, S., Shaw, J., 1982. The problem of recognizing melt-out till. Boreas 11: 261-277.

Hart, J. K., 1996. Proglacial glaciotectonic deformation associated with glaciolacustrine sedimentation, Lake Pukaki, New Zealand. Journal of Quaternary Science 11(2): 149-160.

Hooke, R. L., Pohjola, V.A., 1994. Hydrology of a segment of a glacier situated in an overdeepening, Storglaciären, Sweden. Journal of Glaciology 40(134): 140-148.

Ivy-Ochs, S., Schluechter, C., Kubik, P.W., and Denton, G.H., 1999. Moraine exposure dates imply synchronous Younger Dryas glacier advances in the European Alps and in the Southern Alps of New Zealand. Geografiska Annaler 81A(2): 313-323.

Kamp, P. J. J., 1986. The mid-Cenozoic Challenger Rift System of western New Zealand and its implications for the age of the Alpine Fault inception. Bulletin of the Geological Society of America 97: 255-281.

Kamp, P. J. J., 2001. Possible Jurassic age for part of the Rakaia Terrane: implications for tectonic development of the Torlesse accretionary prism. New Zealand Journal of Geology and Geophysics 44: 185-203.

Krbetschek, M. R., Rieser, U., Zoeller, L., Heinicke, J., 1994. Radiocative disequilibria in palaeodosimetric dating of sediments. Radiation Measurements 24: 485-489.

Mabin, M. C. G., 1996. The age of the Waiho Loop glacial event. Science 271: 668.

Maizels, J. K., 1989. Differentiation of late Pleistocene terrace outwash deposits using geomorphic criteria: Tekapo Valley, South Island, New Zealand. New Zealand Journal of Geology and Geophysics 32: 225-241.

McKay, A., 1890. On the earthquakes of September, 1888, in the Amuri and Marlborough Districts of the South Island., Reports of Geological Explorations, Colonial Museum and Geological Survey of New Zealand 20: 1-16.

McKellar, I. C., 1960. Pleistocene deposits of the upper Clutha Valley, Otago, New Zealand. New Zealand Journal of Geology and Geophysics 3: 432-460.

Mejdahl, V., Funder, S., 1994. Luminescence dating of Late Quaternary sediments from East Greenland. Boreas 23: 525-535.

Nobes, D., Owens, I. F., 1995. Preliminary results of the 1995 programme of radar profiling of the Tasman Glacier and the nevé of the Fanz Josef Glacier. Annual Conference of the Geological Society of New Zealand, Geological Society of New Zealand Annual Conference Programme and Abstracts, pg. 158, Auckland, New Zealand.

Norris, R. J., Koons, P.O., and Cooper, A.F., 1990. The obliquely-convergent plate boundary in the South Island of New Zealand: implications for ancient collision zones. Journal of Structural Geology 12(5/6): 715-725.

Purdie, J., Fitzharris, B., 1999. Processes and rates of ice loss at the terminus of Tasman Glacier, New Zealand. Global and Planetary Change 22: 79-91.

Prescott, J.R., Hutton, J.T., 1995. Cosmic ray contribution to dose rates for luminescence and ESR dating: large depth and long time variations. Radiation Measurements 23: 497-500.

Rother, H ., Jol, H.M., Shulmeister, J. (in press). Stratigraphy and tectonic implications of Late Pleistocene valley fill in the Hope Valley , Canterbury , South Island , New Zealand. Baker, G.S., Jol, H.M., (Ed.) Progress in stratigraphic analyses using ground penetrating radar (GPR), Geological Society of America (GSA), Special Publication.

Shaw, J., 1975. Sedimentary successions in Pleistocene ice-marginal lakes. Glaciofluvial and glaciolacustrine sedimentation. A. V. Jopling, McDonald, B.C (Ed). Tulsa, Oklahoma, U.S.A.: 281-303.

Shaw, J., 1987. Glacial sedimentary processes and environmental reconstruction based on lithofacies. Sedimentology 34: 103-116.

Shulmeister, J., Fink, D., Augustinus, P., 2005a. A cosmogenic nuclide chronology of the last glacial transition in North-West Nelson, New Zealand - new insights in Southern Hemisphere climate forcing during the last deglaciation. Earth and Planetary Science Letters 233: 455-466.

Shulmeister, J., Rother, H. , Rieser, U., Thackray, G., 2005b. Glacial Sedimentology and chronology in the Rakaia and Hope Valleys , Canterbury . Abstract *in* Alloway, B.V., Shulmeister, J. (Ed.) 2005. Proceedings of the 2005 NZ-INTIMATE Meeting, GNS-Rafter Laboratory, Wellington, GNS science report 05/18. 29 p.

Soons, J. M., 1963. The glacial sequence in part of the Rakaia Valley, Canterbury, New Zealand. New Zealand Journal of Geology and Geophysics 6: 735-756.

Spedding, N., Evans, D.J.A., 2002. Sediments and landforms at Kvíárjökull, southeast Iceland: a reappraisal of the glaciated valley landsystem. Sedimentary Geology 149: 21-42.

Speight, R., 1940. Ice wasting and glacier retreat in New Zealand. Journal of Geomorphology 3: 131-143.

Speight, R., 1942. A detail of the Pukaki moraine. Transactions and Proceedings of the Royal Society of New Zealand 72(2): 148 - 157.

Suggate, R. P., 1990. Late Pleistocene and Quaternary glaciations of New Zealand. Quaternary Science Reviews 9: 175-197.

Suggate, R. P., (Ed.), 1978. The Geology of New Zealand, New Zealand Geological Survey, Wellington, 2 volumes: 820 p.

Suggate, R. P., 1965. Late Pleistocene geology of the northern part of the South Island, New Zealand. New Zealand Geological Survey Bulletin 77: 90.

Teller, J. T., 2003. Subaquatic landsystems: large proglacial lakes., Glacial landsystems., D. J. A. E. (Ed.). London, 532 p.

Thomas, G. S. P., Connell, R.J., 1985. Iceberg drop, dump, and grounding structures from Pleistocene glacio-lacustrine sediments, Scotland. Journal of Sedimentary Petrology 55(2): 243-249.

Turney, C. S. M., McGlone, M.S., Wilmhurst, J.M., 2003. Asynchronous climate change between New Zealand and the North Atlantic during the last deglaciation. Geology 31(3): 223-226.

Wellman, H. W., 1979. An uplift map for the South Island of New Zealand, and a model for uplift of the Southern Alps. The origin of the Southern Alps. R. I. Walcott, and Cresswell, M.M. 18: 13-20.

Wood, R. A., Pettinga, J.R., Bannister, S., Lamarche, G., and McMorran, T.J., 1994. Structure of the Hanmer strike-slip basin, Hope Fault, New Zealand. Geological Society of America Bulletin 106: 1459-1473.

Near Surface Geophysics, 2006, 69-74

Radar 'lensing' by a small river: Can a layer of surface water improve the signal?

David C. Nobes[1*], Henrik Rother[1], Jan van der Kruk[2] and Harry M. Jol[3]

[1] *Department of Geological Sciences, University of Canterbury, Private Bag 4800, Christchurch, New Zealand*
[2] *Institute of Geophysics, Swiss Federal Institute of Technology, Hoenggerberg, Zurich*
[3] *Department of Geography and Anthropology, University of Wisconsin – Eau Claire, Eau Claire, Wisconsin 57402-4004, USA*

Received October 2004, revision accepted March 2005

ABSTRACT

A radar survey was carried out on a gravel bar between the Hope and Boyle Rivers near the Hanmer Basin in the central South Island of New Zealand. One of the profiles crossed a shallow stream, where the depth of penetration and resolution both appeared to improve. The water's high dielectric permittivity, and consequent slower velocity, causes the signal to be directed more vertically into the subsurface. The superior resolution is also due in part to the slower average velocity; the water table is at or above the ground surface in the stream channel. Spectral analysis shows that there is a small increase in the amplitude of the higher frequencies in the stream portion of the profile, so that the improved resolution appears to be real. Multiple reflections from the stream may also contribute to the spectral broadening. The apparent increased depth of penetration is partly due to the increased time required for echoes to return at the slower velocity, but the larger two-way traveltime does yield a marginally greater depth of penetration.

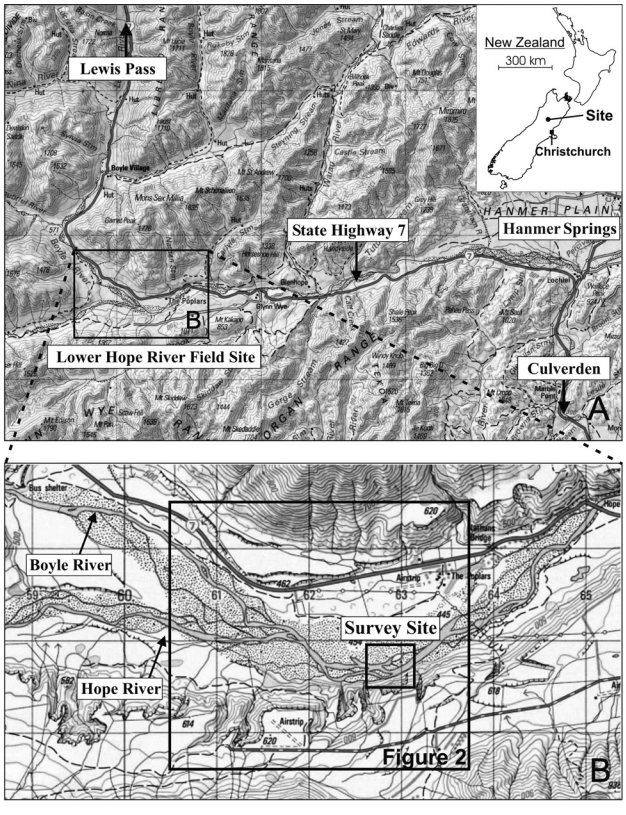

FIGURE 1

(A) The survey site is located in the north central South Island of New Zealand. (inset) upstream from Hanmer Basin, near the confluence of the Hope and Boyle Rivers. (B) A detailed view shows confluence, which has migrated downstream over time and is now located near the survey site (labelled box). The approximate locations of the aerial photograph (Fig. 2) and of the survey site (Fig. 3) are indicated. (Both maps modified from NZMS Series 260, Sheet M32 1989.)

INTRODUCTION

The confluence of the Hope and Boyle Rivers in North Canterbury (South Island, New Zealand) occurs on a broad braid-dominated floodplain (Fig. 1). The 500 m wide braided channel carries a combined mean annual flow of 45.1 m^3/s, but flooding following heavy rainfalls in the upper catchment is frequent and can produce peak discharge in excess of 700 m^3/s (Mosley 2004). As a result, the position of the Hope–Boyle confluence is highly variable and has repeatedly shifted over distances of 1–2 km (Fig. 2). The depositional environment in the valley is characterized by very high annual sediment yields typical of New Zealand rivers, due to rapid tectonic uplift and frequent intense rain storms (Griffiths 1981). The present floodplain is dominated by coarse fluvial gravel and comprises all commonly known types of braid bars in various states of development and decay. Since the last glacial termination, the Hope and Boyle Rivers have incised ca. 150 m into the last glacial valley fill, thus forming large fluvial terraces on both sides of the active channel.

* david.nobes@canterbury.ac.nz

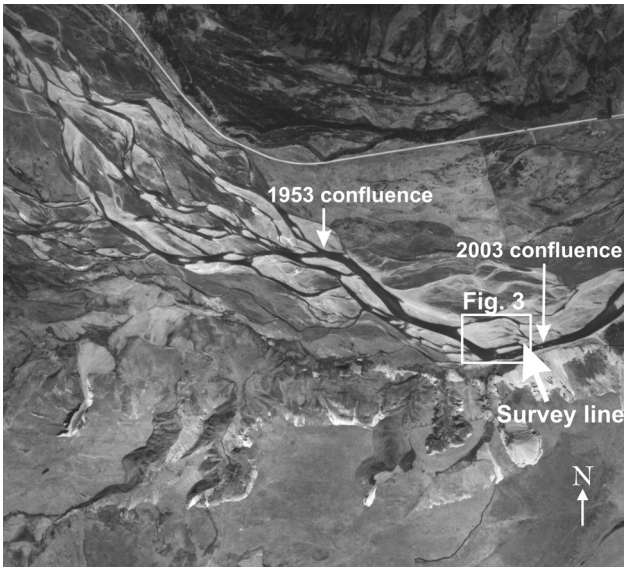

FIGURE 2
A 1950 aerial photograph shows the confluence of the Hope and Boyle Rivers. The general valley configuration is still the same, but the rivers have shifted as indicated. The radar survey site location is boxed and is shown in more detail in Fig. 3. The approximate position of the radar line discussed here is also shown (large arrow).

During a ground-penetrating radar (GPR) survey to investigate the sedimentary channel-fill structures, several GPR lines were recorded across a linguoid bar that was obliquely dissected by a small shallow stream (Fig. 3). The stream was less than 0.5 m at its deepest point (see e.g. Fig. 3B), and was generally less than 0.3 m deep. The resulting enigmatic raw data profile (Fig. 4) seems to have higher resolution and greater penetration where the profile crosses the stream, which appears to be acting almost like a lens for the radar signal. The data were acquired using a pulseEKKO 100 system with 50 MHz antennae, a standard 2 m antenna offset and 0.50 m trace spacing.

In this paper, we report on the results of a more detailed study of this phenomenon as observed in the collected profile. The appearance of improved resolution across the stream may simply be due to the slower average velocity, given that the water table is at or above the ground surface in the stream channel. We investigate the velocity influence, spectral content and focusing of the radar signal due to the high water content. Each step in turn is briefly introduced before the specific set of results is discussed. All profiles shown are de-wowed and use automatic gain control.

GUIDED WAVES, MULTIPLES AND DIFFRACTIONS

Our analysis is complicated by the presence of multiples and of steeply dipping events on either side of the stream. The multiples will be discussed when we consider the spectral content and velocity variations. The dipping events could arise from two possible causes: diffractions and guided waves.

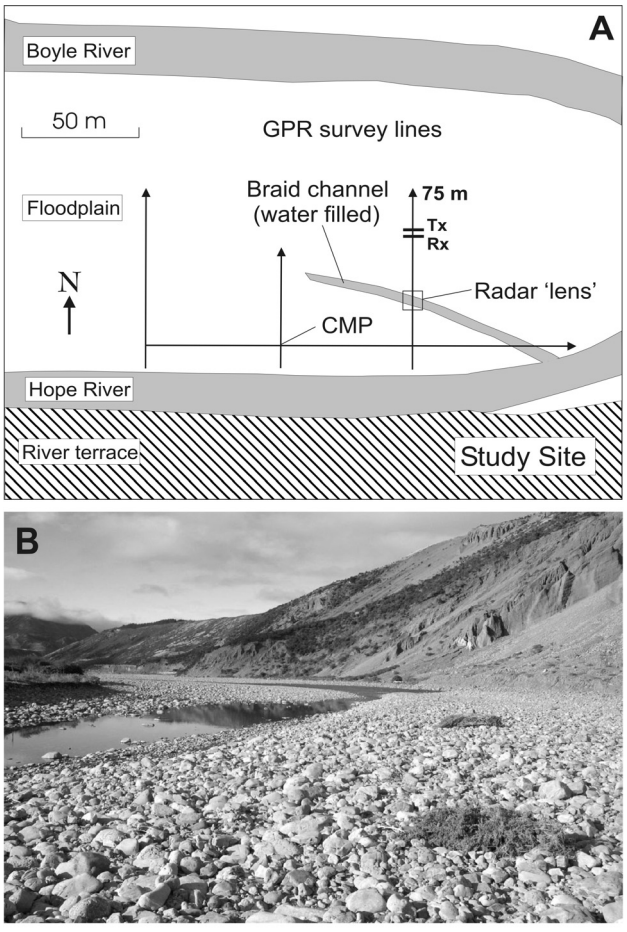

FIGURE 3
(A) Site map showing the position of the radar survey just above the confluence of the Hope and Boyle Rivers. CMP surveys were carried out along the survey baseline. The radar 'lens' (labelled box) occurred along the survey line that crossed a small water-filled braid channel. The antennae (Tx-Rx) were orientated approximately parallel to the shallow stream. (B) Photograph looking SSE from the radar line along the shallow stream.

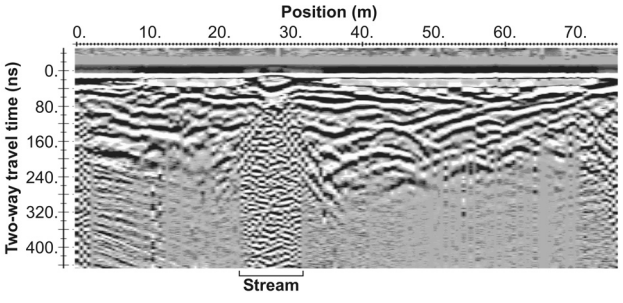

FIGURE 4
The raw profile which crosses the small braid channel shows the 'lensing' effect of the stream.

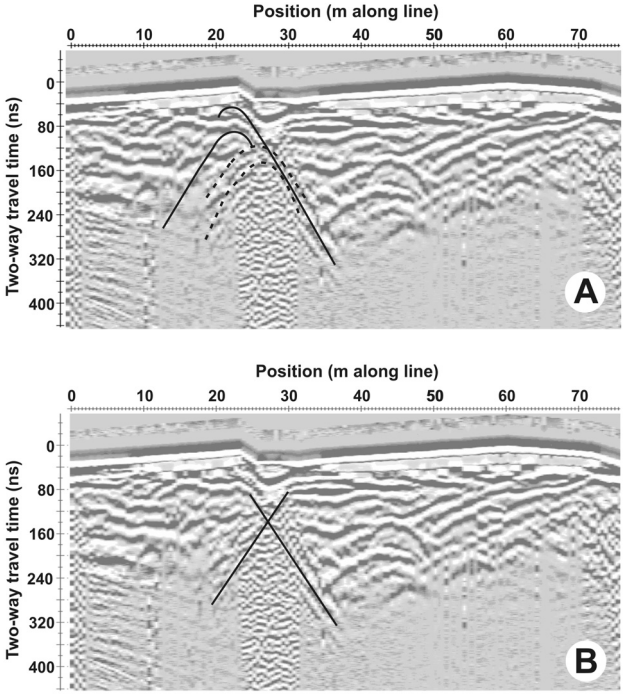

FIGURE 5

The steeply dipping events on either side of the braid channel can have two sources: (A) They are the tails of diffractions from the bottom of the infilled channel and from beds truncated by the channel incision. (B) They are the result of guided waves from the low-velocity waveguide formed by the stream (cf. Arcone *et al*. 2003).

Diffractions

The bottom of the incised channel can cause diffractions, possibly giving rise to 'bow-tie' events. The incised channel has been subsequently infilled with sediment. In addition, channel incision would have eroded and truncated beds that have also been buried, and these could also yield diffractions. Some possible diffractions and their steeply dipping tails are highlighted in Fig. 5(A). The shapes of the diffractions, and in particular the slopes of the proposed tails, yield velocities of 60±10 m/μs for diffractions from the bottom of the buried stream channel. Diffractions from truncated beds yield velocities of 87±5 m/μs. These velocities are consistent with those obtained from a common-midpoint (CMP) profile acquired adjacent to the braid-channel survey line, and with the migration velocity required to collapse diffractions from beneath the stream. The velocity analyses are discussed in more detail in a later section.

Guided waves

Radar energy can propagate in a low-velocity waveguide, as observed by Arcone *et al*. (2003) for a saturated surface soil layer. The radar velocity in the stream would, of course, be the water velocity, 33 m/μs, which is much lower than the air velocity above, 300 m/μs, and the saturated stream bed velocity below,

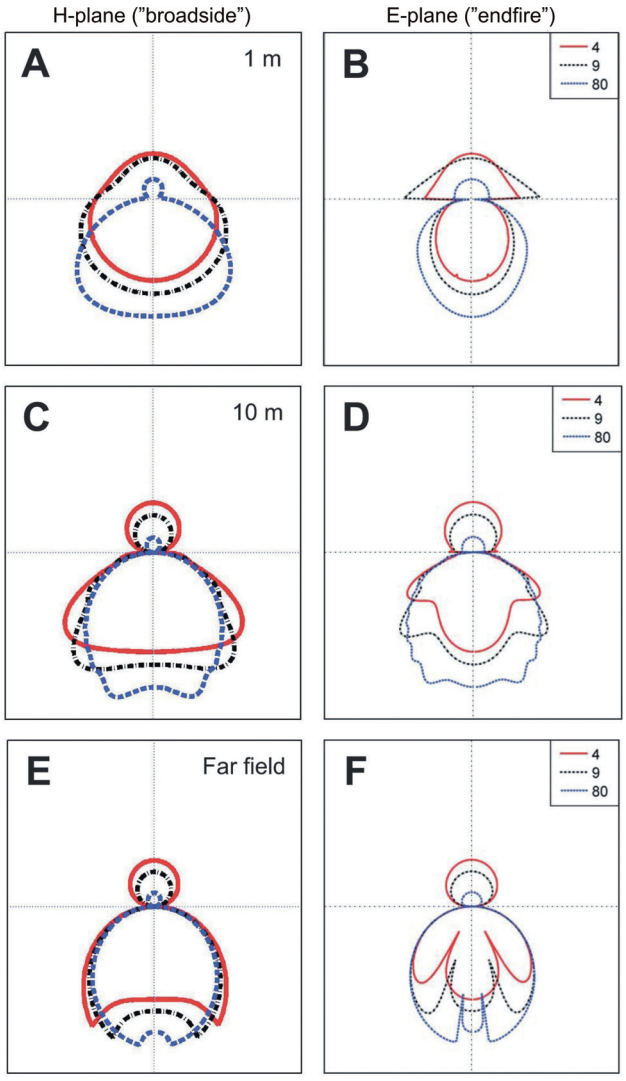

FIGURE 6

Radar antenna radiation patterns for H-plane ('broadside', left) and E-plane ('endfire', right) at 1 m (near field, A and B), 10 m (C and D), and far field (E and F). See text for discussion.

approximately 60 m/μs. Such a waveguide can cause steeply dipping events in a radar profile, as shown by Arcone *et al*. (2003) and as illustrated in Fig. 5(B). There would also be multiple reflections associated with the strong velocity contrasts between air and water and between the water and the stream bed.

PROCESSING, RESULTS AND DISCUSSION

Signal focusing and directionality

The high water content yields a high dielectric coefficient, causing more energy to be directed vertically into the subsurface, as shown in numerous studies of the radar signal directionality (e.g. Annan *et al*. 1975; Nobes and Annan 2000). Our own modelling results (Fig. 6) replicate this greater directionality, which contributes to

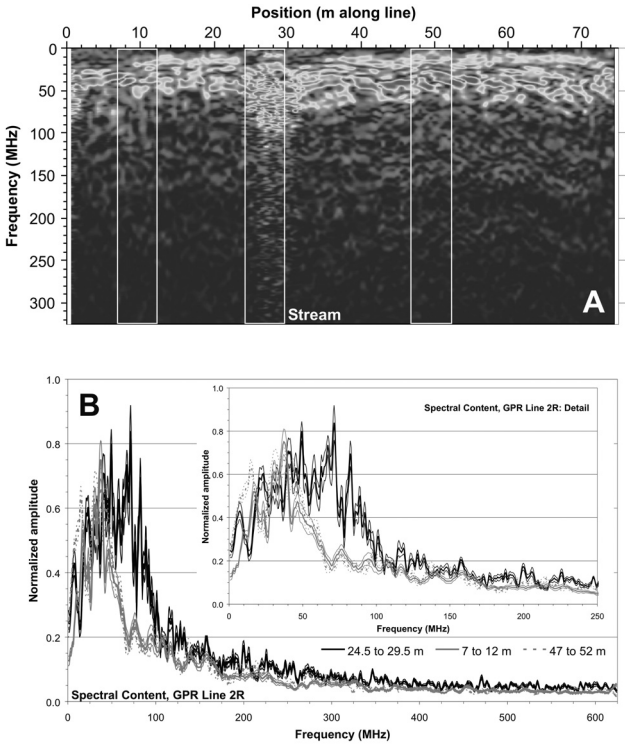

FIGURE 7

(A) The amplitude spectrum is similar across the profile, except for a section across the stream where there is more energy at high frequencies. The spectral content of three sets of profiles, from locations indicated by the white rectangles, were examined in more detail. (B) Amplitude spectra from 7–12 m and from 47–52 m, on either side of the channel, were compared with those from the stream, 24.5–29.5 m. Spectral amplitudes are normalized to the maximum amplitude for the entire profile. The stream spectral content does have broader frequency content, which would yield a more compact signal pulse. (Inset) A detailed subset of the spectra shows that the frequency range is almost doubled.

the greater signal return from within the confines of the stream. The total field has been calculated by evaluating the exact integral expressions (Slob and Fokkema 2002; van der Kruk *et al.* 2003).

The energy from the transmitting antenna is directed more vertically into the ground as the relative dielectric coefficient increases from 4 (v = 150 m/μs, equivalent to dry sand), to 9 (v = 100 m/μs, equivalent to partly saturated sand), to 80 (v = 33 m/μs, the radar velocity in water). For our bistatic GPR survey, where the receiving antenna was offset 1 m from the transmitting antenna, the configuration where both antennae are in each others' H-plane provides the majority of the reflected energy (Figs 6A, C and E) as compared to when the antennae are in each others' E-plane. Only for vertically incident reflections are the energies the same.

Spectral analysis and resolution

A natural next step is to carry out a spectral analysis of the raw data. We want to see if there is a broader amplitude spectrum in the traces that cross the stream when compared to the traces away from the stream, and this indeed is what we observe (Fig. 7). Because the low-frequency content is similar, the broader frequency spectra from the stream traces yield a more compact radar signal pulse, and thus apparently greater resolution.

However, the spectral energy for radar multiples occurs in a bandwidth similar to that for the directly reflected radar energy, thus complicating the situation. We tested the possible effects of the multiples by filtering the traces so that all had a similar bandwidth regardless of position. In other words, a band-pass filter was used to remove the higher frequency energy from the stream-channel traces, so that the resulting spectral content was consistent across the whole profile. There was little evident difference between the filtered and unfiltered profiles, except that the reflections from the stream appeared broader, i.e. less well resolved. We return to the question of multiples in the next section.

Velocity and migration

We migrated the profile for a number of velocities, using the two-dimensional *f–k* migration based on the Stolt (1978) algorithm for a constant velocity which is provided with the pulseEKKO system. By migrating the profiles with a range of velocities, we test the degree to which the velocity can vary.

A CMP velocity survey was carried out along the survey baseline adjacent to the Hope River (see Fig. 3), and these velocities (Fig. 8) are used as the starting point for migration. The layers above the water table have stacking velocities of the order of 150 m/μs (0.15 m/ns) or greater, whereas the CMP velocity below the water table is 90 m/μs (0.09 m/ns). The shallowest velocities, above 50 ns two-way traveltime (TWT), are very high, and may indicate some air-wave influences. A migration velocity of 100 m/μs (0.10 m/ns) yields good results for the profiles away from the stream (Fig. 9), collapsing diffractions and giving good continuity to reflective beds. However, the reflections below the stream take on the appearance of a parallel-banded sequence, akin to a set of multiple reflections from a single reflector, and the edges of the stream reflective sequence are highly overmigrated, causing the 'smiles' on either side of the stream.

To test the hypothesis that we are dealing with a single reflector causing multiple reflections, we migrated the profile with a low velocity, i.e. 33 m/μs (0.033 m/ns), the radar velocity in water. Away from the stream, the profile is highly undermigrated, as expected. Within the stream, however, the segment is only moderately undermigrated. There are subsets of parallel reflectors which are likely to be multiple reflectors:

(i) between 28 and 31 m and from TWTs of 100–160 ns, which appear to be parallel to and thus associated with a deeper buried channel;
(ii) between 25 and 28 m, from TWTs of 160–200 ns, which appear to be parallel or subparallel to the surface channel, but this association is ambiguous;
(iii) from 25 to 28 m, at TWTs of 400 ns or more.

However, we can see that there are a number of subparallel or

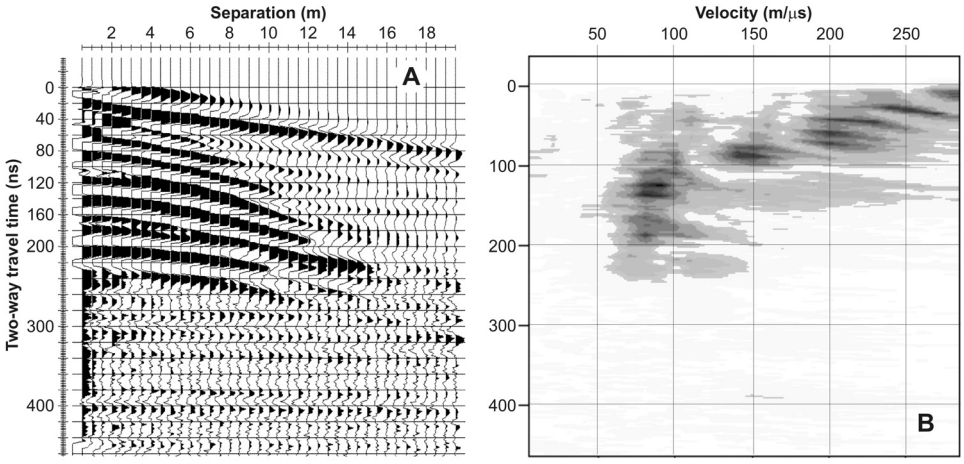

FIGURE 8
(A) The CMP profile acquired adjacent to the survey line contains an obvious air wave and many clear subsurface reflection events. (B) A semblance analysis of the CMP record in (A) yields the velocity structure. The shallowest events are influenced by air-wave events probably arising from the nearby terrace edge. Subsurface velocities are 150 m/μs or higher above 100 ns, and 90 m/μs below.

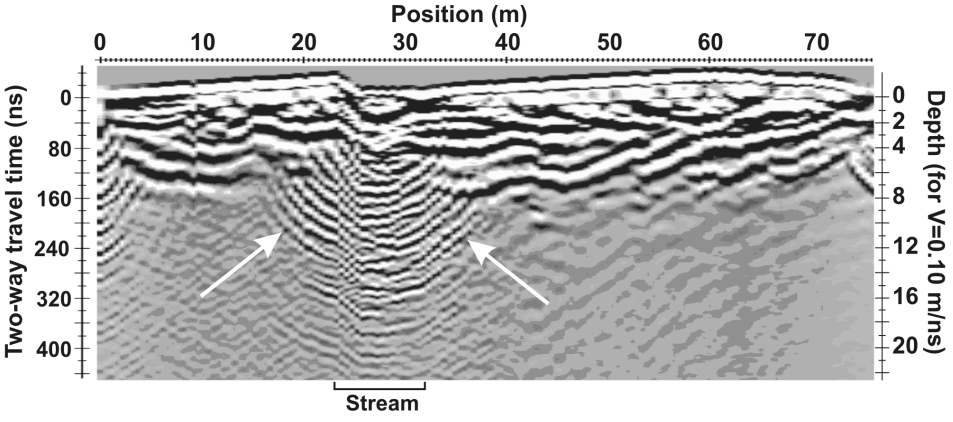

FIGURE 9
When the profile is migrated using an average velocity of 100 m/μs, then diffractions outside the stream zone are collapsed and there is good continuity of bed reflections. Within the stream zone, however, the velocity is too high, yielding 'smiles', as highlighted by the white arrows. The reflections beneath the stream are flattened and appear to be stacked multiples.

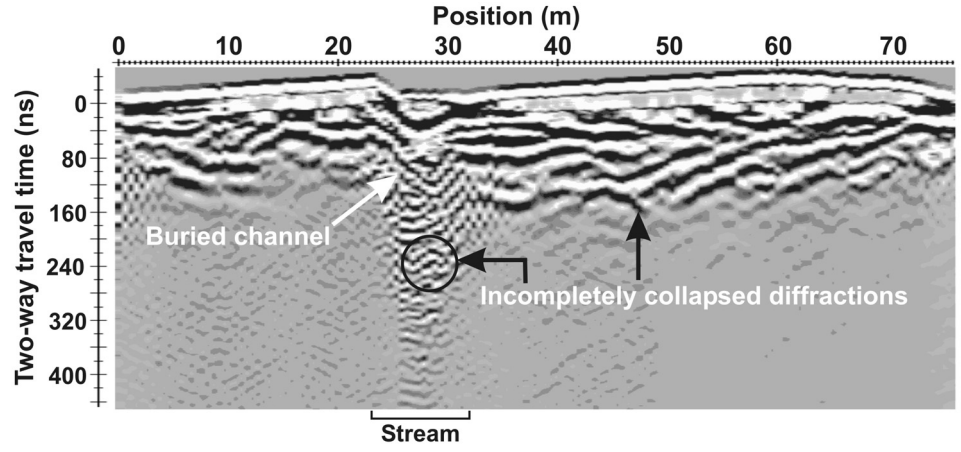

FIGURE 10
When the water velocity (33 m/μs) is used to migrate the profile, the buried incised braid channel is clearer, and there is more structure beneath the stream. Diffractions are incompletely collapsed, including one below the stream, at about 220 ns TWT. This diffraction is collapsed when a velocity of 60 m/μs is used.

undulating reflectors, so that the section of the profile across the stream is not entirely composed of multiples.

In addition, there is a remnant of a hyperbolic diffraction at a TWT of 220 ns, well below the stream bed (Fig. 10). When a velocity of 60 m/μs (0.06 m/ns) is used, the diffraction collapses, suggesting that our depth of penetration exceeds 6.6 m beneath the surface of the stream, deeper than the 4 to 6 m observed elsewhere in the profile. There appear to be reflections as deep as 300 ns (approximately 9 m using the velocity of 60 m/μs), but these may still be multiple reflections, and are thus treated with some caution.

Profile splicing

The stream segment was spliced from the profile migrated at

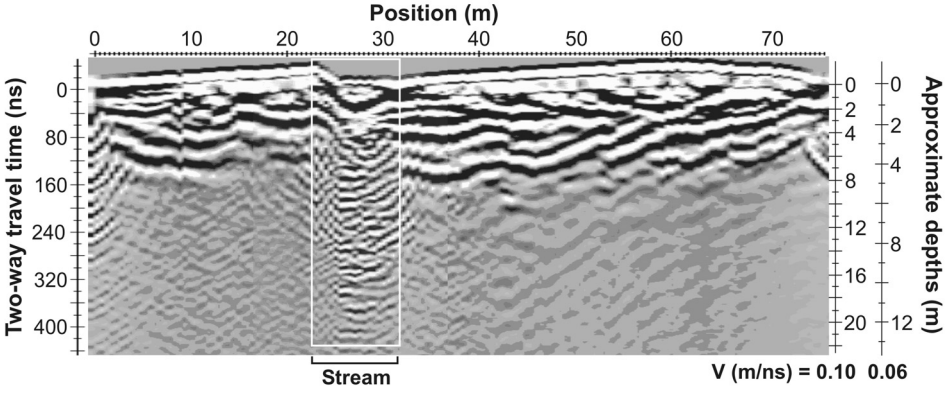

FIGURE 11
The profile migrated using 100 m/μs is overlain by the stream segment cut from the profile migrated using 60 m/μs. The reflections at the margins of the stream splice did not originally match those from the 100 m/μs migrated profile, and the splice was compressed until the reflections on the margins did match. The maximum alignment of reflections occurs for a compression factor of 0.9, equivalent to a velocity of 90 m/μs.

60 m/μs and superimposed on the profile migrated using 100 m/μs. The reflections at the margins of the stream splice did not originally match those from the 100 m/μs migrated profile. The stream segment splice was compressed until reflections at the edges of both the splice and the original profile matched (Fig. 11). The amount of compression yields a velocity of approximately 75 to 90 m/μs, i.e. compression factors of 0.75 to 0.9, depending on the reflectors used for alignment. The higher velocity aligns the greatest number of reflectors. We thus conclude that the velocity varies laterally, decreasing from a layered velocity of 150 m/μs over 90 m/μs, and an overall average migration velocity of 100 m/μs, to a minimum velocity of 60 m/μs in the centre of the stream. A consequence of the varying lateral velocity is that the trace spacing (spatial sampling) must be less across the stream to maintain the spatial Nyquist frequency (e.g. Annan and Cosway 1992).

CONCLUSIONS

We conclude that the stream has had a positive influence on the depth of penetration and the resolution of the signal. The resolution may in part be merely apparent, but at least a portion of it is a genuine improvement in resolution. As we have shown, the spectral content is broader, giving a more compact pulse with better resolution. The velocity of the subsurface within the stream channel was 60 m/μs, compared with 75 to 90 m/μs on the margins, and 150 m/μs above and 90 m/μs below the water table away from the channel. The lower velocity (due to higher dielectric permittivity) causes the radar signal to be more focused into the subsurface, and more energy goes into the area beneath the stream. In addition, the consequent spatial sampling must also vary. Finally, the lower velocity does not lead to decreased penetration; on the contrary, the TWT combined with the stream bed velocity of 60 m/μs yields a depth of penetration in excess of 6.6 m, greater than the 4 to 6 m observed away from the stream. Attenuation losses are proportional to the ratio of the conductivity and the square root of the permittivity. In this case, the former is very low due to the fresh water, whereas the latter is high, and the attenuative energy losses per metre are thus low.

ACKNOWLEDGEMENTS

DCN benefited from the hospitality of the Institute of Geophysics at ETH, during which time most of the work and this paper were completed. HR gratefully acknowledges the support of the Department of Geological Sciences of the University of Canterbury during the course of his PhD. HJ thanks the University of Canterbury for the Erskine Fellowship which provided the opportunity to participate in the research.

REFERENCES

Annan A.P. and Cosway S.W. 1992. Ground penetrating radar survey design. In: *Proceedings of the 5th Symposium on the Application of Geophysics to Engineering and Environmental Problems (SAGEEP)* (ed. R.S. Bell), pp. 329–351.

Annan A.P., Waller W.M., Strangway D.W., Rossiter J.R., Redman J.D. and Watts R.D. 1975. The electromagnetic response of a low-loss, 2-layer, dielectric earth for horizontal electric dipole excitation. *Geophysics* **40**, 285–298.

Arcone S.A., Peapples P.R. and Liu L. 2003. Propagation of a GPR pulse in a thin surface waveguide. *Geophysics* **68**, 1934–1944.

Griffiths G.A. 1981. Some suspended sediment yields from South Island catchments, New Zealand. *Water Resource Bulletin* **17**(4), 662–671.

van der Kruk J., Wapenaar C.P.A., Fokkema J.T. and van den Berg P.M. 2003. Improved three-dimensional reconstruction technique for multi-component ground penetrating radar. *Subsurface Sensing Technologies and Applications* **4**, 61–99.

Mosley M.P. 2004. *Waiau River - instream values and flow regime*. Environment Canterbury Report R04/02, p. 218.

Nobes D.C. and Annan A.P. 2000. 'Broadside' versus 'end-fire' radar response: Some simple illustrative examples. In: *GPR 2000: Proceedings of the 8th International Conference on Ground Penetrating Radar* (eds D.A. Noon, G.F. Stickley and D. Longstaff), *Society of Photo-Optical Instrumentation Engineers (SPIE)* **4084**, pp. 696–701.

Slob E.C. and Fokkema J.T. 2002. Interfacial dipoles and radiated energy. *Subsurface Sensing Technologies and Applications* **3**, 347–367.

Stolt R.H. 1978. Migration by Fourier transform. *Geophysics* **43**, 23–48.

A. Sample details for Infrared Stimulated Luminescence Dating (IRSL)

Field code	Lab. code	Sample location	Sampling method	NZ Grid reference	Elevation (m a.s.l.)	Lithology	Stratigraphic context	Water content	IRSL Age (in ka)
LAT 1	WLL-355	Carlyle Terrace (Lewis Advance aggradation terrace (Clayton, 1968)	Metal cylinder	M32 584590 N 246720 E	435	Laminated fine and cross stratified medium sand	15 m of lacustrine and fluvial sand	Sample from well above the water table	95.7 ± 6.8
HV-L-554	WLL-413	Hope Valley, terrace above Glynn Wye Gorge	Metal cylinder	M32 N 584577 E 246830	554	Fine sand	0.5 m of loess over fluvial gravel	Sample from well above the water table	10.2 ± 0.8
MHV-S-501	WLL-411	Middle Hope Valley, 1.2 m above river level	Sediment block	M32 N 584420 E 245651	501	Lacustrine silt and clay	Lacustrine sediments overlain by deltaic gravel	Sample from 1.2 m above river level	34.4 ± 2.5
GWS 409	WLL-423	Glynn Wye Stream, ~15 m above Hope River	Metal cylinder	M32 N 584609 E 246924	410	Medium sand to fine sand	8 m thick unit of sand within fluvial and alluvial gravel	Sample from well above the water table	89.3 ± 5.0
Hor-615	WLL-422	Hope Valley, east of Manuka Stream	Metal cylinder	M32 N 584403 E 247221	620	Medium to coarse sand	Sand lens within fluvial gravel	Sample from well above the water table	110.5 ± 10.6
PG 2	WLL-353	Poplars Gully	Metal cylinder	M32 584620 N 246290 E	575	Thick unit of Fine sand and silt	glacio-lacustrine (?) sands & silts	Sample from well above the water table	164.7 ± 14.8

Field code	Lab. code	Sample location	Sampling method	NZ Grid reference	Elevation (m a.s.l.)	Lithology	Stratigraphic context	Water content	IRSL Age (in ka)
LHD 1	WLL-356	Kakapo Delta, lower Hope Valley	Sediment block	M32 584460 N 246310 E	465	3 m unit of fine sand and silt	Lacustrine sand & silt within deltaic gravel	Sample from well above the water table	60.3 ± 5.6
G 580	WLL-351	Lower Hope Valley, main aggradational terrace	Metal cylinder	M32 584450 N 246325 E	570	0.6 m bed of fine sand above coarse gravel	Loess at terrace surface above fluvial gravel	Sample from well above the water table	32.1 ± 2.6
GWS 1	WLL-354	Glynn Wye Stream, upper gully section	Metal cylinder	M32 584560 N 246920 E	500	5 m unit of medium to fine sand	Fluvial-lacustrine overbank deposits	Sample from well above the water table	45.5 ± 12.9
PG 1	WLL-352	Poplars Gully	Metal cylinder	M32 584620 N 246290 E	490	Fine sand and silt	Proglacial glacio-lacustrine sand and silt	Sample from well above the water table	127.5 ± 10.7
Poplars F 1	WLL-357	Poplars Gully	Metal cylinder	M32 584620 N 246290 E	495	Medium to coarse sand	Distal fan deposit underlying glacio-fluvial deposits	Sample from well above the water table	119.8 ± 10.5
Poplars F 2	WLL-358	Poplars Gully	Metal cylinder	M32 584620 N 246290 E	545	Medium to coarse sand	Fluvial sand	Sample from well above the water table	164.2 ± 17.4

Field code	Lab. code	Sample location	Sampling method	NZ Grid reference	Elevation (m a.s.l.)	Lithology	Stratigraphic context	Water content	IRSL Age (in ka)
La-Ter-Q-1	WLL-359	Carlyle Terrace (Lewis Advance aggradation terrace (Clayton, 1968)	Metal cylinder	M32 584590 N 246720 E	445	Fine sand	Loess above degradational gravel	Sample from well above the water table	18.2 ± 1.6
GWT-S-2	WLL-412	Lower Hope Valley, Glynn Wye Terrace	Metal cylinder	M32 584449 N 246335 E	617	Fine sand	Loess above aggradational gravel	Sample from well above the water table	14.0 ± 0.8

B. Sample details for cosmogenic ^{10}Be Surface Exposure Dating (SED)

Sample code	Sample location (moraine site, Fig.0)	NZ grid reference	Elevation (m a.s.l.)	Boulder size (cm)	Lithology	Sample material	Horizon shielding	Sample thickness	Age (in ka)
GW-I	Glynn Wye moraine, Lower Hope Valley (7)	M32 246254 E 584339 N	640	560 x 340 x 220	Sandstone	Rock sample	250˚-310˚= 4˚ / 310˚-350˚= 8˚ / 350˚-40˚= 4˚ / 40˚-70˚= 2˚ / 70˚-120˚= 12˚ / 120˚-210˚= 8˚ / 210-250˚= 17˚	top 4 cm	18.6 ± 1.7
GW-II	Glynn Wye moraine, Lower Hope Valley (7)	M32 246254 E 584339 N	645	270 x 330 x 160	Sandstone	Rock sample	230˚-310˚= 4˚ / 310˚-340˚= 4˚ / 340˚-10˚= 7˚ / 10˚-190˚= 24˚ / 190˚-230˚= 18˚	top 4 cm	19.2 ± 2.0
GW-III	Glynn Wye moraine, Lower Hope Valley (7)	M32 246254 E 584339 N	647	270 x 85 x 75	Sandstone	Rock sample	230˚-320˚= 5˚ / 320˚-360˚= 10˚ / 360˚-30˚= 5˚ / 30˚-60˚= 3˚ / 60˚-120˚= 12˚ / 120˚-190˚= 8˚ / 190-230˚= 18˚	top 4 cm	15.5 ± 1.2

Sample code	Sample location (moraine site, Fig. 0)	NZ grid reference	Elevation (m a.s.l.)	Boulder size (cm)	Lithology	Sample material	Horizon shielding	Sample thickness	Age (in ka)
GW-B	Glynn Wye moraine, Lower Hope Valley (7)	M32 246254 E 584339 N	640	560 x 340 x 220	Sandstone	Rock sample	250˚-310˚= 4˚ / 310˚-350˚= 8˚ / 350˚-40˚= 4˚ / 40˚-70˚= 2˚ / 70˚-120˚= 12˚ / 120˚-210˚= 8˚ / 210-250˚= 17˚	top 4 cm	12.8 ± 2.8
LP-I	Lewis Pass moraine, (1)	M31 246066 E 586975 N	870	170 x 120 x 60	Sandstone	Rock sample	250˚-40˚= 14˚ / 40˚-140˚= 25˚ / 140˚-210˚= 11˚ / 210˚-250˚= 23˚	top 4 cm	17.6 ± 1.3
LP-II	Lewis Pass moraine, (1)	M31 246062 E 586980 N	880	200 x 110 x 75	Sandstone	Quartz vein	160˚-340˚= 14˚ / 340˚-20˚= 8˚ / 20˚-160˚= 24˚	top 4 cm	n / a
LP-III	Lewis Pass moraine, (1)	M31 246063 E 586983 N	875	180 x 110 x 75	Sandstone	Rock sample	130˚-230˚= 20˚ / 230˚-340˚= 17˚ / 340˚-10˚= 6˚ / 10˚-130˚= 20˚	top 4 cm	16.5 ± 1.6
KH-I	Kakapo Hill moraine, (5)	M32 246745 E 584362 N	830	250 x 150 x 170	Sandstone	Rock sample / Quartz vein	120˚-84˚= 4˚ / 84˚-10˚= 2˚ / 10˚-352˚= 8˚ / 352˚-172˚=40˚ / 172˚-120˚= 6˚ /	top 3 cm	23.4 ± 1.7
MM-I	Magdalen moraine, Boyle Valley (2)	M32 246979 E 585648 N	750	100 x 100 x 65	Sandstone	Rock sample	150˚-330˚= 20˚ / 330˚-20˚= 28˚ / 20˚-90˚= 12˚ / 90˚-150˚= 18˚	top 3 cm	n / a
MM-II	Magdalen moraine, Boyle Valley (2)	M32 246994 E 585653 N	760	120 x 100 x 55	Sandstone	Rock sample	200˚-240˚= 6˚ / 240˚-280˚= 11˚ / 280˚-320˚= 22˚ / 320˚-30˚= 32˚ / 30˚-100˚= 12˚ / 100˚-180˚= 20˚ / 180-200˚= 6˚	top 4 cm	n / a
MM-III	Magdalen moraine, Boyle Valley (2)	M32 246997 E 585655 N	750	140 x 120 x 50	Sandstone	Rock sample	50˚-90˚= 10˚ / 90˚-180˚= 20˚ / 180˚-210˚= 15˚ / 210˚-250˚= 5˚ / 250˚-300˚= 10˚ / 300˚-320˚= 26˚ / 320-30˚= 36˚ / 30-50˚= 20˚	top 5 cm	n / a

Sample code	Sample location (moraine site, Fig. 0)	NZ grid reference	Elevation (m a.s.l.)	Boulder size (cm)	Lithology	Sample material	Horizon shielding	Sample thickness	Age (in ka)
KS-I	Kiwi Saddle moraine, (8)	L32 244750 E 584050 N	660	200 x 100 x 120	Sandstone	Rock sample	150˚-190˚= 8˚ / 190˚-220˚= 15˚ / 220˚-240˚= 6˚ / 240˚-320˚= 18˚ / 320˚-360˚= 7˚ / 360˚-20˚= 10˚ / 20˚-50˚= 3˚ / 50˚-150˚= 18˚	top 5 cm	n / a
KS-II	Kiwi Saddle moraine, (8)	L32 244750 E 584050 N	661	200 x 110 x 200	Sandstone	Rock sample	140˚-180˚= 6˚ / 180˚-210˚= 12˚ / 210˚-240˚= 5˚ / 240˚-310˚= 19˚ / 310˚-340˚= 9˚ / 340˚-30˚= 10˚ / 30˚-50˚= 2˚ / 50˚-80˚= 14˚ / 80˚-140˚= 19˚	top 5 cm	n / a
KS-III	Kiwi Saddle moraine, (8)	L32 244750 E 584050 N	656	250 x 270 x 90	Sandstone	Rock sample	60˚-130˚= 19˚ / 130˚-180˚= 8˚ / 180˚-200˚= 15˚ / 200˚-240˚= 7˚ / 240˚-310˚= 20˚ / 310˚-340˚= 10˚ / 340˚-10˚= 10˚ / 10˚-60˚= 4˚	top 5 cm	n / a
WP-II	Windy Point moraine, (3)	M32 245795 E 584582 N	599	190 x 140 x 60	Sandstone	Rock sample	275˚-340˚= 10˚ / 340˚-50˚= 12˚ / 50˚-110˚= 2˚ / 110˚-200˚= 8˚ / 200˚-275˚= 18˚	top 4 cm	n / a
WP-III	Windy Point moraine, (3)	M32 245795 E 584582 N	568	250 x 200 x 80	Sandstone	Rock sample	330˚-50˚= 20˚ / 50˚-120˚= 9˚ / 120˚-170˚= 12˚ / 170˚-280˚= 14˚ / 280˚-330˚= 8˚ /	top 4 cm	n / a
WP-IX	Windy Point moraine, (3)	M32 24579 E 58458 N	594	220 x 150 x 150	Sandstone	Rock sample	280˚-320˚= 9˚ / 320˚-30˚= 16˚ / 30˚-150˚= 11˚ / 150˚-280˚= 15˚	top 5 cm	n / a
Ho-I	Horseshoe moraine, (4)	M32 24703 E 58446 N	690	100 x 70 x 40	Sandstone	Rock sample	n / a	n / a	n / a
Ho-II	Horseshoe moraine, (4)	M32 24705 E 58447 N	690	80 x 70 x 40	Sandstone	Rock sample	n / a	n / a	n / a

Sample code	Sample location (moraine site, Fig. 0)	NZ grid reference	Elevation (m a.s.l.)	Boulder size (cm)	Lithology	Sample material	Horizon shielding	Sample thickness	Age (in ka)
Glen-I	Glenhope moraine, (6)	M32 24667 E 58418 N	740	100 x 70 x 60	Sandstone	Rock sample	n / a	n / a	n / a

C. Sample details for ^{14}C-dating

Sample code	Sample location	NZ grid reference	Elevation (m a.s.l.)	Sample material	Stratigraphic context	$d^{14}C$ (in ‰)	$\delta^{13}C$ (in ‰)	Age (in a BP)	Calibrated (in a BP)
Wk-14708	West of Kiwi River, upper Hope Valley	L32 24473 E 58409 N	620	Wood, tree fern	Wood within lacustrine silt	-701.5 ± 2.0	-27.4 ± 0.2	9,672 ± 53	10,963 ± 215
Wk-12669	East of Loch Kathrine, Lake Sumner area	L32 24450 E 58309 N	540	Wood, Phyllocladus	Wood in delta foresets, 14 m above Loch Kathrine	-699.3 ± 2.1	-24.2 ± 0.2	9,665 ± 57	10,956 ± 215

Appendix 3: Compilation of age control for deposits >8 ka BP from absolute dating
(Hope-Waiau, Waimakariri, Rakaia, Rangitata Valleys, and Mackenzie Basin)

Hope-Waiau Valleys

Lab code	Dating technique	Date (a BP) (old T½)	Locality, grid reference and altitude	Material dated	Stratigraphic position	Significance	Collector, reference
K1-354-1	^{14}C	13,309 ± 203 a	West bank of Boyle River, 200 m upstream of Doubtful River junction; M32 E 24562 / N 58511; 548 m	wood	Silty deltaic bottomsets from ca. 10 m above present river. Deposit located near large delta foreset unit	Minimum age of deglaciation of Boyle Valley; age of paleolake in lower Boyle Valley	Clayton (1968)
NZ-6180	^{14}C	10,800 ± 150 a	same as above	wood	Thin carbonaceous band in sandy/silty bottomset deposit. 8 m above present river, 6 m below top of deposit	Minimum age of deglaciation of Boyle Valley; age of paleolake in lower Boyle Valley	C.J. Burrows (1988) L. Clayton
Wk-4965	^{14}C	10,900 ± 80 a	same as above	wood	same as above	Minimum age of deglaciation of Boyle Valley; age of paleolake in lower Boyle Valley	Burrows (1997)
NZ-6092	^{14}C	13,050 ± 200 a	same as above	peat	Thin peat layer underlain by silt/sand overlain by gravel	Minimum age of deglaciation of Boyle Valley; age of paleolake in lower Boyle Valley / organic accumulation during cool conditions	C.J. Burrows (1988)
NZ-6093	^{14}C	12,800 ± 200 a	same as above	peat	Thin peat layer underlain by compact silt and diamicton over bedrock; overlain by silt, sand peat layers	Minimum age of deglaciation of Boyle Valley; age of paleolake in lower Boyle Valley / organic accumulation during cool conditions	C.J. Burrows (1988)
NZ-6091	^{14}C	11,700 ± 200 a	same as above	peat	Bottom of peat layer between sheets of alluvium	Minimum age for stable period between two periods of aggradation	C.J. Burrows (1988)
NZ-3904	^{14}C	10,900 ± 200 a	same as above	peat	Top of peat layer between sheets of alluvium	Age close to end of stable period prior to renewed aggradation possibly indicating climate cooling	C.J. Burrows (1988)
NZ-738	^{14}C	42,100 ± 2,400 a	2.5 km south of Lewis Pass, N of Goings Creek, M31 E 24605 N 58672 ~810 m	organic fragments in silt	Carbonaceous band from between two fans overlain by terrace deposits	Deposit predates LGM advances	P. Suggate, N. Moar in: Grant-Taylor & Rafter (1971)
?	^{14}C	> 45,000 a	North Bank of Hanmer River	organic mud an dpeat	Carbonaceous band between tilted fluvial gravel	Early sedimentarry fill into Hanmer Basin	Wood et al. (1994)

Appendix 3: Compilation of age control for deposits >8 ka BP from absolute dating
(Hope-Waiau, Waimakariri, Rakaia, Rangitata Valleys, and Mackenzie Basin)

Hope-Waiau Valleys (continued)

Lab code	Dating technique	Date (a BP) (old T½)	Locality, grid reference and altitude	Material dated	Stratigraphic position	Significance	Collector, reference
?	^{14}C	13,000 ± 200 a	Drill hole near Hanmer Springs	peat	5.5 m depth in drillhole	Peat deposition in swamp between coalescing fans	Wood et al. (1994)
NZ-5532	^{14}C	12,450 ± 200 a	Doubtful Valley M32 E 24544 N 58516; 560 m	leaves and twigs	Deltaic bottomset ca. 40 cm above present river, below foresets	Indicates presence of paleolake in Boyle and Doubtful valley;	Chinn (1981)
NZ-532	^{14}C	14,100 ± 220 a	1 km east of Handyside Stream M32 E 24812 N 58478; ca. 450 m	organic fragments in silt	Silt layer between terrace deposit (below) and talus fan (above)	Minimum age of end of glacial aggradation	Suggate (1965)
WLL 351	IRSL	32.1 ± 2.6 ka	Lower Hope Valley, M32 E 24633 N 58446; ca. 560 m	silt (feldspar)	Overbank (?) deposit within glacio-fluvial gravel, 25 m below glacial moraine	Dates large scale fluvial aggradation	this study
WLL 356	IRSL	60.3 ± 5.6 ka	Lower Hope Valley, M32 E 24631 N 58446; ca. 475 m	silt (feldspar)	Block of lacustrine silts exposed below large delta foreset unit	Dates paleolake in the lower Hope Valley	this study
WLL 355	IRSL	95.7 ± 6.8 ka	Lower Hope Valley, M32 E24672 N 58459; ca. 435 m	silt (feldspar)	Lacustrine fine sand, overlain by aggradational gravel	Dates paleolake in the lower Hope Valley	this study
WLL 352	IRSL	127.5 ± 10.7 ka	Poplars Gully M32 E24630 / N 58463; 490 m	fine sand / silt	Glacio-lacustrine fine sand and silt	Dates glacio-lacustrine sediments	this study
WLL 357	IRSL	119.8 ± 9.9 ka	Poplars Gully M32 E24630 / N 58463; 495 m	medium / coarse sand	Alluvial gravel over bedrock at base of Poplars Gully sequence	Dates early aggradation near valley floor	this study
WLL 353	IRSL	157.8 ± 14.8 ka	Poplars Gully M32 E24630 / N 58463; 475 m	fine sand / silt	Glacio-lacustrine / glacio-fluvial sand	Dates proglacial sediments	this study
WLL 358	IRSL	164.2 ± 17.4 ka	Poplars Gully M32 E24630 / N 58463; 545 m	medium / coarse sand	Medium sand	Glacio-fluvial sediments	this study
WLL 359	IRSL	18.8 ± 1.6 ka	Lower Hope Valley M32 E24672 N 58459; 450 m	fine sand	Loess above fluvial gravel	Dates degradational terrace level	this study

Appendix 3: Compilation of age control for deposits >8 ka BP from absolute dating
(Hope-Waiau, Waimakariri, Rakaia, Rangitata Valleys, and Mackenzie Basin)

Hope-Waiau Valleys (continued)

Lab code	Dating technique	Date (a BP) (old T½)	Locality, grid reference and altitude	Material dated	Stratigraphic position	Significance	Collector, reference
Wk-8037	^{14}C	10,780 ± 60 a	Confluence Doubtful and Boyle Rivers, M32 E 2456 / N 5851; 530 m	organic bed in lacustrine mud	10 m thick laminated lacustrine deposits, depth 1.9 m	Dates deglaciation and paleolake	Turney et al. (2003)
Wk-8035	^{14}C	10,660 ± 60 a	same as above	organic bed in lacustrine mud	same as above, sample depth 3.1 m	same as above	Turney et al. (2003)
Wk-8036	^{14}C	11,860 ± 140 a	same as above	organic bed in lacustrine mud	same as above, sample depth 4.5 m	same as above	Turney et al. (2003)
Wk-8034	^{14}C	10,780 ± 60 a	same as above	organic bed in lacustrine mud	same as above, sample depth 7.7 m	same as above	Turney et al.(2003)
Wk-8038	^{14}C	10,730 ± 60 a	same as above	organic bed in lacustrine mud	same as above, sample depth 7.7 m	same as above	Turney et al. (2003)
Wk-14708	^{14}C	9,672 ± 53 a	West of Kiwi River, upper Hope Valley L32 E24473 / N 58409, 620 m	wood	Wood within lacustrine mud	Dates age of small paleolake, deglaciation	this study
WLL-354	IRSL	45.5 ± 12.9 ka	Glynn Wye Stream, upper gully M32 N 584560 / E 246920, 500 m	sand (quartz)	Fluvio-lacustrine overbank deposit within aggradational gravel	Dates large scale aggradation	this study
WLL-411	IRSL	34.4 ± 2.5 ka	Middle Hope Valley M32 N 584420 / E 245651, 501 m	silt (feldspar)	lacustrine mud at river level overlain by deltaic and aggradational gravels	Dates paleo-lake and ice free conditions	this study
WLL-412	IRSL	14.0 ± 0.8 ka	Lower Hope Valley, Glynn Wye Terrace M32 N 584449 / E 246335, 617 m	silt (feldspar)	fine sand and silt over aggradational gravel	Dates loess deposition and abondonment of LGM floodplain level	this study
WLL-413	IRSL	10.2 ± 0.8 a	Hope Valley terrace above Glynn Wye gorge, M32 N 584577 / E 246830, 554 m	silt (feldspar)	fine sand and silt over degradational gravel	Dates loess deposition and abondonment of floodplain level	this study
WLL-422	IRSL	110.5 ± 10.6 ka	Hope Valley, east of Manuka Stream M32 N584403 / E 247221, 620	silt (feldspar)	Sand lens within fluvial gravel	Dates Horseshoe glaciation gravels	this study

Appendix 3: Compilation of age control for deposits >8 ka BP from absolute dating
(Hope-Waiau, Waimakariri, Rakaia, Rangitata Valleys, and Mackenzie Basin)

Hope-Waiau Valleys (continued)

Lab code	Dating technique	Date (a BP) (old T½)	Locality, grid reference and altitude	Material dated	Stratigraphic position	Significance	Collector, reference
WLL-423	IRSL	89.3 ± 5.0 ka	Glynn Wye Stream M32 N 584609, E 246924, 410 m	silt (feldspar)	lacustrine sand wiithin alluvial gravel	Dates small paleolake and aggradation	this study
B-1936	^{10}Be SED	18.6 ± 1.7 ka	Glynn Wye Moraine M32 N 584339 / E 246254, 640 m	Greywacke (quartz)	Boulder on moraine ridge	Dates glacial moraine, rescession	this study
B-1917	^{10}Be SED	12.8 ± 2.8 ka	Glynn Wye Moraine M32 N 584339 / E 246254, 645 m	Greywacke (quartz)	Boulder on moraine ridge	Dates glacial moraine, rescession	this study
B-1942	^{10}Be SED	19.2 ± 2.0 ka	Glynn Wye Moraine M32 N 584339 / E 246254, 647 m	Greywacke (quartz)	Boulder on moraine ridge	Dates glacial moraine, rescession	this study
B-1927	^{10}Be SED	15.5 ± 1.2 ka	Glynn Wye Moraine M32 N 584339 / E 246254, 640 m	Greywacke (quartz)	Boulder on moraine ridge	Dates glacial moraine, rescession	this study
B-1937	^{10}Be SED	17.6 ± 1.3 ka	Lewis Pass moraine M31 N 586975 / E 246066, 870 m	Greywacke (quartz)	Boulder on moraine ridge	Dates glacial moraine, rescession	this study
B-1928	^{10}Be SED	16.5 ± 1.6 ka	Lewis Pass moraine M31 N 586983 / E 246063, 875 m	Greywacke (quartz)	Boulder on moraine ridge	Dates glacial moraine, rescession	this study
B-1924	^{10}Be SED	23.4 ± 1.7 ka	Kakapo Hill moraine M32 N 584362 / E 246745, 830 m	Greywacke (quartz)	Boulder on moraine ridge	Dates glacial moraine, rescession	this study
NZ-3969	^{14}C	13,000 ± 200 a	Quenn Mary Hospital, Hanmer Springs S54/193784, 360 m	peat	Peat between 5.1 and 5.5 m depth below surface	Cool climate organic accumulation, herbaceous vegetation	Moar (1980)

Appendix 3: Compilation of age control for deposits >8 ka BP from absolute dating
(Hope-Waiau, Waimakariri, Rakaia, Rangitata Valleys, and Mackenzie Basin)

Waimakariri Valley

Lab code	Dating technique	Date (a BP) (old T½)	Locality, grid reference and altitude	Material dated	Stratigraphic position	Significance	Collector, reference
NZ-5287	^{14}C	13,750 ± 200 a	Kettlehole Bog, 500 m SE of Lake Sarah, L 34 E 24109 N 57941, 579 m	lacustrine detrital mud	Sample from basal section of bog 4.30 m below surface	Minimum age of deglaciation	Burrows (1983)
NZ-1076	^{14}C	8,250 ± 450 a	Kettlehole Bog, 500 m SE of Lake Sarah, L 34 E 24109 N 57941, 579 m	lacustrine detrital mud	sample from ca. 1.8 m core depth from lacustrine mud	Dates dominaent podocarp forest	Moar (1977)
NZ-5295	^{14}C	13,200 ± 250 a	Cass River cut on West bank below Mt. Misery, K 34 E 2406 N 5795, 625 m	organic detritus	Organic layer in laminated silts, clay, and sands which underlie fan gravel, sample from 1.5 m above river	lacustrine silts possibly representing 'Glacial Lake Cass' Gage (1958, 1977) ; Burrows (1983)	Burrows (1983)
WLL-31	IRSL	14.0 ± 0.6 ka	Blackwater outwash adjacent to SH 73	silt	Gravely loess overlying Blackwater-1 outwash	Dates loess on 'Blackwater-1' surface, minimum age for outwash surface	Bell (unpubl) Rieser (2001)
WLL-32	IRSL	17.0 ± 0.9 ka	Blackwater outwash adjacent to SH 73 same as WLL-31 but further into bank	silt	Gravely loess overlying Blackwater-1 outwash	same as above	Bell (unpubl) Rieser (2001)
WLL-34	IRSL	14.3 ± 0.9 ka	near confluence of Winding Creek / Broken River	silt	Gravelly loess on Blackwater-1 outwash	Dates loess on 'Blackwater-1' surface, minimum age for outwash surface	Bell (unpubl) Rieser (2001)
WLL-35	IRSL	20.7 ± 1.0 ka	cutting on Flock Hill - Avoca road	silt	Loess-colluvium draped on Blackwater-2 lateral moraine	Minimum age for 'Blackwater-2' outwash	Bell (unpubl) Rieser (2001)
NZ-1906	^{14}C	9,800 ± 200 a	Poulter River, south bank, L 33 E24135 N58165, 640 m	wood	Wood from buried soil buried under 18 m of alluvium	Dates period of warming (soil) and slope stability	Burrows et al. (1976)
Birm-523	^{14}C	8,960 ± 140 a	Arthurs Pass Summit K 33 E23923 N58097, 914 m	peat	Peat over sand/silt over till	Minimum age for deglaciation and climatic amelioration	Burrows et al. (1976)
NZ-1903	^{14}C	8,090 ± 110 a	Taruahuna Pass, K 33 E24019 N58117, 1219 m	peat	Alluvium overlain by peat and laminated lake silts	Dates a mild period before glacial advance from side valley dammed a lake depositing silts over peat	Burrows et al. (1976)

Appendix 3: Compilation of age control for deposits >8 ka BP from absolute dating
(Hope-Waiau, Waimakariri, Rakaia, Rangitata Valleys, and Mackenzie Basin)

Waimakariri Valley (continued)

Lab code	Dating technique	Date (a BP) (old T½)	Locality, grid reference and altitude	Material dated	Stratigraphic position	Significance	Collector, reference
NZ-1910	^{14}C	9,500 ± 100 a	upper Waimakariri, K33 N2383 N5803, 807 m	wood	Wood from peat layer within alluvium	Dates mild period prior to alluvial aggradation (White Glacier advance?)	Burrows et al. (1976)
NZ-7518	^{14}C	37,000 ± 200 a	N of Broken River bridge K 34 E 23072 N 57784, 670 m	organic silts from buried soil	Soil above rusty alluvium above Miocene sands,	Sample dates approximate onset of Blackwater 1 aggradation	C. Burrows & N.T. Moar (1996)
NZ-98	^{14}C	10,200 ± 120 a	Rubicon River L 35 E2416 N 5765 or 66, 550 m	wood in peat	Peat below aggradational deposit	pre-dates Late Otiran aggradation	Burrows (1979)
NZ-1391	^{14}C	12,750 ± 210 a	Rubicon Creek, northern bank S74/338832	organic beds	0.75 m above stream bed	pre-dates Late Otiran aggradation	Moar & Lintott (1977)
NZ-1392	^{14}C	14,100 ± 240 a	Rubicon Creek, northern bank, S74/338832	organic beds	2.4 m above stream bed	pre-dates Late Otiran aggradation	Moar & Lintott (1977)
NZ-1	^{10}Be SED	12,050 ± 960 a	Lake Misery Moraines, Arthurs Pass K33 N58109 / E 23922, 920 m	Greywacke (quartz)	Boulder on moraine ridge	Dates late glacial re-advance	Ivy-Ochs et al. 1999
NZ-2	^{10}Be SED	12,420 ± 1180 a	Lake Misery Moraines, Arthurs Pass K33 N58109 / E 23922, 920 m	Greywacke (quartz)	Boulder on moraine ridge	Dates late glacial re-advance	Ivy-Ochs et al. 1999
NZ-3	^{10}Be SED	9,300 ± 990 a	Lake Misery Moraines, Arthurs Pass K33 N58109 / E 23922, 920 m	Greywacke (quartz)	Boulder on moraine ridge	Dates late glacial re-advance	Ivy-Ochs et al. 1999
NZ-4	^{10}Be SED	11,000 ± 1360 a	Lake Misery Moraines, Arthurs Pass K33 N58109 / E 23922, 920 m	Greywacke (quartz)	Boulder on moraine ridge	Dates late glacial re-advance	Ivy-Ochs et al. 1999
NZ-5	^{10}Be SED	11,410 ± 1030 a	Lake Misery Moraines, Arthurs Pass K33 N58109 / E 23922, 920 m	Greywacke (quartz)	Boulder on moraine ridge	Dates late glacial re-advance	Ivy-Ochs et al. 1999
Wk-18073	^{14}C	14,070 ± 86 a	Lake Hawdon L34 N578865 / E 241635, 600 m	organic silts	Basal age from core at 4.5 m depth	Minimum age of deglaciation and begin of organic sedimentation	Woodward (unpubl.)

Appendix 3: Compilation of age control for deposits >8 ka BP from absolute dating
(Hope-Waiau, Waimakariri, Rakaia, Rangitata Valleys, and Mackenzie Basin)

Waimakariri Valley (continued)

Lab code	Dating technique	Date (a BP) (old T½)	Locality, grid reference and altitude	Material dated	Stratigraphic position	Significance	Collector, reference
Wk-18074	^{14}C	12,957 ± 77 a	Lake Hawdon L34 N578865 / E 241635, 600 m	organic silts	Sample from core at 4.4 m depth	Minimum age of deglaciation and begin of organic sedimentation	Woodward (unpubl.)
UB-6554	^{14}C	13,689 ± 73 a	Lake Hawdon L34 N578865 / E 241635, 600 m	organic silts	Basal age from core 4.5 m depth	Minimum age of deglaciation and begin of organic sedimentation	Whitehouse (unpubl)
NZ - 94	^{14}C	>45,000 a	Joyce Stream S74 393866, 340 m	wood	Peat below fluvial and morainic gravels	Dates interglacial conditions	Moar & Gage (1973)

Rakaia Valley

Lab code	Dating technique	Date (a BP) (old T½)	Locality, grid reference and altitude	Material dated	Stratigraphic position	Significance	Collector, reference
NZ-3940	^{14}C	22,200 ± 750 a	S bank of Lyndon Stream, K35 E 24027 / N 57628; 780 m	plant fragments (leaves)	Blue silts over till	lacustrine deposits in channel-cut of Bayfield 2, representing intermediate period prior to Bayfield 3 advance	Soons & Burrows (1978)
NZ-4298	^{14}C	19,200 ± 550 a	sames as above, 140 m further west; 790 m	plant fragments	Brown silts overlaying blue silts and till	same as above	Soons & Burrows (1978)
NZ-1290	^{14}C	11,650 ± 200 a	Acheron River K35 E 2394 / N 5755; 365 m	organic fragments	Laminated sand, silt below alluvial gravel; sequence underlain by till	Glacial lake during retreat of Acheron 2	Burrows, in: Soons & Gullentops (1973)
NZ-1652	^{14}C	11,900 ± 200 a	Quagmire Tarn 2 km S of Prospect Hill J35 N 57633 / E 23576, 750 m	organic mud	Organic silts above inorganic mud in tarn	Minimum age for deglaciation	Burrows & Russel (1975)
NZ-1653	^{14}C	10,000 ± 150 a	same as above	organic mud	Organic silt above inorganic silt and sand	NZ-1652 and NZ-1653 bracket Lake Stream Advance'	Burrows & Russel (1975)

Appendix 3: Compilation of age control for deposits >8 ka BP from absolute dating
(Hope-Waiau, Waimakariri, Rakaia, Rangitata Valleys, and Mackenzie Basin)

Rakaia Valley (continued)

Lab code	Dating technique	Date (a BP) (old T½)	Locality, grid reference and altitude	Material dated	Stratigraphic position	Significance	Collector, reference
NZ-4484	^{14}C	9,480 ± 130 a	Meins Knob Ridge J 35 E2341 / N 5766; ca. 1250 m	peat	Sample from basal peat bog 1.34 m depth	Dates organic accumulation, minimum age deglaciation	Burrows & Russel (1990)
BHL-5 (field code)	TL	11,700 ± 1,900 a	Barrhill, ca. 10 km upstream from State Highway 1 Rakaia bridge	silt	Fine sand 3.25 m below surface	Loess overlies Burnham formation	Berger et al. (1996)
NZA-8125	^{14}C	35,170 ± 580 a	West bank of Rakaia River K35 E 24013 / N 57408; 310 m	organic fragments (plant material)	Sample from near the base of Bayfield (Burnham) gravels 40 m above river level	Dates onset of Burnham aggradation	Bal & Browne (1997)
WLL-33	IRSL	18,100 ± 1,700 a	North bank of Lyndon Stream; K35 E 2402 / N 5763, 770 m	silt	Grey lacustrine silts deposited in channel cut of Bayfield 2 surface	Dates intermediate (recessional) period prior to Bayfield 3 advance	Bell D.H., Grapes, R. 1998 (unpubl.)
WLL-389	IRSL	9, 720± 750 a	Landslide deposit SE of Ryton River, K35 E 2391 N 5768, ca. 570 m	silt	Loess overlying till buried by landslide	Dates landslide and provides minimum age for deglaciation	Lee,J.,Bell, D (2004) (unpubl.)
WLL-ZZ-1	IRSL	36,400± 2,800 a	Zig-Zag quarry K35 N 5745 / E 2402	silt	Collapsed glaciofluvial deposits in Kettlehole	Dates proglacial sedimentation	Shulmeister (2005) (unpubl)
WLL-ZZ-2	IRSL	38,700± 1,000 a	Zig-Zag quarry K35 N 5745 / E 2402	silt	Collapsed glaciofluvial deposits in Kettlehole	Dates proglacial sedimentation	Shulmeister (2005) (unpubl)
WLL-ZZ-3	IRSL	52,500± 1,000 a	Zig-Zag quarry K35 N 5745 / E 2402	silt	Collapsed glaciofluvial deposits in Kettlehole	Dates proglacial sedimentation	Shulmeister (2005) (unpubl)
?	^{10}Be SED	12.7 ka	Prospect Hill J35 N 5765 / E 2357, 660 m	Greywacke (Quartz)	Glacial erratic	Dates late glacial readvance	Easterbrook, D INQUA (2003)
LC-1A	^{14}C	17,800 ± 95 a	S bank of Lyndon Stream, K35 E 24027 / N 57628; 780 m	organic silts	Lacustrine silts in terrace	Dates intermediate (recessional) period prior to Bayfield 3 advance	Vandergoes, M (unpubl.)
LC-2b(1)	^{14}C	20,700 ± 75 a	S bank of Lyndon Stream, K35 E 24027 / N 57628; 780 m	organic silts	Lacustrine silts in terrace	Dates intermediate (recessional) period prior to Bayfield 3 advance	Vandergoes, M (unpubl.)

Appendix 3: Compilation of age control for deposits >8 ka BP from absolute dating
(Hope-Waiau, Waimakariri, Rakaia, Rangitata Valleys, and Mackenzie Basin)

Rakaia Valley (continued)

Lab code	Dating technique	Date (a BP) (old T½)	Locality, grid reference and altitude	Material dated	Stratigraphic position	Significance	Collector, reference
LC-2b(2)	^{14}C	20,600 ± 85 a	S bank of Lyndon Stream, K35 E 24027 / N 57628; 780 m	organic silts	Lacustrine silts in terrace	Dates intermediate (recessional) period prior to Bayfield 3 advance	Vandergoes, M (unpubl.)
LC-3b	^{14}C	25,000 ± 150 a	S bank of Lyndon Stream, K35 E 24027 / N 57628; 780 m	organic silts	Lacustrine silts in terrace	Dates intermediate (recessional) period prior to Bayfield 3 advance	Vandergoes, M (unpubl.)
WLL-491	IRSL	181.6 ± 14.5 ka	Rakaia Gorge K35 N 5742 / E 2400, 270 m	sand / silt	Lake silts near river level	Dates paleo-lake	Shulmeister (2005) (unpubl)
WLL-492	IRSL	144.7 ± 13.8 ka	Rakaia Gorge K35 N 5742 / E 2400, 270 m	sand / silt	Lake silts near river level	Dates paleo-lake	Shulmeister (2005) (unpubl)
WLL-487	IRSL	173.5 ± 18.2 ka	Montrose outcrop K35 N 5745 / E 2398, 320 m	sand / silt	Cross laminated silt and sand over matrix supported gravel	Proglacial / ice proximal fluvial deposition	Shulmeister (2005) (unpubl)
WLL-490	IRSL	168.4 ± 15.6 ka	Montrose oucrop K 35 N 5747 / E 2396,	sand / silt	Matrix supported gravel above silt / sand	Proglacial / ice proximal deposition	Shulmeister (2005) (unpubl)
WLL-497	IRSL	79.4 ± 5.6 ka	Montrose outcrop K 35 N 5747 / E 2396,	sand / silt	Cross laminated sand above diamicton	Proglacial fluvial deposition	Shulmeister (2005) (unpubl)
WLL-518	IRSL	151.6 ± 9.8 ka	Cleardale K35 N 5751 / 2394	sand / silt	Interbedded gravel and sandy silt	Proglacial / ice proximal deposition	Shulmeister (2005) (unpubl)
WLL-519	IRSL	92.2 ± 5.1 ka	Cleardale K35 N 5751 / 2394	sand / silt	laminated and cross-bedded sand and silt	Proglacial fluvial / lacustrine deposition	Shulmeister (2005) (unpubl)
WLL-487	IRSL	100.6 ± 8.7 ka	Acheron Bank K35 N5755 / E 2393	sand / silt	Bedded silt over matrix supported angular gravels	Proglacial lacustrine deposition	Shulmeister (2005) (unpubl)
WLL-513	IRSL	48.3 ± 2.5 ka	Acheron Bank K35 N5755 / E 2393	sand / silt	Laminate silts	Proglacial / ice proximal deposition	Shulmeister (2005) (unpubl)

Appendix 3: Compilation of age control for deposits >8 ka BP from absolute dating
(Hope-Waiau, Waimakariri, Rakaia, Rangitata Valleys, and Mackenzie Basin)

Rakaia Valley (continued)

Lab code	Dating technique	Date (a BP) (old T½)	Locality, grid reference and altitude	Material dated	Stratigraphic position	Significance	Collector, reference
WLL-520	IRSL	11.36 ± 0.74 ka	Acheron Bank K35 N5755 / E 2393	sand / silt	Surface forming cover sand	Loess deposition	Shulmeister (2005) (unpubl)
NZ - 484	^{14}C	>39,000 ± 350 a	Front of moraine in upper Selwyn River, S74 / 196668	organic silt	Within angular gravel on front of moraine.	Minimum age of moraine	Grant-Taylor & Rafter (1971)
NZ - 4265	^{14}C	12,950 ± 200 a	200 m upstream from Lyndon Stream site (NZ-3940), S74/ 156807	organic silt	4 m above Lyndon Stream	Organic deposition	Moar (1980)

Rangitata

Lab code	Dating technique	Date (a BP) (old T½)	Locality, grid reference and altitude	Material dated	Stratigraphic position	Significance	Collector, reference
NZ - 5406A	^{14}C	9,780 ± 140 a	2.5 km upstream of Rangitata gorge J36 N 5717 / E 2363, 410 m	leaves and twigs	Lacustrine mud below gravels and loess sample from 3.5 m above river level	Dates paleo-lake	Mabin (1987)
NZ - 4772	^{14}C	9,730 ± 190 a	Synclair Plateau, Clyde River J35 N 57537 / E 23316, 990 m	organic mud	Basal sediment in bog beside tarn 2.8 - 3.2 m below surface	Minimal age for recession of Clyde Glacier	Burrows (1988)
NZA-15192	^{14}C	12624 ± 75 a	upper Rangitata Valley, J36 N 57366 / E 23358, 540 m	leaf litter	Buried soil below fan	Dates organic accumulation and deglaciation	Forsyth et al. (2003)
Wk-10870	^{14}C	8352 ± 60 a	upper Rangitata Valley, J36 N 57366 / E 23358, 540 m	log	Buried soil in / below fan	Dates organic accumulation and deglaciation	Forsyth et al. (2003)
Wk-10871	^{14}C	8578 ± 78 a	upper Rangitata Valley, J36 N 57366 / E 23358, 540 m	peat	Buried soil in / below fan	Dates organic accumulation and deglaciation	Forsyth et al. (2003)
Wk-10872	^{14}C	12552 ± 133 a	upper Rangitata Valley, J36 N 57366 / E 23358, 540 m	peat	Buried soil in / below fan	Dates organic accumulation and deglaciation	Forsyth et al. (2003)

Appendix 3: Compilation of age control for deposits >8 ka BP from absolute dating
(Hope-Waiau, Waimakariri, Rakaia, Rangitata Valleys, and Mackenzie Basin)

Rangitata (continued)

Lab code	Dating technique	Date (a BP) (old T½)	Locality, grid reference and altitude	Material dated	Stratigraphic position	Significance	Collector, reference
Wk-10873	^{14}C	8603 ± 71 a	upper Rangitata Valley, J36 N 57366 / E 23358, 540 m	peat	Buried soil in / below fan	Dates organic accumulation and deglaciation	Forsyth et al. (2003)
Wk-10874	^{14}C	8520 ± 63 a	upper Rangitata Valley, J36 N 57366 / E 23358, 540 m	wood	Buried soil in / below fan	Dates organic accumulation and deglaciation	Forsyth et al. (2003)
NZA-6394	^{14}C	10504±356 cal a	upper Rangitata Valley	organic matter	Buried soil	dates warm pahse and gives minimum age of local ice retreat	Barrell et al. (1996)
NZ-6288	^{14}C	11,340 ± 350 a	Craig Philips, Mt. Potts Station J36 3399374	organic silts	Sample from kettle hole	Minimum age for deglaciation	Burrows (1988)
NZ-688	^{14}C	9,520 ± 95 a	Cameron Valley J 35 E 2352 / N 5755; ca. 1000 m	wood from buried soil	Soil above fluvial gravel and till and below alluvial fan gravel	Soil postdates the Wildman 2 moraine	Burrows (1975)
NZ-1288	^{14}C	9,140 ± 150 a	Cameron Valley near Lochiel Stream J 35 E 2352 / N 5755; 975 m	wood	Buried soil	Dates organic accumulation and local deglaciation	Burrows (1975)

Mackenzie Basin

Lab code	Dating technique	Date (a BP) (old T½)	Locality, grid reference and altitude	Material dated	Stratigraphic position	Significance	Collector, reference
?	^{10}Be SED	27.8 ± 2.5 a	outer Pukaki Moraine H38 N 5662 / E 2285, 510 m	Greywacke / Quartz	Boulder on moraine crest	Dates ice position	Schaefer et al. (2001)
?	^{10}Be SED	18.0 ± 2.0 a	inner Pukaki Moraine H38 N 5665 / E 2384, 580 m	Greywacke / Quartz	Boulder on moraine crest	Dates ice position	Schaefer et al. (2001)
NZ-6473	^{14}C	8,687 ± 101 a	Macaulay River, upper Tekapo	wood	Wood buried by colluvium	Dates warm phase organic accumulation	Burrows et al. (1990)

Appendix 3: Compilation of age control for deposits >8 ka BP from absolute dating
(Hope-Waiau, Waimakariri, Rakaia, Rangitata Valleys, and Mackenzie Basin)

Mackenzie Basin (continued)

Lab code	Dating technique	Date (a BP) (old T½)	Locality, grid reference and altitude	Material dated	Stratigraphic position	Significance	Collector, reference
NZ-1651	^{14}C	11,650 ± 200 a	Tasman Valley	wood	?	Minimum age for ice recession from site	Burrows (1975)
?	^{14}C	36,400 ± 3,150 a	Balmoral moraine east of Mary Range	plant matter	wood fragments in Balmoral till	Minimum age of ice advance	Mansergh (1973) Suggate (1990)
?	^{14}C	34,100 ± 2750 a	Balmoral moraine east of Mary Range	peat	peat between till of Mt John and Balmoral	Minimum age of ice advance	Suggate (1990)
NZ-4508	^{14}C	7,940 ± 70 a	Black Birch Creek Sebastopol (Mt. Cook) 43.45˚ S / 170. 06˚ E, 700 m	wood	wood (in till?)	Dates ice advance in steep tributary valley	Burrows & Gellatly (1982)
HV-10504	^{14}C	8,040 ± 70 a	Black Birch Creek Sebastopol (Mt. Cook) 43.45˚ S / 170.06˚ E, 700 m	wood	wood (in till?)	Dates ice advance in steep tributary valley	Roethlisberger (1987)
NZ-548	^{14}C	8,460 ± 120 a	Macaulay River, upper Tekapo, below jct. with Tom Creek	wood	peat on fan that is overlain by moraine	Dates ice advance	Grant-Taylor & Rafter (1971)
?	^{14}C	11,950 ± 200 a	South end Lake Tekapo, near township	wood	wood in lacustrine mud within Tekapo lobe	Minimum age of Tekapo retreat	Mansergh (1973)
NZ-4541	^{14}C	13,500 ± 250 a	Mt Cook Station Road, S89/847097	wood	Peat from ponded hollow behind kame ridge	Minimum age of ice reteat	Moar (1980)

PRESENT **Snowfall at ELA**	**Precipitation distribution and snow proportion at the 1600 m ELA ; annual precipitation 9000mm**												
	May	**Jun**	**Jul**	**Aug**	**Sep**	**Oct**	**Nov**	**Dec**	**Jan**	**Feb**	**Mar**	**Apr**	**year**
Monthly precip. distrib. (%)*	7	5.3	5.6	4.9	8.7	13.8	12.5	6.6	4.9	5.8	11	13.9	**100%**
Precipitaion at ELA (mm)	630	477	504	441	783	1242	1125	594	441	522	990	1251	**9000mm**
T (°C) Hokitika (39m asl)**	9.8	7.9	7.3	8.3	9.8	11.1	12.8	14.4	15.4	15.8	15	12.6	**11.7°C**
T (°C) at ELA (1600m asl)	0.4	-1.5	-2.1	-1.1	0.4	1.7	3.4	5.0	6.0	6.4	5.6	3.2	**2.3°C**
(lapse rate: 0.6°C/100m)													
% snow at 1600m***	60.8	71.1	74.3	68.9	60.8	53.7	44.5	35.9	30.4	28.3	32.6	45.6	
y = -5.6818x + 63.636													
snow mm (present)	383.0	339.1	374.5	303.8	476.1	667.0	500.6	213.2	134.1	147.7	322.7	570.5	**4432mm**

* distribution data from Ivory Glacier case study, see reference 22, pg. 75
** nearest climate station providing long term monthly and daily data
*** regression for monthly snow-rain proportions based on monthly mean temperatures. See reference 21, pg. 129.

Precipitation scenarios

Scenario 1

Temp. change in °C (annual)	**0**	**-1**	**-2**	**-3**	**-4**	**-5**	**-6**	**-7**	**-8**	**-9**
Annual temp. at ELA (1600m) (°C)	2.3	1.3	0.3	-0.7	-1.7	-2.7	-3.7	-4.7	-5.7	-6.7
Saturation Vapour Press. (mb)	7.20	6.71	6.24	5.80	5.39	5.01	4.65	4.31	3.99	3.70
% change to present	0.0	-6.8	-13.3	-19.4	-25.1	-30.4	-35.4	-40.1	-44.6	-48.6
Annual precipitation (mm)	**9000**	**8388**	**7800**	**7250**	**6738**	**6263**	**5813**	**5388**	**4988**	**4625**

Scenario 2

Temp. change in °C (annual)	**0**	**-1**	**-2**	**-3**	**-4**	**-5**	**-6**	**-7**	**-8**	**-9**
Annual temp. at ELA (1600m) (°C)	2.3	1.3	0.3	-0.7	-1.7	-2.7	-3.7	-4.7	-5.7	-6.7
Saturation Vapour Press. (mb)	7.20	6.71	6.24	5.80	5.39	5.01	4.65	4.31	3.99	3.70
0.5 x (% change to present)	0.0	-3.4	-6.7	-9.7	-12.6	-15.2	-17.7	-20.1	-22.3	-24.4
Annual precipitation (mm)	**9000**	**8694**	**8400**	**8125**	**7869**	**7631**	**7406**	**7194**	**6994**	**6813**

Scenario 3

Temp. change in °C (annual)	**0**	**-1**	**-2**	**-3**	**-4**	**-5**	**-6**	**-7**	**-8**	**-9**
Annual temp. at ELA (1600m) (°C)	2.3	1.3	0.3	-0.7	-1.7	-2.7	-3.7	-4.7	-5.7	-6.7
Annual precipitation (mm)	**9000**	**9000**	**9000**	**9000**	**9000**	**9000**	**9000**	**9000**	**9000**	**9000**

1°C cooling

Annual total precipitation: 8388mm (-6.8%)

	May	Jun	Jul	Aug	Sep	Oct	Nov	Dec	Jan	Feb	Mar	Apr	year
Monthly temperature (-1°C)	-0.6	-2.5	-3.1	-2.1	-0.6	0.7	2.4	4.0	5.0	5.4	4.6	2.2	1.3°C
% snow*	67	78	81	75	67	59	50	41	35	33	37	51	
Monthly total precipitation	587	445	470	411	730	1158	1049	554	411	487	923	1166	8388mm
Snow (mm water equivalent)	393	345	381	310	488	688	522	225	144	159	344	594	**4594mm**

* regression for monthly snow-rain proportions based on monthly mean temperatures. see: Sevruk, B., (ed.) 1992.

Annual total precipitation: 8694mm (-3.4%)

	May	Jun	Jul	Aug	Sep	Oct	Nov	Dec	Jan	Feb	Mar	Apr	year
Monthly temperature (-1°C)	-0.6	-2.5	-3.1	-2.1	-0.6	0.7	2.4	4.0	5.0	5.4	4.6	2.2	1.3°C
% snow	67	78	81	75	67	59	50	41	35	33	37	51	
Monthly total precipitation	609	461	487	426	756	1200	1087	574	426	504	956	1208	8694mm
Snow (water equivalent)	407	358	395	321	506	713	541	234	149	165	357	616	**4761mm**

Annual total precipitation: 9000mm

	May	Jun	Jul	Aug	Sep	Oct	Nov	Dec	Jan	Feb	Mar	Apr	year
Monthly temperature (-1°C)	-0.6	-2.5	-3.1	-2.1	-0.6	0.7	2.4	4.0	5.0	5.4	4.6	2.2	1.3°C
% snow	67	78	81	75	67	59	50	41	35	33	37	51	
Monthly total precipitation	630	477	504	441	783	1242	1125	594	441	522	990	1251	9000mm
Snow (water equivalent)	421	370	409	332	523	739	560	242	154	171	369	637	**4929mm**

2°C cooling

Annual total precipitation: 7800mm (-13.3%)

	May	Jun	Jul	Aug	Sep	Oct	Nov	Dec	Jan	Feb	Mar	Apr	year
Monthly temperature (-2°C)	-1.6	-3.5	-4.1	-3.1	-1.6	-0.3	1.4	3.0	4.0	4.4	3.6	1.2	0.3°C
% snow	73	83	87	81	73	65	55	46	41	38	43	57	
Monthly total precipitation	546	413	437	382	679	1076	975	515	382	452	858	1084	7800mm
Snow (mm water equivalent)	396	344	379	310	492	701	541	239	156	174	369	614	**4714mm**

Annual total precipitation: 8400mm (-6.7%)

	May	Jun	Jul	Aug	Sep	Oct	Nov	Dec	Jan	Feb	Mar	Apr	year
Monthly temperature (-2°C)	-1.6	-3.5	-4.1	-3.1	-1.6	-0.3	1.4	3.0	4.0	4.4	3.6	1.2	0.3°C
% snow	73	83	87	81	73	65	55	46	41	38	43	57	
Monthly total precipitation	588	445	470	412	731	1159	1050	554	412	487	924	1168	8400mm
Snow (water equivalent)	426	371	408	334	530	755	583	257	168	187	397	661	**5078mm**

Annual total precipitation: 9000mm

	May	Jun	Jul	Aug	Sep	Oct	Nov	Dec	Jan	Feb	Mar	Apr	year
Monthly temperature (-2°C)	-1.6	-3.5	-4.1	-3.1	-1.6	-0.3	1.4	3.0	4.0	4.4	3.6	1.2	0.3°C
% snow	73	83	87	81	73	65	55	46	41	38	43	57	
Monthly total precipitation	630	477	504	441	783	1242	1125	594	441	522	990	1251	9000mm
Snow (water equivalent)	457	397	437	357	568	809	624	276	180	201	426	708	**5440mm**

3°C cooling

Annual total precipitation: 7250mm (-19.4%)

	May	Jun	Jul	Aug	Sep	Oct	Nov	Dec	Jan	Feb	Mar	Apr	year
Monthly temperature (-3°C)	-2.6	-4.5	-5.1	-4.1	-2.6	-1.3	0.4	2.0	3.0	3.4	2.6	0.2	-0.7°C
% snow	78	89	92	87	78	71	61	52	46	44	49	62	
Monthly total precipitation	508	384	406	355	631	1001	906	479	355	421	798	1008	7250mm
Snow (water equivalent)	397	342	375	308	493	709	554	249	165	186	388	628	**4794mm**

Annual total precipitation: 8125mm (-9.7%)

	May	Jun	Jul	Aug	Sep	Oct	Nov	Dec	Jan	Feb	Mar	Apr	year
Monthly temperature (-3°C)	-2.6	-4.5	-5.1	-4.1	-2.6	-1.3	0.4	2.0	3.0	3.4	2.6	0.2	-0.7°C
% snow	78	89	92	87	78	71	61	52	46	44	49	62	
Monthly total precipitation	569	431	455	398	707	1121	1016	536	398	471	894	1129	8125mm
Snow (water equivalent)	445	383	421	345	553	794	621	279	185	208	435	704	**5373mm**

Annual total precipitation: 9000mm

	May	Jun	Jul	Aug	Sep	Oct	Nov	Dec	Jan	Feb	Mar	Apr	year
Monthly temperature (-3°C)	-2.6	-4.5	-5.1	-4.1	-2.6	-1.3	0.4	2.0	3.0	3.4	2.6	0.2	-0.7°C
% snow	78	89	92	87	78	71	61	52	46	44	49	62	
Monthly total precipitation	630	477	504	441	783	1242	1125	594	441	522	990	1251	9000mm
Snow (water equivalent)	493	425	466	383	612	880	688	309	205	230	482	779	**5952mm**

4°C cooling

Annual total precipitation: 6738mm (-25.1%)

	May	Jun	Jul	Aug	Sep	Oct	Nov	Dec	Jan	Feb	Mar	Apr	year
Monthly temperature (-4°C)	-3.6	-5.5	-6.1	-5.1	-3.6	-2.3	-0.6	1.0	2.0	2.4	1.6	-0.8	-1.7°C
% snow	84	95	98	92	84	77	67	58	52	50	54	68	
Monthly total precipitation	472	357	377	330	586	930	842	445	330	391	741	937	6738mm
Snow (water equivalent)	396	338	370	305	492	711	563	257	172	195	403	637	**4838mm**

Annual total precipitation: 7869mm (-12.6%)

	May	Jun	Jul	Aug	Sep	Oct	Nov	Dec	Jan	Feb	Mar	Apr	year
Monthly temperature (-4°C)	-3.6	-5.5	-6.1	-5.1	-3.6	-2.3	-0.6	1.0	2.0	2.4	1.6	-0.8	-1.7°C
% snow	84	95	98	92	84	77	67	58	52	50	54	68	
Monthly total precipitation	551	417	441	386	685	1086	984	519	386	456	866	1094	7869mm
Snow (water equivalent)	462	395	432	356	574	831	658	300	201	227	470	744	**5651mm**

Annual total precipitation: 9000mm

	May	Jun	Jul	Aug	Sep	Oct	Nov	Dec	Jan	Feb	Mar	Apr	year
Monthly temperature (-4°C)	-3.6	-5.5	-6.1	-5.1	-3.6	-2.3	-0.6	1.0	2.0	2.4	1.6	-0.8	-1.7°C
% snow	84	95	98	92	84	77	67	58	52	50	54	68	
Monthly total precipitation	630	477	504	441	783	1242	1125	594	441	522	990	1251	9000mm
Snow (water equivalent)	529	452	494	408	657	950	752	343	230	260	538	851	**6463mm**

5°C cooling

Annual total precipitation: 6263mm (-30.4%)

	May	Jun	Jul	Aug	Sep	Oct	Nov	Dec	Jan	Feb	Mar	Apr	year
Monthly temperature (-5°C)	-4.6	-6.5	-7.1	-6.1	-4.6	-3.3	-1.6	0.0	1.0	1.4	0.6	-1.8	-2.7°C
% snow	90	100	100	98	90	82	73	63	58	55	60	74	
Monthly total precipitation	438	332	351	307	545	864	783	413	307	363	689	871	6263mm
Snow (water equivalent)	393	332	351	301	488	710	568	262	177	202	414	641	**4838mm**

Annual total precipitation: 7631mm (-15.2%)

	May	Jun	Jul	Aug	Sep	Oct	Nov	Dec	Jan	Feb	Mar	Apr	year
Monthly temperature (-5°C)	-4.6	-6.5	-7.1	-6.1	-4.6	-3.3	-1.6	0.0	1.0	1.4	0.6	-1.8	-2.7°C
% snow	90	100	100	98	90	82	73	63	58	55	60	74	
Monthly total precipitation	534	404	427	374	664	1053	954	504	374	443	839	1061	7631mm
Snow (water equivalent)	479	404	427	367	595	866	692	320	216	246	504	781	**5896mm**

Annual total precipitation: 9000mm

	May	Jun	Jul	Aug	Sep	Oct	Nov	Dec	Jan	Feb	Mar	Apr	year
Monthly temperature (-5°C)	-4.6	-6.5	-7.1	-6.1	-4.6	-3.3	-1.6	0.0	1.0	1.4	0.6	-1.8	-2.7°C
% snow	90	100	100	98	90	82	73	63	58	55	60	74	
Monthly total precipitation	630	477	504	441	783	1242	1125	594	441	522	990	1251	9000mm
Snow (water equivalent)	564	477	504	433	701	1021	816	377	255	290	594	922	**6953mm**

6°C cooling

Annual total precipitation: 5813mm (-35.4%)

	May	Jun	Jul	Aug	Sep	Oct	Nov	Dec	Jan	Feb	Mar	Apr	year
Monthly temperature (-6°C)	-5.6	-7.5	-8.1	-7.1	-5.6	-4.3	-2.6	-1.0	0.0	0.4	-0.4	-2.8	-3.7°C
% snow	95	100	100	100	95	88	78	69	63	61	66	79	
Monthly total precipitation	407	308	326	285	506	802	727	384	285	337	639	808	5813mm
Snow (water equivalent)	388	308	326	285	482	705	568	265	181	206	420	641	**4774mm**

Annual total precipitation: 7406mm (-17.7%)

	May	Jun	Jul	Aug	Sep	Oct	Nov	Dec	Jan	Feb	Mar	Apr	year
Monthly temperature (-6°C)	-5.6	-7.5	-8.1	-7.1	-5.6	-4.3	-2.6	-1.0	0.0	0.4	-0.4	-2.8	-3.7°C
% snow	95	100	100	100	95	88	78	69	63	61	66	79	
Monthly total precipitation	518	393	415	363	644	1022	926	489	363	430	815	1029	7406mm
Snow (water equivalent)	494	393	415	363	614	898	724	338	230	263	535	817	**6083mm**

Annual total precipitation: 9000mm

	May	Jun	Jul	Aug	Sep	Oct	Nov	Dec	Jan	Feb	Mar	Apr	year
Monthly temperature (-6°C)	-5.6	-7.5	-8.1	-7.1	-5.6	-4.3	-2.6	-1.0	0.0	0.4	-0.4	-2.8	-3.7°C
% snow	95	100	100	100	95	88	78	69	63	61	66	79	
Monthly total precipitation	630	477	504	441	783	1242	1125	594	441	522	990	1251	9000mm
Snow (water equivalent)	600	477	504	441	746	1091	880	411	280	319	651	993	**7392mm**

7°C cooling

Annual total precipitation: 5388mm (-40.1%)

	May	Jun	Jul	Aug	Sep	Oct	Nov	Dec	Jan	Feb	Mar	Apr	year
Monthly temperature (-7°C)	-6.6	-8.5	-9.1	-8.1	-6.6	-5.3	-3.6	-2.0	-1.0	-0.6	-1.4	-3.8	-4.7°C
% snow	100	100	100	100	100	94	84	75	69	67	71	85	
Monthly total precipitation	377	286	302	264	469	744	674	356	264	313	593	749	5388mm
Snow (water equivalent)	377	286	302	264	469	696	565	266	182	209	423	637	**4675mm**

Annual total precipitation: 7194mm (-20.1%)

	May	Jun	Jul	Aug	Sep	Oct	Nov	Dec	Jan	Feb	Mar	Apr	year
Monthly temperature (-7°C)	-6.6	-8.5	-9.1	-8.1	-6.6	-5.3	-3.6	-2.0	-1.0	-0.6	-1.4	-3.8	-4.7°C
% snow	100	100	100	100	100	94	84	75	69	67	71	85	
Monthly total precipitation	504	381	403	353	626	993	899	475	353	417	791	1000	7194mm
Snow (water equivalent)	504	381	403	353	626	929	754	355	244	279	565	850	**6243mm**

Annual total precipitation: 9000mm

	May	Jun	Jul	Aug	Sep	Oct	Nov	Dec	Jan	Feb	Mar	Apr	year
Monthly temperature (-7°C)	-6.6	-8.5	-9.1	-8.1	-6.6	-5.3	-3.6	-2.0	-1.0	-0.6	-1.4	-3.8	-4.7°C
% snow	100	100	100	100	100	94	84	75	69	67	71	85	
Monthly total precipitation	630	477	504	441	783	1242	1125	594	441	522	990	1251	9000mm
Snow (water equivalent)	630	477	504	441	783	1162	944	444	305	349	707	1064	**7810mm**

8°C cooling

Annual total precipitation: 4988mm (-44.6%)

	May	Jun	Jul	Aug	Sep	Oct	Nov	Dec	Jan	Feb	Mar	Apr	year
Monthly temperature (-8°C)	-7.6	-9.5	-10.1	-9.1	-7.6	-6.3	-4.6	-3.0	-2.0	-1.6	-2.4	-4.8	-5.7°C
% snow	100	100	100	100	100	99	90	80	75	73	77	91	
Monthly total precipitation	349	264	279	244	434	688	624	329	244	289	549	693	4988mm
Snow (water equivalent)	349	264	279	244	434	683	559	265	183	210	423	629	**4522mm**

Annual total precipitation: 6994mm (-22.3%)

	May	Jun	Jul	Aug	Sep	Oct	Nov	Dec	Jan	Feb	Mar	Apr	year
Monthly temperature (-8°C)	-7.6	-9.5	-10.1	-9.1	-7.6	-6.3	-4.6	-3.0	-2.0	-1.6	-2.4	-4.8	-5.7°C
% snow	100	100	100	100	100	99	90	80	75	73	77	91	
Monthly total precipitation	490	371	392	343	608	965	874	462	343	406	769	972	6994mm
Snow (water equivalent)	490	371	392	343	608	958	783	372	256	294	593	882	**6341mm**

Annual total precipitation: 9000mm

	May	Jun	Jul	Aug	Sep	Oct	Nov	Dec	Jan	Feb	Mar	Apr	year
Monthly temperature (-8°C)	-7.6	-9.5	-10.1	-9.1	-7.6	-6.3	-4.6	-3.0	-2.0	-1.6	-2.4	-4.8	-5.7°C
% snow	100	100	100	100	100	99	90	80	75	73	77	91	
Monthly total precipitation	630	477	504	441	783	1242	1125	594	441	522	990	1251	9000mm
Snow (water equivalent)	630	477	504	441	783	1233	1008	478	330	379	763	1135	**8160mm**

9°C cooling

Annual total precipitation: 4625mm (-48.8%)

	May	Jun	Jul	Aug	Sep	Oct	Nov	Dec	Jan	Feb	Mar	Apr	year
Monthly temperature (-9°C)	-8.6	-10.5	-11.1	-10.1	-8.6	-7.3	-5.6	-4.0	-3.0	-2.6	-3.4	-5.8	-6.7°C
% snow	100	100	100	100	100	100	95	86	80	78	83	96	
Monthly total precipitation	324	245	259	227	402	638	578	305	227	268	509	643	4625mm
Snow (water equivalent)	324	245	259	227	402	638	551	263	182	210	421	620	**4342mm**

Annual total precipitation: 6813mm (-24.4%)

	May	Jun	Jul	Aug	Sep	Oct	Nov	Dec	Jan	Feb	Mar	Apr	year
Monthly temperature (-9°C)	-8.6	-10.5	-11.1	-10.1	-8.6	-7.3	-5.6	-4.0	-3.0	-2.6	-3.4	-5.8	-6.7°C
% snow	100	100	100	100	100	100	95	86	80	78	83	96	
Monthly total precipitation	477	361	382	334	593	940	852	450	334	395	749	947	6813mm
Snow (water equivalent)	477	361	382	334	593	940	811	387	269	309	620	913	**6396mm**

Annual total precipitation: 9000mm

	May	Jun	Jul	Aug	Sep	Oct	Nov	Dec	Jan	Feb	Mar	Apr	year
Monthly temperature (-9°C)	-8.6	-10.5	-11.1	-10.1	-8.6	-7.3	-5.6	-4.0	-3.0	-2.6	-3.4	-5.8	-6.7°C
% snow	100	100	100	100	100	100	95	86	80	78	83	96	
Monthly total precipitation	630	477	504	441	783	1242	1125	594	441	522	990	1251	9000mm
Snow (water equivalent)	630	477	504	441	783	1242	1072	512	355	408	819	1206	**8449mm**

Summary Precipitation Scenario 1 (Fig. 1)

cooling (annual) (°C)	0	-1	-2	-3	-4	-5	-6	-7	-8	-9
snowfall (annual) (mm)	4432	4594	4714	4794	4838	4838	4774	4675	4522	4342

Summary Precipitation Scenario 2 (Fig. 2)

cooling (annual) (°C)	0	-1	-2	-3	-4	-5	-6	-7	-8	-9
snowfall (annual) (mm)	4432	4761	5078	5373	5651	5896	6083	6243	6341	6396

Summary Precipitation Scenario 3 (Fig. 3)

cooling (annual) (°C)	0	-1	-2	-3	-4	-5	-6	-7	-8	-9
snowfall (annual) (mm)	4432	4929	5440	5952	6463	6953	7392	7810	8160	8449

Fig. 1

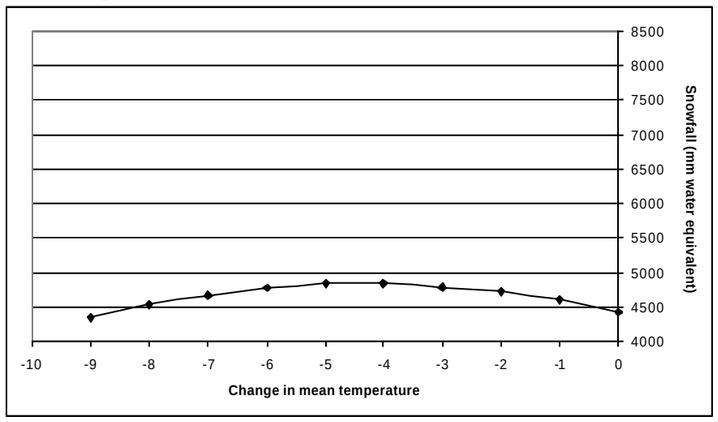

Fig. 2

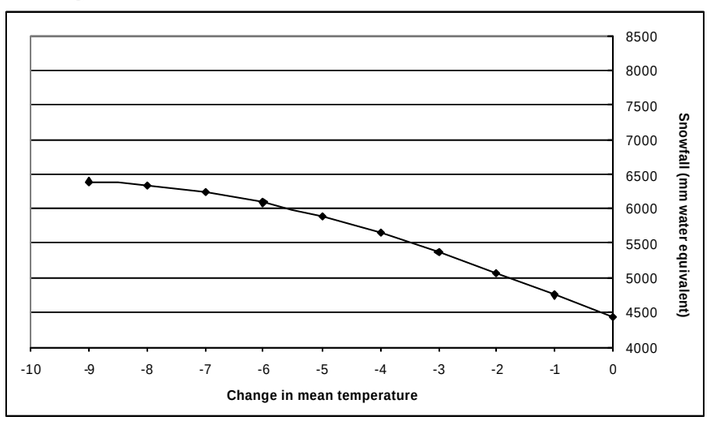

Fig. 3

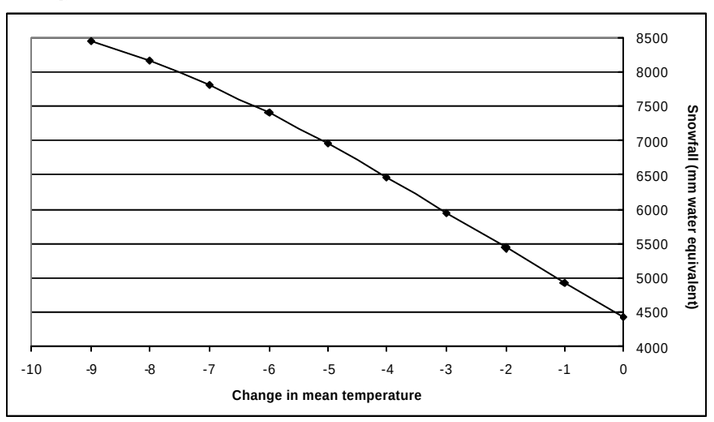

Summary

	Present	Scenario (- 1)	Scenario (- 2)	Scenario (- 3)	Scenario (- 4)	Scenario (- 5)	Scenario (- 6)	Scenario (- 7)	Scenario (- 8)	Scenario (- 9)
Positive degree days (Pdd)*	969	727	520	346	204	92	18	0	0	0
Pdd x 4.5 mm/d/°C**	4360	3270	2338	1559	919	416	79	0	0	0
Corrected ablation***	**4432**	**3326**	**2379**	**1586**	**935**	**423**	**80**	**0**	**0**	**0**
Snowfall										
Precipitation Scenario 1	4432	4594	4714	4794	4838	4838	4774	4675	4522	4342
Precipitation Scenario 2	4432	4761	5078	5373	5651	5896	6083	6243	6341	6396
Precipitation Scenario 3	4432	4929	5440	5952	6463	6953	7392	7810	8160	8449
Net accumulation										
Precipitation Scenario 1	**0**	**1268**	**2335**	**3208**	**3903**	**4415**	**4694**	**4675**	**4522**	**4342**
Precipitation Scenario 2	**0**	**1435**	**2699**	**3787**	**4716**	**5473**	**6003**	**6243**	**6341**	**6396**
Precipitation Scenario 3	**0**	**1603**	**3061**	**4366**	**5528**	**6530**	**7312**	**7810**	**8160**	**8449**

* Temperature data from Hokitika station (39m asl) lapsed to 1600m asl using 6K/km
** The Degree Day Factor (4.5 mm/d/°C) was measured at Franz Josef Glacier. See reference 29
*** Calculated present snowfall at ELA is 4432mm. The degree day calculated ablation is 4359.8mm underestimating ablation by 1.7%.

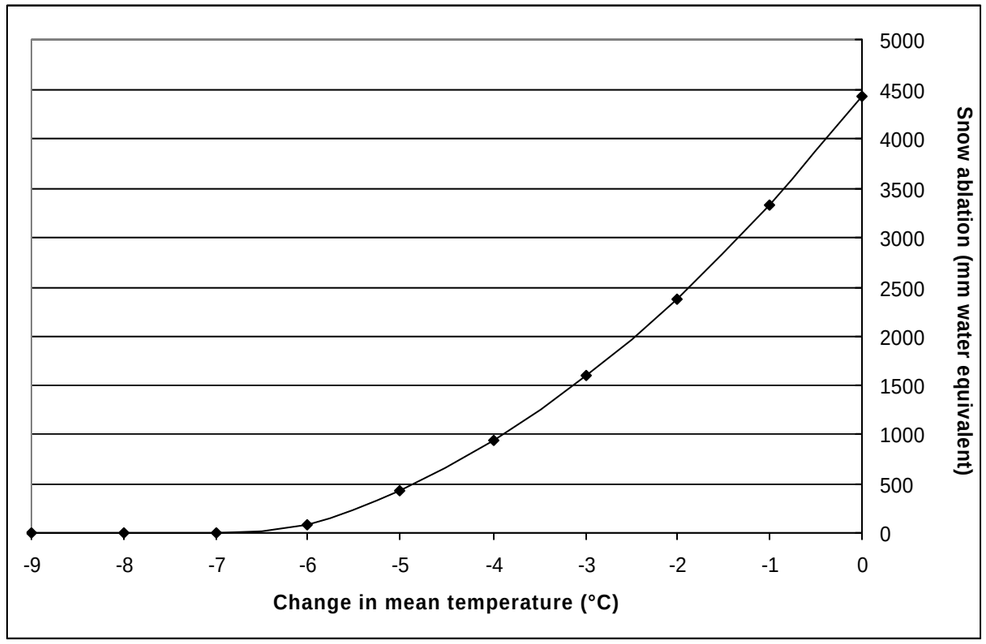

Figure 1

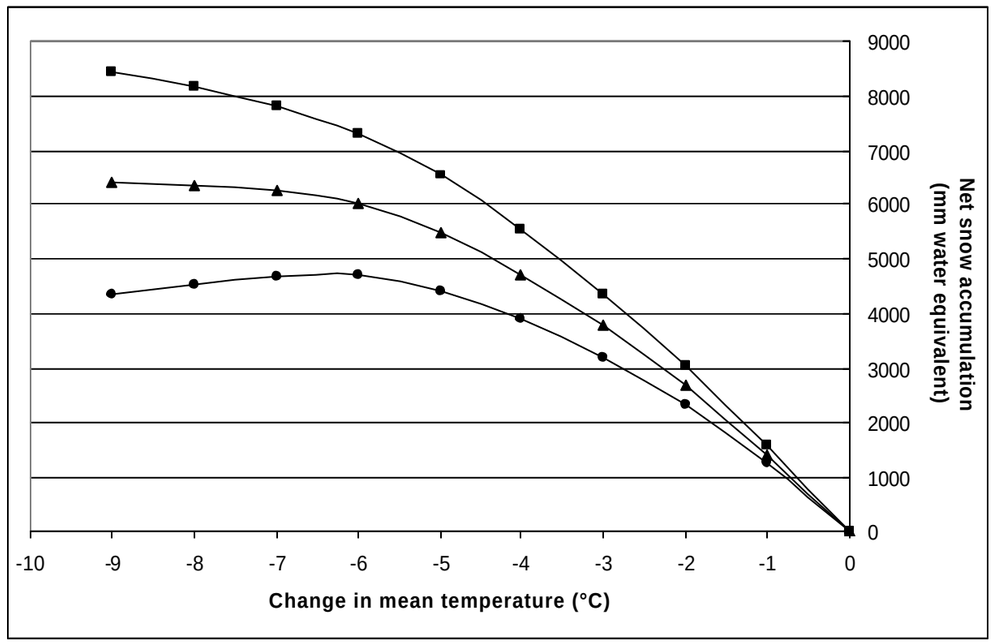

Figure 2

DEGREE DAY ABLATION CALCULATION

January Day	Mean Daily Temperature (Hokitika Station 39masl) (30 year average)	at ELA (1600m) (6K/km lapse rate)	Positive Degree Days (present)	PDD Scenario (- 1)	PDD Scenario (- 2)	PDD Scenario (- 3)	PDD Scenario (- 4)	PDD Scenario (- 5)	PDD Scenario (- 6)	PDD Scenario (- 7)	PDD Scenario (- 8)	PDD Scenario (- 9)
1-Jan	14.9	5.6	5.6	4.6	3.6	2.6	1.6	0.6	0.0	0.0	0.0	0.0
2-Jan	15.0	5.6	5.6	4.6	3.6	2.6	1.6	0.6	0.0	0.0	0.0	0.0
3-Jan	15.0	5.6	5.6	4.6	3.6	2.6	1.6	0.6	0.0	0.0	0.0	0.0
4-Jan	15.0	5.7	5.7	4.7	3.7	2.7	1.7	0.7	0.0	0.0	0.0	0.0
5-Jan	15.1	5.7	5.7	4.7	3.7	2.7	1.7	0.7	0.0	0.0	0.0	0.0
6-Jan	15.1	5.8	5.8	4.8	3.8	2.8	1.8	0.8	0.0	0.0	0.0	0.0
7-Jan	15.2	5.8	5.8	4.8	3.8	2.8	1.8	0.8	0.0	0.0	0.0	0.0
8-Jan	15.2	5.8	5.8	4.8	3.8	2.8	1.8	0.8	0.0	0.0	0.0	0.0
9-Jan	15.2	5.9	5.9	4.9	3.9	2.9	1.9	0.9	0.0	0.0	0.0	0.0
10-Jan	15.3	5.9	5.9	4.9	3.9	2.9	1.9	0.9	0.0	0.0	0.0	0.0
11-Jan	15.3	5.9	5.9	4.9	3.9	2.9	1.9	0.9	0.0	0.0	0.0	0.0
12-Jan	15.3	6.0	6.0	5.0	4.0	3.0	2.0	1.0	0.0	0.0	0.0	0.0
13-Jan	15.4	6.0	6.0	5.0	4.0	3.0	2.0	1.0	0.0	0.0	0.0	0.0
14-Jan	15.4	6.0	6.0	5.0	4.0	3.0	2.0	1.0	0.0	0.0	0.0	0.0
15-Jan	15.4	6.1	6.1	5.1	4.1	3.1	2.1	1.1	0.1	0.0	0.0	0.0
16-Jan	15.5	6.1	6.1	5.1	4.1	3.1	2.1	1.1	0.1	0.0	0.0	0.0
17-Jan	15.5	6.1	6.1	5.1	4.1	3.1	2.1	1.1	0.1	0.0	0.0	0.0
18-Jan	15.5	6.1	6.1	5.1	4.1	3.1	2.1	1.1	0.1	0.0	0.0	0.0
19-Jan	15.5	6.2	6.2	5.2	4.2	3.2	2.2	1.2	0.2	0.0	0.0	0.0
20-Jan	15.5	6.2	6.2	5.2	4.2	3.2	2.2	1.2	0.2	0.0	0.0	0.0
21-Jan	15.6	6.2	6.2	5.2	4.2	3.2	2.2	1.2	0.2	0.0	0.0	0.0
22-Jan	15.6	6.2	6.2	5.2	4.2	3.2	2.2	1.2	0.2	0.0	0.0	0.0
23-Jan	15.6	6.3	6.3	5.3	4.3	3.3	2.3	1.3	0.3	0.0	0.0	0.0
24-Jan	15.7	6.3	6.3	5.3	4.3	3.3	2.3	1.3	0.3	0.0	0.0	0.0
25-Jan	15.7	6.3	6.3	5.3	4.3	3.3	2.3	1.3	0.3	0.0	0.0	0.0
26-Jan	15.7	6.3	6.3	5.3	4.3	3.3	2.3	1.3	0.3	0.0	0.0	0.0
27-Jan	15.7	6.4	6.4	5.4	4.4	3.4	2.4	1.4	0.4	0.0	0.0	0.0
28-Jan	15.7	6.4	6.4	5.4	4.4	3.4	2.4	1.4	0.4	0.0	0.0	0.0
29-Jan	15.8	6.4	6.4	5.4	4.4	3.4	2.4	1.4	0.4	0.0	0.0	0.0
30-Jan	15.8	6.4	6.4	5.4	4.4	3.4	2.4	1.4	0.4	0.0	0.0	0.0
31-Jan	15.8	6.4	6.4	5.4	4.4	3.4	2.4	1.4	0.4	0.0	0.0	0.0

(Continued)

February Day	Mean Daily Temperature (Hokitika Station 39masl) (30 year average)	at ELA (1600m) (6K/km lapse rate)	Positive Degree Days (present)	PDD Scenario (- 1)	PDD Scenario (- 2)	PDD Scenario (- 3)	PDD Scenario (- 4)	PDD Scenario (- 5)	PDD Scenario (- 6)	PDD Scenario (- 7)	PDD Scenario (- 8)	PDD Scenario (- 9)
1-Feb	15.8	6.5	6.5	5.5	4.5	3.5	2.5	1.5	0.5	0.0	0.0	0.0
2-Feb	15.8	6.5	6.5	5.5	4.5	3.5	2.5	1.5	0.5	0.0	0.0	0.0
3-Feb	15.8	6.5	6.5	5.5	4.5	3.5	2.5	1.5	0.5	0.0	0.0	0.0
4-Feb	15.9	6.5	6.5	5.5	4.5	3.5	2.5	1.5	0.5	0.0	0.0	0.0
5-Feb	15.9	6.5	6.5	5.5	4.5	3.5	2.5	1.5	0.5	0.0	0.0	0.0
6-Feb	15.9	6.5	6.5	5.5	4.5	3.5	2.5	1.5	0.5	0.0	0.0	0.0
7-Feb	15.9	6.5	6.5	5.5	4.5	3.5	2.5	1.5	0.5	0.0	0.0	0.0
8-Feb	15.9	6.5	6.5	5.5	4.5	3.5	2.5	1.5	0.5	0.0	0.0	0.0
9-Feb	15.9	6.5	6.5	5.5	4.5	3.5	2.5	1.5	0.5	0.0	0.0	0.0
10-Feb	15.9	6.5	6.5	5.5	4.5	3.5	2.5	1.5	0.5	0.0	0.0	0.0
11-Feb	15.9	6.6	6.6	5.6	4.6	3.6	2.6	1.6	0.6	0.0	0.0	0.0
12-Feb	15.9	6.6	6.6	5.6	4.6	3.6	2.6	1.6	0.6	0.0	0.0	0.0
13-Feb	15.9	6.5	6.5	5.5	4.5	3.5	2.5	1.5	0.5	0.0	0.0	0.0
14-Feb	15.9	6.5	6.5	5.5	4.5	3.5	2.5	1.5	0.5	0.0	0.0	0.0
15-Feb	15.9	6.5	6.5	5.5	4.5	3.5	2.5	1.5	0.5	0.0	0.0	0.0
16-Feb	15.9	6.5	6.5	5.5	4.5	3.5	2.5	1.5	0.5	0.0	0.0	0.0
17-Feb	15.9	6.5	6.5	5.5	4.5	3.5	2.5	1.5	0.5	0.0	0.0	0.0
18-Feb	15.9	6.5	6.5	5.5	4.5	3.5	2.5	1.5	0.5	0.0	0.0	0.0
19-Feb	15.8	6.5	6.5	5.5	4.5	3.5	2.5	1.5	0.5	0.0	0.0	0.0
20-Feb	15.8	6.4	6.4	5.4	4.4	3.4	2.4	1.4	0.4	0.0	0.0	0.0
21-Feb	15.8	6.4	6.4	5.4	4.4	3.4	2.4	1.4	0.4	0.0	0.0	0.0
22-Feb	15.8	6.4	6.4	5.4	4.4	3.4	2.4	1.4	0.4	0.0	0.0	0.0
23-Feb	15.7	6.4	6.4	5.4	4.4	3.4	2.4	1.4	0.4	0.0	0.0	0.0
24-Feb	15.7	6.3	6.3	5.3	4.3	3.3	2.3	1.3	0.3	0.0	0.0	0.0
25-Feb	15.7	6.3	6.3	5.3	4.3	3.3	2.3	1.3	0.3	0.0	0.0	0.0
26-Feb	15.6	6.3	6.3	5.3	4.3	3.3	2.3	1.3	0.3	0.0	0.0	0.0
27-Feb	15.6	6.2	6.2	5.2	4.2	3.2	2.2	1.2	0.2	0.0	0.0	0.0
28-Feb	15.6	6.2	6.2	5.2	4.2	3.2	2.2	1.2	0.2	0.0	0.0	0.0
29-Feb	15.5	6.2	6.2	5.2	4.2	3.2	2.2	1.2	0.2	0.0	0.0	0.0

(Continued)

March Day	Mean Daily Temperature (Hokitika Station 39masl) (30 year average)	at ELA (1600m) (6K/km lapse rate)	Positive Degree Days (present)	PDD Scenario (- 1)	PDD Scenario (- 2)	PDD Scenario (- 3)	PDD Scenario (- 4)	PDD Scenario (- 5)	PDD Scenario (- 6)	PDD Scenario (- 7)	PDD Scenario (- 8)	PDD Scenario (- 9)
1-Mar	15.5	6.1	6.1	5.1	4.1	3.1	2.1	1.1	0.1	0.0	0.0	0.0
2-Mar	15.5	6.1	6.1	5.1	4.1	3.1	2.1	1.1	0.1	0.0	0.0	0.0
3-Mar	15.4	6.1	6.1	5.1	4.1	3.1	2.1	1.1	0.1	0.0	0.0	0.0
4-Mar	15.4	6.0	6.0	5.0	4.0	3.0	2.0	1.0	0.0	0.0	0.0	0.0
5-Mar	15.3	6.0	6.0	5.0	4.0	3.0	2.0	1.0	0.0	0.0	0.0	0.0
6-Mar	15.3	5.9	5.9	4.9	3.9	2.9	1.9	0.9	0.0	0.0	0.0	0.0
7-Mar	15.3	5.9	5.9	4.9	3.9	2.9	1.9	0.9	0.0	0.0	0.0	0.0
8-Mar	15.2	5.8	5.8	4.8	3.8	2.8	1.8	0.8	0.0	0.0	0.0	0.0
9-Mar	15.2	5.8	5.8	4.8	3.8	2.8	1.8	0.8	0.0	0.0	0.0	0.0
10-Mar	15.1	5.7	5.7	4.7	3.7	2.7	1.7	0.7	0.0	0.0	0.0	0.0
11-Mar	15.1	5.7	5.7	4.7	3.7	2.7	1.7	0.7	0.0	0.0	0.0	0.0
12-Mar	15.0	5.6	5.6	4.6	3.6	2.6	1.6	0.6	0.0	0.0	0.0	0.0
13-Mar	15.0	5.6	5.6	4.6	3.6	2.6	1.6	0.6	0.0	0.0	0.0	0.0
14-Mar	14.9	5.5	5.5	4.5	3.5	2.5	1.5	0.5	0.0	0.0	0.0	0.0
15-Mar	14.9	5.5	5.5	4.5	3.5	2.5	1.5	0.5	0.0	0.0	0.0	0.0
16-Mar	14.8	5.4	5.4	4.4	3.4	2.4	1.4	0.4	0.0	0.0	0.0	0.0
17-Mar	14.8	5.4	5.4	4.4	3.4	2.4	1.4	0.4	0.0	0.0	0.0	0.0
18-Mar	14.7	5.3	5.3	4.3	3.3	2.3	1.3	0.3	0.0	0.0	0.0	0.0
19-Mar	14.6	5.3	5.3	4.3	3.3	2.3	1.3	0.3	0.0	0.0	0.0	0.0
20-Mar	14.6	5.2	5.2	4.2	3.2	2.2	1.2	0.2	0.0	0.0	0.0	0.0
21-Mar	14.5	5.1	5.1	4.1	3.1	2.1	1.1	0.1	0.0	0.0	0.0	0.0
22-Mar	14.4	5.1	5.1	4.1	3.1	2.1	1.1	0.1	0.0	0.0	0.0	0.0
23-Mar	14.4	5.0	5.0	4.0	3.0	2.0	1.0	0.0	0.0	0.0	0.0	0.0
24-Mar	14.3	4.9	4.9	3.9	2.9	1.9	0.9	0.0	0.0	0.0	0.0	0.0
25-Mar	14.2	4.9	4.9	3.9	2.9	1.9	0.9	0.0	0.0	0.0	0.0	0.0
26-Mar	14.2	4.8	4.8	3.8	2.8	1.8	0.8	0.0	0.0	0.0	0.0	0.0
27-Mar	14.1	4.7	4.7	3.7	2.7	1.7	0.7	0.0	0.0	0.0	0.0	0.0
28-Mar	14.0	4.7	4.7	3.7	2.7	1.7	0.7	0.0	0.0	0.0	0.0	0.0
29-Mar	14.0	4.6	4.6	3.6	2.6	1.6	0.6	0.0	0.0	0.0	0.0	0.0
30-Mar	13.9	4.5	4.5	3.5	2.5	1.5	0.5	0.0	0.0	0.0	0.0	0.0
31-Mar	13.8	4.5	4.5	3.5	2.5	1.5	0.5	0.0	0.0	0.0	0.0	0.0

(Continued)

April Day	Mean Daily Temperature (Hokitika Station 39masl) (30 year average)	at ELA (1600m) (6K/km lapse rate)	Positive Degree Days (present)	PDD Scenario (- 1)	PDD Scenario (- 2)	PDD Scenario (- 3)	PDD Scenario (- 4)	PDD Scenario (- 5)	PDD Scenario (- 6)	PDD Scenario (- 7)	PDD Scenario (- 8)	PDD Scenario (- 9)
1-Apr	13.7	4.4	4.4	3.4	2.4	1.4	0.4	0.0	0.0	0.0	0.0	0.0
2-Apr	13.7	4.3	4.3	3.3	2.3	1.3	0.3	0.0	0.0	0.0	0.0	0.0
3-Apr	13.6	4.2	4.2	3.2	2.2	1.2	0.2	0.0	0.0	0.0	0.0	0.0
4-Apr	13.5	4.2	4.2	3.2	2.2	1.2	0.2	0.0	0.0	0.0	0.0	0.0
5-Apr	13.4	4.1	4.1	3.1	2.1	1.1	0.1	0.0	0.0	0.0	0.0	0.0
6-Apr	13.4	4.0	4.0	3.0	2.0	1.0	0.0	0.0	0.0	0.0	0.0	0.0
7-Apr	13.3	3.9	3.9	2.9	1.9	0.9	0.0	0.0	0.0	0.0	0.0	0.0
8-Apr	13.2	3.8	3.8	2.8	1.8	0.8	0.0	0.0	0.0	0.0	0.0	0.0
9-Apr	13.1	3.8	3.8	2.8	1.8	0.8	0.0	0.0	0.0	0.0	0.0	0.0
10-Apr	13.0	3.7	3.7	2.7	1.7	0.7	0.0	0.0	0.0	0.0	0.0	0.0
11-Apr	12.9	3.6	3.6	2.6	1.6	0.6	0.0	0.0	0.0	0.0	0.0	0.0
12-Apr	12.8	3.5	3.5	2.5	1.5	0.5	0.0	0.0	0.0	0.0	0.0	0.0
13-Apr	12.8	3.4	3.4	2.4	1.4	0.4	0.0	0.0	0.0	0.0	0.0	0.0
14-Apr	12.7	3.3	3.3	2.3	1.3	0.3	0.0	0.0	0.0	0.0	0.0	0.0
15-Apr	12.6	3.2	3.2	2.2	1.2	0.2	0.0	0.0	0.0	0.0	0.0	0.0
16-Apr	12.5	3.2	3.2	2.2	1.2	0.2	0.0	0.0	0.0	0.0	0.0	0.0
17-Apr	12.4	3.1	3.1	2.1	1.1	0.1	0.0	0.0	0.0	0.0	0.0	0.0
18-Apr	12.4	3.0	3.0	2.0	1.0	0.0	0.0	0.0	0.0	0.0	0.0	0.0
19-Apr	12.3	2.9	2.9	1.9	0.9	0.0	0.0	0.0	0.0	0.0	0.0	0.0
20-Apr	12.2	2.8	2.8	1.8	0.8	0.0	0.0	0.0	0.0	0.0	0.0	0.0
21-Apr	12.1	2.7	2.7	1.7	0.7	0.0	0.0	0.0	0.0	0.0	0.0	0.0
22-Apr	12.0	2.6	2.6	1.6	0.6	0.0	0.0	0.0	0.0	0.0	0.0	0.0
23-Apr	11.9	2.6	2.6	1.6	0.6	0.0	0.0	0.0	0.0	0.0	0.0	0.0
24-Apr	11.8	2.5	2.5	1.5	0.5	0.0	0.0	0.0	0.0	0.0	0.0	0.0
25-Apr	11.8	2.4	2.4	1.4	0.4	0.0	0.0	0.0	0.0	0.0	0.0	0.0
26-Apr	11.7	2.3	2.3	1.3	0.3	0.0	0.0	0.0	0.0	0.0	0.0	0.0
27-Apr	11.6	2.2	2.2	1.2	0.2	0.0	0.0	0.0	0.0	0.0	0.0	0.0
28-Apr	11.5	2.1	2.1	1.1	0.1	0.0	0.0	0.0	0.0	0.0	0.0	0.0
29-Apr	11.4	2.1	2.1	1.1	0.1	0.0	0.0	0.0	0.0	0.0	0.0	0.0
30-Apr	11.3	2.0	2.0	1.0	0.0	0.0	0.0	0.0	0.0	0.0	0.0	0.0

(Continued)

May Day	Mean Daily Temperature (Hokitika Station 39masl) (30 year average)	at ELA (1600m) (6K/km lapse rate)	Positive Degree Days (present)	PDD Scenario (- 1)	PDD Scenario (- 2)	PDD Scenario (- 3)	PDD Scenario (- 4)	PDD Scenario (- 5)	PDD Scenario (- 6)	PDD Scenario (- 7)	PDD Scenario (- 8)	PDD Scenario (- 9)
1-May	11.3	1.9	1.9	0.9	0.0	0.0	0.0	0.0	0.0	0.0	0.0	0.0
2-May	11.2	1.8	1.8	0.8	0.0	0.0	0.0	0.0	0.0	0.0	0.0	0.0
3-May	11.1	1.7	1.7	0.7	0.0	0.0	0.0	0.0	0.0	0.0	0.0	0.0
4-May	11.0	1.7	1.7	0.7	0.0	0.0	0.0	0.0	0.0	0.0	0.0	0.0
5-May	10.9	1.6	1.6	0.6	0.0	0.0	0.0	0.0	0.0	0.0	0.0	0.0
6-May	10.9	1.5	1.5	0.5	0.0	0.0	0.0	0.0	0.0	0.0	0.0	0.0
7-May	10.8	1.4	1.4	0.4	0.0	0.0	0.0	0.0	0.0	0.0	0.0	0.0
8-May	10.7	1.3	1.3	0.3	0.0	0.0	0.0	0.0	0.0	0.0	0.0	0.0
9-May	10.6	1.2	1.2	0.2	0.0	0.0	0.0	0.0	0.0	0.0	0.0	0.0
10-May	10.5	1.2	1.2	0.2	0.0	0.0	0.0	0.0	0.0	0.0	0.0	0.0
11-May	10.4	1.1	1.1	0.1	0.0	0.0	0.0	0.0	0.0	0.0	0.0	0.0
12-May	10.4	1.0	1.0	0.0	0.0	0.0	0.0	0.0	0.0	0.0	0.0	0.0
13-May	10.3	0.9	0.9	0.0	0.0	0.0	0.0	0.0	0.0	0.0	0.0	0.0
14-May	10.2	0.8	0.8	0.0	0.0	0.0	0.0	0.0	0.0	0.0	0.0	0.0
15-May	10.1	0.8	0.8	0.0	0.0	0.0	0.0	0.0	0.0	0.0	0.0	0.0
16-May	10.1	0.7	0.7	0.0	0.0	0.0	0.0	0.0	0.0	0.0	0.0	0.0
17-May	10.0	0.6	0.6	0.0	0.0	0.0	0.0	0.0	0.0	0.0	0.0	0.0
18-May	9.9	0.5	0.5	0.0	0.0	0.0	0.0	0.0	0.0	0.0	0.0	0.0
19-May	9.8	0.5	0.5	0.0	0.0	0.0	0.0	0.0	0.0	0.0	0.0	0.0
20-May	9.8	0.4	0.4	0.0	0.0	0.0	0.0	0.0	0.0	0.0	0.0	0.0
21-May	9.7	0.3	0.3	0.0	0.0	0.0	0.0	0.0	0.0	0.0	0.0	0.0
22-May	9.6	0.2	0.2	0.0	0.0	0.0	0.0	0.0	0.0	0.0	0.0	0.0
23-May	9.5	0.2	0.2	0.0	0.0	0.0	0.0	0.0	0.0	0.0	0.0	0.0
24-May	9.5	0.1	0.1	0.0	0.0	0.0	0.0	0.0	0.0	0.0	0.0	0.0
25-May	9.4	0.0	0.0	0.0	0.0	0.0	0.0	0.0	0.0	0.0	0.0	0.0
26-May	9.3	-0.1	0.0	0.0	0.0	0.0	0.0	0.0	0.0	0.0	0.0	0.0
27-May	9.2	-0.1	0.0	0.0	0.0	0.0	0.0	0.0	0.0	0.0	0.0	0.0
28-May	9.2	-0.2	0.0	0.0	0.0	0.0	0.0	0.0	0.0	0.0	0.0	0.0
29-May	9.1	-0.3	0.0	0.0	0.0	0.0	0.0	0.0	0.0	0.0	0.0	0.0
30-May	9.0	-0.4	0.0	0.0	0.0	0.0	0.0	0.0	0.0	0.0	0.0	0.0
31-May	8.9	-0.4	0.0	0.0	0.0	0.0	0.0	0.0	0.0	0.0	0.0	0.0

(Continued)

June Day	Mean Daily Temperature (Hokitika Station 39masl) (30 year average)	at ELA (1600m) (6K/km lapse rate)	Positive Degree Days (present)	PDD Scenario (- 1)	PDD Scenario (- 2)	PDD Scenario (- 3)	PDD Scenario (- 4)	PDD Scenario (- 5)	PDD Scenario (- 6)	PDD Scenario (- 7)	PDD Scenario (- 8)	PDD Scenario (- 9)
1-Jun	8.9	-0.5	0.0	0.0	0.0	0.0	0.0	0.0	0.0	0.0	0.0	0.0
2-Jun	8.8	-0.6	0.0	0.0	0.0	0.0	0.0	0.0	0.0	0.0	0.0	0.0
3-Jun	8.7	-0.6	0.0	0.0	0.0	0.0	0.0	0.0	0.0	0.0	0.0	0.0
4-Jun	8.7	-0.7	0.0	0.0	0.0	0.0	0.0	0.0	0.0	0.0	0.0	0.0
5-Jun	8.6	-0.8	0.0	0.0	0.0	0.0	0.0	0.0	0.0	0.0	0.0	0.0
6-Jun	8.5	-0.8	0.0	0.0	0.0	0.0	0.0	0.0	0.0	0.0	0.0	0.0
7-Jun	8.5	-0.9	0.0	0.0	0.0	0.0	0.0	0.0	0.0	0.0	0.0	0.0
8-Jun	8.4	-0.9	0.0	0.0	0.0	0.0	0.0	0.0	0.0	0.0	0.0	0.0
9-Jun	8.4	-1.0	0.0	0.0	0.0	0.0	0.0	0.0	0.0	0.0	0.0	0.0
10-Jun	8.3	-1.1	0.0	0.0	0.0	0.0	0.0	0.0	0.0	0.0	0.0	0.0
11-Jun	8.2	-1.2	0.0	0.0	0.0	0.0	0.0	0.0	0.0	0.0	0.0	0.0
12-Jun	8.1	-1.2	0.0	0.0	0.0	0.0	0.0	0.0	0.0	0.0	0.0	0.0
13-Jun	8.1	-1.3	0.0	0.0	0.0	0.0	0.0	0.0	0.0	0.0	0.0	0.0
14-Jun	8.0	-1.3	0.0	0.0	0.0	0.0	0.0	0.0	0.0	0.0	0.0	0.0
15-Jun	8.0	-1.4	0.0	0.0	0.0	0.0	0.0	0.0	0.0	0.0	0.0	0.0
16-Jun	8.0	-1.4	0.0	0.0	0.0	0.0	0.0	0.0	0.0	0.0	0.0	0.0
17-Jun	7.9	-1.5	0.0	0.0	0.0	0.0	0.0	0.0	0.0	0.0	0.0	0.0
18-Jun	7.9	-1.5	0.0	0.0	0.0	0.0	0.0	0.0	0.0	0.0	0.0	0.0
19-Jun	7.8	-1.5	0.0	0.0	0.0	0.0	0.0	0.0	0.0	0.0	0.0	0.0
20-Jun	7.8	-1.6	0.0	0.0	0.0	0.0	0.0	0.0	0.0	0.0	0.0	0.0
21-Jun	7.7	-1.6	0.0	0.0	0.0	0.0	0.0	0.0	0.0	0.0	0.0	0.0
22-Jun	7.7	-1.7	0.0	0.0	0.0	0.0	0.0	0.0	0.0	0.0	0.0	0.0
23-Jun	7.7	-1.7	0.0	0.0	0.0	0.0	0.0	0.0	0.0	0.0	0.0	0.0
24-Jun	7.6	-1.7	0.0	0.0	0.0	0.0	0.0	0.0	0.0	0.0	0.0	0.0
25-Jun	7.6	-1.7	0.0	0.0	0.0	0.0	0.0	0.0	0.0	0.0	0.0	0.0
26-Jun	7.6	-1.8	0.0	0.0	0.0	0.0	0.0	0.0	0.0	0.0	0.0	0.0
27-Jun	7.6	-1.8	0.0	0.0	0.0	0.0	0.0	0.0	0.0	0.0	0.0	0.0
28-Jun	7.5	-1.8	0.0	0.0	0.0	0.0	0.0	0.0	0.0	0.0	0.0	0.0
29-Jun	7.5	-1.9	0.0	0.0	0.0	0.0	0.0	0.0	0.0	0.0	0.0	0.0
30-Jun	7.5	-1.9	0.0	0.0	0.0	0.0	0.0	0.0	0.0	0.0	0.0	0.0

(Continued)

July Day	Mean Daily Temperature (Hokitika Station 39masl) (30 year average)	at ELA (1600m) (6K/km lapse rate)	Positive Degree Days (present)	PDD Scenario (- 1)	PDD Scenario (- 2)	PDD Scenario (- 3)	PDD Scenario (- 4)	PDD Scenario (- 5)	PDD Scenario (- 6)	PDD Scenario (- 7)	PDD Scenario (- 8)	PDD Scenario (- 9)
1-Jul	7.5	-1.9	0.0	0.0	0.0	0.0	0.0	0.0	0.0	0.0	0.0	0.0
2-Jul	7.5	-1.9	0.0	0.0	0.0	0.0	0.0	0.0	0.0	0.0	0.0	0.0
3-Jul	7.4	-1.9	0.0	0.0	0.0	0.0	0.0	0.0	0.0	0.0	0.0	0.0
4-Jul	7.4	-1.9	0.0	0.0	0.0	0.0	0.0	0.0	0.0	0.0	0.0	0.0
5-Jul	7.4	-2.0	0.0	0.0	0.0	0.0	0.0	0.0	0.0	0.0	0.0	0.0
6-Jul	7.4	-2.0	0.0	0.0	0.0	0.0	0.0	0.0	0.0	0.0	0.0	0.0
7-Jul	7.4	-2.0	0.0	0.0	0.0	0.0	0.0	0.0	0.0	0.0	0.0	0.0
8-Jul	7.4	-2.0	0.0	0.0	0.0	0.0	0.0	0.0	0.0	0.0	0.0	0.0
9-Jul	7.4	-2.0	0.0	0.0	0.0	0.0	0.0	0.0	0.0	0.0	0.0	0.0
10-Jul	7.4	-2.0	0.0	0.0	0.0	0.0	0.0	0.0	0.0	0.0	0.0	0.0
11-Jul	7.4	-2.0	0.0	0.0	0.0	0.0	0.0	0.0	0.0	0.0	0.0	0.0
12-Jul	7.4	-2.0	0.0	0.0	0.0	0.0	0.0	0.0	0.0	0.0	0.0	0.0
13-Jul	7.4	-2.0	0.0	0.0	0.0	0.0	0.0	0.0	0.0	0.0	0.0	0.0
14-Jul	7.4	-2.0	0.0	0.0	0.0	0.0	0.0	0.0	0.0	0.0	0.0	0.0
15-Jul	7.4	-2.0	0.0	0.0	0.0	0.0	0.0	0.0	0.0	0.0	0.0	0.0
16-Jul	7.4	-2.0	0.0	0.0	0.0	0.0	0.0	0.0	0.0	0.0	0.0	0.0
17-Jul	7.4	-2.0	0.0	0.0	0.0	0.0	0.0	0.0	0.0	0.0	0.0	0.0
18-Jul	7.4	-2.0	0.0	0.0	0.0	0.0	0.0	0.0	0.0	0.0	0.0	0.0
19-Jul	7.4	-2.0	0.0	0.0	0.0	0.0	0.0	0.0	0.0	0.0	0.0	0.0
20-Jul	7.4	-2.0	0.0	0.0	0.0	0.0	0.0	0.0	0.0	0.0	0.0	0.0
21-Jul	7.4	-2.0	0.0	0.0	0.0	0.0	0.0	0.0	0.0	0.0	0.0	0.0
22-Jul	7.4	-2.0	0.0	0.0	0.0	0.0	0.0	0.0	0.0	0.0	0.0	0.0
23-Jul	7.4	-1.9	0.0	0.0	0.0	0.0	0.0	0.0	0.0	0.0	0.0	0.0
24-Jul	7.4	-1.9	0.0	0.0	0.0	0.0	0.0	0.0	0.0	0.0	0.0	0.0
25-Jul	7.5	-1.9	0.0	0.0	0.0	0.0	0.0	0.0	0.0	0.0	0.0	0.0
26-Jul	7.5	-1.9	0.0	0.0	0.0	0.0	0.0	0.0	0.0	0.0	0.0	0.0
27-Jul	7.5	-1.9	0.0	0.0	0.0	0.0	0.0	0.0	0.0	0.0	0.0	0.0
28-Jul	7.5	-1.8	0.0	0.0	0.0	0.0	0.0	0.0	0.0	0.0	0.0	0.0
29-Jul	7.5	-1.8	0.0	0.0	0.0	0.0	0.0	0.0	0.0	0.0	0.0	0.0
30-Jul	7.6	-1.8	0.0	0.0	0.0	0.0	0.0	0.0	0.0	0.0	0.0	0.0
31-Jul	7.6	-1.8	0.0	0.0	0.0	0.0	0.0	0.0	0.0	0.0	0.0	0.0

(Continued)

August Day	Mean Daily Temperature (Hokitika Station 39masl) (30 year average)	at ELA (1600m) (6K/km lapse rate)	Positive Degree Days (present)	PDD Scenario (- 1)	PDD Scenario (- 2)	PDD Scenario (- 3)	PDD Scenario (- 4)	PDD Scenario (- 5)	PDD Scenario (- 6)	PDD Scenario (- 7)	PDD Scenario (- 8)	PDD Scenario (- 9)
1-Aug	7.6	-1.7	0.0	0.0	0.0	0.0	0.0	0.0	0.0	0.0	0.0	0.0
2-Aug	7.6	-1.7	0.0	0.0	0.0	0.0	0.0	0.0	0.0	0.0	0.0	0.0
3-Aug	7.7	-1.7	0.0	0.0	0.0	0.0	0.0	0.0	0.0	0.0	0.0	0.0
4-Aug	7.7	-1.7	0.0	0.0	0.0	0.0	0.0	0.0	0.0	0.0	0.0	0.0
5-Aug	7.7	-1.6	0.0	0.0	0.0	0.0	0.0	0.0	0.0	0.0	0.0	0.0
6-Aug	7.8	-1.6	0.0	0.0	0.0	0.0	0.0	0.0	0.0	0.0	0.0	0.0
7-Aug	7.8	-1.6	0.0	0.0	0.0	0.0	0.0	0.0	0.0	0.0	0.0	0.0
8-Aug	7.8	-1.5	0.0	0.0	0.0	0.0	0.0	0.0	0.0	0.0	0.0	0.0
9-Aug	7.9	-1.5	0.0	0.0	0.0	0.0	0.0	0.0	0.0	0.0	0.0	0.0
10-Aug	7.9	-1.5	0.0	0.0	0.0	0.0	0.0	0.0	0.0	0.0	0.0	0.0
11-Aug	8.0	-1.4	0.0	0.0	0.0	0.0	0.0	0.0	0.0	0.0	0.0	0.0
12-Aug	8.0	-1.4	0.0	0.0	0.0	0.0	0.0	0.0	0.0	0.0	0.0	0.0
13-Aug	8.0	-1.3	0.0	0.0	0.0	0.0	0.0	0.0	0.0	0.0	0.0	0.0
14-Aug	8.1	-1.3	0.0	0.0	0.0	0.0	0.0	0.0	0.0	0.0	0.0	0.0
15-Aug	8.1	-1.3	0.0	0.0	0.0	0.0	0.0	0.0	0.0	0.0	0.0	0.0
16-Aug	8.1	-1.2	0.0	0.0	0.0	0.0	0.0	0.0	0.0	0.0	0.0	0.0
17-Aug	8.2	-1.2	0.0	0.0	0.0	0.0	0.0	0.0	0.0	0.0	0.0	0.0
18-Aug	8.2	-1.2	0.0	0.0	0.0	0.0	0.0	0.0	0.0	0.0	0.0	0.0
19-Aug	8.3	-1.1	0.0	0.0	0.0	0.0	0.0	0.0	0.0	0.0	0.0	0.0
20-Aug	8.3	-1.1	0.0	0.0	0.0	0.0	0.0	0.0	0.0	0.0	0.0	0.0
21-Aug	8.4	-1.0	0.0	0.0	0.0	0.0	0.0	0.0	0.0	0.0	0.0	0.0
22-Aug	8.4	-1.0	0.0	0.0	0.0	0.0	0.0	0.0	0.0	0.0	0.0	0.0
23-Aug	8.4	-0.9	0.0	0.0	0.0	0.0	0.0	0.0	0.0	0.0	0.0	0.0
24-Aug	8.5	-0.9	0.0	0.0	0.0	0.0	0.0	0.0	0.0	0.0	0.0	0.0
25-Aug	8.5	-0.8	0.0	0.0	0.0	0.0	0.0	0.0	0.0	0.0	0.0	0.0
26-Aug	8.6	-0.8	0.0	0.0	0.0	0.0	0.0	0.0	0.0	0.0	0.0	0.0
27-Aug	8.6	-0.7	0.0	0.0	0.0	0.0	0.0	0.0	0.0	0.0	0.0	0.0
28-Aug	8.7	-0.7	0.0	0.0	0.0	0.0	0.0	0.0	0.0	0.0	0.0	0.0
29-Aug	8.7	-0.6	0.0	0.0	0.0	0.0	0.0	0.0	0.0	0.0	0.0	0.0
30-Aug	8.8	-0.6	0.0	0.0	0.0	0.0	0.0	0.0	0.0	0.0	0.0	0.0
31-Aug	8.8	-0.5	0.0	0.0	0.0	0.0	0.0	0.0	0.0	0.0	0.0	0.0

(Continued)

September Day	Mean Daily Temperature (Hokitika Station 39masl) (30 year average)	at ELA (1600m) (6K/km lapse rate)	Positive Degree Days (present)	PDD Scenario (- 1)	PDD Scenario (- 2)	PDD Scenario (- 3)	PDD Scenario (- 4)	PDD Scenario (- 5)	PDD Scenario (- 6)	PDD Scenario (- 7)	PDD Scenario (- 8)	PDD Scenario (- 9)
1-Sep	8.9	-0.5	0.0	0.0	0.0	0.0	0.0	0.0	0.0	0.0	0.0	0.0
2-Sep	9.0	-0.4	0.0	0.0	0.0	0.0	0.0	0.0	0.0	0.0	0.0	0.0
3-Sep	9.0	-0.4	0.0	0.0	0.0	0.0	0.0	0.0	0.0	0.0	0.0	0.0
4-Sep	9.1	-0.3	0.0	0.0	0.0	0.0	0.0	0.0	0.0	0.0	0.0	0.0
5-Sep	9.1	-0.3	0.0	0.0	0.0	0.0	0.0	0.0	0.0	0.0	0.0	0.0
6-Sep	9.2	-0.2	0.0	0.0	0.0	0.0	0.0	0.0	0.0	0.0	0.0	0.0
7-Sep	9.2	-0.2	0.0	0.0	0.0	0.0	0.0	0.0	0.0	0.0	0.0	0.0
8-Sep	9.3	-0.1	0.0	0.0	0.0	0.0	0.0	0.0	0.0	0.0	0.0	0.0
9-Sep	9.3	0.0	0.0	0.0	0.0	0.0	0.0	0.0	0.0	0.0	0.0	0.0
10-Sep	9.4	0.0	0.0	0.0	0.0	0.0	0.0	0.0	0.0	0.0	0.0	0.0
11-Sep	9.5	0.1	0.1	0.0	0.0	0.0	0.0	0.0	0.0	0.0	0.0	0.0
12-Sep	9.5	0.2	0.2	0.0	0.0	0.0	0.0	0.0	0.0	0.0	0.0	0.0
13-Sep	9.6	0.2	0.2	0.0	0.0	0.0	0.0	0.0	0.0	0.0	0.0	0.0
14-Sep	9.6	0.3	0.3	0.0	0.0	0.0	0.0	0.0	0.0	0.0	0.0	0.0
15-Sep	9.7	0.3	0.3	0.0	0.0	0.0	0.0	0.0	0.0	0.0	0.0	0.0
16-Sep	9.7	0.4	0.4	0.0	0.0	0.0	0.0	0.0	0.0	0.0	0.0	0.0
17-Sep	9.8	0.4	0.4	0.0	0.0	0.0	0.0	0.0	0.0	0.0	0.0	0.0
18-Sep	9.8	0.5	0.5	0.0	0.0	0.0	0.0	0.0	0.0	0.0	0.0	0.0
19-Sep	9.9	0.5	0.5	0.0	0.0	0.0	0.0	0.0	0.0	0.0	0.0	0.0
20-Sep	9.9	0.5	0.5	0.0	0.0	0.0	0.0	0.0	0.0	0.0	0.0	0.0
21-Sep	10.0	0.6	0.6	0.0	0.0	0.0	0.0	0.0	0.0	0.0	0.0	0.0
22-Sep	10.0	0.6	0.6	0.0	0.0	0.0	0.0	0.0	0.0	0.0	0.0	0.0
23-Sep	10.0	0.7	0.7	0.0	0.0	0.0	0.0	0.0	0.0	0.0	0.0	0.0
24-Sep	10.1	0.7	0.7	0.0	0.0	0.0	0.0	0.0	0.0	0.0	0.0	0.0
25-Sep	10.1	0.8	0.8	0.0	0.0	0.0	0.0	0.0	0.0	0.0	0.0	0.0
26-Sep	10.2	0.8	0.8	0.0	0.0	0.0	0.0	0.0	0.0	0.0	0.0	0.0
27-Sep	10.2	0.9	0.9	0.0	0.0	0.0	0.0	0.0	0.0	0.0	0.0	0.0
28-Sep	10.3	0.9	0.9	0.0	0.0	0.0	0.0	0.0	0.0	0.0	0.0	0.0
29-Sep	10.3	0.9	0.9	0.0	0.0	0.0	0.0	0.0	0.0	0.0	0.0	0.0
30-Sep	10.4	1.0	1.0	0.0	0.0	0.0	0.0	0.0	0.0	0.0	0.0	0.0

(Continued)

October Day	Mean Daily Temperature (Hokitika Station 39masl) (30 year average)	at ELA (1600m) (6K/km lapse rate)	Positive Degree Days (present)	PDD Scenario (- 1)	PDD Scenario (- 2)	PDD Scenario (- 3)	PDD Scenario (- 4)	PDD Scenario (- 5)	PDD Scenario (- 6)	PDD Scenario (- 7)	PDD Scenario (- 8)	PDD Scenario (- 9)
1-Oct	10.4	1.0	1.0	0.0	0.0	0.0	0.0	0.0	0.0	0.0	0.0	0.0
2-Oct	10.4	1.1	1.1	0.1	0.0	0.0	0.0	0.0	0.0	0.0	0.0	0.0
3-Oct	10.5	1.1	1.1	0.1	0.0	0.0	0.0	0.0	0.0	0.0	0.0	0.0
4-Oct	10.5	1.2	1.2	0.2	0.0	0.0	0.0	0.0	0.0	0.0	0.0	0.0
5-Oct	10.6	1.2	1.2	0.2	0.0	0.0	0.0	0.0	0.0	0.0	0.0	0.0
6-Oct	10.6	1.3	1.3	0.3	0.0	0.0	0.0	0.0	0.0	0.0	0.0	0.0
7-Oct	10.7	1.3	1.3	0.3	0.0	0.0	0.0	0.0	0.0	0.0	0.0	0.0
8-Oct	10.7	1.3	1.3	0.3	0.0	0.0	0.0	0.0	0.0	0.0	0.0	0.0
9-Oct	10.8	1.4	1.4	0.4	0.0	0.0	0.0	0.0	0.0	0.0	0.0	0.0
10-Oct	10.8	1.4	1.4	0.4	0.0	0.0	0.0	0.0	0.0	0.0	0.0	0.0
11-Oct	10.8	1.4	1.4	0.4	0.0	0.0	0.0	0.0	0.0	0.0	0.0	0.0
12-Oct	10.9	1.5	1.5	0.5	0.0	0.0	0.0	0.0	0.0	0.0	0.0	0.0
13-Oct	10.9	1.5	1.5	0.5	0.0	0.0	0.0	0.0	0.0	0.0	0.0	0.0
14-Oct	11.0	1.6	1.6	0.6	0.0	0.0	0.0	0.0	0.0	0.0	0.0	0.0
15-Oct	11.0	1.6	1.6	0.6	0.0	0.0	0.0	0.0	0.0	0.0	0.0	0.0
16-Oct	11.0	1.7	1.7	0.7	0.0	0.0	0.0	0.0	0.0	0.0	0.0	0.0
17-Oct	11.1	1.7	1.7	0.7	0.0	0.0	0.0	0.0	0.0	0.0	0.0	0.0
18-Oct	11.1	1.8	1.8	0.8	0.0	0.0	0.0	0.0	0.0	0.0	0.0	0.0
19-Oct	11.2	1.8	1.8	0.8	0.0	0.0	0.0	0.0	0.0	0.0	0.0	0.0
20-Oct	11.2	1.8	1.8	0.8	0.0	0.0	0.0	0.0	0.0	0.0	0.0	0.0
21-Oct	11.3	1.9	1.9	0.9	0.0	0.0	0.0	0.0	0.0	0.0	0.0	0.0
22-Oct	11.3	1.9	1.9	0.9	0.0	0.0	0.0	0.0	0.0	0.0	0.0	0.0
23-Oct	11.4	2.0	2.0	1.0	0.0	0.0	0.0	0.0	0.0	0.0	0.0	0.0
24-Oct	11.4	2.0	2.0	1.0	0.0	0.0	0.0	0.0	0.0	0.0	0.0	0.0
25-Oct	11.4	2.1	2.1	1.1	0.1	0.0	0.0	0.0	0.0	0.0	0.0	0.0
26-Oct	11.5	2.1	2.1	1.1	0.1	0.0	0.0	0.0	0.0	0.0	0.0	0.0
27-Oct	11.5	2.2	2.2	1.2	0.2	0.0	0.0	0.0	0.0	0.0	0.0	0.0
28-Oct	11.6	2.2	2.2	1.2	0.2	0.0	0.0	0.0	0.0	0.0	0.0	0.0
29-Oct	11.6	2.3	2.3	1.3	0.3	0.0	0.0	0.0	0.0	0.0	0.0	0.0
30-Oct	11.7	2.3	2.3	1.3	0.3	0.0	0.0	0.0	0.0	0.0	0.0	0.0
31-Oct	11.7	2.4	2.4	1.4	0.4	0.0	0.0	0.0	0.0	0.0	0.0	0.0

(Continued)

November Day	Mean Daily Temperature (Hokitika Station 39masl) (30 year average)	at ELA (1600m) (6K/km lapse rate)	Positive Degree Days (present)	PDD Scenario (- 1)	PDD Scenario (- 2)	PDD Scenario (- 3)	PDD Scenario (- 4)	PDD Scenario (- 5)	PDD Scenario (- 6)	PDD Scenario (- 7)	PDD Scenario (- 8)	PDD Scenario (- 9)
1-Nov	11.8	2.4	2.4	1.4	0.4	0.0	0.0	0.0	0.0	0.0	0.0	0.0
2-Nov	11.8	2.5	2.5	1.5	0.5	0.0	0.0	0.0	0.0	0.0	0.0	0.0
3-Nov	11.9	2.5	2.5	1.5	0.5	0.0	0.0	0.0	0.0	0.0	0.0	0.0
4-Nov	11.9	2.6	2.6	1.6	0.6	0.0	0.0	0.0	0.0	0.0	0.0	0.0
5-Nov	12.0	2.6	2.6	1.6	0.6	0.0	0.0	0.0	0.0	0.0	0.0	0.0
6-Nov	12.0	2.7	2.7	1.7	0.7	0.0	0.0	0.0	0.0	0.0	0.0	0.0
7-Nov	12.1	2.7	2.7	1.7	0.7	0.0	0.0	0.0	0.0	0.0	0.0	0.0
8-Nov	12.1	2.8	2.8	1.8	0.8	0.0	0.0	0.0	0.0	0.0	0.0	0.0
9-Nov	12.2	2.8	2.8	1.8	0.8	0.0	0.0	0.0	0.0	0.0	0.0	0.0
10-Nov	12.2	2.9	2.9	1.9	0.9	0.0	0.0	0.0	0.0	0.0	0.0	0.0
11-Nov	12.3	2.9	2.9	1.9	0.9	0.0	0.0	0.0	0.0	0.0	0.0	0.0
12-Nov	12.3	3.0	3.0	2.0	1.0	0.0	0.0	0.0	0.0	0.0	0.0	0.0
13-Nov	12.4	3.0	3.0	2.0	1.0	0.0	0.0	0.0	0.0	0.0	0.0	0.0
14-Nov	12.4	3.1	3.1	2.1	1.1	0.1	0.0	0.0	0.0	0.0	0.0	0.0
15-Nov	12.5	3.1	3.1	2.1	1.1	0.1	0.0	0.0	0.0	0.0	0.0	0.0
16-Nov	12.5	3.2	3.2	2.2	1.2	0.2	0.0	0.0	0.0	0.0	0.0	0.0
17-Nov	12.6	3.2	3.2	2.2	1.2	0.2	0.0	0.0	0.0	0.0	0.0	0.0
18-Nov	12.6	3.3	3.3	2.3	1.3	0.3	0.0	0.0	0.0	0.0	0.0	0.0
19-Nov	12.7	3.3	3.3	2.3	1.3	0.3	0.0	0.0	0.0	0.0	0.0	0.0
20-Nov	12.8	3.4	3.4	2.4	1.4	0.4	0.0	0.0	0.0	0.0	0.0	0.0
21-Nov	12.8	3.5	3.5	2.5	1.5	0.5	0.0	0.0	0.0	0.0	0.0	0.0
22-Nov	12.9	3.5	3.5	2.5	1.5	0.5	0.0	0.0	0.0	0.0	0.0	0.0
23-Nov	13.0	3.6	3.6	2.6	1.6	0.6	0.0	0.0	0.0	0.0	0.0	0.0
24-Nov	13.0	3.6	3.6	2.6	1.6	0.6	0.0	0.0	0.0	0.0	0.0	0.0
25-Nov	13.1	3.7	3.7	2.7	1.7	0.7	0.0	0.0	0.0	0.0	0.0	0.0
26-Nov	13.1	3.8	3.8	2.8	1.8	0.8	0.0	0.0	0.0	0.0	0.0	0.0
27-Nov	13.2	3.8	3.8	2.8	1.8	0.8	0.0	0.0	0.0	0.0	0.0	0.0
28-Nov	13.2	3.9	3.9	2.9	1.9	0.9	0.0	0.0	0.0	0.0	0.0	0.0
29-Nov	13.3	3.9	3.9	2.9	1.9	0.9	0.0	0.0	0.0	0.0	0.0	0.0
30-Nov	13.3	4.0	4.0	3.0	2.0	1.0	0.0	0.0	0.0	0.0	0.0	0.0

(Continued)

December Day	Mean Daily Temperature (Hokitika Station 39masl) (30 year average)	at ELA (1600m) (6K/km lapse rate)	Positive Degree Days (present)	PDD Scenario (- 1)	PDD Scenario (- 2)	PDD Scenario (- 3)	PDD Scenario (- 4)	PDD Scenario (- 5)	PDD Scenario (- 6)	PDD Scenario (- 7)	PDD Scenario (- 8)	PDD Scenario (- 9)
1-Dec	13.4	4.0	4.0	3.0	2.0	1.0	0.0	0.0	0.0	0.0	0.0	0.0
2-Dec	13.5	4.1	4.1	3.1	2.1	1.1	0.1	0.0	0.0	0.0	0.0	0.0
3-Dec	13.5	4.1	4.1	3.1	2.1	1.1	0.1	0.0	0.0	0.0	0.0	0.0
4-Dec	13.6	4.2	4.2	3.2	2.2	1.2	0.2	0.0	0.0	0.0	0.0	0.0
5-Dec	13.6	4.3	4.3	3.3	2.3	1.3	0.3	0.0	0.0	0.0	0.0	0.0
6-Dec	13.7	4.3	4.3	3.3	2.3	1.3	0.3	0.0	0.0	0.0	0.0	0.0
7-Dec	13.7	4.4	4.4	3.4	2.4	1.4	0.4	0.0	0.0	0.0	0.0	0.0
8-Dec	13.8	4.4	4.4	3.4	2.4	1.4	0.4	0.0	0.0	0.0	0.0	0.0
9-Dec	13.8	4.5	4.5	3.5	2.5	1.5	0.5	0.0	0.0	0.0	0.0	0.0
10-Dec	13.9	4.5	4.5	3.5	2.5	1.5	0.5	0.0	0.0	0.0	0.0	0.0
11-Dec	14.0	4.6	4.6	3.6	2.6	1.6	0.6	0.0	0.0	0.0	0.0	0.0
12-Dec	14.0	4.7	4.7	3.7	2.7	1.7	0.7	0.0	0.0	0.0	0.0	0.0
13-Dec	14.1	4.7	4.7	3.7	2.7	1.7	0.7	0.0	0.0	0.0	0.0	0.0
14-Dec	14.1	4.8	4.8	3.8	2.8	1.8	0.8	0.0	0.0	0.0	0.0	0.0
15-Dec	14.2	4.8	4.8	3.8	2.8	1.8	0.8	0.0	0.0	0.0	0.0	0.0
16-Dec	14.2	4.9	4.9	3.9	2.9	1.9	0.9	0.0	0.0	0.0	0.0	0.0
17-Dec	14.3	4.9	4.9	3.9	2.9	1.9	0.9	0.0	0.0	0.0	0.0	0.0
18-Dec	14.3	4.9	4.9	3.9	2.9	1.9	0.9	0.0	0.0	0.0	0.0	0.0
19-Dec	14.4	5.0	5.0	4.0	3.0	2.0	1.0	0.0	0.0	0.0	0.0	0.0
20-Dec	14.4	5.0	5.0	4.0	3.0	2.0	1.0	0.0	0.0	0.0	0.0	0.0
21-Dec	14.5	5.1	5.1	4.1	3.1	2.1	1.1	0.1	0.0	0.0	0.0	0.0
22-Dec	14.5	5.1	5.1	4.1	3.1	2.1	1.1	0.1	0.0	0.0	0.0	0.0
23-Dec	14.5	5.2	5.2	4.2	3.2	2.2	1.2	0.2	0.0	0.0	0.0	0.0
24-Dec	14.6	5.2	5.2	4.2	3.2	2.2	1.2	0.2	0.0	0.0	0.0	0.0
25-Dec	14.6	5.3	5.3	4.3	3.3	2.3	1.3	0.3	0.0	0.0	0.0	0.0
26-Dec	14.7	5.3	5.3	4.3	3.3	2.3	1.3	0.3	0.0	0.0	0.0	0.0
27-Dec	14.7	5.4	5.4	4.4	3.4	2.4	1.4	0.4	0.0	0.0	0.0	0.0
28-Dec	14.8	5.4	5.4	4.4	3.4	2.4	1.4	0.4	0.0	0.0	0.0	0.0
29-Dec	14.8	5.4	5.4	4.4	3.4	2.4	1.4	0.4	0.0	0.0	0.0	0.0
30-Dec	14.9	5.5	5.5	4.5	3.5	2.5	1.5	0.5	0.0	0.0	0.0	0.0
31-Dec	14.9	5.5	5.5	4.5	3.5	2.5	1.5	0.5	0.0	0.0	0.0	0.0
		Total	**969**	**727**	**520**	**346**	**204**	**92**	**18**	**0**	**0**	**0**